ADSORPTION OF ORGANOTIN COMPOUNDS ON NANO METAL OXIDE/SILICA, ACTIVATED CARBON AND FLY ASH COMPOSITE MATERIALS

by

OLUSHOLA SUNDAY AYANDA
B.Sc. (Hons.), M.Sc. (Ind. Chem.) (Ilorin), *miccon*

Thesis submitted in fulfilment of the requirements for the degree

Doctor of Technology: Chemistry

in the Faculty of Applied Sciences

at the Cape Peninsula University of Technology

Supervisor: Prof Olalekan Fatoki
Co-supervisor: Dr Bhekumusa J. Ximba
External co-supervisor: Prof Folahan A. Adekola

Cape Town
August 2013

DECLARATION

I, Olushola Sunday Ayanda, declare that the contents of this dissertation/thesis represent my own unaided work, and that the dissertation/thesis has not previously been submitted for academic examination towards any qualification. Furthermore, it represents my own opinions and not necessarily those of the Cape Peninsula University of Technology.

Signed **Date**

ABSTRACT

In this present study, the physicochemical properties, nature and morphology of prepared composite materials involving activated carbon, fly ash, nFe_3O_4, $nSiO_2$ and nZnO in the 1:1 ratio for two components composite materials and 1:1:1 for three components composite materials were investigated. The nature, morphology and elemental characterizations of these materials were carried out by means of modern analytical methods such as scanning electron and transmission electron microscopy (SEM and TEM), x-ray diffraction (XRD), x-ray fluorescence (XRF), inductively coupled plasma mass spectrometry (ICP-MS), inductively coupled plasma atomic emission spectroscopy (ICP-AES) and Fourier transform infrared spectroscopy (FTIR). Other physicochemical characterizations undertaken were CNH analysis, ash content, pH, point of zero charge and surface area and porosity determination by Brunauer, Emmett and Teller (BET). The precursors and composite materials were then applied to the sorption (remediation) of tributyltin (TBT) and triphenyltin (TPT) from artificial seawater and wastewater and the adsorption efficiencies for the precursors and the composites compared. The adsorption of TBT and TPT onto these materials as a function of adsorbent amount, contact time, pH, stirring speed, initial adsorbate concentration and temperature was investigated. Maximum organotin adsorption was recorded within the pH range of normal saline water (pH 8). Approximately 99.95 %, 95.75 %, 96.78 %, 99.88 %, 96.96 %, 99.98 %, 99.99 %, 99.99 % and 99.99 % TBT were removed from 25 mL of 100 mg/L TBT-contaminated artificial seawater using 0.5 g adsorbents at a contact time of 60 min, pH 8, stirring speed 200 rpm and temperature of 80 ^oC by activated carbon, fly ash, nFe_3O_4, $nSiO_2$, nZnO, fly ash/activated carbon, nFe_3O_4/activated carbon, $nSiO_2$/activated carbon and nZnO/activated carbon composite, respectively and the adsorption of TBT onto these adsorbents was endothermic. Approx. 99.99 %, 96.54 %, 95.50 %, 96.92 %, 97.14 %, 99.99 %, 98.44 %, 98.98 % and 99.66 % TPT were also removed from 25 mL of 100 mg/L TPT-contaminated artificial seawater using 0.5 g adsorbents at a contact time of 60 min, pH 8, stirring speed 200 rpm and a temperature of 20 ^oC by the activated carbon, fly ash, nFe_3O_4, $nSiO_2$, nZnO, fly ash/activated carbon, nFe_3O_4/fly ash, $nSiO_2$/fly ash and nZnO/fly ash composite, respectively. The adsorption of TPT onto activated carbon and fly ash/activated carbon composite from TPT – contaminated artificial seawater was endothermic while TPT adsorption onto fly ash, nFe_3O_4, $nSiO_2$, nZnO, nFe_3O_4/fly ash, $nSiO_2$/fly ash and nZnO/fly ash composites from TPT – contaminated artificial seawater was exothermic. The adsorption of TBT and TPT onto nFe_3O_4/fly ash/activated carbon and $nSiO_2$/fly ash/activated carbon composites from TBT – and TPT – contaminated water, respectively were endothermic and approx. 99.98 % and 99.99 % of TBT and TPT, respectively were removed from the initial concentration of 100 mg/L OTC by the composites at a temperature of 80 ^oC, 60 min contact time, pH 8 and a stirring speed of 200 rpm. The adsorption kinetics of all the precursors and composite materials fitted well with the pseudo

second-order kinetic model while the adsorption isotherm data could be well described by the Freundlich isotherm model except TBT adsorption onto nZnO/activated carbon and nFe_3O_4/activated carbon composite from TBT contaminated artificial seawater, TPT adsorption onto activated carbon and fly ash/activated carbon from TPT contaminated artificial seawater, and TPT sorption onto $nSiO_2$/fly ash/activated carbon composite from TPT – contaminated water which could be described by both the Freundlich and Dubinin-Radushkevich (D-R) isotherm models. Optimal conditions for the adsorption of TBT and TPT from artificial seawater were further applied to TBT and TPT removal from TBT – and TPT – contaminated natural seawater obtained from Cape Town harbour and the results obtained show that 99.71 %, 79.23 %, 80.11 %, 82.86 %, 80.42 %, 99.75 %, 99.88 %, 99.83 % and 99.88 % TBT were removed from TBT – contaminated natural seawater by activated carbon, fly ash, nFe_3O_4, $nSiO_2$, nZnO, fly ash/activated carbon, nFe_3O_4/activated carbon, $nSiO_2$/activated carbon and nZnO/activated carbon composite, respectively while 99.90 %, 96.44 %, 95.37 %, 96.75 %, 97.03 %, 99.92 %, 98.42 %, 98.92 % and 99.58 % TPT were removed from TPT – contaminated natural seawater by activated carbon, fly ash, nFe_3O_4, $nSiO_2$, nZnO, fly ash/activated carbon, nFe_3O_4/fly ash, $nSiO_2$/fly ash and nZnO/fly ash composite, respectively. Experimental results therefore show that the composite materials present higher organotin adsorption efficiency than the precursors due to the nature and improved properties of the composite materials and can therefore be utilized for the remediation of organotin contamination from industrial and/or shipyards process wastewater to > 99 % reduction before discharge into the environment.

ACKNOWLEDGEMENTS

I wish to thank:

- Almighty God, for his wonderful work in my life. I thank him for his guidance, protection, care, provision, his love and peace over my life.
- My excellent and hardworking supervisor, Prof O.S. Fatoki for his sacrifice of time, energy and laboratory assistance towards the completion of this project. The God almighty be with him and his families. Amen.
- My mentor and external co-supervisor, Prof F.A. Adekola who helped me in many ways. His comments, suggestions and supervision during this research work expose me to a lot of interesting things that will be of great use in future. The Lord almighty will continue to promote him in every areas of life. Amen
- My admirable co-supervisor, Dr B.J. Ximba. He gave me necessary laboratory assistance. The lord almighty will continue to help him in all his endeavors. Amen.
- Cape Peninsula University of Technology, for the award of 2011, 2012 and 2013 bursary and 2012 University Research Fund to study Doctor of Tech., Chemistry in the institution.
- Department of Chemistry, CPUT, Bellville campus, for supporting me financially in terms of lecturing position at the Department.
- The CPUT staff members, I will like to say special thanks to Prof Tjaart N. Van Der Walt, Dr F. Wewers, Mrs Shirley Le Roux, Mr Xolani Mdoda, Mr Peter Frank, Mr Christoffel J. Van Zyl, Dr Tobie Oosthuysen, Merichia Peterson, Liziwe Poni, Ivy Juta, Mrs Lorna Marshall, Dawn Petersen, Zandile Lorraine Mthembu, A. Solomon, Llewellyn Anthony, S. Adonis, Gillian Fennesy-Yon, Andre Spies, Kanyisa Nohako, and Luyanda Mnyaka. I appreciate the moral and technical support given to me by colleagues; Mr O.S. Akinsoji, Adeyi Oladayo, Mr. Ogidan, Mrs Olafisoye Oladunni, Dr L. Olujimi, Dr A. Daso, Eric Jondiko, Oputu Ochuko, Awe Tunji, Fred Okumu, Dr Hussein Okoro, Mr A. Musengi, and Sumbu Kakalanga. My special appreciation goes to Prof. Fakunle, Dr B.O. Opeolu, Mr Godwin Olutona, Dr O. Olatunji, Dr Olawale Ajuwon and Dr. Ayeleso and I also thank my students, Erica Suana, Tangouna L.B. Marie-Louise and Christele L. Komba for their laboratory assistance.
- Prof L. Petrik and Dr O. Fatoba for providing the fly ash. Mrs W. Miranda and Mr Francoius of the Electron Microscope Unit. Prof David Reid of Department of Geology, and the BET Unit, Chemical Engineering Department, University of Cape Town for their assistance towards the analytical characterization of my materials.
- Central Analytical Facility, Stellenbosch University for their assistance towards the ICP-MS, ICP-AES, GC-MS and Euro Ea elemental analysis of my samples.
- My parents, Mr and Mrs Ayanda for their advice, encouregment and financial support. Their prayers also contributed to the success of this research work.
- My wife, Mrs Ayanda Folashade Bunmi for her patience, love, care and for standing by me. Her advice and contribution is also of great benefit. Nothing will ever separate us in Jesus name. Amen.
- My daughter and Love, Miss Loveth Omoshewa Ayanda for her love and patience. Love you so much my Love.
- Mr and Mrs Yahaya, for their calls and word of encouragement.
- The Redeemed Christian Church of God (RCCG), Latter House Parish, Cape Town, South Africa and RCCG, Wonder Area Headquarter, Iwo, Osun State, Nigeria for their prayers.
- My sisters and brothers: Ayanda Omolola Temitope, Ayanda Odunayo, Ayanda Motunrayo, Funmilayo Ogunmokun, Alexander Ayanda, Tobi Lateef and Damola Simeon. We shall all live long and not die young in Jesus name. Amen.
- My late sister, Miss Aduke Oluwatoyin, My late grandmother, Deaconess Elizabeth Ajala and late Pa Ajala. They all contributed a lot to my childhood and my life. May their souls rest in perfect peace. Amen.
- My friends: Isaac Adeniyi, Gcobisa Tame, Ncumisa Nabi, Mr Nandi of DTL, Akobe Philip, Muritala Aliu, and Azeez Obasola for their calls and friendship support.

DEDICATION

This thesis is dedicated to Almighty God who started with me and assisted me throughout this research

TABLE OF CONTENTS

LIST OF FIGURES

LIST OF TABLES

LIST OF APPENDICES

GLOSSARY

OTC	OTC
TBT	Tributyltin
TTBT	Tetrabutyltin
DBT	Dibutyltin
TBTO	Tributyltin oxide
MBT	Monobutyltin
TPT	Triphenyltin
MPT	Monophenyltin
DMTC	Dimethyl dichloride
PVC	Polyvinyl chloride
CVD	Chemical vapour deposition
TBTN	Tributyltin naphthanate
IMO	International of Marine Organization
BET	Brunauer, Emmett and Teller
D-R	Dubinin-Radushkevich
GC	Gas chromatography
LC	Liquid chromatography
SFC	Supercritical fluid chromatography
MS	Mass spectroscopy
ICP-MS	Inductively coupled plasma mass spectrometry
ICP-AES	inductively coupled plasma atomic emission spectroscopy
AAS	Atomic adsorption Spectrometry
MIP-AES	Microwave induced plasma atomic emission spectrometry
FPD	Flame photometric detector
PFPD	Pulsed flame photometric detector
QFAA	Quartz furnace atomic adsorption spectroscopy
XRD	Powder x-ray diffractometer

XRF	X-ray fluorescence spectrophotometer
SEM	Scanning electron microscope
TEM	Transmission electron microscope
FTIR	Fourier transform infrared spectroscopy
CNH	Carbon, nitrogen and hydrogen
EDX	Energy-dispersive X-ray spectroscopy
q_e	amount of adsorbate adsorbed at equilibrium per unit weight of the adsorbent (mg/g)
q_t	amount of adsorbate adsorbed at any time (mg/g)
k_1	pseudo first - order rate constant/min
k_2	rate constant of pseudo second - order adsorption (g/mg min)
h_o	initial adsorption rate (mg/g/min)
α_E	constant in Elovich rate equation (g min^2/mg)
β	constant in Elovich rate equation (g min/mg)
k_p	rate coefficient for particle-diffusion controlled process
k	Fractional power rate constant
c_a	amount of adsorbed adsorbate on the adsorbent (mg/g)
c_e	equilibrium concentration of adsorbate in the bulk solution (mg/L)
c_o	initial concentration of the adsorbate aqueous solution
R	gas constant (J/mole K)
k_L	Langmuir isotherm constant
$A_{\max}$	maximum monolayer adsorbate adsorption capacity (mg/g)
k_F	Freundlich isotherm constant
n_F	exponent in Freundlich isotherm

k_T	Temkin isotherm constant
b_T	constant in Temkin isotherm (J/mol)
n_T	constant in Temkin isotherm
k_{D-R}	Dubinin-Radushkevich (D-R) isotherm constant
ε	Polanyi potential = $RT \ln\left(1+\frac{1}{C_e}\right)$
E	mean free energy (J/mol)
q_m	maximal substance amount of adsorbate per gram of the adsorbent
ΔG^o	standard Gibbs free energy (kJ/mol)
ΔH^o	standard enthalpy change (kJ/mol)
ΔS^o	standard entropy change (J/K/mol)
T	absolute temperature
K_c	thermodynamic equilibrium constant.

CHAPTER ONE
INTRODUCTION

1.1 Background

Organotin compounds (OTCs) are chemical compounds based on tin with hydrocarbon substituents. They are characterized by the presence of strong carbon-tin bonds and have the general formula: $R_x - SnL_{(4-x)}$, where R denotes an organic alkyl or aryl group and L denotes one or more organic (or sometimes inorganic) ligands, which may or may not be the same. The first organotin compound (OTC) was diethyltin diiodide, which was discovered by Edward Frankland in 1849 (Sander et al., 2004). Other OTCs include tributyltin chloride (TBT), tetrabutyltin (TTBT), tributyltin oxide (TBTO), triphenyltin chloride (TPT), tetraethyltin (TET) and trimethyltin chloride (TMTC) (Hoch, 2001). The physical and chemical properties of some tributyltin and triphenyltin compounds are represented in Tables 1.1 and 1.2, respectively while the chemical properties of some organotin chlorides are provided in Table 1.3. They are amongst the most widely used organometallic compounds. They have been utilized for a variety of industrial and agricultural applications including pesticides, fungicides and anti-fouling agents. The use of antifouling paints in the ship building industry has led to a significant concentration of OTCs in the marine environment while run off from agriculture is another means by which OTCs enter the ecosystem (Bosselmann, 1996). Organotin-based antifouling paints are highly effective against fouling organisms and are used to prevent the growth of fouling organisms on marine structures and vessels. High concentrations of OTCs thus have a negative effect on the aquatic environment. They cause imposex, calcification abnormalities in mollusks and exposure through consumption of sea food is thought to be the most probable source of OTCs in humans (Mimura et al., 2008). It is therefore preferable to reduce the concentration of OTCs in shipyard process wastewater to > 99 % reduction before discharge into the aquatic environment.

Table 1.1: Physical properties of tributyltin compounds

	Bis(n-tributyltin)oxide	**Tributyltinchloride**
Solubility	4 mg/L (20^{o}C, pH 7) 18-19.5 mg/L	17 mg/L 5.7±2.3 mg/L in distilled water with varying temperature
Partition coefficient octanol/water (log K_{ow})	3.7 in 32 % seawater 4.1 at pH 7	3.54 in seawater 4.2 at pH>7.4, 18 % salinity
Vapor pressure (20^{o}C)	0.1 mPa at 20^{o}C	<1 Pa at 20^{o}C
Organic carbon-water partition coefficient (K_{oc})	90 800	N/A

(Adapted from WHO, 1990)

Table 1.2: Physical and chemical properties of some triphenyltin compounds

	Triphenyltin hydroxide	Triphenyltin acetate	Triphenyltin chloride
Synonyms	Fentin hydroxides; TPTH	Fentin acetate; TPTA	Fentin Chloride; TPTC
(CAS) Registry No	76-87-9	900-95-8	639-58-7
Molecular formula	$C_{18}H_{16}OSn$	$C_{20}H_{18}O_2Sn$	$C_{18}H_{15}ClSn$
Molecular weight	367.0	409.1	385.5
Melting point	122-123.5 ^oC	122-124 ^oC	106 ^oC
Solubility in water (20^{o}C)	1 mg/L at pH 7 Greater at lower pH	9 mg/L at pH 5	40 mg/L (pH not given)
Solubility in other solvents (20^{o}C)	10 g/L (ethanol) 171 g/L (dichloromethane) 28 g/L (diethyl ether) 50 g/L (acetone)	22 g/L (ethanol) 82 g/L (ethyl acetate) 5 g/L (hexane) 460 g/L (dichloromethane) 89 g/L (toluene)	moderately soluble in organic solvent
Vapor pressure	0.047 mPa (50 ^oC)	1.9 mPa (60 ^oC)	0.021 mPa
Log K_{ow}	3.43	3.43	-

(Adapted from Tomlin, 1997 & NLM, 1998)

Table 1.3: Chemical properties of some organotin chlorides

	Monomethylin trichloride	Dimethyltin dichloride	Monobutyltin trichloride	Dibutyltin dichloride	Monooctyltin trichloride	Dioctyltin dichloride
Synonyms	MMTC	DMTC	MBTC	DBTC	MOTC	DOTC
Chemical formula	CH_3Cl_3Sn	$(CH3)_2Cl_2Sn$	$C_4H_9Cl_3Sn$	$(C_4H_9)_2Cl_2Sn$	$C_8H_{17}Cl_3Sn$	$(C_8H_{17})Cl_2Sn$
CAS No.	993-16-8	753-73-1	1118-46-3	683-18-1	3091-25-6	3542-36-7
Molecular weight	240.8	219.7	282.2	303.8	338.3	416
Melting point (^{o}C)	47	105	-63	40	10	47
Boiling point (^{o}C)	173	189	250	250	250	250
Solubility (g/l)	$1X10^5$	$1X10^5$	8.2	36	0.1	1.0
Vapor pressure at 25^{o}C (Pa)	33.3	30.0	5.84	0.15	0.55	$1.35X10^{-4}$
LogK_{ow}	-2.15	-2.18 to -3.1	0.18	1.89	2.14	5.82
K_{oc} (l/kg)	0.2	0.2; 21 537[b]	1.76; 75 354[c]	42.8; 61 664[b] 223.867[c]	68.2	65200; 292 556[b]
Henry's law constant (Pa.m^3/mol)	0.08	0.066	201	1.27	1420	0.056
Air/water partition coefficient	$3.38X10^{-5}$	$2.78X10^{-5}$	$8.48X10^{-2}$	$4.34X10^{-4}$	$5.98X10^{-1}$	$2.37X10^{-5}$

(Adapted from WHO, 1990 & Ayanda et al., 2012a)

1.2 Toxicity of organotin compounds

Tin (Sn) in its inorganic form is believed as being non-toxic. Inorganic Sn compounds are of low toxicological risk due to their low solubility, poor absorption, low accumulations in tissue, and rapid excretion (Kimbrough, 1976) but the toxicological pattern of organotins is very

complex. The biological effects of the substances depend on the nature, number and type of organic groups R (alkyl or aryl group) bound to the Sn cation. Inorganic anion X plays a secondary role. Organotin toxicity to microorganisms decreases in the order $R_3Sn\ X > R_2Sn\ X_2 > RSn\ X_3$, with R_4Sn compounds being of low toxicity. In general, tributyl-, triphenyl- and tripropyltins are the most toxic, with an association with cell membranes being an important prerequisite for toxicity. The inhibition of microbial processes by TBT has been recorded for all major groups, with the main interactions occurring at cellular membranes and chloroplasts, or the mitochondria in eukaryotes (Gadd, 2000).

Occupational exposure is the most likely point of exposure to OTCs to humans. OTCs can be inhaled in commercial/industrial work environments where OTCs are produced or used. Ingestion is considered to be an unlikely route in these environments. Some skin absorption may occur when direct contact with OTCs takes place (DEWHA, 2008). Human exposure to non-point sources of OTCs occurs through contaminated dietary sources (seafood and shellfish), fungicides on food crops, and antifungal agents in wood treatments, industrial water systems, and textile (Golub and Doherty, 2004). Irrigation waters from rivers can expose cultivated plant to OTCs (Lespes et al., 2003). Pesticides such as acaricides, fungicides e.t.c. contain compounds such as TPT.

1.2.1 Effect of organotin compounds on aquatic plants, marine invertebrates and birds

Aquatic plants growing in effluents of urban treatment plants are polluted by butyltins, but fruits and vegetables also have been found contaminated by organotin-based pesticides (Waite et al., 1989). Phenylated species were also found in pecan leaves: ten days after spraying with a TPT hydroxide solution, leaf samples contained from 6 to 50 mg/kg of the mono-, di-, and triphenylated species respectively (Kannan and Lee, 1996).

TBT is very toxic to marine invertebrates (Maguire, 1991 & Fent, 1996) and because of its persistence in sediment; there is still a concern about its impact on organism (Meador, 2000). It has been established that marine species exhibit a range in responses when exposed to TBT in water (Meador 1997 & Fent, 1996), but their responses to sediment-associated TBT has not been fully studied (Meador, 2000). Mortality responses for TBT in water exposures have been reported to be approx. 0.5 ng/mL to over 200 ng/mL (Cardwell and Meador, 1989). Most of this variability is due to differences in the uptake and elimination kinetics between species; however some of these values underestimate the toxic response because of insufficient time of exposure (Meador, 2000). Meador (1997) reported that it takes about 75 days for tissue concentrations to reach steady state in *Eohaustorius washingtonianus*, an amphipod with a slow rate of elimination.

TBT adverse effects were noted at concentrations of 0.001 to 0.06 µg/L on bivalve molluscs and marine gastropod and 0.1 to 1.0 µg/L on algae, echinoderms, fish, coelenterates and crustaceans (Eisler, 1989 & Meador, 2000). Bioconcentration of organotins was high, but degradation was sufficiently rapid to preclude food chain biomagnifications (Eisler, 1989). Fent and Hunn (1995) noted that clams had disappeared in areas where sediment TBT exceeded 800 ng/g dry weight. Similarly, Meador and Rice (2001) noted moderate to severe reductions in growth for the polychaete *Armandia brevis* for sediment concentration in this range (100 -1000 ng/g dry wt.). It has also been reported that some populations of bivalves such as *Macoma balthica* and *Scrobicularia plana* have disappeared in locations with TBT sediment concentrations over 700 ng/g dry wt.

TBT act as endocrine disruptor, for instance, trialkyl organotins have the capability to cause imposex, the abnormal induction of male sex characteristics in female marine invertebrates (Grun and Blumger, 2006). Bioaccumulation of TBT was demonstrated to decrease the activity of P450 aromatase, the key step in conversion of androgens to estrogens, with a consequent increase in testosterone and decrease in estrogen levels (Matthiessen and Gibbs, 1998); induce masculinization in fish species (McAllister and Kime, 2003).

Current environmental concentrations of some OTCs are not likely to be directly toxic to birds and mammals. Birds seem to be relatively resistant to OTCs but data are scarce. Studies of 75 days duration revealed that diets containing 50 mg tin as trimethyltin chloride/kg were fatal to ducklings; 5 mg/kg killed 40 %, and 0.5 mg/kg was not lethal (Eisler, 1989).

1.2.2 Effect of organotin compounds on mammals

In mammals, OTCs have modest adverse effects on both the male and female reproductive tracts and do not affect the sex ratios but hepatic, neutral, and immunotoxicity are the predominant indicators of high levels of OTCs exposure (Boyer, 1989 & Ogata et al., 2001). Diorganotin compounds cause cerebral edema and inhibit mitochondra respiration by preventing the oxidation of keto acids, presumably through inhibition of alpha-keto oxidase activity (WHO, 1980). Trimethyltin, triethyltin, and tributyltin compounds are highly toxic to animals (Eisler, 1989). Trimethyltin and triethyltin compounds are more toxic to mammals than are the higher triorganotin homologues, probably because of poorer absorption to higher trialkytin compounds from the gastrointestinal tract (Kimbrough, 1976 & WHO, 1980). Trimethyltin and triethyltin compounds are potent inhibitors of oxidative phosphorylation in the mitochondria for which these compounds have a high binding affinity (WHO, 1980).

Triethyltins were the most potent organotins tested on mammals, although other organotins produced similar signs of poisoning (Eisler, 1989). Mammals poisoned by triethyltin compounds showed muscle weakness within hours of dosing; after a short period of recovery, tremors developed, leading to convulsions and death two to five days after dosing (Eisler, 1989). Tetraorganotin compounds produce muscular weakness, paralysis, respiratory failure, tremors, and hyperexcitability as acute effects in mice and dogs; latent effects are similar to those seen in triorganotin poisoning (WHO, 1980).

Toxicity of the butyl- and phenyltin derivatives in live organisms depends on dose, time of exposure, the type and specificity of a given species, the age and resistance of an individual and the physiological processes undergoing in a given organism. It should be pointed out that mollusks and snails accumulate the most organotins, and are the main source of pollutants delivered to the remaining links in the food chain. Next are the crustaceans and fishes. Lipophilicity of organotins results in their propensity to persist and bioaccumulate in the sequential links of the food chain. This may lead to the spread of toxic substances in the food web, and in particular cases, to the poisoning of specific organisms. Several organotins are strongly immunosuppressive, display developmental and reproductive effects, and are neurotoxic.

OTCs get easily absorbed through the skin, which may manifest itself by a skin rash. Particularly, the R_3SnX type compounds bind quickly to proteins, most likely via sulphur of the amino acids cysteine and histidine. Interactions with mitochondrial functions through various mechanisms are probably the biochemical pathways that lead to toxic responses (Radke et al., 2008). Alkyltin compounds are known to affect the cardiovascular and respiratory systems. An acute toxic dose has been reported to cause a drop in the rectal temperature of both rat and rabbit. Diethyltin dichloride has been found to produce nasal irritation, headache and it also has an emetic action on the gut. Triethyltin compounds may cause cerebral edema in human. Common symptoms of triethyltin compounds are headaches, vomiting, abdominal pain, visual disturbance and rapid loss of weight, while the symptoms of TPT include sluggishness, unsteadiness, moderate diarrhea, anorexia, wheezing, etc.

1.3 Organotin antifouling paints

Organotin-based antifouling paints are highly effective against most fouling organisms, and their application results in a large amount of savings for the shipping industry (Sonak et al., 2009). In fact, TBT - based paints are described as the most effective antifouling paints ever devised for use on boat hulls (Bosselmann, 1996). On the contrary, TBT has also been described as the most toxic substance ever introduced into the marine environment,

especially since it is directly released into the aquatic environment (Goldberg, 1986). Organotin antifouling paint will cause harm to the environment if inappropriately used.

Antifouling paints are used to prevent the growth of fouling organisms on marine structures and vessels. The paints are directed at 'target' organisms, which are essentially any marine organisms that settle on solid surfaces after a period of mobility in the sea. The growth of fouling organisms on the hulls of vessels adversely affects the movement of vessels in water, resulting in increased fuel costs and transit time for the shipping industry. Fouling organisms can also interfere with the operation of submerged equipment and lead to the increased corrosion of marine structures.

A consequence of the effectiveness of organotin antifoulants is their exceptional toxicity to nontarget marine organisms (Sheikh et al., 2007). Organotins interfere with biological processes in a diverse range of species. Scientific evidence demonstrates the extreme negative impacts of OTCs on the marine environment.

1.3.1 Adverse effect of organotin antifoulants

Recent studies have shown high elevations of OTCs in the tissues of marine mammals, and the presence of organotin has been linked to mass mortalities of marine mammals (seals, dolphins) through the weakening of their immune systems. It causes the superimposition of male genital organs (penis and vas deferens) on female gastropods. Imposex is cause-specific and occurs at low concentrations of organotins such as TBT and TPT. Reproductive failure is known to occur in severely affected stages. Imposex has been reported all over the world for more than 140 species. The main cause of population decline in at least seven of these species is considered to be reproductive failure related to imposex (Horiguchi et al., 2001). Calcification anomalies in mollusks are also known to be caused by TBT.

1.3.2 International controls on organotin antifouling paints

Due to the highly toxic effect of OTCs on the marine environment, TBT restrictions apply in many countries around the world. For example, the Notifiable Chemical Order in Victoria restricts the sale, supply and application of organotin antifouling paints. Countries of the European Union, Canada, Scandinavia and South Africa have banned the use of TBT on vessels of less than 25 metres in length. Japan and New Zealand have banned the use of TBT antifouling paints on all vessels. Therefore, the International of Maritime Organization (IMO) prohibited the use of such OTCs as antifouling biocides after 1st January 2008 (Mimura et al., 2008). This has resulted in highly restricted worldwide application of organotin antifoulant paints to vessels less than 25 metres in length. Although tightened controls on the

application of organotin antifouling paints to small vessels have been positive in reducing the TBT load to the environment, organotin paints are still applied to large shipping vessels (e.g. tankers and container ships). The release of TBT from these vessels remains a significant environmental concern.

1.4 Fate and Degradation of organotin compounds

A sequential removal of the consecutive organic groups from the organotin molecule until reaching a complete metamorphosis into inorganic and non-toxic Sn (IV) can be transcribed as follows (Gadd, 2000):

$$R_4Sn \rightarrow R_3SnX \rightarrow R_2SnX_2 \rightarrow RSnX_3 \rightarrow SnX_4$$

Degradation takes place under the influence of radiation, biological and chemical factors. Photolysis is considered the fastest degradation process of OTCs in the aquatic environment. It has been established that photolysis is faster in phenyltin derivatives as compared to butyltin compounds. The degradation of organotins may also occur as a result of interactions among molecules of nucleophilic and electrophilic character and the polarized Sn-C bond of an organotin compound.

The most important mechanism of TBT elimination from sediment is biodegradation. It has been established that biochemical degradation due to microbial activity (i.e. activity of bacteria, algae and fungi) is faster in the water column as compared to sediment. This results from the higher light intensity and better oxygenation of the water column in comparison to sediment. The half-life of OTCs in seawater ranges from a couple of days to a couple of weeks. In the case of TBT, it may reach 15 days, while DBT and TPT may reach 10 to 60 days (Harino et al., 1997).

The reversal process to degradation is methylation. Methyltin derivatives form in the marine environment via biomethylation, e.g. biomethylation of inorganic tin by sulphur bacteria which results in the accumulation of mono- and dimethyltin in sediments.

1.4.1 Biomethylation

Methyltin compounds are widely found in the environment, although it is usually difficult to ascertain the proportions that arise from anthropogenic sources, abiotic or biotic methylation reactions, or the degradation of complex OTCs, including tributyl derivatives. Several biotic and abiotic methylation agents are known. They include methycobalamin and methyliodide. Methylcobalamin (CH_3B_{12}) is a carbanion donor and is able to convert inorganic Sn (IV) to several methyltin species. Methyliodide (CH_3I) which is produced by certain algae and seaweeds can also methylate inorganic Sn (II) salts in an aqueous medium to produce

monomethyltin species while certain Pseudomonas bacteria are also able to form various methyltin compounds (Ayanda et al., 2012a).

1.4.2 Bioaccumulation and soil/sediments trap of organotin compounds

Most studies on bioaccumulation deals with TBT because of its extremely toxicity to several organisms. Some marine bacteria display a remarkable ability to accumulate OTCs. Research on TBT accumulation by aquatic invertebrate has been mostly to mollusks (bivalves) and crustaceans (decapods) because these groups are important seafood resources and are ecologically dominant in many habitats. Marine bivalves are able to accumulate significant amounts of TBT (up to > 5 µg/g) while crustaceans and fish accumulate much lower amounts of TBT because of their possession of efficient enzymatic mechanism that degrade TBT in the body (Hoch, 2001). The accumulation of TBT by higher tropic aquatic organisms proceeds through either uptake from solution alone or a combination by diet ingestion. Studies have also shown that marine mammals and birds also accumulate high levels of toxic butyltins in various tissues and organs.

Large proportions of OTCs are found to be associated with clay fraction of particulate matter, indicating that adsorption and concentration unto fraction is an important control fraction mechanism. Thus, soil and sediments serve as trap for OTCs but to what extent have these compounds accumulated in the sediments over the last decades. The adsorption behavior of organotin species is thus important in determining the transport processes as well as their bioavailability especially to aquatic organisms. Experimental results have also shown that clay minerals and metal oxides bearing a net negative charge are effective adsorbents for OTC under environmentally relevant conditions.

1.5 Adsorption

Adsorption is the adhesion of atoms, ions, biomolecules or molecules of gas, liquid, or dissolved solids to a surface (Brandt et al., 1993). It is a process that occurs when a gas or liquid solute accumulates on the surface of a solid or a liquid (adsorbent), forming a molecular or atomic film (the adsorbate). Adsorption is operative in most natural, physical, biological, and chemical systems, and is widely used in industrial applications such as water purification. Adsorption has been found to be superior to other techniques for water purification in terms of cost, simplicity of design and use of operation (Meshko et al., 2001). Adsorption has been used extensively in industrial processes for separation and purification. The removal of coloured and colourless organic pollutants from industrial wastewater is considered an important application of adsorption processes (Al-Qodah, 2000). Adsorption has advantages over other methods for remediation of heavy metals from wastewater

because its design is simple, and it is sludge-free and is not capital intensive (Viraraghvan and Dronamraju, 1993).

Adsorption is usually described through isotherms, that is, functions which connect the amount of adsorbate on the adsorbent (Knaebel, 2008). Isotherms can be grouped into two-parameter and three-parameter models. Two-parameter models are Freundlich (Ho, 2006 & Zawani et al., 2009), Langmuir, Temkin and Dubinin-Radushkevich (D-R) (Sutcu, 2005) adsorption isotherms while three-parameter models are Redlich-Peterson (Sathishkumar et al., 2007), Langmuir-Freundlich or Sips (Foo and Hameed, 2010) and Toth (Toth, 1971 & Foo and Hameed, 2010) adsorption isotherms. These isotherms are linearized and the linearized forms are plotted on a graph from which the unknown constants are determined from the slope and intercept of the graphs.

1.5.1 Adsorbents

Adsorbents are substances, usually porous in nature and with a high surface area that can adsorb substances by intermolecular forces. The most important parameters of an adsorbent for any application are: capacity, selectivity, regenerability, kinetics, compatibility and cost. Rarely will a single adsorbent be optimal for all these parameters. Frequently it will be possible to narrow the choice of one or two classes of adsorbents, but that still commonly leaves a vast array of possibilities (Knaebel, 2008). Adsorbents can either be inorganic or organic. The inorganic adsorbents include alumina, silica and zeolite while the organic adsorbents are activated carbon and synthetic polymers.

1.5.1.1 Nano particles

Nano oxides are sized between 1 and 100 nm. Conventional metal oxides typically have grain sizes that fall within the micrometer range and often are supplied in the form of particles having particle sizes greater than the micrometer range. It is believed that metal oxides that are comprised of nanometer sized grains will have important advantages over conventional metal oxides. These advantages include lower sintering temperatures, potentially very high surface areas etc. Methods for the synthesis of nano materials include gas phase synthesis, ball milling, co-precipitation, sol gel, and micro emulsion methods. The methods are typically applicable to different groups of materials, such as metals, alloys, intermetallics, oxides and non-oxides.

1.5.1.2 Activated Carbon

Activated carbon is a highly porous, amorphous solid consisting of microcrystallites with a graphite lattice. It is a black solid substance resembling granular or powdered charcoal. It is a processed carbon material with a highly developed porous structure and a large internal specific surface area (Helena et al., 1991). In practice, activated carbon is used as an adsorbent for the adsorption of mainly organic compounds along with some larger molecular weight inorganic compounds. Activated carbon, also called activated charcoal or activated coal, is a general term that includes carbon material mostly derived from charcoal. It has an exceptionally high surface area. One gram of activated carbon has a surface area of approximately 500 m^2. The three main physical carbon types are granular, powder and extruded (pellet). Activated carbon has been reported to have high and fast adsorption capacities due to its well-developed porous structure and large surface area.

1.5.1.2.1 Preparation of activated carbon

The preparation of activated carbon with different pore sizes can be achieved by physical or chemical activation processes. In physical activation, the generation of porosity is by selective elimination of the more reactive carbon of the structure and further gasification which leads to the production of the activated carbon with the required pore structure. In the chemical activation process, the precursor is mixed with a chemical such as $ZnCl_2$ or H_3PO_4, carbonized and washed to produce the activated carbon. Following the thermal decomposition of the precursor, the chemical reacts with the product causing a reduction in the evolution of the volatile matter and inhibition of the particle shrinkage. Once the chemical is removed by exhaustive washing, a large amount of porosity is formed (Abdullah et al., 2001).

1.5.1.2.2 Uses of activated carbon

All three types of activated carbon (granular, powder and pellet) can have their properties tailored for the intended the application. Activated carbon is used for adsorption of organic substances and non-polar adsorbates and it is also usually used for waste gas and waste water treatment. It is the most widely used adsorbent. Its usefulness derives mainly from its large micropore and mesopore volumes and the resulting high surface area. It is frequently used in everyday life, in industry, food production, medicine, pharmacy, military, etc. In pharmacy, activated charcoal is considered to be the most effective single agent available as an emergency decontaminant in the gastrointestinal tract. It is used after a person swallows or absorbs almost any toxic drug or chemical (Eddleston et al., 2008).

1.5.1.3 Fly ash

Fly ash consists of fine, powdery particles that are predominantly spherical in shape, either solid or hollow, and mostly glassy (amorphous) in nature. It is the by-product of the coal combustion process for energy generation, and is recognized as an environmental pollutant. Because of the environmental problem of fly ash, a good deal of work and applications on the utilization of fly ash has been undertaken. One of the uses of fly ash is the adsorption of metallic ions at the liquid/solid interface (Sutcu, 2005).

The fly ash produced from the burning of pulverized coal in a coal-fired boiler is a fine-grained, powdery particulate material that is carried off in the flue gas and usually collected from the flue gas by means of electrostatic precipitators, bag houses, or mechanical collection devices such as cyclones. The term fly ash is not applied to the residue extracted from the bottom of boilers usually referred to as bottom ash.

1.6 Statement of research problems

Organotin-based antifouling paints are highly effective against fouling organisms and are used to prevent the growth of fouling organisms on marine structures and vessels. Their toxicity has been a great problem in the aquatic environment. High concentrations of OTCs have been correlated with growth abnormalities in mussels and oysters and have also resulted in a decline in their populations. High levels of OTCs have also been found in the tissues of marine mammals and the presence of organotin has been linked to mass mortalities of marine mammals (Ayanda et al., 2012a). They cause imposex and calcification abnormalities in mollusks. In humans, exposure through consumption of seafood is thought to be the most probable source of OTCs.

South Africa has one of the world's busiest shipment routes and most of these ships are probably coated with organotin-based antifouling paint. Wastewater from the antifouling paint industry is also another means by which OTCs are released into the marine system. There is therefore a need to investigate how OTCs could be removed from organotin contaminated shipyard process and industrial wastewater before discharge into the environment. A study of appropriate and effective adsorbent and/or adsorbent composite materials for the adsorption of OTCs from contaminated seawater by the use of nano metal oxides/silica, activated carbon and fly ash composite materials will constitute the research problems to be solved.

1.7 Justification for the project

Although tightened controls on the use of organotin antifouling paints to ships less than 25 metres have been positive in reducing the OTCs release to the environment, organotin paints are still applied to tankers and container ships. The main source of OTCs (TBT and TPT) is the release from painted ships at the harbour. However, a major point source of pollution is high-pressure hosing in shipyards. The majority of biocide released during hosing activities is in the form of paint particles that can become incorporated in sediments. Although the physicochemical properties of antifouling compounds differ significantly and some are rapidly degraded, they will accumulate in marine sediments if introduced as paint particles. Treating wastewater in shipyards and anti-fouling paint manufacturing industries by adsorption will thus prevent a significant part of the introduction of antifouling compounds into the marine ecosystem.

1.8 Research Questions

- How can composite adsorbent materials be prepared from activated carbon, nano metal oxide/silica and fly ash to be of high quality in term of nature, morphology and properties?
- Could the properties of these composite materials be tailored towards better remediation of OTCs and other pollutants from wastewater?
- Which of the adsorbents or adsorbent composite materials will give the highest adsorption capacity of OTCs and at what optimal conditions?
- How can the adsorption of OTCs by the adsorbents be explained isothermally and which of the adsorption isotherms fit the adsorption process?
- Which of the kinetic models best described the adsorption data?
- What is the entropy and free energy of the various adsorbents and adsorbent composite materials during the adsorption processes?
- Will the adsorbent composite materials be capable of adsorbing OTCs when the laboratory findings are practically applied to wastewater and how efficient is the process of adsorption?

1.9 Research Objectives

The main aim of this project is to prepare and characterize adsorbent composite materials and optimize their adsorption capacity of OTCs in organotin – contaminated wastewater.

Specific objectives:

- To prepare composite materials using activated carbon, nano metal oxides, nano silica and fly ash as precursors.
- To characterize the adsorbents and the prepared composite materials by modern analytical techniques.
- To prepare artificial seawater and organotin – contaminated water.
- To establish the processes of interaction of OTCs on the adsorbents so as to understand all their properties and the properties that could be useful for future applications.
- To investigate the adsorption capacities of the adsorbents and adsorbent composite materials for the direct adsorption of OTCs.
- To establish the adsorption equilibrium and removal efficiency of OTCs by the adsorbents and composite materials.
- To quantify and analyse the adsorption data by adsorption isotherms, investigation of the adsorption kinetics, determination of standard entropy change (ΔS^{o}), standard enthalpy change (ΔH^{o}) as well as the determination of the standard Gibbs free energy (ΔG^{o}) of the adsorbents.

1.10 Significance of the study

To prepare adsorbent composite materials of high adsorption capacity, capable of enhancing the adsorption of OTCs from organotin contaminated seawater and wastewater and to give public education on the preparation of adsorbent composites, characterization of adsorbents and application of the precursors and adsorbent composite materials to the sorption of OTCs.

1.11 Expected outcomes and contributions of the research

- Adsorbent composite materials would be prepared using activated carbon, nano metal oxides, nano silica and fly ash as precursors.
- The precursors and the adsorbent composite materials would be characterized by modern analytical methods such as surface area and porosity determination, elemental and mineralogical characterization, morphological characterization of adsorbents before and after adsorption processes, particle size distribution measurement, pH determination and ash content determination. Optimal conditions for the adsorption of OTCs would be established**.**
- Adsorption experiments would be conducted by the use of artificial organotin contaminated seawater and wastewater, and experimental parameters such as contact time between the adsorbate and the adsorbents, adsorbent amount, temperature, pH, and stirring speed would be investigated to understand the conditions and process required for maximum adsorption capacity.
- The adsorption capacity of precursors and adsorbent composite materials would be quantified and the experimental data points fitted to the linearized form of the adsorption isotherms including Langmuir, Freundlich, Temkin, and D-R adsorption Isotherms.
- Investigation of the adsorption kinetics, the removal efficiency, basic thermodynamic functions such as ΔH^{o}, ΔS^{o}, and ΔG^{o} of the precursors and composite materials would be carried out.
- Optimal condition for the adsorption of OTCs would be applied to the adsorption of OTCs from organotin – contaminated natural seawater.

1.12 Delimitations

The research was based on the remediation of OTCs at Cape Town harbour by adsorption. Optimum conditions obtained from the laboratory studies (adsorption of OTCs from simulated seawater) were applied to organotin removal from real matrices (organotin – contaminated seawater). However, contaminated water was also considered but the optimal conditions for the sorption of organotins from organotin – contaminated water were not applied to organotins removal from real matrices because organotin – contaminated industrial wastewater and/or organotin polluted streams/river water were not available during the course of this study, the reason being that we could not find organotin industries or any industries generating OTCs as waste at Cape Town environ.

CHAPTER TWO
LITERATURE REVIEW

2.1 Analysis of organotin compounds

OTCs are present in water at ng/L levels; their analysis therefore requires highly sensitive techniques. Several techniques, based on species specific analytical methods, have been developed for the determination of OTCs in environmental matrices. Hyphenated systems, based on on-line coupling of gas chromatography (GC), liquid chromatography (LC), or supercritical fluid chromatography (SFC), to mass spectrometry (MS) (Munoz et al., 2004 & Mizukawa et al., 2009), inductively coupled plasma mass spectrometry (ICPMS) (Xiao et al., 2008), pulsed flame photometric detection (PFPD) (Vreysen et al., 2008 & Oliveira et al., 2010), Quartz Furnace Atomic Absorption Spectroscopy (QFAA) (Park and Hahn, 1996), atomic absorption spectrometry (AAS) (Donald et al., 1993), tandem mass spectrometry (MS-MS) (Tsunoi et al., 2002), atomic emission detector (AED) (Rodriguez et al., 1997, Brack, 2002 & Campillo et al., 2004), flame photo detector (FPD) (Bancon-Montigny et al., 2000), and microwave induced plasma atomic emission spectrometry (MIP-AES) (Zachariadis and Rosenber, 2009) are in current use. Among the different techniques, the coupling of GC to ICP-MS appears to be one of the most popular techniques, due to high sensitivity and multi-elemental and multi-isotopic capabilities (Tesfalidet, 2004).

Sheikh et al. (2007) used gas chromatography (GC) equipped with an HP-1 methyl siloxane column (30 m length, 320 µm i.d., 0.25 µm film thickness) with a flame photometric detector (FPD) fitted with a 610 nm optical filter for the analysis of OTCs. Vreysen et al. (2008) analysed OTCs by gas chromatography with pulsed flame photometric detection (GC–PFPD). Park and Hahn (1996) analyzed butyltin compounds in seawater, sediment and biosamples in the south coast of Korea by the use of GC/QFAA (Gas Chromatography/Quartz Furnace Atomic Absorption Spectroscopy) system. Vidal et al. (2003) reported the determination of OTCs in water, sediments and mussels using low-pressure gas chromatography/tandem mass spectrometry (LPGC/MS/MS). The method was based on sodium diethyldithiocarbamate (DDTC) complexation of the ionic organotins, followed by extraction of the target matrices and derivatization by a Grignard reagent.

Brack (2002) reported the analysis of OTCs in sediment by the use of an atomic emission detector coupled with a gas chromatograph. Mizukawa et al. (2009) quantified OTCs by the use of a gas chromatograph-mass spectrometer (GC/MS).

2.2 Nano oxides, fly ash, activated carbon and composites in adsorption studies

2.2.1 Nano oxides

Nano oxides are sized between 1 and 100 nanometers; metal oxides that comprised of nanometer sized grains have important advantages over conventional metal oxides. These advantages include lower sintering temperatures, high surface areas, and improved or unusual physical properties. Owing to the large surface area and unique physicochemical properties, nano and ultrafine particles have drawn much attention in recent years for their roles in adsorption/desorption of contaminants in the environment (Yu-huan et al., 2007)

Peng et al. (2004) studied the adsorption of lysozyme onto nano-sized magnetic particles (Fe_3O_4) at different pH. The surface area of the nFe_3O_4 magnetic particles by Brunauer, Emmett and Teller (BET) was 108 m^2/g. Yang et al. (2009) examined the adsorption of humic acid by TiO_2, SiO_2, Al_2O_3, and ZnO nano metal oxides. The surface area of nano α-Al_2O_3, nano TiO_2, nano ZnO, nano s-SiO_2, and nano p-SiO_2 was 4.73, 324, 30, 191 and 570 mg/m^2, respectively. They showed that the adsorption of humic acid was a function of surface characteristics and specific surface area. Ghasemi et al. (2011) reported the adsorption of Hg (II) on nano-TiO_2 from aqueous solution, the specific surface area of the nano-TiO_2 was 98.743 m^2/g and about 96 % of Hg (II) was removed by nano-TiO_2. Rakhshaee et al. (2011) modified Fe_3O_4 nano-particles by extracted pectin of Azolla for the adsorption of methyl orange. Liang et al. (2011) investigated the adsorption and desorption of humic and fulvic acids on SiO_2 particles at nano and micro-scales and reported that the adsorption of humic acid and fulvic acids on 20 nm SiO_2 was much stronger compared with their adsorption on 100 and 500 nm SiO_2 due to the specific surface properties of the nano metal oxides. Boparai et al. (2010) investigated the use of nano zerovalent iron particles for the adsorption of cadmium ion. The freshly prepared nano zerovalent iron particles have a specific surface area of 26.3 m^2/g and the maximum adsorption capacity of Cd^{2+} was found to be 769.2 mg/g at 297 K.

2.2.2 Activated carbon

Activated carbon is widely used in a variety of areas, viz, as an adsorbent in air and water pollution control, a catalyst in the chemical and petrochemical industries, and a purifier in the food and pharmaceutical industries (Zhang et al., 2007). In the water treatment field, activated carbon is often used as an adsorbent for the removal of various synthetic and naturally occurring organic chemicals in drinking water (Li et al., 2002). In wastewater treatment, activated carbon is a powerful adsorbent because of its large surface area and pore volume, which allows the removal of liquid-phase contaminants, including organic

compounds, heavy metal ions and colours. Adsorption on activated carbon has been investigated extensively due to their use in many applications including the removal of toxic volatile organic compounds (VOCs) and pollutants in water and air (Stenzel, 1993, Hsieh and Teng, 2000, Newcombe et al., 2002 & Shukla et al., 2009).

2.2.3 Fly ash

Fly ash, generated during the combustion of coal for energy production consists of fine, powdery particles predominantly spherical in shape, either solid or hollow, and mostly glassy (amorphous) in nature (Ahmaruzzaman, 2010 & Ayanda et al., 2012b). Fly ash has been proposed as a good adsorbent for NOx, SOx and mercury removal from flue gases as well as adsorption of organic gas (Lu and Do, 1991 & Ahmaruzzaman, 2010). Fly ash has a potential application in wastewater treatment because of its major chemical components, which are alumina, silica, ferric oxide, calcium oxide, magnesium oxide and carbon, and its physical properties such as porosity, particle size distribution and surface area. Hence, it has been used as a low-cost adsorbent for the removal of heavy metals (Panday et al., 1985, Ricou et al., 1999, Ricou et al., 2001 & Nascimento et al., 2008), dyes (Mall et al., 2006), phenolic compounds (Wang and Wu, 2006), and humic acids (Wang et al., 2008) in wastewater. Coal firing power thermal stations are still the main source of power generation in South Africa (Bada et al., 2008).

2.2.4 Composite materials

Within the last few years, intensive wide spread contamination of the atmosphere and surface water related to adverse industrial operations has been of great concern, and as such there have been calls for the development of better adsorbents. Many researchers have therefore focused on the search for better adsorbents with very high adsorption capacities, the use of nano metal oxides as adsorbents as well as the surface modification of existing adsorbents. Limited work has thus been reported on the use of composite materials for wastewater treatments as is outlined in the following paragraphs.

Shin and Song (2011) reported the use of adsorbent consisting of silver nano-particles attached onto the surface of granular activated carbon for the removal of formaldehyde. The BET surface area were 907 ± 5 m^2/g for the granular activated carbon and 641 ± 12 m^2/g for the Ag-granular activated carbon. They reported that the silver nano-particle deposited on the granular activated carbon (GAC) blocked the pores of the GAC, thus reducing the available surface area for adsorption. However, the overall mass of formaldehyde removed by the Ag-granular activated carbon composite was increased due to catalytic oxidation as a function of the ratio of the surface coverage by the nano-particles. Wang et al. (2002)

prepared nano-sized coupled oxides ZnO/SnO_2 for the adsorption of methyl orange. The BET surface areas of ZnO, SnO_2, and ZnO/SnO_2 in molar ratio of 1:1 and ZnO/SnO_2 in molar ratio of 2:1 were 6.25, 20.89, 20.13 and 30.95, respectively. Shi et al. (2012) prepared composite adsorbent for the removal of phosphate ions from aqueous solutions by loading iron oxide onto activated carbon. They reported that the composite adsorbent showed fast adsorption rates and high adsorption capacities for the removal of phosphate ions.

Zhang et al. (2007) reported the preparation of $CuFe_2O_4$/activated carbon magnetic adsorbents with mass ratios of 1:1, 1:1.5 and 1:2 for the adsorption of acid orange II (AO7) in water and subsequent separation of adsorbent from the medium by a magnetic technique. Their results suggest that the composite has much higher catalytic activity than that of activated carbon, and this is attributed to the presence of $CuFe_2O_4$. Shukla et al. (2009) studied the synthesis of composites of carbon and natural zeolite with varying amounts of carbon as prospective adsorbents of organic contaminants from waste water such as phenol. They reported that the adsorption isotherm indicated an enhanced adsorption of phenol on the composites as compared with the natural zeolite, and that adsorption increased with increase in carbon content of the composite materials. The adsorption and degradation of trichloroethylene (TCE) through dechlorination using synthetic granular activated carbon and zerovalent iron (GAC–ZVI) composites was reported by Tseng et al. (2011). They found that the usage of granular activated carbon – zerovalent iron composites liberated a greater amount of Cl than when zerovalent iron was used alone. Jha et al. (2008) also investigated the preparation of composite materials of activated carbon and zeolite by activating coal fly ash by fusion and reported that the composites of activated carbon and zeolite proved to be suitable for the uptake of toxic metal ions.

The use of nano metal oxides for adsorption processes is expensive. The adsorption capacity of adsorbents for the remediation of pollutants is also dependent on the surface area of the adsorbents in the absence of other chemical reactions such as oxidation, reduction, etc. The surface area of fly ash and nano metal oxides is thus exceptionally low compared to widely used activated carbon. Hence, there is a need to increase the surface area of nano metal oxides as well as reducing the cost of using nano metal oxides alone for adsorption processes. These can be achieved by the preparation of a composite material of nano metal oxides with fly ash and/or activated carbon. The use of composite materials for the remediation of environmental pollutants might also combine the adsorption characteristics of activated carbon with the magnetic and catalytic properties of the metal oxides.

2.3 Remediation of organotin compounds

2.3.1 Remediation using activated carbon and oxides

Honda and Takahashi (2006) investigated the treatment of OTCs in liquid using iron oxides. They reported that the addition of iron oxide into a liquid containing an organotin compound allows trapping of the organotin compound in the liquid by the iron oxide, and reduction of the organotin compound concentration in the liquid. In the reported work, 870 ng of a TBT compound standard substance and 340 ng of a TPT compound standard substance were added to 30 mL of a 3% saline solution to prepare a test liquid. 1 g of iron oxide black (Fe_3O_4) was added to the test liquid, and the system was stirred for 1 hour. The test liquid was then subjected to centrifugation and separated into a supernatant and iron oxide black. Contents of TBT and TPT in the supernatant were then measured with a gas chromatograph mass spectrometer (GC/MS). As a result, the contents of TBT and TPT in the supernatant were 210 ng (removal rate of 76%) and 150 ng (removal rate of 56%), respectively.

Maes and Vreysen (2007) developed and optimized a sorption-flocculation process for the removal of organotins and heavy metals from shipyard wastewater. They tested a clay-based sorbent and powdered activated carbon with artificial and real dockyard wastewater and managed to reach a discharge limit of 100 ng Sn/L to the effluent. They reported that powdered activated carbon could be replaced by the installation of a granular activated carbon (GAC) column after the settlement tank. The sorption-flocculation process was economically favorable at relatively low organotin concentrations (<10 mg Sn/L). At medium to high organotin concentrations the installation of a GAC column would be preferred.

Vreysen et al. (2008) investigated the removal of DBT and TBT from shipyard wastewater by a one-step adsorption–flocculation method. He reported that activated carbon adsorbents showed the largest ability to remove OTCs from wastewater. He stated that the powdered activated carbons showed larger organotin adsorption capacity than granular activated carbons which can be attributed to their larger surface area. He also indicated that organotins are mainly removed from wastewater by hydrophobic adsorption onto the activated carbon.

Fang et al. (2010) investigated the adsorption of TBT to well characterized soot and charcoals with specific surface area in the range of 62-111 m^2/g with the main focus on pH effects. The charcoals, but not soot, were reported to possess acidic functional groups. TBT adsorption reaches a maximum at pH 6-7 for charcoals, and at pH > 6 for soot. Soot was reported to have between 1.5 and 15 times higher adsorption capacity (0.09-1.77 $mmolm^{-2}$) than charcoals, while charcoals show up to 17 times higher sorption affinities than soot.

2.3.2 Remediation using mineral surfaces

Weidenhaupt et al. (1997) investigated the sorption of triorganotin biocides from aqueous solution to mineral surfaces in batch sorption experiments using homoionic clay minerals (kaolinites, montmorillonites, illites), and aluminium, iron, and silicon hydroxides. For all minerals investigated, sorption kinetics of triorganotin biocides was reported to be fast and reversible.

Hoch et al. (2002) studied the adsorption and desorption behaviour of TBT from aqueous solution to clay-rich sediments under varying conditions of pH and salinity using the batch technique. Sediments containing illite, kaolinite, and montmorillonite in different proportions were used as sorbent materials. Several physicochemical parameters of the sediments were evaluated to assess the influence of sediment characteristics to the adsorption capacity for TBT. He reported that the adsorption isotherms were linear over the concentration range of 100 to 1,000 ng(Sn)/mL, the adsorption coefficient (K_d) values range from 29 to 70 at the pH value generally found in marine systems (pH 8) and that the adsorption capacity shows a maximum in the pH range of 6 and 7. The adsorption mechanism was reported to be controlled by the properties of the clay minerals as well as the aquatic chemistry of TBT.

2.3.3 Remediation using microorganisms

The removal of TBT from artificial wastewater by dead and live cells of four microalgal species, *Chlorella miniata, C. sorokiniana, Scenedesmus dimorphus* and *S. platydiscus* was investigated by Tam et al. (2002). They reported that dead cells were generally more efficient in removing TBT during three days of exposure. More than 90% and 85% TBT were reported to be removed by dead cells of *Scenedesmus* and *Chlorella*, respectively. They reported that degradation products, DBT and MBT, were recorded mainly inside the cells, and intracellular MBT concentrations were significantly higher than DBT. In terms of TBT removal, *Scenedesmus* cells were reported to be more effective than *Chlorella*, probably due to larger cell sizes and biomass. However, TBT specific uptake and degradation by *Chlorella* was higher than in *Scenedesmus*.

Tam et al. (2003) investigated the biosorption and biodegradation of TBT by free cells of a resistant microalgal species, *Chlorella sorokiniana* at low and high densities. They reported that TBT in contaminated water was continuously removed by microalgal cells and reached a 54% and 74% removal at the end of 14 days of treatment in low and high density cultures, respectively. The pattern of TBT removal in both densities was similar. A decrease in the

concentration of TBT in water, resulted to an increase in TBT uptake by the algal cells, reached a peak and declined to low levels towards the end of the treatment period.

Hala et al. (2009) investigated the biosorption and biodegradation of TBT at its sublethal concentration of unicellular algae *Nannochloropsis oculata* and *Dunaliella parva*. He reported that the initial concentration of tributyltin in the culture media of *N. oculata* was reduced by 46% within 2 days, while in *D. parva* it decreased stepwise reaching 50% within 6 days. He reported that at the end of 12 days both algae adsorbed nearly 80% of the initial TBT content.

2.3.4 Remediation using municipal solid waste compost

Said-Pullicino and Vella (2005) investigated the sorption behaviour of TBT from reconstituted seawater onto municipal solid waste compost. They investigated the rate of adsorption, the influence of pH, and the adsorbate hydrophobicity on the partitioning process and reported that the adsorption capacity for TBT onto compost was highest at pH 6.7, and for other organotins it increased with increasing adsorbate hydrophobicity, following the trend tripropyltin < tributyltin < tripentyltin. The use of washed municipal solid waste water compost as a sorbent for the purification of TBT-contaminated wash water as generated in large quantities during hull cleaning in dry docks was suggested as a mitigatory measure against pollution of the marine environment by TBT.

2.3.5 Other remediation processes

Ottosen et al. (2006) observed a decrease in TBT concentration after coagulation with iron salts (1.4 mL/L of a 1.0 M $FeCl_3$ solution). He reported that the significant reduction in TBT is not sufficient to reach strict discharge criteria. Song et al. (2005) reported the removal of TBT from wastewater by extraction with diesel oil. He reported that OTCs could be more effectively removed from artificial wastewater by solvent extraction with diesel oil. He stated that, after 5 hour extraction time the level of TBT decreased from 4 mg/L to 0.8 µg/L.

Prasad and Schafran (2006) used a full-scale process train consisting of coagulation–flocculation, dissolved air flotation, sand filtration and a series of two granular activated carbon (GAC) filters for removal of TBT. About 50% of the TBT was reported to have been removed after the sand filtration step (initial TBT concentration: 400–500 µg/L). The GAC filters decreased the TBT concentration further to less than 0.1% of the TBT concentration in the influent (final TBT concentration: 0.3–0.4 µg/L).

Arevalo and Calmano (2007) tested different anode materials to evaluate their suitability to eliminate OTCs electrochemically from shipyard process water. The capacity of two types of anode materials was investigated: niobium coated with boron-doped diamond (BDD) and titanium coated with iridium dioxide, (Ti/IrO2). The processes were tested on synthetic and real shipyard water containing approximately 25,000 ng/L of TBT (as Sn) and 5000 ng/L DBT. The range of current densities was between 6 and 70 $mAcm^{-2}$. The results showed that electrochemical treatment is suitable to eliminate organotins down to very low concentrations following a stepwise debutylation mechanism. Both anode materials exhibited a similar performance with energy consumption in the range of 7–10 $kWhm^{-3}$ in order to decrease organotins down to 100 ng/L (as Sn).

Haug et al. (2007) reported the use of hydrogen peroxide (H_2O_2) as a photocatalyst to enhance the rate of photodegradation of TBT, whereas the use of titanium oxide (TiO_2) or Fe (III) catalyst did not show any improvement in the reaction. A sufficiently strong UV source, in combination with H_2O_2 dosing (300 mg/L), resulted in a reduction of the organotin compound concentrations in real wastewater below the discharge criterion of 100 ng/L within a 2.5 min treatment period. These conditions are considered realistic for the application in full-scale treatment processes for wastewater streams ranging from 10 to 60 m^3/h. Bioassays, however, showed no clear reduction in toxicity after the treatment. The presence of other contaminants in the wastewater stream as well as the formation of intermediates is thought to be responsible for the observed toxicity. Thus, additional treatment steps are required before the treated wastewater can be discharged.

Adsorption and degradation of TPT by Pseudomonas chiororaphis immobilized in alginate beads was reported by Takimura et al., 2003. Han et al. (2007) also reported the adsorption of TPT onto modified chitosan and reported that the adsorption fitted well with Freundlich adsorption isotherm equation, showing that the biosorbent and TPT combined with functional groups. The adsorption of phenyltin compounds onto phosphatidylcholine/cholesterol bilayers have also been reported by Langner et al., 2000.

2.4 Critical appraisal of previous studies on the adsorption of organotin

It is preferable to dispose TBT and TPT wastewater after treatment with 99 % reduction on its concentration (Ayanda et al., 2012a). The use of oxides, especially iron oxides, for the remediation of OTCs as reported usually resulted to between 56-76% removal of OTCs (Honda and Takahashi, 2006). Vreysen et al. (2008) reported powdered activated carbon to show high ability in removing OTCs. Microbial remediation also appears to be possible but only if the concentration of organotin compound is not too high. Some of the available organotin remediation techniques take between 1-2 weeks of adsorption processes before a notable percentage of OTCs could be removed.

No work has also been reported on the remediation of OTCs from organotin contaminated seawater or shipyard process wastewater at Cape Town harbour. Kinetics and equilibrium data on the sorption of OTCs from seawater to oxides and carbon are limited and no work has also been reported on the use of nano metal oxides and/or nano metal oxide/fly ash/activated carbon composite materials for the adsorption of OTCs from seawater. The use of adsorbent composite materials i.e. powdered activated carbon, nano particles and/or fly ash composites for the adsorption of OTCs are therefore expected to result in fast and more efficient technique in OTCs remediation.

CHAPTER THREE
RESEARCH DESIGN AND METHODOLOGY

3.1 Materials and chemical reagents

The fly ash used in this study was obtained from Matla power station, Mpumalanga, South Africa. Activated carbon (100-400 mesh), iron (III) oxide nanopowder (particle size < 50 nm), silica nanopowder (particle size 12 nm), zinc oxide NanoGard (particle size 40 - 100 nm APS powder), TBT (purity 98%), TPT (purity 98%), methanol, hexane, sodium nitrate ($NaNO_3$), potassium bromide (KBr), acetic acid, sodium hydroxide and sodium tetraethylborate ($NaBEt_4$) were all purchased from Sigma Aldrich, USA.

Carbonate, sulphate and chloride salts for the preparation of artificial seawater were supplied by Merck. Stock solutions containing 1000 mg/L TBT (Figure 3.1a) and TPT (Figure 3.1b) were prepared by dissolving the organotin compound in methanol and stored in the dark at 4 ^{o}C. Working solutions were prepared daily. A solution of the derivatizing agent was made up daily by dissolving 1.0 g $NaBEt_4$ in 100 mL of methanol while acetate buffer (3 mL acetic acid, 4.0 g sodium acetate, filled up to 1 L with deionised water resulting in a pH 4.5) was also prepared.

a)

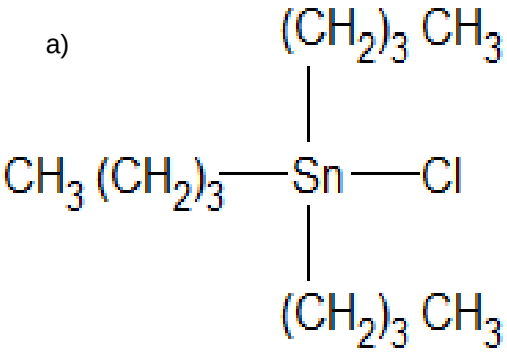

b)

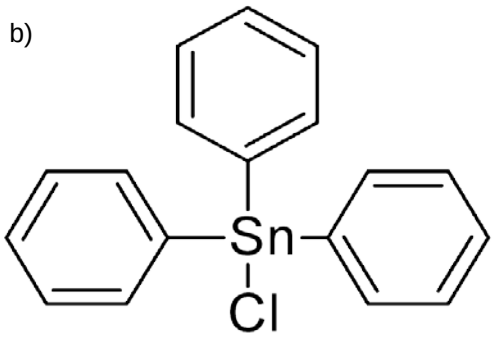

Figure 3.1: Tributyltin chloride (a) and triphenyltin chloride (b)

3.2 Preparation of Composite Materials

Activated carbon, fly ash and nano metal oxides in the ratio 1:1 for two components and 1:1:1 for three components composite materials were dispersed in 0.5 M HCl to form slurries. The slurries were stirred and evaporated to dryness in an oven. The composite materials were washed with deionised (Milli-Q) water, filtered and further dried in an oven at 100 ^{o}C for 24 hours. They were finally ground to fine powder using agate mortar and pestle (Westerhoff et al., 2006, Fungaro and Graciano, 2007, Oh et al., 2007, Fatoki et al., 2012 & Ayanda et al., 2013a).

Figure 3.2 is the photograph of the prepared composite materials.

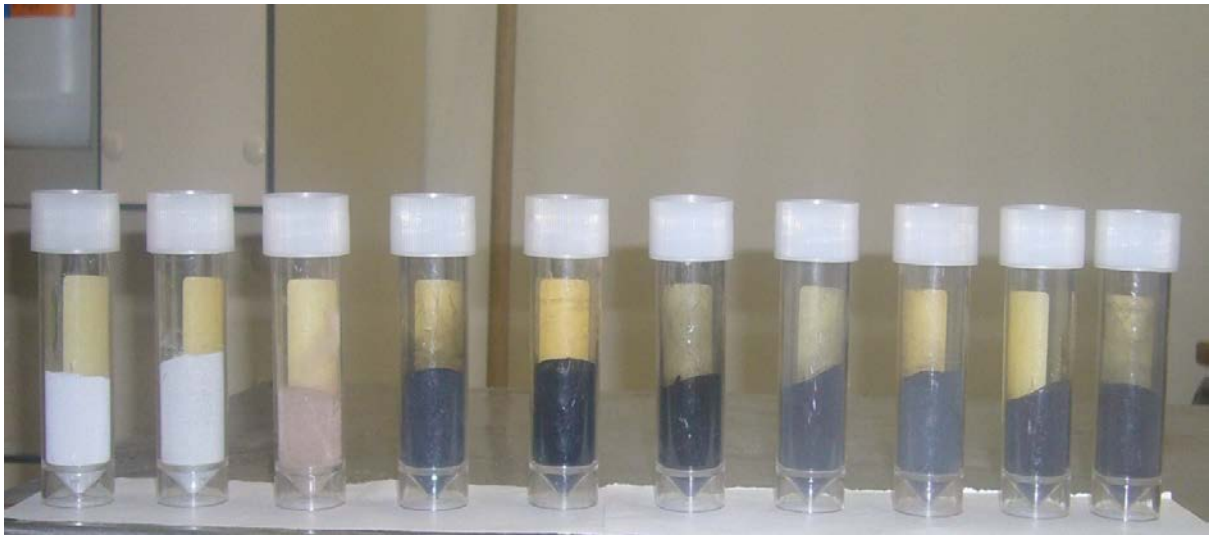

Figure 3.2: Composite materials

From L-R: nZnO/fly ash, $nSiO_2$/fly ash, nFe_3O_4/Fly ash, nZnO/activated carbon, SiO_2/activated carbon, nFe_3O_4/activated carbon, fly ash/activated carbon, nZnO/fly ash/activated carbon, $nSiO_2$/fly ash/activated carbon, nFe_3O_4/fly ash/activated carbon composite materials

3.3 Preparation of artificial seawater

A litre solution of artificial seawater (pH 8, marine water condition) was prepared by adding 86.6 mL of 5 M NaCl, 9.0 mL of 1.0 M KCl, 9.27 mL of 1.0 M $CaCl_2.2H_2O$, 4.68 mL of 4.9 M $MgCl_2.2H_2O$, 12.75 mL of 2.0 M $MgSO_4.7H_2O$ and 2.15 mL of 1.0 M $NaHCO_3$ to a volumetric flask and diluting to the mark with deionised water. TrisHCl-buffer was not used because it resulted in a lower pH (Brandli et al., 2009). However, TrisHCl-buffer and NaOH solution were used to adjust the pH during the study of the effect of pH.

3.3.1 Organotin – contaminated artificial seawater and wastewater

Different concentrations of TBT and TPT contaminated artificial seawater were prepared by spiking appropriate volume of artificial seawater with appropriate concentration of OTCs (prepared in methanol). Cloudy solution was formed and the resulting pH of TBT – contaminated, TPT – contaminated and TBT/TPT – contaminated artificial seawater was around 7. Activated carbon and its composites (2 components) were used for the sorption of TBT from TBT – contaminated artificial seawater, fly ash and its composites (2 components) were used for the sorption of TPT from TPT – contaminated artificial seawater while nZnO/fly ash/activated carbon was used for the sorption of TBT and TPT from TBT/TPT – contaminated artificial seawater. The sorption data are presented in appendices A, B and E.

For the organotin – contaminated water, appropriate concentration of TBT and TPT were spiked in deionized water. A clear solution was formed and the TBT – contaminated and TPT – contaminated water resulted to a pH of around 4.5. nFe_3O_4/fly ash/activated carbon composite was used for the sorption of TBT from TBT – contaminated water while $nSiO_2$/fly ash/activated carbon was used for the sorption of TPT from TPT – contaminated water. The sorption data are presented in appendices C and D.

3.4 Instrumentation

3.4.1 Scanning and Transmission Electron Microscopy

The scanning electron micrograph (SEM) and the transmission electron micrograph (TEM) analysis of the materials were carried out at Electron Microscope Unit, University of Cape Town, South Africa.

3.4.1.1 SEM sample preparation

A thin layer of carbon glue was spread on a stub. A small quantity of the sample was spread on the thin layer of the glue and excess particles were dusted off by means of a compressed gas duster. The stubs were coated with carbon to make the samples conductive by means of a carbon coater (Balzers model BSV 202) for 1 hr. The micrographs of the samples were viewed with a FEI^{TM} scanning electron microscope (Nova Nano SEM 230) (Appendix F (a)).

3.4.1.2 TEM sample preparation

0.1 g of the sample was put into a microcentrifuge tube-snap cap follow by the addition of 0.6 mL methanol. The mixture was dispersed for 30 s by means of a whirlimixer (FISSONS model BP 931963). Few drops of the suspension were added on a carbon coated copper grid by means of micropipette and allowed to dry. The dried carbon coated copper grid was placed on a single tilt sample holder and the vacuum seal cleaned by means of compressed gas duster. The single tilt sample holder was then loaded on the transmission electron microscope (TECNAI G^2 20) (Appendix F (b)) and the micrograph of the particles viewed.

3.4.2 Particle size distribution determination

The particle size distribution of $nSiO_2$, nZnO and nFe_3O_4 was carried out by the use of TEM while SEM was used for the particle size distribution of fly ash. The particle size distribution of activated carbon could not be calculated as the SEM and TEM micrographs of activated carbon do not show any particles that can be measured.

The micrographs were analysed by the use of IMAGEJ software. The software was used to determine the diameter of the various particle sizes on the micrograph. A plot of the percentage population (obtained from the number of particles) was plotted against the diameter (nm).

3.4.3 Carbon, Nitrogen and Hydrogen (CNH) Analysis

Samples of approximately ± 3 mg were measured into tin capsules. The tin capsules were sealed and were loaded on Euro Ea elemental analyser (Appendix F (c)) where the samples were combusted and analyzed for the percentage carbon, nitrogen and hydrogen contents. The CNH analysis of the precursors and composite materials was carried out at Environmental Laboratory, Central Analytical Facility, Stellenbosch University, South Africa.

3.4.4 X-ray fluorescence (XRF)

Major elements in the Matla fly ash such as Fe, Mn, Ti, Ca, K, S, P, Si, Al, Mg and Na (with Ni and Cr when Ni and Cr concentrations exceed -2000 mg/L or 0.2%) were determined using fusion disks prepared with LiT-LiM flux in the proportion 57:43 (Sigma Chemicals) and LiBr as releasing agent, according to the method of Claisse and Blanchette, 2004. The disks are analyzed on a Philips PW1480 wavelength dispersive XRF spectrometer with a dual target Mo/Sc x-ray tube. All measurements were made with the tube at 50 kV, 50 mA.

3.4.5 ICP-MS and ICP-AES

Inductively coupled plasma mass spectrometry (ICP-MS) (Agilent 7700) and inductively coupled plasma atomic emission spectroscopy (ICP-AES) (Thermo Icap 6300) instruments were used to determine trace and major elements in the fly ash, respectively at Environmental Laboratory, Central Analytical Facility, Stellenbosch University, South Africa. Nitric acid - hydrogen peroxide digestion method was used for ICP-MS and ICP-AES sample preparation. Appendices F (d) and F (e) shows the photographs of ICP-MS and ICP-AES used in this study.

Approximately ± 1.0 g of fly ash was added to 10 mL of 1:1 HNO_3 in a 200 mL tube, put in 90 ^oC water bath for 5 min and allow cooling for 5 min. After cooling, 5 mL of concentrated HNO_3 was added, put in hot water bath for 5 min and allow cooling, these processes were repeated until fumes disappeared. The sample was then put in the hot water bath; 2 mL of H_2O_2 was added and heated in the bath for 2 hrs. The sample was cooled and transferred into a 100 - mL volumetric flask, made up to the mark with deionized water and then filtered to remove very tiny particulate matter that might be present in the sample solution.

3.4.6 Fourier Transform Infrared Spectroscopy (FTIR)

FTIR absorption spectra were obtained using the potassium bromide (KBr) pellet method. In this method, ± 1 mg of adsorbent samples before and after adsorption were mixed with ± 250 mg of dry potassium bromide and ground to fine powder in an agate mortal. The mixture was transferred into a clean dry die with the shiny face of the metal pellet upwards and the powder distributed by shaking lightly. It was covered by a second metal pellet and the plunge was inserted.

The die was placed into the hydraulic press. Making sure the hydraulic valve was closed, the handle was pumped until the die was fairly tightly secure (8 tons pressure gauge). The vacuum pump was prepared by closing the top bleed valve and opening bottom suction valve. Pump rubber hose was connected to the die nipple and exhausted for 10 min to remove water from the mixture. With pump still exhausting, pressure was supplied using the handle back to the initial pressure gauge (8 ton) and exhausted for a further 20 min.

After 20 minutes, the hydraulic valve was released to allow the pressure to drop gradually. The hose was then disconnected and the pump switched off. The formed pellet (13 mm diameter) was carefully removed from the die and placed in the holder. The spectra were recorded over 4 000 – 400 cm^{-1} range using a Perkin Elmer^{TM} Spectrum 1000 FTIR instrument (Appendix F (f)).

3.4.7 pH determination

The pH was determined by gently boiling 50 mL of Milli-Q water in a flask containing 0.1 g of the samples for 5 minutes. The pH was measured after the solutions were cooled to room temperature using a Mettler Toledo pH meter.

3.4.8 Point of Zero Charge (PZC) determination by mass titration

Increasing amounts of samples from 0 to 2.0 g were added to 10 mL of 0.01 M $NaNO_3$ solution. The resulting pH of each suspension was measured after 24 hours. The pH plateau for the highest concentrations of solid in a successive series of mass titrations was taken as the PZC (Adekola et al., 2011). When the pH is lower than the PZC value, the acidic water donates more protons than hydroxide groups, and so the adsorbent surface is positively charged (attracting anions). Conversely, above PZC the surface is negatively charged (attracting cations/repelling anions) (Zheng et al., 2009).

3.4.9 Ash content determination

Approximately ± 0.1 g of samples were measured into crucibles and were heated in a muffle furnace (Carbolite Sheffied model LMF 4) at a temperature of 600 ± 1 ºC for 4 hours. After ashing, the samples were withdrawn from the furnace, allowed to cool in a desiccator and were reweighed. The ash content of the samples was calculated by difference and the experiments carried out in triplicate (Ayanda and Adekola, 2011).

3.4.10 X-ray diffraction

X-ray diffraction analysis for the qualitative evaluation of the common and predominant phases within the precursors and composite materials was determined using a PANalytical PW 3830 diffractometer (Appendix F (g)) at Geology Department, University of Cape Town. The diffractometer was operated at 40 kV and 25 mA for 1 h over the range of 2θ from 0° to 80°.

3.4.11 Surface area and porosity determination

The specific surface area of the precursors and composite materials were obtained using a TriStar 3000 analyser (Micromeritics Instrument Corp) (Appendix F (h)) at Chemical Engineering Department, University of Cape Town, with N_2 adsorption at - 196 ºC. The sample was first degassed at 200 ºC for 4 hours. TriStar 3000 is an automated gas analyser which contains three ports, allowing up to three samples to be analyse simultaneously. The TriStar 3000 system consists of the TriStar analyser, a SmartPrep degasser that is used for samples preparation, a vacuum pump and a control module for entering analysis and report options.

3.5 Analysis of organotin compounds

The concentration of OTCs (TBT and TPT) in artificial or natural wastewater before and after the adsorption studies was determined after derivatization by the addition of 1 mL of acetate buffer (pH = 4.5) and 1.0 mL of 1 % $NaBEt_4$ and extraction into hexane by horizontal shaking in a separation funnel. The extracts were reduced to 1 mL and analyse by the use of GC-FPD (Shimadzu GC-2010 Plus) (Appendix F (i)) with a capillary column HP 5 (5 % phenyl methyl siloxane, 30 m X 0.25 mm, i.d., film thickness 0.25 µm), and the temperature was programmed as follows: initially at 60 ^{o}C hold for 1 min, then heated to 280 ^{o}C at 10 ^{o}C/min, hold for 4 minutes. The injection and detector temperatures were 270^{o}C and 300^{o}C, respectively and the carrier gas was high purity helium.

TBT and TPT were analyzed by the use of gas chromatography flame photometric detection (GC–FPD) and a working curve was generated. Table 3.1a shows the GC – FPD operating parameters used for the analysis of TBT and TPT compounds.

Table 3.1a: GC – FPD operating parameters

GC injection parameters	
Mode	Splitless
Volume	1.0 µL
Sampling time	1.00 min
Temperature	270 ^{o}C
Flow control mode	Linear velocity
Pressure	121.3 kPa
Total flow	20.2 mL/min
Column flow	1.56 mL/min
Linear velocity	35.5 cm/sec
Purge flow	3.0 mL/min
Column parameters	
Column information	HP 5
Temperature	60 ^{o}C
Carrier gas	Helium
Equilbration time	1.0 min
Length	30.0 m
Film thickness	0.25 µL
Inner diameter	0.25 mmID
Oven programme	initially at 60 ^{o}C hold for 1 min, then heated to 280 ^{o}C at 10 ^{o}C/min, hold for 4 min
Detector (FPD) parameters	
Temperature	300 ^{o}C
Sampling rate	80.0 msec
Stop time	27.00 min
Delay time	0.00 min
H_2 flow	120.0 mL/min
Air flow	100.0 mL/min

The retention time of TBT and TPT was 12.87 and 21.19 min, respectively and the calibration curve obtained from the GC-FPD is as shown in Appendix G and H. The limit of detection and quantification of the analytical method were determined according to EURACHEM guidelines (1998). Blank matrices without sample were injected, and the blank signal measured. The limit of detection (LOD = 0.0001 mg/L) and limit of quantification (LOQ = 0.0010 mg/L) were calculated from the mean and standard deviation of 10 blank measurements with 95 % confidence level.

The regression analysis carried out on signal intensities obtained for 6.25, 12.5, 25, 50 and 100 mg/L working standards of TBT, showed a correlation coefficient of 0.9985. The linearity of the standards calibrations concentration of TBT analyzed under the same conditions was

38.75 ± 0.05 mg/L and the precision of measurement was represented by the relative standard deviation (RSD) which ranged 8.83 – 10.50 % for the between sample reproducibility aliquots of TBT.

3.5.1 Organotin confirmation by Gas chromatography mass spectrometry

Gas chromatography mass spectrometry (GC – MS) was used for the confirmation of TBT and TPT in the filtrate after adsorption. Table 3.1b shows the GC – MS instrument (Agilent 6890N GC with CTC CombiPAL autosampler and Agilent 5975B MS) operating parameters used for the confirmation of TBT and TPT.

Table 3.1b: GC – MS operating parameters

GC injection parameters	
Mode	Splitless
Temperature	270 ^{o}C
Pressure	98.6 kPa
Purge flow	50.0 mL/min
Purge time	10.00 min
Total flow	54.3 mL/min
Gas saver	On
Saver flow	50.0 mL/min
Saver time	2.00 min
Gas type	Helium
Column parameters	
Column information	**Rtx®-5MS,** Restek 12723-127
Max. temperature	330 ^{o}C
Normal Length	30 m, 0.25 mm ID, 0.25 µm film thickness
Oven programme	initially at 60 ^{o}C hold for 1 min, then heated to 280 ^{o}C at 10 ^{o}C/min, hold for 7 min
Mode	Constant flow
Initial flow	1.6 mL/min
Normal initial pressure	98.6 kPa
Average velocity	46 cm/sec
Inlet	Front inlet
Outlet	MSD
Outlet pressure	Vacuum

The analysis was conducted to investigate if the adsorption by the adsorbents result in the degradation of OTCs into other compounds or derivatives and to check that the use of the adsorbents has not resulted to the production of a more severe pollutants during the treatment process. Filtrate samples were randomly picked (7 samples) and analysed.

3.6 Adsorption experiments

Adsorption experiment was carried out by shaking on an orbital shaker (Labotec OrbiShake) 0.5 g of adsorbents in 25 mL of adsorbate solutions with an initial concentration of 100 mg/L at room temperature (20 ^{o}C). After 60 minutes, the aqueous samples were filtrated and the concentrations of the adsorbate in the filtrates were analysed. The solid residues before and after adsorption (optimal conditions) were subjected to SEM and FTIR analysis.

The amount of adsorbate adsorbed (mg/g) was calculated based on a mass balance equation as given in Equation 3.1 (Ayanda et al., 2012d):

$$q = \frac{\left(C_o - C_e\right)}{W} V \qquad (3.1)$$

where q is the equilibrium adsorption capacity per gram dry weight of the adsorbent, mg/g; C_o is the initial concentration of the adsorbate in the solution, mg/L; C_e is the final or equilibrium concentration of adsorbate in the solution, mg/L; V is the volume of the solution, L; and W is the dry weight of the adsorbent, g. All adsorption studies were carried out in triplicate.

3.6.1 Effect of adsorbent amount

The amount of adsorbents (adsorbent dose) ranging from 0.0625 – 1.0 g per 25 mL of organotin solution were investigated on the efficiency of the adsorption process. Graphs of the percentage of organotin compound adsorbed (C_a), mg/g on the adsorbents were plotted against the adsorbent amount.

3.6.2 Effect of contact time

The effect of contact time was carried out by shaking 0.5 g of the adsorbents in 25 mL of organotin solutions with an initial concentration of 100 mg/L, temperature of 20 ^{o}C at different contact time. After pre-defined contact time (10 – 70 min), the aqueous samples were filtered, and the concentration of adsorbate in the filtrate was determined. The results obtained on the effect of contact time were used for the adsorption kinetics studies. Pseudo first – order, pseudo second – order, Elovich, Fractional Power and Intra-particle diffusivity kinetic rate equations were used for modelling the kinetics of organotin adsorption.

3.6.3 Effect of pH

The adsorption behaviour of OTCs on the adsorbents was studied at different pH values in the range of pH 3 – 9. The percentage of adsorbed organotin compound (C_a), mg/g on the adsorbent was plotted against pH.

3.6.4 Effect of stirring speed

Studies on mixing speed were also performed by comparing the adsorption efficiency of OTCs on the precursors and composite materials at various mixing speeds from 160 – 200 rpm.

3.6.5 Effect of initial concentration

The effect of initial concentration were investigated by varying the initial organotin concentration from 12.5 to 200 mg/L at optimized adsorbent amount, contact time, pH and stirring speed established after the optimization of working parameters. The results obtained on the effect of initial concentration were used for the adsorption isotherm studies. The equilibrium data were fitted by Langmuir, Freundlich, Temkin and D-R isotherm models.

3.6.6 Effect of temperature

The effect of temperature on the adsorption of OTCs was also evaluated after the optimization of all the working parameters for organotin adsorption at initial concentration of 100 mg/L solution with 0.5 g of adsorbents per 25 mL, contact time of 60 min and stirring speed of 200 rpm from where the thermodynamic parameters of organotin adsorption were obtained.

3.7 Theory

3.7.1 Adsorption kinetics

Pseudo first-order, pseudo second-order, Elovich, fractional power and intraparticle diffusion rate equations have been used for modelling the kinetic of organotin adsorption.

3.7.1.1 Pseudo first-order

The pseudo first - order equation is generally expressed as follows (Ayanda et al., 2012d):

$$\frac{d_q}{d_t} = k_1\left(q_e - q_t\right) \qquad (3.2)$$

where, q_e is the amount of organotin adsorbed at equilibrium per unit weight of the adsorbent (mg/g); q_t is the amount of organotin adsorbed at any time (mg/g) and k_1 is the pseudo first - order rate constant/min.

After integration and applying boundary conditions t = 0 to t = t and q_t = 0 to q_t = q_t, the integrated form of Equation 3.2 becomes:

$$\log\left(q_e - q_t\right) = \log q_e - \frac{k_1}{2.303}(t) \qquad (3.3)$$

The values of $\log\left(q_e - q_t\right)$ were linearly correlated with t. The plot of $\log\left(q_e - q_t\right)$ versus t should give a linear relationship from which k_1 and q_e can be determined from the slope and intercept of the plot, respectively.

3.7.1.2 Pseudo second – order

The pseudo second - order adsorption kinetic rate equation is expressed as Equation 3.4:

$$\frac{d_q}{d_t} = k_2\left(q_e - q_t\right)^2 \qquad (3.4)$$

where, k_2 is the rate constant of pseudo second - order adsorption (g/mg min). For the boundary conditions t = 0 to t = t and q_t = 0 to q_t = q_t, the integrated form of Equation 3.4 becomes Equation 3.5:

$$\frac{t}{q} = \frac{1}{h_o} + \frac{1}{q_e}(t) \qquad (3.5)$$

where, h_o is the initial adsorption rate. If the second-order kinetics is applicable, the plot $\frac{t}{q}$ against t in Equation 3.5 should give a linear relationship from which the constants q_e and h_o can be determined.

When t tends to 0, h_o is defined as Equation 3.6 (Basha and Murthy, 2007):

$$h_o = k_2 q_e^{\ 2} \qquad (3.6)$$

where, k_2 is the pseudo second-order rate constant (g/mg/min), k_2 was calculated for the adsorption of organotin in artificial seawater.

3.7.1.3 Elovich

The Elovich model is generally described by Equation 3.7 (Aboul-Kassim and Simoneit, 2001 & Ho and McKay, 2002):

$$\left(d_{q_t} / d_t\right) = \alpha e^{(-\beta q_t)} \qquad (3.7)$$

And applying the boundary conditions q_t = 0 at t = 0 and q_t = q_t at t = t, the simplified form of the Elovich equation is expressed as Equation 3.8:

$$q_t = \frac{1}{\beta}.\ln\frac{\alpha_E}{\beta} + \frac{1}{\beta}.\ln t \qquad (3.8)$$

where, q_t is the amount of adsorbate per unit mass of sorbent at time (*t*), and α_E and β are the constants during any one experiment (α_E is the initial adsorbate sorption rate and β is the desorption constant). A plot of q_t vs $\ln t$ should give a linear relationship with a slope of $\frac{1}{\beta}$ and an intercept of $\frac{1}{\beta}.\ln\frac{\alpha_E}{\beta}$.

3.7.1.4 Fractional Power

The Fractional Power or Power Function model can be expressed as Equation 3.9:

$$q_t = k_3 t^{v} \qquad (3.9)$$

The linearized form is given as Equation 3.10:

$$\log q_t = \log k_3 + v \log t \quad (3.10)$$

where, q_t is the amount of sorbate per unit mass of sorbent, k_3 is a constant, t is time, and v is a positive constant (< 1). A plot of $\log q_t$ vs $\log t$ should give a linear relationship with a slope (v) and an intercept of $\log k_3$.

3.7.1.5 Intra-particle diffusivity

The equation (Equation 3.11) used to model the intraparticle diffusion is that which was developed using the linear driving force concept by Chanda et al., as reported by Okieimen and Orhorhoro, 1986 & Igwe et al., 2008.

$$\ln(1-\alpha) = -k_p t \quad (3.11)$$

where, α is fractional attainment to equilibrium and k_p is the rate coefficient for particle-diffusion controlled process corresponding to the particle size of the adsorbent; t is time and $\ln(1-\alpha)$ is a measure of the intra-particulate diffusivity. $\ln(1-\alpha)$ will be plotted against time t and the rate coefficient k_p calculated from the slope of the graph.

3.7.2 Adsorption isotherm modelling

Isotherms are the equilibrium relations between the concentration of adsorbate on the solid phase and its concentration in the liquid phase. From the isotherms the maximum adsorption capacity can be obtained. These data provide information on the capacity of the sorbent or the amount required to remove a unit mass of pollutant under the system conditions. Data has been subjected to four different adsorption isotherms.

3.7.2.1 Langmuir isotherm

Langmuir isotherm is usually used to describe the adsorption of solute from liquid solutions and this model assumes monolayer adsorption onto a homogeneous surface with finite number of identical sites. The Langmuir isotherm is represented as Equation 3.12a and the linearized form of the model can be written as Equation 3.12b (Lin et al., 2011):

$$C_a = \frac{A_{\max} k_L C_e}{1 + k_L C_e} \quad (3.12a)$$

$$\frac{c_e}{c_a} = \frac{1}{A_{\max} k_L} + \frac{1}{A_{\max}} c_e \quad (3.12b)$$

where, c_e (mg/L) is the equilibrium concentration of adsorbate in the solution, c_a (mg/g) is the adsorbate adsorption capacity for the adsorbents at equilibrium, $A_{\max}$ (mg/g) is the maximum monolayer adsorbate adsorption capacity, and k_L (L/mg) is the Langmuir isotherm constant related to the free energy of adsorption. The values of $A_{\max}$ and k_L can be calculated from the intercept and the slope of the straight line of the linearized form of the Langmuir isotherm.

3.7.2.2 Freundlich isotherm

The Freundlich isotherm is applicable to both monolayer (chemisorption) and multilayer adsorption (physisorption) and is based on the assumption that the adsorbate adsorbs onto the heterogeneous surface of an adsorbent. The Freundlich isotherm is represented as Equation 3.13a while the linearized form of model can be written as Equation 3.13b (Sheela et al., 2012):

$$c_a = k_F c_e^{1/n} \quad (3.13a)$$

$$\log c_a = \log k_F + \frac{1}{n_F} \log c_e \quad (3.13b)$$

where, k_F [mg/g (L/mg)$^{1/n}$] and n_F are the Freundlich constants which are related to the adsorption capacity and adsorption intensity, respectively. The values of k_F and n_F can be calculated from the intercept and the slope of the straight line of the linearized form of the Freundlich isotherm, respectively.

3.7.2.3 Temkin isotherm

The Temkin isotherm model assumes that the adsorption energy decreases linearly with the surface coverage due to adsorbent–adsorbate interactions. The Temkin isotherm equation is given in Equation 3.14a and the linearized form of model can be written as Equation 3.14b (Boparai et al., 2010):

$$c_a = k_T (n_T c_e) \quad (3.14a)$$

$$c_a = n_T \ln k_T + n_T \ln c_e \quad (3.14b)$$

where, $n_T = \frac{RT}{b_T}$, b_T is the Temkin constant related to the heat of sorption (J/mol) and k_T is the Temkin isotherm constant (L/g). The values of n_T, b_T and k_T can be obtained from the intercept and the slope of the straight line of the linearized form of the Temkin isotherm.

3.7.2.4 Dubinin-Radushkevich isotherm

The D–R isotherm model is a semi-empirical equation where adsorption follows a pore filling mechanism. It assumes that the adsorption has a multilayer character involving vander Waals forces and is applicable for physical adsorption processes (Hutson and Yang, 1997). The D-R isotherm is defined as Equation 3.15a while the linear form of the model is expressed as Equation 3.15b:

$$c_a = q_m e^{(-k_{D-R}\varepsilon^2)} \quad (3.15a)$$

$$\ln c_a = \ln q_m - k_{D-R}\varepsilon^2 \quad (3.15b)$$

where q_m is the is the maximum OTC adsorption capacity (mg/g), k_{D-R} is the D–R constant related to free energy, R (8.314 J/mol K) is the gas constant, T (K) is the absolute temperature and ε is the Polanyi potential which is defined as:

$$\varepsilon = RT \ln\left(1 + \frac{1}{c_e}\right) \quad (3.16)$$

The values of q_m, and k_{D-R} can be calculated from the intercept and the slope of the straight line of the linearized form of the D-R isotherm while the mean free energy (E) can be calculated using Equation 3.17:

$$E = \frac{1}{\sqrt{2k_{D-R}}} \quad (3.17)$$

3.7.3 Thermodynamic parameters

The thermodynamic parameters can be determined from the thermodynamic equilibrium constant, K_c. The standard Gibbs free energy ΔG^o (kJ/mol) was calculated using Equation 3.18 while the values of the standard enthalpy change ΔH^o (kJ/mol) and standard entropy change ΔS^o (J/K/mol) can be calculated from the intercept and the slope of the linear plot of $\log K_c$ versus $\frac{1}{T}$ (Equation 3.19b). K_c was calculated by the use of Equation 3.19a.

$$\Delta G^o = -RT \ln K_c \qquad (3.18)$$

$$K_c = \frac{C_a}{C_e} \qquad (3.19a)$$

$$\log K_c = \frac{\Delta S^o}{2.303R} - \frac{\Delta H^o}{2.303R}.\frac{1}{T} \qquad (3.19b)$$

where, C_a (mg/L) is the amount of the OTC (mg) adsorbed on the adsorbent per liter of the solution at equilibrium, C_e (mg/L) is the equilibrium concentration of OTC in the solution, R is the universal gas constant, 8.314 J/mol K; T is absolute temperature and K_c is the thermodynamic equilibrium constant.

3.8 Application of optimized conditions to the sorption of organotin compounds

Optimal conditions (with respect to the laboratory findings) for the adsorption of OTCs (TBT and TPT) from artificial seawater were applied to organotins removal from organotin – contaminated natural seawater (shipyard wastewater) obtained from Cape Town harbour.

CHAPTER FOUR
RESULTS AND DISCUSSION

4.1 SEM and TEM micrographs of the precursors and composite materials

Figures 4.1a – 4.5a show the SEM micrographs of activated carbon, fly ash, $nSiO_2$, nZnO, nFe_3O_4 while Figures 4.1b – 4.5b show the corresponding TEM micrographs.

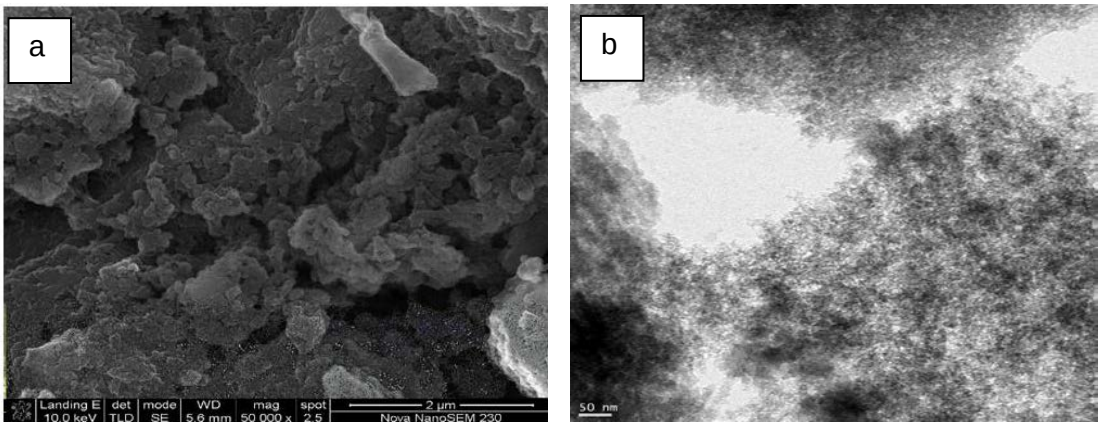

Figure 4.1: SEM (a) and TEM (b) of activated carbon

The SEM of activated carbon (Figure 4.1a) shows that activated carbon exhibits aggregated irregular surfaces with large number of micropores and crevices of various sizes at the surface (Fatoki et al., 2012). The micropores confirm activated carbon as a good adsorbent for the adsorption of pollutants from wastewater. The SEM (Figure 4.1a) and TEM of activated carbon (Figure 4.1b) do not show any carbon nanotubes and the particles could not be classified as nanospheres.

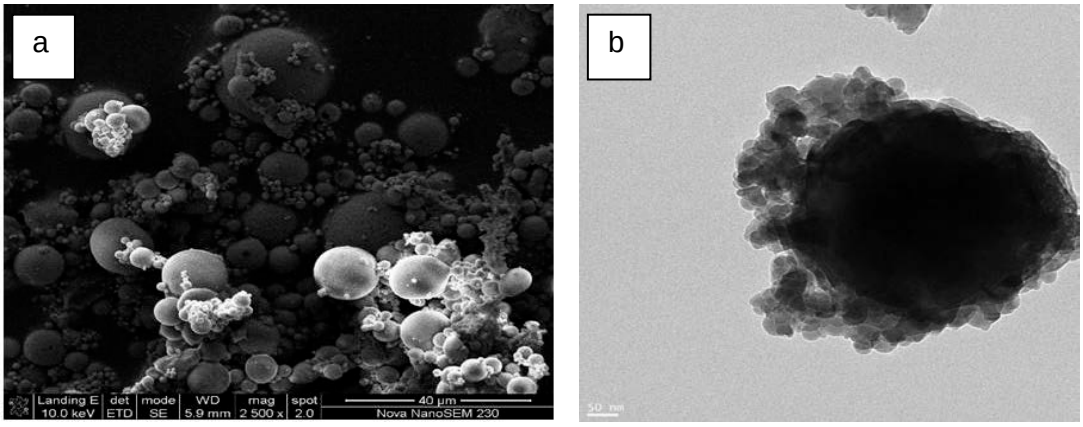

Figure 4.2: SEM (a) and TEM (b) of fly ash

The SEM of fly ash (Figure 4.2a) shows that each of the particles of Matla fly ash is spherical with smooth and regular surfaces (Ayanda et al., 2012b). The size of the spheres is 0.6 - 26.2 µm and mean particle size is 3.2 ± 3.9 µm. The cracks of some of the spheres show that the inner part of the spheres is hollow. The TEM of fly ash (Figure 4.2b) presents

agglomeration of different particle sizes. The fly ash particles show several size distributions and spherical shapes as shown in Figure 4.2a and 4.2b.

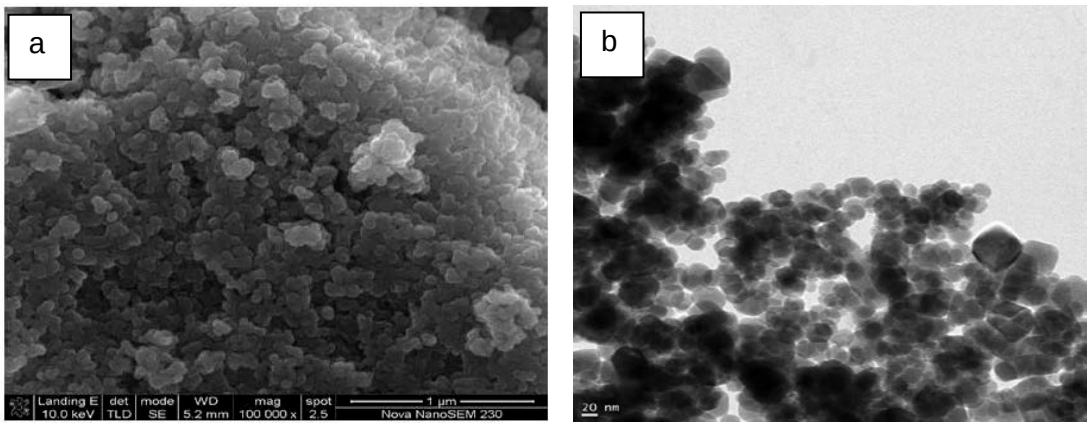

Figure 4.3: SEM (a) and TEM (b) of nFe_3O_4

The SEM of nFe_3O_4 (Figure 4.3a) shows that nFe_3O_4 consists of agglomerated globules with irregular and rough surfaces. The TEM of nFe_3O_4 (Figure 4.3b) shows agglomeration of particle sizes of various shapes (square, sphere, and hexagon) and sizes (10.8 - 77.3 nm) with an average diameter of 34.1 ± 13.7 nm.

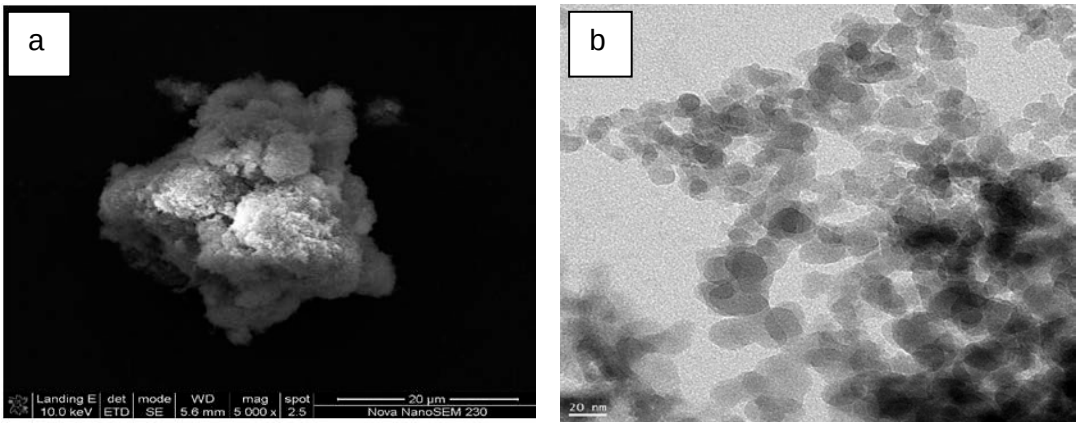

Figure 4.4: SEM (a) and TEM (b) of $nSiO_2$

Figure 4.4a is a SEM of $nSiO_2$ which shows agglomerated irregular surfaces and a large number of micropores and a few voids and crevices (Ayanda et al., 2013a). The TEM of $nSiO_2$ (Figure 4.4b) thus shows a bimodal distribution of particles size. This is in support of the result of Gianina et al. (2003) who reported the TEM result of SiO_2 powder. Figure 4.4b also shows that the particle size of $nSiO_2$ ranges between 9.8 - 33.9 nm with a mean particle size of 19.3 ± 6.0 nm.

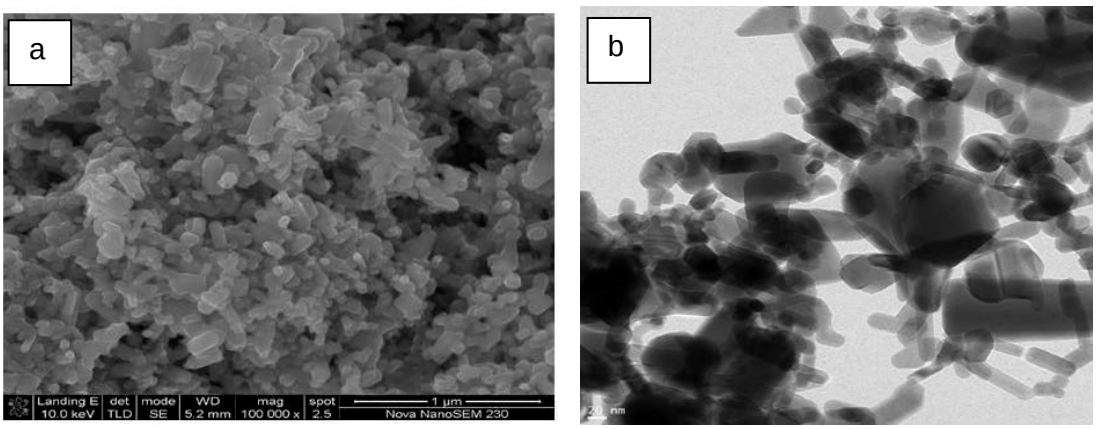

Figure 4.5: SEM (a) and TEM (b) of nZnO

The SEM and TEM micrographs of nZnO (Figure 4.5a and 4.5b) show that nZnO particles consist of uniform granules and more regular surfaces (Ayanda et al., 2012e). The TEM of nZnO (Figure 4.5b) confirms the various shapes of nZnO particles which are spherical, rectangular, hexagonal and rod-like in shape. TEM thus presents granules of particle sizes ranging from between 15.9 - 144.7 nm with a mean particle size of 53.5 ± 26.6 nm.

Figures 4.6a to 4.12a show the SEMs of the composite materials involving two precursors whereas Figures 6b to 12b show their corresponding TEMs.

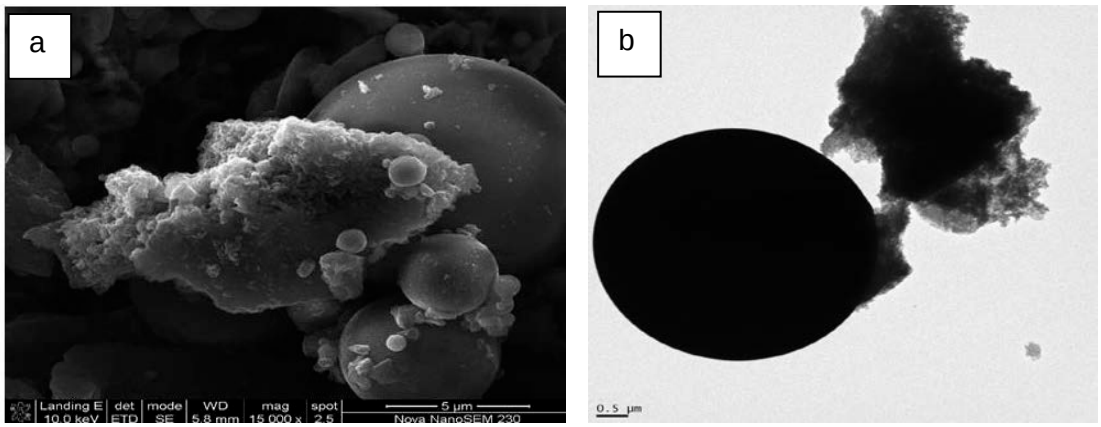

Figure 4.6: SEM (a) and TEM (b) of fly ash/activated carbon composite material

Figure 4.6a is a SEM of fly ash/activated carbon composite material and shows that the composite material is made up of smooth surface materials (activated carbon) and spherical materials (fly ash) deposited at various positions throughout the surface of the activated carbon. The TEM of fly ash/activated carbon composite material (Figure 4.6b) shows that the activated carbon (irregular surface) is aggregated with the spherical particle of fly ash. The SEM and TEM (Figure 4.6a and 4.6b) also show that the particles of fly ash maintain their spherical morphology after the preparation of the composite material.

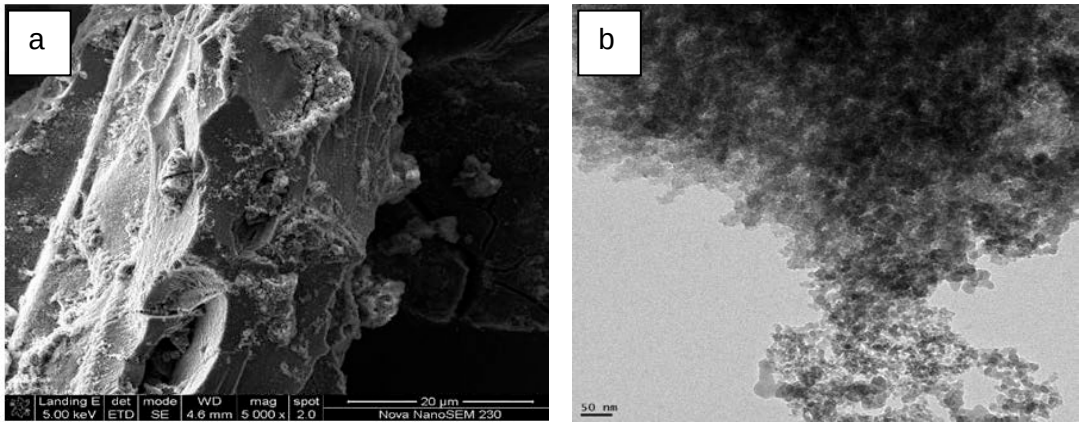

Figure 4.7: SEM (a) and TEM (b) of $nSiO_2$/activated carbon composite material

Figure 4.7a shows that the $nSiO_2$/activated carbon composite material is made up of irregular surfaces with crevices and few macropores. The micrograph also shows that $nSiO_2$ is deposited throughout the surface of the activated carbon. The TEM of $nSiO_2$/activated carbon composite material (Figure 4.7b) indicates that activated carbon is aggregated with $nSiO_2$.

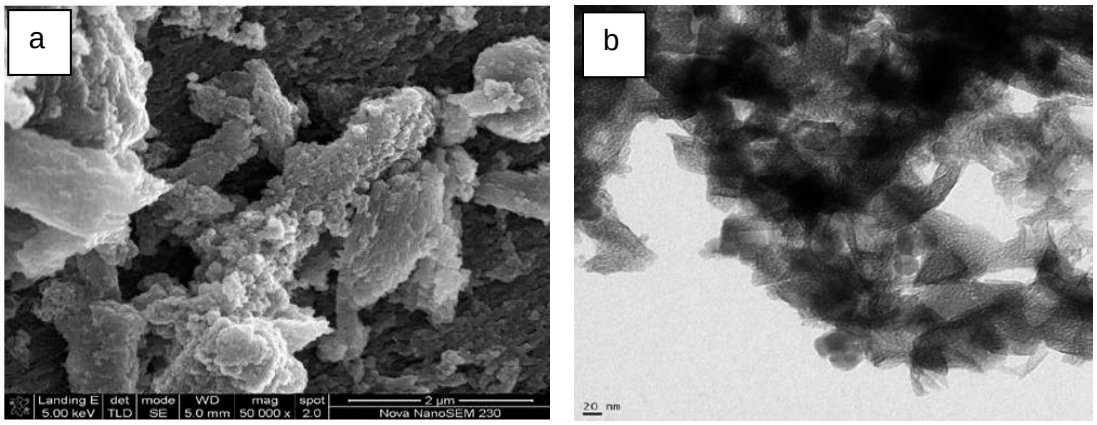

Figure 4.8: SEM (a) and TEM (b) of nFe_3O_4/activated carbon composite material

The SEM of nFe_3O_4/activated carbon composite material (Figure 4.8a) shows that nFe_3O_4/activated carbon composite material exhibits irregular surfaces with a large number of micropores and crevices of various sizes at the surface. The SEM and TEM (Figure 4.8b) of this composite material also shows that the various nFe_3O_4 particles are embedded in the porous activated carbon.

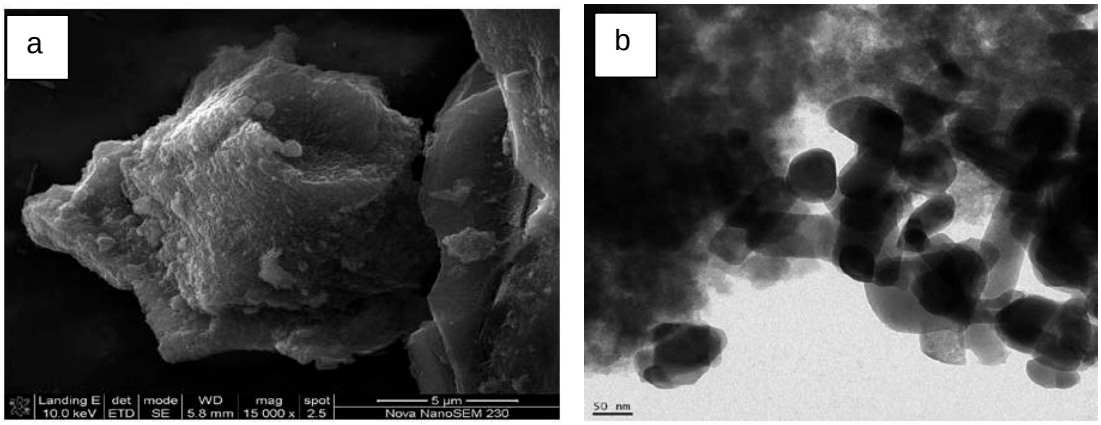

Figure 4.9: SEM (a) and TEM (b) of nZnO/activated carbon composite material

Figure 4.9a shows that nZnO/activated carbon composite material is made up of smooth surface materials (activated carbon) with nZnO deposited at various positions throughout the surface of the activated carbon. The TEM of nZnO/activated carbon composite material (Figure 4.9b) shows an aggregate of the activated carbon and nZnO. The TEM also shows that the nZnO particles maintained their morphology after the preparation of the composite material (Ayanda et al., 2012e).

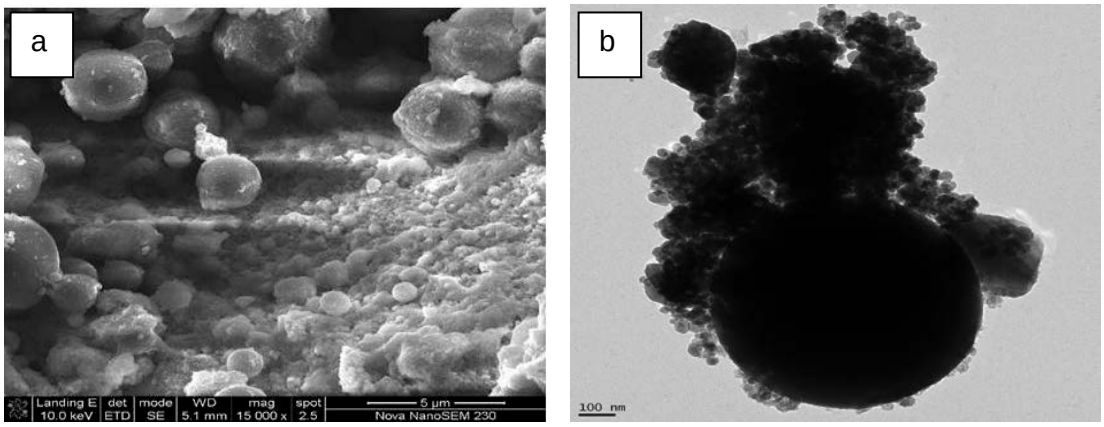

Figure 4.10: SEM (a) and TEM (b) of nFe_3O_4/fly ash composite material

The SEM of nFe_3O_4/fly ash composite material (Figure 4.10a) shows an aggregated nFe_3O_4 and fly ash particles. The figure also shows that the nFe_3O_4 particles exhibit irregular surfaces whereas the fly ash retains its spherical and smooth surface. The TEM of nFe_3O_4/fly ash composite material (Figure 4.10b) shows an aggregate of spherical fly ash and nFe_3O_4 with large crevices. The nFe_3O_4/fly ash composite material particles show several size distributions of the fly ash and the micrographs also show that the fly ash particles maintained their spherical morphology after preparation of the composite material.

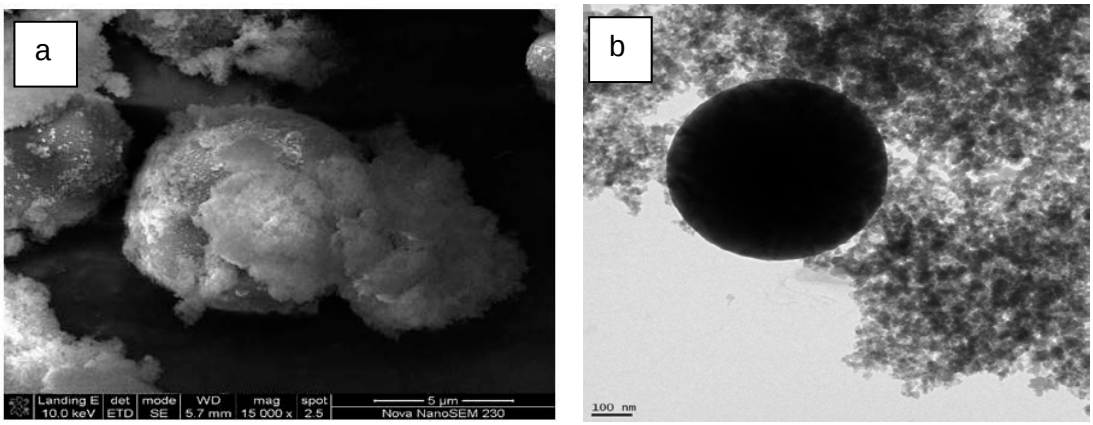

Figure 4.11: SEM (a) and TEM (b) of $nSiO_2$/fly ash composite material

The SEM of $nSiO_2$/fly ash (Figure 4.11a) shows that $nSiO_2$ with irregular surfaces and large number of micropores is deposited at various positions throughout the spherical surface of the fly ash. The TEM of $nSiO_2$/fly ash composite material (Figure 4.11b) thus shows a highly porous $nSiO_2$ surrounding the spherical fly ash.

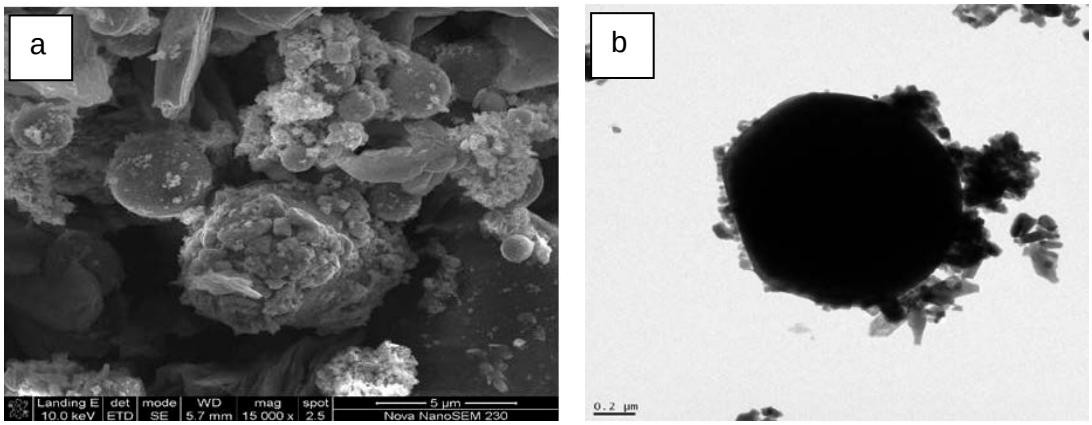

Figure 4.12: SEM (a) and TEM (b) of nZnO/fly ash composite material

The SEM of nZnO/fly ash composite material (Figure 4.12a) shows that each of the fly ash and nZnO particles are clustered together with large intergranular voids and crevices. The TEM (Figure 4.12b) also confirms the clustered nZnO/fly ash composite. The SEM and TEM (Figure 4.12a and 4.12b) thus shows the fly ash and nZnO particles maintain their morphology after preparation of the composite material.

Figures 4.13 – 4.15 show the SEM and TEM of composite materials involving three precursors.

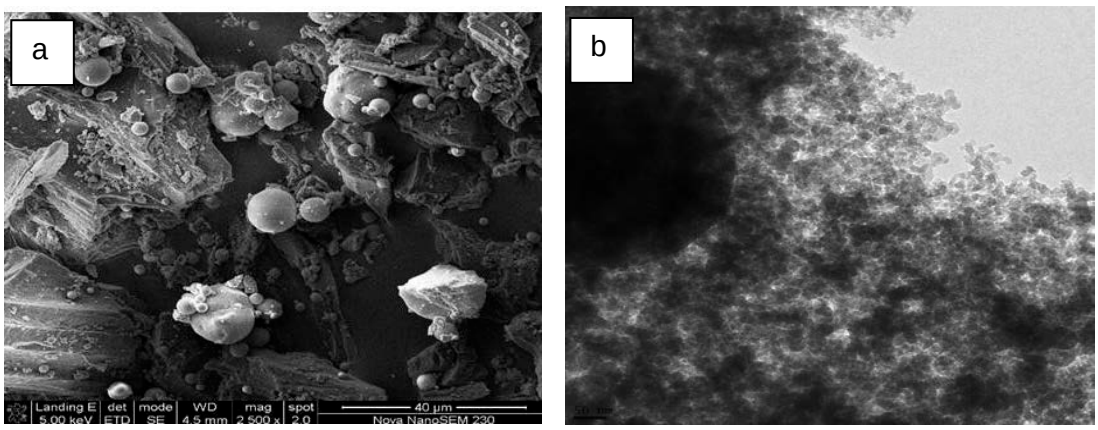

Figure 4.13: SEM (a) and TEM (b) of nFe_3O_4/fly ash/activated carbon composite material

The SEM of nFe_3O_4/fly ash/activated carbon composite material (Figure 4.13a) shows that the composite material exhibits aggregated irregular surfaces with large number of micropores and crevices at the surface. Few fly ash and nFe_3O_4 are found at the surface of the composite material. The TEM of nFe_3O_4/fly ash/activated carbon composite material (Figure 4.13b) thus shows fly ash and nFe_3O_4 embedded in the activated carbon.

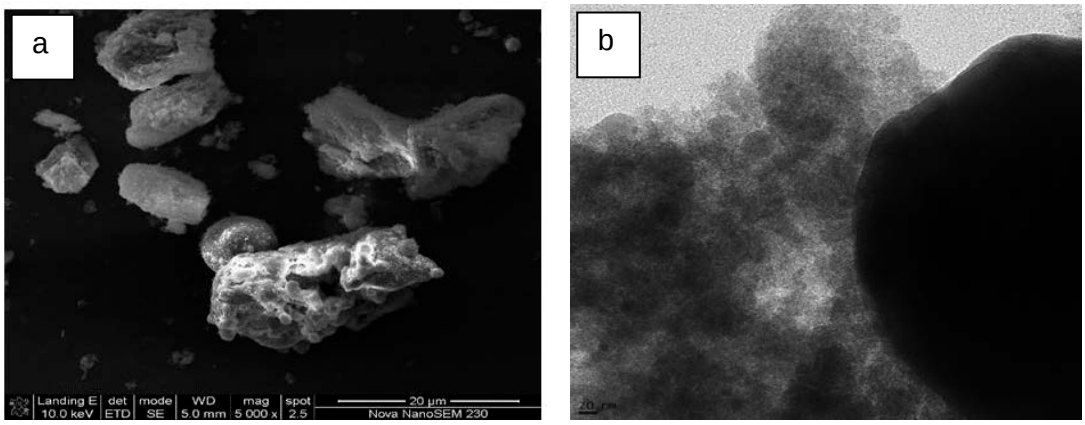

Figure 4.14: SEM (a) and TEM (b) of $nSiO_2$/fly ash/activated carbon composite material

The SEM of $nSiO_2$/fly ash/activated carbon composite material (Figure 4.14a) shows that the composite material also exhibits aggregated irregular surfaces with large number of micropores and crevices at the surface. The $nSiO_2$ and fly ash are distributed at the surface of the activated carbon. Fly ash is also found at the surface of the material. The TEM of $nSiO_2$/fly ash/activated carbon composite material (Figure 4.13b) also shows that fly ash and $nSiO_2$ are embedded in the activated carbon.

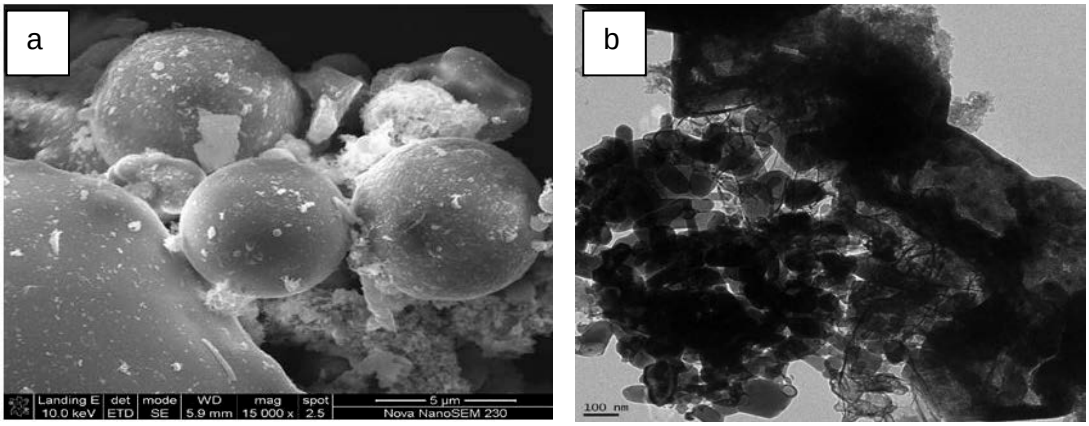

Figure 4.15: SEM (a) and TEM (b) of nZnO/fly ash/activated carbon composite material

The SEM of nZnO/fly ash/activated carbon composite material (Figure 4.15a) shows that the activated carbon, fly ash and nZnO particles are fused together. Large intergranular voids and crevices are associated with the nZnO/fly ash/activated carbon composite material with the fly ash maintaining its spherical regular shape. The TEM of nZnO/fly ash/activated carbon composite material (Figure 4.15b) also shows a clustered activated carbon, fly ash and nZnO composite material with large intergranular voids and crevices. In this composite material, the fly ash and the nZnO are not embedded in the activated carbon.

4.2 Particle size distribution

Figure 4.16 – 4.19 show the particle size distribution of fly ash, nFe_3O_4, $nSiO_2$ and nZnO. Figure 4.16 shows that the particle size of fly ash range from 0.6 - 26.2 µm, mean particle size is 3.2 µm and the standard deviation is 3.9. The graph on the particle size distribution of fly ash shows that the fly ash particles are mostly between 1.1 – 1.2 µm particle sizes while particles greater than 10 µm size are also present but very minute in the sample.

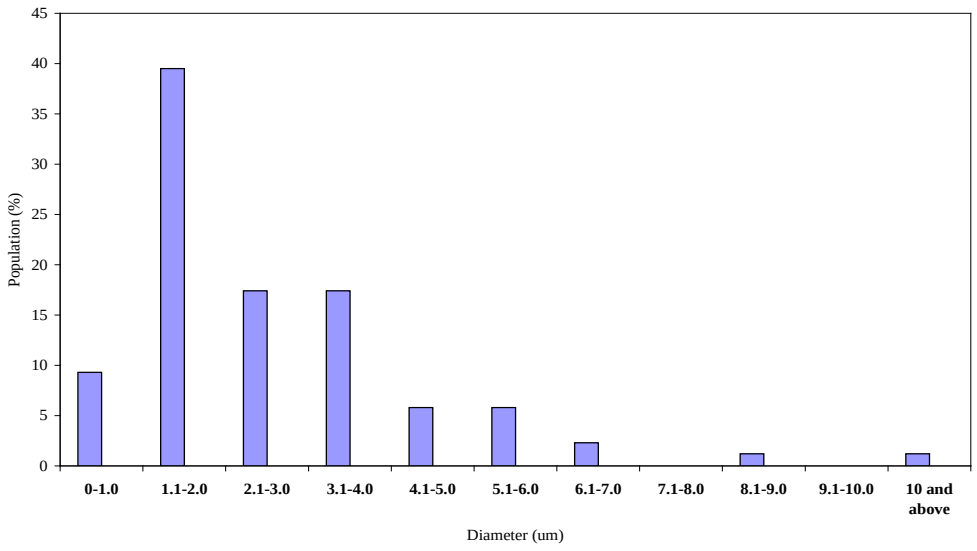

Figure 4.16: Particle size distribution of fly ash

Though the particle size of nFe_3O_4 used in this research work was specified by the manufacturer to be < 50 nm, Figure 4.17 shows that the particle size of nFe_3O_4 is between 10.8 – 77.3 nm, mean particle size is 34.1 nm and a standard deviation of 13.7. The graph on the particle size distribution of nFe_3O_4 shows that nFe_3O_4 is mostly between 20.1 – 30.0 nm particle sizes.

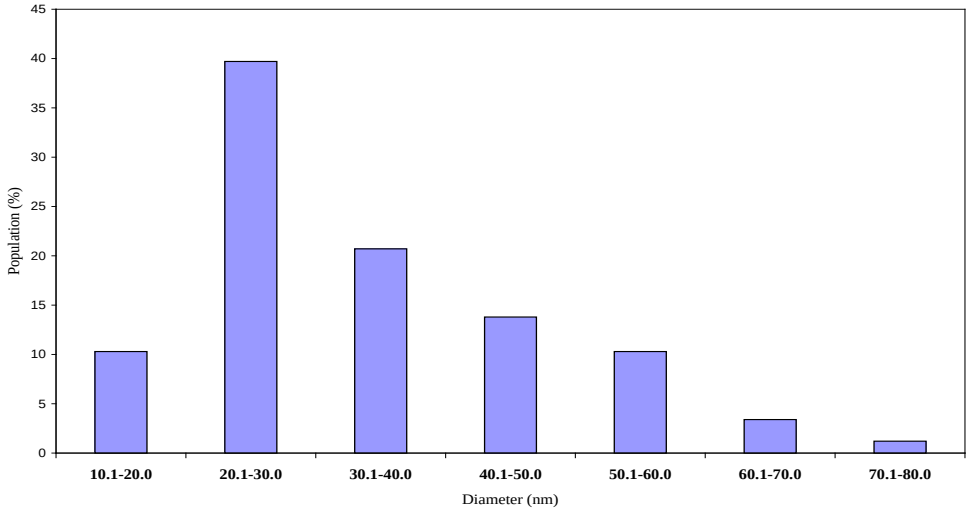

Figure 4.17: Particle size distribution of nFe_3O_4

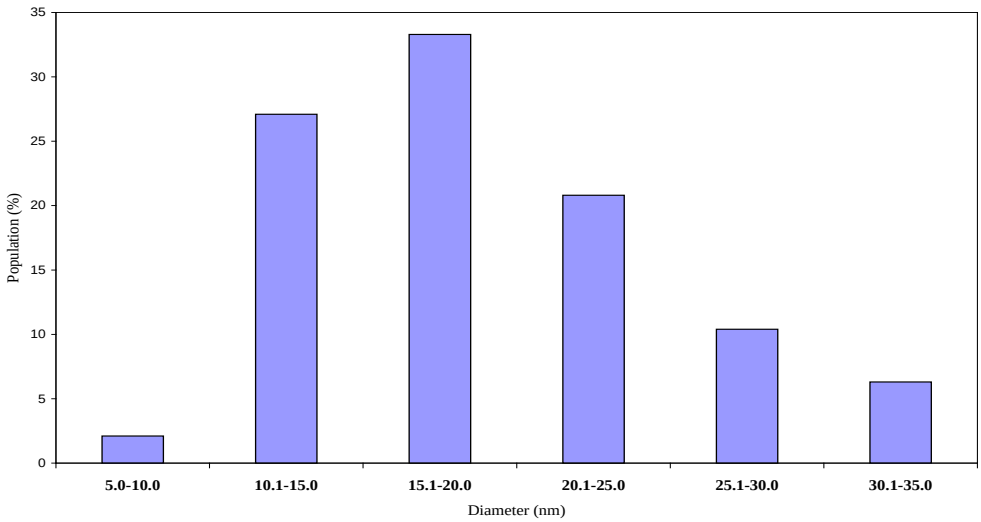

Figure 4.18: Particle size distribution of $nSiO_2$

Figure 4.18 shows that the particle size of $nSiO_2$ range from 9.8 – 33.9 nm, mean particle size is 19.3 nm and the standard deviation is 6.0. The graph of Figure 4.18 shows that $nSiO_2$ is mostly distributed between 10.1 – 20.0 nm particle sizes whereas the $nSiO_2$ was specified and labelled by the manufacturer as 12 nm particle size.

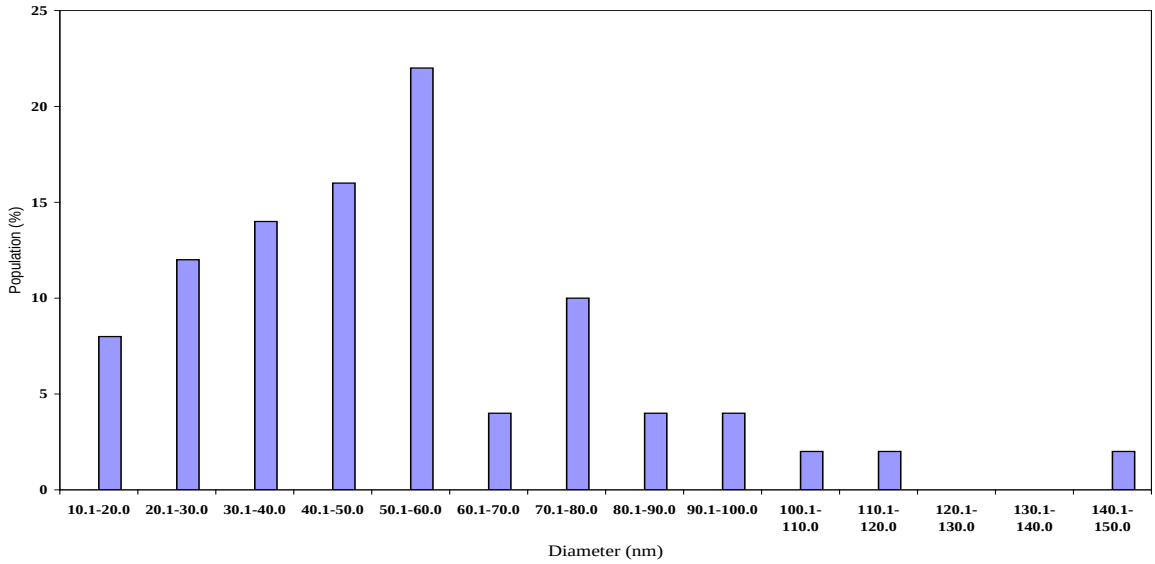

Figure 4.19: Particle size distribution of nZnO

From Figure 4.19, the particle size of nZnO is between 15.9 – 144.7 nm, mean particle size is 53.5 and a standard deviation of 26.6. The graph on the particle size distribution of nZnO shows that nZnO is slightly evenly distributed between 20.1 – 60.1 nm particle sizes. The nZnO was specified by the manufacturer as 40 – 100 nm particle size, many particles are found to be lesser than 40 nm while few particles are greater than 100 nm.

4.3 CNH analysis

The results of the percentage carbon, nitrogen and hydrogen of the precursors and composite materials are presented in Table 4.1.

Table 4.1 and Figure 4.20 show that activated carbon used in this research work contains 71.40 % percentage carbon, 0.35 % percentage nitrogen and 2.82 % hydrogen. The nitrogen contents of nFe_3O_4, $nSiO_2$ and nZnO are all below the detection limit, the carbon and hydrogen content of $nSiO_2$ is 0.76 % each while the hydrogen percentage content of nFe_3O_4 and nZnO is also below the detection limit. Upon preparation of nano oxides/activated carbon composite materials, the nFe_3O_4/activated carbon composite contains 33.28 % carbon, 0.19 % nitrogen and 1.91 % hydrogen; $nSiO_2$/activated carbon composite on the other hand contains 37.95 % carbon, 2.03 % hydrogen while the nitogen content is below the detection limit. nZnO/activated carbon composite material thus contains 34.72 % carbon, 0.23 % nitrogen and 2.08 % hydrogen contents.

Table 4.1: Percentage carbon, nitrogen and hydrogen of precursors and composite materials

Samples	% C	% N	% H
Activated carbon	71.40	0.35	2.82
Fly ash	1.54	BD	BD
nFe_3O_4	0.46	BD	BD
$nSiO_2$	0.76	BD	0.76
nZnO	0.42	BD	BD
nFe_3O_4 **/activated carbon**	33.28	0.19	1.91
$nSiO_2$**/activated carbon**	37.95	BD	2.03
nZnO/activated carbon	34.72	0.23	2.08
nFe_3O_4 **/fly ash**	0.55	BD	1.00
$nSiO_2$**/fly ash**	0.80	BD	1.43
nZnO/fly ash	0.79	BD	1.07
Fly ash/activated carbon	36.83	BD	2.72
nFe_3O_4 **/fly ash/activated carbon**	29.34	0.19	2.24
$nSiO_2$**/fly ash/activated carbon**	34.04	0.26	0.51
nZnO/fly ash/activated carbon	30.69	0.20	0.89

BD - Below Detection of 0.001 wt%

Quality control: Acetalinide std. measured: C – 73.00 %, N - 10.85 % and H – 6.42%

Acetalinide std value: C – 71.10 %, N - 10.40 % and H – 6.70%

The results obtained show that the carbon content of activated carbon decreases by 53.39 %, 46.85 % and 51.37% in the prepared nFe_3O_4/activated carbon, $nSiO_2$/activated carbon and nZnO/activated carbon composite materials, respectively. Upon the preparation of the adsorbent composite materials, the percentage nitrogen content of nFe_3O_4 and nZnO in the corresponding composite material is raised to 0.19 % and 0.23 %, respectively while the nitrogen content of $nSiO_2$ still remain below the detection limit. The hydrogen content of nFe_3O_4/activated carbon, $nSiO_2$/activated carbon and nZnO/activated carbon composite materials is also raised to 1.91 %, 2.03 % and 2.08 %, respectively.

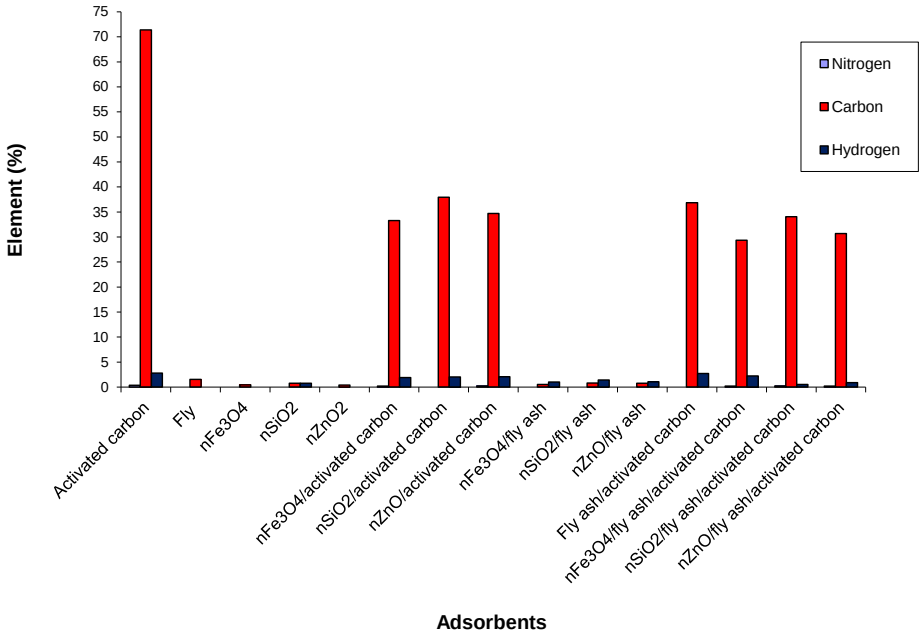

Figure 4.20: Plot of element (%) against the precursors and composite materials

The fly ash used contains 1.54 % percentage carbon while the nitrogen and hydrogen content are below the detection limit. As in the case of activated carbon, the nitrogen contents of nFe_3O_4, $nSiO_2$ and nZnO are all below the detection limit, the carbon and hydrogen contents of $nSiO_2$ are 0.76 % each while the hydrogen percentage content of nFe_3O_4 and nZnO is also below the detection limit but the preparation of fly ash composite materials involving nFe_3O_4, $nSiO_2$ and nZnO, the nFe_3O_4/fly ash composite contains 0.55 % carbon, 1.0 % hydrogen and nitrogen below the detection limit; $nSiO_2$/fly ash composite material on the other hand contains 0.80 % carbon, 1.43 % hydrogen while nitrogen content is below the detection limit. nZnO/fly ash composite material thus contains 0.79 % carbon, 1.07 % hydrogen content and nitrogen content below the detection limit.

The results show that the carbon content of fly ash decreases by 64.29 %, 48.05 % and 48.70 % in the prepared nFe_3O_4/fly ash, $nSiO_2$/fly ash and nZnO/fly ash composite materials, respectively. The nitrogen content in all the fly ash composite material is below the detection limit. The percentage hydrogen content of nFe_3O_4, $nSiO_2$ and nZnO in their corresponding composite material is raised to 1.00 %, 1.43 % and 1.07 %, respectively.

The Table 4.1 and the Figure 4.20 also show that fly ash/activated composite materials involving nFe_3O_4, $nSiO_2$, nZnO, and fly ash/activated composite contain 29.34 %, 34.04 %, 30.69% and 36.83 % carbon content, respectively. Values of 0.91 %, 0.26 % and 0.20 % are recorded for the nitrogen content of nFe_3O_4/fly ash/activated carbon, $nSiO_2$/fly ash/activated

carbon and nZnO/fly ash/activated carbon, respectively while the nitrogen content of fly ash/activated carbon composite material is below the detection limit. The fly ash/activated carbon, nFe_3O_4/fly ash/activated carbon, nSiO_2/fly ash/activated carbon and nZnO/fly ash/activated carbon thus contain 2.72 %, 0.51% and 0.89 % hydrogen contents, respectively. The results show that the very high carbon content of activated carbon plays a dominant role in the carbon contents of the composite materials.

4.4 XRF analysis of fly ash

The major elemental composition of fly ash is as shown in Table 4.2 which has alkaline (Na_2O + K_2O) of 1.31 % and alkaline rare earth's (CaO + MgO) of 8.70 %. The major constituents are SiO_2 51.43 % and alumina 30.93 %. TiO_2 and Fe_2O_3 do not exceed 1.74 and 2.29 %, respectively. The fly ash sample also contains MnO, P_2O_5, SO_3, Cr_2O_3 and NiO at 0.02, 1.08, 0.54, 0.02 and 0.01 percent, respectively.

Table 4.2 Elemental composition of Matla fly ash

Oxides	**wt %**
SiO_2	51.43
TiO_2	1.74
Al_2O_3	30.93
Fe_2O_3	2.29
MnO	0.02
MgO	1.95
CaO	6.75
Na_2O	0.54
K_2O	0.77
P_2O_5	1.08
SO_3	0.54
Cr_2O_3	0.02
NiO	0.01
LOI	1.21

Total = 99.28

The loss of mass on ignition (LOI) is 1.21 % while the ratio of SiO_2/Al_2O_3 is 1.66. The obtained result is similar to the result obtained by Gitari et al. (2008) who reported the XRF analysis of fly ash from two South African power plants (Arnot and Matla) and Vimlesh and Giri (2011) who reported the elemental concentration of fly ash generated from Parichha thermal power station in Jhansi, India.

4.5 ICP-MS and ICP- AES analysis of fly ash

The results of major and trace metals contained in the fly ash samples by ICP-AES and ICP-MS are presented in Table 4.3.

Table 4.3 Elemental concentration in fly ash

Elements	Conc. (mg/L)	Error (%)
Al	29320.00	20.16
As	16.61	1.37
B	354.70	3.06
Ba	1453.00	6.91
Ca	53010.00	3.51
Cd	0.16	1.02
Co	5.45	1.65
Cr	72.97	1.08
Cu	18.76	8.14
Fe	6144.00	0.56
K	763.50	9.53
Mg	9503.00	8.97
Mn	148.10	0.23
Mo	18.31	3.74
Na	1491.00	11.03
Ni	13.94	1.47
P	3715.00	0
Pb	24.38	1.62
Sb	0.54	1.02
Se	8.88	1.80
Si	2432.00	3.85
Sr	1696.00	0
Ti	2003.00	6.53
V	103.85	4.64
Zn	20.03	0.41

The Matla fly ash contains detectable concentrations of all the toxic and potentially toxic elements analysed for. Cobalt (Co), copper (Cu), iron (Fe), manganese (Mn), molybdenum (Mo), vanadium (V), titanium (Ti), Selenium (Se), strontium (Sr), and zinc (Zn) present are essential to health in trace amounts while arsenic (As), antimony (Sb), cadmium (Cd), chromium (Cr), and lead (Pb) are harmful to health in excessive amounts. Heavy metals can readily be leached into waterways such as rivers, lakes and by dissolving in rain, thereby causing harmful effect on the environments and human health.

4.6 FTIR results

FTIR was applied to reveal the systematic changes in the spectra features upon preparation of composite materials. By comparing the FTIR spectra of the precursors and the composite materials (Figure 4.21 - 4.30), there are slight shift in the wavenumber (bands).

In the FTIR spectrum of activated carbon, nFe_3O_4 and nFe_3O_4/activated carbon composite material (Figure 4.21), the absorption at 1616 cm^{-1} is assigned to the C=C stretching of activated carbon (Collin et al., 2007 & Mopoung and Nogklai, 2008), the absorption at 586 cm^{-1} is assigned to the Fe – O stretching of nFe_3O_4. The wavenumber of Fe – O stretching changed from 586 cm^{-1} of nFe_3O_4 to 558 cm^{-1} of the nFe_3O_4/activated carbon composite material. The wavenumber of the absorption peak decreases by 28 cm^{-1}. This shows that a new C–O–Fe bond was formed during the preparation of the nFe_3O_4/activated carbon composite material.

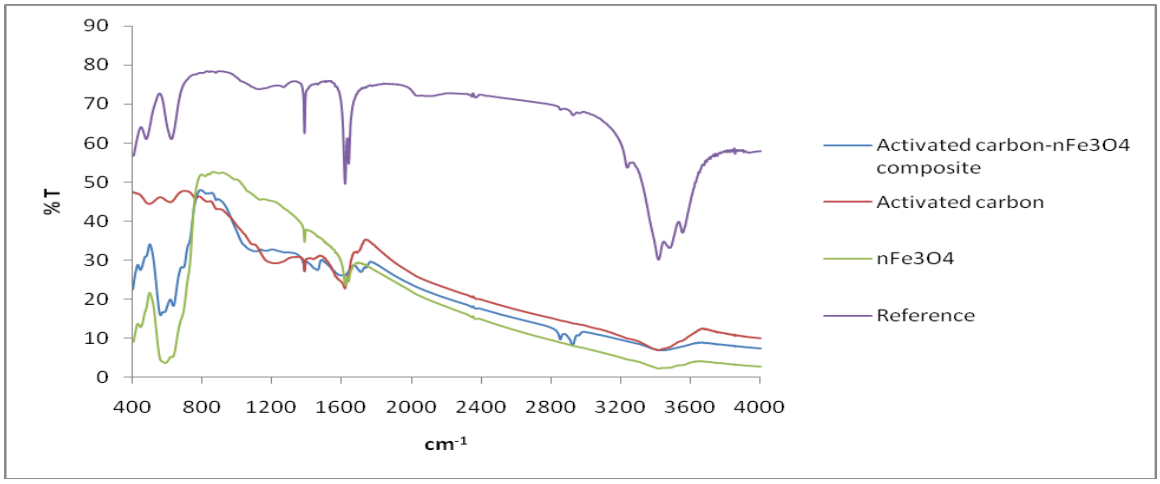

Figure 4.21: FTIR spectrum of activated carbon, nFe_3O_4 and nFe_3O_4/activated carbon composite material

In the FTIR spectrum of activated carbon, $nSiO_2$ and $nSiO_2$/activated carbon composite material (Figure 4.22), the absorption at 1616 cm^{-1} is assigned to the C=C stretching of activated carbon, and the absorption at 1101 cm^{-1} and 809 cm^{-1} is assigned to the asymmetric and symmetric vibration of Si – O, respectively (Beganskiene et al., 2004). The wavenumber of the asymmetric vibration of Si – O changed from 1101 cm^{-1} of $nSiO_2$ to 1110 cm^{-1} of the $nSiO_2$/activated carbon composite material. The wavenumber of the absorption peak therefore increases by 9 cm^{-1}. The increase wavenumber for the absorption peak indicates that the intensity of Si – O bond increases. It shows that a new C–O–Si bond was formed during the preparation of the $nSiO_2$/activated carbon composite material.

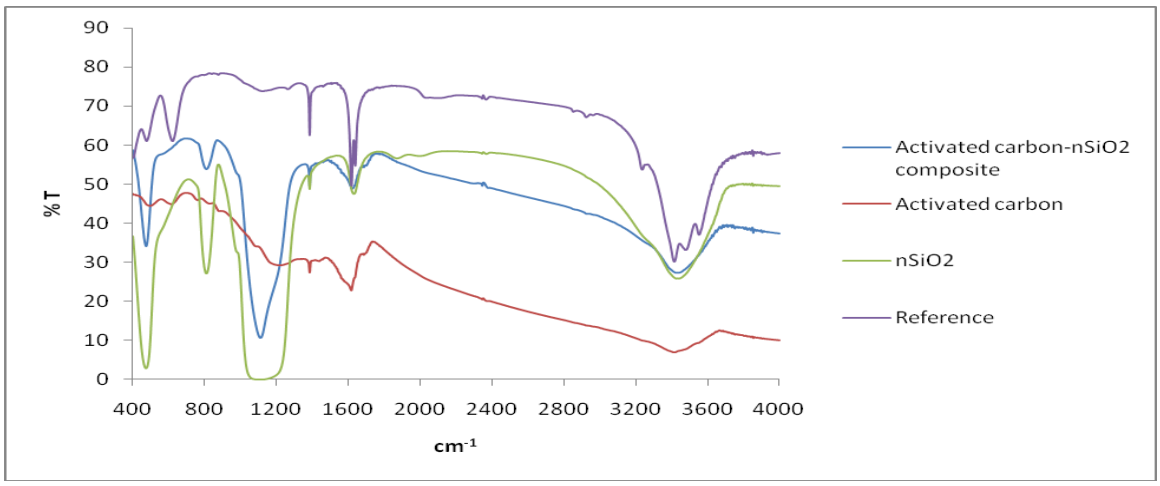

Figure 4.22: FTIR spectrum of activated carbon, $nSiO_2$ and $nSiO_2$/activated carbon composite material

In the FTIR spectrum of activated carbon, nZnO and nZnO/activated carbon composite material (Figure 4.23), the absorption at 1616 cm^{-1} is assigned to the C=C stretching of activated carbon, the adsorption at 1110 cm^{-1} is assigned to the asymmetric vibration of Zn – O, and the absorption at 808 cm^{-1} is assigned to the Zn – O stretching of nZnO (Hamedani and Farzaneh, 2006). The wavenumber of Zn – O stretching changed from 808 cm^{-1} of nZnO to 720 cm^{-1} (curve (g)) of the nZnO/activated carbon composite material. The wavenumber of the absorption peak decreases by 88 cm^{-1}. It could be explained that a new C–O–Zn bond was formed during the preparation of the nZnO/activated carbon composite material.

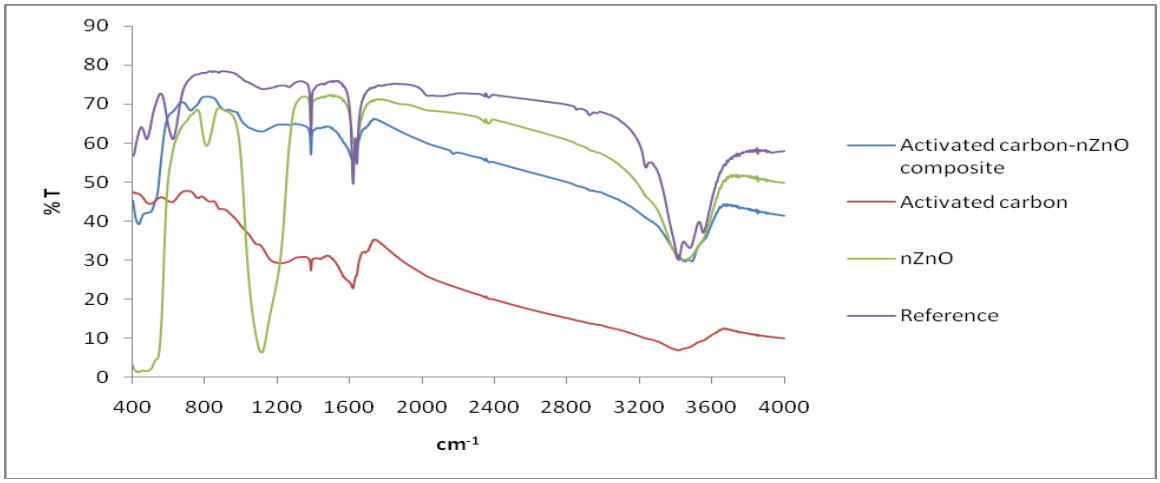

Figure 4.23: FTIR spectrum of activated carbon, nZnO and nZnO/activated carbon composite material

In the FTIR spectrum of fly ash, nFe_3O_4 and nFe_3O_4/fly ash composite material (Figure 4.24), the absorption at 1097 cm^{-1} is assigned to the C–C stretching of fly ash, the absorption at 586 cm^{-1} is assigned to the Fe – O stretching of nFe_3O_4. It was found that the wavenumber of Fe – O stretching changed from 586 cm^{-1} of nFe_3O_4 to 556 cm^{-1} of the nFe_3O_4/fly ash composite material. The wavenumber of the absorption peak decreases by 30 cm^{-1}. The

decrease wavenumber for the absorption peak indicates that the intensity of Fe–O bond decreases. It explains that a new C–O–Fe bond was formed during the preparation of the nFe_3O_4/fly ash composite material.

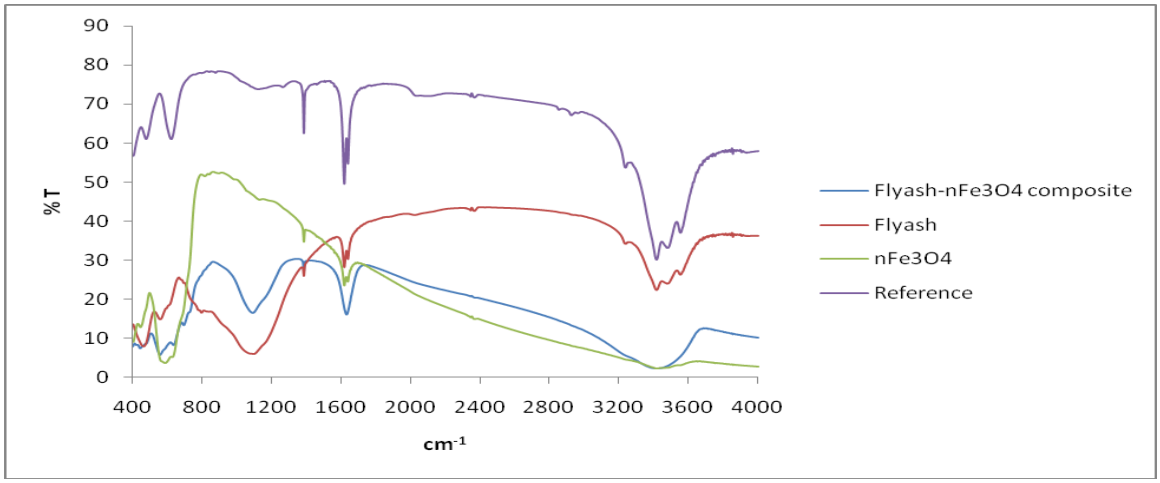

Figure 4.24: FTIR spectrum of fly ash, nFe_3O_4 and nFe_3O_4/fly ash composite material

In the FTIR spectrum of fly ash, $nSiO_2$ and $nSiO_2$/fly ash composite material (Figure 4.25), the absorption at 1097 cm^{-1} is assigned to the C–C stretching of fly ash while the absorption at 1101 cm^{-1} and 809 cm^{-1} is assigned to the asymmetric and symmetric vibration of Si – O, respectively. It was found that the wavenumber of symmetric vibration of Si – O changed from 809 cm^{-1} of $nSiO_2$ to 805 cm^{-1} of the $nSiO_2$/fly ash composite material. The wavenumber of the absorption peak decreased 4 cm^{-1}. The decrease wavenumber for the absorption peak indicates that the intensity of Si–O bond decreases and could be described that a new C–O–Si bond was formed during the preparation of the $nSiO_2$/fly ash composite material.

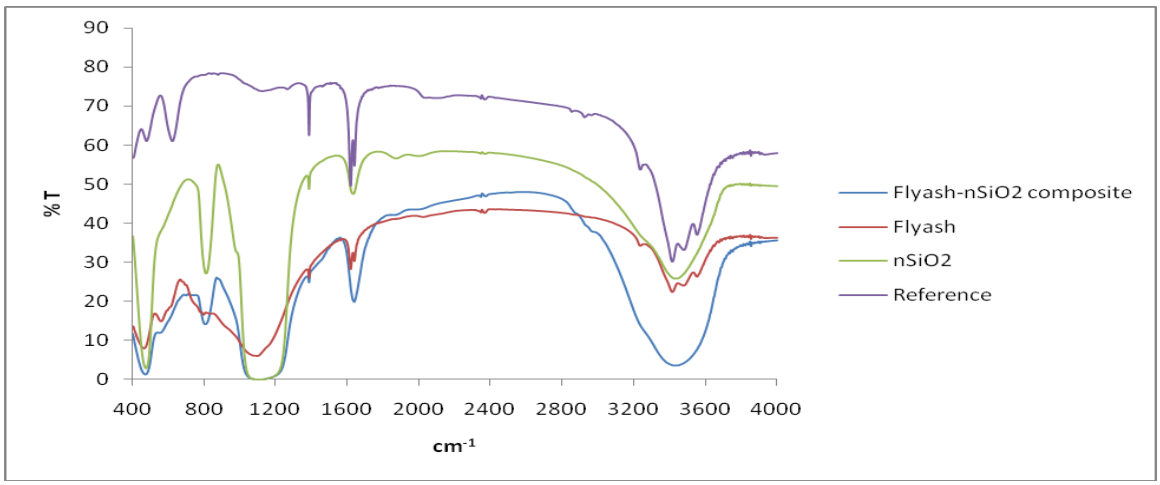

Figure 4.25: FTIR spectrum of fly ash, $nSiO_2$ and $nSiO_2$/fly ash composite material

In the FTIR spectrum of fly ash, nZnO and nZnO/fly ash composite material (Figure 4.26), the absorption at 1097 cm^{-1} is assigned to the C–C stretching of fly ash while the adsorption at 1110 cm^{-1} is assigned to the asymmetric vibration of Zn – O, and the absorption at 808 cm^{-1} is assigned to the Zn – O stretching of nZnO. It was found that the wavenumber of Zn – O stretching changed from 808 cm^{-1} of nZnO to 722 cm^{-1} of the nZnO/fly ash composite material. The wavenumber of the absorption peak decreased 86 cm^{-1}. The decrease wavenumber for the absorption peak indicates that the intensity of Zn – O bond decreases. This shows that a new C–O–Zn bond was formed during the preparation of the nZnO/fly ash composite material.

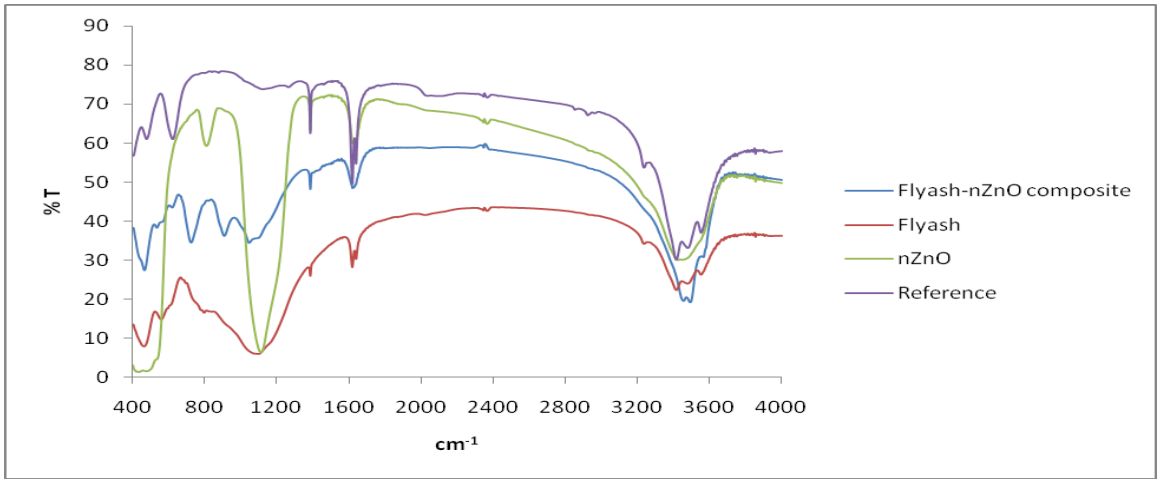

Figure 4.26: FTIR spectrum of fly ash, nZnO and nZnO/fly ash composite material

In the FTIR spectrum of activated carbon, fly ash and fly ash/activated carbon composite material (Figure 4.27), the absorption at 1616 cm^{-1} is assigned to the C=C stretching of activated carbon while the absorption at 1097 cm^{-1} is assigned to the C–C stretching of fly ash. The wavenumber of C–C stretching of fly ash changed slightly from 1097 cm^{-1} of fly ash to 1093 cm^{-1} of the fly ash/activated carbon composite material. The wavenumber of the absorption peak decreased 4 cm^{-1}. The slight change in the wavenumber suggests that a new bond was formed during the preparation of the fly ash/activated carbon composite material.

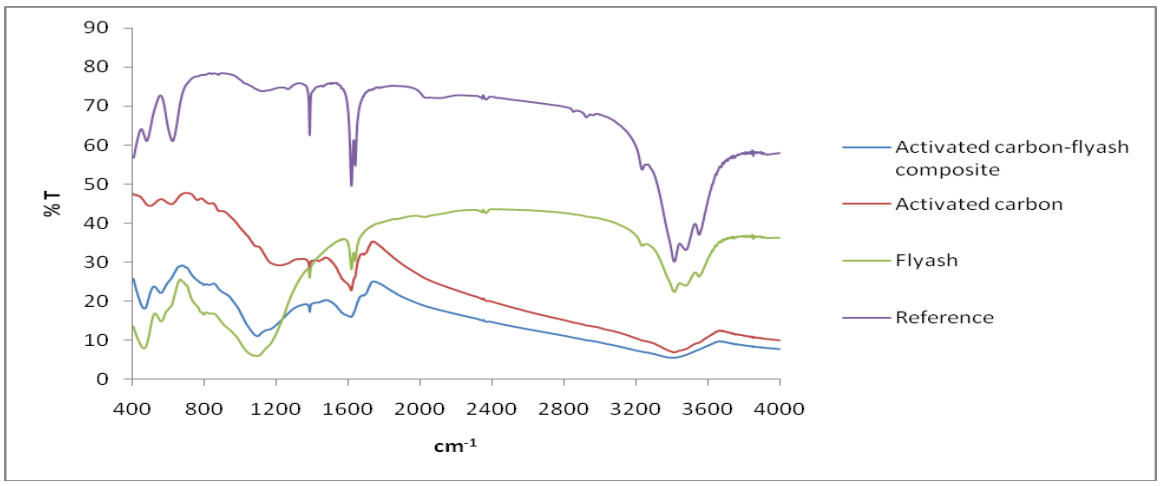

Figure 4.27: FTIR spectrum of activated carbon, fly ash and fly ash/activated carbon composite material

In the FTIR spectrum of activated carbon, fly ash, nFe_3O_4 and nFe_3O_4/fly ash/activated carbon composite material (Figure 4.28), the absorption at 1616 cm^{-1} is assigned to the C=C stretching of activated carbon, the absorption at 1097 cm^{-1} is assigned to the C–C stretching of fly ash while the absorption at 586 cm^{-1} is assigned to the Fe – O stretching of nFe_3O_4. It was found that the wavenumber of Fe – O stretching changed from 586 cm^{-1} of nFe_3O_4 to 560 cm^{-1} of the nFe_3O_4/fly ash/activated carbon composite material. The wavenumber of the absorption peak decreased 26 cm^{-1}. The decrease in the wavenumber suggests that a new bond was formed during the preparation of the nFe_3O_4/fly ash/activated carbon composite material.

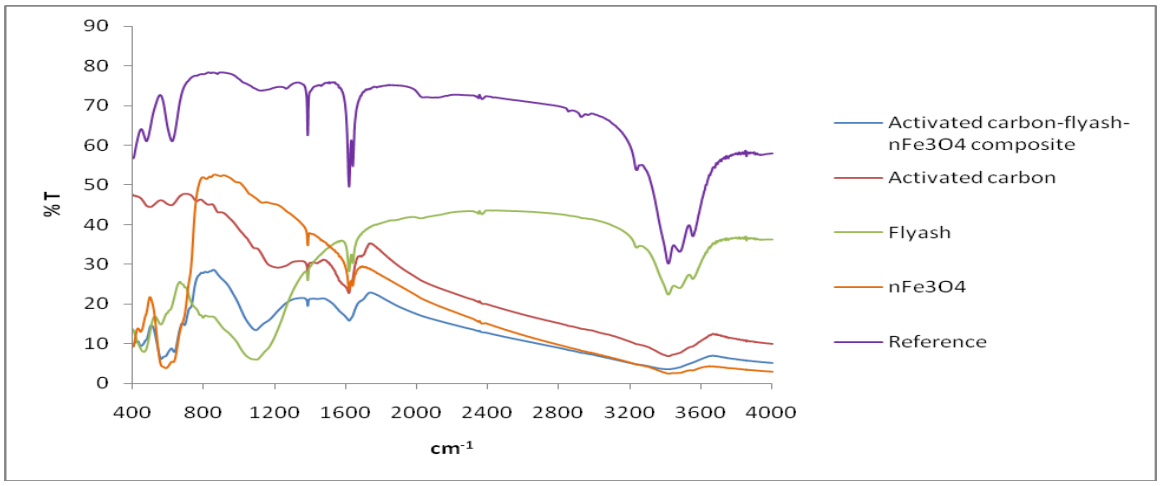

Figure 4.28: FTIR spectrum of activated carbon, fly ash, nFe_3O_4 and nFe_3O_4/fly ash/activated carbon composite material

In the FTIR spectrum of activated carbon, fly ash, $nSiO_2$ and $nSiO_2$/fly ash/activated carbon composite material (Figure 4.29), the absorption at 1616 cm^{-1} is assigned to the C=C stretching of activated carbon, the absorption at 1097 cm^{-1} is assigned to the C–C stretching of fly ash while the absorption at 1101 cm^{-1} and 809 cm^{-1} is assigned to the asymmetric and symmetric vibration of Si – O, respectively. It was found that the wavenumber of symmetric vibration of Si – O changed from 809 cm^{-1} of $nSiO_2$ to 805 cm^{-1} of the $nSiO_2$/fly ash/activated carbon composite material. The wavenumber of the absorption peak decreased 4 cm^{-1}. A decrease in the wavenumber suggests that a new bond was formed during the preparation of the $nSiO_2$/fly ash/activated carbon composite material.

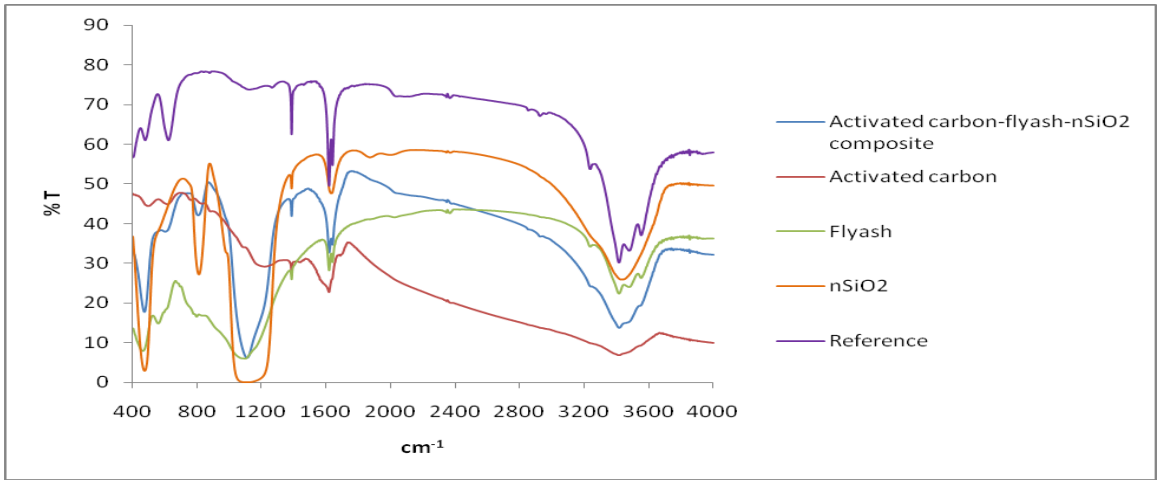

Figure 4.29: FTIR spectrum of activated carbon, fly ash, $nSiO_2$ and $nSiO_2$/fly ash/activated carbon composite material

In the FTIR spectrum of activated carbon, fly ash, nZnO and nZnO/fly ash/activated carbon composite material (Figure 4.30), the absorption at 1616 cm^{-1} is assigned to the C=C stretching of activated carbon, the absorption at 1097 cm^{-1} is assigned to the C–C stretching of fly ash while the adsorption at 1110 cm^{-1} is assigned to the asymmetric vibration of Zn – O, and the absorption at 808 cm^{-1} is assigned to the Zn – O stretching of nZnO. It was found that the wavenumber of asymmetric vibration of Zn – O changed from 1110 cm^{-1} of nZnO to 1094 cm^{-1} of the nZnO/fly ash/activated carbon composite material. The wavenumber of the absorption peak decreases by 16 cm^{-1}. A decrease in the wavenumber suggests that a new bond was formed during the preparation of the nZnO/fly ash/activated carbon composite material.

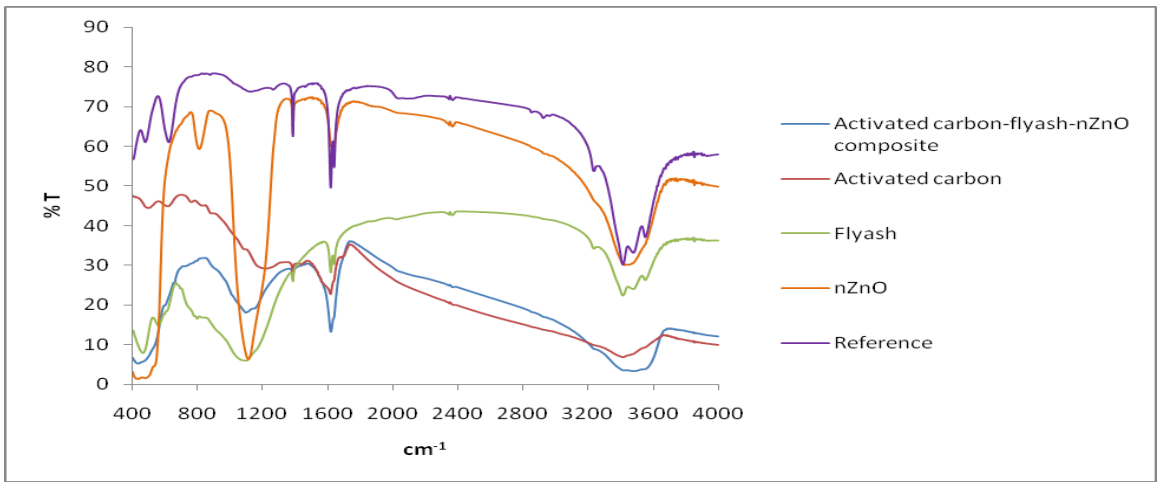

Figure 4.30: FTIR spectrum of activated carbon, fly ash, nZnO and nZnO/fly ash/activated carbon composite material

The results (Figure 4.21 – 4.30) show that the shift in the band is a function of the metal ions present in the composite materials. The FTIR also confirms the absence of impurity in both the precursors and the prepared composite materials.

4.7 pH

The pH of the precursors and composite materials are shown in Table 4.4 while Figures 4.31 – 4.33 show the relationship between the pH of the precursors and the composite materials. The figures also show how the pH of individual precursors is altered upon the preparation of the composite materials.

Table 4.4: pH of precursors and composite materials

Samples	pH
Activated carbon	3.30
Fly ash	10.70
nFe_3O_4	5.95
$nSiO_2$	5.53
nZnO	6.71
nFe_3O_4/activated carbon	2.58
$nSiO_2$/activated carbon	3.34
nZnO/activated carbon	6.47
nFe_3O_4/fly ash	3.54
$nSiO_2$/fly ash	3.48
nZnO/fly ash	6.96
fly ash/activated carbon	3.51
nFe_3O_4/fly ash/activated carbon	3.41
$nSiO_2$/fly ash/activated carbon	3.81
nZnO/fly ash/activated carbon	6.42

Figure 4.31 shows that the pH of fly ash (10.70) is very much higher compared to all other adsorbent (precursors) while a very low pH is recorded by the activated carbon (3.30). The pH of the nano oxides and silica all falls within the same range with the pH of nZnO slightly higher than that of $nSiO_2$ and nFe_3O_4.

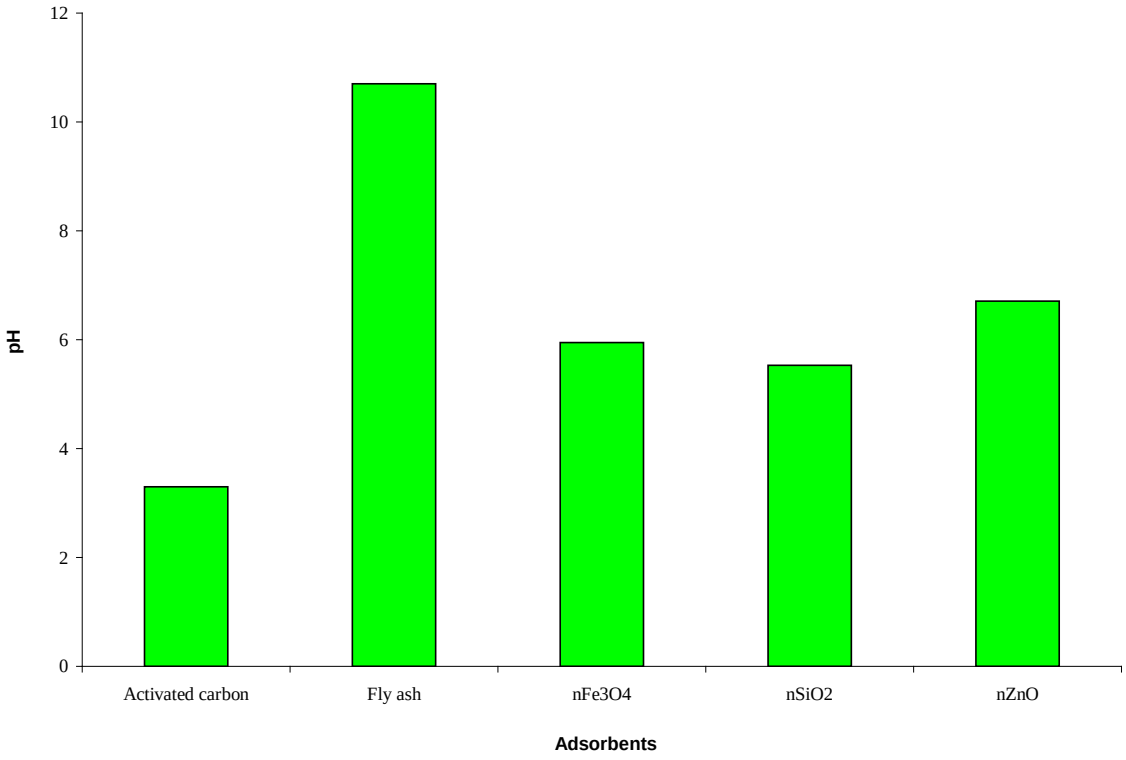

Figure 4.31: pH of the precursors

Upon the preparation of composite materials, Figure 4.32 shows that the pH of activated carbon is higher than the pH of nFe_3O_4/activated carbon composite material by 21.80 % while the pH of the nFe_3O_4/activated carbon composite material (2.58) is in turn lower than the pH of nFe_3O_4 by 56.60 %. The low acidic nature of nFe_3O_4 (5.95) tends to bring down the acidic nature of activated carbon (3.3) to form a composite material of pH 2.58.

The preparation of $nSiO_2$/activated carbon composite material using activated carbon (pH 3.3) and $nSiO_2$ (5.53) as precursors results in $nSiO_2$/activated carbon composite material of pH 3.38, the pH is higher than the pH of activated carbon by 23.70 % and lower than the pH of $nSiO_2$ by 38.90 %.

The pH of activated carbon is lower than the pH of nZnO/activated carbon composite material by 48.90 %, the acidic nature of activated carbon (3.3) slightly lowers the pH of nZnO (6.71) to form nZnO/activated carbon composite material of pH 6.47. The pH of nZnO/activated carbon composite material is thus lower than the pH of nZnO by 3.60 %.

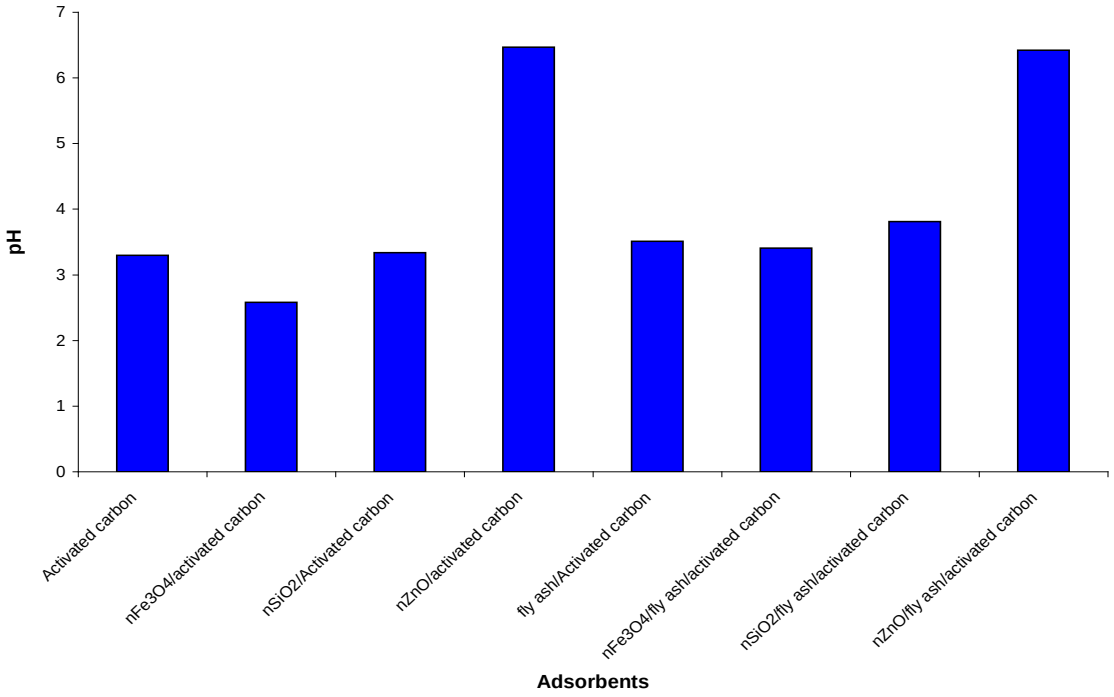

Figure 4.32: pH of activated carbon and its composites

From Figure 4.33, the preparation of nFe_3O_4/fly ash composite material using fly ash (10.70) and nFe_3O_4 (5.95) as precursors results in nFe_3O_4/fly ash composite material of pH 3.54, the pH is lower than the pH of fly ash and nFe_3O_4 by 66.90 % and 40.50 %, respectively.

The preparation of nZnO/fly ash composite material by the use of fly ash (10.70) and nZnO (6.71) as precursors results in nZnO/fly ash composite material of pH 6.96, the pH is lower than pH of fly ash by 34.90 % but higher than the pH of nZnO by 3.59 %.

The preparation of $nSiO_2$/fly ash composite material using fly ash (10.70) and $nSiO_2$ (5.53) as precursors results in $nSiO_2$/fly ash composite material of pH 3.48, the pH is lower than pH of fly ash by 67.50 % and also lower than pH of $nSiO_2$ by 37.10 %.

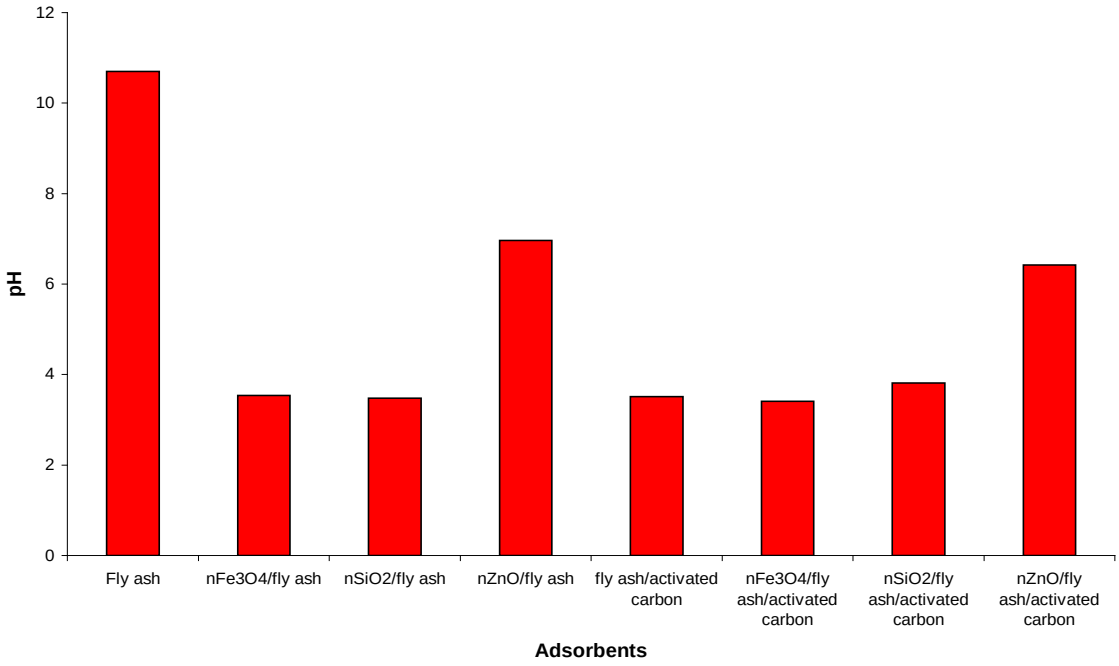

Figure 4.33: pH of fly ash and its composite

From Figures 4.32 and 4.33, the preparation of fly ash/activated carbon composite material by the use of activated carbon (pH 3.3) and fly ash (10.70) as precursors resulted to fly ash/activated carbon composite material of pH 3.51, the pH is higher than the pH of activated carbon by 59.80 % and lower than the pH of fly ash by 67.20 %. The preparation of nFe_3O_4/fly ash/activated carbon composite material using activated carbon (pH 3.3), fly ash (10.70) and nFe_3O_4 (5.95) as precursors results in nFe_3O_4/fly ash/activated carbon composite material of pH 3.41, the pH is higher than pH of activated carbon by 32.30 %, lower than the pH of fly ash by 68.10 % and lower than pH of nFe_3O_4 by 42.70 %. The preparation of $nSiO_2$/fly ash/activated carbon composite material using activated carbon (pH 3.3), fly ash (10.70) and $nSiO_2$ (5.53) as precursors results in $nSiO_2$/fly ash/activated carbon composite material of pH 3.34, the pH is higher than pH of activated carbon by 1.20 %, lower than pH of fly ash and $nSiO_2$ by 68.80 % and 39.60 %, respectively. The preparation of nZnO/fly ash/activated carbon composite material using activated carbon (pH 3.3), fly ash (10.70) and nZnO (6.71) as precursors also results in nZnO/fly ash/activated carbon composite material of pH 6.42, the pH is higher than the pH of activated carbon by 48.60 %, lower than pH of fly ash and nZnO by 40.00 % and 4.30 %, respectively.

Comparing the pH values of the precursors and composite materials, it is evident that it is not the presence of the nano particles alone that is responsible for the pH changes but the pH value of each of the component precursors that made up the composite materials.

4.8 Point of zero charge

Addition of a metal oxide powder to an aqueous solution would cause a change in pH. At a certain high mass concentration, the pH value would reach the plateau (pH_{∞}) that was found to be equal to PZC if the powder was sufficiently purified (Noh and Schwarz, 1989). When the pH is lower than the PZC value, the acidic water donates more protons than hydroxide groups, and so the adsorbent surface is positively charged (attracting anions). Conversely, above PZC the surface is negatively charged (attracting cations/repelling anions) (Zheng et al., 2009).

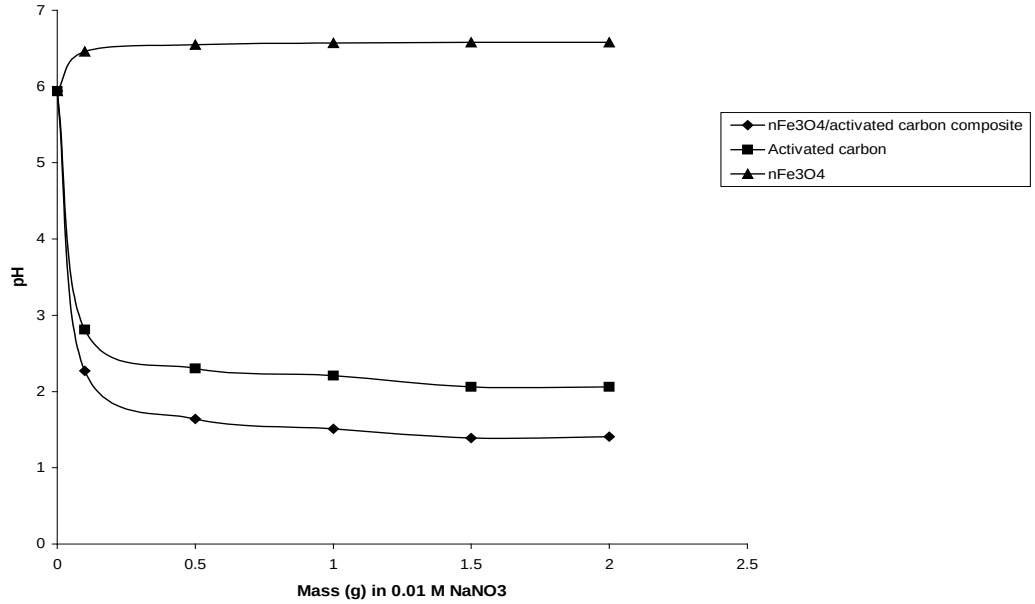

Figure 4.34: Result of mass titration experiments with activated carbon, nFe_3O_4 and nFe_3O_4/activated carbon composite material. Variation of pH versus mass of solid in 0.01 M $NaNO_3$

Figure 4.34 shows that the PZC of activated carbon, nFe_3O_4 and nFe_3O_4/activated carbon composite material are 2.06, 6.58 and 1.39, respectively. The value of the point of zero charge of nFe_3O_4 (6.58) is in support of the result by Kosmulski, 2009 who reported that the average PZC of commercial nFe_3O_4 is 6.6. The PZC of nFe_3O_4/activated carbon composite material is lower than the PZC of activated carbon by 32.52 % and lower than the PZC of nFe_3O_4 by 78.88 %. The graph shows that the presence of nFe_3O_4 in the activated carbon further lowers the PZC to form nFe_3O_4/activated carbon composite material with PZC 1.39. The presence of nFe_3O_4 is therefore responsible for the decrease in the point of zero charge of the nFe_3O_4/activated carbon composite material.

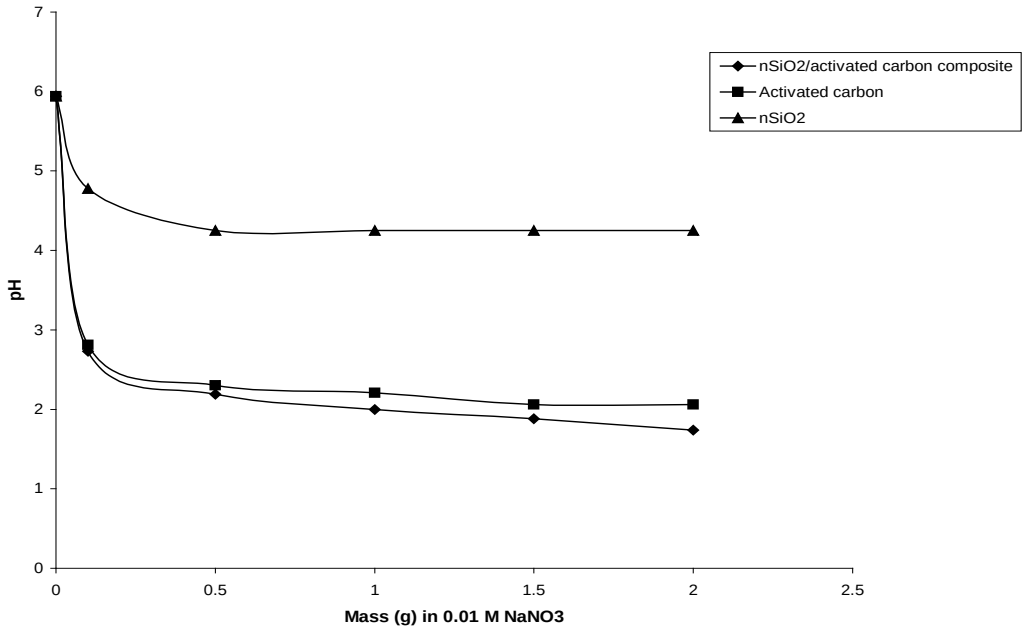

Figure 4.35: Result of mass titration experiments with activated carbon, $nSiO_2$ and $nSiO_2$/activated carbon composite material. Variation of pH versus mass of solid in 0.01 M $NaNO_3$

From Figure 4.35, the point of zero charge of activated carbon, $nSiO_2$ and $nSiO_2$/activated carbon composite material are 2.06, 4.25 and 1.74, respectively. The PZC of $nSiO_2$/activated carbon composite material is therefore lower than PZC of activated carbon by 15.53 % and also lower than the PZC of $nSiO_2$ by 59.06 %. The graph also shows that the presence of $nSiO_2$ in the activated carbon further lowers the PZC to form $nSiO_2$/activated carbon composite material with PZC 1.74. The presence of $nSiO_2$ is therefore responsible for the decrease in the point of zero charge of the $nSiO_2$/activated carbon composite material.

Figure 4.36 shows that the PZC of nZnO/activated carbon composite material is 6.24. This PZC value on the other hand is higher than the PZC of activated carbon (2.06) but lower than the PZC of nZnO (6.80) by 66.99 and 8.24 %, respectively. In the case of nZnO/activated carbon composite material, the presence of nZnO in the activated carbon brings about an increase in PZC of nZnO/activated carbon composite material. Hence, the presence of nZnO is accountable for the increase in the PZC of the nZnO/activated carbon composite material.

Figure 4.37 shows that the PZC of fly ash, nFe_3O_4 and nFe_3O_4/fly ash composite material are 12.17, 6.58, and 3.57, respectively. The PZC of nFe_3O_4/fly ash composite material is lower than PZC of fly ash by 70.67 % and lower than the PZC of nFe_3O_4 by 45.74 %. The graph shows that the presence of nFe_3O_4 in the fly ash revert the increasing PZC nature of fly ash and thereby lowers PZC to form nFe_3O_4/fly ash composite material of PZC 3.57. The presence of nFe_3O_4 is therefore responsible for the decrease in the PZC of the nFe_3O_4/fly ash composite material.

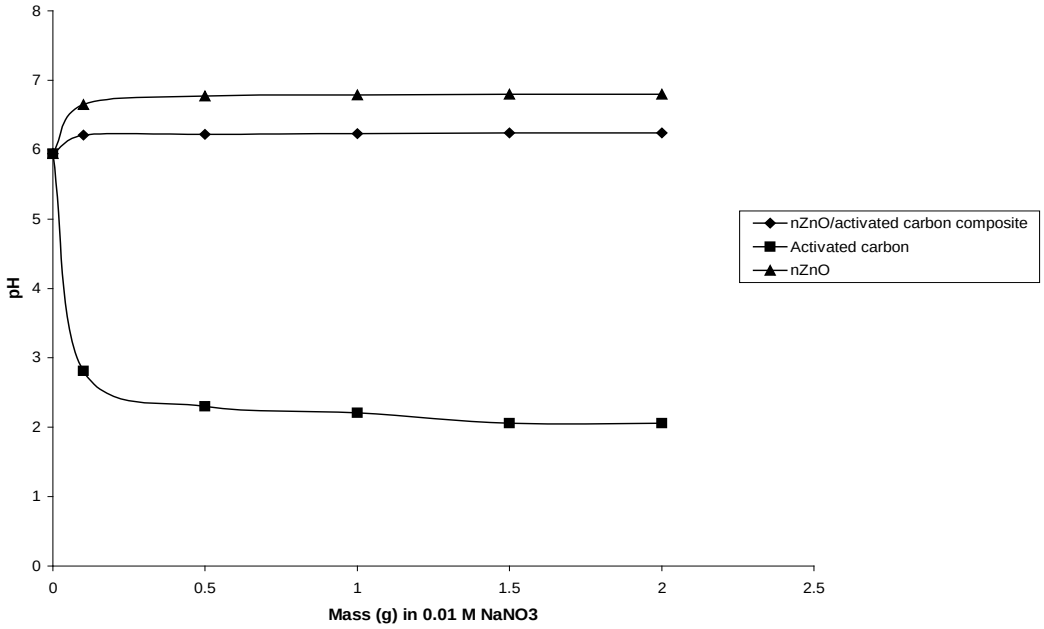

Figure 4.36: Result of mass titration experiments with activated carbon, nZnO and nZnO/activated carbon composite material. Variation of pH versus mass of solid in 0.01 M $NaNO_3$

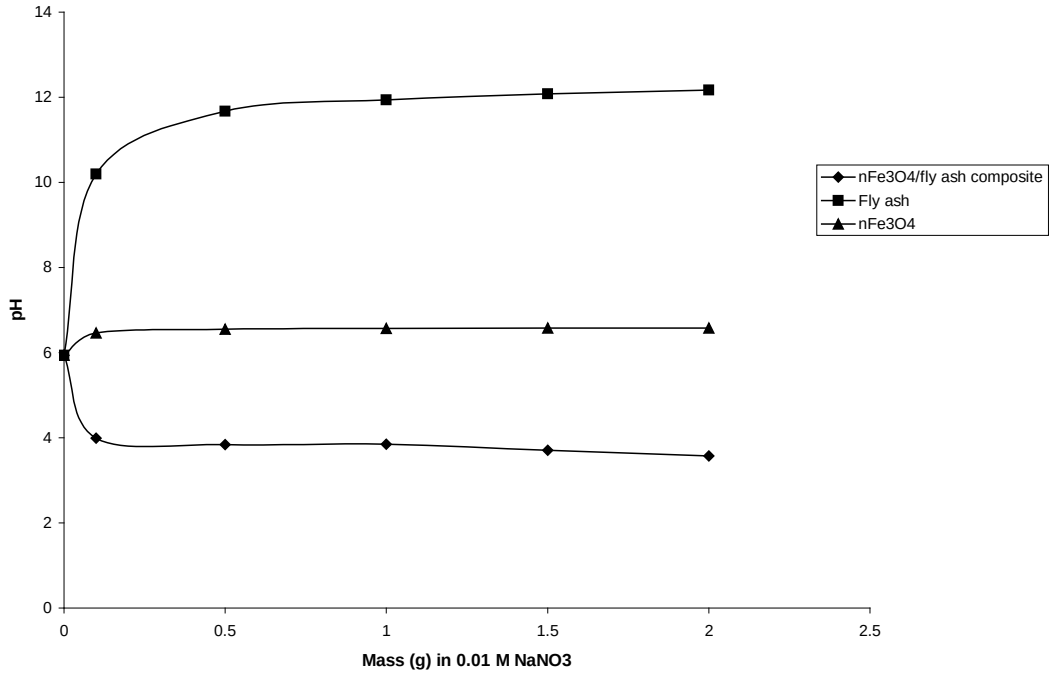

Figure 4.37: Result of mass titration experiments with fly ash, nFe_3O_4 and nFe_3O_4/fly ash composite material. Variation of pH versus mass of solid in 0.01 M $NaNO_3$

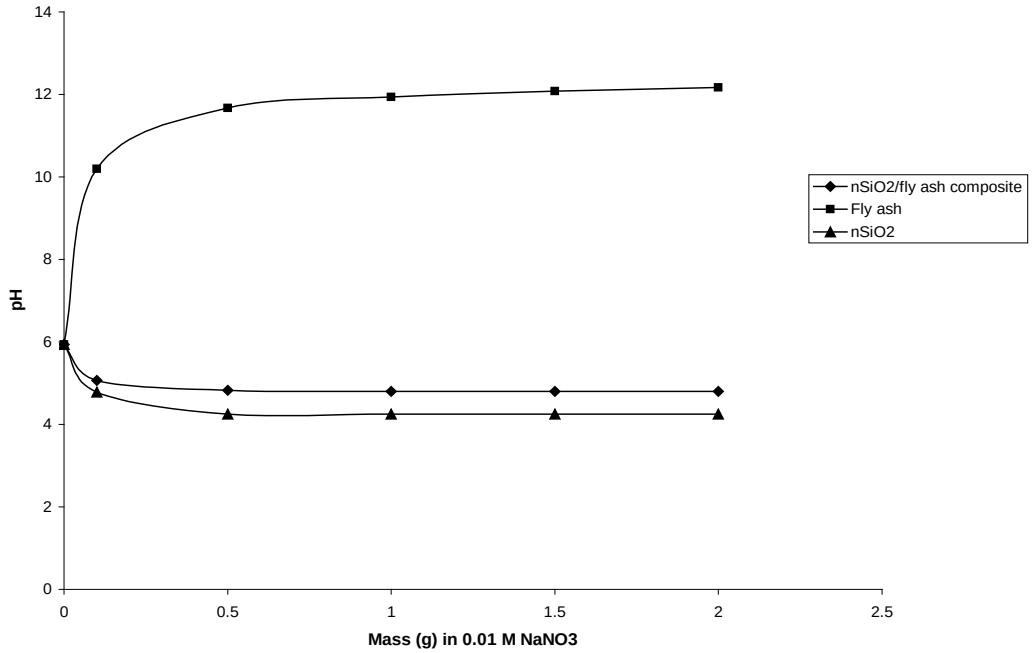

Figure 4.38: Result of mass titration experiments with fly ash, $nSiO_2$ and $nSiO_2$/fly ash composite material. Variation of pH versus mass of solid in 0.01 M $NaNO_3$

From Figure 4.38, the PZC of fly ash, $nSiO_2$ and $nSiO_2$/fly ash composite material are 12.17, 4.25 and 4.80, respectively. The PZC of $nSiO_2$/fly ash composite material is therefore lower than PZC of fly ash by 60.56 % but higher than the PZC of $nSiO_2$ by 11.46 %. The graph also shows that the presence of $nSiO_2$ in the fly ash also revert the increasing PZC nature of fly ash and brings about a decrease in the PZC to form $nSiO_2$/fly ash composite material of PZC 4.80. The presence of $nSiO_2$ is therefore responsible for the decrease in the PZC of the $nSiO_2$/fly ash composite material.

Figure 4.39 shows that the PZC of nZnO/fly ash composite material is 6.70. This PZC value is lower than the PZC of fly ash (12.17) and lower than the PZC of nZnO (6.80) by 44.95 % and 1.47 %, respectively. In the case of nZnO/fly ash composite material, the presence of nZnO in fly ash brings about a decrease in PZC of nZnO/fly ash composite material (Figure 4.39). The presence of nZnO is also accountable for the decrease in the PZC of the nZnO/fly ash composite material.

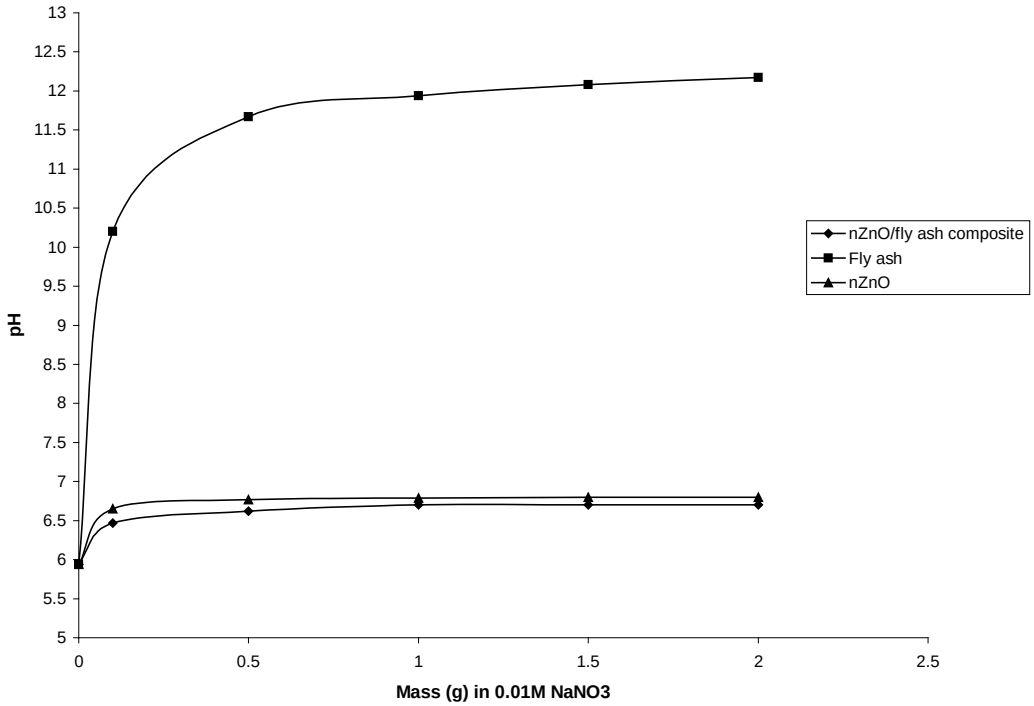

Figure 4.39 Result of mass titration experiments with fly ash, nZnO and nZnO/fly ash composite material. Variation of pH versus mass of solid in 0.01 M $NaNO_3$

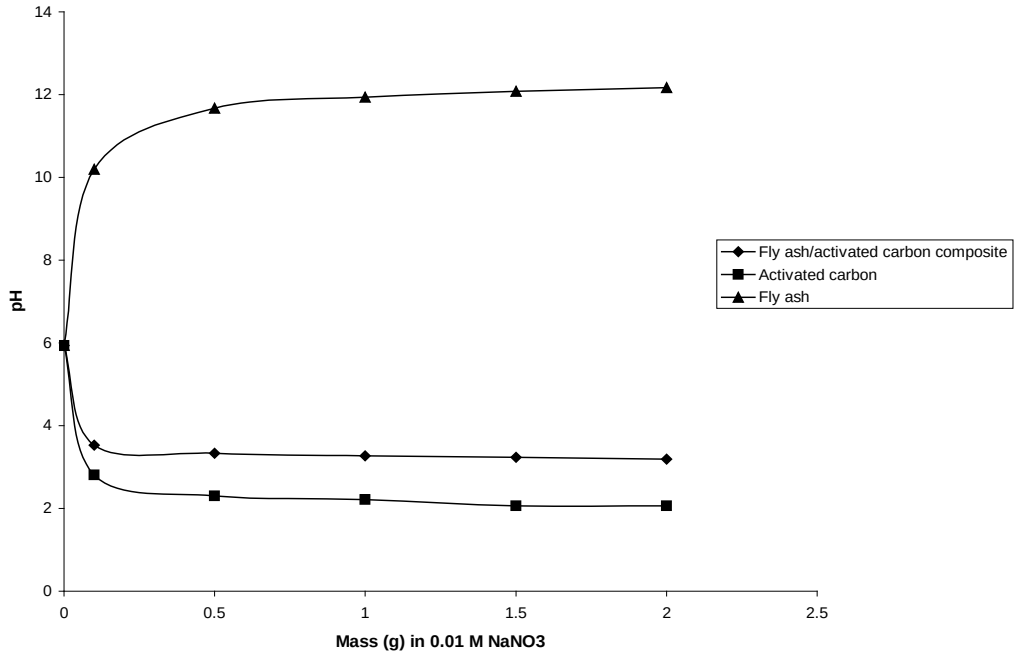

Figure 4.40: Result of mass titration experiments with activated carbon, fly ash and fly ash/activated carbon composite material. Variation of pH versus mass of solid in 0.01 M $NaNO_3$

Figure 4.40 shows that the PZC of activated carbon, fly ash and fly ash/activated carbon composite material are 2.06, 12.17 and 3.19, respectively. The PZC of fly ash/activated carbon composite material is higher than PZC of activated carbon by 35.42 % but lower than the PZC of fly ash by 73.79 %. The graph shows that the presence of fly ash (high PZC value

and basic) in the activated carbon (acidic) raise the PZC of activated carbon to form fly ash/activated carbon composite material with PZC of 3.19.

Figure 4.41 also shows that the PZC of activated carbon, fly ash, nFe_3O_4 and nFe_3O_4/fly ash/activated carbon composite material are 2.06, 12.17, 6.58 and 2.84, respectively. The PZC of nFe_3O_4/fly ash/activated carbon composite material is higher than the PZC of activated carbon by 27.46 %, lower than PZC of fly ash by 76.66 % and also lower than the PZC of nFe_3O_4 by 56.84 %.

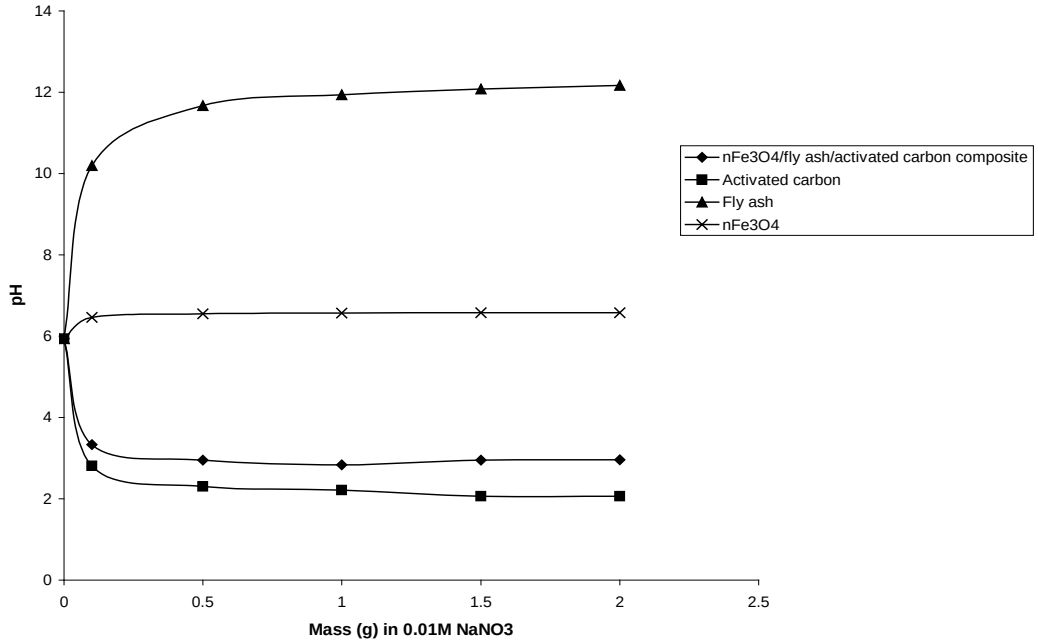

Figure 4.41: Result of mass titration experiments with activated carbon, fly ash, nFe_3O_4 and nFe_3O_4/fly ash/activated carbon composite material. Variation of pH versus mass of solid in 0.01 M $NaNO_3$

Comparing the PZC values of nFe_3O_4/activated carbon and nFe_3O_4/fly ash composite materials which are 1.39 and 3.57, respectively with the PZC of nFe_3O_4/fly ash/activated carbon composite material (2.84), it is evident that the presence of the nano oxides alone is not responsible for the PZC changes but the PZC of each of the component precursors that made up the composite materials.

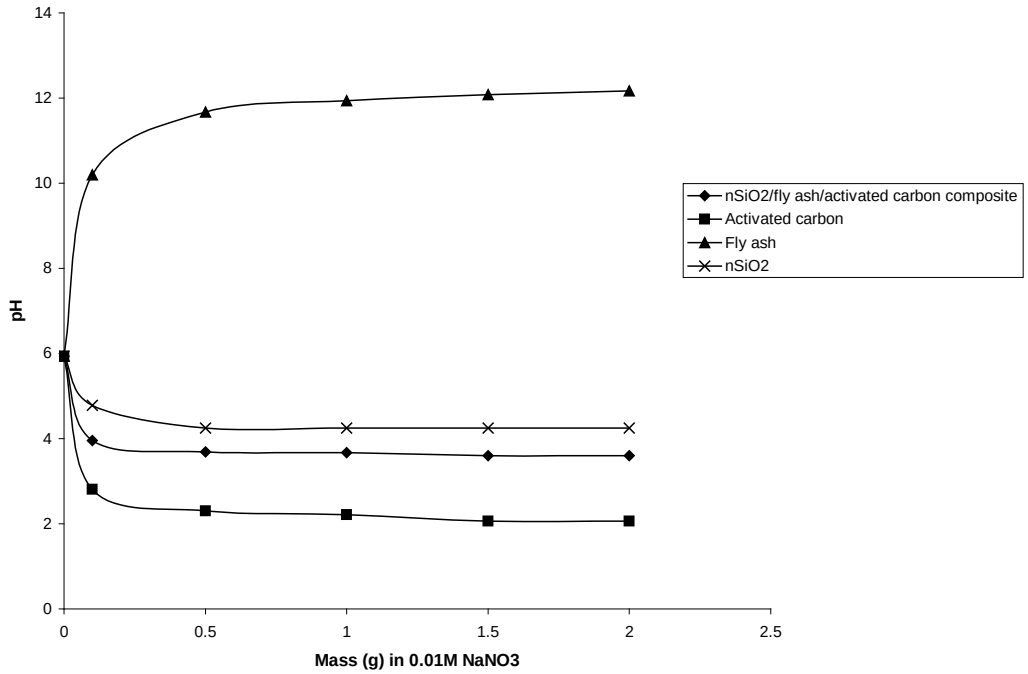

Figure 4.42: Result of mass titration experiments with activated carbon, fly ash, $nSiO_2$ and $nSiO_2$/fly ash/activated carbon composite material. Variation of pH versus mass of solid in 0.01 M $NaNO_3$

From Figure 4.42, the PZC of activated carbon, fly ash, $nSiO_2$ and $nSiO_2$/fly ash/activated carbon composite material are 2.06, 12.17, 4.25 and 3.60, respectively. The PZC of $nSiO_2$/fly ash/activated carbon composite material is therefore higher than the PZC of activated carbon by 42.78 % and lower than PZC of fly ash and $nSiO_2$ by 70.42 % and 15.29 %, respectively.

Comparing the PZC values of $nSiO_2$/activated carbon and $nSiO_2$/fly ash composite materials which are 1.74 and 4.80 respectively with the PZC of $nSiO_2$/fly ash/activated carbon composite material (3.60), it could also be affirmed that the PZC of each of the component precursors that made up the composite materials determines the PZC changes.

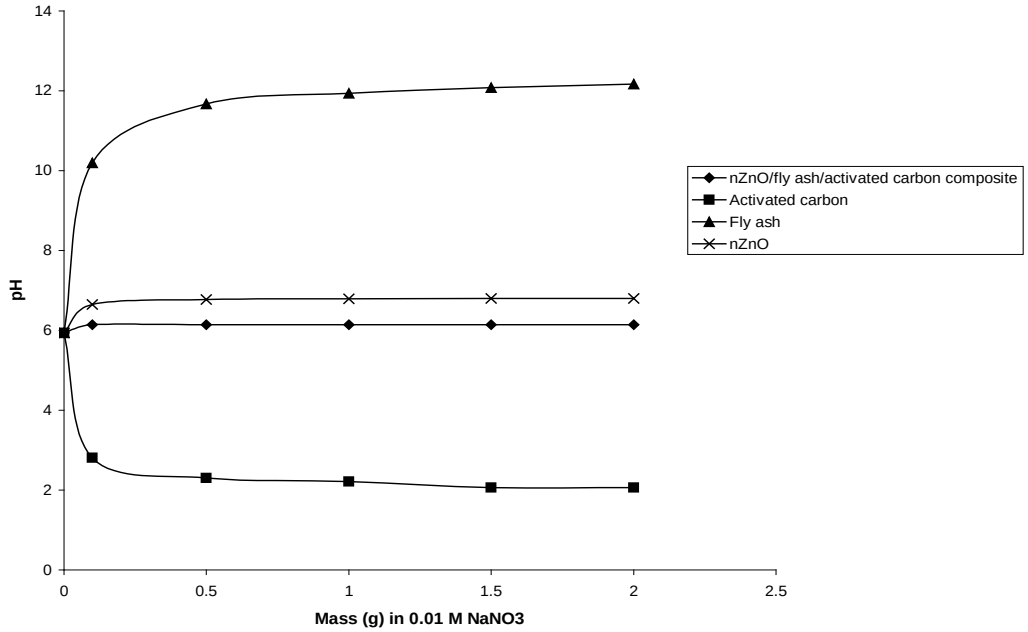

Figure 4.43: Result of mass titration experiments with activated carbon, fly ash, nZnO and nZnO/fly ash/activated carbon composite material. Variation of pH versus mass of solid in 0.01 M $NaNO_3$

From Figure 4.43, the PZC of activated carbon, fly ash, nZnO and nZnO/fly ash/activated carbon composite material are 2.06, 12.17, 6.80 and 6.14, respectively. The PZC of nZnO/fly ash/activated carbon composite material is therefore higher than the PZC of activated carbon by 66.45 %, lower than PZC of fly ash by 49.55 % and also lower than the PZC of nZnO by 9.71 %.

Comparing the PZC values of nZnO/activated carbon (6.24) and nZnO/fly ash composite (6.70) materials with the PZC of nZnO/fly ash/activated carbon composite material (6.14), it could also be asserted that the PZC of each of the component precursors that made up the composite materials determines the PZC changes. The change in PZC is as a result of type and number of functional groups present on the adsorbents (Kaya et al., 2012).

4.8.1 Comparison of the pH and PZC of the precursors and the composite materials

Table 4.5 and Figure 4.44 represent a comparison between the pH and PZC of the precursors and the composite materials.

Table 4.5 and Figure 4.44 show that the pH values of activated carbon, $nSiO_2$, nFe_3O_4/activated carbon, $nSiO_2$/activated carbon, nZnO/activated carbon, nZnO/fly ash, fly ash/activated carbon, nFe_3O_4/fly ash/activated carbon, $nSiO_2$/fly ash/activated carbon and nZnO/fly ash/activated carbon are slightly higher than their corresponding PZC values. This

suggests that the surface of these adsorbents is negatively charged and will therefore attract cations.

Table 4.5: pH and PZC of precursors and composite materials

Samples	pH	PZC
Activated carbon	3.30	2.06
Fly ash	10.70	12.17
nFe_3O_4	5.95	6.58
$nSiO_2$	5.53	4.25
nZnO	6.71	6.80
nFe_3O_4/activated carbon	2.58	1.39
$nSiO_2$/activated carbon	3.34	1.74
nZnO/activated carbon	6.47	6.24
nFe_3O_4/fly ash	3.54	3.57
$nSiO_2$/fly ash	3.48	4.80
nZnO/fly ash	6.96	6.70
fly ash/activated carbon	3.51	3.19
nFe_3O_4/fly ash/activated carbon	3.41	2.84
$nSiO_2$/fly ash/activated carbon	3.81	3.60
nZnO/fly ash/activated carbon	6.42	6.14

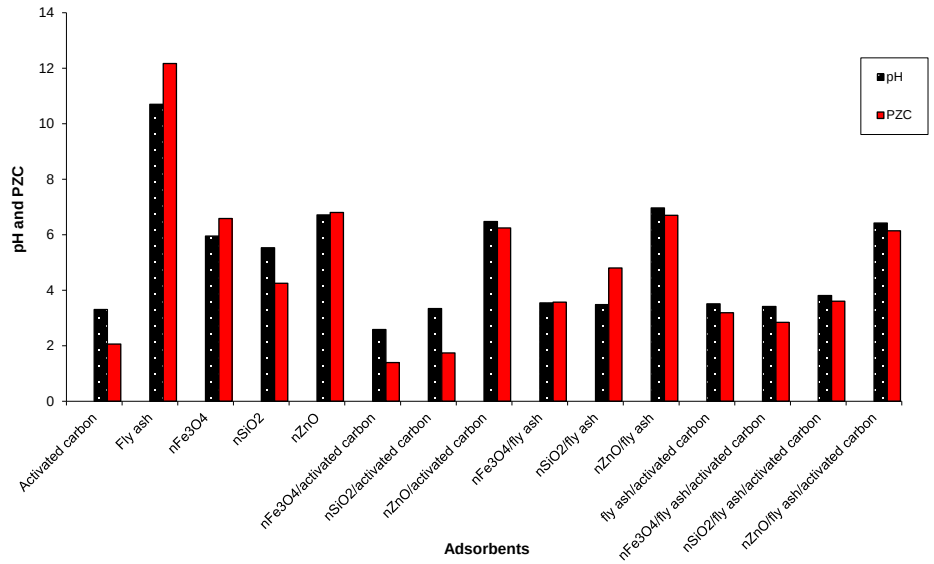

Figure 4.44: pH and PZC of the precursors and composite materials

Conversely, the pH values of fly ash, nFe_3O_4, nZnO, nFe_3O_4/fly ash and $nSiO_2$/fly ash are slightly lower than their corresponding PZC values. This suggests that the surface of these adsorbents is positively charged and will therefore attract anions.

4.9 Ash content

The ash content of the precursors and composite materials are presented in Table 4.6. Table 4.6 shows that the ash content of activated carbon is 0.45 ± 0.07 % with a relative percentage difference (RPD) of 22.0 %. The result shows that the activated carbon contains 0.45 % inorganic material while 99.55 % could be attributed to the organic components of the activated carbon.

Fly ash has a ash content of 97.40 ± 0.14 % and a relative percentage difference of 0.20 %. The amount of inorganic materials (ash content) thus present in the fly ash is 97.40 % while the organic material present amount to 2.60 %.

Table 4.6: Ash content of the precursors and composite materials

Samples	Ash content (%)	RPD (%)
Activated carbon	0.45 ± 0.07	22
Fly ash	97.4 ± 0.14	0.2
nFe_3O_4	97.2 ± 0.0 %	0.0
$nSiO_2$	98.3 ± 0.07 %	0.1
nZnO	99.2 ± 0.14 %	0.2
nFe_3O_4/activated carbon	45.15 ± 0.21	0.7
$nSiO_2$/activated carbon	52.75 ± 0.07	0.2
nZnO/activated carbon	44.25 ± 0.07	0.2
nFe_3O_4/fly ash	89.25 ± 0.07	0.1
$nSiO_2$/fly ash	88.15 ± 0.07	0.1
nZnO/fly ash	85.9 ± 0.0 %	0.0
fly ash/activated carbon	46.3 ± 0.14	0.4
nFe_3O_4/fly ash/activated carbon	58.5 ± 0.0	0.0
$nSiO_2$/fly ash/activated carbon	61.45 ± 0.07	0.2
nZnO/fly ash/activated carbon	61.9 ± 0.14	0.3

The ash content of nFe_3O_4, $nSiO_2$, and nZnO are 97.20 ± 0.0 %, 98.30 ± 0.07 % and 99.20 ± 0.14 %, respectively. 0.0 %, 0.10 % and 0.20 % are recorded as the corresponding RPD values of the nano oxides. The results obtained indicate that nFe_3O_4 contains 97.20 % inorganic material while the remaining 2.80 % can be attributed to the organic materials present in the nFe_3O_4 sample. The $nSiO_2$ contains 98.30 ± 0.07 % inorganic components and 1.70 % organic materials while nZnO contains 99.20 % inorganic material and 0.80 % organic materials.

The ash content of nFe_3O_4/activated carbon, $nSiO_2$/activated carbon and nZnO/activated carbon are 45.15 ± 0.21 %, 52.75 ± 0.07 % and 44.25 ± 0.07 %, respectively. 0.70 %, 0.20 % and 0.20 % are also recorded as the RPD values of the nFe_3O_4/activated carbon, $nSiO_2$/activated carbon and nZnO/activated carbon, respectively. The results obtained indicate that nFe_3O_4/activated carbon contains 45.15 % inorganic material while 54.87 % can be attributed to the organic materials present in the nFe_3O_4/activated carbon sample. The $nSiO_2$/activated carbon contains 52.75 % inorganic components and 47.25 % organic materials while nZnO/activated carbon contains 44.25 % inorganic material and 55.75 % organic materials.

The ash content of nFe_3O_4/fly ash, $nSiO_2$/fly ash and nZnO/fly ash composite materials are 89.25 ± 0.07 %, 88.15 ± 0.07 % and 85.90 ± 0.0 %, respectively. 0.10 %, 0.10 % and 0.0 % are recorded as the RPD values of the nFe_3O_4/fly ash, $nSiO_2$/fly ash and nZnO/fly ash, respectively. The results obtained indicate that nFe_3O_4/fly ash contains 89.25 % inorganic material and 10.75 % can be attributed to the organic materials present in the nFe_3O_4/fly ash sample. The $nSiO_2$/fly ash contains 88.15 % inorganic components and 11.85 % organic materials while nZnO/fly ash composite material contains 85.90 % inorganic material and 14.10 % organic materials.

The ash content of fly ash/activated carbon, nFe_3O_4/fly ash/activated carbon, $nSiO_2$/fly ash/activated carbon and nZnO/fly ash/activated carbon composite materials are 46.30 ± 0.14 %, 58.50 ± 0.0 %, 61.45 ± 0.07 % and 61.90 ± 0.14 %, respectively. 0.40 %, 0.0 %, 0.20 % and 0.30 % are also recorded as the RPD values of the fly ash/activated carbon, nFe_3O_4/fly ash/activated carbon, $nSiO_2$/fly ash/activated carbon and nZnO/fly ash/activated carbon composites, respectively. The results obtained indicate that the fly ash/activated carbon composite contain 46.30 % inorganic material while 53.70 % may be attributed to the presence of organic materials in the sample. nFe_3O_4/fly ash/activated carbon contains 58.50 % inorganic components and 41.50 % organic materials, $nSiO_2$/fly ash/activated carbon contains 61.45 % inorganic components and 38.55 % organic materials while nZnO/fly ash/activated carbon composite contains 61.90 % inorganic material and 38.10 % organic materials.

Figure 4.45 thus shows a graphical comparison of the ash content of activated carbon, fly ash, nano oxides and the composite materials.

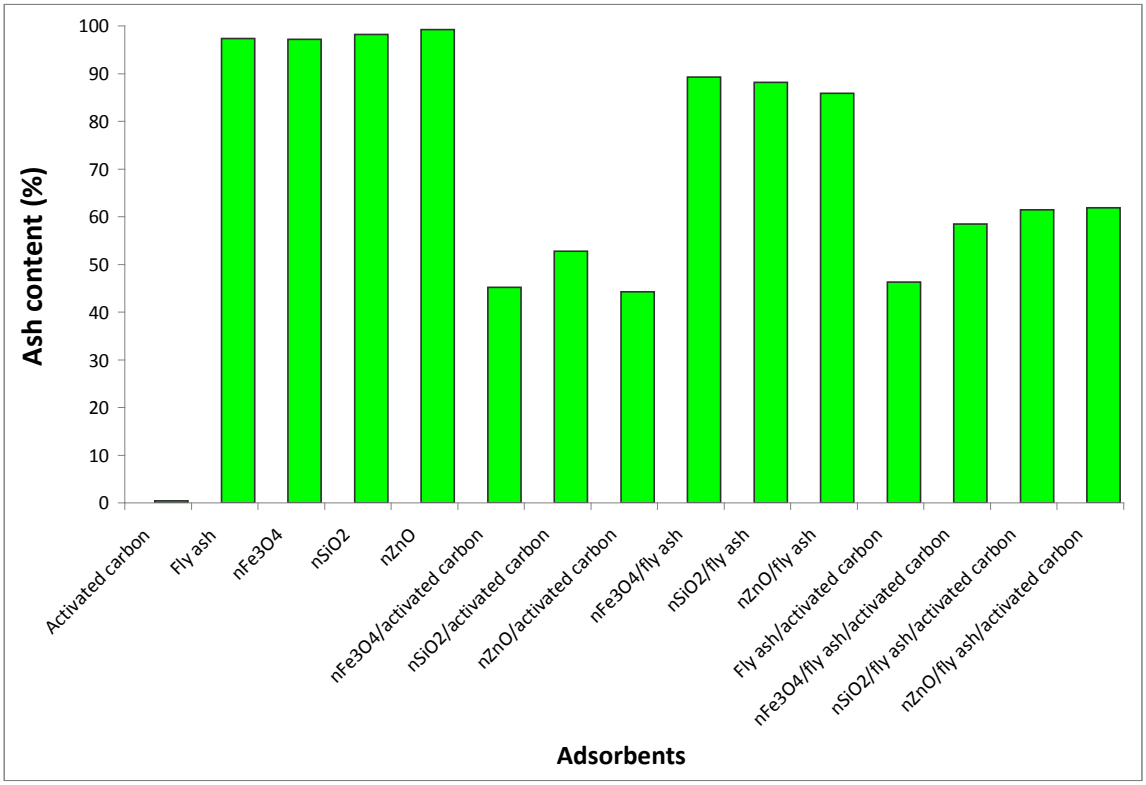

Figure 4.45: Ash content (%) versus adsorbents

The graph shows that all the precursors have very high percentage of inorganic components except activated carbon. Activated carbon is thus richer in water and organic materials as compared to all other precursors. The graph also shows that the composite materials involving fly ash and nano oxides have the highest inorganic material followed by those involving activated carbon, fly ash and nano particles and then the composite materials involving activated carbon and nano oxides. It is therefore evident that the level of inorganic materials present in the composite materials is a function of the precursors that constitute the composite materials.

4.10 XRD

The x-ray diffractogram of activated carbon, nFe_3O_4, $nSiO_2$, nZnO, nFe_3O_4/activated carbon, $nSiO_2$/activated carbon and nZnO/activated carbon are represented in Figure 4.46 – 4.52.

Figure 4.46 shows the absence of crystalline substances in the activated carbon. The absence of crystalline minerals confirms the amorphous nature of the activated carbon. Figure 4.47 which is the XRD of nFe_3O_4 shows that the nano iron oxide consists mainly of magnetite. The intensity of the magnetite is also very strong with sharp peaks. The diffractogram of nano silica (Figure 4.48) shows that $nSiO_2$ consists of quartz (SiO_2) and cristobalite (SiO_2) while Figure 4.49 shows that the nano zinc oxide consists of ZnO with sharp peaks.

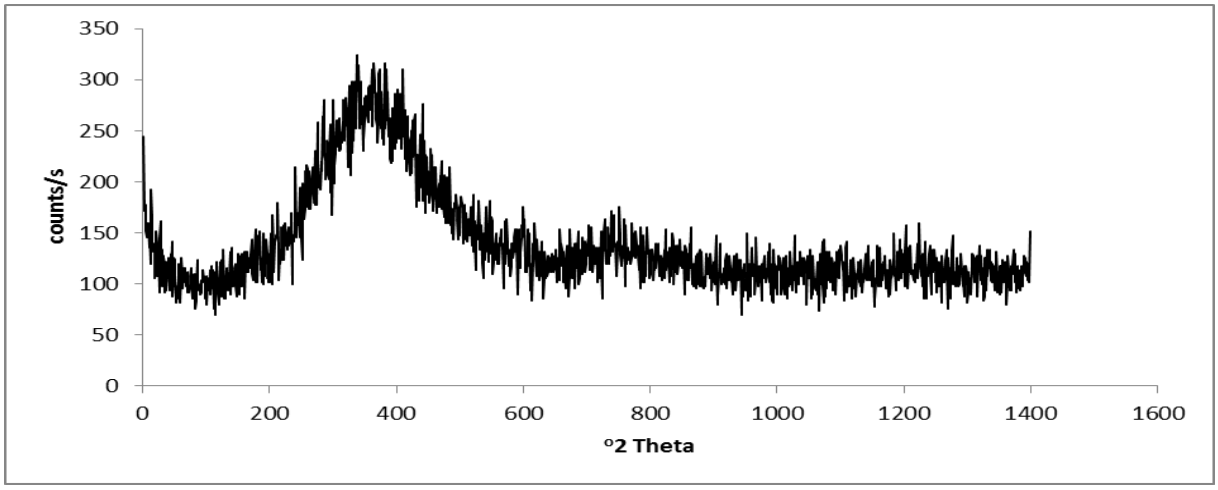

Figure 4.46: XRD of activated carbon

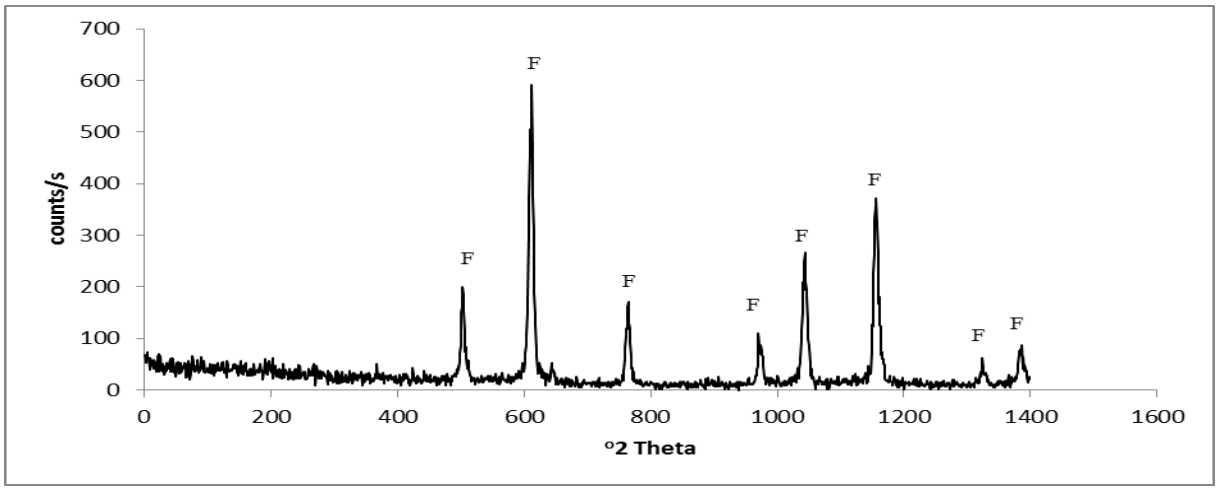

F – Magnetite (Fe_3O_4)

Figure 4.47: XRD diffraction of nFe_3O_4

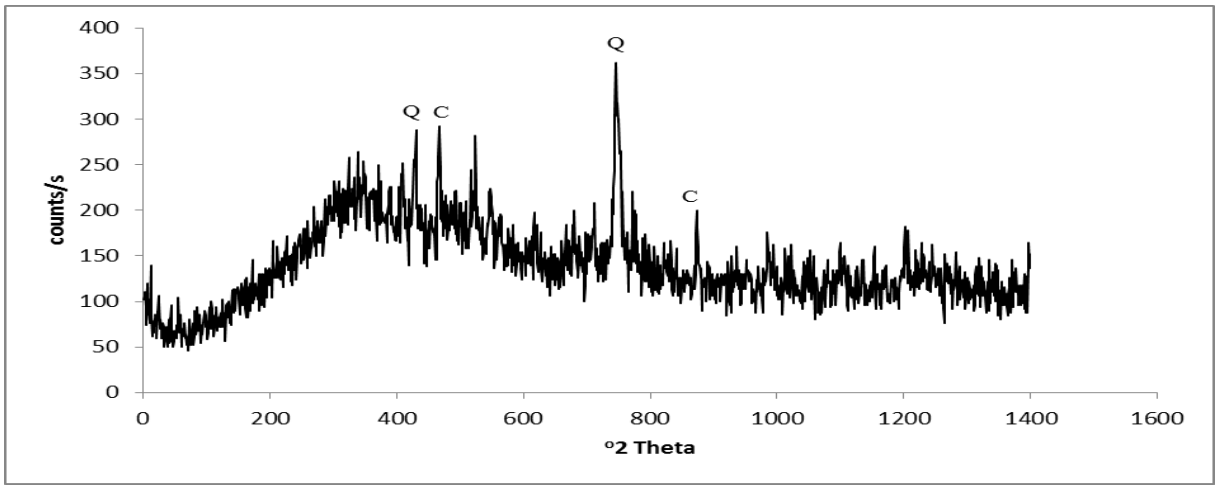

Q – Quartz (SiO_2), C – Cristobalite (SiO_2)

Figure 4.48: XRD of $nSiO_2$

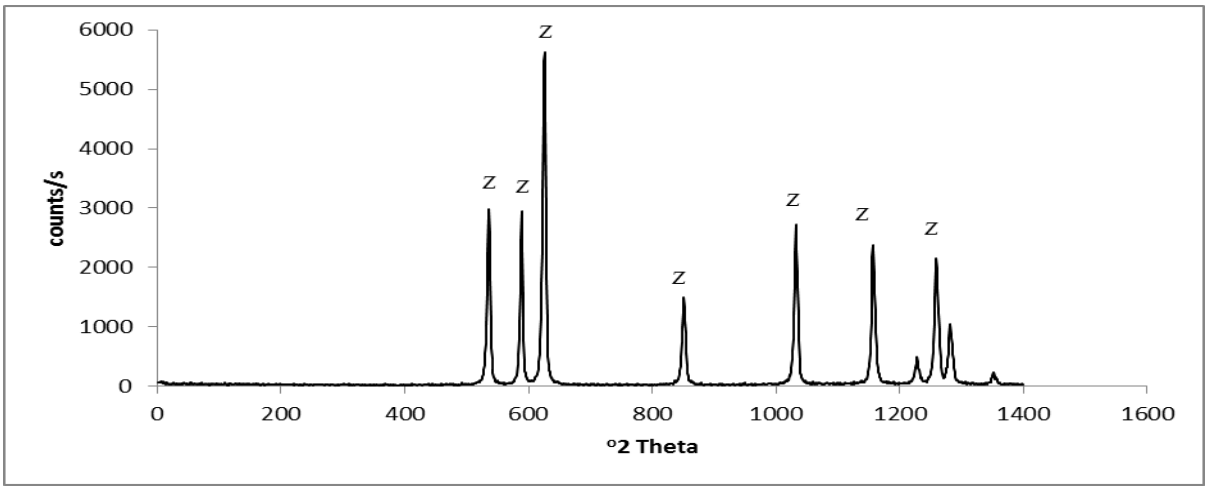

Z – Zinc Oxide (ZnO)

Figure 4.49: XRD of nZnO

Upon the preparation of composite materials involving activated carbon and nano oxides, the x-ray diffractogram of nFe_3O_4/activated carbon, $nSiO_2$/activated carbon and nZnO/activated carbon composite materials contains crystalline substances corresponding to the nano oxides involved in the preparation of the composite materials. The diffractogram of nFe_3O_4/activated carbon composite material (Figure 4.50) shows that the activated carbon been an amorphous substance is dominated with nFe_3O_4 i.e. peaks corresponding to nFe_3O_4 are the only peaks that appear on the nFe_3O_4/activated carbon composite material diffractogram.

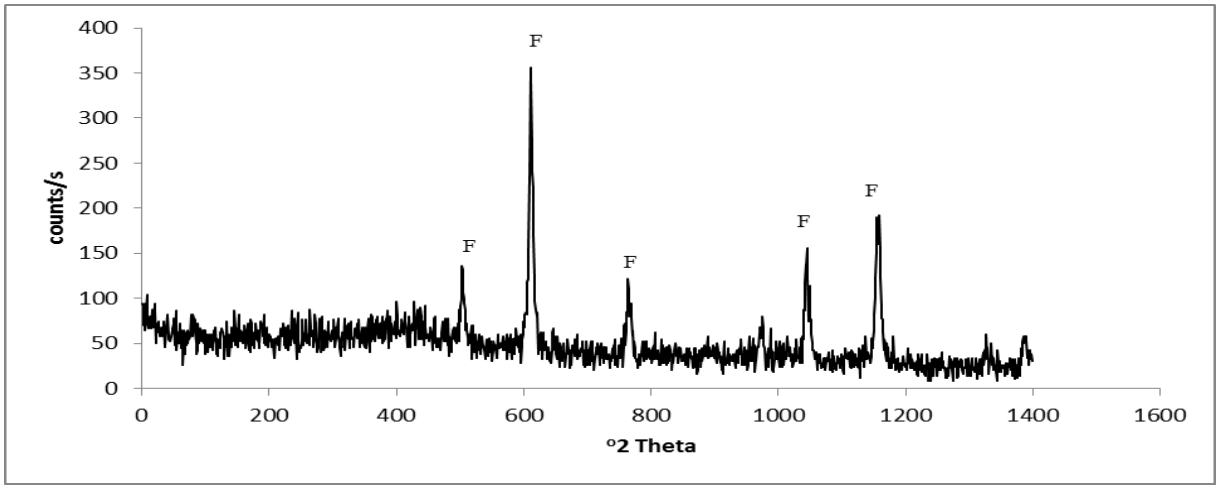

F – Magnetite (Fe_3O_4)

Figure 4.50 XRD of nFe_3O_4/activated carbon composite material

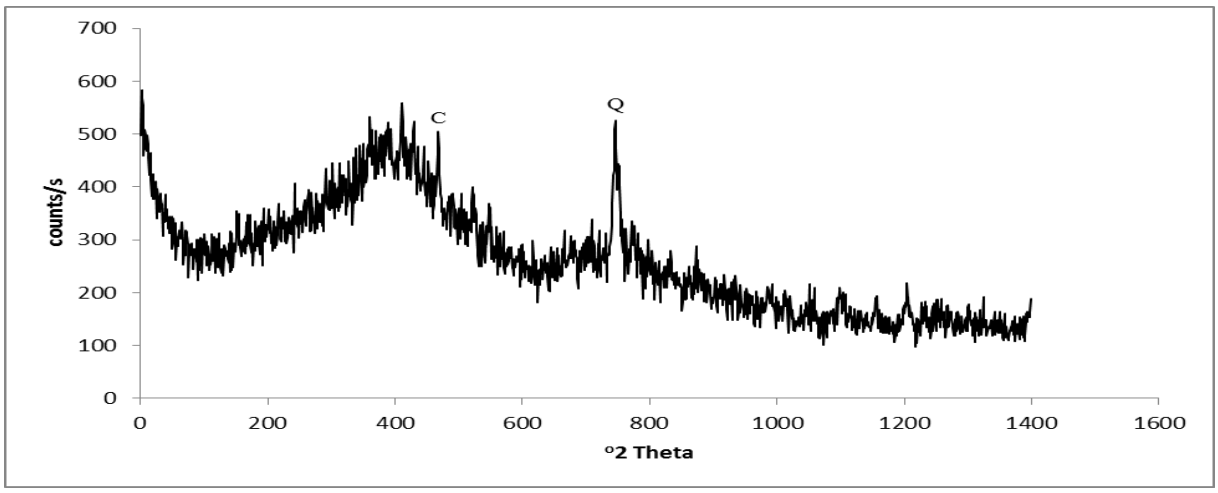

Q – Quartz (SiO_2), C – Cristobalite (SiO_2)

Figure 4.51: XRD of $nSiO_2$/activated carbon composite material

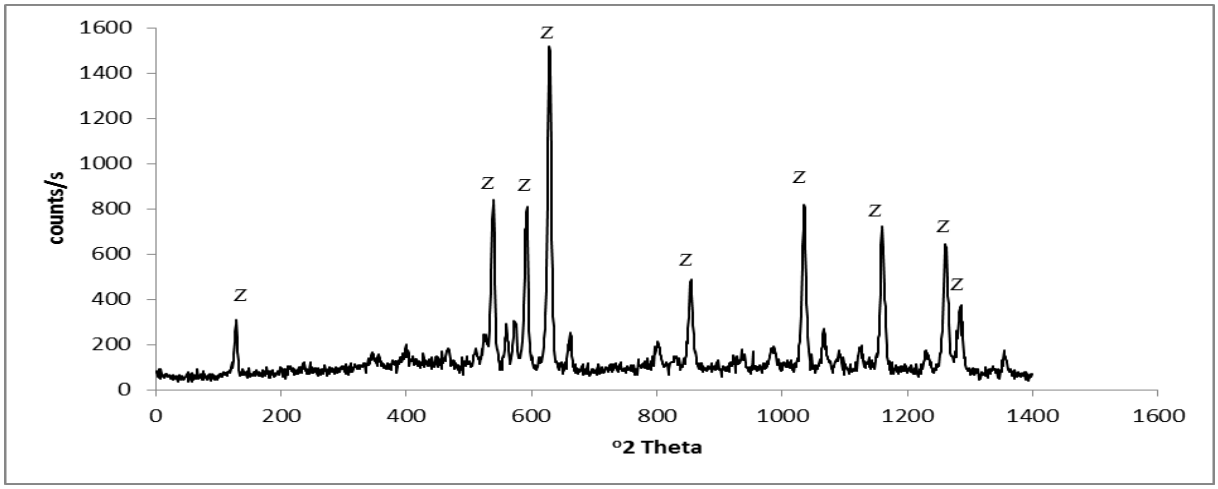

Z – Zinc Oxide (ZnO)

Figure 4.52: XRD of nZnO/activated carbon composite material

The diffractogram of $nSiO_2$/activated carbon composite material (Figure 4.51) shows that the prepared $nSiO_2$/activated carbon composite material consists of quartz (SiO_2) and cristobalite (SiO_2) which are attributed to the presence of $nSiO_2$ in the activated carbon. Figure 4.52 thus shows that nZnO/activated carbon composite material consists of nZnO. The XRD analysis also confirms the absence of impurities in the prepared composite materials.

The diffractogram of fly ash, nFe_3O_4/fly ash, $nSiO_2$/fly ash and nZnO/fly ash composite materials are represented in Figures 4.53 – 4.57. The diffractogram of fly ash (Figure 4.53) shows that the fly ash is dominated mainly of crystalline minerals mullite and quartz with large characteristic peaks of quartz (SiO_2). The intensity of quartz is also very strong. This result is similar to that reported for a fly ash investigated by Reynolds, 2004, Ward and French, 2005, and Sarkar et al., 2006.

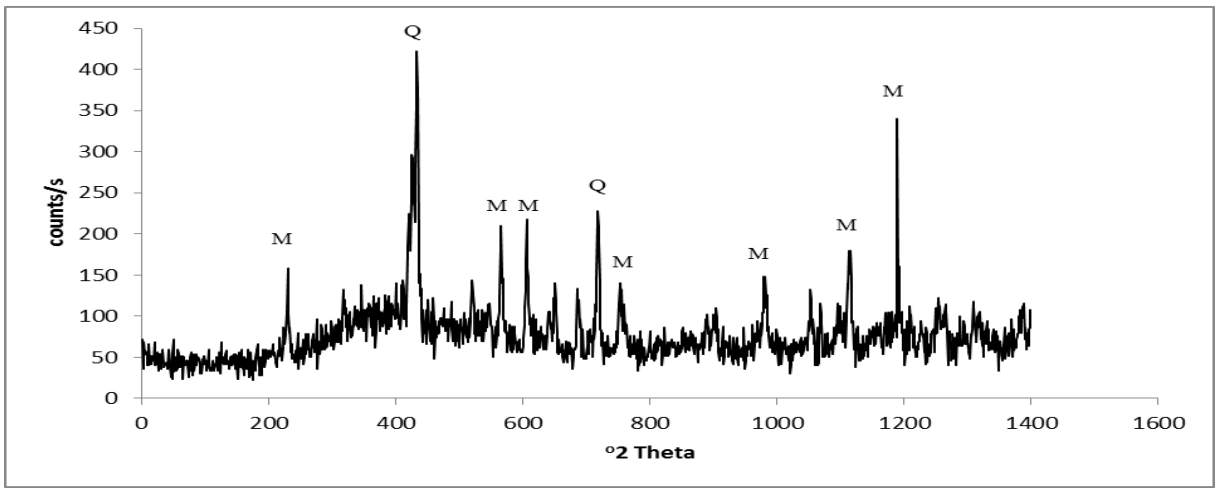

M - Mullite ($Al_6Si_2O_{13}$), Q – Quartz (SiO_2)

Figure 4.53: XRD of fly ash

The diffractogram of fly ash composite materials shows that nFe_3O_4/fly ash composite material (Figure 4.54) consists of mullite ($Al_6Si_2O_{13}$), quartz (SiO_2) and magnetite (Fe_3O_4). $nSiO_2$/fly ash composite material (Figure 4.55) consists of mullite ($Al_6Si_2O_{13}$), quartz (SiO_2) and cristobalite (SiO_2) while nZnO/fly ash composite material likewise consists of mullite ($Al_6Si_2O_{13}$), quartz (SiO_2) and zinc oxide (nZnO) (Figure 4.56). Mullite and quartz are from the fly ash while magnetite, cristobalite and zinc oxide are from the corresponding nano oxides involved in the composite preparations.

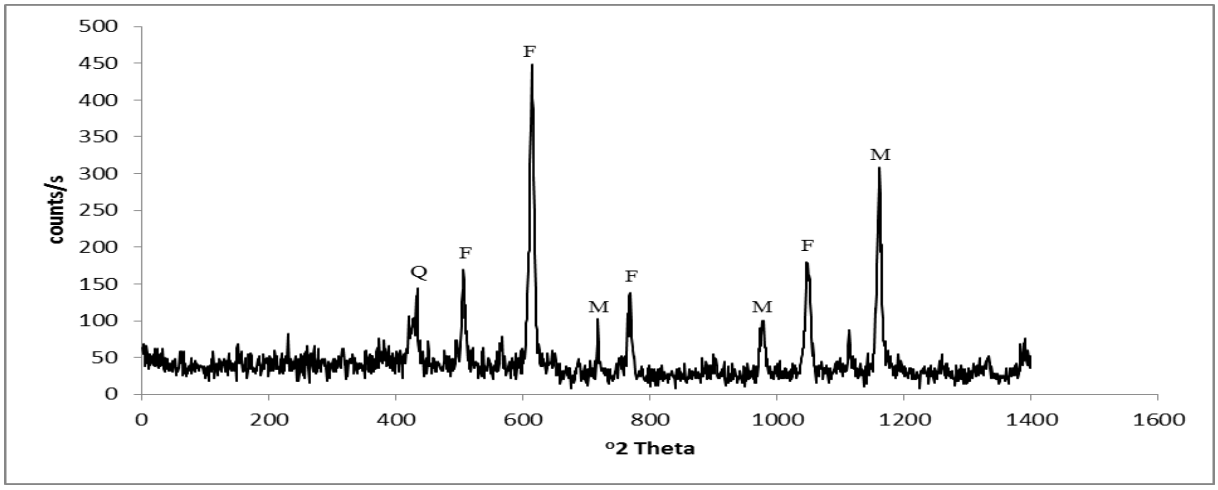

M – Mullite ($Al_6Si_2O_{13}$), Q – Quartz (SiO_2), F – Magnetite (Fe_3O_4)

Figure 4.54: XRD of nFe_3O_4/fly ash composite material

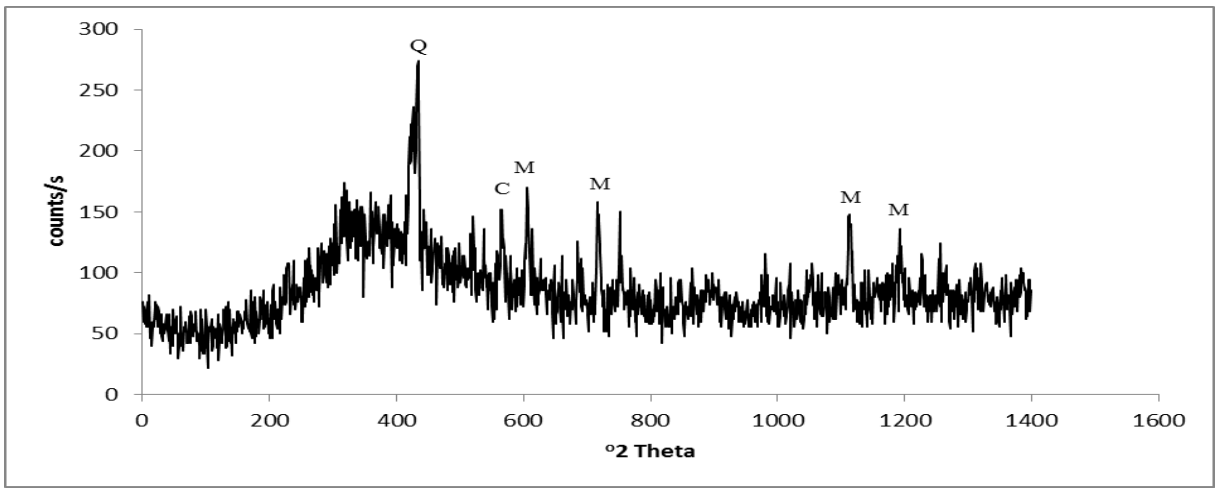

M – Mullite ($Al_6Si_2O_{13}$), Q – Quartz (SiO_2), C – Cristobalite (SiO_2)

Figure 4.55: XRD of $nSiO_2$/fly ash composite material

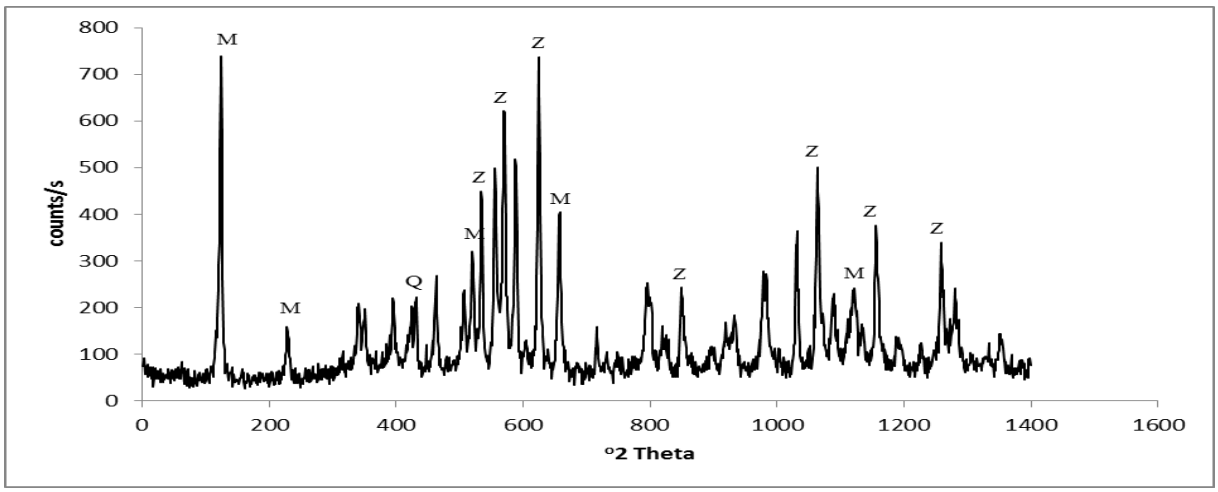

M - Mullite ($Al_6Si_2O_{13}$), Q – Quartz (SiO_2), Z – Zinc Oxide (nZnO)

Figure 4.56: XRD of nZnO/fly ash composite material

The diffractogram of fly ash/activated carbon, nFe_3O_4/fly ash/activated carbon, $nSiO_2$/fly ash/activated carbon and nZnO/fly ash/activated carbon composite materials are represented in Figure 4.57 – 4.60. The diffractogram of fly ash/activated carbon (Figure 4.57) shows that the crystalline minerals mullite and quartz of fly ash are dominant. The x-ray diffractogram of nFe_3O_4/fly ash/activated carbon composite material (Figure 4.58) consists of mullite ($Al_6Si_2O_{13}$), quartz (SiO_2) and Magnetite (Fe_3O_4). The mullite and quartz are from fly ash while magnetite is from nFe_3O_4.

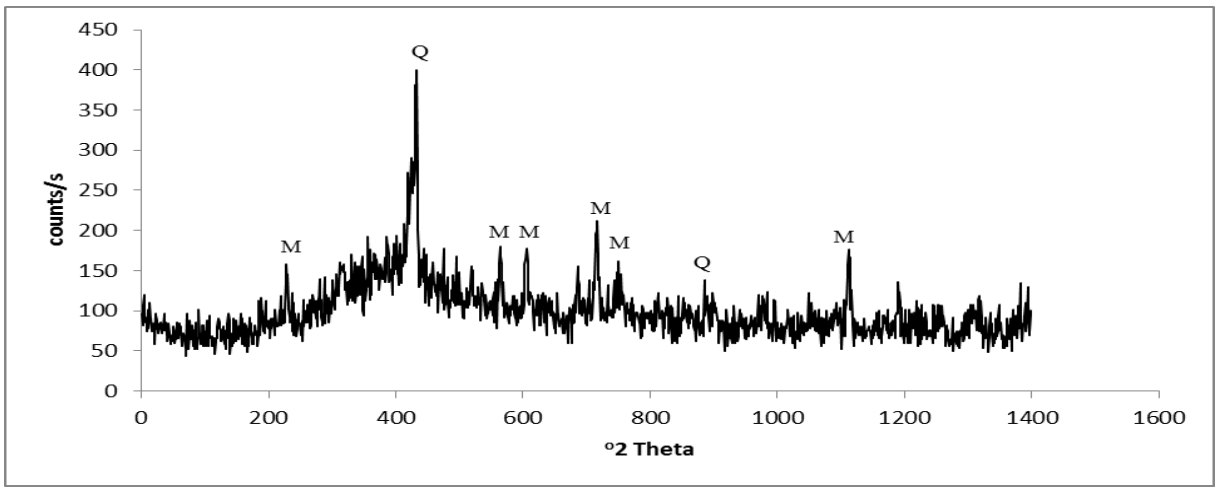

M - Mullite ($Al_6Si_2O_{13}$), Q – Quartz (SiO_2)

Figure 4.57: XRD of fly ash/activated carbon composite material

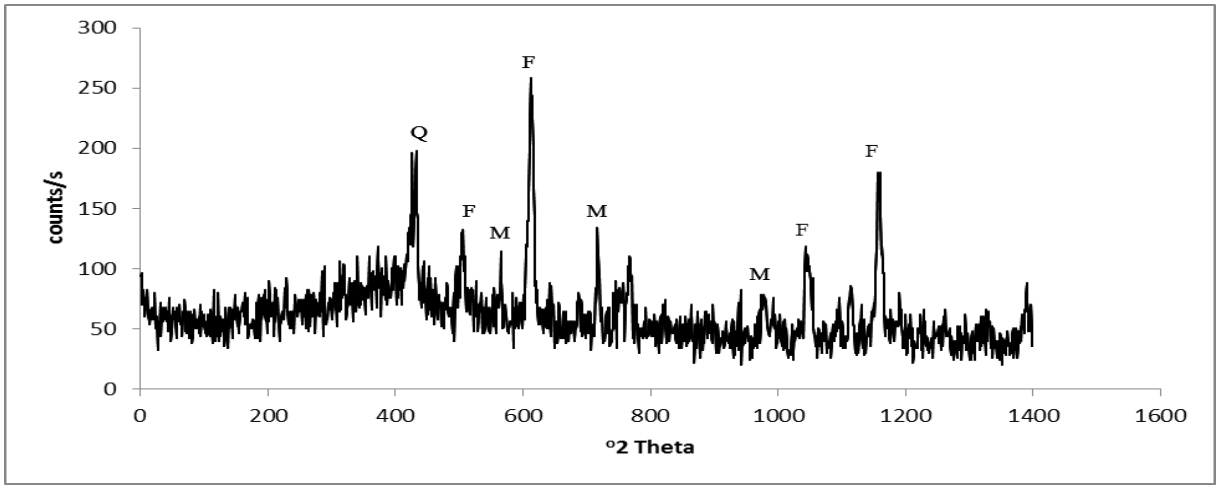

M - Mullite ($Al_6Si_2O_{13}$), Q – Quartz (SiO_2), F – Magnetite (Fe_3O_4)

Figure 4.58: XRD of nFe_3O_4/fly ash/activated carbon composite material

The diffractogram of $nSiO_2$/fly ash/activated carbon composite material (Figure 4.59) consists of mullite ($Al_6Si_2O_{13}$), quartz (SiO_2) and cristobalite (SiO_2). The mullite and quartz are from fly ash while some quartz and cristobalite peaks are from $nSiO_2$. The diffractogram of nZnO/fly ash/activated carbon composite material (Figure 4.60) consists of mullite ($Al_6Si_2O_{13}$), quartz (SiO_2) and zinc oxide (nZnO). The mullite and quartz are from fly ash while zinc oxide peak is from nZnO.

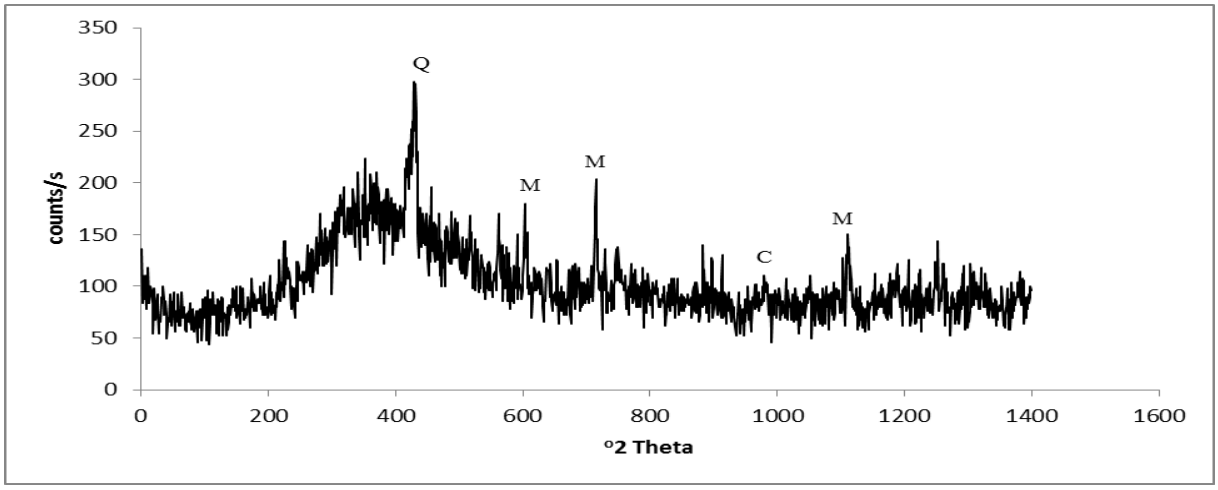

M - Mullite ($Al_6Si_2O_{13}$), Q – Quartz (SiO_2), C – Cristobalite (SiO_2)

Figure 4.59: XRD of $nSiO_2$/fly ash/activated carbon composite material

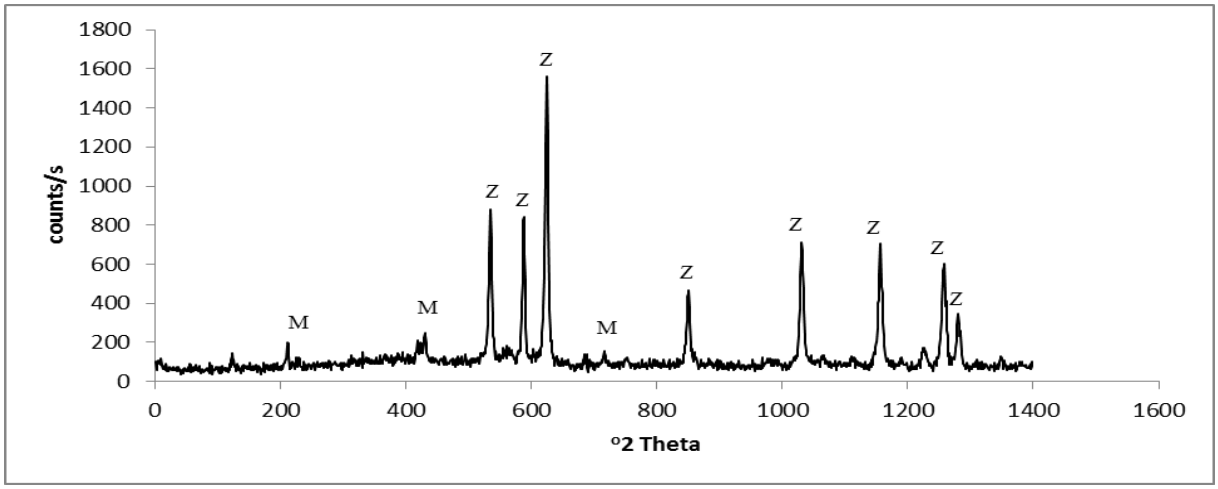

M - Mullite ($Al_6Si_2O_{13}$), Q – Quartz (SiO_2), Z – Zinc Oxide (nZnO)

Figure 4.60: XRD of nZnO/fly ash/activated carbon composite material

All the diffractograms obtained show defined characteristic peaks corresponding to the mineral constituents of the precursors and the composite materials. This shows that the precursors and all the prepared composite materials are pure.

4.11 Surface area and porosity

A summary of BET surface area and porosity determination of precursors and nano oxides/activated carbon composite materials are as shown in Table 4.7 and Figure 4.61.

Table 4.7: BET results of precursors and nano oxides/activated carbon composite materials

Samples	BET Surface area m^2/g	Micropore Volume cm^3/g	Micropore Area m^2/g	External Surface Area m^2/g	Average pore Diameter Á
Activated carbon	1156.64 ± 8.70	0.182	442.75	713.89	48.89
nFe_3O_4	37.18 ± 0.19	0.0017	3.981	33.20	217.42
$nSiO_2$	217.62 ± 1.76	0.0060	16.127	201.50	88.076
nZnO	14.41 ± 0.04	0.0014	3.1780	11.23	98.50
nFe_3O_4/activated carbon	361.12 ± 1.66	0.0499	122.86	238.25	56.73
$nSiO_2$/activated carbon	605.59 ± 3.11	0.0832	205.49	400.097	56.086
nZnO/activated carbon	275.49 ± 1.56	0.0335	82.617	192.87	53.296

From Table 4.7 and Figure 4.61, the surface area of nFe_3O_4, $nSiO_2$, nZnO and activated carbon are 37.18 ± 0.19, 217.62 ± 1.76, 14.41 ± 0.04 and 1156.64 ± 8.70 m^2/g, respectively while the surface area of nFe_3O_4/activated carbon, $nSiO_2$/activated carbon and nZnO/activated carbon are 361.12 ± 1.66, 605.59 ± 3.11 and 275.49 ± 1.56, respectively. The results show that the composition of activated carbon with nano oxides greatly accelerated the surface area of nano oxides. The surface area of nFe_3O_4, $nSiO_2$ and nZnO are all improved by 89.71 %, 64.06 % and 94.77 %, respectively. The highest increase in the surface area is observed for the nZnO composited with activated carbon.

The micropore area of nFe_3O_4/activated carbon is 122.86 m^2/g, $nSiO_2$/activated carbon has a micropore area of 205.49 m^2/g while nZnO/activated carbon micropore area is 82.62 m^2/g. If compared with the micropore area of nFe_3O_4, $nSiO_2$ and nZnO which are 3.98, 16.13 and 3.18 m^2/g, respectively, then it could be proven that the presence of activated carbon as in the case of surface area also improve the micropore areas of the nano oxides.

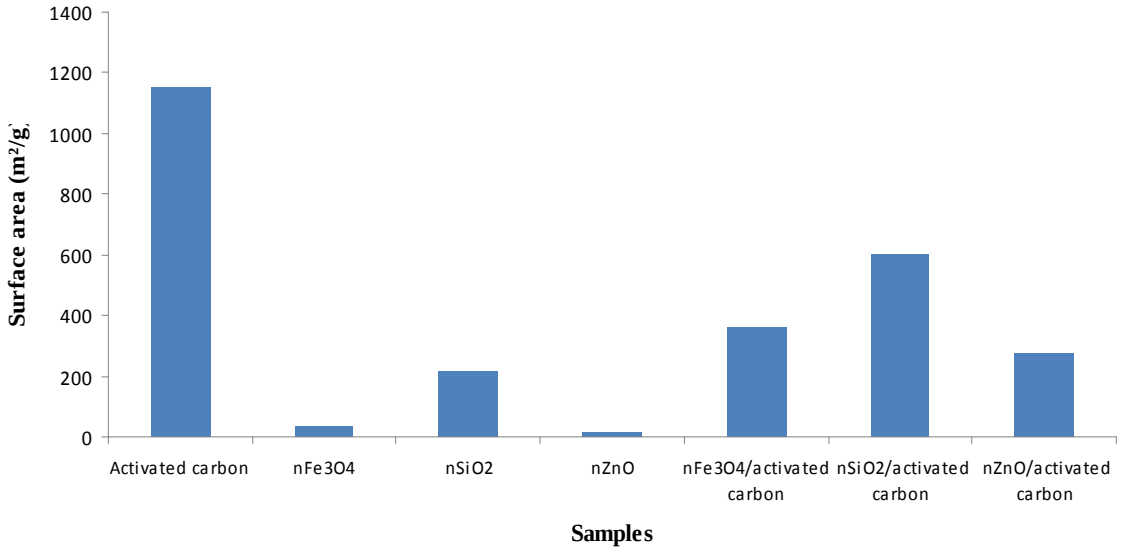

Figure 4.61: Surface area (m^2/g) versus precursors and nano oxides/activated carbon composites

Results obtained on the BET surface area and porosity determination of nano oxides/fly ash composite materials as well as the precursors is as presented in Table 4.8 and Figure 4.62.

Table 4.8: BET results of precursors and nano oxides/fly ash composite materials

Samples	BET Surface area m^2/g	Micropore Volume cm^3/g	Micropore Area m^2/g	External Surface Area m^2/g	Average pore Diameter Á
Fly ash	1.06 ± 0.003	0.00016	0.38	0.68	89.43
nFe_3O_4	37.18 ± 0.19	0.0017	3.98	33.20	217.42
$nSiO_2$	217.62 ± 1.76	0.0060	16.13	201.50	88.08
nZnO	14.41 ± 0.04	0.0014	3.18	11.23	98.50
nFe_3O_4/fly ash	207.01 ± 1.20	0.085	209.41	197.60	50.99
$nSiO_2$/fly ash	343.75 ± 0.16	0.057	35.21	414.97	148.93
nZnO/fly ash	198.45 ± 0.094	0.002	5.44	73.72	74.10

From Table 4.8 and Figure 4.62, the surface area of nFe_3O_4, $nSiO_2$, nZnO and fly ash are 37.18 ± 0.19, 217.62 ± 1.76, 14.41 ± 0.04 and 1.06 ± 0.003 m^2/g, respectively while the surface area of nFe_3O_4/fly ash, $nSiO_2$/fly ash and nZnO/fly ash are 207.01 ± 1.20, 343.75 ± 0.16 and 198.45 ± 0.09, respectively. The results show that the use of nano oxides for the preparation of nano oxides/fly ash composites greatly accelerated the surface area of fly ash. The surface area of fly ash is therefore improved by 99.49 % for nFe_3O_4/fly ash, 99.69 % for $nSiO_2$/fly ash and 99.47 % for nZnO/fly ash composites.

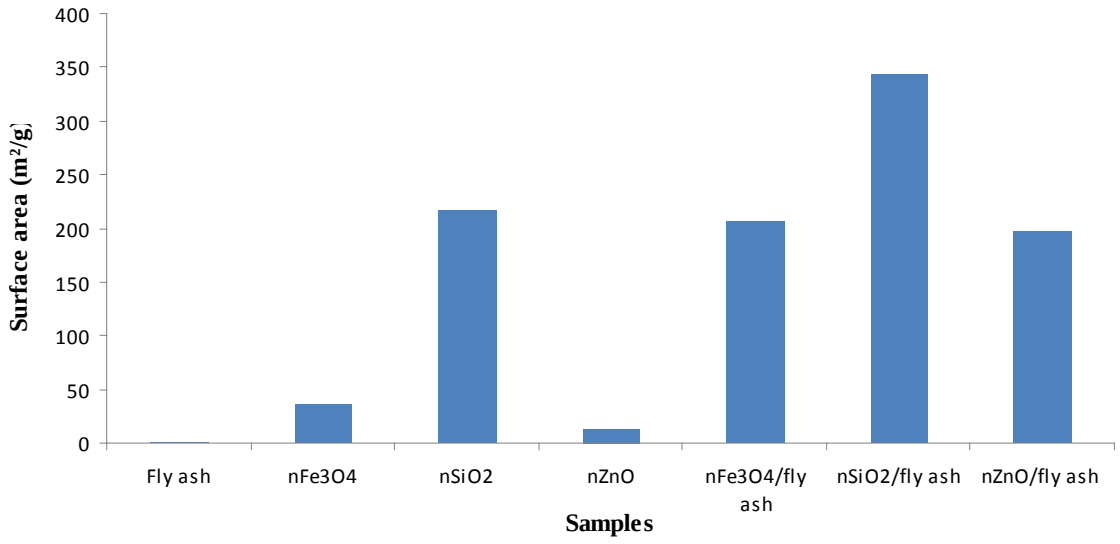

Figure 4.62: Surface area (m^2/g) versus precursors and nano oxides/fly ash composites

The micropore area of nFe_3O_4/fly ash is 209.41 m^2/g, $nSiO_2$/fly ash has a micropore area of 35.21 m^2/g while nZnO/fly ash micropore area is 5.44 m^2/g. The micropore areas of fly ash, nFe_3O_4, $nSiO_2$ and nZnO which are 0.38, 3.98, 16.13 and 3.18 m^2/g, respectively are thus

smaller than the micropore area of the corresponding composites. It could therefore be affirmed that the composition of nano oxides with fly ash also improved the micropore area of fly ash.

Results obtained on the BET surface area and porosity determinations of nano oxides/fly ash/activated carbon composite materials as well as their precursors are presented in Table 4.9 and Figure 4.63. From Table 4.9 and Figure 4.63, the surface area of fly ash, activated carbon, nFe_3O_4, $nSiO_2$, nZnO, are 1.06 ± 0.0030, 1156.64 ± 8.70, 37.18 ± 0.19, 217.62 ± 1.76 and 14.41 ± 0.04 m^2/g, respectively while the surface area of fly ash/activated carbon, nFe_3O_4/fly ash/activated carbon, $nSiO_2$/fly ash/activated carbon and nZnO/fly ash/activated carbon are 5.30 ± 0.03, 299.76 ± 1.09, 352.61 ± 1.01 and 240.81 ± 1.15 m^2/g, respectively. The results show that the use of activated carbon, fly ash and nano oxides for the preparation of nano oxides/fly ash/activated carbon composites greatly accelerated the surface area of fly ash.

Table 4.9: BET results of precursors and nano oxides/fly ash/activated carbon composite materials

Samples	BET Surface area m^2/g	Micropore Volume cm^3/g	Micropore Area m^2/g	External Surface Area m^2/g	Average pore Diameter Á
Activated carbon	1156.64 ± 8.70	0.18	442.75	713.89	48.89
Fly ash	1.06 ± 0.003	0.0002	0.38	0.68	89.43
nFe_3O_4	37.18 ± 0.19	0.0017	3.98	33.20	217.42
$nSiO_2$	217.62 ± 1.76	0.0060	16.13	201.50	88.08
nZnO	14.41 ± 0.04	0.0014	3.18	11.23	98.50
fly ash/activated carbon	5.30 ± 0.03	0.00002	0.19	5.11	210.01
nFe_3O_4/fly ash/activated carbon	299.76 ± 1.09	0.048	118.89	180.86	63.55
$nSiO_2$/fly ash/activated carbon	352.61 ± 1.01	0.063	154.21	198.41	64.78
nZnO/fly ash/activated carbon	240.81 ± 1.15	0.033	82.17	158.64	51.84

The surface area of fly ash is therefore improved by 99.65 % for nFe_3O_4/fly ash/activated carbon, 99.70 % for $nSiO_2$/fly ash/activated carbon and 99.56 % for nZnO/fly ash/activated carbon composites.

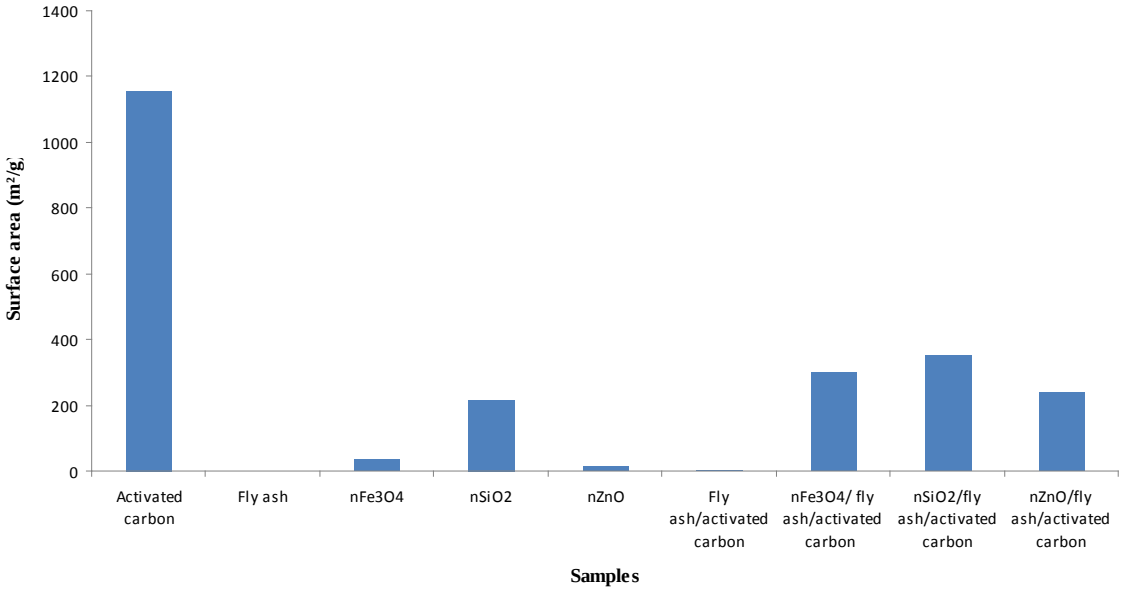

Figure 4.63: Surface area (m^2/g) versus precursors and nano oxides/fly ash/activated carbon composites materials

The micropore area of nFe_3O_4/fly ash/activated carbon is 118.89 m^2/g, $nSiO_2$/fly ash/activated carbon has a micropore area of 154.21 m^2/g while nZnO/fly ash/activated carbon micropore area is 82.17 m^2/g. The micropore areas of fly ash, nFe_3O_4, $nSiO_2$ and nZnO which are 0.38, 3.98, 16.13 and 3.18 m^2/g, respectively are thus smaller than the micropore area of the corresponding composites. It could therefore be asserted that the composition of activated carbon and nano oxides with fly ash also improve the micropore area of fly ash and nano oxides.

The increase in the surface area for all the composites is in support of the work by Wang et al., 2013 who reported the deposition of iron–nickel nanoparticles onto carbon nanotubes (CNTs) to form nano composite materials.

4.12 Adsorption studies

4.12.1 Adsorption of TBT from TBT-contaminated artificial seawater onto activated carbon

4.12.1.1 Effect of adsorbent amount

Adsorbent amount is one of the vital parameters in this study. The amount of activated carbon was varied from 0.0625 – 1 g to investigate the effect on the adsorption of TBT from TBT – contaminated artificial seawater. To study this effect, the concentration of TBT was taken as 100 mg/L and other parameters were kept constant. The amount adsorbed and percentage removal of TBT by the activated carbon increases as the amount of adsorbent increases from 0.0625 - 0.5 g. The adsorbent amount directly affects the adsorption capacity; this is because as the adsorbent dosage increases, more active sites become available for the adsorbate (TBT). Figure 4.64 shows that 0.5 g of activated carbon remove 99.71 % of TBT from TBT – contaminated artificial seawater (Ayanda et al., 2013b). After 0.5 g (which is the value of the activated carbon used for the rest of the experiment), the adsorption of TBT onto the activated carbon has already attained equilibration.

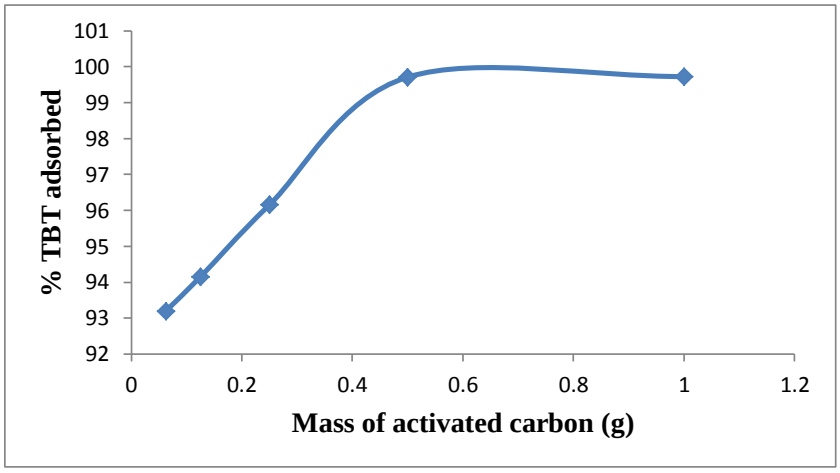

Figure 4.64: Adsorption efficiencies of TBT onto activated carbon

Experimental conditions: Concentration of TBT = 100 mg/L; Volume of TBT solution = 25 mL, Contact time = 60 min; Stirring speed = 160 rpm, Temperature = 20 ^{o}C.

4.12.1.2 Effect of contact time

It is a normal observation among all adsorption studies that as the contact time increases, there is enhancement in the amount of adsorbate adsorbed. This is probably due to a larger surface area of the adsorbent being available at the beginning for the adsorption of the adsorbate. As the surface adsorption sites become exhausted, the uptake rate tends to be controlled by the rate at which the adsorbate is transported from the exterior to the interior sites of the adsorbent particles. To study the effect of contact time, the TBT concentration

was 100 mg/L while, other remaining conditions pH = 8, stirring speed 160 rpm etc. were kept constant. The effect of contact time was carried out at various time intervals from 10 min – 70 min. The increase in the amount adsorbed from 4.49 mg/g (89.88 % TBT removal) to 4.84 mg/g (96.81 % TBT removal) (Figure 4.65) was observed up to 60 min. After that, there was no significant change observed. Therefore, 60 min was fixed as the contact time for subsequent studies.

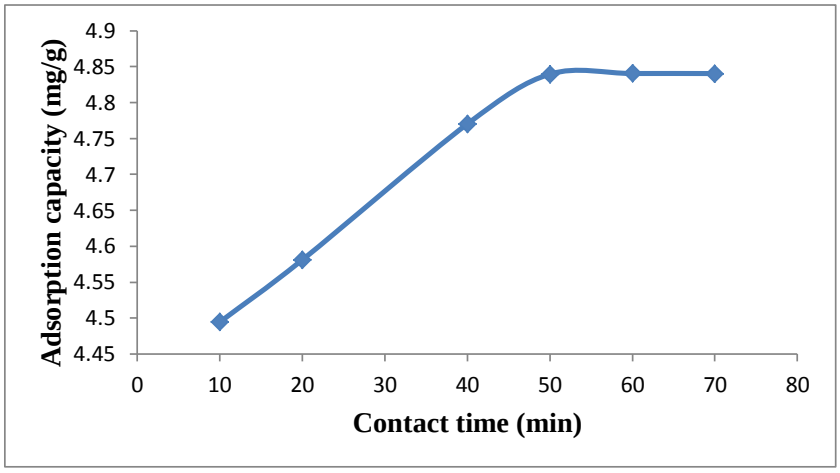

Figure 4.65: Effect of contact time on TBT adsorption onto activated carbon

Experimental conditions: Concentration of TBT = 100 mg/L; Volume of TBT solution = 25 mL, Mass of activated carbon = 0.5 g; Stirring speed = 160 rpm, Temperature = 20 ^{o}C.

4.12.1.2.1 Adsorption kinetics

In order to investigate the mechanism and to determine the rate controlling step of the adsorption of TBT onto the activated carbon, kinetic models were used. The rate constants were calculated by pseudo first-order, pseudo second-order, Elovich and fractional power kinetic models (Equaions 3.3, 3.5, 3.8 and 3.10) and the rate controlling steps were determined by intra-particle diffusion model (Equation 3.11).

Figures 4.66 – 4.70 thus show the pseudo first-order, pseudo second-order, Elovich, fractional power and intraparticle diffusivity kinetic plots, respectively and Table 4.10 provides the evaluated parameters of all the kinetics models.

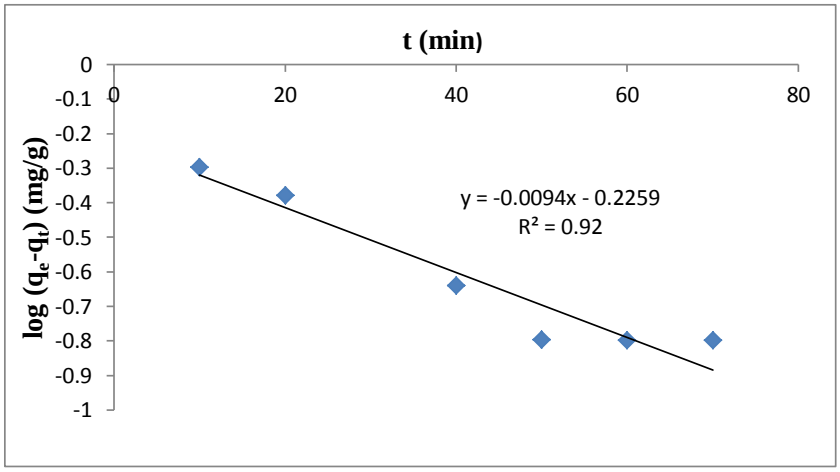

Figure 4.66: Pseudo first-order rate equation plot for TBT adsorption onto activated carbon

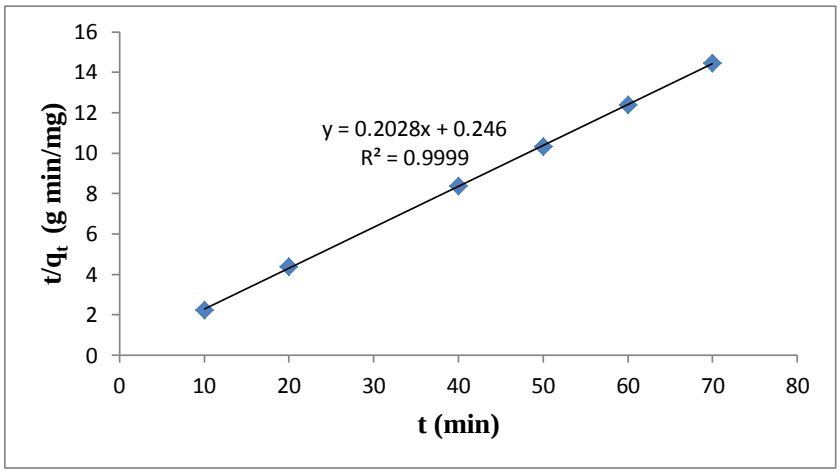

Figure 4.67: Pseudo second-order rate equation plot for TBT adsorption onto activated carbon

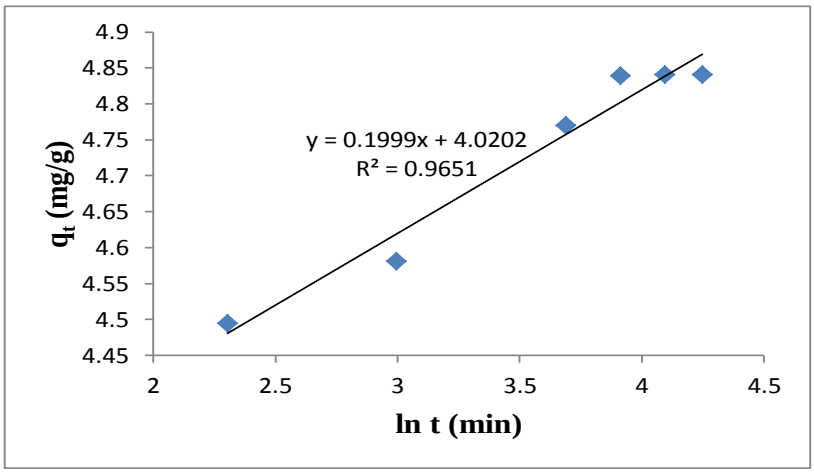

Figure 4.68: Elovich rate equation plot for TBT adsorption onto activated carbon

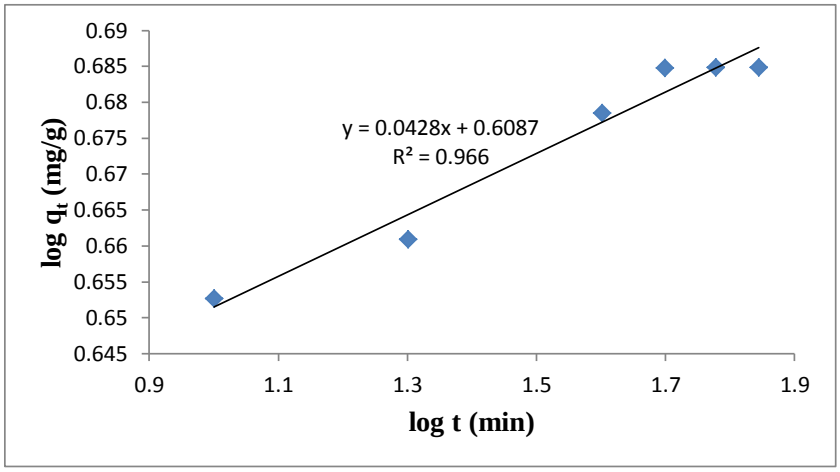

Figure 4.69: Fractional Power rate equation plot for TBT adsorption onto activated carbon

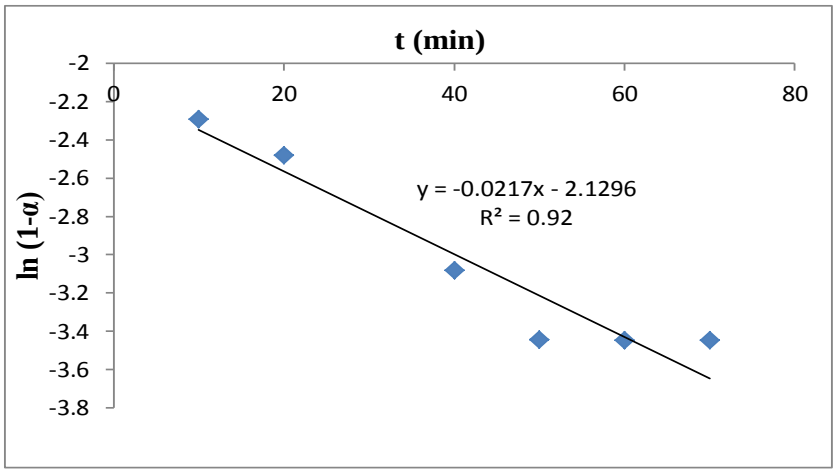

Figure 4.70: Intraparticle diffusivity plot for TBT adsorption onto activated carbon

The value of correlation coefficient (R^2) of pseudo second-order kinetic model (> 0.99) is higher than the correlation coefficients of all other models indicating that the kinetic model for the adsorption of TBT onto the activated carbon is pseudo second-order. The intraparticle coefficient for the adsorption of TBT by the activated carbon is also calculated and presented in Table 4.10.

The results indicate that the power function model satisfactorily describes the time-dependence of TBT on the activated carbon since the value of the constant v is less than 1, and the regression coefficient is greater than 0.96 (Ayanda et al., 2013c).

Table 4.10: Kinetic model parameters for TBT adsorption onto activated carbon

Kinetic models	
Pseudo first-order	
k_1 (min^{-1})	0.0216
q_e (mg/g)	0.5944
R^2	0.9200
Pseudo second-order	
q_e (mg/g)	4.9309
h_o (mg/g/min)	4.0650
k_2 (g/mg/min)	0.1672
R^2	0.9999
Elovich	
β (g min/mg)	5.0025
α (g min^2/mg)	2.712×10^9
R^2	0.9651
Fractional Power	
v (min^{-1})	0.0428
k_3 (mg/g)	4.0616
k_3v (mg/g/min)	0.1738
R^2	0.9660
Intraparticle diffusivity	
kp (min^{-1})	0.0217
R^2	0.9200

The value of the initial adsorption rate, h_o, obtained for the pseudo second-order kinetics is 4.0650 mg/g/min indicating a rapid adsorption of TBT onto the activated carbon. The amount of TBT adsorbed at equilibrium per unit weight of the adsorbent (q_e) is 4.9309 mg/g and the rate constant of pseudo second - order adsorption (k_2) is 0.1672 g/mg/min.

4.12.1.3 Effect of pH

The effect of pH on the adsorption of TBT onto the activated carbon was studied at pH 3 – 9. It was observed (Figure 4.71) that the percentage of TBT adsorbed by activated carbon steadily increases as the pH of the solution increases from pH 3 to pH 8, and reaches equilibration at pH ≥ 8. This is in support of the results obtained by Fang et al. (2010) and Weidenhaupt et al. (1997).

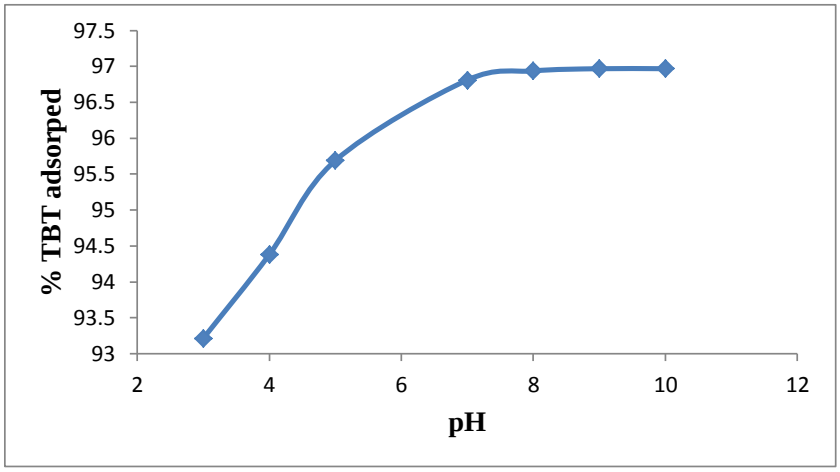

Figure 4.71: Effect of pH on TBT adsorption onto activated carbon

Experimental conditions: Concentration of TBT = 100 mg/L; Volume of TBT solution = 25 mL, Mass of activated carbon = 0.5 g; Contact time = 60 min; Stirring speed = 160 rpm, Temperature = 20 ^{o}C.

Maximum adsorption capacity was therefore recorded within the pH range of normal saline water (pH 8). About 96.94 % of TBT was removed from the initial concentration of 100 mg/L TBT by the activated carbon at a contact time of 60 min, stirring speed of 160 rpm, temperature of 20 ^{o}C and pH 8. pH 8 was chosen as the optimum pH and was utilized for further studies.

4.12.1.4 Effect of stirring speed

The stirring speed on the adsorption of TBT onto the activated carbon was studied at a stirring speed of 160 – 200 rpm.

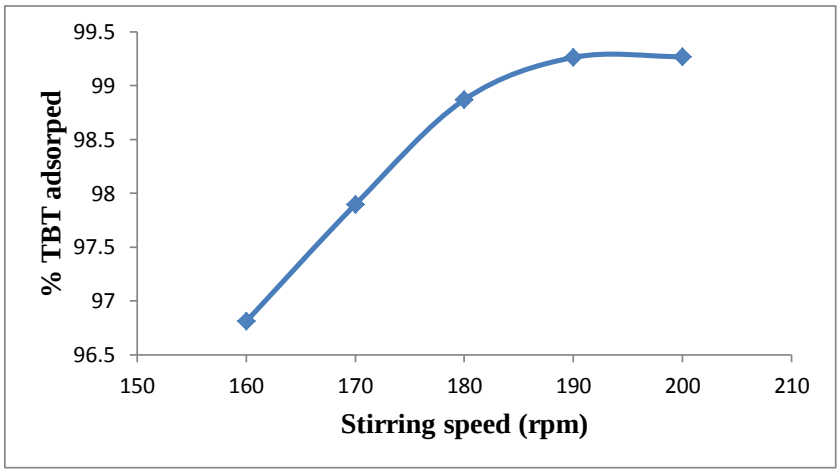

Figure 4.72: Effect of stirring speed on TBT adsorption onto activated carbon

Experimental conditions: Concentration of TBT = 100 mg/L; Volume of TBT solution = 25 mL, Mass of activated carbon = 0.5 g; Contact time = 60 min; Temperature = 20 ^{o}C.

The adsorption capacity of TBT onto activated carbon increases as the stirring speed of the mixture increases, reaching equilibration at 190 - 200 rpm (Figure 4.72). Maximum amount of 4.963 mg/g (99.27 %) of TBT was removed from the initial concentration of 5 mg/g TBT by the activated carbon at a contact time of 60 min, pH 8, temperature of 20 ^{o}C and a stirring speed of 200 rpm (Figure 4.72). A stirring speed of 200rpm was therefore used for further studies.

4.12.1.5 Effect of initial concentration

The adsorption isotherms were investigated by varying the initial TBT concentration from 12.5 to 200 mg/L at optimized adsorbent dose, contact time, pH and stirring speed established after optimization of working parameters. The equilibrium data were fitted by Langmuir, Freundlich, Temkin and D-R isotherm models (Equations 3.12 – 3.15).

Figure 4.73 shows that the adsorption of TBT onto activated carbon increases as the initial TBT concentration increases from 12.5 to 100 mg/L, indicating that adsorption is also favourable for the higher TBT concentrations that have been investigated.

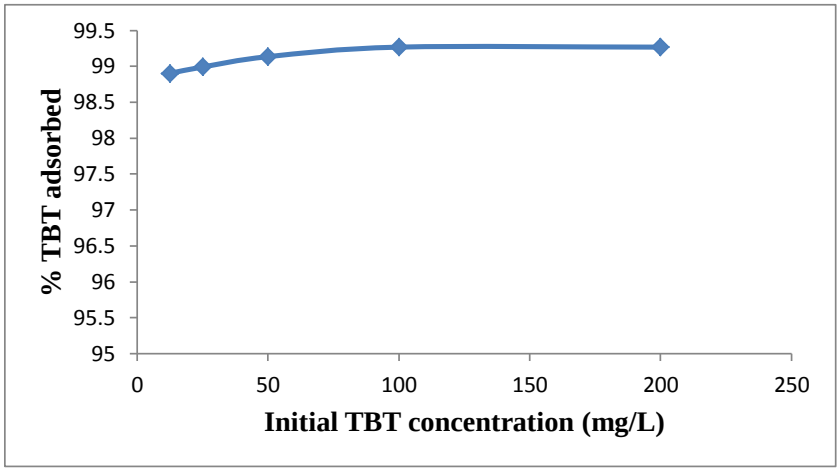

Figure 4.73: Percentage TBT adsorbed by activated carbon at various initial TBT concentrations

Experimental conditions: Volume of TBT solution = 25 mL, Mass of activated carbon = 0.5 g; pH = 8; Stirring speed = 200 rpm; Contact time = 60 min; Temperature = 20 ^{o}C.

The increase in the adsorption capacity with an increase in initial TBT concentration is as a result of the increase in driving force due to concentration gradient developed between the bulk solution and surface of the adsorbents. At higher concentration of TBT, the active sites of the adsorbents were surrounded by much more TBT and the process of adsorption continues, leading to an increased uptake of TBT from the solution.

4.12.1.5.1 Adsorption isotherms

The adsorption isotherm plots are presented in Figures 4.74 – 4.77 and parameters obtained for all the models were given in Table 4.11. The experimental data fitted well with Freundlich model, probably due to the real heterogeneous nature of the surface sites involved in the process of adsorption. It is the suitable model for describing the adsorption process because the regression coefficient (R^2) value (> 0.99) is higher than other models (Table 4.11). The value of n_F, for activated carbon, falling in the range 1 -10 indicates favourable adsorption.

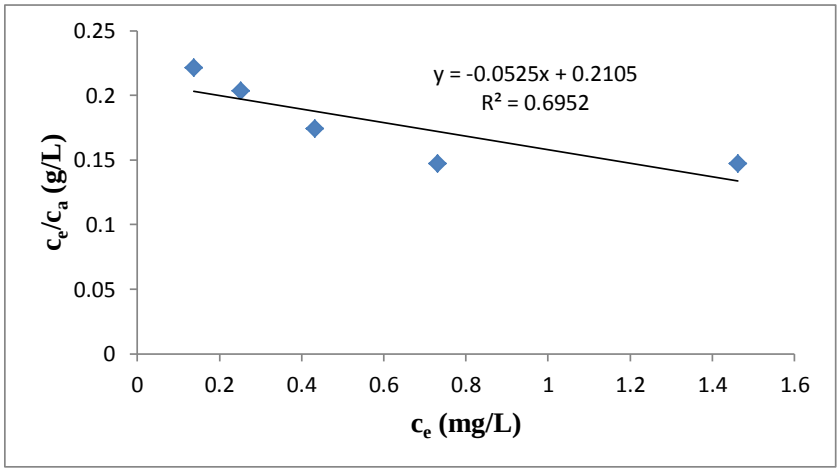

Figure 4.74: Langmuir isotherm for adsorption of TBT onto activated carbon

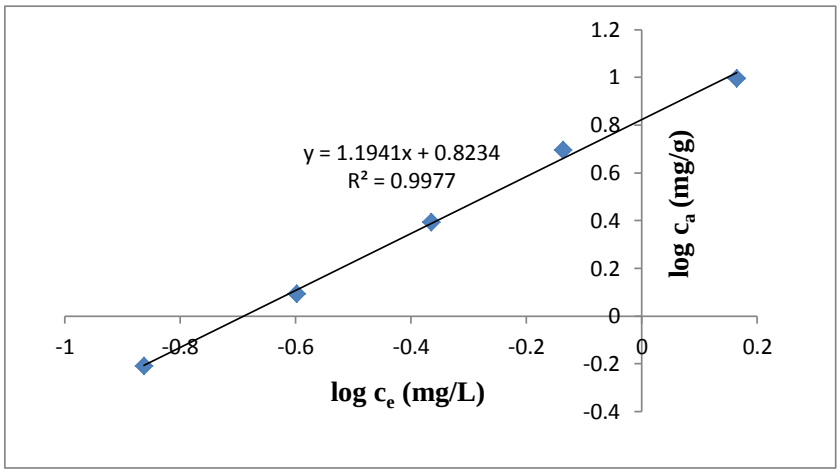

Figure 4.75: Freundlich isotherm for adsorption of TBT onto activated carbon

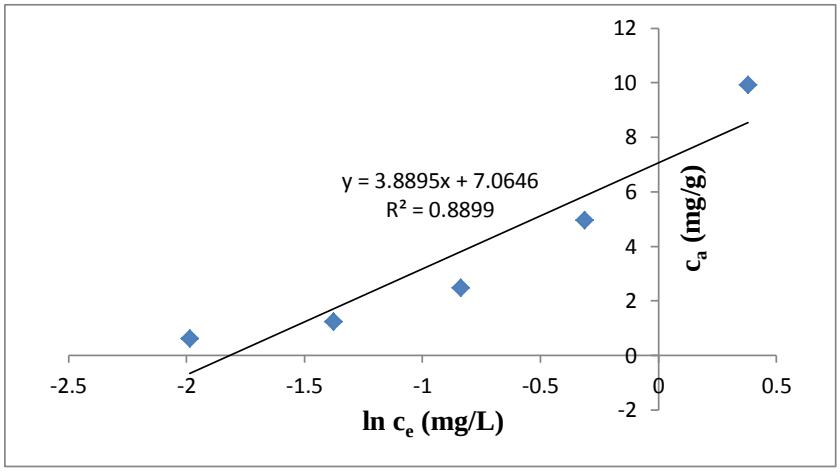

Figure 4.76: Temkin isotherm for adsorption of TBT onto activated carbon

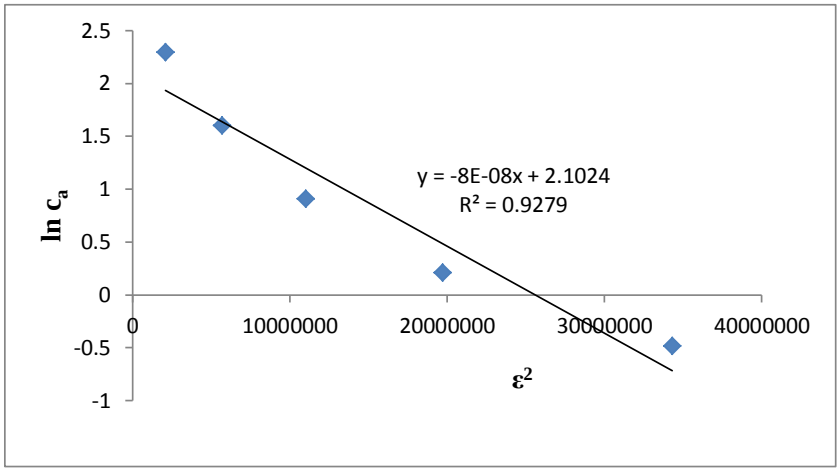

Figure 4.77: D-R isotherm for adsorption of TBT onto activated carbon

Moreover, the negative value of the Langmuir constants, A_{max} (mg/g) and k_L (L/mg) for TBT adsorption indicate the inadequacy fitting of experimental data to Langmuir model (Maarof and Hameed, 2004). Thus, Freundlich model is the best model to explain the adsorption behaviour of TBT onto activated carbon.

Table 4.11: Isotherms constants for the adsorption of TBT onto activated carbon

Equilibrium models	
Freundlich	
k_F [mg/g (L/mg)$^{1/n}$]	6.6589
n_F	0.8375
R^2	0.9977
Langmuir	
K_L (L/mg)	- 0.2494
A_{max} (mg/g)	-19.0476
R^2	0.6952
Temkin	
n_T (L/g)	3.8895
k_T (mg/L)	6.1492
b_T (J/mol)	626.30
R^2	0.8899
Dubinin-Redushkevich	
k_{D-R} (J^2/mol^2)	8×10^{-8}
q_m (mg/g)	8.1858
E (J/mol)	2500
R^2	0.9279

4.12.1.6 Effect of temperature

The experimental results obtained on the effect of temperature show that the adsorption capacity of TBT onto activated carbon increases with increase in the solution temperature (Figure 4.78). This indicates that the adsorption of TBT onto the activated carbon is endothermic. The increase in the rate of adsorption with the increase in temperature may be attributed to the strong adsorptive forces between the active sites of the adsorbents and adsorbate species and also between the adjacent molecules of the adsorbed phases.

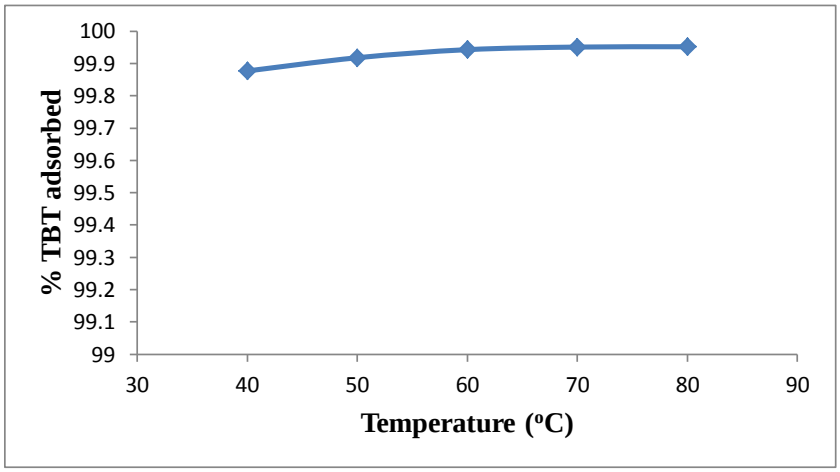

Figure 4.78: Effect of temperature on TBT adsorption onto activated carbon

Experimental conditions: Concentration of TBT = 100 mg/L; Volume of TBT solution = 25 mL, Mass of activated carbon = 0.5 g; Contact time = 60 min; pH = 8; Stirring speed = 200 rpm.

Approx. 99.95 % of TBT was removed from the initial concentration of 100 mg/L TBT by the activated carbon at a temperature of 80 ^{o}C, 60 min contact time, pH 8 and a stirring speed of 200 rpm.

Figure 4.79 thus shows the Van't Hoff plot (Sheela et al., 2012) for the adsorption of TBT and the variation in the extent of adsorption with respect to temperature has been explained on the basis of ΔH^{o}, ΔS^{o}, and ΔG^{o} as shown in Table 4.12.

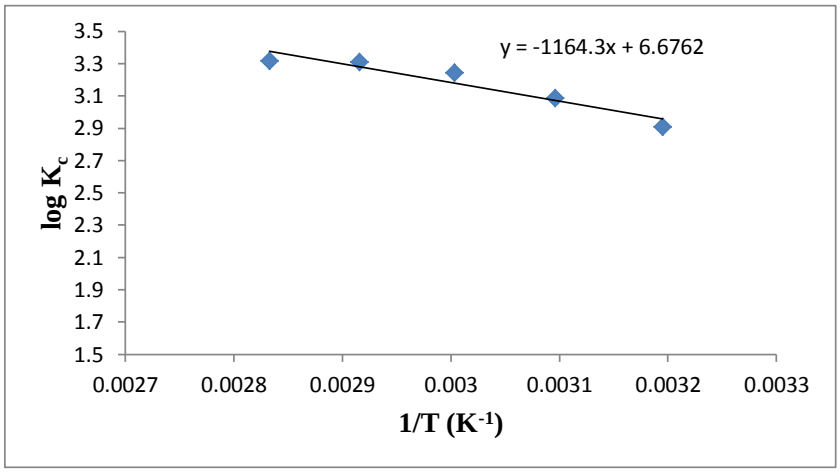

Figure 4.79: Van't Hoff Plot for the adsorption of TBT onto activated carbon

The positive value of ΔH^{o} for the intervals of temperatures also shows the endothermic nature of the adsorption process. The positive value of ΔS^{o} corresponds to increase in degree of freedom of the adsorbed TBT and suggest the increase in concentration of adsorbate in solid–solution interface indicating an increase in adsorbate concentration onto the solid phase. It is evident from Table 4.12 that ΔG^{o} values were found to be more negative as the temperature increases, this indicates that the adsorption efficiency of TBT onto activated carbon increases with increase in temperature. K_c also ranged 812.0 – 2082.3.

Table 4.12: Thermodynamic parameters for adsorption of TBT onto activated carbon

Temperature (°C)	ΔG° (kJ/mol)	ΔS° (J/K/mol)	ΔH° (kJ/mol)	K_c
40	-17.434	127.830	22.293	812.0
50	-19.080			1218.5
60	-20.679			1753.4
70	-21.731			2039.8
80	-22.425			2082.3

The solid residue of activated carbon before and after the adsorption processes were subjected to SEM analysis and are presented in Figure 4.80 while a representative TBT chromatogram after adsorption of 100 mg/L TBT with 0.5 g of activated carbon, contact time of 60min, temperature 20 ^{o}C and a stirring speed of 200 rpm is as shown in Figure 4.81.

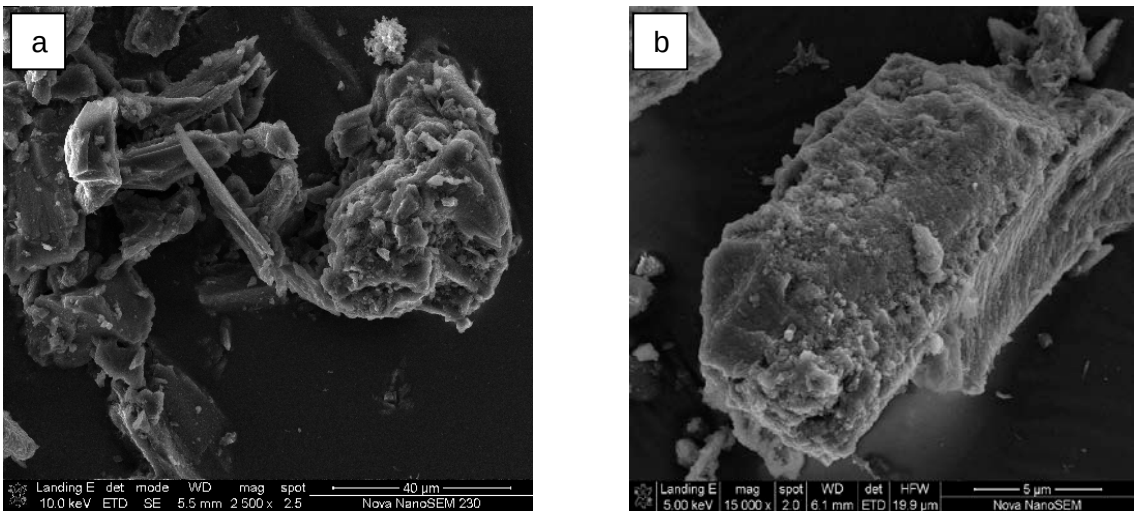

Figure 4.80: Activated carbon before (a) and after (b) TBT adsorption

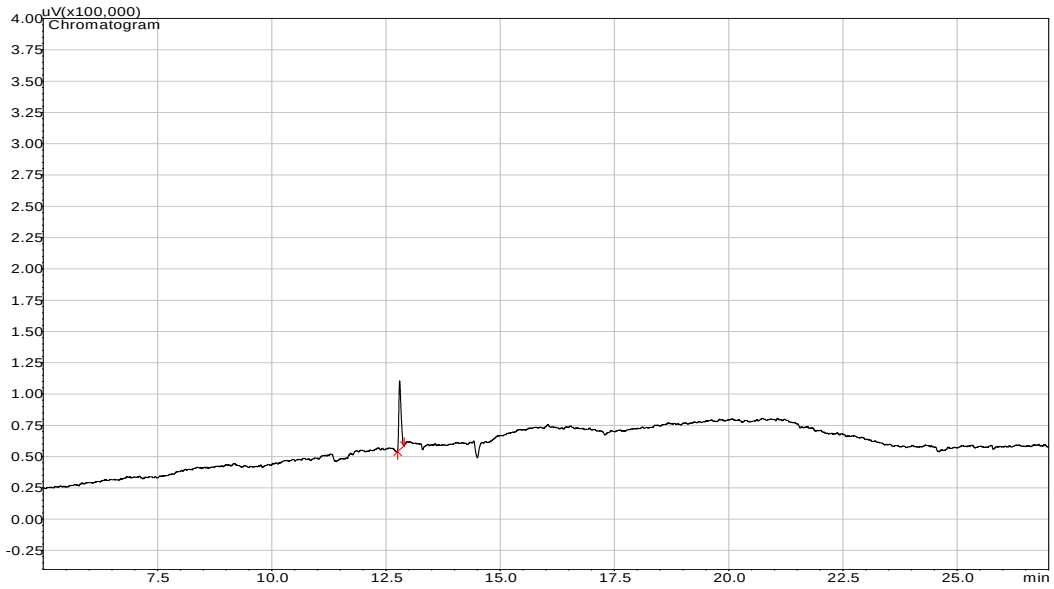

Figure 4.81: Representative TBT chromatogram after adsorption of 100 mg/L TBT with 0.5g of activated carbon, contact time of 60min, temperature 20 ^{o}C and a stirring speed of 200 rpm

4.12.2 Adsorption of TBT from TBT-contaminated artificial seawater onto fly ash

4.12.2.1 Effect of adsorbent amount

The effect of adsorbent amount on the adsorption of TBT by the fly ash is as shown in Figure 4.82. It was observed that the percentage adsorption of TBT increases with increasing amount of fly ash, reaching an optimum at 0.5 g for the fly ash, corresponding to 89.07 % removal. 0.5 g was therefore selected as the optimum adsorbent amount utilized for further studies.

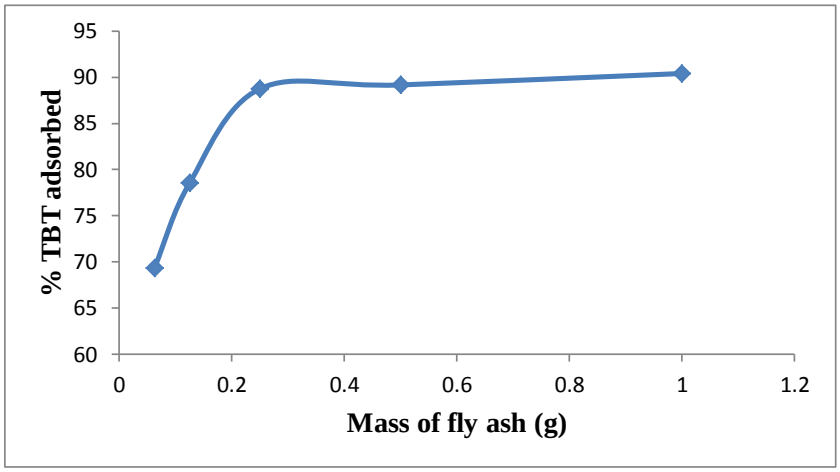

Figure 4.82: Adsorption efficiencies of TBT onto fly ash

Experimental conditions: Concentration of TBT = 100 mg/L; Volume of TBT solution = 25 mL, Contact time = 60 min; Stirring speed = 160 rpm, Temperature = 20 ^{o}C.

4.12.2.2 Effect of contact time

Figure 4.83 shows the effect of contact time on the adsorption of TBT by the fly ash. The TBT removal efficiency at different time intervals ranging from 10 – 70 min were obtained. Figure 4.83 also shows that the adsorption of TBT onto fly ash increases with time and gradually attains equilibrium after 50 - 60 minutes. The TBT removal efficiency for fly ash reaches 4.84 mg/g (89.17 %). A contact time of 60 min was therefore fixed for further studies.

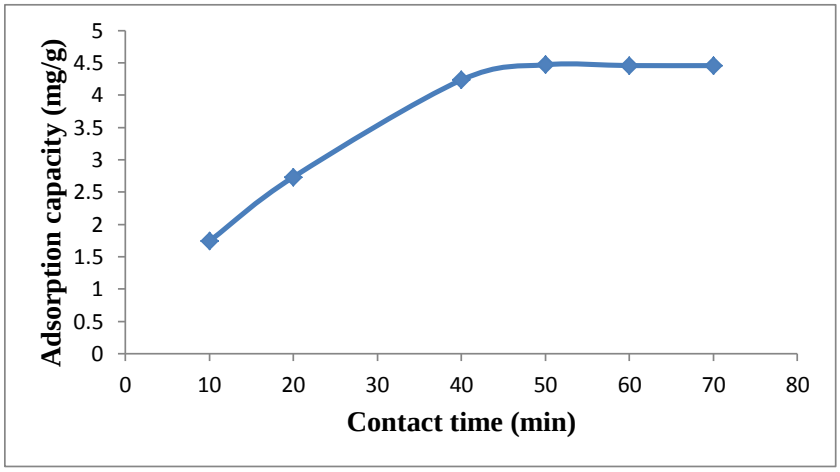

Figure 4.83: Effect of contact time on TBT adsorption onto fly ash

Experimental conditions: Concentration of TBT = 100 mg/L; Volume of TBT solution = 25 mL, Mass of fly ash = 0.5 g; Stirring speed = 160 rpm, Temperature = 20 ^{o}C.

4.12.2.2.1 Adsorption kinetics

Figures 4.84 – 4.88 show the pseudo first-order, pseudo second-order, Elovich, fractional power and intraparticle diffusivity kinetic plots, respectively and Table 4.13 provides the evaluated parameters of the kinetic models. The R^2 value obtained for pseudo second-order kinetic model is very high (R^2 > 0.97) when compared with other models, showing the applicability of the pseudo second-order kinetic model to describe the adsorption kinetic data of TBT onto the fly ash.

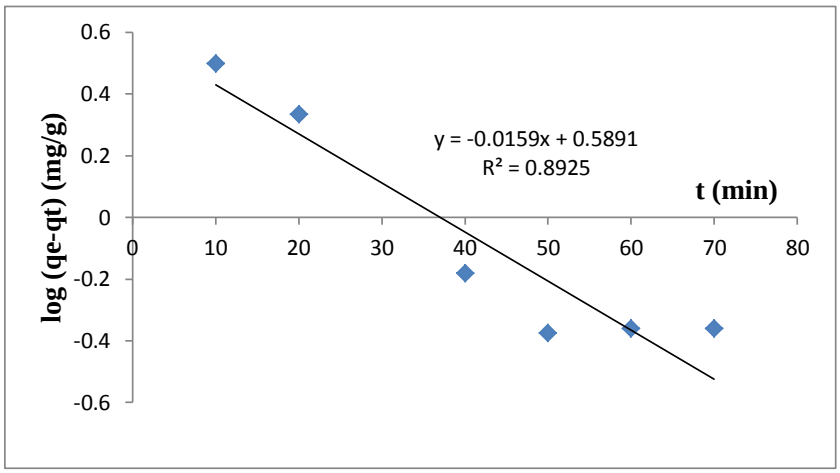

Figure 4.84: Pseudo first-order rate equation plot for TBT adsorption onto fly ash

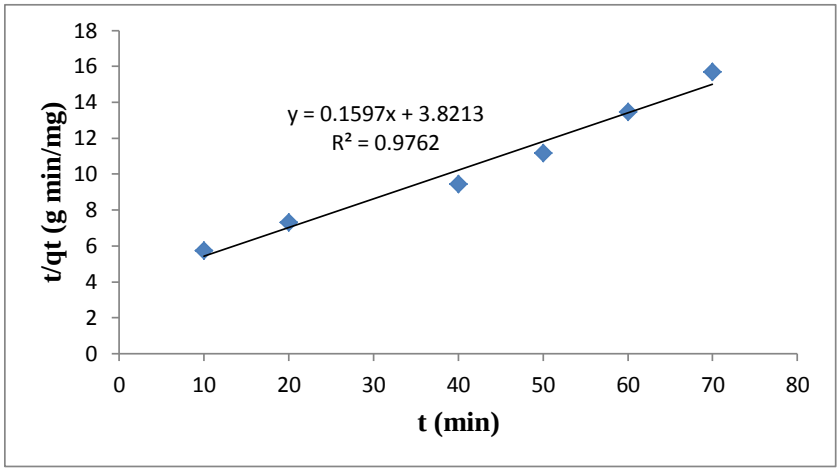

Figure 4.85: Pseudo second-order rate equation plot for TBT adsorption onto fly ash

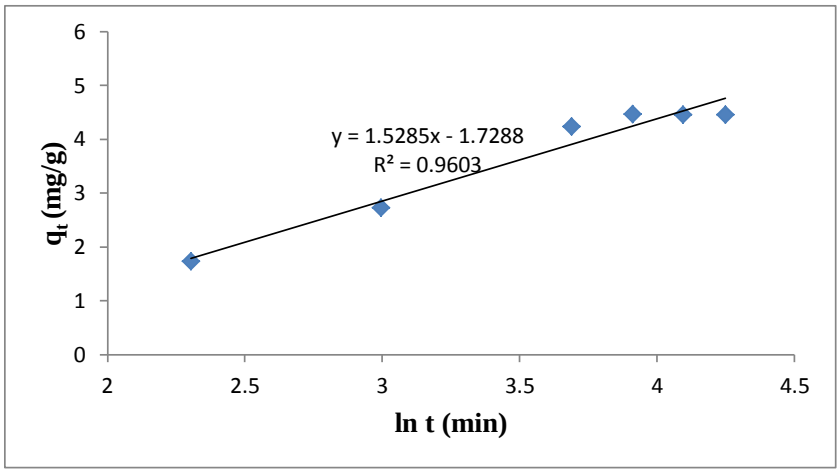

Figure 4.86: Elovich rate equation plot for TBT adsorption onto fly ash

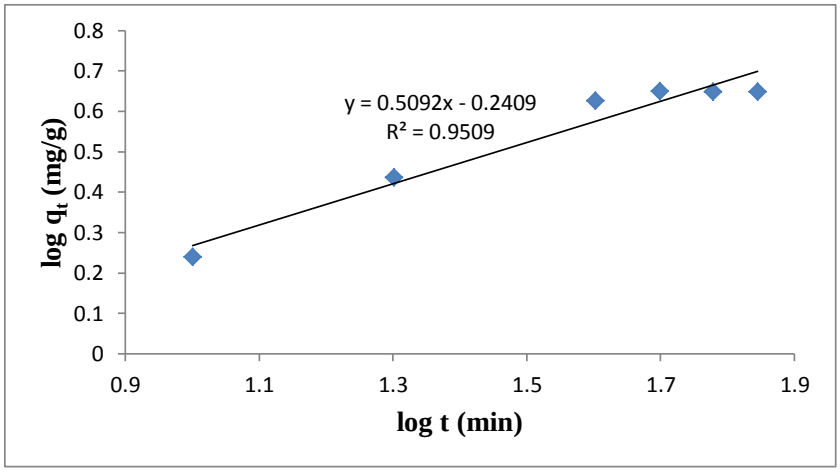

Figure 4.87: Fractional Power rate equation plot for TBT adsorption onto fly ash

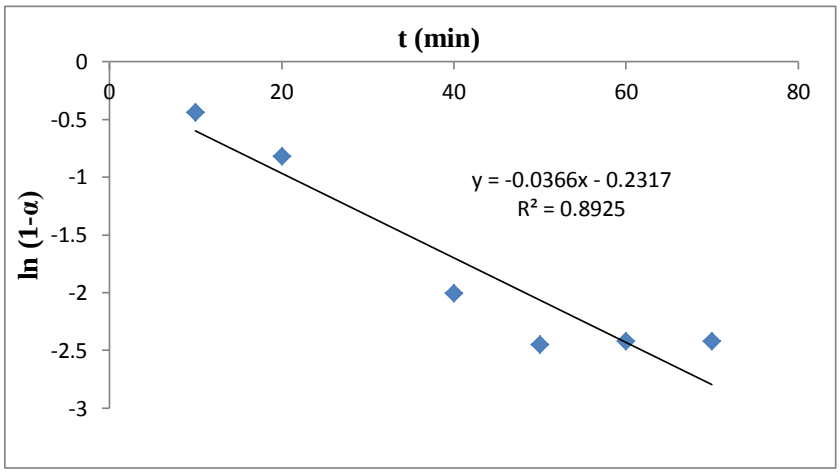

Figure 4.88: Intraparticle diffusivity plot for TBT adsorption onto fly ash

The intraparticle coefficient for the adsorption of TBT by the fly ash was also calculated (Table 4.13). The initial adsorption rate (h_o) calculated from the pseudo second-order rate equation for TBT adsorption onto fly ash is 0.2617 mg/g/min.

Table 4.13: Kinetic model parameters for TBT adsorption onto fly ash

Kinetic models	
Pseudo first-order	
k_1 (min^{-1})	0.0366
q_e (mg/g)	3.8824
R^2	0.8925
Pseudo second-order	
q_e (mg/g)	6.2617
h_o (mg/g/min)	0.2617
k_2 (g/mg/min)	0.006675
R^2	0.9762
Elovich	
β (g min/mg)	0.6542
α (g min^2/mg)	0.2111
R^2	0.9603
Fractional Power	
v (min^{-1})	0.5092
k_3 (mg/g)	0.5742
k_3v (mg/g/min)	0.2924
R^2	0.9509
Intraparticle diffusivity	
k_p (min^{-1})	0.0366
R^2	0.8925

The results also indicate that the power function model satisfactorily describes the time-dependence of TBT on fly ash since the value of the constant v is less than 1, and the regression coefficient for fly ash is greater than 0.95. From Table 4.13, k_1, k_2, β, α_E, k_3 and k_p are 0.0366 min^{-1}, 0.0067 g/mg/min, 0.654 gmin/mg, 0.211 $gmin^2/mg$, 0.574 mg/g and 0.0366 min^{-1}, respectively.

4.12.2.3 Effect of pH

The pH of an aqueous solution is an important variable that governs the adsorption of TBT onto the adsorbents. The pH affects both the adsorbent and adsorbate chemistry in solution. The effect of pH on the adsorption of TBT onto fly ash was studied at pH 3 – 9. It was observed from Figure 4.89 that the percentage of TBT adsorbed by the fly ash steadily increases as the pH of the solution increases from pH 3 to pH 8 where the equilibrium was attained. It is therefore evident from Figure 4.89 that maximum adsorption was recorded within the pH range of normal saline water (pH 8). About 89.47 % of TBT was removed from the initial concentration of 5 mg/g TBT by the fly ash at a contact time of 60 min, stirring speed of 160 rpm, temperature of 20 ^oC and pH 8. pH of 8 was therefore chosen as the optimum pH and was used for further studies.

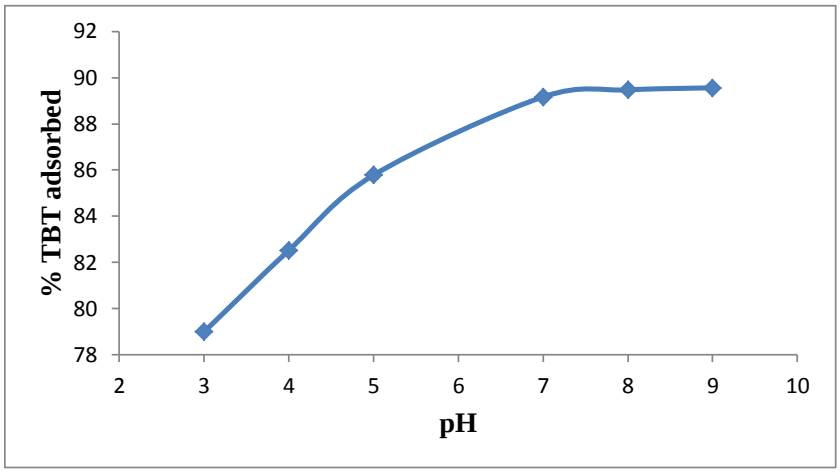

Figure 4.89: Effect of pH on TBT adsorption onto fly ash

Experimental conditions: Concentration of TBT = 100 mg/L; Volume of TBT solution = 25 mL, Mass of fly ash = 0.5 g; Contact time = 60 min; Stirring speed = 160 rpm, Temperature = 20 ^oC.

4.12.2.4 Effect of stirring speed

The effect of stirring speed on the adsorption of TBT onto fly ash was studied at a stirring speed of 160 – 200 rpm. The adsorption capacity of the fly ash increases as the stirring speed of the mixture increases. Maximum amount of 4.726 mg/g (94.53 %) of TBT was removed from the initial concentration of 5 mg/g TBT by the fly ash at a contact time of 60

min, pH 8, temperature of 20 ^{o}C and a stirring speed of 200 rpm (Figure 4.90). A stirring speed of 200rpm was therefore used for further studies.

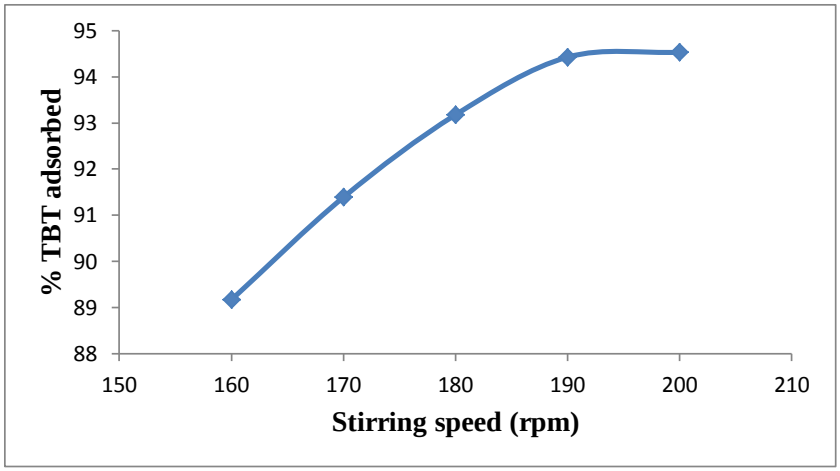

Figure 4.90: Effect of stirring speed on TBT adsorption onto fly ash

Experimental conditions: Concentration of TBT = 100 mg/L; Volume of TBT solution = 25 mL, Mass of fly ash = 0.5 g; Contact time = 60 min; Temperature = 20 ^{o}C.

4.12.2.5 Effect of initial concentration

The effect of initial TBT concentration in the range of 12.5 to 100 mg/L on adsorption was investigated. Along with pH, all parameters were kept constant in this study. It is evident from Figure 4.91 that, as the concentration of TBT increases, the amount adsorbed increases and an increase in percentage removal was also observed. This is due to the fact that the initial TBT concentration provides the necessary driving force to overcome the resistances to the mass transfer of TBT between the aqueous phase and the solid phase.

The increase in the initial TBT concentration also enhances the interaction between TBT and the fly ash adsorbent. Therefore, an increase in the initial concentration of TBT enhances the adsorption uptake of TBT and resulted to higher adsorption. The percentage TBT adsorbed increases from 93.21 to 94.53 % (Figure 4.91) as the initial TBT concentration increases.

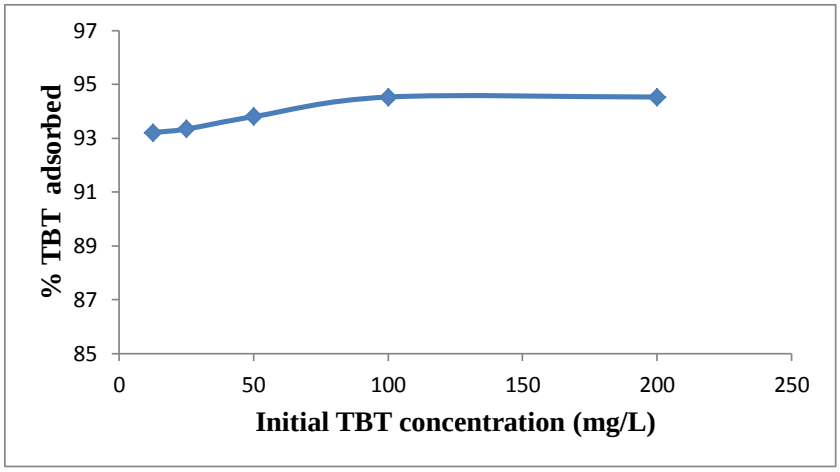

Figure 4.91: Percentage TBT adsorbed by fly ash at various initial TBT concentrations

Experimental conditions: Volume of TBT solution = 25 mL, Mass of fly ash = 0.5 g; pH = 8; Stirring speed = 200 rpm; Contact time = 60 min; Temperature = 20 ^{o}C.

4.12.2.5.1 Adsorption isotherms

The adsorption isotherm plots were presented in Figures 4.92 – 4.95 and parameters obtained for the models were given in Table 4.14. Based on values of correlation coefficient, R^2, summarized in Table 4.14, the adsorption of TBT onto fly ash can be described by the Freundlich adsorption isotherm, probably due to the real heterogeneous nature of the surface sites involved in the process of adsorption.

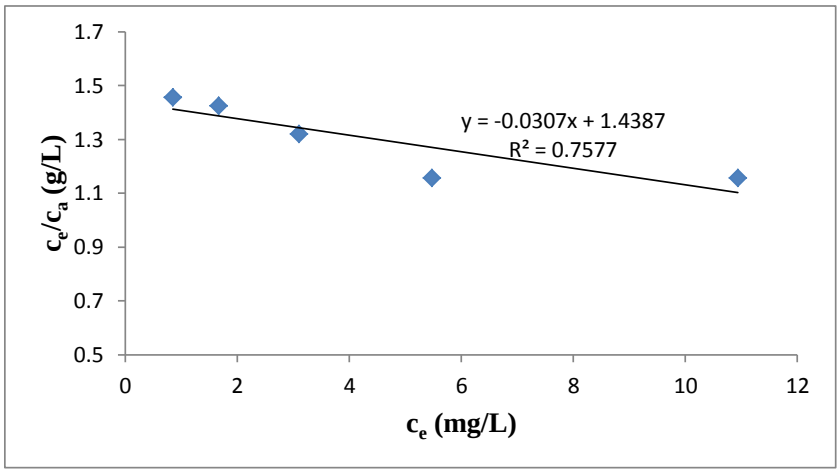

Figure 4.92: Langmuir isotherm for adsorption of TBT onto fly ash

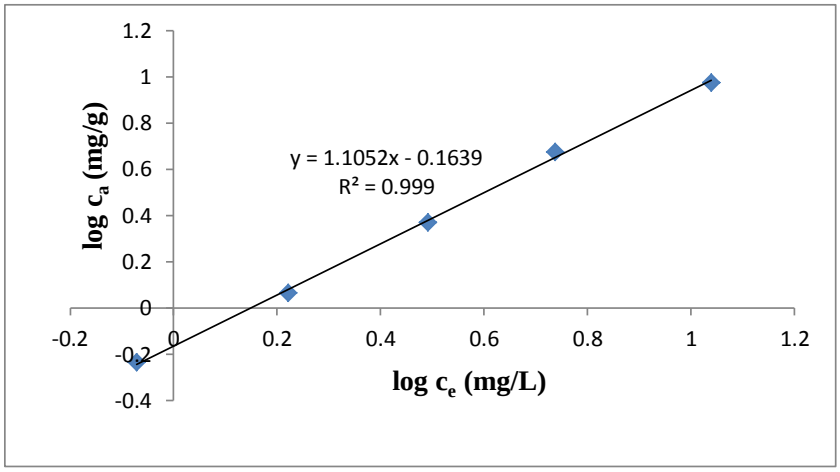

Figure 4.93: Freundlich isotherm for adsorption of TBT onto fly ash

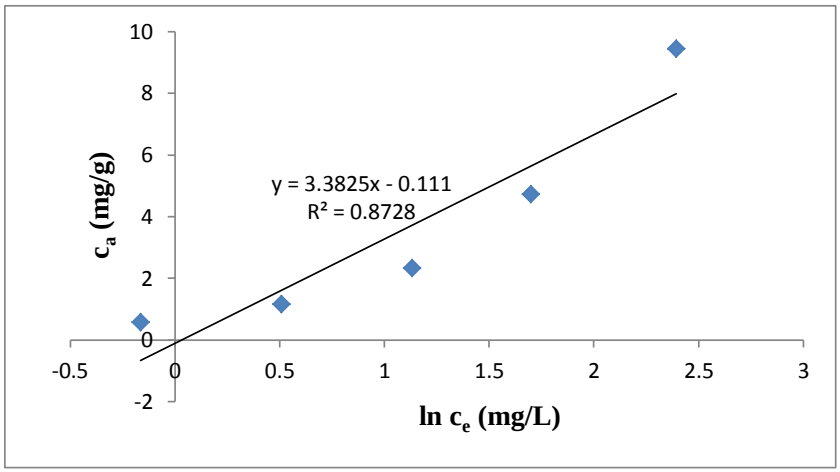

Figure 4.94: Temkin isotherm for adsorption of TBT onto fly ash

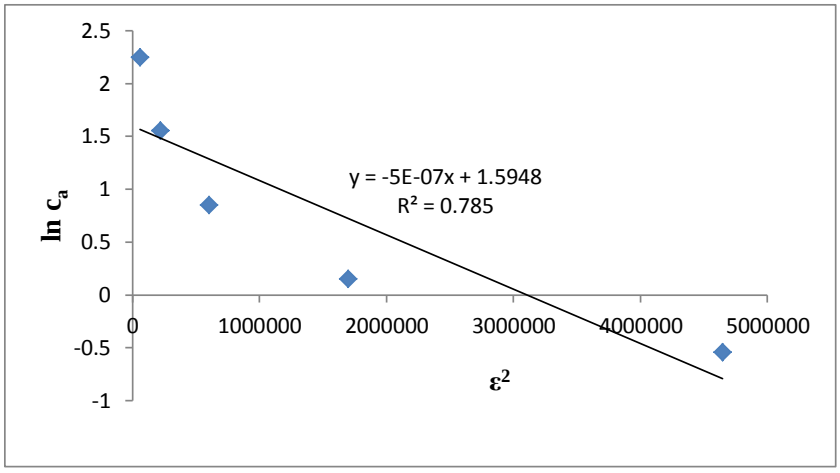

Figure 4.95: D-R isotherm for adsorption of TBT onto fly ash

The values of k_F, k_L, k_T and k_{D-R} constants obtained are 0.6856 mg/g (L/mg)$^{1/n}$, -0.02134 L/mg, 0.9677 mg/L and 5 x 10-7 J^2/mol^2, respectively (Table 4.14). Moreover, the negative value of the Langmuir constants, A_{max} (mg/g) and k_L (L/mg) for TBT adsorption

onto fly ash indicate the inadequacy of the Langmuir model to fit the process (Maarof and Hameed, 2004). Thus, Freundlich model is the best model to explain the adsorption behaviour of TBT onto fly ash.

Table 4.14: Isotherms constants for the adsorption of TBT onto fly ash

Equilibrium models	
Freundlich	
k_F [mg/g (L/mg)$^{1/n}$]	0.6856
n_F	0.9048
R^2	0.9990
Langmuir	
K_L (L/mg)	-0.02134
A_{max} (mg/g)	-32.5733
R^2	0.7577
Temkin	
n_T (L/g)	3.3825
k_T (mg/L)	0.9677
b_T (J/mol)	720.18
R^2	0.8728
Dubinin-Redushkevich	
k_{D-R} (J^2/mol^2)	5 x 10^{-7}
q_m (mg/g)	4.9273
E (J/mol)	1000
R^2	0.7850

4.12.2.6 Effect of temperature

The experimental results obtained on the effect of temperature (Figure 4.96) show that the adsorption capacity of fly ash increases with increase in the solution temperature. This indicates that the adsorption of TBT onto fly ash is endothermic in nature. The increase in the rate of adsorption with the increase in temperature may be attributed to the strong adsorptive forces between the active sites of fly ash and TBT and also between the adjacent molecules of the adsorbed phases. Approx. 95.75 % of TBT was removed from the initial concentration of 100 mg/L TBT by the fly ash at a contact time of 60 min, pH 8, stirring speed of 200 rpm and a temperature of 80 ^oC.

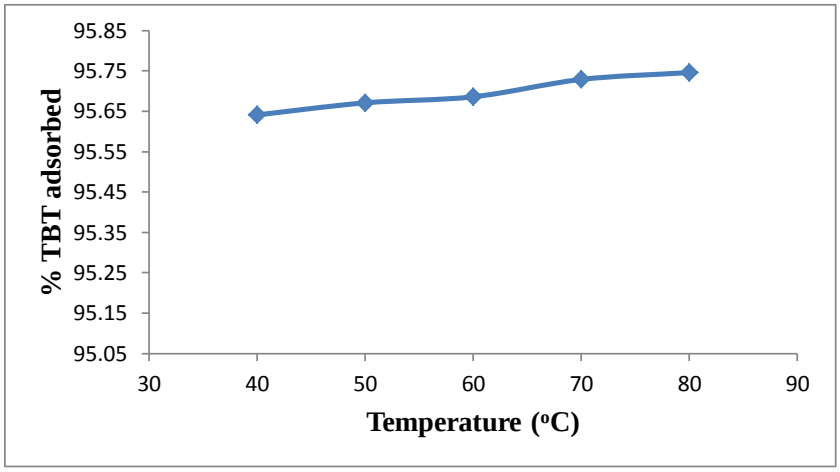

Figure 4.96: Effect of temperature on TBT adsorption onto fly ash

Experimental conditions: Concentration of TBT = 100 mg/L; Volume of TBT solution = 25 mL, Mass of fly ash = 0.5 g; Contact time = 60 min; pH = 8; Stirring speed = 200 rpm.

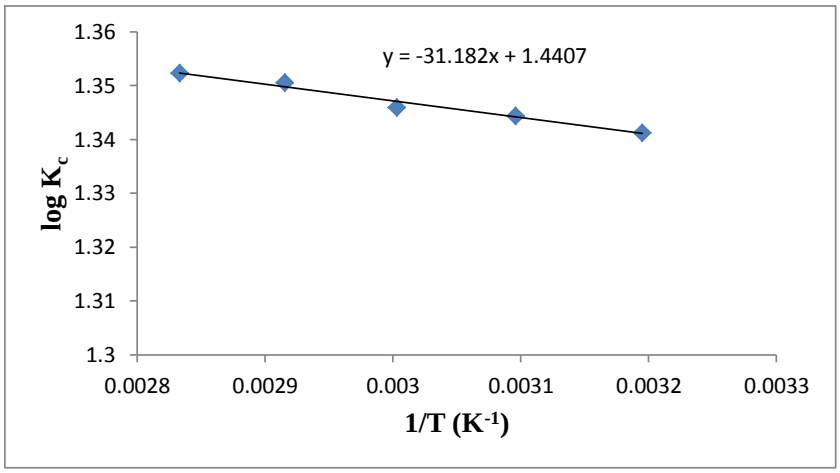

Figure 4.97: Van't Hoff plot for the adsorption of TBT onto fly ash

Figure 4.97 thus shows the Van't Hoff plot for the adsorption of TBT onto fly ash and the variation in the extent of adsorption with respect to temperature (ΔH^{o}, ΔS^{o}, and ΔG^{o}) are presented in Table 4.15.

Table 4.15: Thermodynamic parameters for adsorption of TBT onto fly ash

Temperature (°C)	ΔG° (kJ/mol)	ΔS° (J/K/mol)	ΔH° (kJ/mol)	K_c
40	-8.036	27.5853	0.5970	21.94
50	-8.312			22.10
60	-8.580			22.18
70	-8.867			22.41
80	-9.138			22.51

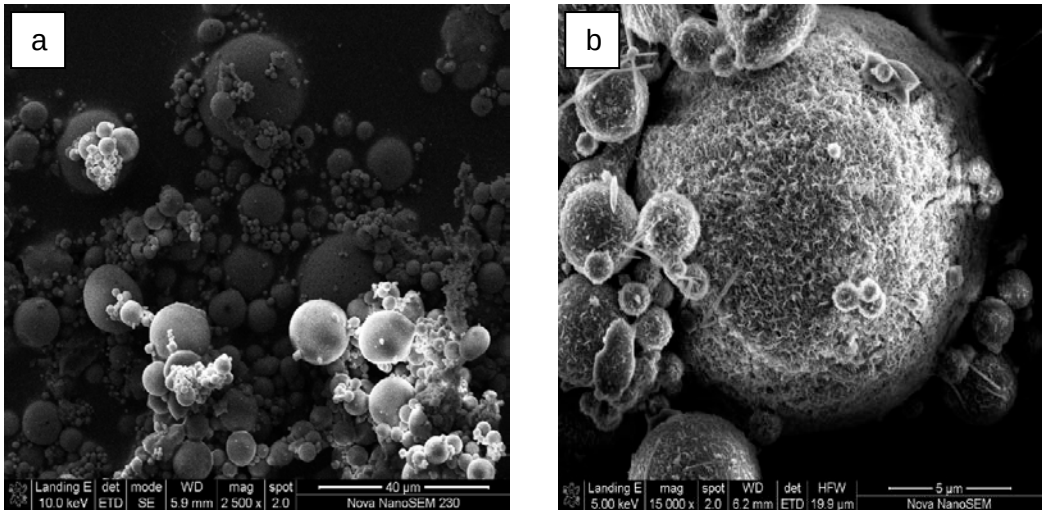

Figure 4.98: SEM of fly ash before (a) and after (b) TBT adsorption

The positive value of ΔH^{o} (0.5970 kJ/mol) for the intervals of temperatures (Table 4.15) shows the endothermic nature of the adsorption process. The positive value of ΔS^{o} (27.5853 J/K/mol) corresponds to increase in degree of freedom of the adsorbed TBT and suggest the increase in concentration of adsorbate in solid–solution interface indicating an increase in adsorbate concentration onto the solid phase. ΔG^{o} values were found to be more negative as the temperature increases, which indicates spontaneous adsorption and the degree of spontaneity of the reaction increases with increase in temperature.

The SEM analysis of the fly ash before and after adsorption (optimal condition) is presented in Figure 4.98 while the TBT chromatogram after adsorption of 100 mg/L TBT with 0.5g of fly ash, contact time of 60min, temperature 20 ^{o}C and a stirring speed of 200 rpm is as shown in Figure 4.99.

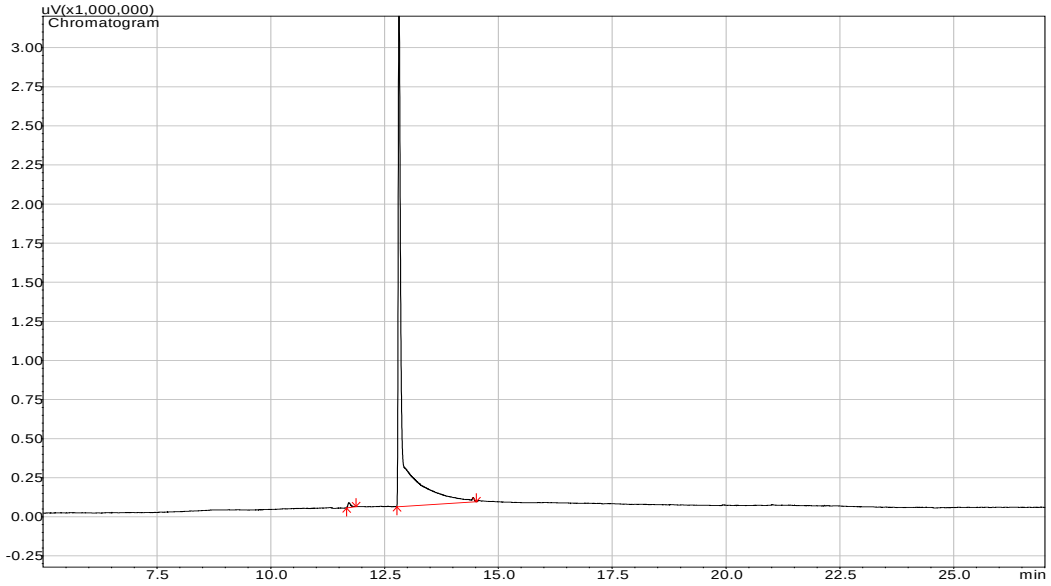

Figure 4.99: Representative TBT chromatogram after adsorption of 100 mg/L TBT with 0.5g of fly ash, contact time of 60min, temperature 20 ^{o}C and a stirring speed of 200 rpm

4.12.3 Adsorption of TBT from TBT-contaminated artificial seawater onto nFe_3O_4

4.12.3.1 Effect of adsorbent amount

The amount of adsorbent (adsorbent dose) ranging from 0.0625 – 1.0 g per 25 mL of TBT solution was investigated on the efficiency of the adsorption process. A graph of the percentage of TBT adsorbed (C_a), mg/g on the adsorbent was plotted against the adsorbent amount (Figure 4.100).

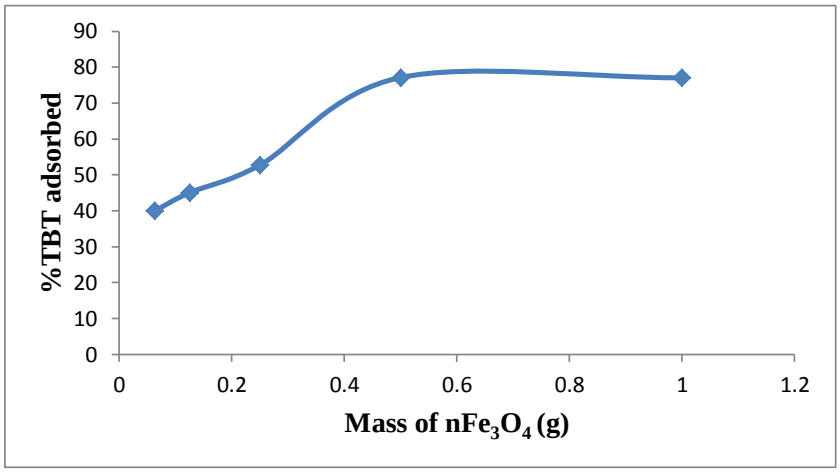

Figure 4.100: Adsorption efficiencies of TBT onto nFe_3O_4

Experimental conditions: Concentration of TBT = 100 mg/L; Volume of TBT solution = 25 mL, Contact time = 60 min; Stirring speed = 160 rpm, Temperature = 20 ^{o}C.

It was observed that the percentage adsorption increases with increasing adsorbent amount, reaching an optimum at 0.5 g for the nFe_3O_4, corresponding to 77.15 %. 0.5 g was selected as the optimum adsorbent amount utilized for further studies.

4.12.3.2 Effect of contact time

Adsorption kinetic study was carried out by shaking 0.5 g of the adsorbents in 25 mL of TBT solutions with an initial concentration of 100 mg/L (pH 8) at 20 ^oC. After pre-defined contact time (10 – 70 min), the aqueous samples were filtered, and the concentration of TBT in the filtrate was determined.

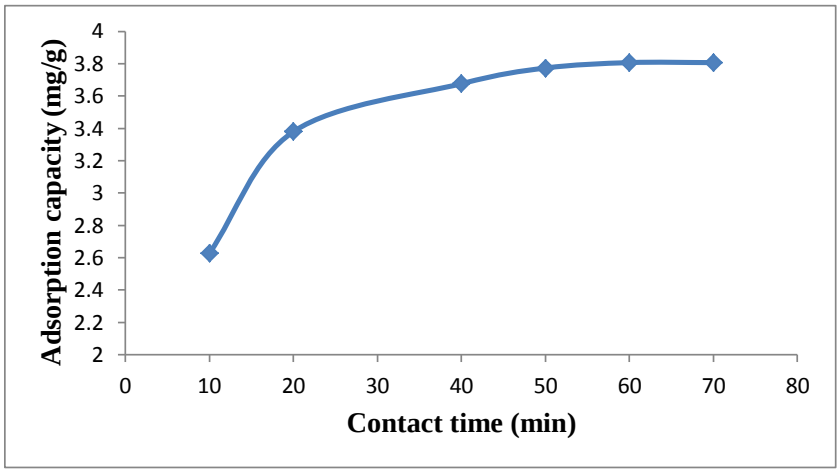

Figure 4.101: Effect of contact time on TBT adsorption onto nFe_3O_4

Experimental conditions: Concentration of TBT = 100 mg/L; Volume of TBT solution = 25 mL, Mass of nFe_3O_4 = 0.5 g; Stirring speed = 160 rpm, Temperature = 20 ^oC.

Figure 4.101 thus shows the effect of contact time on the adsorption of TBT by nano iron (III) oxide (nFe_3O_4). The TBT removal efficiencies at different time intervals ranging from 10 – 70 min were obtained. It was observed that equilibrium was approximately achieved within 60 min and the corresponding TBT removal efficiency for nFe_3O_4 from the initial concentration of 100 mg/L TBT by the nFe_3O_4 reaches 3.81 mg/g (76.15 %).

4.12.3.2.1 Adsorption Kinetics

Figures 4.102 – 4.105 show the pseudo first-order, pseudo second-order, Elovich, fractional power and intraparticle diffusivity kinetic plots, respectively while Table 4.16 provides the evaluated parameters of all the kinetics models. The value of correlation coefficient (R^2) of the pseudo second-order kinetic model (> 0.999) is higher than that of all other models indicating that the kinetic model for the adsorption of TBT onto nFe_3O_4 is pseudo second-order.

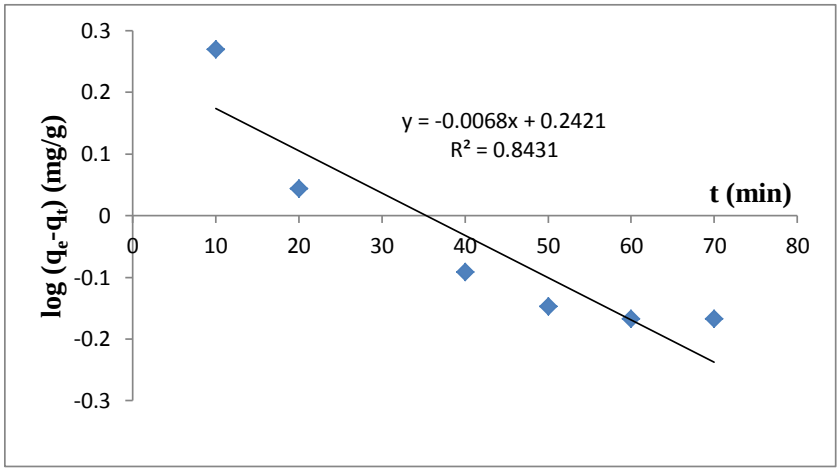

Figure 4.102: Pseudo first-order rate equation plot for TBT adsorption onto nFe_3O_4

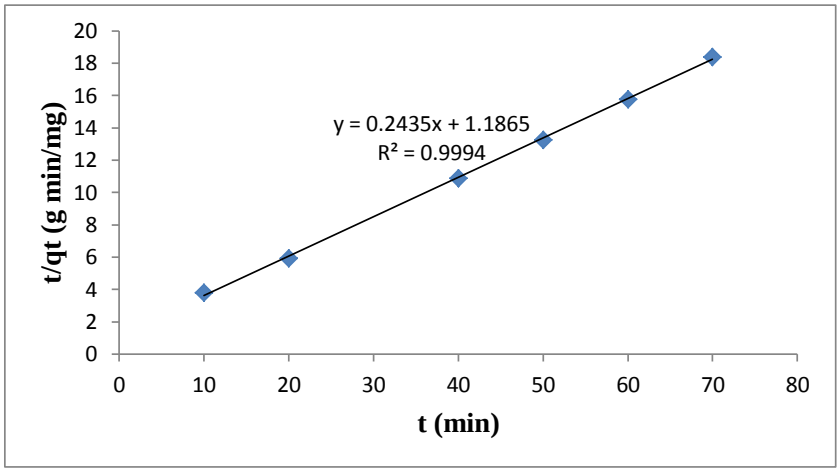

Figure 4.103: Pseudo second-order rate equation plot for TBT adsorption onto nFe_3O_4

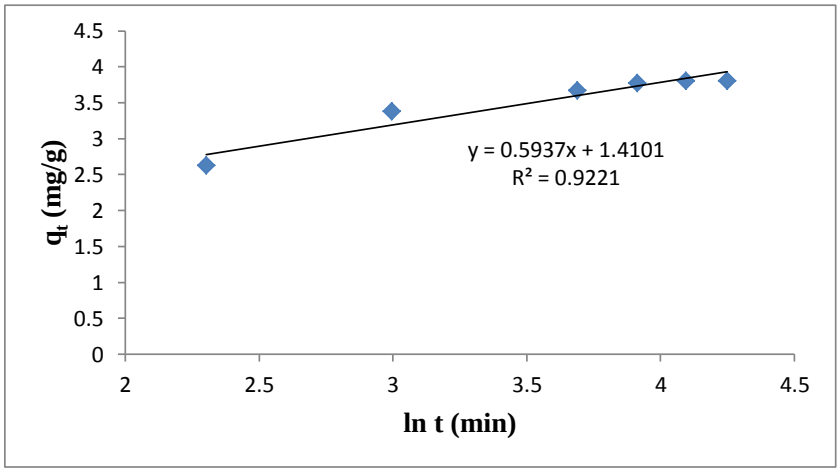

Figure 4.103: Elovich rate equation plot for TBT adsorption onto nFe_3O_4

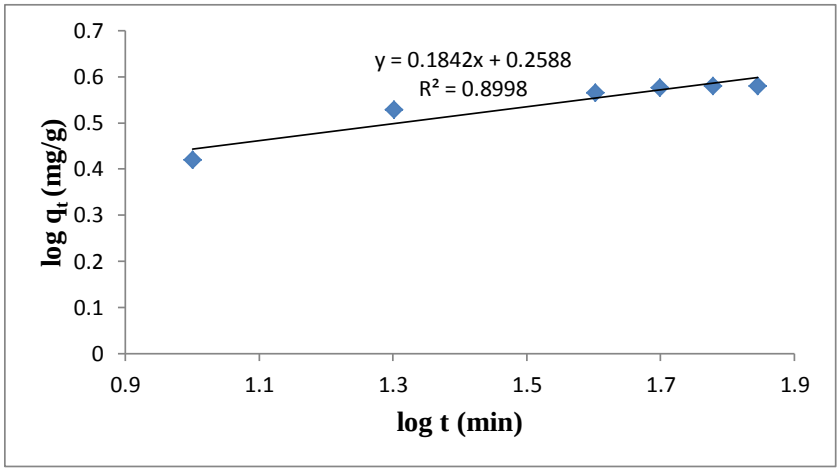

Figure 4.104: Fractional Power rate equation plot for TBT adsorption onto nFe_3O_4

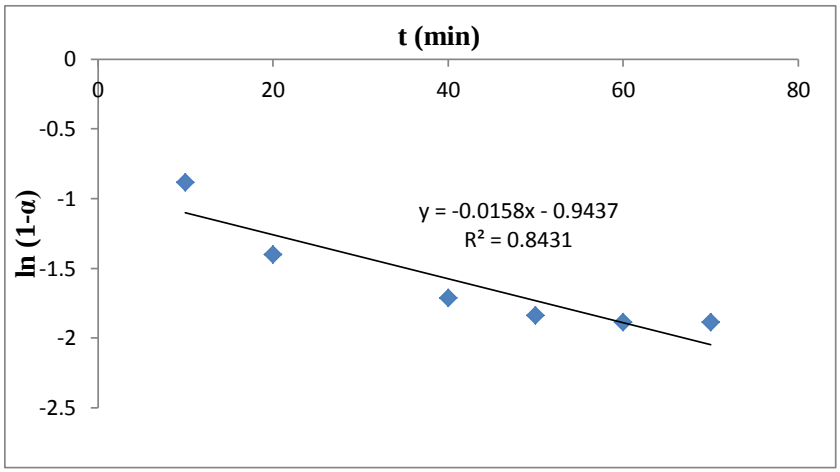

Figure 4.105: Intraparticle diffusivity plot for TBT adsorption onto nFe_3O_4

The results also indicate that the power function model satisfactorily describes the time-dependence of TBT on the nFe_3O_4 as the value of the constant v is less than 1. In the present study, the value of the initial adsorption rates, h_o, obtained for the pseudo second-order kinetics is 0.8428 mg/g/min (nFe_3O_4). The kinetic model constants k_1, k_2, β, α_E, k_3 and k_p are 0.0157 min^{-1}, 0.05 g/mg/min, 1.684 gmin/mg, 18.11 $gmin^2/mg$, 1.815 mg/g and 0.0158 min^{-1}, respectively.

Table 4.16: Kinetic model parameters for TBT adsorption onto nFe_3O_4

Kinetic models	
Pseudo first-order	
k_1 (min^{-1})	0.0157
q_e (mg/g)	1.7462
R^2	0.8431
Pseudo second-order	
q_e (mg/g)	4.1068
h_o (mg/g/min)	0.8428
k_2 (g/mg/min)	0.0500
R^2	0.9994
Elovich	
β (g min/mg)	1.6844
α (g min^2/mg)	18.1109
R^2	0.9221
Fractional Power	
v (min^{-1})	0.1842
k_3 (mg/g)	1.8147
k_3v (mg/g/min)	0.3343
R^2	0.8998
Intraparticle diffusivity	
k_p (min^{-1})	0.0158
R^2	0.8431

4.12.3.3 Effect of pH

The effect of pH on the adsorption of TBT onto nFe_3O_4 was studied at pH 3 – 9. It was observed from Figure 4.106 that the percentage of TBT adsorbed by the adsorbents steadily increases as the pH of the solution increases from pH 3 – 8, and reaches equilibration at pH ≥ 8. It is also evident that maximum adsorption was recorded within the pH range of normal saline water (pH 8) and pH 8 was used for further studies.

About 77.30 % of TBT was removed from the initial concentration of 100 mg/L TBT by the nFe_3O_4 at a contact time of 60 min, stirring speed of 160 rpm, pH 8 and a temperature of 20 ^oC.

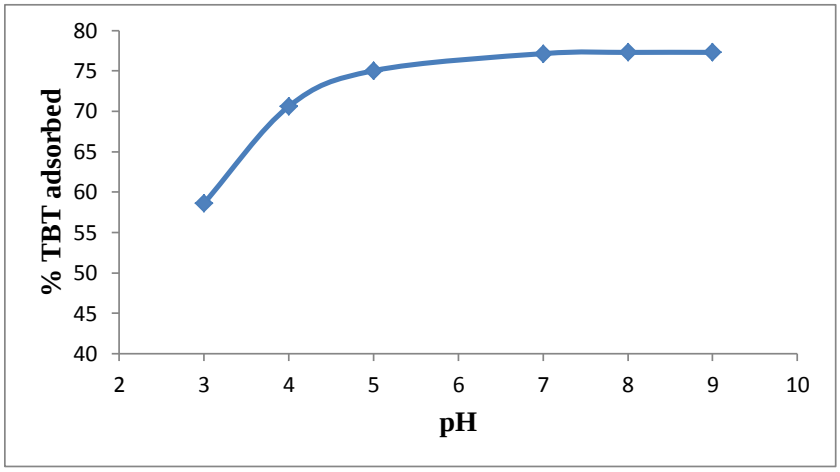

Figure 4.106: Effect of pH on TBT adsorption onto nFe_3O_4

Experimental conditions: Concentration of TBT = 100 mg/L; Volume of TBT solution = 25 mL, Mass of nFe_3O_4 = 0.5 g; Contact time = 60 min; Stirring speed = 160 rpm, Temperature = 20 ^oC.

4.12.3.4 Effect of stirring speed

The effect of stirring speed on the adsorption of TBT onto the nFe_3O_4 was studied at a stirring speed of 160 – 200 rpm.

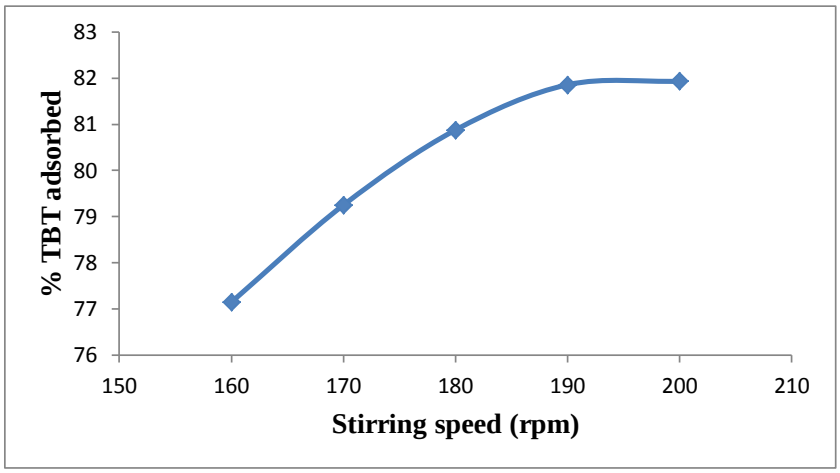

Figure 4.107: Effect of stirring speed on TBT adsorption onto nFe_3O_4

Experimental conditions: Concentration of TBT = 100 mg/L; Volume of TBT solution = 25 mL, Mass of nFe_3O_4 = 0.5 g; Contact time = 60 min; Temperature = 20 ^oC.

The adsorption capacity of nFe_3O_4 also increases with increase in the stirring speed and maximum amount of 81.93 % of TBT was removed from the initial concentration of 100 mg/L TBT by the nFe_3O_4 at a contact time of 60 min, pH 8, a temperature of 20 ^oC and a stirring speed of 200 rpm (Figure 4.107).

4.12.3.5 Effect of initial concentration

Figure 4.108 therefore shows that the adsorption of TBT onto the nFe_3O_4 increases as the initial TBT concentration increases from 12.5 to 100 mg/L, indicating that adsorption is also favourable for the higher TBT concentrations that have been investigated.

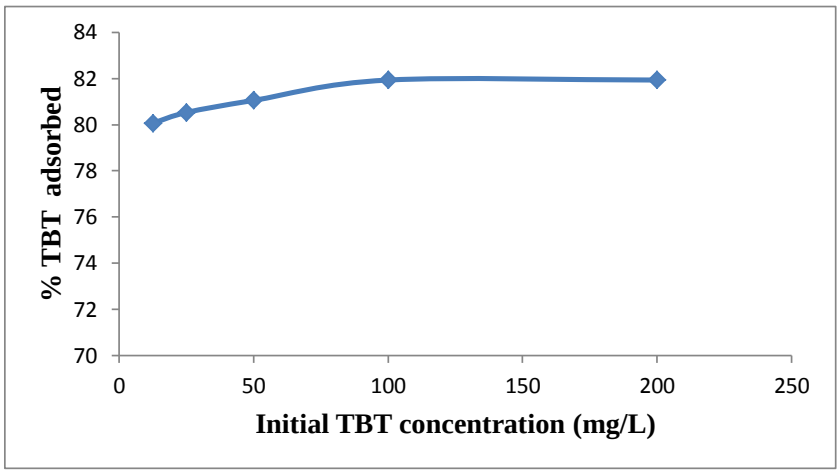

Figure 4.108: Percentage TBT adsorbed by nFe_3O_4 at various initial TBT concentrations

Experimental conditions: Volume of TBT solution = 25 mL, Mass of nFe_3O_4 = 0.5 g; pH = 8; Stirring speed = 200 rpm; Contact time = 60 min; Temperature = 20 ^{o}C.

The increase in the adsorption capacity of nFe_3O_4 with an increase in the initial TBT concentration can be attributed to increase in the driving force due to concentration gradient developed between the bulk solution and surface of the adsorbents (Kumar et al., 2010). At higher concentration of TBT, the active sites of the nFe_3O_4 were surrounded by much more TBT and the process of adsorption continues, leading to an increased uptake of TBT from the solution. Therefore, the values of C_a increased with the increase in the initial TBT concentrations.

4.12.3.5.1 Adsorption isotherms

The adsorption isotherm parameters obtained from all the equilibrium models for the adsorption of TBT onto nFe_3O_4 were given in Table 4.17 and the plots are presented in Figures 4.109 – 4.112. The figures show that the experimental data fitted well with Freundlich model for the nFe_3O_4 used and the value of n_F, for the adsorbent, falling in the range 1 -10 indicates favourable adsorption.

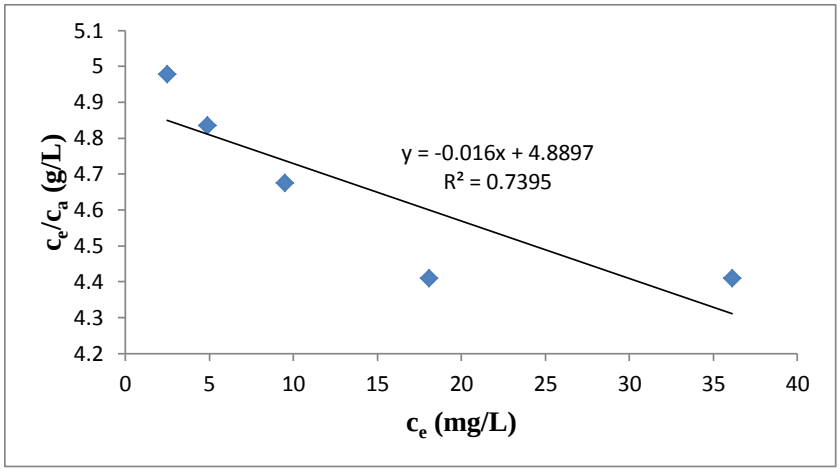

Figure 4.109: Langmuir isotherm for adsorption of TBT onto nFe_3O_4

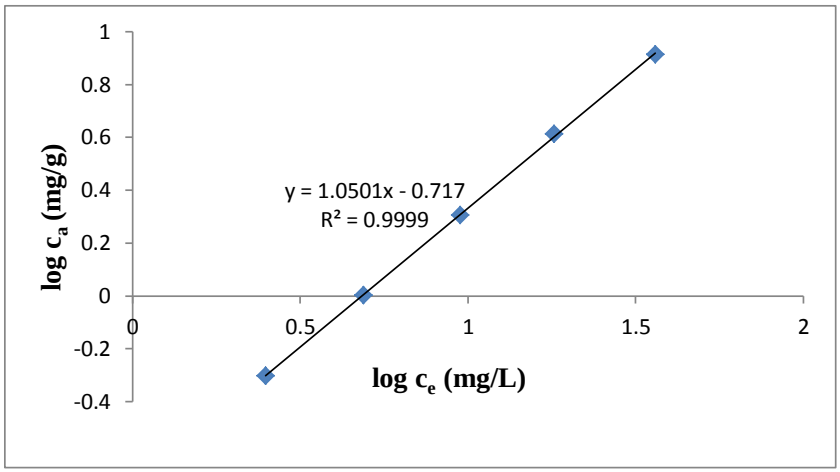

Figure 4.110: Freundlich isotherm for adsorption of TBT onto nFe_3O_4

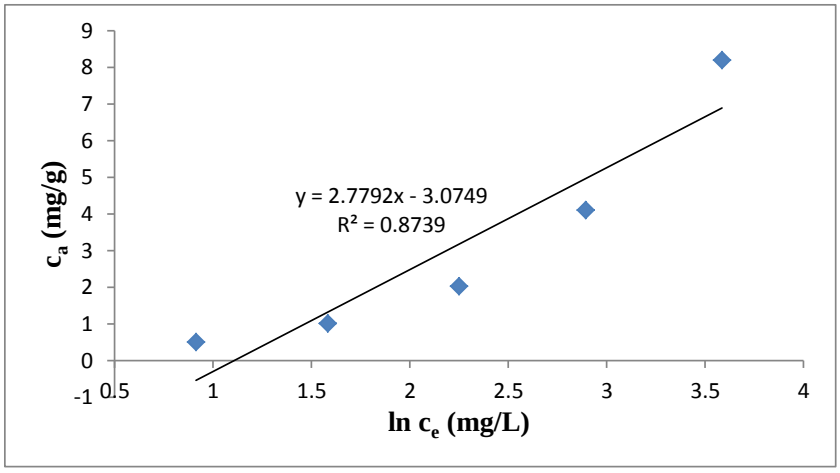

Figure 4.111: Temkin isotherm for adsorption of TBT onto nFe_3O_4

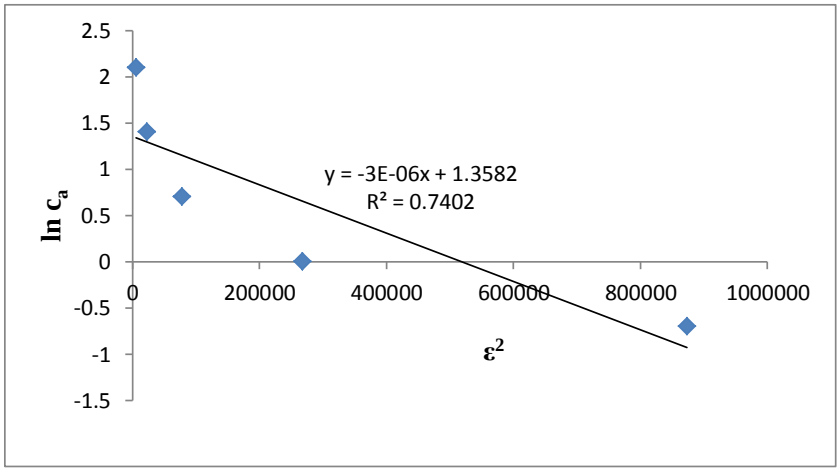

Figure 4.112: D-R isotherm for adsorption of TBT onto nFe_3O_4

Table 4.17: Isotherms constants for the adsorption of TBT onto nFe_3O_4

Equilibrium models	
Freundlich	
k_F [mg/g (L/mg)$^{1/n}$]	0.1919
n_F	0.9523
R^2	0.9999
Langmuir	
K_L (L/mg)	-0.0033
A_{max} (mg/g)	-62.5
R^2	0.7395
Temkin	
n_T (L/g)	2.7792
k_T (mg/L)	0.3307
b_T (J/mol)	876.51
R^2	0.8739
Dubinin-Redushkevich	
k_{D-R} (J^2/mol^2)	3 x 10^{-6}
q_m (mg/g)	3.8892
E (J/mol)	408.25
R^2	0.7402

Moreover, the negative value of the Langmuir constant, A_{max} (mg/g) for TBT adsorption onto nFe_3O_4 also indicates the inadequacy of the Langmuir model to fit the process. Thus, Freundlich model is the best model to explain the adsorption behaviour of TBT onto the nFe_3O_4. The negative value obtained for the Langmuir model is supported by the work reported by Maarof and Hameed, 2004.

4.12.3.6 Effect of temperature

The experimental results obtained on the effect of temperature for the adsorption of TBT onto nFe_3O_4 (Figure 4.113) show that the adsorption capacity increases with increase in the solution temperature from 40 ^oC – 60 ^oC after which equilibration was attained. This indicates that the adsorption of TBT onto nFe_3O_4 is endothermic. The increase in the rate of adsorption with the increase in temperature may be attributed to the strong adsorptive forces between the active sites of nFe_3O_4 and TBT species and also between the adjacent molecules of the adsorbed phases.

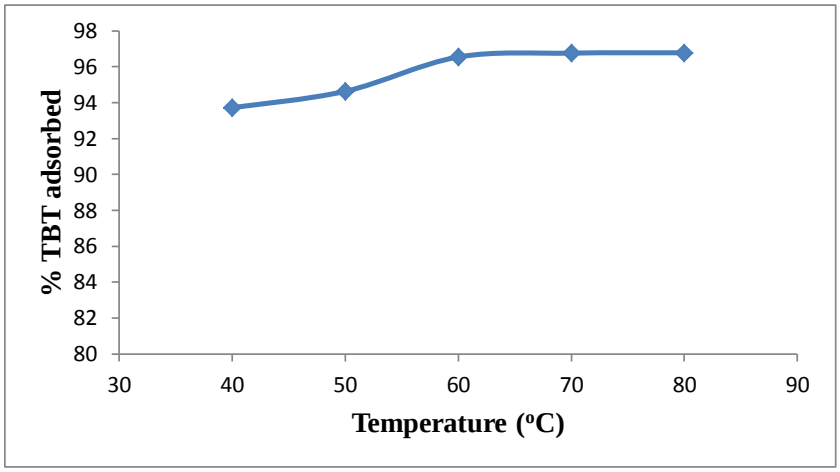

Figure 4.113: Effect of temperature on TBT adsorption onto nFe_3O_4

Experimental conditions: Concentration of TBT = 100 mg/L; Volume of TBT solution = 25 mL, Mass of nFe_3O_4 = 0.5 g; Contact time = 60 min; pH = 8; Stirring speed = 200 rpm.

Approximately 96.78 % of TBT was removed from the initial concentration of 100 mg/L TBT by nFe_3O_4 at a temperature of 80 ^oC, contact time of 60 min, pH 8 and a stirring speed of 200 rpm. Figure 4.114 thus shows the Van't Hoff plot for the adsorption of TBT onto nFe_3O_4 while ΔH^o , ΔS^o , and ΔG^o are presented in Table 4.18.

Table 4.18: Thermodynamic parameters for the adsorption of TBT onto nFe_3O_4

Temperature (°C)	ΔG° (kJ/mol)	ΔS° (J/K/mol)	ΔH° (kJ/mol)	K_c
40	-7.036	79.9259	17.885	14.94
50	-7.708			17.64
60	-9.221			27.96
70	-9.688			29.88
80	-9.989			30.08

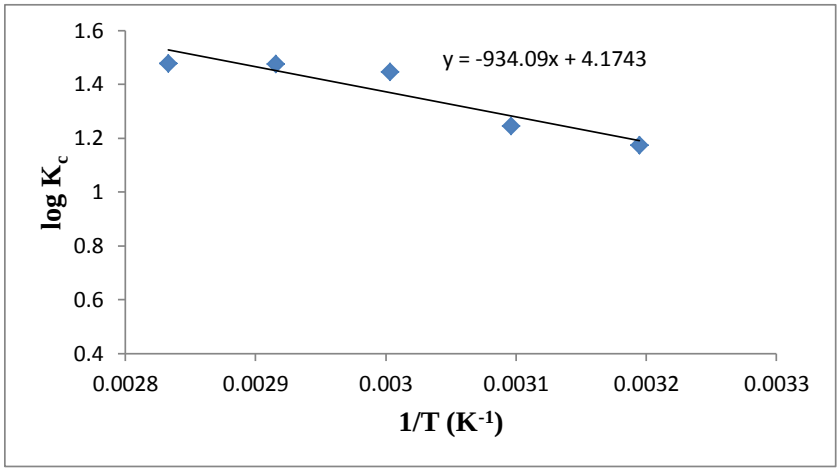

Figure 4.114: Van't Hoff plot for the adsorption of TBT onto nFe_3O_4

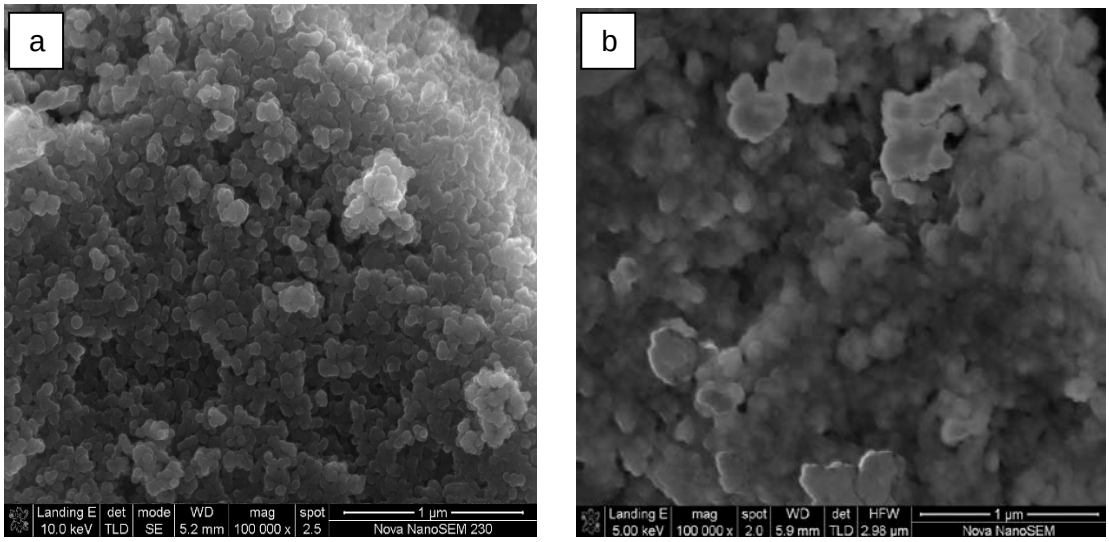

Figure 4.115: SEM of nFe_3O_4 before (a) and after (b) TBT adsorption

The positive value of ΔH^{o} for the intervals of temperatures (17.89 kJ/mol) also shows the endothermic nature of the adsorption process. The positive value of ΔS^{o} (79.73 J/K/mol) corresponds to increase in degree of freedom of the adsorbed TBT onto the nFe_3O_4 and suggest the increase in concentration of adsorbate in solid–solution interface indicating an increase in adsorbate concentration onto the solid phase. It is evident from Table 4.18 that ΔG^{o} values were found to be more negative as the temperature increases, which indicates that the adsorption efficiency of TBT onto nFe_3O_4 increases with increase in temperature.

The SEM analysis of nFe_3O_4 before and after adsorption (optimal condition) is presented in Figure 4.115 while the TBT chromatogram after adsorption of 100 mg/L TBT with 0.5g of nFe_3O_4, contact time of 60min, temperature 20 ^{o}C and a stirring speed of 200 rpm is as shown in Figure 4.116.

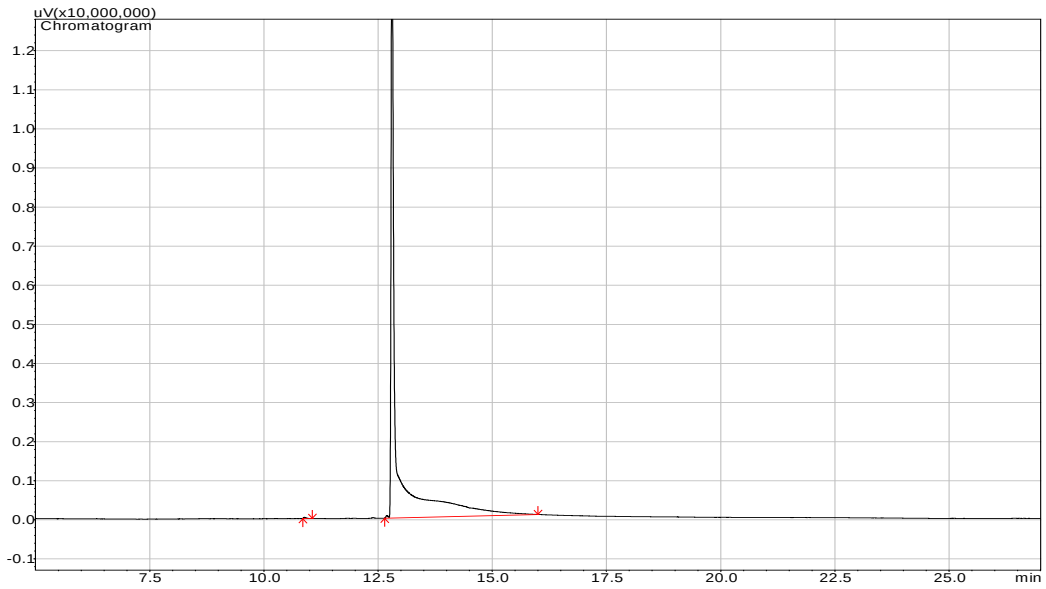

Figure 4.116: Representative TBT chromatogram after adsorption of 100 mg/L TBT with 0.5g of nFe_3O_4, contact time of 60min, temperature 20 ^oC and a stirring speed of 200 rpm

4.12.4 Adsorption of TBT from TBT-contaminated artificial seawater onto $nSiO_2$

4.12.4.1 Effect of adsorbent amount

The results on the effect of adsorbent amount on the adsorption of TBT by the nano silica oxide ($nSiO_2$) as shown in Figure 4.117 indicate that the percentage of TBT adsorption increases with increasing adsorbent amount, reaching an optimum at 0.5 g, corresponding to 87.40 % removal by the $nSiO_2$. 0.5 g was selected as the optimum adsorbent amount and was utilized for further studies.

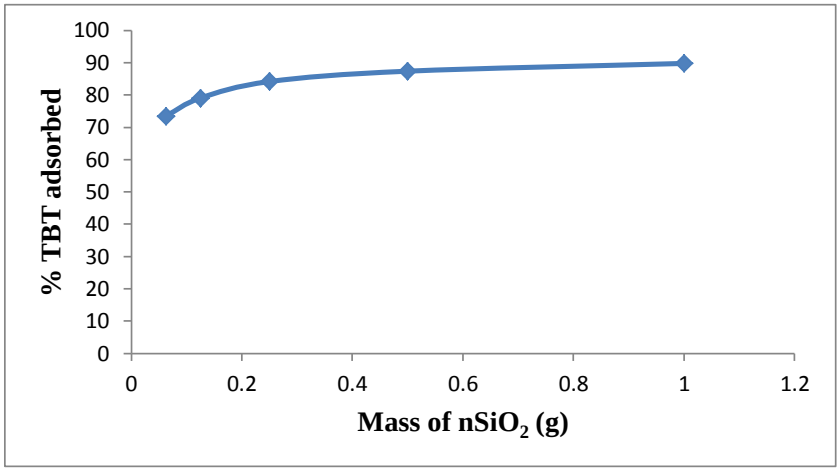

Figure 4.117: Adsorption efficiencies of TBT onto $nSiO_2$

Experimental conditions: Concentration of TBT = 100 mg/L; Volume of TBT solution = 25 mL, Contact time = 60 min; Stirring speed = 160 rpm, Temperature = 20 ^oC.

4.12.4.2 Effect of contact time

Figure 4.118 shows the effect of contact time on the adsorption of TBT by $nSiO_2$. The TBT removal efficiency at different time intervals ranging from 10 to 70 min were obtained.

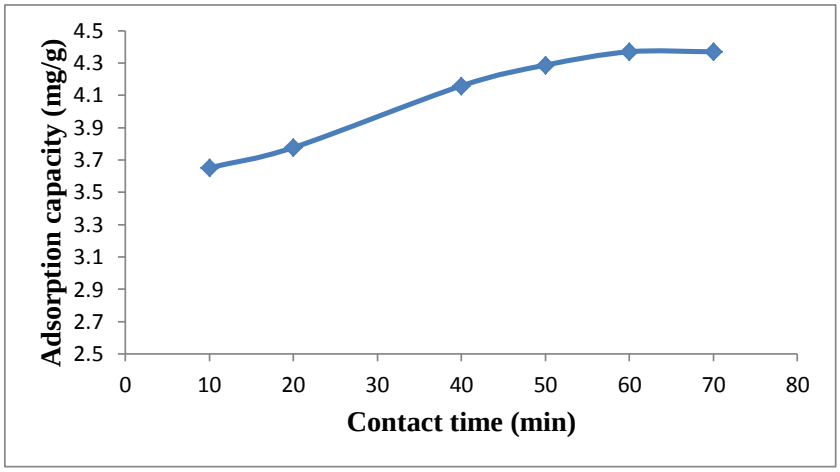

Figure 4.118: Effect of contact time on TBT adsorption onto $nSiO_2$

Experimental conditions: Concentration of TBT = 100 mg/L; Volume of TBT solution = 25 mL, Mass of $nSiO_2$ = 0.5 g; Stirring speed = 160 rpm, Temperature = 20 ^{o}C.

It was observed that equilibrium was approximately achieved within 60 min (Figure 4.118). The amount of TBT removed at a contact time of 60 min from the initial TBT concentration of 5.0 mg/g by the $nSiO_2$ is 4.37 mg/g (87.40 %). 60 min was used for further studies.

4.12.4.2.1 Adsorption kinetics

Figures 4.119 – 4.123 show the pseudo first-order, pseudo second-order, Elovich, fractional power and intraparticle diffusivity kinetic plots and Table 4.19 provides the evaluated parameters of all the kinetics models.

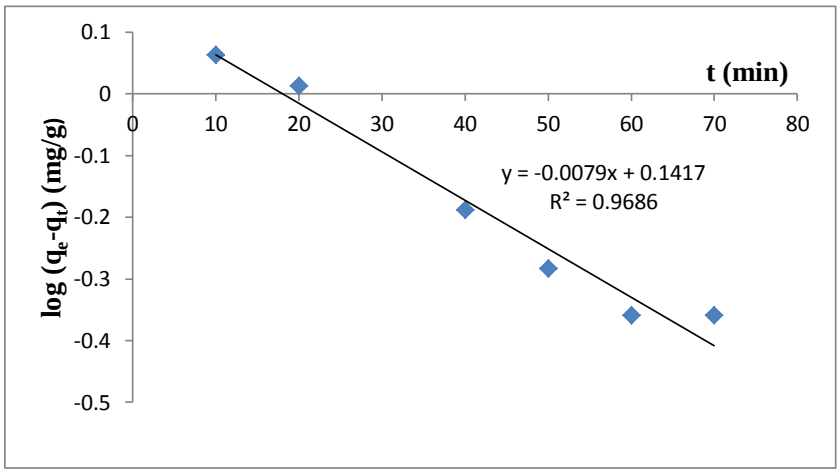

Figure 4.119: Pseudo first-order rate equation plot for TBT adsorption onto $nSiO_2$

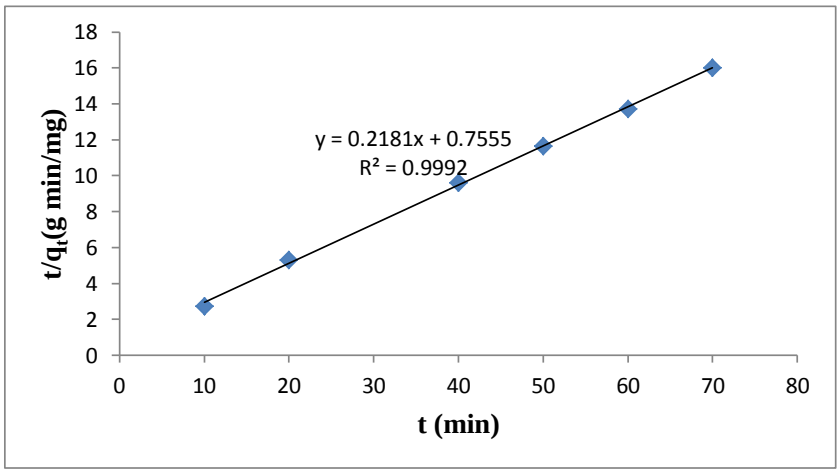

Figure 4.120: Pseudo second-order rate equation plot for TBT adsorption onto $nSiO_2$

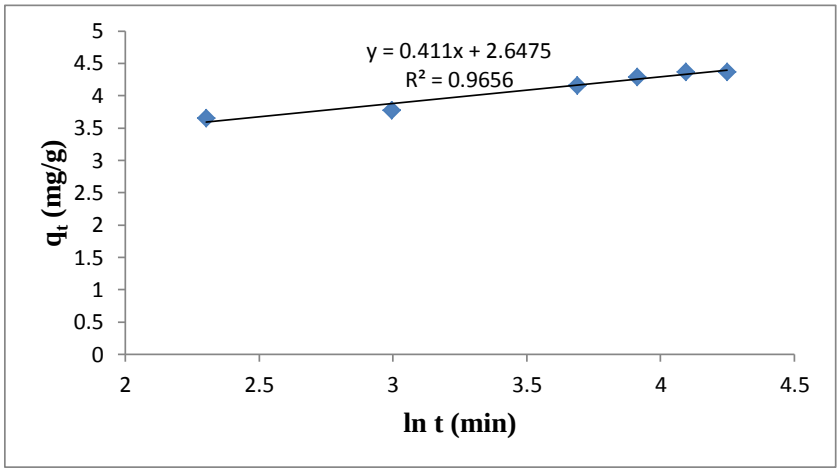

Figure 4.121: Elovich rate equation plot for TBT adsorption onto $nSiO_2$

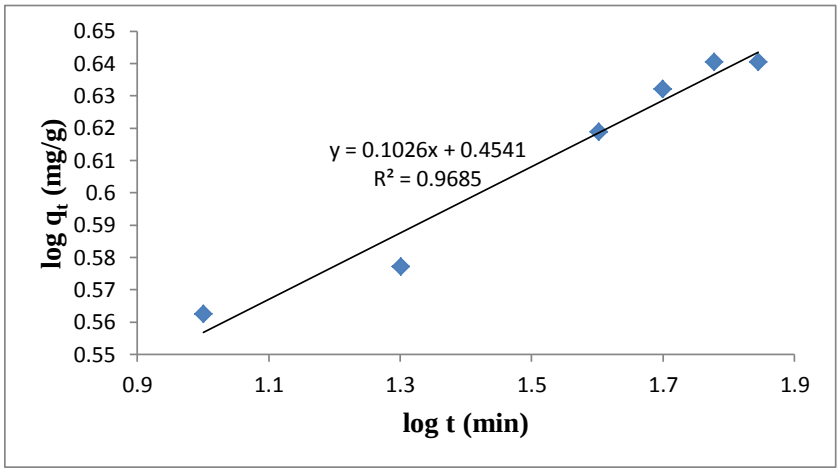

Figure 4.122: Fractional Power rate equation plot for TBT adsorption onto $nSiO_2$

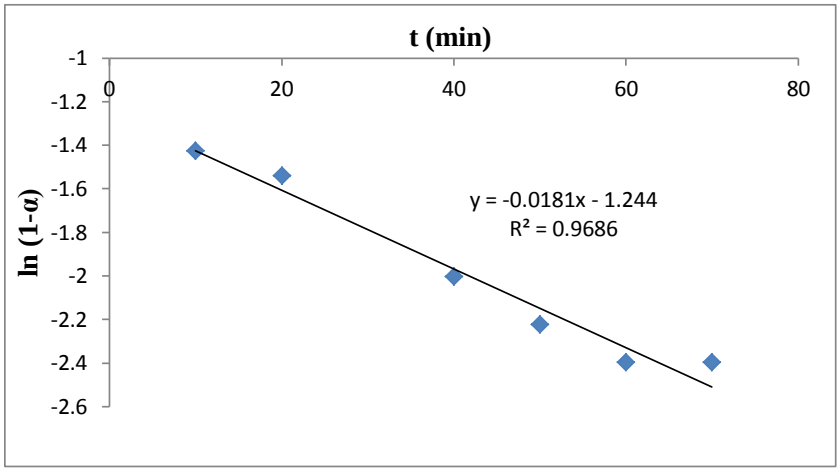

Figure 4.123: Intraparticle diffusivity plot for TBT adsorption onto $nSiO_2$

The results in Table 4.19 show the adsorption rate constant, k_2, initial adsorption rate, h_o, and equilibrium adsorption capacity, q_e, of the pseudo second-order model. The results show a very good compliance with pseudo second-order equation with high regression coefficient (> 0.999) whereas the pseudo first-order and Elovich models were not applicable as low regression coefficients (< 0.97) were observed. The value of q_e obtained for the pseudo second-order kinetics for the adsorption of TBT by the $nSiO_2$ is 1.3236 mg/g/min.

Table 4.19: Kinetic model parameters for TBT adsorption onto $nSiO_2$

Kinetic models	
Pseudo first-order	
k_1 (min^{-1})	0.0182
q_e (mg/g)	1.3858
R^2	0.9686
Pseudo second-order	
q_e (mg/g)	4.5851
h_o (mg/g/min)	1.3236
k_2 (g/mg/min)	0.06296
R^2	0.9992
Elovich	
β (g min/mg)	2.4331
α (g min^2/mg)	1.5266×10^3
R^2	0.9656
Fractional Power	
v (min^{-1})	0.1026
k_3 (mg/g)	2.8451
k_3v (mg/g/min)	2.9477
R^2	0.9685
Intraparticle diffusivity	
k_p (min^{-1})	0.0181
R^2	0.9686

A simple kinetic analysis of the adsorption of TBT onto $nSiO_2$ was also tested according to fractional power model and Table 4.19 shows the estimated parameters of the model. The results indicate that the power model satisfactorily described the time-dependent of TBT on the $nSiO_2$ as the value of the constant v is less than 1 and the regression coefficient is greater than 0.96. The intraparticle diffusivity parameters also show that the adsorption is diffusion controlled (R^2 > 0.96). The kinetic model constants k_1, k_2, β, α_E, k_3 and k_p for the adsorption of TBT onto $nSiO_2$ are therefore 0.0182 min^{-1}, 0.063 g/mg/min, 2.433 gmin/mg, 1.53 x 10^3 $gmin^2/mg$, 2.85 mg/g and 0.0181 min^{-1}, respectively.

4.12.4.3 Effect of pH

The pH is a critical factor that affects both the adsorbent and adsorbate chemistry in solution. The effect of pH on the adsorption of TBT onto $nSiO_2$ was studied at pH 3 – 9. It was observed from Figure 4.124 that the percentage of TBT adsorbed by the adsorbents steadily increases as the pH of the solution increases from pH 3 to pH 8, and reaches equilibration at pH > 8.

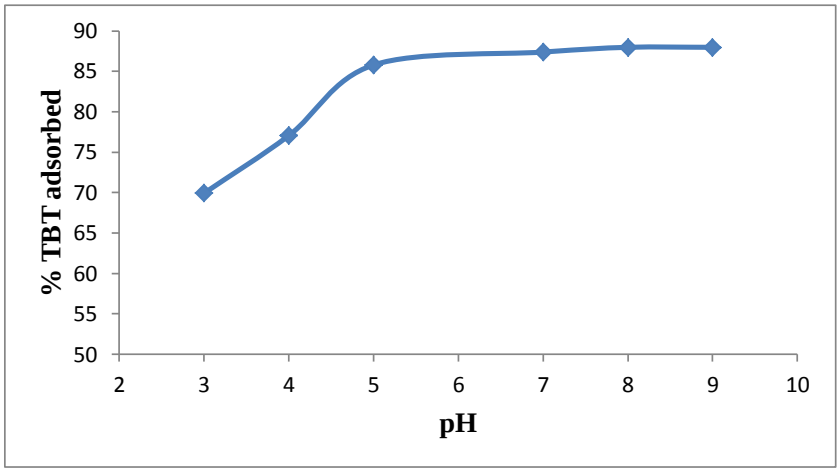

Figure 4.124: Effect of pH on TBT adsorption onto $nSiO_2$

Experimental conditions: Concentration of TBT = 100 mg/L; Volume of TBT solution = 25 mL, Mass of $nSiO_2$ = 0.5 g; Contact time = 60 min; Stirring speed = 160 rpm, Temperature = 20 ^oC.

Maximum adsorption capacity was therefore recorded within the pH range of normal saline water (pH 8). About 87.97 % TBT was removed from the initial concentration of 100 mg/L TBT by the $nSiO_2$ at a contact time of 60 min, stirring speed of 160 rpm and a temperature of 20 ^oC.

4.12.4.4 Effect of stirring speed

The stirring speed of the adsorption process was also studied and optimized. The stirring speed on the adsorption of TBT onto the $nSiO_2$ was studied at a stirring speed of 160 – 200 rpm. The adsorption capacity of the adsorbents therefore increases as the stirring speed of the mixture increases.

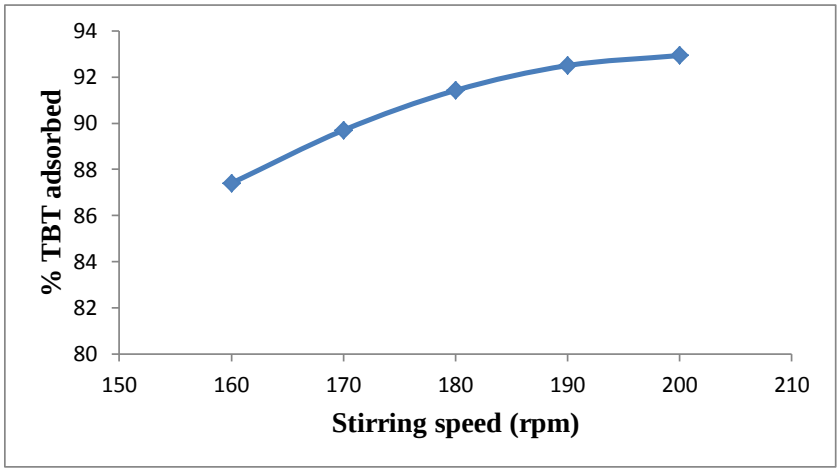

Figure 4.125: Effect of stirring speed on TBT adsorption onto $nSiO_2$

Experimental conditions: Concentration of TBT = 100 mg/L; Volume of TBT solution = 25 mL, Mass of $nSiO_2$ = 0.5 g; Contact time = 60 min; Temperature = 20 ^{o}C.

Approx. 4.65 mg/g (92.93 %) TBT was removed from the initial concentration of 5 mg/g TBT by the $nSiO_2$ at a contact time of 60 min, pH 8, temperature of 20 ^{o}C and a stirring speed of 200 rpm (Figure 4.125).

4.12.4.5 Effect of initial concentration

Figure 4.126 shows that the adsorption of TBT onto $nSiO_2$ increases as the initial TBT concentration increases from 12.5 to 100 mg/L, indicating that the adsorption is also favourable for the higher TBT concentrations that have been investigated.

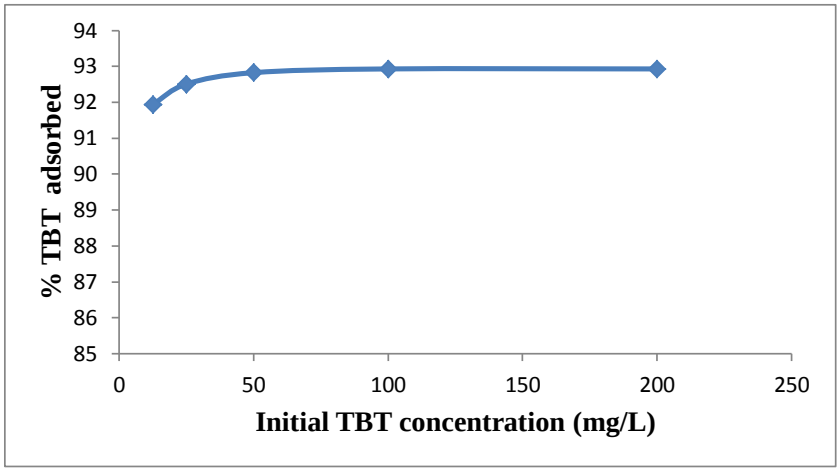

Figure 4.126: Percentage TBT adsorbed by $nSiO_2$ at various initial TBT concentrations

Experimental conditions: Volume of TBT solution = 25 mL, Mass of $nSiO_2$ = 0.5 g; pH = 8; Stirring speed = 200 rpm; Contact time = 60 min; Temperature = 20 ^{o}C.

The increase in the adsorption capacity with an increase in the initial TBT concentration is a result of the increase in the driving force due to concentration gradient developed between the bulk solution and surface of $nSiO_2$.

4.12.4.5.1 Adsorption isotherms

The results indicate that the Freundlich model fit the experiment data well. It is the suitable model for describing this adsorption process, as R^2 value is higher than for other models (Figures 4.127 – 4.130 and Table 4.20), probably due to the real heterogeneous nature of the surface sites involved in the process of adsorption. The value of n_F falling in the range 1 -10 indicates favourable adsorption.

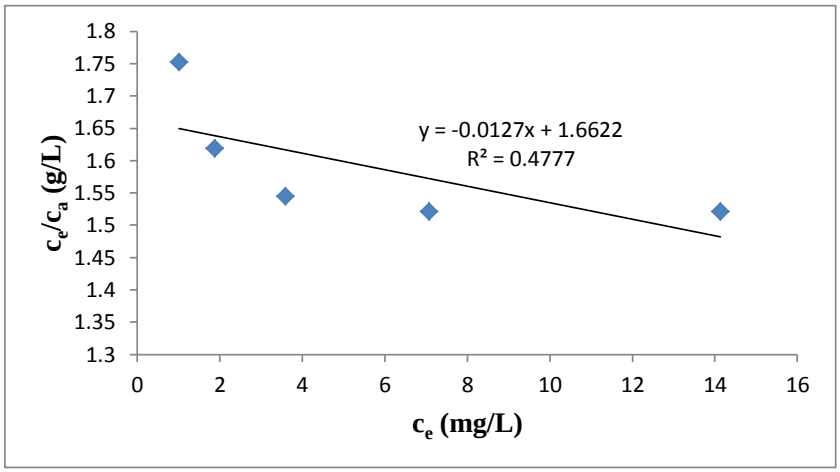

Figure 4.127: Langmuir isotherm for adsorption of TBT onto $nSiO_2$

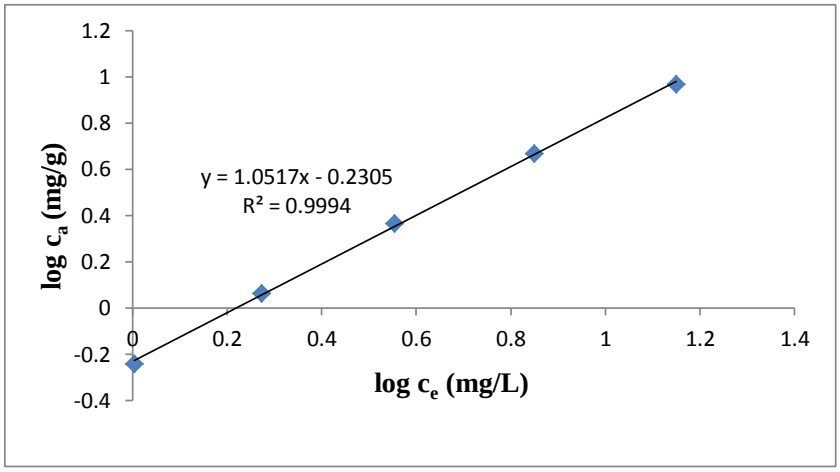

Figure 4.128: Freundlich isotherm for adsorption of TBT onto $nSiO_2$

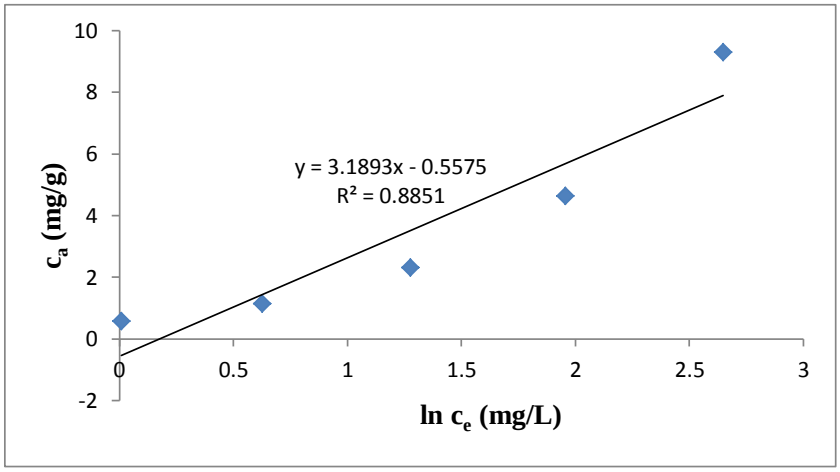

Figure 4.129: Temkin isotherm for adsorption of TBT onto $nSiO_2$

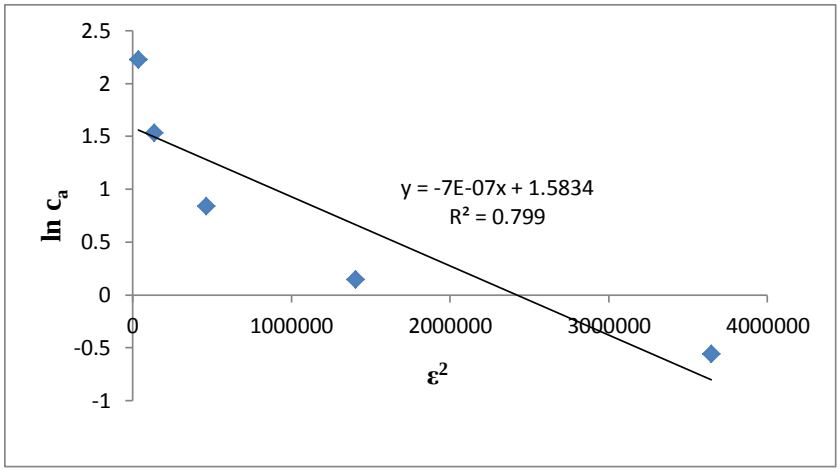

Figure 4.130: D-R isotherm for adsorption of TBT onto $nSiO_2$

The experimental data (Table 4.20) does not fit the Langmuir model, as the R^2 value is very low (< 0.5). Moreover, the negative value of the Langmuir constant, A_{max} (mg/g) for TBT adsorption onto $nSiO_2$ indicates the inadequacy of the Langmuir model to fit the equilibrium

data. The Temkin and D-R isotherm models also gave low R^2 value (< 0.90 for Temkin and < 0.80 for D-R) and can also not be used to describe the adsorption process.

Table 4.20: Isotherms constants for the adsorption of TBT onto $nSiO_2$

Equilibrium models	
Freundlich	
k_F [mg/g (L/mg)$^{1/n}$]	0.5882
n_F	0.9508
R^2	0.9994
Langmuir	
K_L (L/mg)	-0.00764
A_{max} (mg/g)	-78.74
R^2	0.4777
Temkin	
n_T (L/g)	3.1893
k_T (mg/L)	0.8396
b_T (J/mol)	763.80
R^2	0.8851
Dubinin-Redushkevich	
k_{D-R} (J^2/mol^2)	7x 10^{-7}
q_m (mg/g)	4.871
E (J/mol)	845.15
R^2	0.7990

The equilibrium model constants k_F, k_L, k_T and k_{D-R} for the adsorption of TBT by $nSiO_2$ are 0.59 mg/g (L/mg)$^{1/n}$, -0.008 L/mg, 0.840 mg/L and 7 x 10^{-7} J^2/mol^2, respectively.

4.12.4.6 Effect of temperature

The experimental results obtained on the effect of temperature show that the adsorption capacity of TBT onto $nSiO_2$ increases with increase in the solution temperature (Figure 4.131). This indicates that the adsorption of TBT onto the $nSiO_2$ is endothermic. The increase in the rate of adsorption with the increase in temperature may be attributed to the strong adsorptive forces between the active sites of the adsorbents and adsorbate species and also between the adjacent molecules of the adsorbed phases.

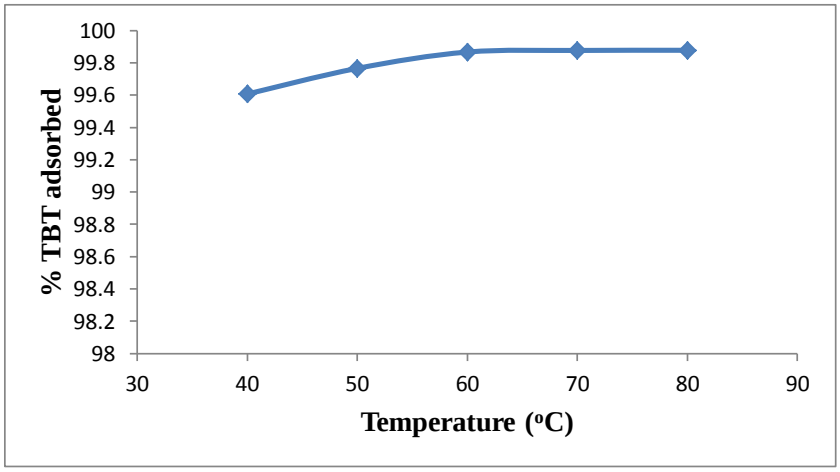

Figure 4.131: Effect of temperature on TBT adsorption onto $nSiO_2$

Experimental conditions: Concentration of TBT = 100 mg/L; Volume of TBT solution = 25 mL, Mass of $nSiO_2$ = 0.5 g; Contact time = 60 min; pH = 8; Stirring speed = 200 rpm.

Approx. 99.88 % TBT was removed from the initial concentration of 100 mg/L TBT by $nSiO_2$ at 80 ^{o}C, contact time of 60 min, pH 8 and a stirring speed of 200 rpm. Figure 4.132 thus shows the Van't Hoff plot (Sheela et al., 2012) for the adsorption of TBT and the variation in the extent of adsorption with respect to temperature has been explained on the basis of ΔH^{o}, ΔS^{o}, and ΔG^{o} as shown in Table 4.21.

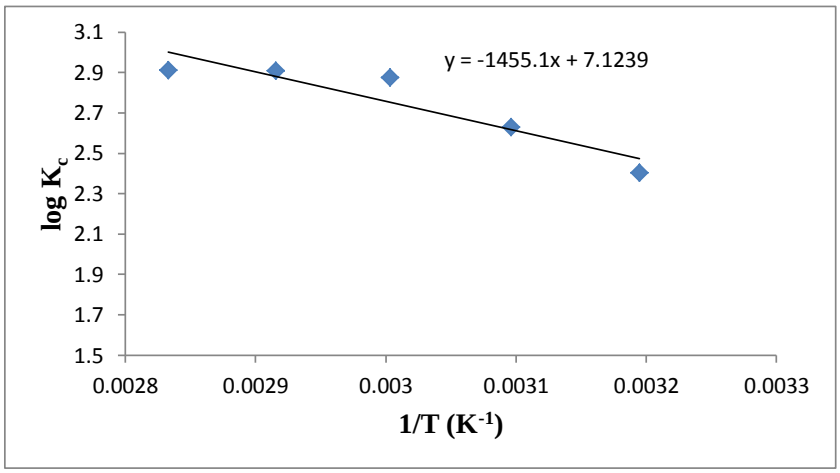

Figure 4.132: Van't Hoff plot for the adsorption of TBT onto $nSiO_2$

The positive value of ΔH^{o} for the intervals of temperatures (27.861 kJ/mol) also shows the endothermic nature of the adsorption process. The positive value of ΔS^{o} (136.402 J/K/mol) corresponds to an increase in degree of freedom of the adsorbed TBT. It is evident from Table 4.21 that ΔG^{o} values were found to be more negative as the temperature increases,

this indicates that the adsorption efficiency of TBT onto $nSiO_2$ increases with increase in temperature and K_c ranged 243.45 – 818.67.

Table 4.21: Thermodynamic parameters for the adsorption of TBT onto $nSiO_2$

Temperature (°C)	ΔG° (kJ/mol)	ΔS° (J/K/mol)	ΔH° (kJ/mol)	K_c
40	-14.40	136.402	27.861	253.45
50	-16.26			4226.4
60	-18.33			750.88
70	-19.11			812.01
80	-19.69			818.67

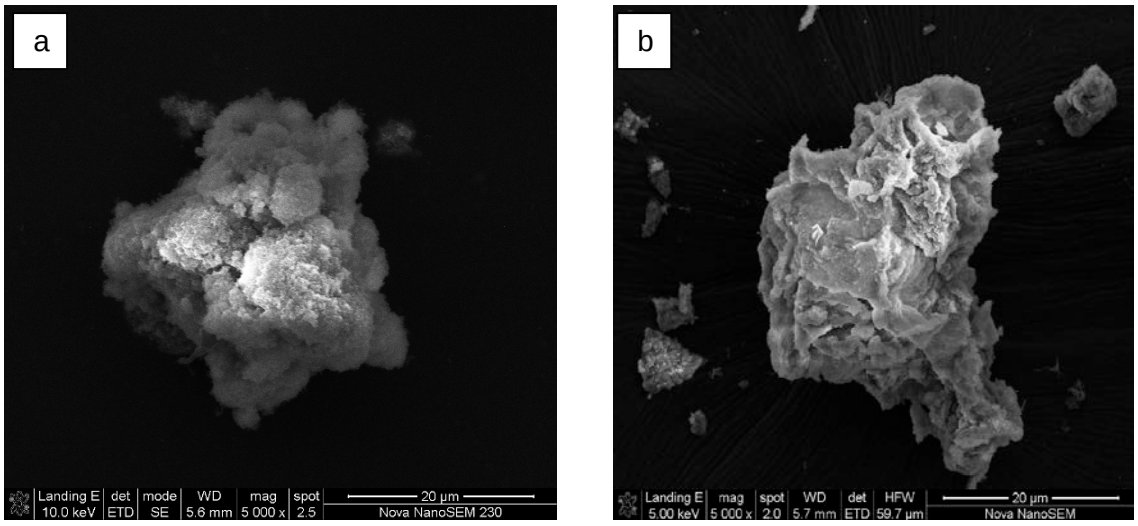

Figure 4.133: SEM of $nSiO_2$ before (a) and after (b) TBT adsorption

The SEM analysis of $nSiO_2$ before and after adsorption studies (optimal condition) is presented in Figure 4.133. A representative TBT chromatogram after adsorption of 100 mg/L TBT onto 0.5g of $nSiO_2$, contact time of 60min, temperature 20 ^oC and a stirring speed of 200 rpm is as shown in Figure 4.134.

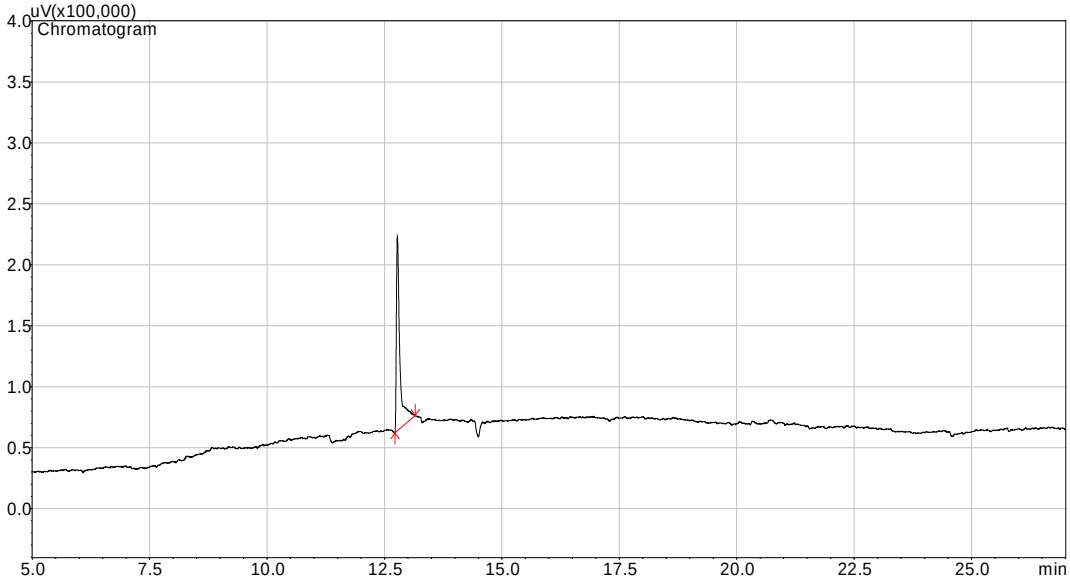

Figure 4.134: Representative TBT chromatogram after adsorption of 100 mg/L TBT with 0.5g of $nSiO_2$, contact time of 60min, temperature 20 ^oC and a stirring speed of 200 rpm

4.12.5 Adsorption of TBT from TBT-contaminated artificial seawater onto nZnO

4.12.5.1 Effect of Adsorption amount

To study the effect of the amount of nZnO on the adsorption of TBT from TBT – contaminated artificial seawater, the amount of nZnO was varied from 0.0625 – 1 g, the concentration of TBT was taken as 100 mg/L and other parameters were also kept constant.

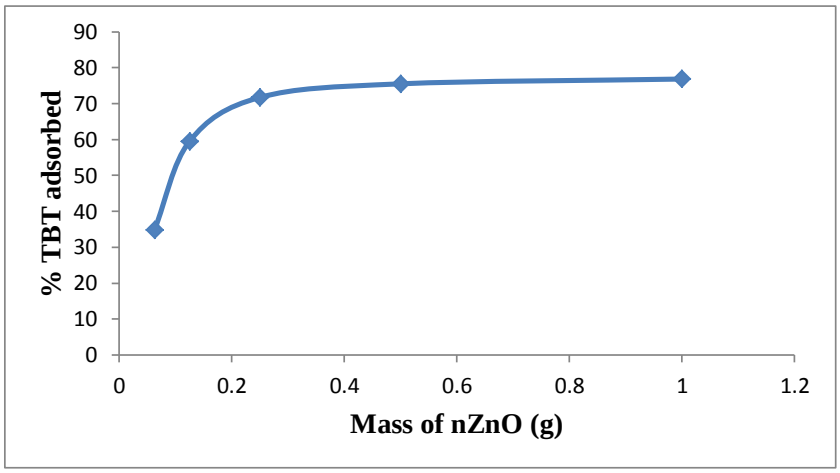

Figure 4.135: Adsorption efficiencies of TBT onto nZnO

Experimental conditions: Concentration of TBT = 100 mg/L; Volume of TBT solution = 25 mL, Contact time = 60 min; Stirring speed = 160 rpm, Temperature = 20 ^{o}C.

Figure 4.135 shows that the amount of TBT adsorbed and percentage removal of TBT by the nZnO increases as the amount of adsorbent increases from 0.0625 - 0.5 g after which equilibration was attained. Figure 4.135 thus shows that 0.5 g of nZnO removed 75.53 % of TBT from TBT – contaminated artificial seawater (Ayanda et al., 2013c).

4.12.5.2 Effect of contact time

To study the effect of contact time on the adsorption of TBT onto nZnO, the TBT concentration was 100 mg/L while, other remaining conditions are constant. The effect of contact time was carried out at various time intervals from 10 – 70 min.

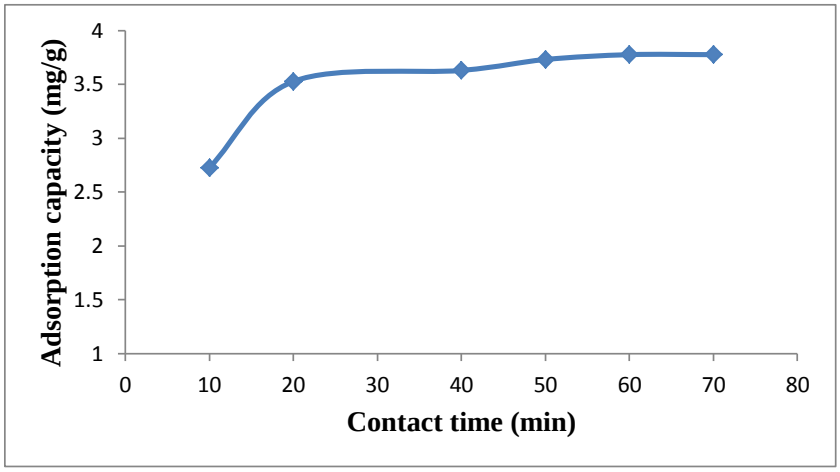

Figure 4.136: Effect of contact time on TBT adsorption onto nZnO

Experimental conditions: Concentration of TBT = 100 mg/L; Volume of TBT solution = 25 mL, Mass of nZnO = 0.5 g; Stirring speed = 160 rpm, Temperature = 20 ^{o}C.

The increase in the amount adsorbed from 2.73 mg/g (54.53 %) to 3.78 mg/g (75.53 %) (Figure 4.136) was observed up to 60 min. After that, there is no significant change observed. 60 min was therefore fixed as the contact time for further studies.

4.12.5.2.1 Adsorption kinetics

Figures 4.137 – 4.141 thus show the pseudo first-order, pseudo second-order, Elovich, fractional power and intraparticle diffusivity kinetic plots, respectively and Table 4.22 provides the evaluated parameters of all the kinetics models.

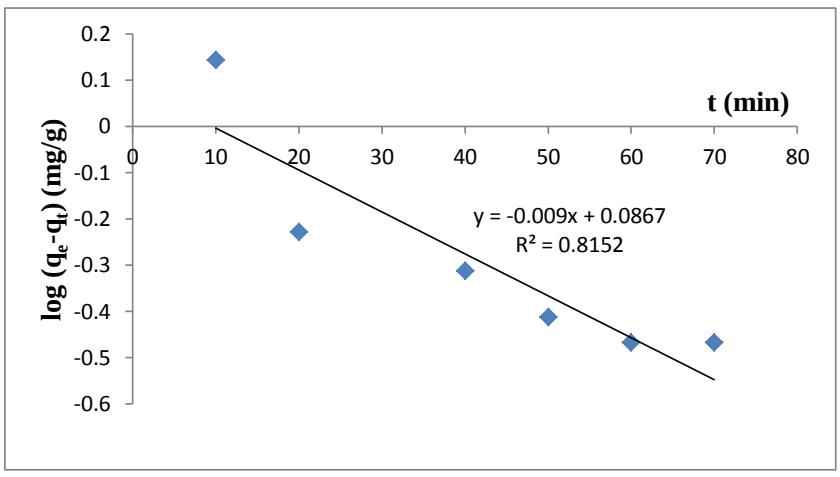

Figure 4.137: Pseudo first-order rate equation plot for TBT adsorption onto nZnO

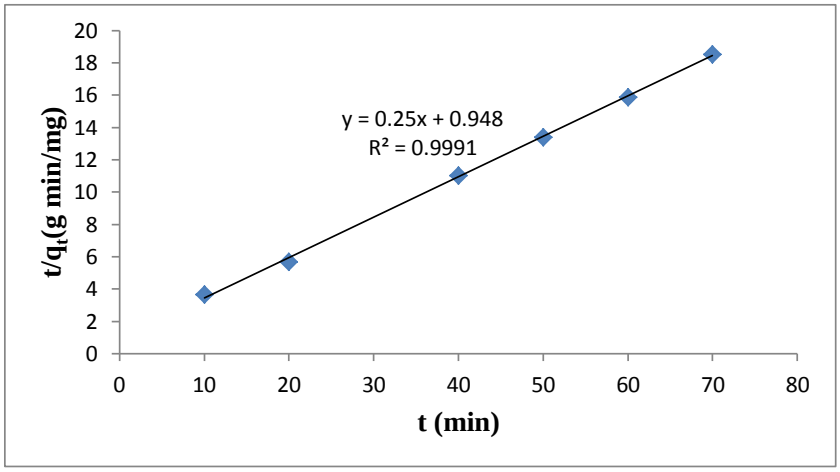

Figure 4.138: Pseudo second-order rate equation plot for TBT adsorption onto nZnO

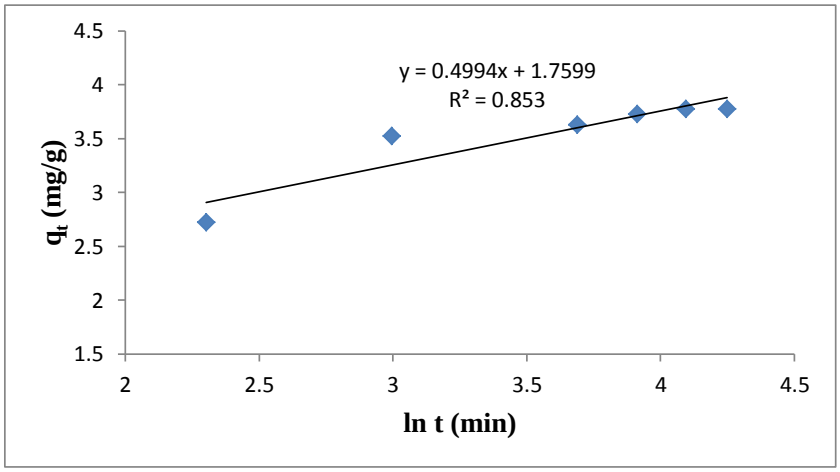

Figure 4.139: Elovich rate equation plot for TBT adsorption onto nZnO

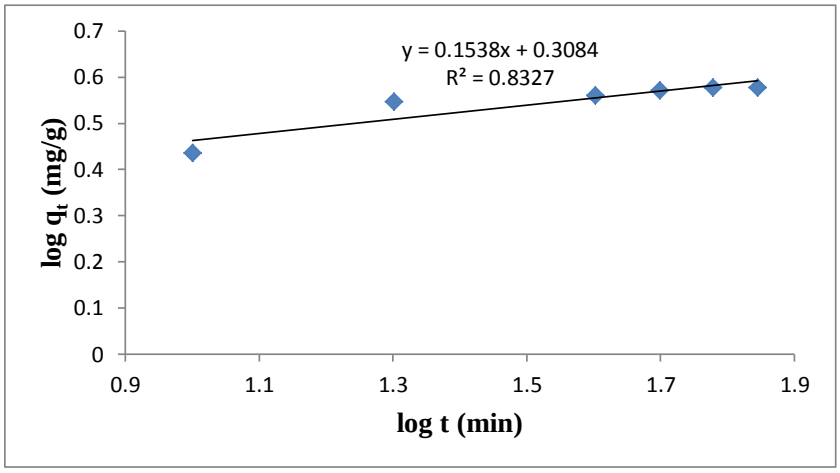

Figure 4.140: Fractional Power rate equation plot for TBT adsorption onto nZnO

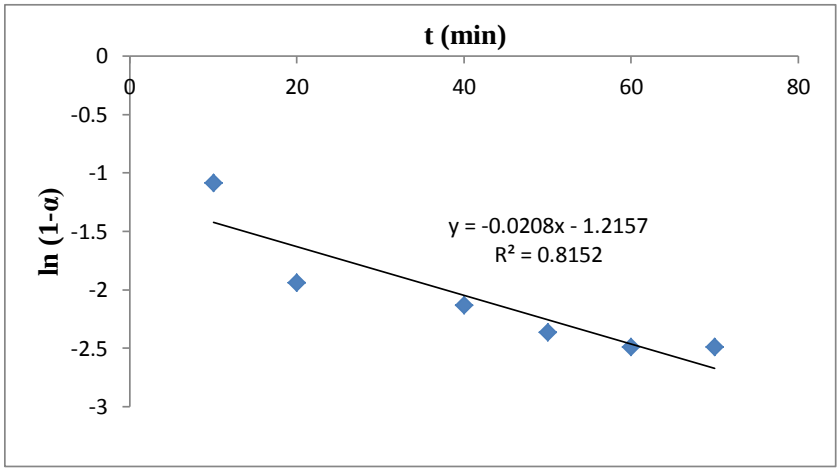

Figure 4.141: Intraparticle diffusivity plot for TBT adsorption onto nZnO

The value of correlation coefficient (R^2) of pseudo second-order kinetic model (> 0.99) is higher than the correlation coefficients of all other models indicating that the kinetic model for the adsorption of TBT onto the nZnO is pseudo second-order. The intraparticle coefficient for the adsorption of TBT by the nZnO as also calculated and presented in Table 4.22 and the results also indicate that the power function model satisfactorily describes the time-dependence of TBT on the nZnO since the value of the constant v is less than 1.

Table 4.22: Kinetic model parameters for TBT adsorption onto nZnO

Kinetic models	
Pseudo first-order	
k_1 (min^{-1})	0.02073
q_e (mg/g)	1.2209
R^2	0.8152
Pseudo second-order	
q_e (mg/g)	4.00
h_o (mg/g/min)	1.0549
k_2 (g/mg/min)	0.0659
R^2	0.9991
Elovich	
β (g min/mg)	2.002
α (g min^2/mg)	67.9095
R^2	0.8530
Fractional Power	
v (min^{-1})	0.1538
k_3 (mg/g)	2.0342
k_3v (mg/g/min)	0.3129
R^2	0.8327
Intraparticle diffusivity	
kp (min^{-1})	0.0208
R^2	0.8152

The value of the initial adsorption rate, h_o, obtained for the pseudo second-order kinetics is 1.0549 mg/g/min. The amount of TBT adsorbed at equilibrium per unit weight of the adsorbent (q_e) is 4.00 mg/g and the rate constant of pseudo second - order adsorption (k_2) is 0.0659 g/mg/min.

4.12.5.3 Effect of pH

The effect of pH on the adsorption of TBT onto the nZnO was studied at pH 3 – 9. It was observed in Figure 4.142 that the percentage of TBT adsorbed by nZnO steadily increases as the pH of the solution increases from pH 3 to pH 8, and reaches equilibration at pH ≥ 8.

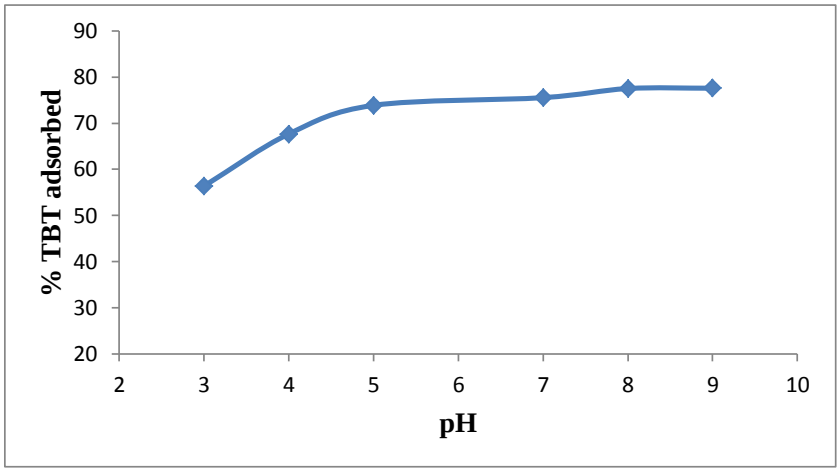

Figure 4.142: Effect of pH on TBT adsorption onto nZnO

Experimental conditions: Concentration of TBT = 100 mg/L; Volume of TBT solution = 25 mL, Mass of nZnO = 0.5 g; Contact time = 60 min; Stirring speed = 160 rpm, Temperature = 20 ^{o}C.

Maximum adsorption capacity was recorded within the pH range of normal saline water (pH 8). About 77.50 % of TBT was removed from the initial concentration of 100 mg/L TBT by nZnO at a contact time of 60 min, stirring speed of 160 rpm, temperature of 20 ^{o}C and pH 8. pH 8 was chosen as the optimum pH and was utilized for further studies.

4.12.5.4 Effect of stirring speed

The stirring speed on the adsorption of TBT onto nZnO was studied at a stirring speed of 160 – 200 rpm. The adsorption capacity of nZnO increases as the stirring speed of the mixture increases, reaching equilibration at 190 - 200 rpm (Figure 4.143).

3.9949 mg/g of TBT was removed from the initial concentration of 5 mg/g TBT by nZnO at a contact time of 60 min, pH 8, temperature of 20 ^{o}C and a stirring speed of 200 rpm (Figure 4.143). A stirring speed of 200rpm was therefore used for further studies.

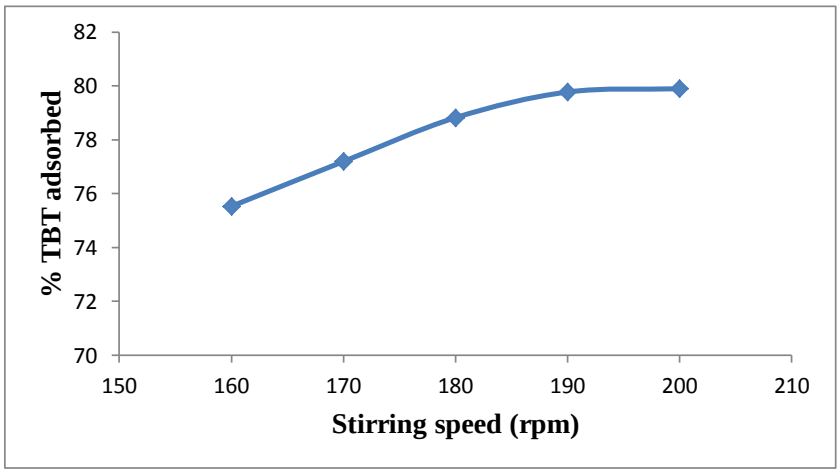

Figure 4.143: Effect of stirring speed on TBT adsorption onto nZnO

Experimental conditions: Concentration of TBT = 100 mg/L; Volume of TBT solution = 25 mL, Mass of nZnO = 0.5 g; Contact time = 60 min; Temperature = 20 ^{o}C.

4.12.5.5 Effect of initial concentration

The adsorption isotherms of the adsorption of TBT onto nZnO were investigated by varying the initial TBT concentration from 12.5 to 200 mg/L at optimized adsorbent dose, contact time, pH and stirring speed established after optimization of working parameters. The equilibrium data were fitted by Langmuir, Freundlich, Temkin and D-R isotherm models as presented in Figures 4.145 – 4.148.

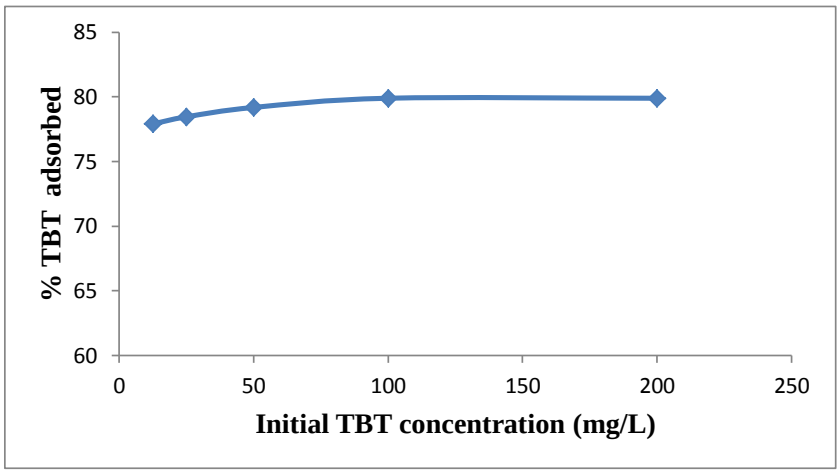

Figure 4.144: Percentage TBT adsorbed by nZnO at various initial TBT concentrations

Experimental conditions: Volume of TBT solution = 25 mL, Mass of nZnO = 0.5 g; pH = 8; Stirring speed = 200 rpm; Contact time = 60 min; Temperature = 20 ^{o}C.

Figure 4.144 shows that the adsorption of TBT onto nZnO steadily increases as the initial TBT concentration increases from 12.5 to 100 mg/L, indicating that adsorption is also favourable for the higher TBT concentrations that have been investigated.

4.12.5.5.1 Adsorption isotherms

The adsorption isotherm plots presented in Figures 4.145 – 4.148 and parameters obtained for all the models were given in Table 4.23. The experimental data fitted well with Freundlich model because the regression coefficient (R^2 > 0.99) is higher than other models (Table 4.11). The value of n_F, for the nZnO, falling in the range 1 -10 also indicates favourable adsorption (Ayanda et al., 2013c).

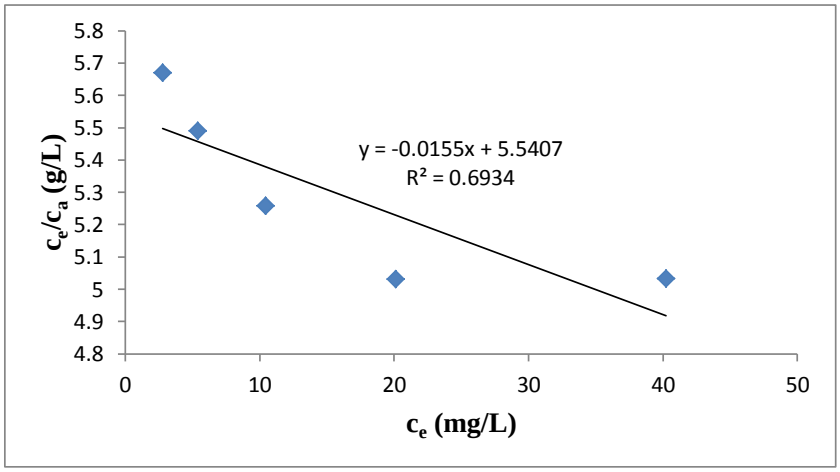

Figure 4.145: Langmuir isotherm for adsorption of TBT onto nZnO

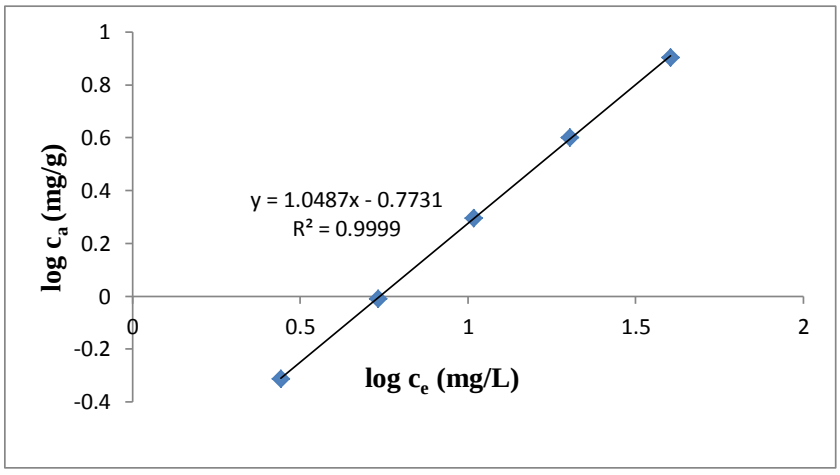

Figure 4.146: Freundlich isotherm for adsorption of TBT onto nZnO

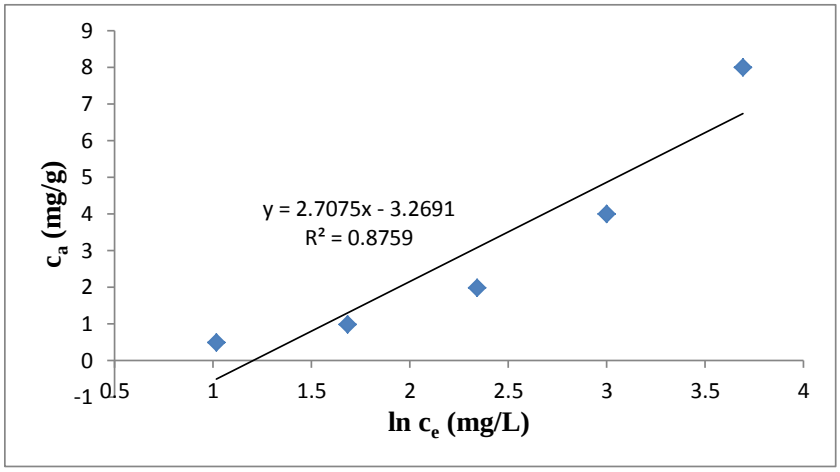

Figure 4.147: Temkin isotherm for adsorption of TBT onto nZnO

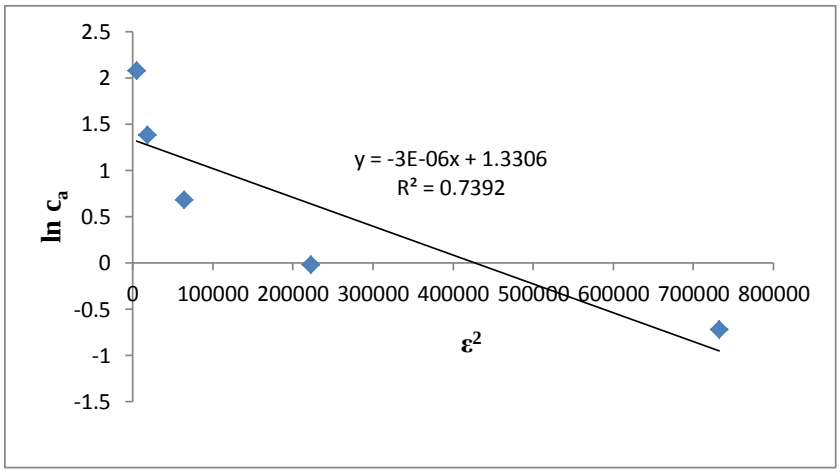

Figure 4.148: D-R isotherm for adsorption of TBT onto nZnO

The negative value of the Langmuir constants, A_{max} (mg/g) and k_L (L/mg) for TBT adsorption (Table 4.23) indicate the inadequacy fitting of experimental data to Langmuir model (Maarof and Hameed, 2004).

Table 4.23: Isotherms constants for the adsorption of TBT onto nZnO

Equilibrium models	
Freundlich	
k_F [mg/g (L/mg)$^{1/n}$]	0.1686
n_F	0.9536
R^2	0.9999
Langmuir	
K_L (L/mg)	-0.002797
A_{max} (mg/g)	-64.52
R^2	0.6934
Temkin	
n_T (L/g)	2.7075
k_T (mg/L)	0.2989
b_T (J/mol)	899.72
R^2	0.8759
Dubinin-Redushkevich	
k_{D-R} (J^2/mol^2)	3 x 10^{-6}
q_m (mg/g)	3.7833
E (J/mol)	408.25
R^2	0.7392

4.12.5.6 Effect of temperature

The experimental results obtained on the effect of temperature show that the adsorption capacity of TBT onto nZnO increases with increase in the solution temperature (Figure 4.149). This indicates that the adsorption of TBT onto the nZnO is endothermic.

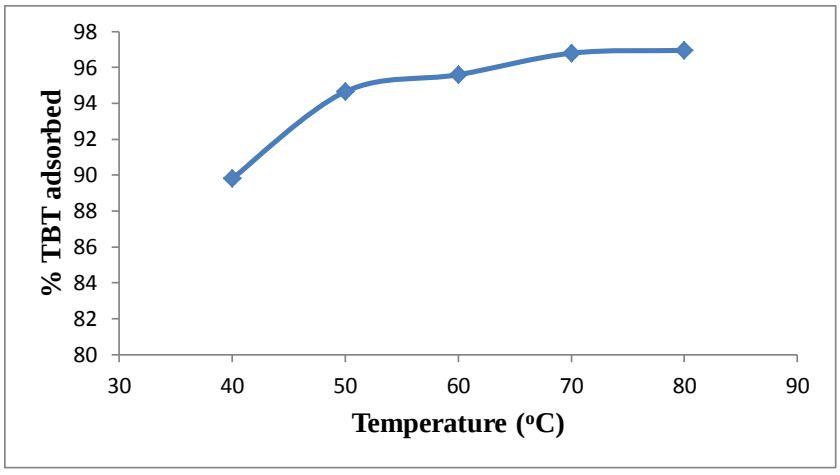

Figure 4.149: Effect of temperature on TBT adsorption onto nZnO

Experimental conditions: Concentration of TBT = 100 mg/L; Volume of TBT solution = 25 mL, Mass of nZnO = 0.5 g; Contact time = 60 min; pH = 8; Stirring speed = 200 rpm.

Approx. 96.96 % of TBT was removed from the initial concentration of 100 mg/L TBT by the nZnO at a temperature of 80 ^{o}C, contact time of 60 min, pH 8 and a stirring speed of 200 rpm. Figure 4.150 show the Van't Hoff plot for the adsorption of TBT and the variation in the extent of adsorption with respect to temperature has been explained on the basis of ΔH^{o}, ΔS^{o}, and ΔG^{o} as shown in Table 4.24.

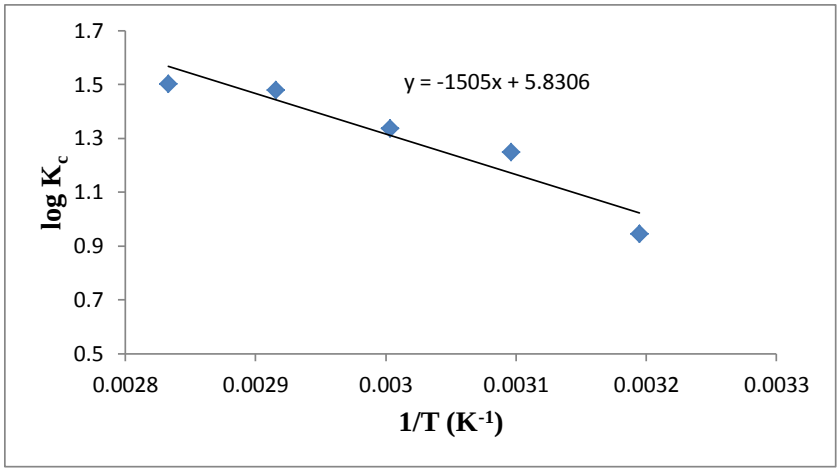

Figure 4.150: Van't Hoff plot for the adsorption of TBT onto nZnO

The positive value of ΔH^{o} for the intervals of temperatures also shows the endothermic nature of the adsorption process. The positive value of ΔS^{o} corresponds to an increase in degree of freedom of the adsorbed TBT and suggest the increase in concentration of adsorbate in solid–solution interface indicating an increase in adsorbate concentration onto the solid phase. ΔG^{o} values (Table 4.24) are found to be more negative as the temperature increases which indicates that the adsorption efficiency of TBT onto nZnO increases with increase in temperature. K_c also ranged 8.81 – 31.85 (Table 4.24).

Table 4.24: Thermodynamic parameters for the adsorption of TBT onto nZnO

Temperature (°C)	ΔG° (kJ/mol)	ΔS° (J/K/mol)	ΔH° (kJ/mol)	K_c
40	-5.663	111.639	28.816	8.81
50	-7.719			17.71
60	-8.523			21.73
70	-9.719			30.21
80	-10.158			31.85

The solid residue of nZnO before and after the adsorption processes were subjected to SEM analysis (Figure 4.151) while a representative TBT chromatogram after adsorption of 100 mg/L TBT with 0.5 g of nZnO, contact time of 60min, temperature 20 ^{o}C and a stirring speed of 200 rpm is as shown in Figure 4.152.

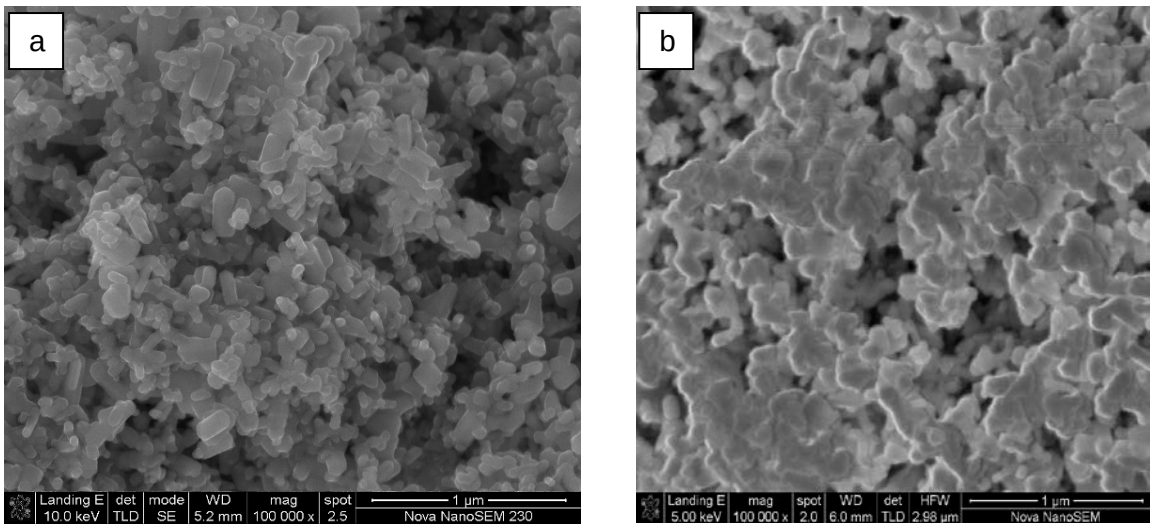

Figure 4.151: SEM of nZnO before (a) and after (b) TBT adsorption

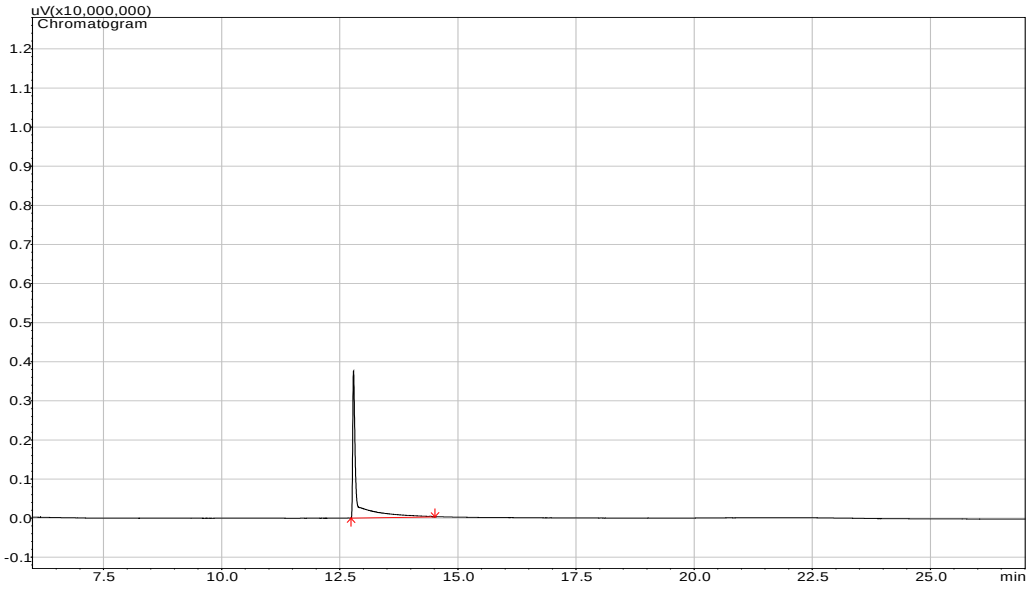

Figure 4.152: Representative TBT chromatogram after adsorption of 100 mg/L TBT with 0.5g of nZnO, contact time of 60min, temperature 20 ^{o}C and a stirring speed of 200 rpm

4.12.6 Adsorption of TBT from TBT-contaminated artificial seawater onto fly ash/activated carbon composite

4.12.6.1 Effect of adsorbent amount

The effect of adsorbent amount on the adsorption of TBT by the fly ash/activated carbon composite is shown in Figure 4.153. It was observed that the percentage adsorption of TBT increased with increasing amount of fly ash/activated carbon composite, reaching an optimum at 0.5 g for the fly ash/activated carbon composite, corresponding to 99.58 % removal. 0.5 g was therefore selected as the optimum adsorbent amount utilized for further studies.

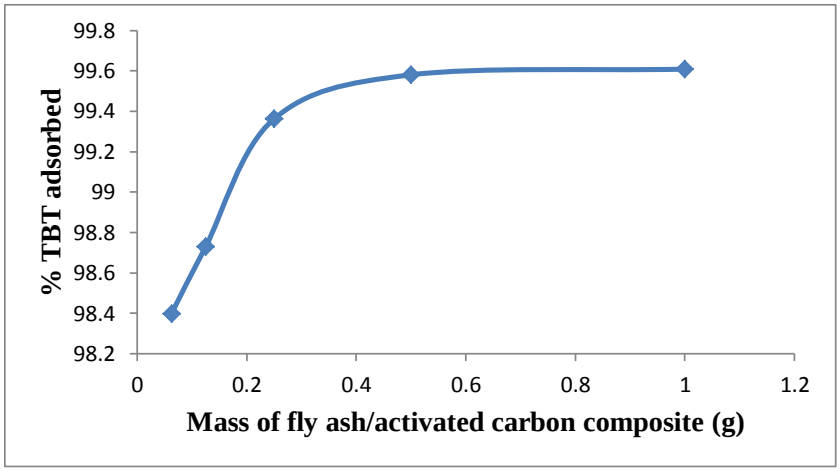

Figure 4.153: Adsorption efficiencies of TBT onto fly ash/activated carbon composite

Experimental conditions: Concentration of TBT = 100 mg/L; Volume of TBT solution = 25 mL, Contact time = 60 min; Stirring speed = 160 rpm, Temperature = 20 ^{o}C.

4.12.6.2 Effect of contact time

Figure 4.154 shows the effect of contact time on adsorption of TBT by the fly ash/activated carbon composite material. The TBT removal efficiency at different time intervals ranging from 10 – 70 min are obtained. The figure also shows that the adsorption of TBT onto fly ash/activated carbon composite increases with time and gradually attains equilibrium after 60 minutes. The TBT removal efficiency for the fly ash/activated carbon composite reaches 4.979 mg/g (99.58 %) (Ayanda et al., 2013b). A contact time of 60 min was therefore fixed for further studies.

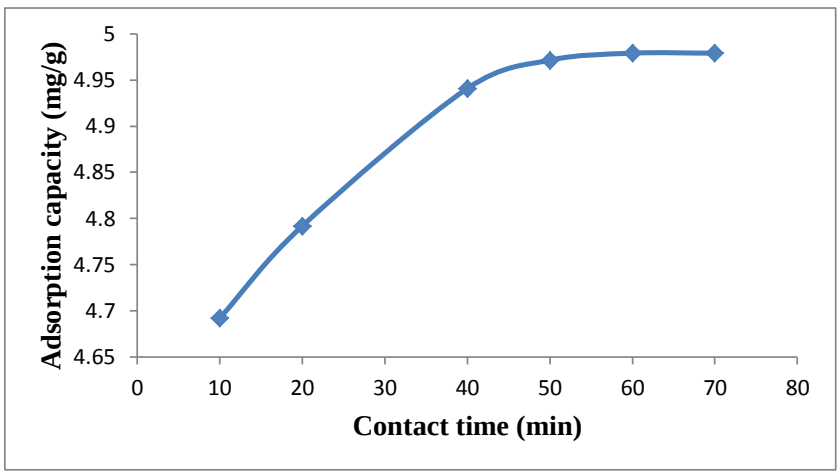

Figure 4.154: Effect of contact time on TBT adsorption onto fly ash/activated carbon

Experimental conditions: Concentration of TBT = 100 mg/L; Volume of TBT solution = 25 mL, Mass of composite = 0.5 g; Stirring speed = 160 rpm, Temperature = 20 ^{o}C.

4.12.6.2.1 Adsorption kinetics

Figures 4.155 – 4.159 shows the pseudo first-order, pseudo second-order, Elovich, fractional power and intraparticle diffusivity kinetic plots, respectively and Table 4.25 provides the evaluated parameters of all the kinetic models. The R^2 value obtained for pseudo second-order kinetic model is very high (R^2 > 0.99) when compared with other models, showing the applicability of the pseudo second-order kinetic model to describe the adsorption kinetic data of TBT onto the fly ash/activated carbon composite material (Ayanda et al., 2013b).

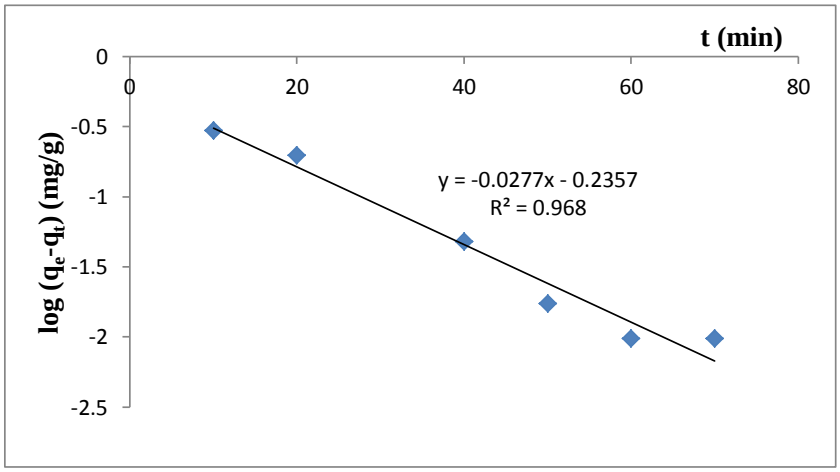

Figure 4.155: Pseudo first-order rate equation plot for TBT adsorption onto fly ash/activated carbon composite

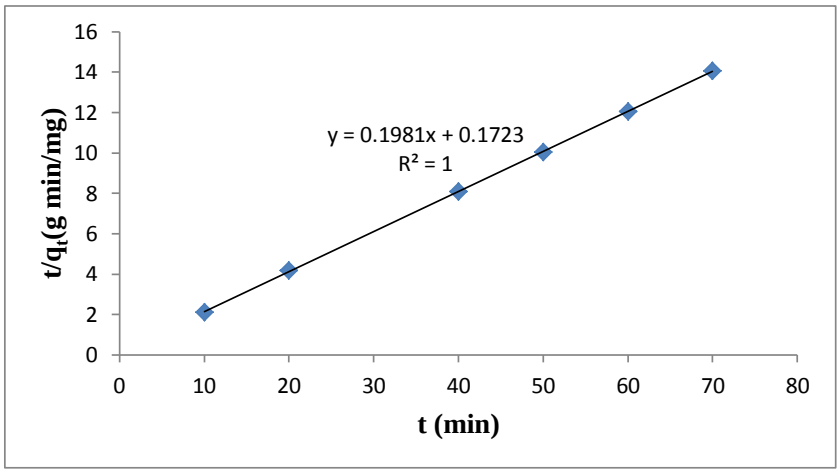

Figure 4.156: Pseudo second-order rate equation plot for TBT adsorption onto fly ash/activated carbon composite

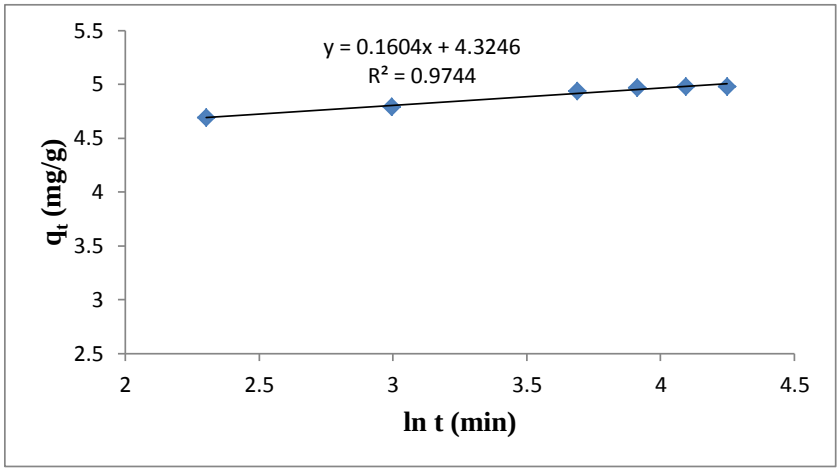

Figure 4.157: Elovich rate equation plot for TBT adsorption onto fly ash/activated carbon composite

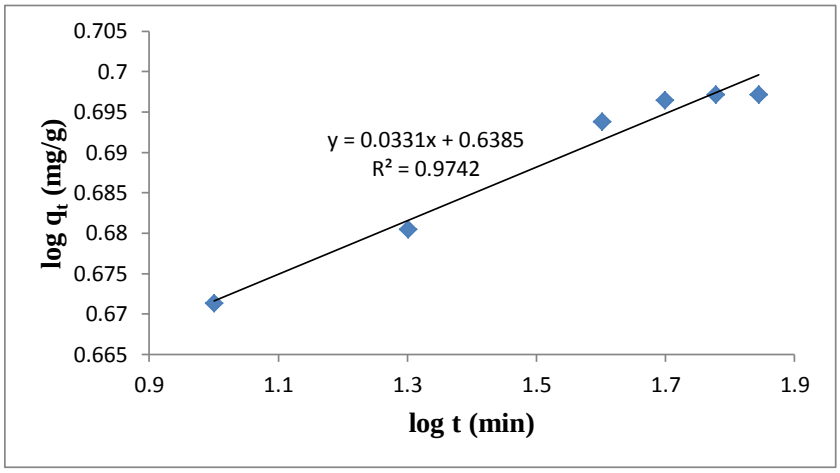

Figure 4.158: Fractional Power rate equation plot for TBT adsorption onto fly ash/activated carbon composite

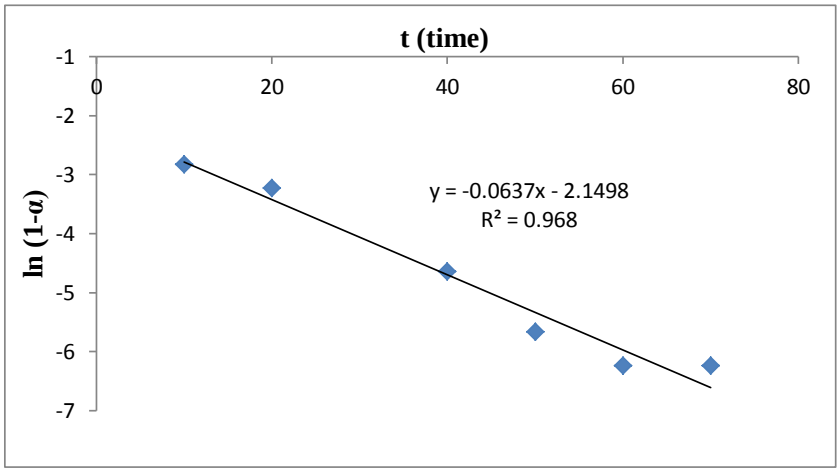

Figure 4.159: Intraparticle diffusivity plot for TBT adsorption onto fly ash/activated carbon composite

Table 4.25: Kinetic model parameters for TBT adsorption onto fly ash/activated carbon composite

Kinetic models	
Pseudo first-order	
k_1 (min^{-1})	0.0638
q_e (mg/g)	0.5812
R^2	0.9680
Pseudo second-order	
q_e (mg/g)	5.0480
h_o (mg/g/min)	5.8038
k_2 (g/mg/min)	0.2278
R^2	1.000
Elovich	
β (g min/mg)	6.2344
α (g min^2/mg)	3.19×10^{12}
R^2	0.9744
Fractional Power	
v (min^{-1})	0.0331
k_3 (mg/g)	4.3501
k_3v (mg/g/min)	0.1440
R^2	0.9742
Intraparticle diffusivity	
k_p (min^{-1})	0.0637
R^2	0.968

The intraparticle coefficient for the adsorption of TBT by the fly ash/activated carbon composite was also computed (Table 4.25). The initial adsorption rate (h_o) calculated from pseudo second-order rate equation for TBT adsorption onto fly ash/activated carbon composite is 5.8038 mg/g/min. The results also indicate that the power function model satisfactorily describes the time-dependence of TBT onto fly ash/activated carbon composite since the value of the constant v is less than 1, and the regression coefficient is greater than 0.97. From Table 4.25, k_1, k_2, β, α_E, k_3 and k_p are 0.0638 min^{-1}, 0.2278 g/mg/min, 6.2344 gmin/mg, 3.19×10^{12} $gmin^2/mg$, 4.3501 mg/g and 0.0637 min^{-1}, respectively.

4.12.6.3 Effect of pH

The effect of pH on the adsorption of TBT onto fly ash/activated carbon composite was studied at pH 3 – 9. It was observed from Figure 4.160 that the percentage of TBT adsorbed by the fly ash/activated carbon composite increases as the pH of the solution increases from pH 3 to pH 8 and tends to falls afterwards. It is therefore evident from Figure 4.160 that maximum adsorption was also recorded within the pH range of normal saline water (pH 8).

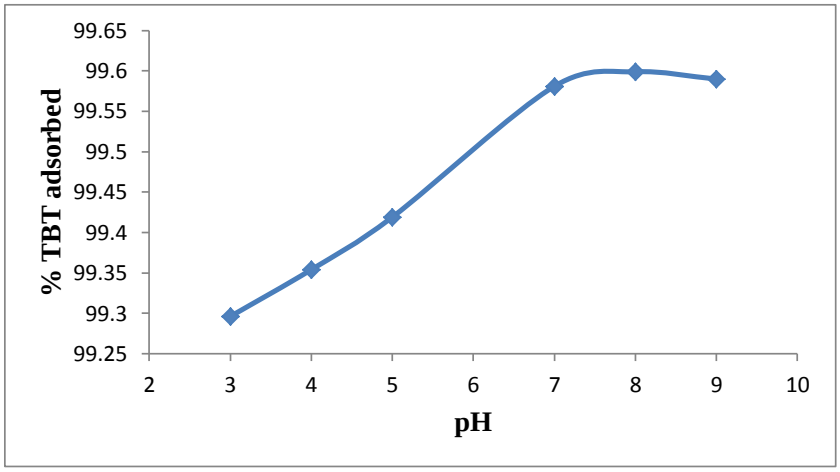

Figure 4.160: Effect of pH on TBT adsorption onto fly ash/activated carbon composite

Experimental conditions: Concentration of TBT = 100 mg/L; Volume of TBT solution = 25 mL, Mass of composite = 0.5 g; Contact time = 60 min; Stirring speed = 160 rpm, Temperature = 20 ^{o}C.

About 99.60 % of TBT was removed from the initial concentration of 100 mg/L TBT by the fly ash/activated carbon composite at a contact time of 60 min, stirring speed of 160 rpm, temperature of 20 ^{o}C and pH 8. pH 8 was therefore chosen as the optimum pH and was used for further studies.

4.12.6.4 Effect of stirring speed

The effect of stirring speed on the adsorption of TBT onto fly ash/activated carbon composite was studied at a stirring speed of 160 – 200 rpm. The adsorption capacity of the fly ash/activated carbon composite increases as the stirring speed of the mixture increases (Figure 4.161).

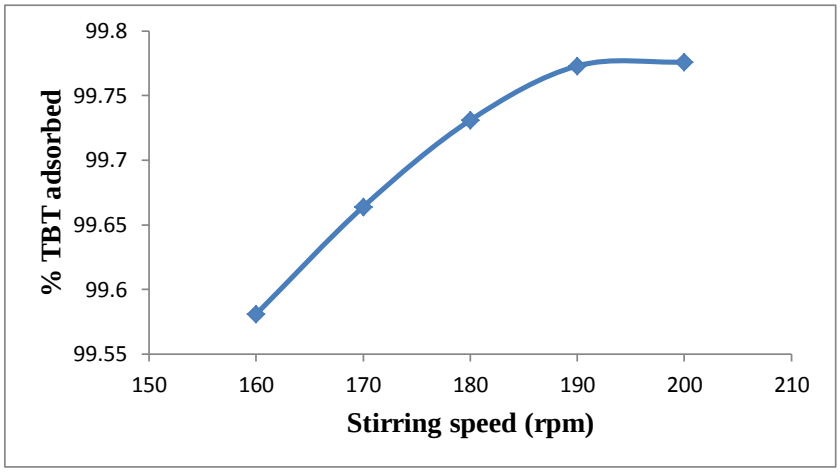

Figure 4.161: Effect of stirring speed on TBT adsorption onto fly ash/activated carbon composite

Experimental conditions: Concentration of TBT = 100 mg/L; Volume of TBT solution = 25 mL, Mass of composite = 0.5 g; Contact time = 60 min; Temperature = 20 ^{o}C.

4.989 mg/g (99.78 %) of TBT was therefore removed from the initial concentration of 5 mg/g TBT by the fly ash/activated carbon composite material at a contact time of 60 min, pH 8, temperature of 20 ^{o}C and a stirring speed of 200 rpm (Figure 4.161). A stirring speed of 200 rpm was therefore used for further studies.

4.12.6.5 Effect of initial concentration

The effect of initial TBT concentration in the range of 12.5 to 100 mg/L on adsorption was investigated. Along with pH, all parameters were kept constant in this study. It is evident from the Figure 4.162 that, as the concentration of TBT increases, the amount of TBT adsorbed by fly ash/activated carbon composite material was increased and an increase in percentage removal was also observed. The percentage TBT adsorbed increases from 99.49 to 99.78 % as the initial TBT concentration increases.

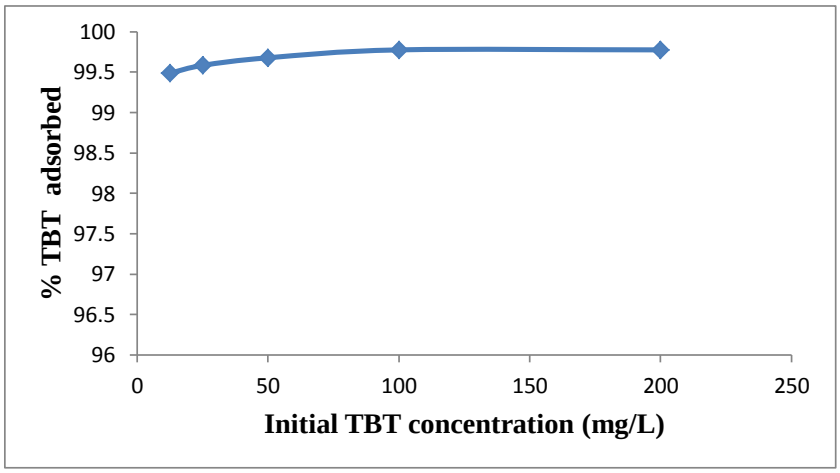

Figure 4.162: Percentage TBT adsorbed by fly ash/activated carbon composite at various initial TBT concentrations

Experimental conditions: Volume of TBT solution = 25 mL, Mass of composite = 0.5 g; pH = 8; Stirring speed = 200 rpm; Contact time = 60 min; Temperature = 20 ^{o}C.

4.12.6.5.1 Adsorption isotherms

The adsorption isotherm plots are presented in Figures 4.163 – 4.166 and parameters obtained for the models were given in Table 4.26. Based on values of correlation coefficient, R^2, summarized in Table 4.26, the adsorption of TBT onto fly ash/activated carbon composite can be described by the Freundlich adsorption isotherm, probably due to the real heterogeneous nature of the surface sites involved in the process of adsorption.

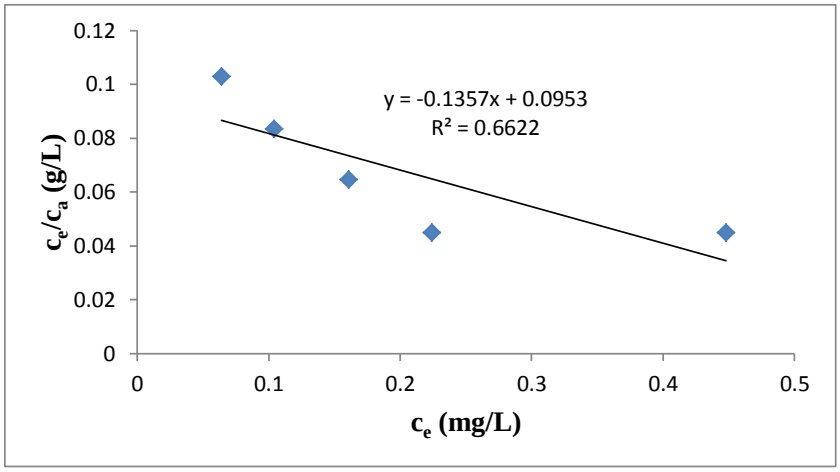

Figure 4.163: Langmuir isotherm for adsorption of TBT onto fly ash/activated carbon composite

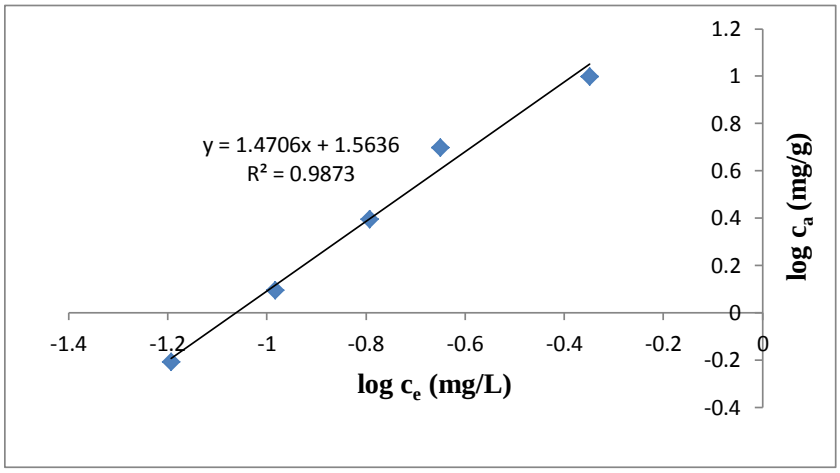

Figure 4.164: Freundlich isotherm for adsorption of TBT onto fly ash/activated carbon composite

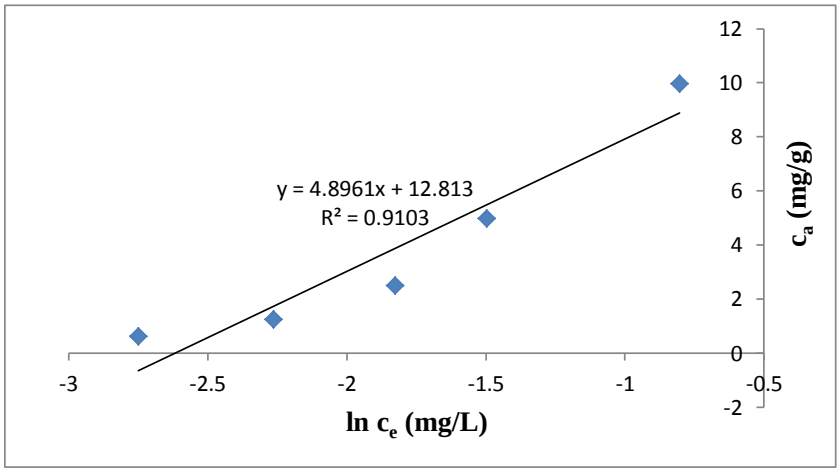

Figure 4.165: Temkin isotherm for adsorption of TBT onto fly ash/activated carbon composite

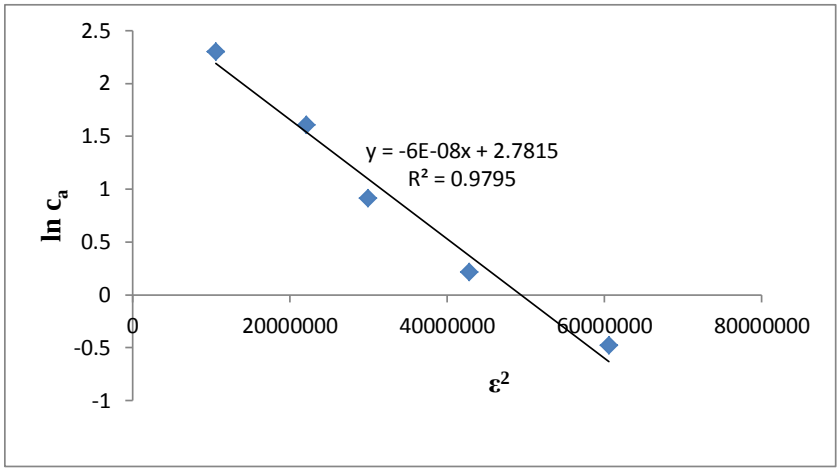

Figure 4.166: D-R isotherm for adsorption of TBT onto fly ash/activated carbon composite

Table 4.26: Isotherms constants for the adsorption of TBT onto fly ash/activated carbon composite

Equilibrium models	
Freundlich	
k_F [mg/g (L/mg)$^{1/n}$]	36.610
n_F	0.6799
R^2	0.9873
Langmuir	
K_L (L/mg)	-1.4239
A_{max} (mg/g)	-7.3692
R^2	0.6622
Temkin	
n_T (L/g)	4.8961
k_T (mg/L)	13.6943
b_T (J/mol)	497.54
R^2	0.9103
Dubinin-Redushkevich	
k_{D-R} (J^2/mol^2)	6 x 10^{-8}
q_m (mg/g)	16.1432
E (J/mol)	2886.75
R^2	0.9795

The values of k_F, k_L, k_T and k_{D-R} constants obtained are 36.610 mg/g (L/mg)$^{1/n}$, -1.4239 L/mg, 13.6943 mg/L and 6 x 10^{-8} J^2/mol^2, respectively (Table 4.26). Moreover, the negative value of the Langmuir constants, A_{max} (mg/g) and k_L (L/mg) for TBT adsorption onto fly ash/activated carbon composite indicate the inadequacy of the Langmuir model to explain the process. Thus, Freundlich model is the best model to explain the adsorption behaviour of TBT onto the fly ash/activated carbon composite material.

4.12.6.6 Effect of temperature

The experimental results obtained on the effect of temperature (Figure 4.167) show that the adsorption capacity of fly ash/activated carbon composite increases with increase in the solution temperature. This indicates that the adsorption of TBT onto fly ash/activated carbon composite is endothermic in nature. Approx. 99.98 % of TBT was removed from the initial concentration of 5 mg/g TBT by the fly ash/activated carbon composite at a contact time of 60 min, pH 8, stirring speed 200 rpm and temperature of 80 ^{o}C (Ayanda et al., 2013b).

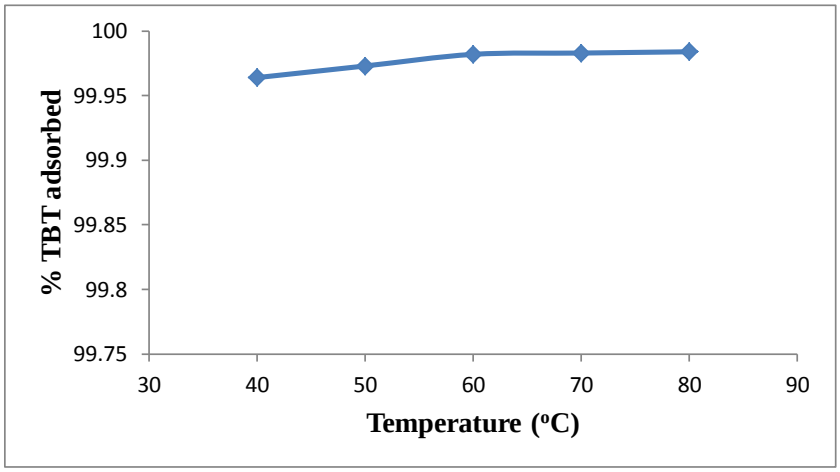

Figure 4.167: Effect of temperature on TBT adsorption onto fly ash/activated carbon composite

Experimental conditions: Concentration of TBT = 100 mg/L; Volume of TBT solution = 25 mL, Mass of composite = 0.5 g; Contact time = 60 min; pH = 8; Stirring speed = 200 rpm.

Figure 4.168 thus shows the Van't Hoff plot for the adsorption of TBT onto fly ash/activated carbon composite and the variation in the extent of adsorption with respect to temperature were explained on the basis of ΔH^{o} , ΔS^{o}, and ΔG^{o} as presented in Table 4.27.

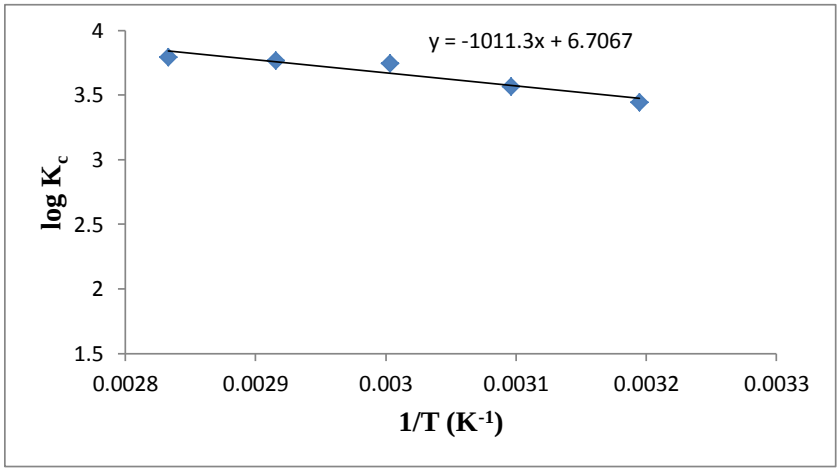

Figure 4.168: Van't Hoff plot for the adsorption of TBT onto fly ash/activated carbon composite

Table 4.27: Thermodynamic parameters for the adsorption of TBT onto fly ash/activated carbon composite

Temperature (°C)	ΔG° (kJ/mol)	ΔS° (J/K/mol)	ΔH° (kJ/mol)	K_c
40	-20.63	128.414	19.363	2776.8
50	-22.07			3702.7
60	-23.87			5554.6
70	-24.75			5881.4
80	-25.65			6249.0

The positive value of ΔH^{o} (19.363 kJ/mol) for the intervals of temperatures (Table 4.27) also shows the endothermic nature of the adsorption process. The positive value of ΔS^{o} (128.414 J/K/mol) corresponds to an increase in degree of freedom of the adsorbed TBT and suggests the increase in concentration of adsorbate in solid–solution interface indicating an increase in adsorbate concentration onto the solid phase. ΔG^{o} values are found to be more negative as the temperature increases, which indicate spontaneous adsorption and the degree of spontaneity of the reaction increases with increase in temperature.

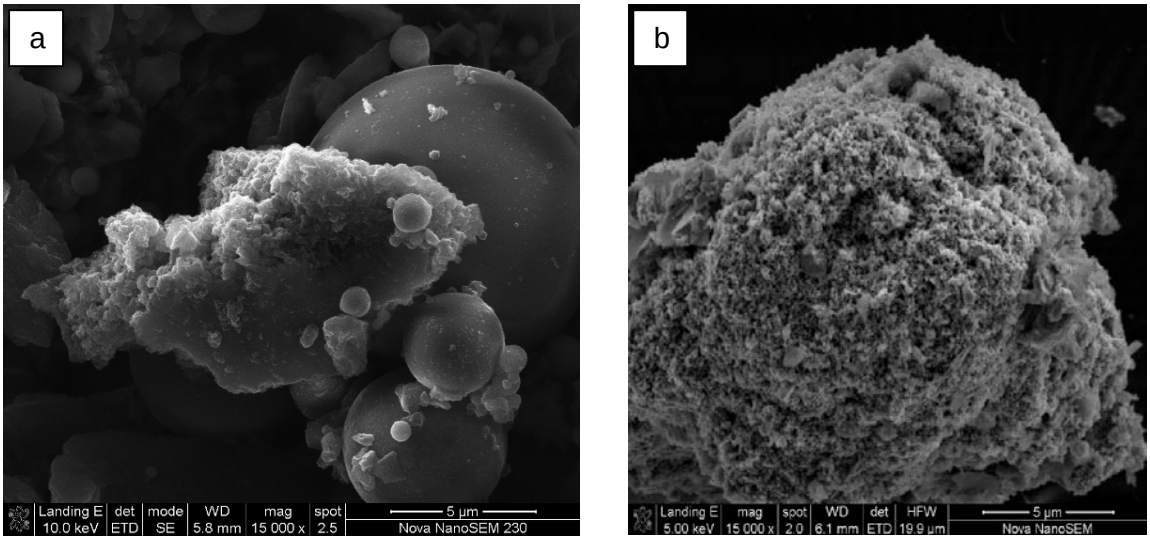

Figure 4.169: SEM of fly ash/activated carbon composite before (a) and after (b) TBT adsorption

The SEM analysis of the solid residues before and after adsorption (optimal condition) is presented in Figure 4.169 while a representative TBT chromatogram after adsorption of 100 mg/L TBT with 0.5 g of fly ash/activated carbon composite, contact time of 60min, temperature 20 ^{o}C and a stirring speed of 200 rpm is as shown in Figure 4.170.

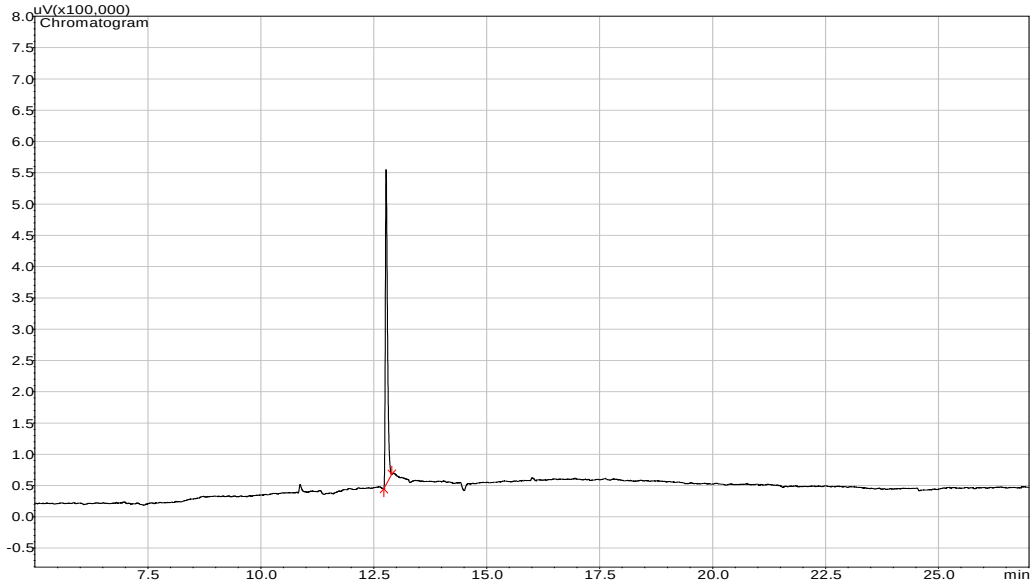

Figure 4.170: Representative TBT chromatogram after adsorption of 100 mg/L TBT with 0.5g of fly ash/activated carbon composite, contact time of 60min, temperature 20 ^{o}C and a stirring speed of 200 rpm

4.12.7 Adsorption of TBT from TBT-contaminated artificial seawater onto nFe_3O_4/activated carbon composite

4.12.7.1 Effect of adsorbent amount

The amount of nFe_3O_4/activated carbon composite (adsorbent dose) ranging from 0.0625 – 1.0 g per 25 mL of TBT solution was investigated on the efficiency of the adsorption process. A graph of the percentage of TBT adsorbed (C_a), mg/g on nFe_3O_4/activated carbon composite was plotted against the adsorbent amount (Figure 4.171).

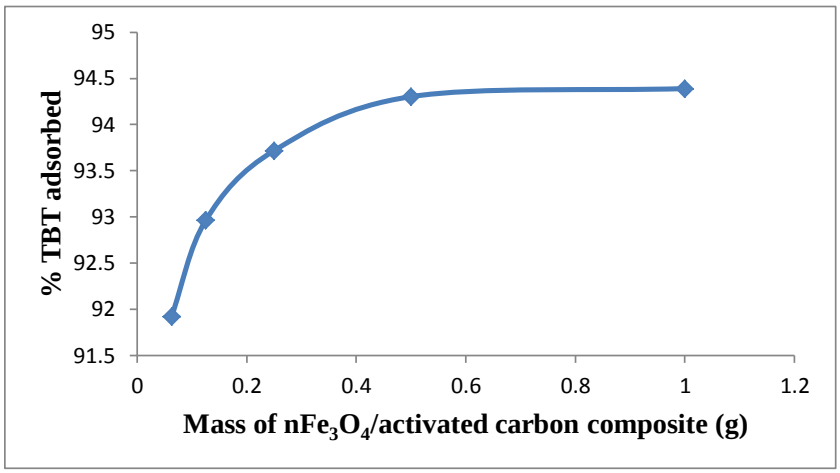

Figure 4.171: Adsorption efficiencies of TBT onto nFe_3O_4/activated carbon composite

Experimental conditions: Concentration of TBT = 100 mg/L; Volume of TBT solution = 25 mL, Contact time = 60 min; Stirring speed = 160 rpm, Temperature = 20 ^{o}C.

It was observed that the percentage adsorption increased with increasing adsorbent amount, reaching an optimum at 0.5 g for the nFe_3O_4/activated carbon composite material, corresponding to 94.30 %. 0.5 g was therefore selected as the optimum nFe_3O_4/activated carbon composite amount used for further studies.

4.12.7.2 Effect of contact time

The kinetic study of TBT onto nFe_3O_4/activated carbon composite was carried out by shaking 0.5 g of the adsorbents in 25 mL of TBT solutions with an initial concentration of 100 mg/L (pH 8) at 20 ^oC. After pre-defined contact time (10-70 min), the aqueous samples were filtered, and the concentration of TBT in the filtrate was determined.

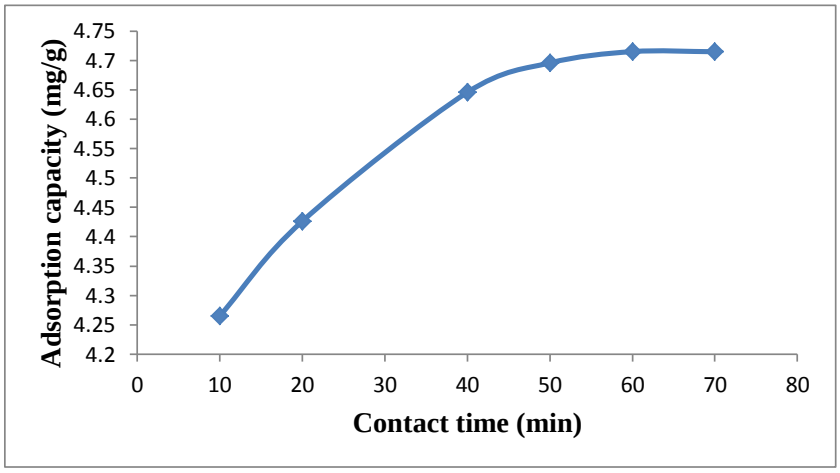

Figure 4.172: Effect of contact time on TBT adsorption onto nFe_3O_4/activated carbon composite

Experimental conditions: Concentration of TBT = 100 mg/L; Volume of TBT solution = 25 mL, Mass of composite = 0.5 g; Stirring speed = 160 rpm, Temperature = 20 ^oC.

Figure 4.171 thus shows the effect of contact time on adsorption of TBT by nFe_3O_4/activated carbon composite material. The TBT removal efficiencies at different time intervals ranging from 10 to 70 min were obtained. It was observed that equilibrium was achieved within 60 min and the corresponding TBT removal efficiency for nFe_3O_4/activated carbon composite from the initial concentration of 100 mg/L TBT reaches 4.72 mg/g (94.30 %).

4.12.7.2.1 Adsorption kinetics

Figures 4.173 – 4.177 show the pseudo first-order, pseudo second-order, Elovich, fractional power and intraparticle diffusivity kinetic plots, respectively while Table 4.28 provides the evaluated parameters of the kinetics models. The value of correlation coefficient (R^2) of pseudo second-order kinetic model (> 0.99) is higher than that of all other models indicating that the kinetic model for the adsorption of TBT onto nFe_3O_4/activated carbon composite is pseudo second-order.

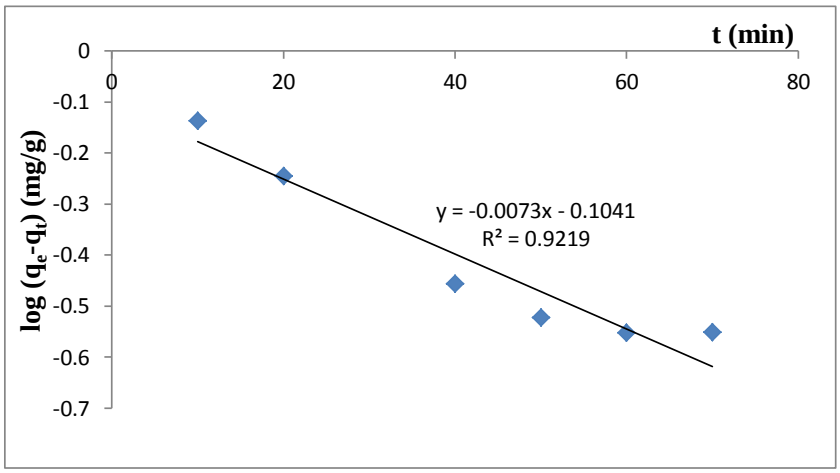

Figure 4.173: Pseudo first-order rate equation plot for TBT adsorption onto nFe_3O_4/activated carbon composite

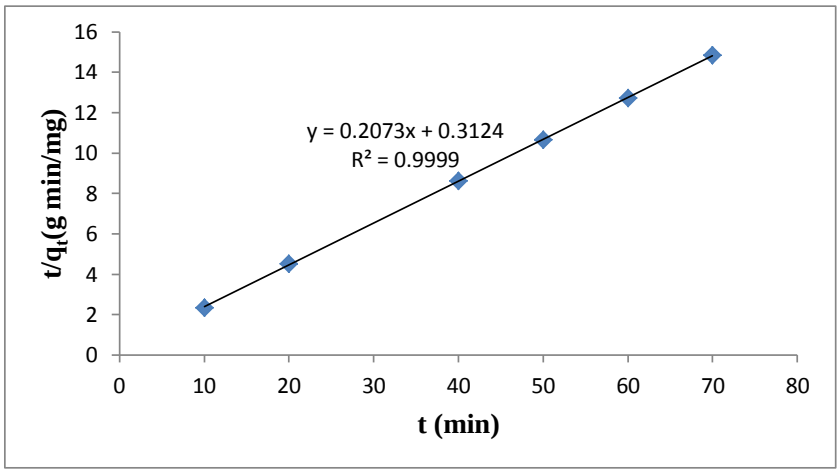

Figure 4.174: Pseudo second-order rate equation plot for TBT adsorption onto nFe_3O_4/activated carbon composite

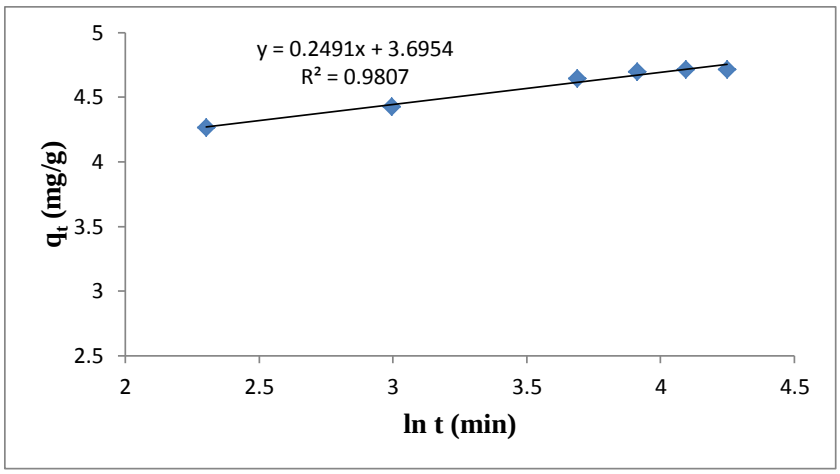

Figure 4.175: Elovich rate equation plot for TBT adsorption onto nFe_3O_4/activated carbon composite

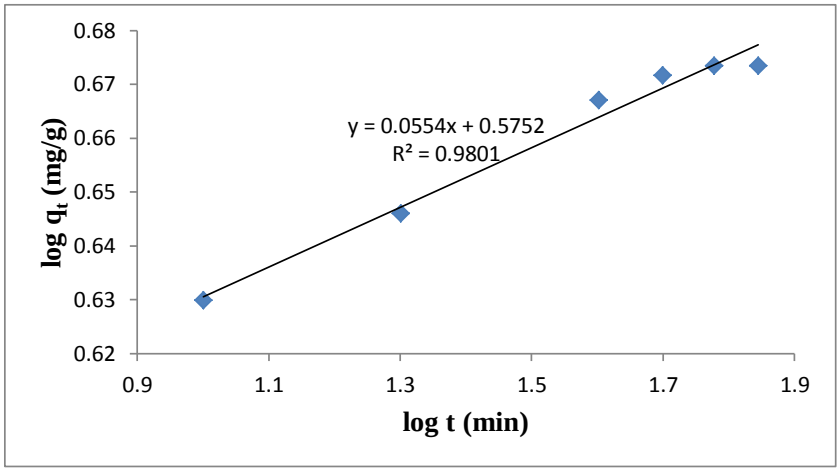

Figure 4.176: Fractional Power rate equation plot for TBT adsorption onto nFe_3O_4/activated carbon composite

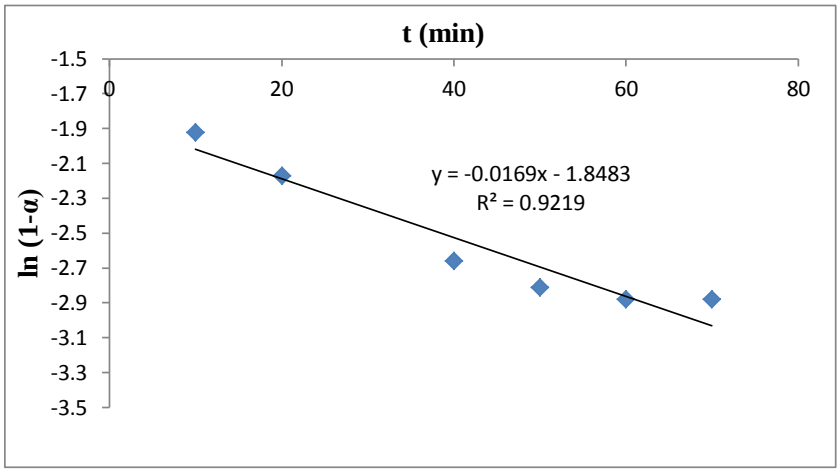

Figure 4.177: Intraparticle diffusivity plot for TBT adsorption onto nFe_3O_4/activated carbon composite

The intraparticle coefficient for the adsorption of TBT by the nFe_3O_4/activated carbon composite was calculated and the results also indicate that the power function model satisfactorily describes the time-dependence of TBT onto the nFe_3O_4/activated carbon composite as the value of the constant v is less than 1.

In the present study, the value of the initial adsorption rates, h_o, obtained for the pseudo second-order kinetics of the adsorption of TBT onto nFe_3O_4/activated carbon composite is 3.2010 mg/g/min. The kinetic model constants k_1, k_2, β, α_E, k_3 and k_p are 0.0168 min^{-1}, 0.1376 g/mg/min, 4.0145 gmin/mg, 1.11 x 10^7 $gmin^2/mg$, 3.7601 mg/g and 0.0169 min^{-1}, respectively.

Table 4.28: Kinetic model parameters for TBT adsorption onto nFe_3O_4/activated carbon composite

Kinetic models	
Pseudo first-order	
k_1 (min^{-1})	0.0168
q_e (mg/g)	0.7869
R^2	0.9219
Pseudo second-order	
q_e (mg/g)	4.8239
h_o (mg/g/min)	3.2010
k_2 (g/mg/min)	0.1376
R^2	0.9999
Elovich	
β (g min/mg)	4.0145
α (g min^2/mg)	1.11×10^7
R^2	0.9807
Fractional Power	
v (min^{-1})	0.0554
k_3 (mg/g)	3.7601
k_3v (mg/g/min)	0.2083
R^2	0.9801
Intraparticle diffusivity	
k_p (min^{-1})	0.0169
R^2	0.9219

4.12.7.3 Effect of pH

The effect of pH on the adsorption of TBT onto the nFe_3O_4/activated carbon composite was studied at pH 3 – 9. It was observed from Figure 4.178 that the percentage of TBT adsorbed by nFe_3O_4/activated carbon composite steadily increases as the pH of the solution increases from pH 3 to pH 8, and reaches equilibration at pH ≥ 8. It is also evident that maximum adsorption was recorded within the pH range of normal saline water and pH 8 was utilized for further studies.

About 94.46 % of TBT was removed from the initial concentration of 100 mg/L TBT by nFe_3O_4/activated carbon composite at a contact time of 60 min, stirring speed of 160 rpm, pH 8 and a temperature of 20 ^oC.

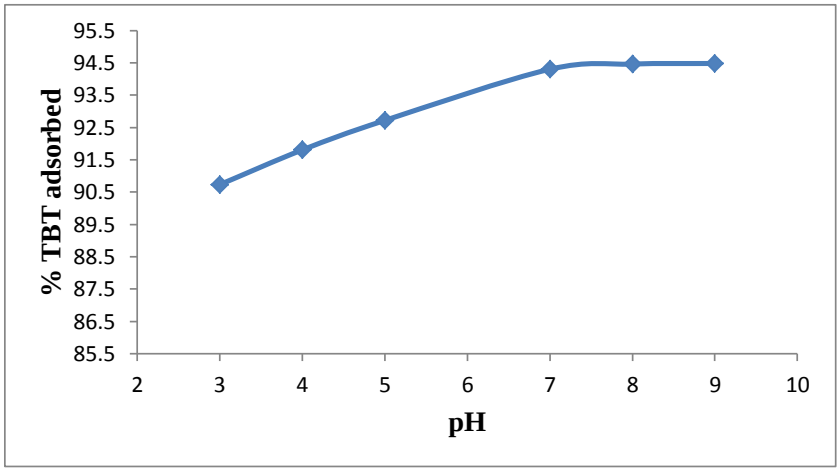

Figure 4.178: Effect of pH on TBT adsorption onto nFe_3O_4/activated carbon composite

Experimental conditions: Concentration of TBT = 100 mg/L; Volume of TBT solution = 25 mL, Mass of composite = 0.5 g; Contact time = 60 min; Stirring speed = 160 rpm, Temperature = 20 ^oC.

4.12.7.4 Effect of stirring speed

The effect of stirring speed on the adsorption of TBT onto the nFe_3O_4/activated carbon composite was studied at a stirring speed of 160 – 200 rpm.

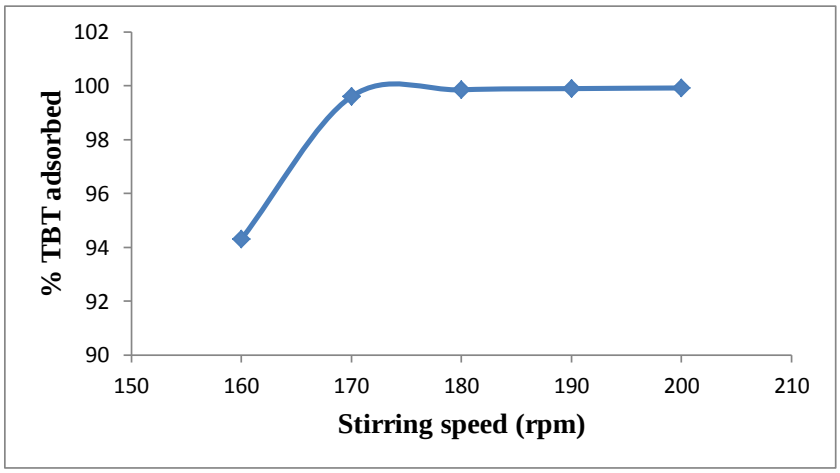

Figure 4.179: Effect of stirring speed on TBT adsorption onto nFe_3O_4/activated carbon composite

Experimental conditions: Concentration of TBT = 100 mg/L; Volume of TBT solution = 25 mL, Mass of composite = 0.5 g; Contact time = 60 min; Temperature = 20 ^oC.

The adsorption capacity of TBT onto nFe_3O_4/activated carbon composite increases with increasing stirring speed from 160 rpm to 180 rpm after which equilibration was attained (Figure 4.179). The figure thus shows that about 99.92 % TBT was removed from the initial concentration of 100 mg/L TBT by nFe_3O_4/activated carbon composite material at a contact time of 60 min, pH 8, a temperature of 20 ^oC and a stirring speed of 200 rpm. 200rpm was therefore used for further studies.

4.12.7.5 Effect of initial concentration

The results on the effect of initial TBT concentration (Figure 4.180) show that the adsorption of TBT on the nFe_3O_4/activated carbon composite increases as the initial TBT concentration increases from 12.5 to 100 mg/L, indicating that adsorption is also favourable for the higher TBT concentrations that have been investigated.

The increase in the adsorption capacity of nFe_3O_4/activated carbon composite with an increase in the initial TBT concentration can also be attributed to increase in the driving force due to concentration gradient developed between the bulk solution and surface of nFe_3O_4/activated carbon composite material.

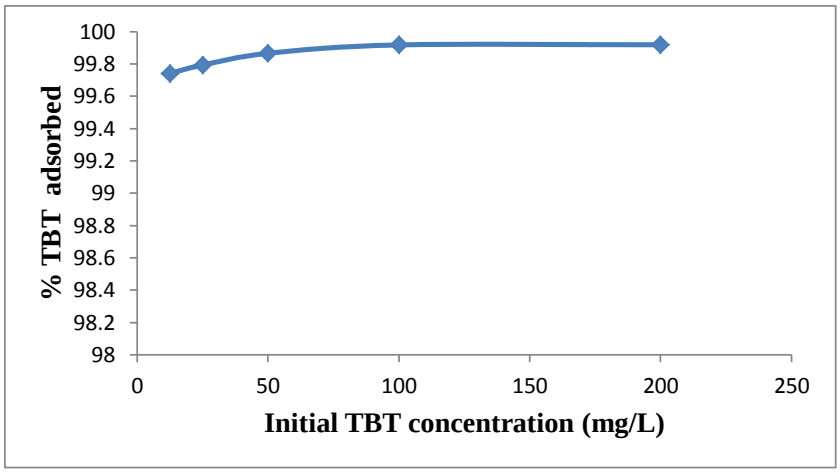

Figure 4.180: Percentage TBT adsorbed by nFe_3O_4/activated carbon composite at various initial TBT concentrations

Experimental conditions: Volume of TBT solution = 25 mL, Mass of composite = 0.5 g; pH = 8; Stirring speed = 200 rpm; Contact time = 60 min; Temperature = 20 ^{o}C.

4.12.7.5.1 Adsorption isotherms

The adsorption isotherm parameters obtained from all the equilibrium models for the adsorption of TBT onto nFe_3O_4/activated carbon composite were given in Table 4.29 and the plots are presented in Figures 4.181 – 4.184. The figures and table show that the experimental data fitted well with Freundlich and D-R isotherm models and the value of n_F, for the nFe_3O_4/activated carbon composite material, falling in the range 1 -10 indicates favourable adsorption.

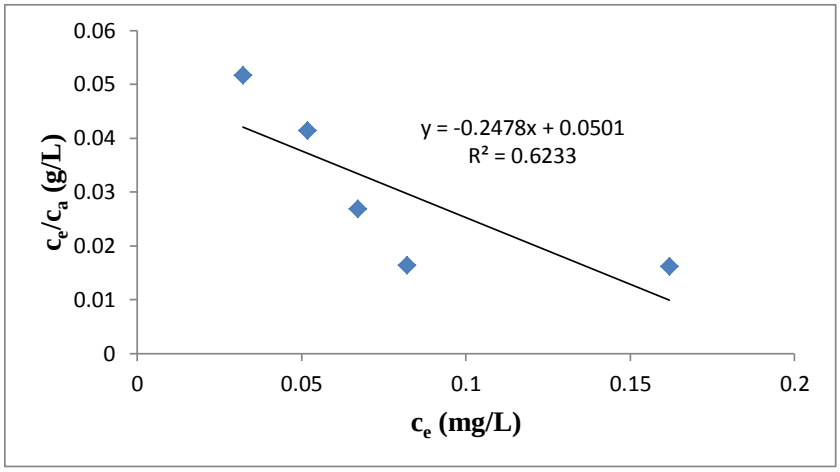

Figure 4.181: Langmuir isotherm for adsorption of TBT onto nFe_3O_4/activated carbon composite

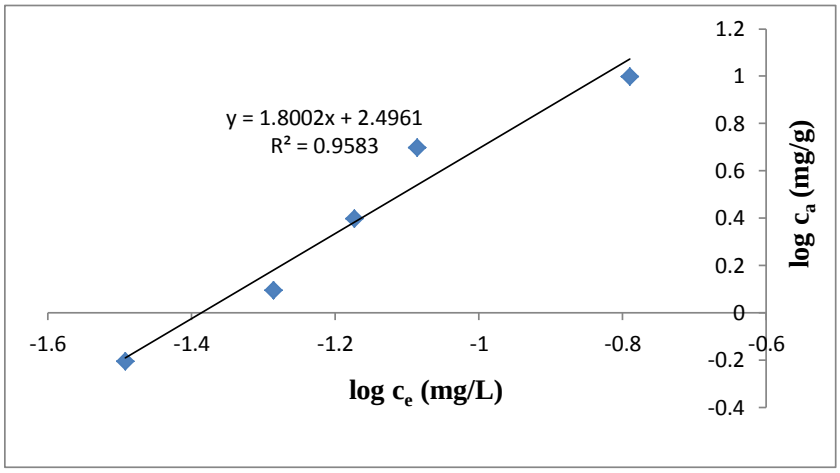

Figure 4.182: Freundlich isotherm for adsorption of TBT onto nFe_3O_4/activated carbon composite

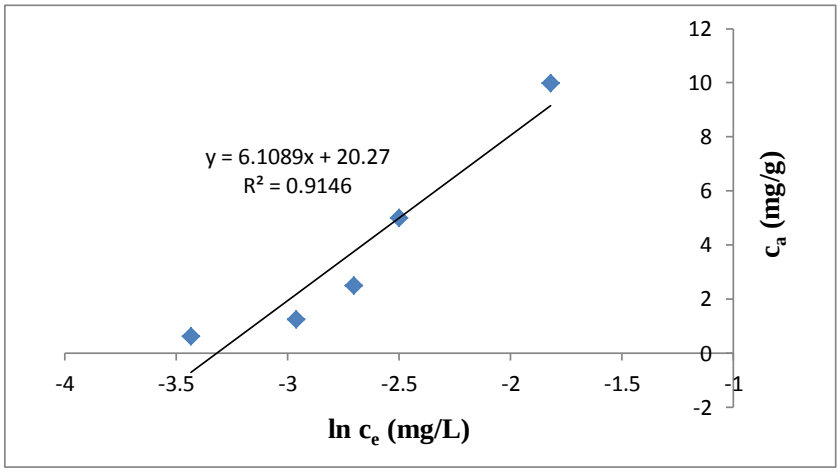

Figure 4.183: Temkin isotherm for adsorption of TBT onto nFe_3O_4/activated carbon composite

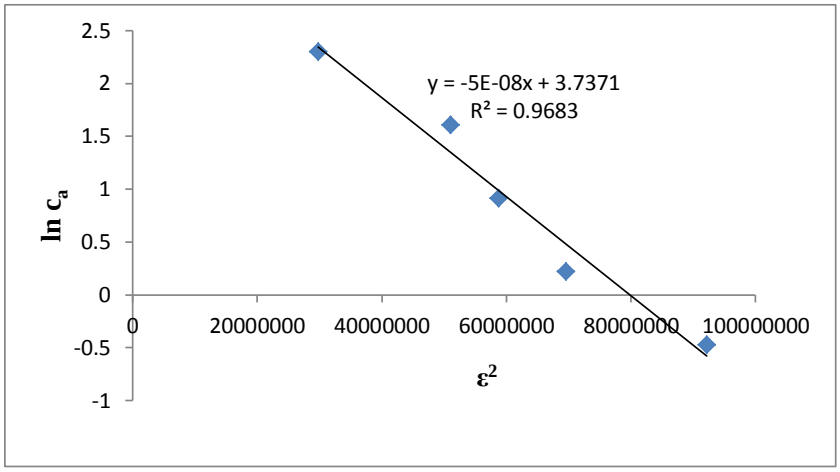

Figure 4.184: D-R isotherm for adsorption of TBT onto nFe_3O_4/activated carbon composite

Table 4.29: Isotherms constants for the adsorption of TBT onto nFe_3O_4/activated carbon composite

Equilibrium models	
Freundlich	
k_F [mg/g (L/mg)$^{1/n}$]	313.40
n_F	0.5554
R^2	0.9583
Langmuir	
K_L (L/mg)	-4.9461
A_{max} (mg/g)	-4.0355
R^2	0.6233
Temkin	
n_T (L/g)	6.1089
k_T (mg/L)	27.6081
b_T (J/mol)	398.76
R^2	0.9146
Dubinin-Redushkevich	
k_{D-R} (J^2/mol^2)	5 x 10^{-8}
q_m (mg/g)	41.9761
E (J/mol)	3162.2
R^2	0.9683

Moreover, the negative value of the Langmuir constants, A_{max} (mg/g) and k_L (L/mg) for TBT adsorption onto nFe_3O_4/activated carbon composite indicate the inadequacy of the Langmuir model to fit the process.

4.12.7.6 Effect of temperature

The experimental results obtained on the effect of temperature for the adsorption of TBT onto nFe_3O_4/activated carbon composite (Figure 4.185) show that the adsorption capacity of the composite increases with increase in the solution temperature. This indicates that the adsorption of TBT onto nFe_3O_4/activated carbon composite is endothermic.

Approximately 99.99 % of TBT was removed from the initial concentration of 100 mg/L TBT by nFe_3O_4/activated carbon composite at a temperature of 80 ^oC, 60 min contact time, pH 8 and a stirring speed of 200 rpm. Figure 4.186 thus shows the Van't Hoff plot for the adsorption of TBT onto nFe_3O_4/activated carbon composite material while ΔH^o , ΔS^o, and ΔG^o are presented in Table 4.30.

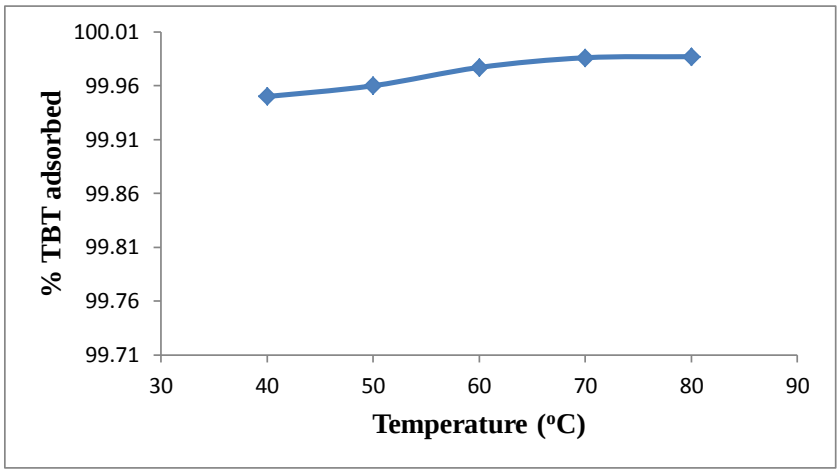

Figure 4.185: Effect of temperature on TBT adsorption onto nFe_3O_4/activated carbon composite

Experimental conditions: Concentration of TBT = 100 mg/L; Volume of TBT solution = 25 mL, Mass of composite = 0.5 g; Contact time = 60 min; pH = 8; Stirring speed = 200 rpm.

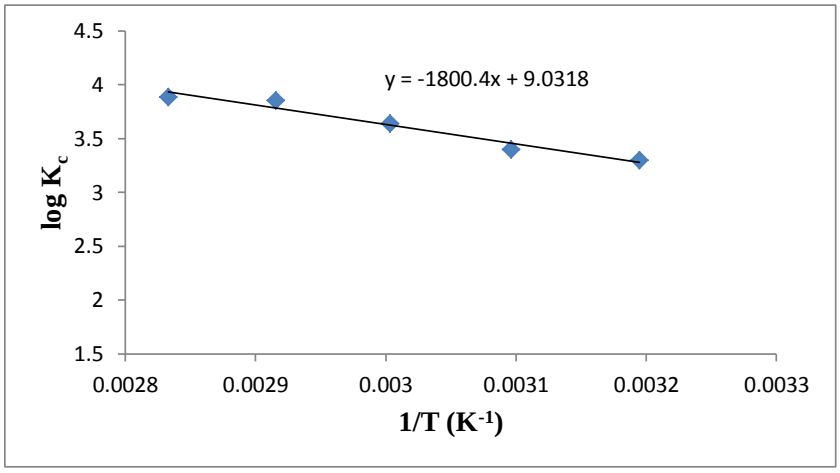

Figure 4.186: Van't Hoff plot for the adsorption of TBT onto nFe_3O_4/activated carbon composite

Table 4.30: Thermodynamic parameters for the adsorption of TBT onto nFe_3O_4/activated carbon composite

Temperature (°C)	ΔG° (kJ/mol)	ΔS° (J/K/mol)	ΔH° (kJ/mol)	K_c
40	-19.78	172.933	34.473	1999.0
50	-21.01			2499.0
60	-23.19			4346.8
70	-25.31			7141.9
80	-26.26			7691.3

The positive value of ΔH^{o} for the intervals of temperatures (34.473 kJ/mol) also shows the endothermic nature of the adsorption process. The positive value of ΔS^{o} (172.933 J/K/mol) corresponds to increase in degree of freedom of the adsorbed TBT onto nFe_3O_4/activated carbon composite and suggest the increase in concentration of adsorbate in solid–solution interface indicating an increase in adsorbate concentration onto the solid phase. It is evident from Table 4.30 that ΔG^{o} values were found to be more negative as the temperature increases, which indicates that the adsorption efficiency of TBT onto nFe_3O_4/activated carbon composite increases with increase in temperature.

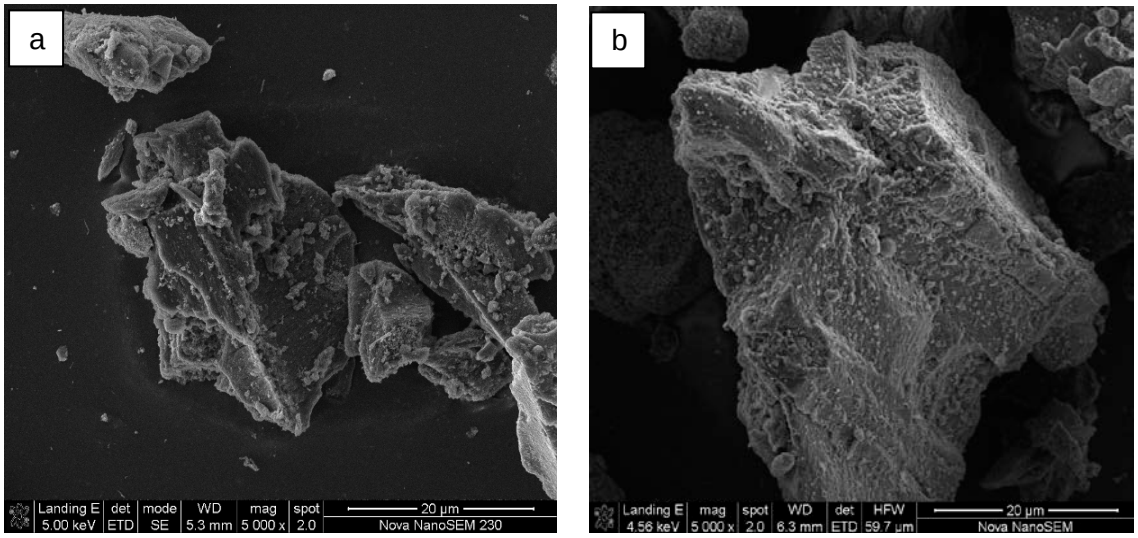

Figure 4.187: SEM of nFe_3O_4/activated carbon composite before (a) and after (b) TBT adsorption

The SEM analysis of nFe_3O_4/activated carbon composite before and after adsorption (optimal condition) is presented in Figure 4.187 and the TBT chromatogram after adsorption of 100 mg/L TBT with 0.5 g of nFe_3O_4/activated carbon composite, 60 min contact time, temperature 20 ^{o}C and a stirring speed of 200 rpm is as shown in Figure 4.188.

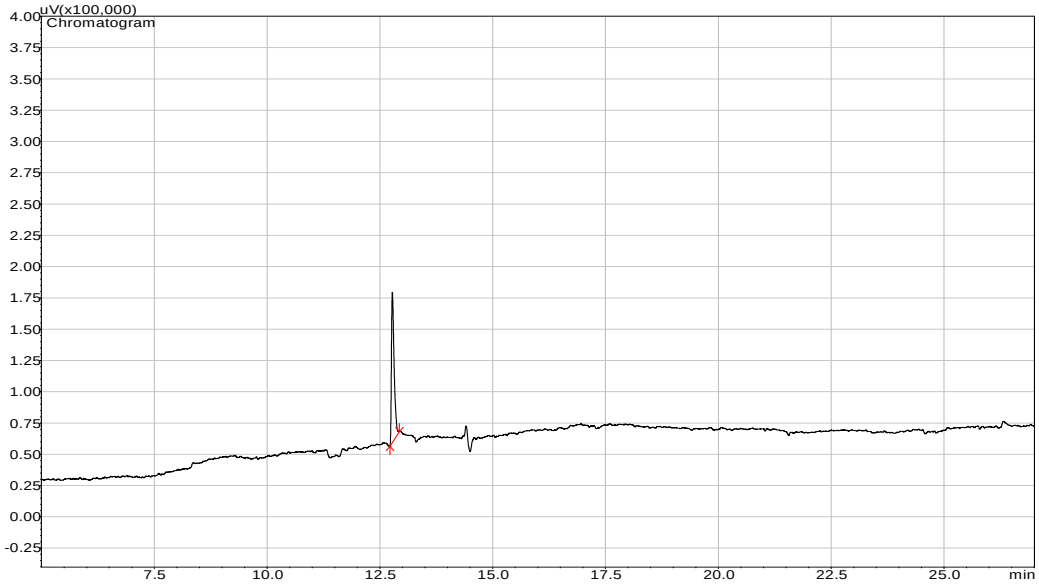

Figure 4.188: Representative TBT chromatogram after adsorption of 100 mg/L TBT with 0.5g of nFe_3O_4/activated carbon composite, contact time of 60min, temperature 20 ^oC and a stirring speed of 200 rpm

4.12.8 Adsorption of TBT from TBT-contaminated artificial seawater onto $nSiO_2$/activated carbon composite

4.12.8.1 Effect of adsorbent amount

The results on the effect of adsorbent amount on the adsorption of TBT by the $nSiO_2$/activated carbon composite material as shown in Figure 4.189 indicates that the percentage of TBT adsorption increases with increasing $nSiO_2$/activated carbon composite amount, reaching an optimum at 0.5 g, corresponding to 99.74 % removal.

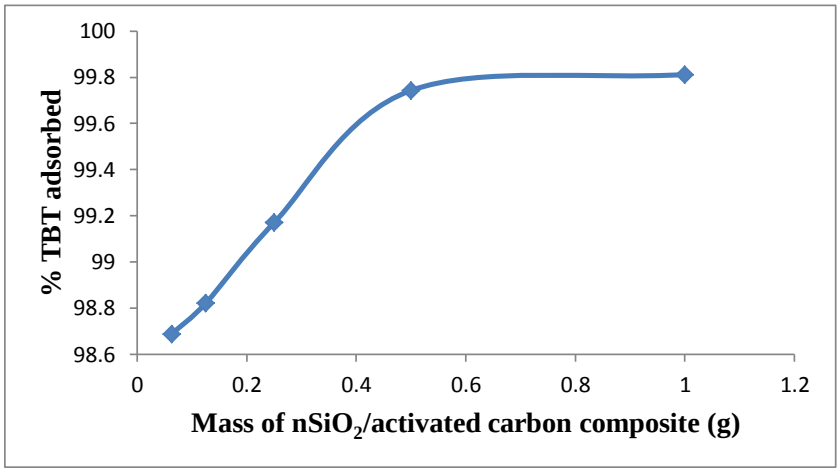

Figure 4.189: Adsorption efficiencies of TBT onto $nSiO_2$/activated carbon composite

Experimental conditions: Concentration of TBT = 100 mg/L; Volume of TBT solution = 25 mL, Contact time = 60 min; Stirring speed = 160 rpm, Temperature = 20 ^oC.

4.12.8.2 Effect of contact time

Figure 4.190 shows the effect of contact time on the adsorption of TBT onto $nSiO_2$/activated carbon composite material. The TBT removal efficiency at different time intervals ranging from 10 – 70 min were obtained.

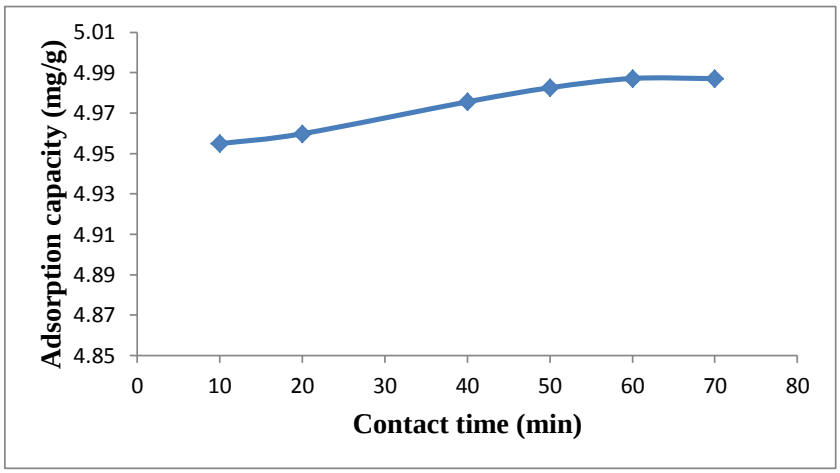

Figure 4.190: Effect of contact time on TBT adsorption onto $nSiO_2$/activated carbon composite

Experimental conditions: Concentration of TBT = 100 mg/L; Volume of TBT solution = 25 mL, Mass of composite = 0.5 g; Stirring speed = 160 rpm, Temperature = 20 ^{o}C.

It was therefore observed from Figure 4.190 that equilibrium was approximately achieved within 60 min. The amount of TBT removed at a contact time of 60 min from the initial TBT concentration of 5.0 mg/g by the $nSiO_2$/activated carbon composite is 4.987 mg/g (99.74 %). 60 min was therefore used for further studies.

4.12.8.2.1 Adsorption kinetics

Figures 4.191 – 4.195 show the pseudo first-order, pseudo second-order, Elovich, fractional power and intraparticle diffusivity kinetic plots while Table 4.31 provides the evaluated parameters of the kinetics models.

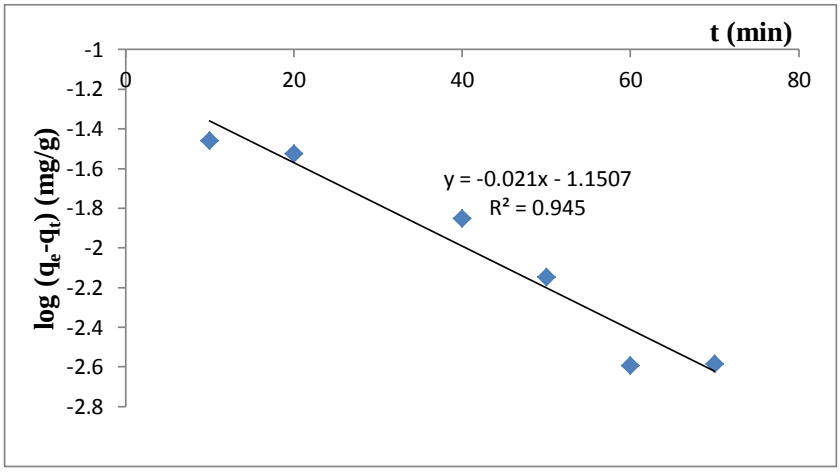

Figure 4.191: Pseudo first-order rate equation plot for TBT adsorption onto $nSiO_2$/activated carbon composite

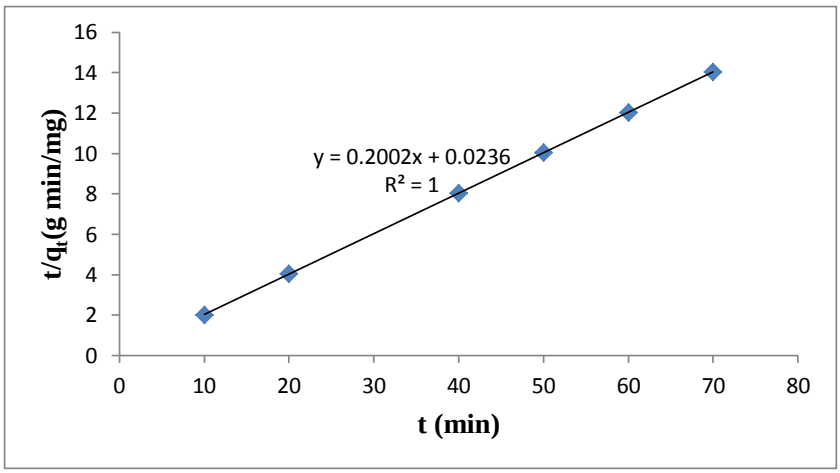

Figure 4.192: Pseudo second-order rate equation plot for TBT adsorption onto $nSiO_2$/activated carbon composite

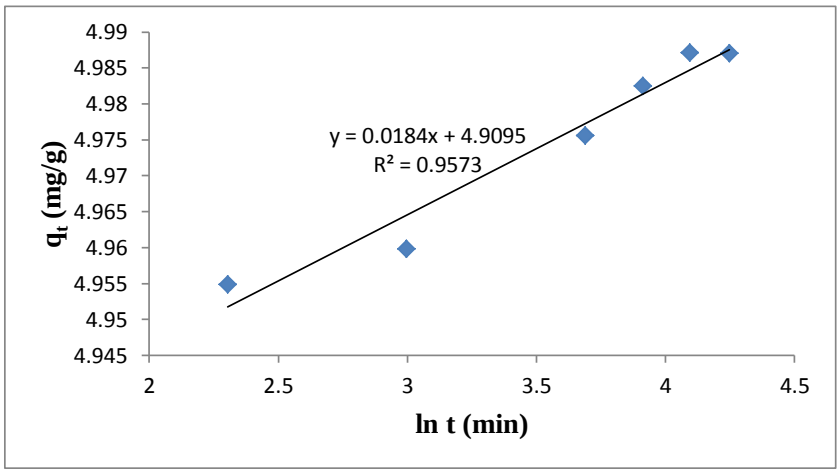

Figure 4.193: Elovich rate equation plot for TBT adsorption onto $nSiO_2$/activated carbon composite

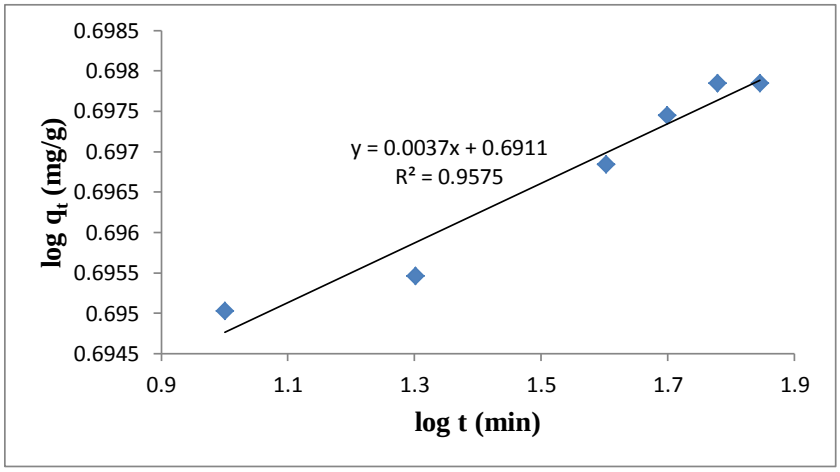

Figure 4.194: Fractional Power rate equation plot for TBT adsorption onto nSiO$_2$/activated carbon composite

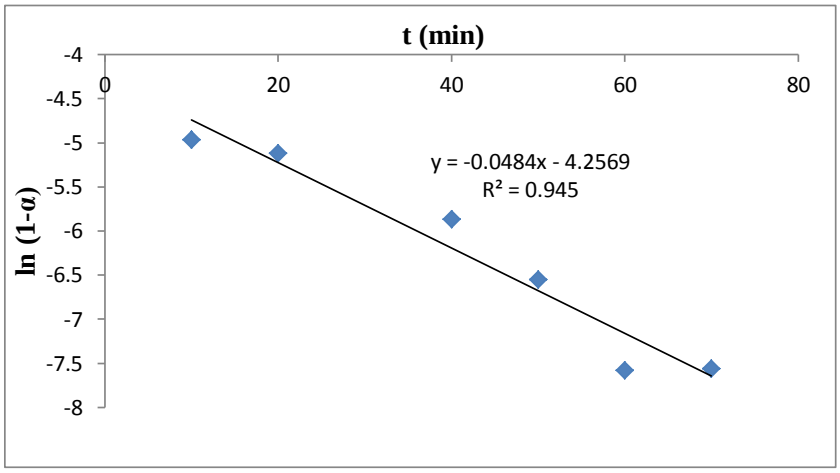

Figure 4.195: Intraparticle diffusivity plot for TBT adsorption onto nSiO$_2$/activated carbon composite

The results obtained show a very good compliance with pseudo second-order equation with high regression coefficient (> 0.999) whereas the pseudo first-order and Elovich models were not applicable as low regression coefficients (< 0.96) were observed. The results also show that the adsorption rate constant, k_2, initial adsorption rate, h_o, and equilibrium adsorption capacity, q_e, of the pseudo second-order model are 1.6983 g/mg/min, 42.373 mg/g/min and 4.9950 mg/g, respectively.

A simple kinetic analysis of the adsorption of TBT onto nSiO$_2$/activated carbon composite was also tested according to fractional power model and Table 4.31 shows the estimated parameters of the model. The results indicate that the power model satisfactorily described the time-dependent of TBT on the nSiO$_2$/activated carbon composite as the value of the constant v is less than 1 and the regression coefficient is greater than 0.95.

The kinetic model constants k_1, k_2, β, α_E, k_3 and k_p as presented in Table 4.31 for the adsorption of TBT onto $nSiO_2$/activated carbon composite material are therefore 0.0484 min^{-1}, 1.6983 g/mg/min, 54.3478 gmin/mg, 4.11 x 10^{117} $gmin^2/mg$, 4.9102 mg/g and 0.0484 min^{-1}, respectively.

Table 4.31: Kinetic model parameters for TBT adsorption onto $nSiO_2$/activated carbon composite

Kinetic models	
Pseudo first-order	
k_1 (min^{-1})	0.0484
q_e (mg/g)	0.07068
R^2	0.9450
Pseudo second-order	
q_e (mg/g)	4.9950
h_o (mg/g/min)	42.373
k_2 (g/mg/min)	1.6983
R^2	1.000
Elovich	
β (g min/mg)	54.3478
α (g min^2/mg)	4.11 x 10^{117}
R^2	0.9573
Fractional Power	
v (min^{-1})	0.0037
k_3 (mg/g)	4.9102
k_3v (mg/g/min)	0.0182
R^2	0.9575
Intraparticle diffusivity	
k_p (min^{-1})	0.0484
R^2	0.9450

4.12.8.3 Effect of pH

The effect of pH on the adsorption of TBT onto $nSiO_2$/activated carbon composite material was studied at pH 3 – 9. It was observed from Figure 4.196 that the percentage of TBT adsorbed by $nSiO_2$/activated carbon composite material increases as the pH of the solution increases from pH 3 to pH 8, and reaches equilibration at pH ≥ 8.

Higher adsorption capacity was therefore recorded within the pH range of normal saline water. About 99.74 % TBT was removed from the initial concentration of 100 mg/L TBT by the $nSiO_2$/activated carbon composite at pH 8, a contact time of 60 min, 160 rpm stirring speed and a temperature of 20 ^oC.

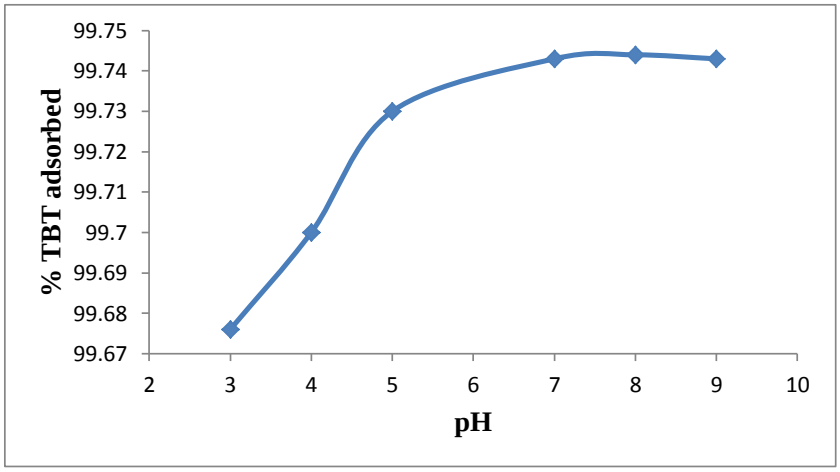

Figure 4.196: Effect of pH on TBT adsorption onto $nSiO_2$/activated carbon composite

Experimental conditions: Concentration of TBT = 100 mg/L; Volume of TBT solution = 25 mL, Mass of composite = 0.5 g; Contact time = 60 min; Stirring speed = 160 rpm, Temperature = 20 ^{o}C.

4.12.8.4 Effect of stirring speed

The stirring speed of the adsorption process was also studied and optimized. The stirring speed on the adsorption of TBT onto $nSiO_2$/activated carbon composite was studied at a stirring speed of 160 – 200 rpm. Figure 4.197 therefore shows that the adsorption capacity of $nSiO_2$/activated carbon composite increases as the stirring speed of the mixture increases.

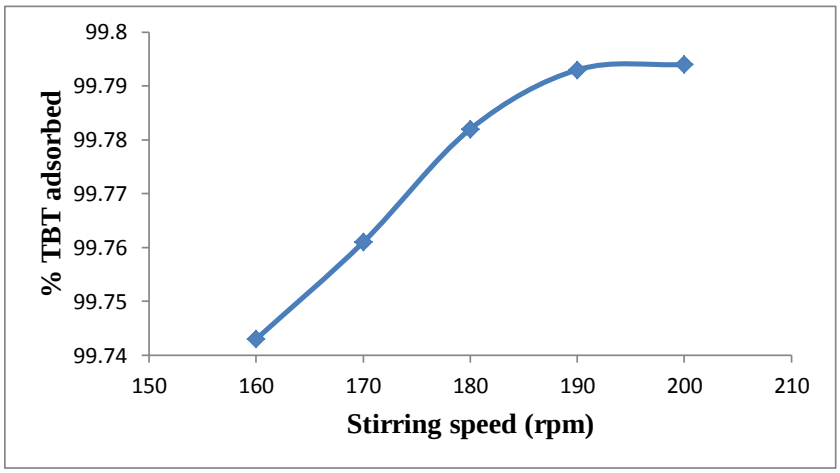

Figure 4.197: Effect of stirring speed on TBT adsorption onto $nSiO_2$/activated carbon composite

Experimental conditions: Concentration of TBT = 100 mg/L; Volume of TBT solution = 25 mL, Mass of composite = 0.5 g; Contact time = 60 min; Temperature = 20 ^{o}C.

Approx. 4.989 mg/g (99.79 %) TBT was removed from the initial concentration of 5 mg/g TBT by the $nSiO_2$/activated carbon composite at a contact time of 60 min, pH 8, temperature of 20 ^{o}C and a stirring speed of 200 rpm (Figure 4.197).

4.12.8.5 Effect of initial concentration

Figure 4.198 shows that the adsorption of TBT onto $nSiO_2$/activated carbon composite material increases as the initial TBT concentration increases from 12.5 to 100 mg/L, indicating that the adsorption is also favourable for the higher TBT concentrations that have been investigated.

The increase in the adsorption capacity with an increase in initial TBT concentration is a result of the increase in the driving force due to concentration gradient developed between the bulk solution and surface of $nSiO_2$/activated carbon composite adsorbent.

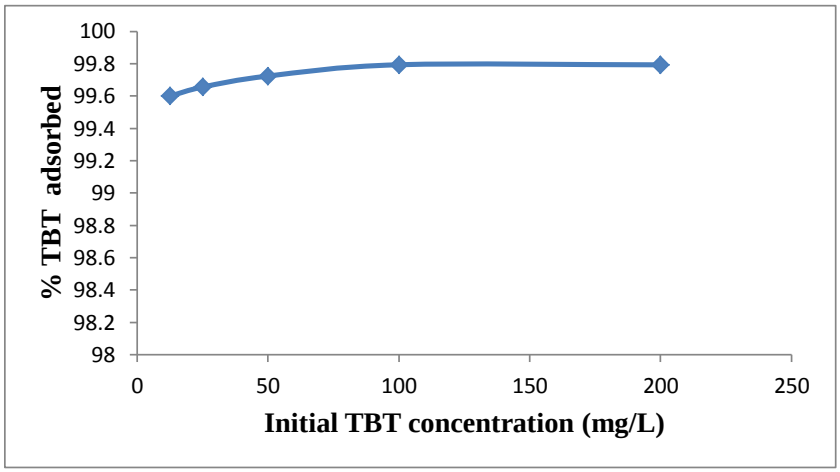

Figure 4.198: Percentage TBT adsorbed by $nSiO_2$/activated carbon composite at various initial TBT concentrations

Experimental conditions: Volume of TBT solution = 25 mL, Mass of composite = 0.5 g; pH = 8; Stirring speed = 200 rpm; Contact time = 60 min; Temperature = 20 ^{o}C.

4.12.8.5.1 Adsorption isotherms

The present study indicates that the Freundlich model fit the experiment data well. It is the suitable model for describing this adsorption process, as R^2 value is higher than the R^2 values obtained for other models (Figures 4.199 – 4.202 and Table 4.32), probably due to the real heterogeneous nature of the surface sites involved in the process of adsorption. The value of n_F falling in the range 1 -10 also indicates favourable adsorption.

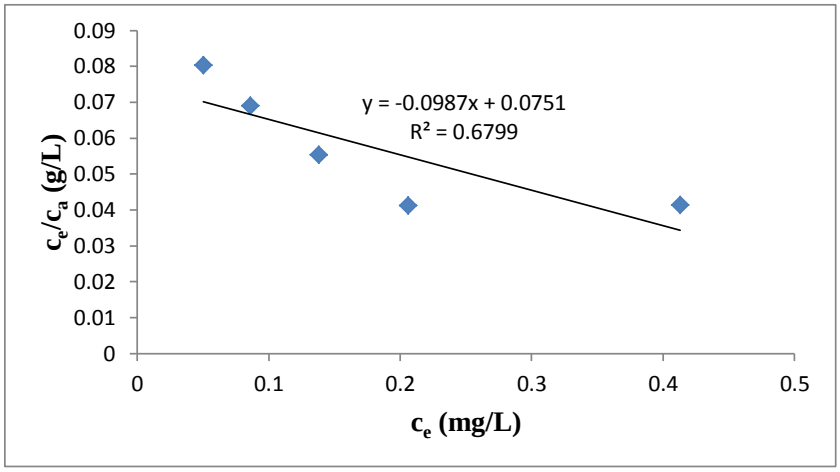

Figure 4.199: Langmuir isotherm for adsorption of TBT onto $nSiO_2$/activated carbon composite

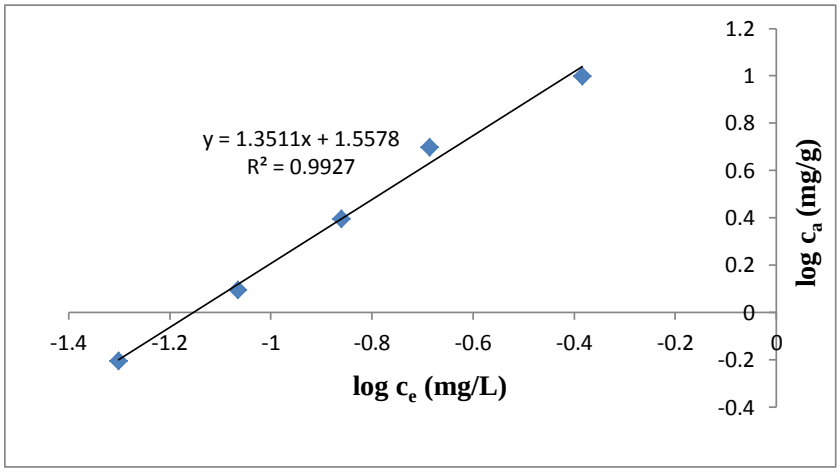

Figure 4.200: Freundlich isotherm for adsorption of TBT onto $nSiO_2$/activated carbon composite

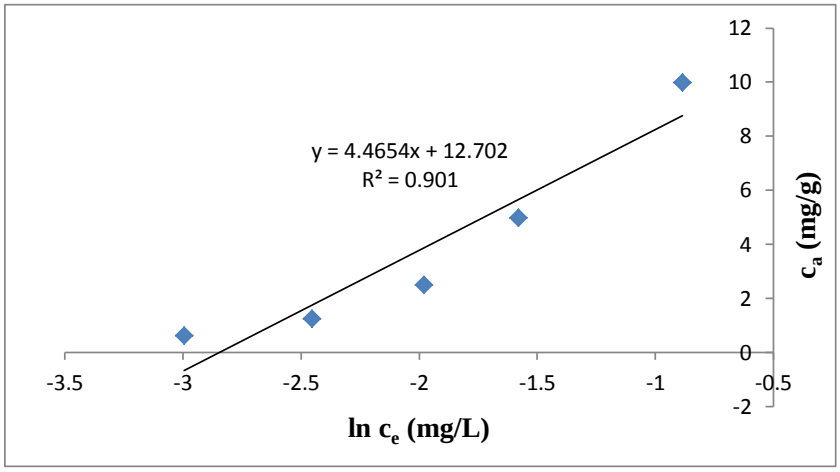

Figure 4.201: Temkin isotherm for adsorption of TBT onto $nSiO_2$/activated carbon composite

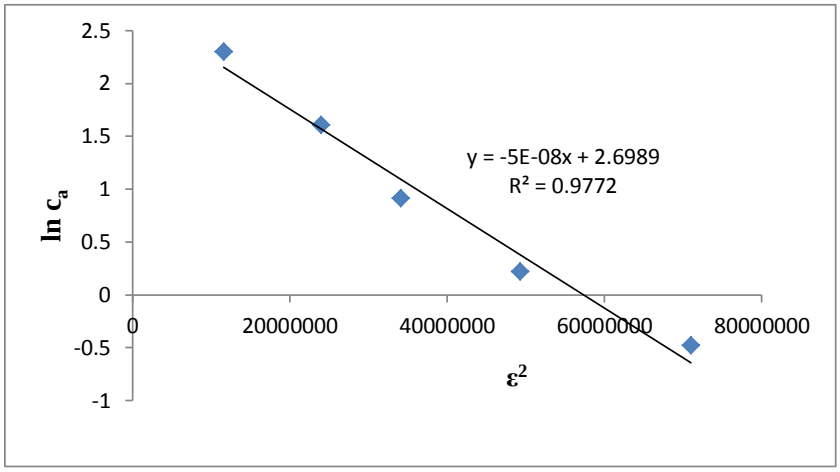

Figure 4.202: D-R isotherm for adsorption of TBT onto $nSiO_2$/activated carbon composite

Table 4.32: Isotherms constants for the adsorption of TBT onto $nSiO_2$/activated carbon composite

Equilibrium models	
Freundlich	
k_F [mg/g (L/mg)$^{1/n}$]	36.12
n_F	0.7401
R^2	0.9927
Langmuir	
K_L (L/mg)	-1.3142
A_{max} (mg/g)	-10.1317
R^2	0.6799
Temkin	
n_T (L/g)	4.4654
k_T (mg/L)	17.1936
b_T (J/mol)	545.53
R^2	0.9010
Dubinin-Redushkevich	
k_{D-R} (J^2/mol^2)	5 x 10^{-8}
q_m (mg/g)	14.8634
E (J/mol)	3162.28
R^2	0.9772

The experimental data (Table 4.32) does not fit the Langmuir model, as the R^2 value is very low (< 0.7) and Langmuir constants, $A_{\max}$ (mg/g) and k_L (L/mg) for TBT adsorption onto $nSiO_2$/activated carbon composite are negative. The Temkin and D-R isotherm models also gave low R^2 value (< 0.91 for Temkin and < 0.98 for D-R) and can also not be used to describe the adsorption process. The equilibrium model constants k_F, k_L, k_T and k_{D-R} for the adsorption of TBT onto $nSiO_2$/activated carbon composite are 36.12 mg/g (L/mg)$^{1/n}$, -1.3142 L/mg, 17.1936 mg/L and 5 x 10^{-8} J^2/mol^2, respectively.

4.12.8.6 Effect of temperature

The experimental results obtained on the effect of temperature show that the adsorption capacity of TBT onto $nSiO_2$/activated carbon composite adsorbent increases with increase in the solution temperature (Figure 4.203). This indicates that the adsorption of TBT onto the $nSiO_2$/activated carbon composite material is endothermic.

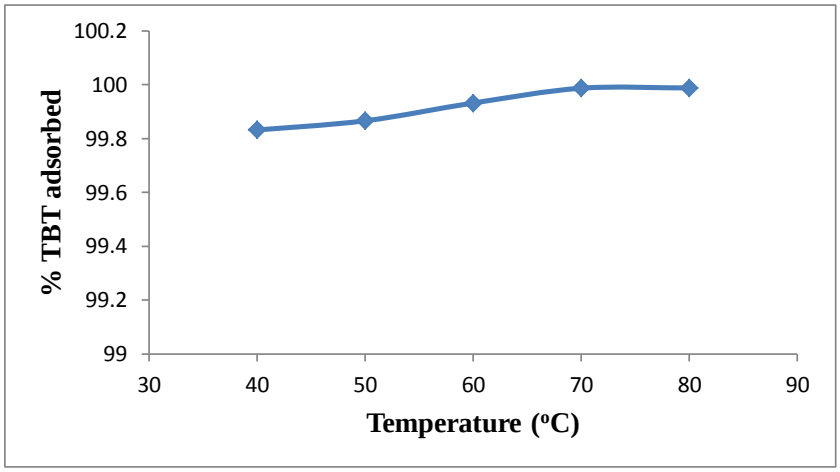

Figure 4.203: Effect of temperature on TBT adsorption onto $nSiO_2$/activated carbon composite

Experimental conditions: Concentration of TBT = 100 mg/L; Volume of TBT solution = 25 mL, Mass of composite = 0.5 g; Contact time = 60 min; pH = 8; Stirring speed = 200 rpm.

Approx. 99.99 % TBT was removed from the initial concentration of 100 mg/L TBT by $nSiO_2$/activated carbon composite at 80 ^oC, contact time of 60 min, pH 8 and a stirring speed of 200 rpm. Figure 4.204 thus shows the Van't Hoff plot for the adsorption of TBT and the variation in the extent of adsorption with respect to temperature has been explained on the basis of ΔH^o , ΔS^o, and ΔG^o as shown in Table 4.33.

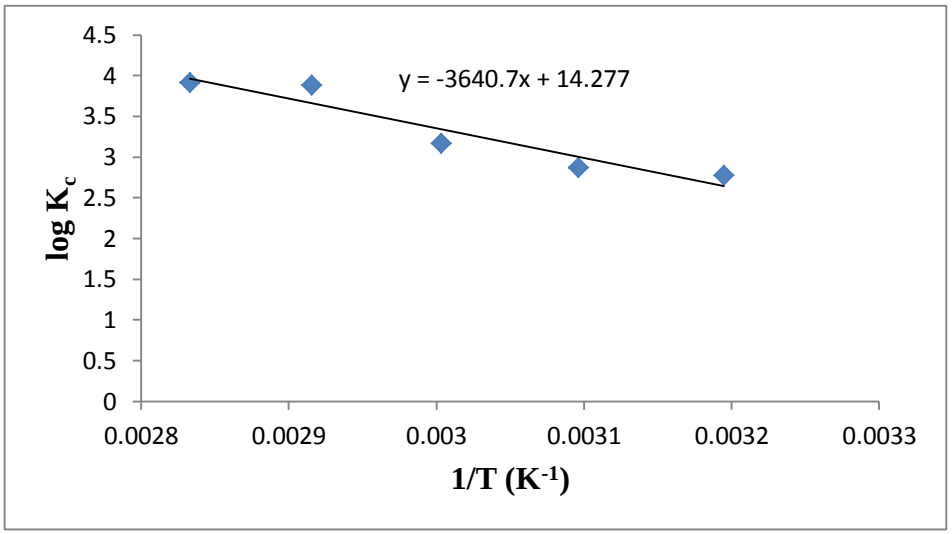

Figure 4.204: Van't Hoff plot for the adsorption of TBT onto $nSiO_2$/activated carbon composite

Table 4.33: Thermodynamic parameters for the adsorption of TBT onto $nSiO_2$/activated carbon composite

Temperature (°C)	ΔG° (kJ/mol)	ΔS° (J/K/mol)	ΔH° (kJ/mol)	K_c
40	-16.62	273.364	69.709	594.2
50	-17.76			745.3
60	-20.19			1469.6
70	-25.52			7691.3
80	-26.50			8332.3

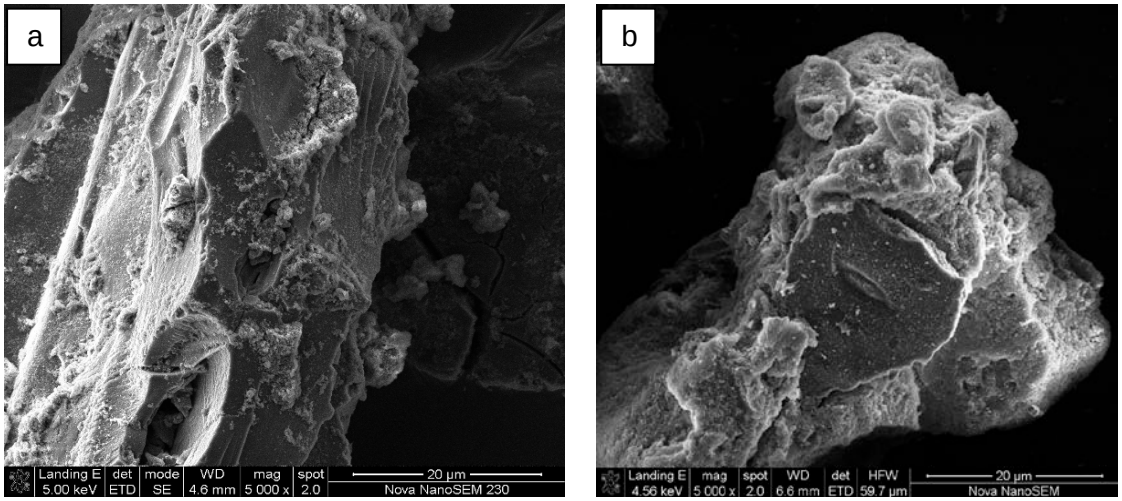

Figure 4.205: SEM of $nSiO_2$/activated carbon composite before (a) and after (b) TBT adsorption

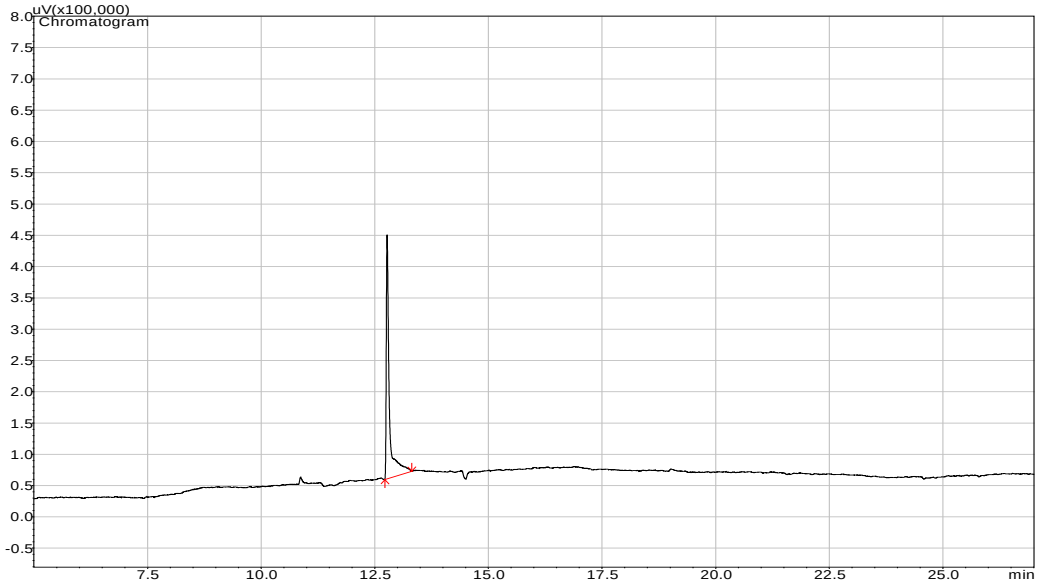

Figure 4.206: Representative TBT chromatogram after adsorption of 100 mg/L TBT with 0.5g of $nSiO_2$/activated carbon composite, contact time of 60min, temperature 20 ^oC and a stirring speed of 200 rpm

The positive value of ΔH^o for the intervals of temperatures (69.709 kJ/mol) also shows the endothermic nature of the adsorption process. The positive value of ΔS^o (273.364 J/K/mol) corresponds to an increase in degree of freedom of the adsorbed TBT. It is also evident from

Table 4.33 that ΔG^{o} values were found to be more negative as the temperature increases and this indicates that the adsorption efficiency of TBT onto $nSiO_2$/activated carbon composite increases with increase in temperature. K_c ranged 594.2 – 8332.3.

The SEM analysis of $nSiO_2$/activated carbon composite before and after the adsorption studies is presented in Figure 4.205. A representative TBT chromatogram after adsorption of 100 mg/L TBT onto 0.5 g of $nSiO_2$/activated carbon composite material, contact time of 60min, temperature of 20 ^{o}C and a stirring speed of 200 rpm is as shown in Figure 4.206.

4.12.9 Adsorption of TBT from TBT-contaminated artificial seawater onto nZnO/activated carbon composite

4.12.9.1 Effect of adsorbent amount

To study the effect of nZnO/activated carbon composite amount on the adsorption of TBT from TBT – contaminated artificial seawater, the amount of the adsorbent was varied from 0.0625 – 1 g, the concentration of TBT was taken as 100 mg/L and other parameters were also kept constant. Figure 4.207 shows that the amount of TBT adsorbed and percentage removal of TBT by nZnO/activated carbon composite increases as the amount of adsorbent increases from 0.0625 - 0.5 g after which equilibration was attained (Ayanda et al., 2013c).

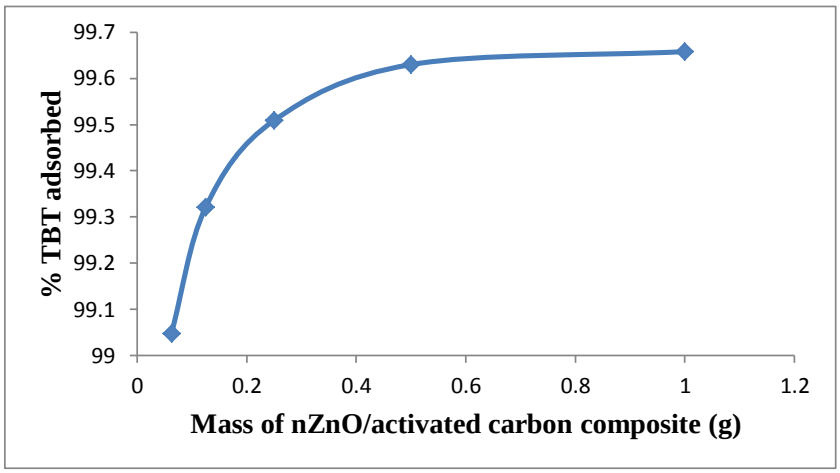

Figure 4.207: Adsorption efficiencies of TBT onto nZnO/activated carbon composite

Experimental conditions: Concentration of TBT = 100 mg/L; Volume of TBT solution = 25 mL, Contact time = 60 min; Stirring speed = 160 rpm, Temperature = 20 ^{o}C.

Figure 4.207 therefore shows that 0.5 g of nZnO/activated carbon composite removed 99.63 % of TBT from TBT – contaminated artificial seawater.

4.12.9.2 Effect of contact time

To study the effect of contact time on the adsorption of TBT onto nZnO/activated carbon composite, the TBT concentration was 100 mg/L while, other remaining conditions such as pH, stirring speed etc. were constant. The effect of contact time was carried out at various time intervals from 10 – 70 min.

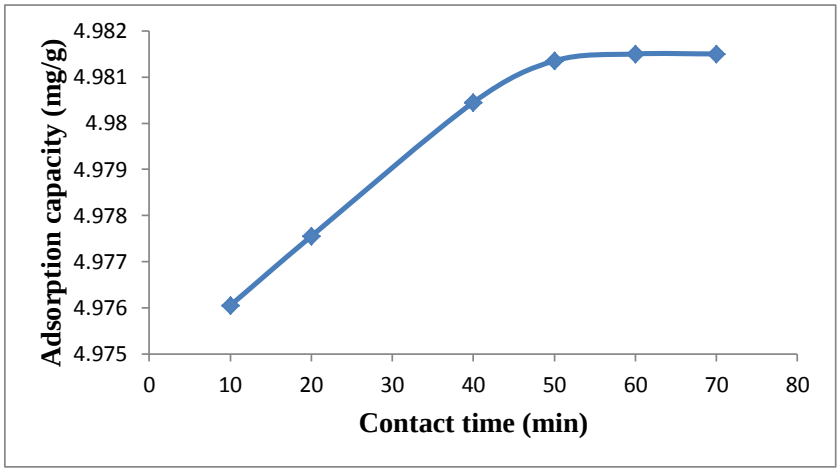

Figure 4.208: Effect of contact time on TBT adsorption onto nZnO/activated carbon composite

Experimental conditions: Concentration of TBT = 100 mg/L; Volume of TBT solution = 25 mL, Mass of composite = 0.5 g; Stirring speed = 160 rpm, Temperature = 20 ^{o}C.

The increase in the amount of TBT adsorbed by nZnO/activated carbon composite material from 4.976 mg/g (99.52 %) to 4.982 mg/g (99.63 %) (Figure 4.208) was observed up to 60 min. After that, there is no significant change observed. 60 min was therefore fixed as the contact time for further studies.

4.12.9.2.1 Adsorption kinetics

Figures 4.209 – 4.213 thus show the pseudo first-order, pseudo second-order, Elovich, fractional power and intraparticle diffusivity kinetic plots, respectively and Table 4.34 provides the evaluated parameters of the kinetics models.

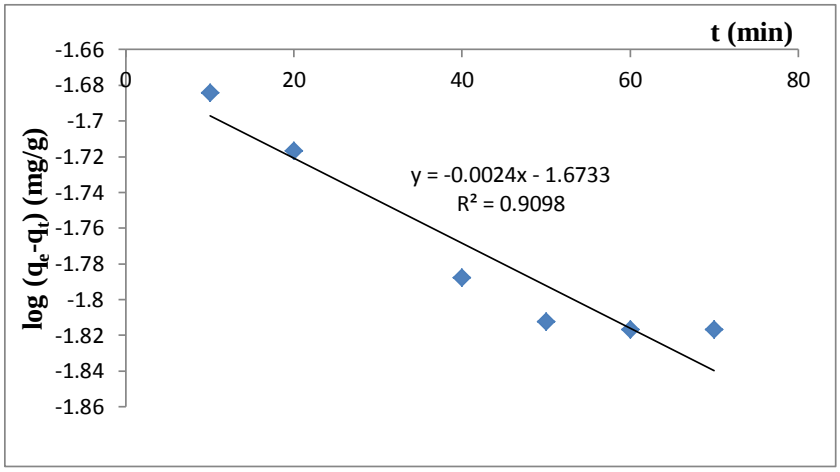

Figure 4.209: Pseudo first-order rate equation plot for TBT adsorption onto nZnO/activated carbon composite

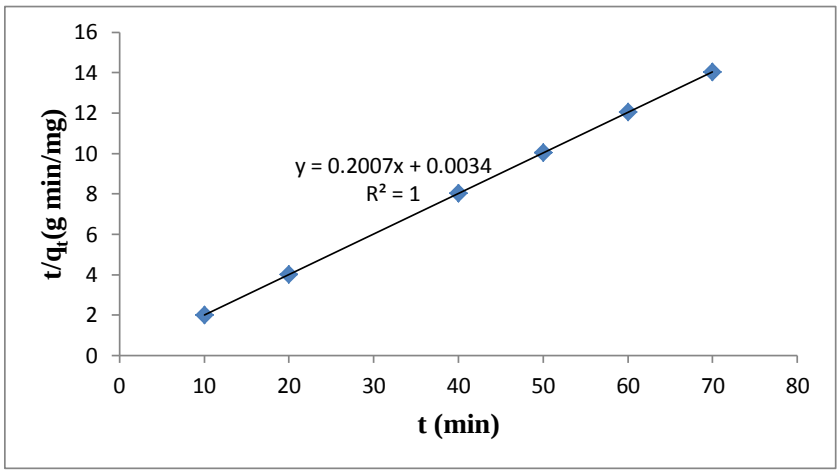

Figure 4.210: Pseudo second-order rate equation plot for TBT adsorption onto nZnO/activated carbon composite

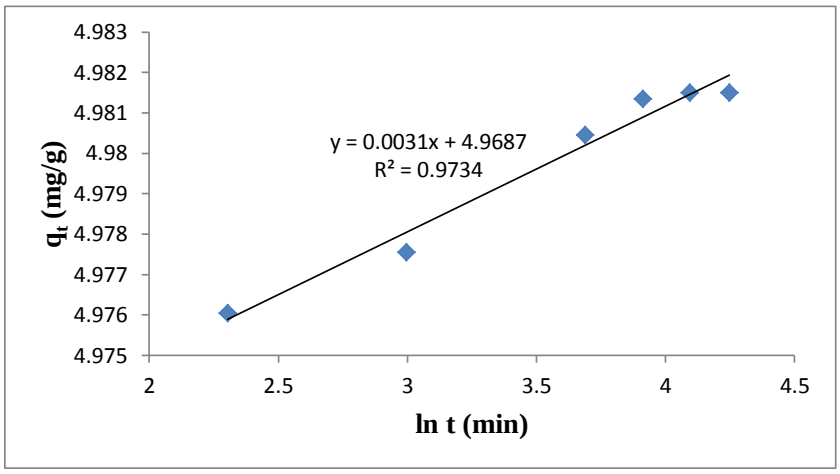

Figure 4.211: Elovich rate equation plot for TBT adsorption onto nZnO/activated carbon composite

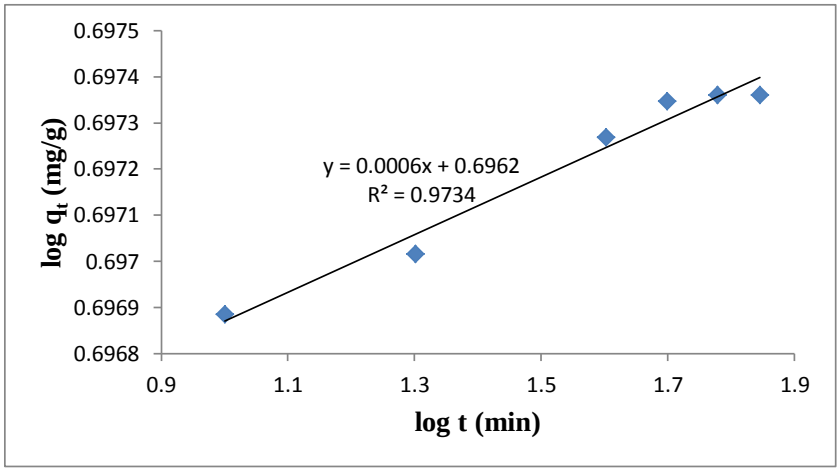

Figure 4.212: Fractional Power rate equation plot for TBT adsorption onto nZnO/activated carbon composite

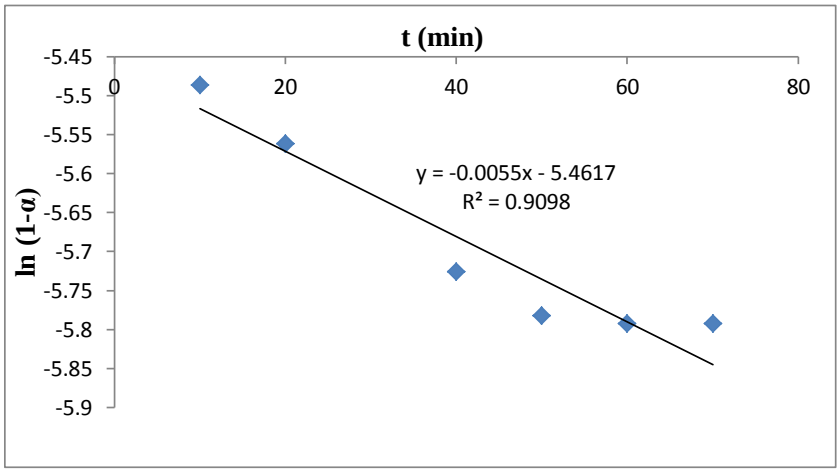

Figure 4.213: Intraparticle diffusivity plot for TBT adsorption onto nZnO/activated carbon composite

The value of correlation coefficient (R^2) of pseudo second-order kinetic model (> 0.99) is higher than the correlation coefficients of all other models indicating that the kinetic model for the adsorption of TBT onto the nZnO/activated carbon composite is pseudo second-order. The intraparticle coefficient for the adsorption of TBT by the nZnO/activated carbon composite is also calculated and presented in Table 4.34 and the results also indicate that the power function model satisfactorily describes the time-dependence of TBT on the nZnO/activated carbon composite since the value of the constant v is less than 1.

The value of the initial adsorption rate, h_o, obtained for the pseudo second-order kinetics is 294.12 mg/g/min. The amount of TBT adsorbed at equilibrium per unit weight of the adsorbent (q_e) is 4.9826 mg/g and the rate constant of pseudo second - order adsorption (k_2) is 11.8470 g/mg/min.

Table 4.34: Kinetic model parameters for TBT adsorption onto nZnO/activated carbon composite

Kinetic models	
Pseudo first-order	
k_1 (min^{-1})	0.005527
q_e (mg/g)	0.02122
R^2	0.9098
Pseudo second-order	
q_e (mg/g)	4.9826
h_o (mg/g/min)	294.12
k_2 (g/mg/min)	11.8470
R^2	1.000
Elovich	
β (g min/mg)	322.58
α (g min^2/mg)	3.9431×10^{698}
R^2	0.9734
Fractional Power	
v (min^{-1})	0.0006
k_3 (mg/g)	4.9682
k_3v (mg/g/min)	0.00298
R^2	0.9734
Intraparticle diffusivity	
k_p (min^{-1})	0.0055
R^2	0.9098

4.12.9.3 Effect of pH

The effect of pH on the adsorption of TBT onto nZnO/activated carbon composite was studied at pH 3 – 9.

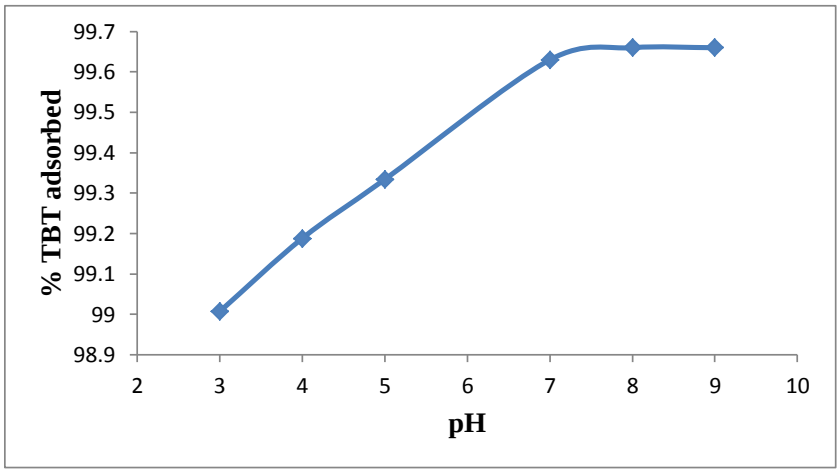

Figure 4.214: Effect of pH on TBT adsorption onto nZnO/activated carbon composite

Experimental conditions: Concentration of TBT = 100 mg/L; Volume of TBT solution = 25 mL, Mass of composite = 0.5 g; Contact time = 60 min; Stirring speed = 160 rpm, Temperature = 20 ^{o}C.

It was observed in Figure 4.214 that the percentage of TBT adsorbed by the composite steadily increases as the pH of the solution increases from pH 3 to pH 7, and reaches equilibration at pH ≥ 8. Maximum adsorption capacity was recorded at pH 8. About 99.66 % of TBT was removed from the initial concentration of 100 mg/L TBT by nZnO/activated carbon composite material at a contact time of 60 min, stirring speed of 160 rpm, temperature of 20 ^{o}C and pH 8. pH 8 was chosen as the optimum pH and was used for further studies.

4.12.9.4 Effect of stirring speed

The stirring speed on the adsorption of TBT onto nZnO/activated carbon composite was studied at a stirring speed of 160 – 200 rpm. The adsorption capacity of TBT onto the composite material increases as the stirring speed of the mixture increases, reaching equilibration at 190 - 200 rpm. Figure 4.215 shows that 99.94 % of TBT was removed from the initial concentration of 100 mg/L TBT by the nZnO/activated carbon composite at a contact time of 60 min, pH 8, temperature of 20 ^{o}C and a stirring speed of 200 rpm (Figure 4.215). A stirring speed of 200rpm was therefore used for further studies.

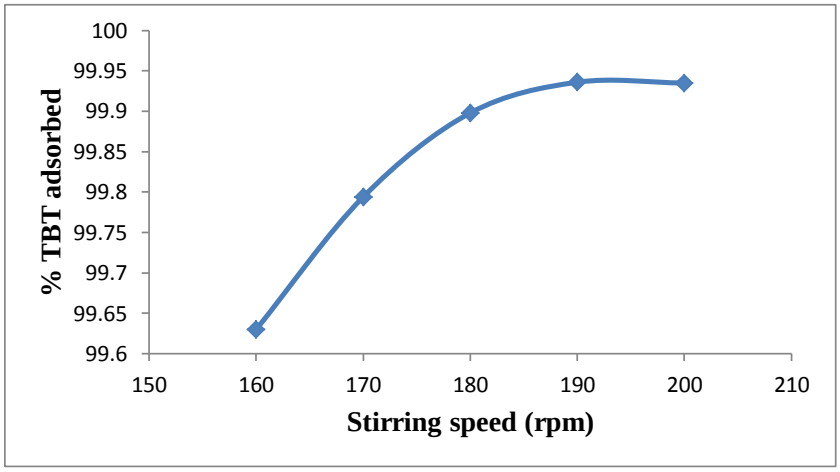

Figure 4.215: Effect of stirring speed on TBT adsorption onto nZnO/activated carbon composite

Experimental conditions: Concentration of TBT = 100 mg/L; Volume of TBT solution = 25 mL, Mass of composite = 0.5 g; Contact time = 60 min; Temperature = 20 ^{o}C.

4.12.9.5 Effect of initial concentration

The adsorption isotherms of the adsorption of TBT onto nZnO/activated carbon composite were investigated by varying the initial TBT concentration from 12.5 to 200 mg/L at optimized adsorbent dose, contact time, pH and stirring speed established after optimization of working parameters. The equilibrium data were fitted by Langmuir, Freundlich, Temkin and D-R isotherm models as presented in Figures 4.217 – 4.220.

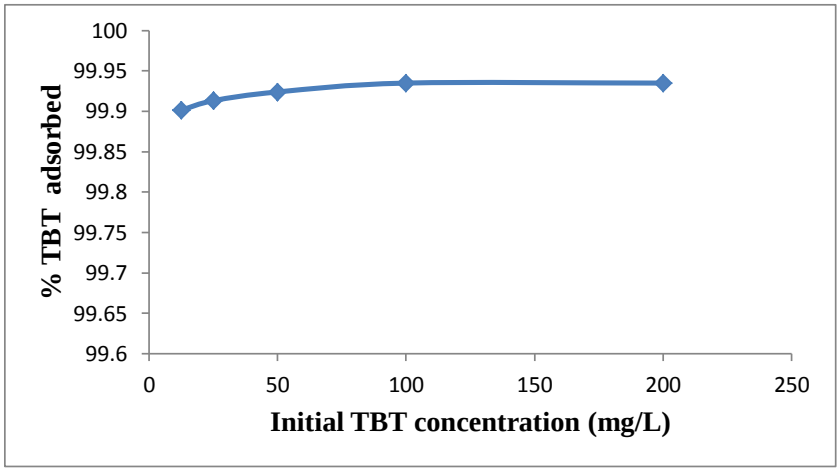

Figure 4.216: Percentage TBT adsorbed by nZnO/activated carbon composite at various initial TBT concentrations

Experimental conditions: Volume of TBT solution = 25 mL, Mass of composite = 0.5 g; pH = 8; Stirring speed = 200 rpm; Contact time = 60 min; Temperature = 20 ^{o}C.

Figure 4.216 therefore shows that the adsorption of TBT onto nZnO/activated carbon composite steadily increases as the initial TBT concentration increases from 12.5 to 100 mg/L, indicating that adsorption is also favourable for the higher TBT concentrations that have been investigated.

4.12.9.5.1 Adsorption isotherms

The adsorption isotherm plots as presented in Figures 4.217 – 4.220 and parameters obtained for the models were given in Table 4.35. The experimental data fitted well with Freundlich and D-R isotherm models because the regression coefficients (R^2 > 0.99) are higher than for other models (Table 4.35). The value of n_F, for the nZnO/activated carbon composite, falling in the range 1 -10 also indicates favourable adsorption.

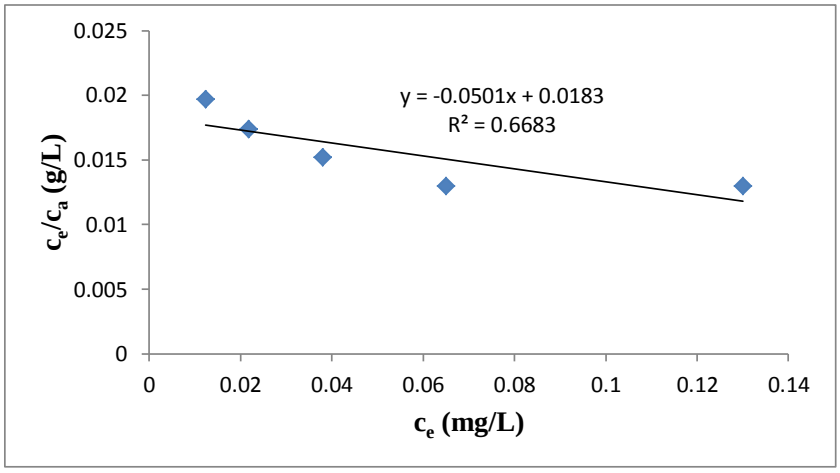

Figure 4.217: Langmuir isotherm for adsorption of TBT onto nZnO/activated carbon composite

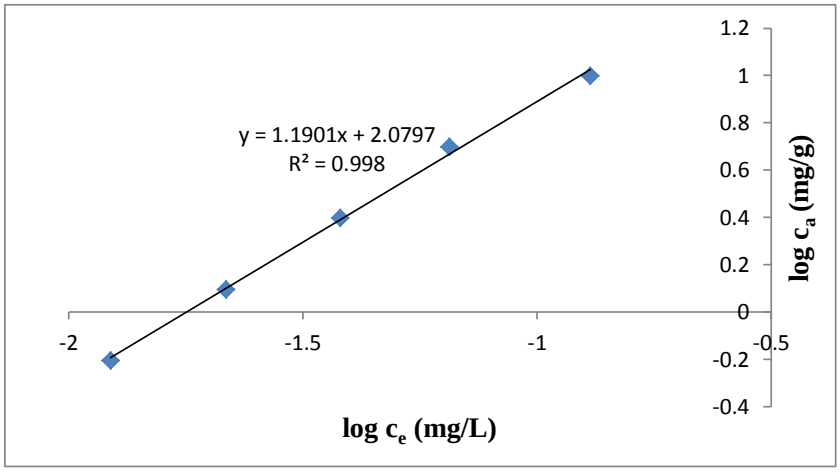

Figure 4.218: Freundlich isotherm for adsorption of TBT onto nZnO/activated carbon composite

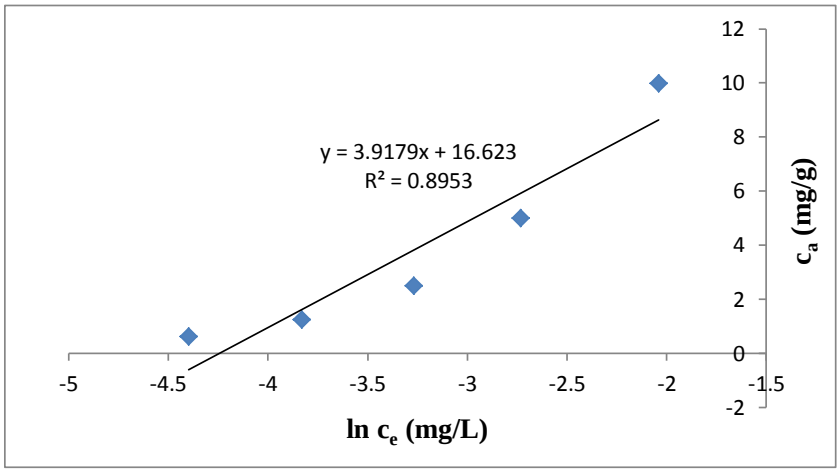

Figure 4.219: Temkin isotherm for adsorption of TBT onto nZnO/activated carbon composite

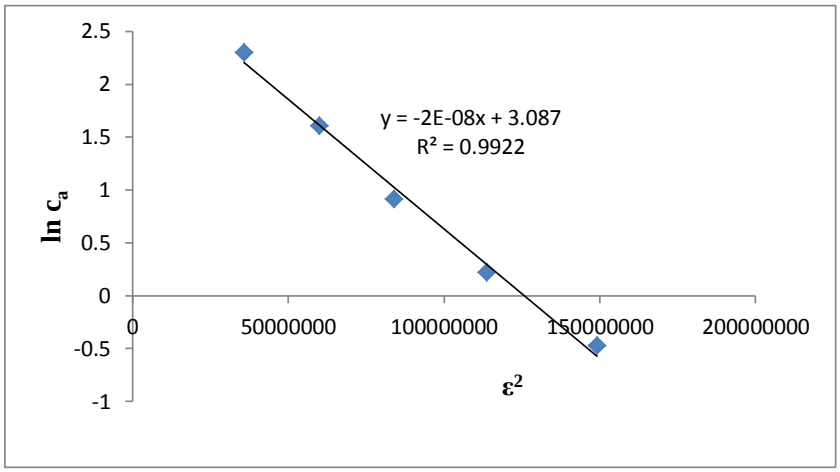

Figure 4.220: D-R isotherm for adsorption of TBT onto nZnO/activated carbon composite

The negative value of the Langmuir constants, A_{max} (mg/g) and k_L (L/mg) for TBT adsorption (Table 4.35) onto nZnO/activated carbon composite indicate the inadequacy fitting of experimental data to Langmuir model.

The equilibrium model constants k_F, k_L, k_T and k_{D-R} for the adsorption of TBT onto nZnO/activated carbon composite (Table 4.35) are 120.14 mg/g $(L/mg)^{1/n}$, -2.7377 L/mg, 69.6048 mg/L and 2 x 10^{-8} J^2/mol^2, respectively.

Table 4.35: Isotherms constants for the adsorption of TBT onto nZnO/activated carbon composite

Equilibrium models	
Freundlich	
k_F [mg/g $(L/mg)^{1/n}$]	120.14
n_F	0.8403
R^2	0.9980
Langmuir	
K_L (L/mg)	-2.7377
A_{max} (mg/g)	-19.960
R^2	0.6683
Temkin	
n_T (L/g)	3.9179
k_T (mg/L)	69.6048
b_T (J/mol)	621.76
R^2	0.8953
Dubinin-Redushkevich	
k_{D-R} (J^2/mol^2)	2 x 10^{-8}
q_m (mg/g)	21.91
E (J/mol)	5000
R^2	0.9922

4.12.9.6 Effect of temperature

The experimental results obtained on the effect of temperature show that the adsorption capacity of TBT onto nZnO/activated carbon composite increases with increase in the solution temperature (Figure 4.221). This indicates that the adsorption of TBT onto the nZnO/activated carbon composite is also endothermic.

Approx. 99.99 % of TBT was removed from the initial concentration of 100 mg/L TBT by nZnO/activated carbon composite at a temperature of 80 ^oC, contact time of 60 min, pH 8 and a stirring speed of 200 rpm (Ayanda et al., 2013c).

Figure 4.222 thus shows the Van't Hoff plot for the adsorption of TBT and the variation in the extent of adsorption with respect to temperature has been explained on the basis of ΔH^o, ΔS^o, and ΔG^o as shown in Table 4.36.

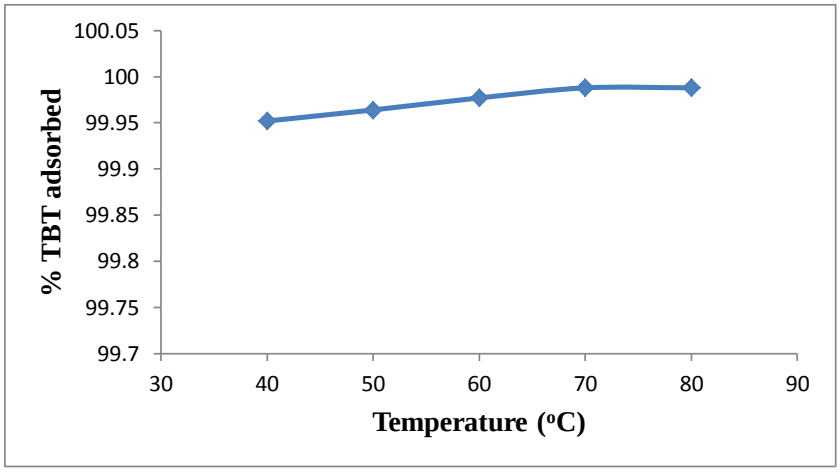

Figure 4.221: Effect of temperature on TBT adsorption onto nZnO/activated carbon composite

Experimental conditions: Concentration of TBT = 100 mg/L; Volume of TBT solution = 25 mL, Mass of composite = 0.5 g; Contact time = 60 min; pH = 8; Stirring speed = 200 rpm.

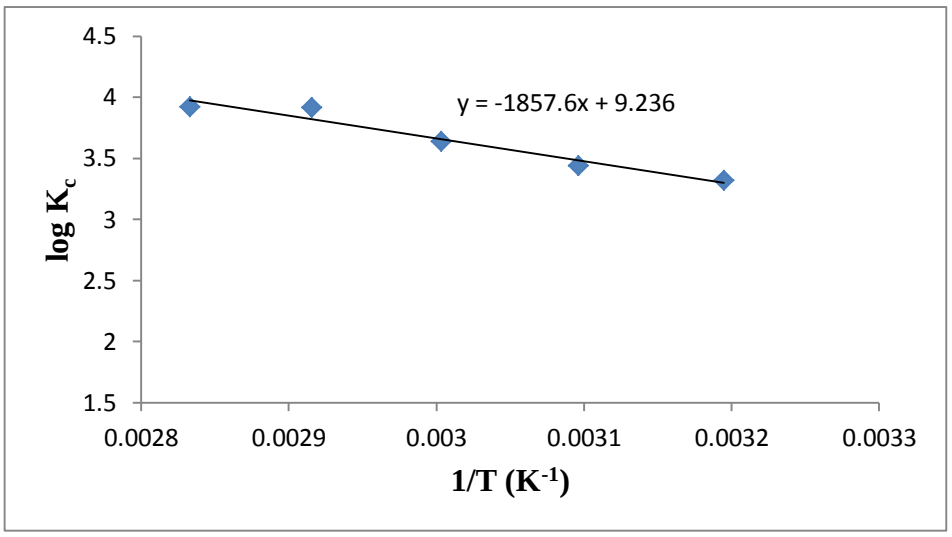

Figure 4.222: Van't Hoff plot for the adsorption of TBT onto nZnO/activated carbon composite

Table 4.36: Thermodynamic parameters for the adsorption of TBT onto nZnO/activated carbon composite

Temperature (°C)	ΔG° (kJ/mol)	ΔS° (J/K/mol)	ΔH° (kJ/mol)	K_c
40	-19.88	176.843	35.568	2082.3
50	-21.29			2776.8
60	-23.19			4346.8
70	-25.72			8263.5
80	-26.50			8332.3

The positive value of ΔH^{o} for the intervals of temperatures also shows the endothermic nature of the adsorption process. The positive value of ΔS^{o} corresponds to increase in degree of freedom of the adsorbed TBT and suggest the increase in concentration of adsorbate in solid–solution interface indicating an increase in adsorbate concentration onto the solid phase. ΔG^{o} values were found to be more negative as the temperature increases

which indicate that the adsorption efficiency of TBT onto nZnO/activated carbon composite increases with increase in temperature. K_c also ranged 2082.3 – 8332.3 (Table 4.36).

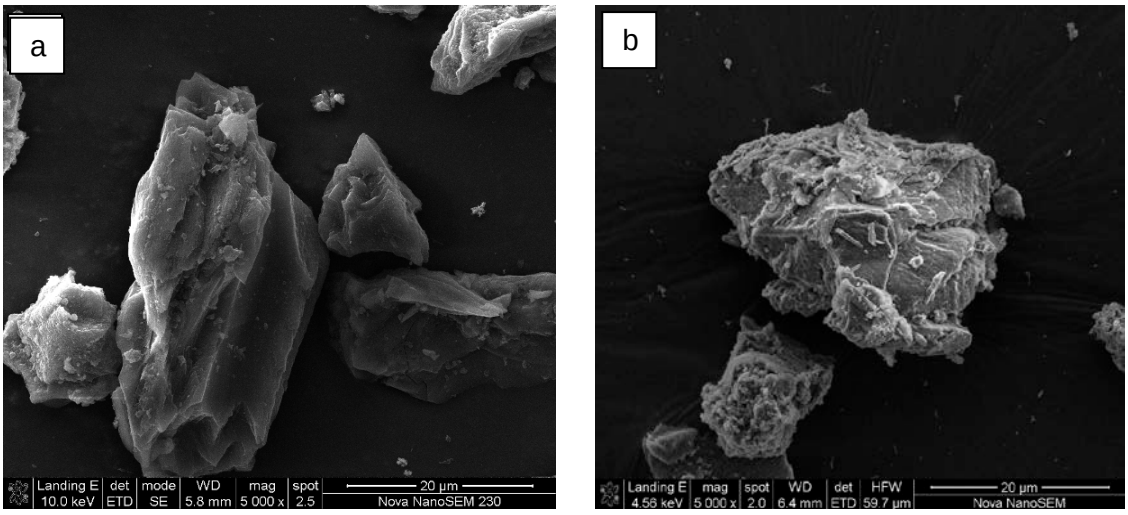

Figure 4.223: SEM of nZnO/activated carbon composite before (a) and after (b) TBT adsorption

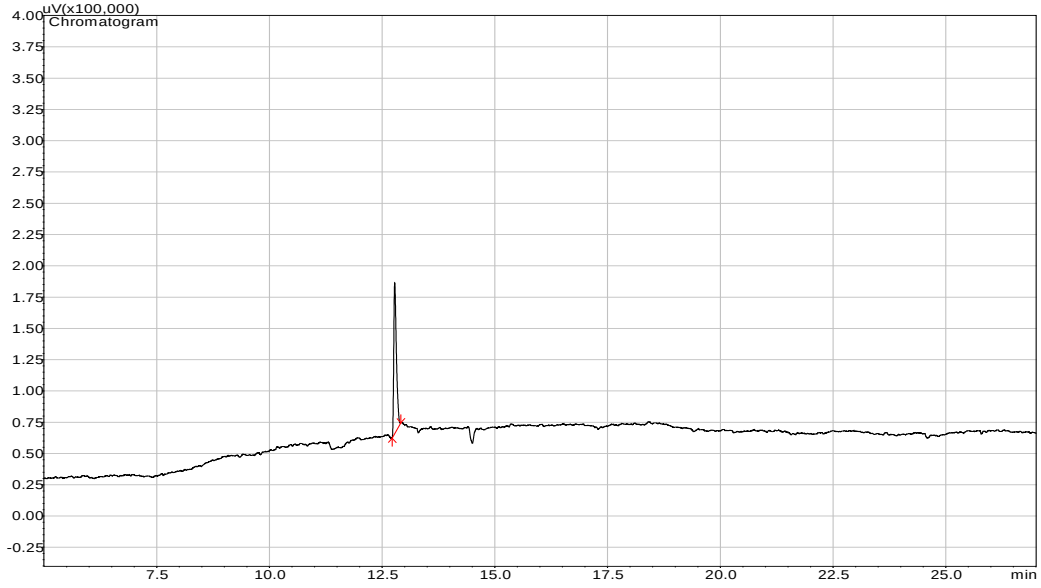

Figure 4.224: Representative TBT chromatogram after adsorption of 100 mg/L TBT with 0.5g of nZnO/activated carbon composite, contact time of 60min, temperature 20 ^{o}C and a stirring speed of 200 rpm

The solid residue of nZnO/activated carbon composite material before and after the adsorption processes were subjected to SEM analysis as shown in Figure 4.223 while a representative TBT chromatogram after adsorption of 100 mg/L TBT with 0.5 g of nZnO/activated carbon composite material, contact time of 60min, temperature 20 ^{o}C and a stirring speed of 200 rpm is as shown in Figure 4.224.

4.12.10 Comparison of TBT adsorption capacity of the precursor and composite materials

Figure 4.225 thus shows that 99.95 %, 95.75 %, 96.78 %, 99.88 %, 96.96 %, 99.98 %, 99.99 %, 99.99 % and 99.99 % TBT were removed from 25 mL of 100 mg/L TBT-contaminated artificial seawater using 0.5 g adsorbents at a contact time of 60 min, pH 8, stirring speed 200 rpm and temperature of 80^{o}C by the activated carbon, fly ash, nFe_3O_4, $nSiO_2$, nZnO, fly ash/activated carbon, nFe_3O_4/activated carbon, $nSiO_2$/activated carbon and nZnO/activated carbon composite, respectively. The adsorption of TBT onto all the adsorbents is endothermic.

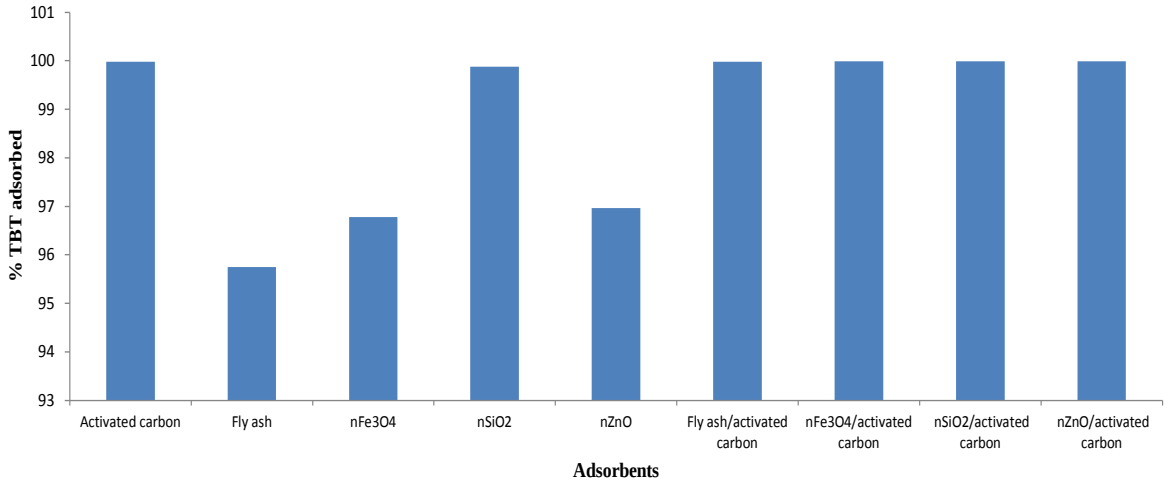

Figure 4.225: Percentage TBT removed from TBT-contaminated artificial seawater

Experimental conditions: Concentration of TBT = 100 mg/L; Volume of TBT solution = 25 mL, Mass of composite = 0.5 g; Contact time = 60 min; pH = 8; Stirring speed = 200 rpm; Temperature 80 ^{o}C.

The value of h_o calculated from pseudo second-order rate equation for TBT by activated carbon, fly ash, nFe_3O_4, $nSiO_2$, nZnO, fly ash/activated carbon, nFe_3O_4/activated carbon, $nSiO_2$/activated carbon and nZnO/activated carbon composites are 4.065, 0.262, 0.843, 1.324, 1.055, 5.804, 3.201, 42.37 and 294.118 mg/g min, respectively, thus indicating the higher TBT adsorption rate of nZnO/activated carbon composite compared to all other composites and the precursors.

The adsorption of TBT by all the adsorbents follows a pseudo second-order kinetics model. This model depends on the assumption that chemisorption may be the rate-limiting step. In chemisorption, the TBT ions stick to the adsorbent surface by forming a chemical (usually covalent) bond and tend to find sites that maximize their coordination number with the surface (Atkins, 1995). The applicability of Freundlich isotherm model to the adsorption of

TBT onto the adsorbents is based on the assumption that TBT adsorbs onto the heterogeneous surface of the adsorbents.

4.12.10.1 Application to the sorption of TBT from natural seawater

Optimal conditions for the adsorption of TBT from artificial seawater were applied to TBT removal from TBT – contaminated natural seawater (shipyard wastewater) obtained from Cape Town harbour. The physicochemical properties of wastewater is presented in Table 4.37 and the percentage of TBT removed after adsorption of TBT contain in 25 mL of natural seawater by 0.5 g of adsorbents, contact time of 60 min and stirring speed of 200 rpm under natural condition is as shown in Figure 4.226.

Table 4.37: Physicochemical properties of TBT – contaminated natural seawater

Parameters	
Turbidity (NTU)	3.26
pH	7.5
Conductivity (mS/cm)	37.56
TDS (ppt)	18.78
Salinity (psu)	22.65
Resistivity (ohms)	26.6
TBT conc. (mg/L)	4.615

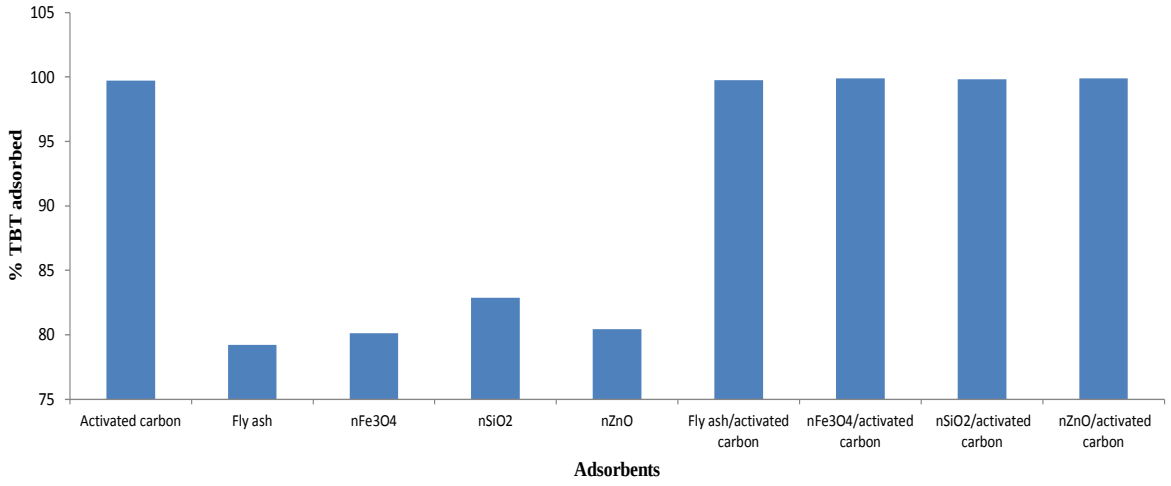

Figure 4.226: Percentage TBT removed from TBT-contaminated natural seawater

Experimental conditions: Concentration of TBT = 4.6148 mg/L; Volume of natural seawater = 25 mL, Mass of composite = 0.5 g; Contact time = 60 min; pH = 7.286; Stirring speed = 200 rpm; Temperature = 20 ^{o}C.

Figure 4.226 shows that 99.71 %, 79.23 %, 80.11 %, 82.86 %, 80.42 %, 99.75 %, 99.88 %, 99.83 % and 99.88 % TBT were removed from natural seawater by activated carbon, fly ash, nFe_3O_4, $nSiO_2$, nZnO, fly ash/activated carbon, nFe_3O_4/activated carbon, $nSiO_2$/activated carbon and nZnO/activated carbon composites, respectively. All the composites including activated carbon therefore show higher TBT sorption capacity from TBT – contaminated natural seawater than the precursors. The TBT removal efficiency is in the order: nZnO/activated carbon composite ≈ nFe_3O_4/activated carbon > $nSiO_2$/activated carbon composite > fly ash/activated carbon composite > activated carbon > $nSiO_2$ > nZnO > nFe_3O_4 > fly ash. Fly ash therefore recorded the least TBT removal efficiency which may probably be as a result of its very low surface area as compared to all other adsorbents.

The percentage TBT adsorbed from the contaminated natural seawater was slightly lower than the percentage removed from TBT – contaminated artificial seawater, this could be attributed to the adsorption of other species such as metal ions that might be present in the contaminated natural seawater.

4.12.11 Adsorption of TPT from TPT-contaminated artificial seawater onto activated carbon

4.12.11.1 Effect of adsorbent amount

To study the effect of adsorbent amount on the adsorption of TPT from TPT-contaminated artificial seawater, the amount of activated carbon was varied from 0.0625 – 1 g, the concentration of TPT was taken as 100 mg/L and other parameters were kept constant. Figure 4.227 shows that the percentage removal of TPT by the activated carbon as the case for TBT adsorption unto activated carbon increases as the amount of adsorbent increases from 0.0625 - 0.5 g, after which equilibration was attained. The figure (Figure 4.227) shows that 0.5 g of activated carbon is able to remove 99.98 % of TPT from TPT – contaminated artificial seawater.

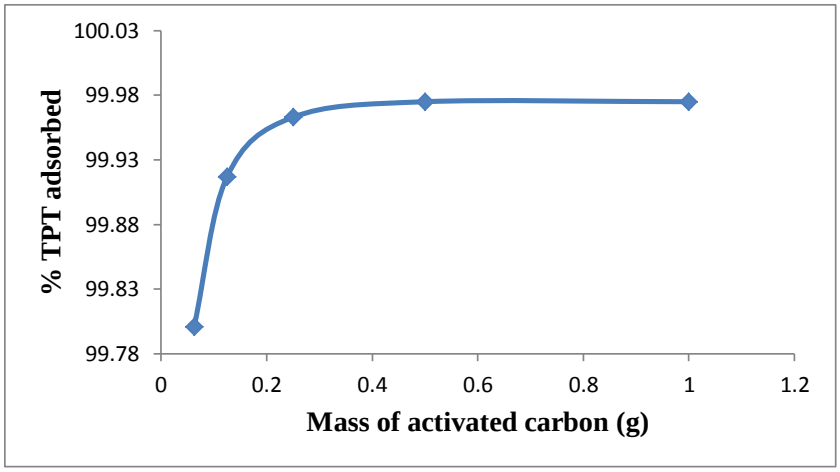

Figure 4.227: Adsorption efficiencies of TPT onto activated carbon

Experimental conditions: Concentration of TPT = 100 mg/L; Volume of TPT solution = 25 mL, Contact time = 60 min; Stirring speed = 160 rpm, Temperature = 20 ^{o}C.

4.12.11.2 Effect of contact time

The effect of contact time on the adsorption of TPT from TPT-contaminated artificial seawater onto activated carbon was studied at various time intervals from 10 – 70 min. The TPT concentration was 100 mg/L while other remaining conditions were constant. The increase in the amount of TPT adsorbed from 4.9945 mg/g (99.89 %) to 4.9987 mg/g (99.98 %) (Figure 4.228) was observed up to 60 min. After 60 min, there is no significant change observed. 60 min was therefore fixed as contact time for further studies.

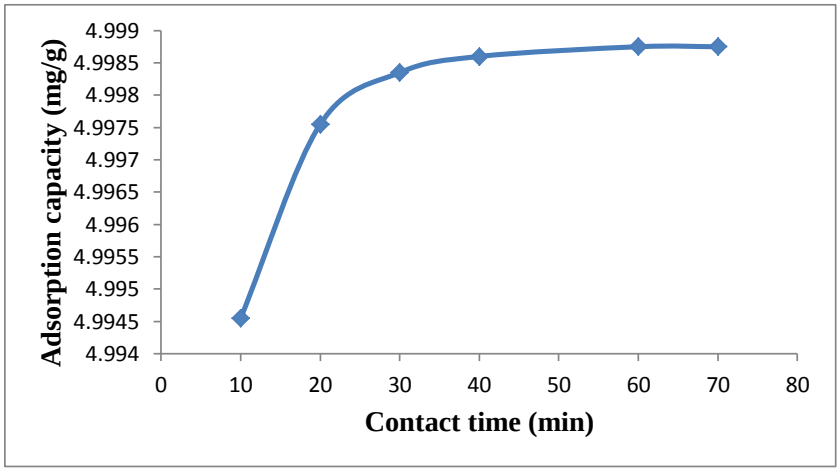

Figure 4.228: Effect of contact time on TPT adsorption onto activated carbon

Experimental conditions: Concentration of TPT = 100 mg/L; Volume of TPT solution = 25 mL, Mass of activated carbon = 0.5 g; Stirring speed = 160 rpm, Temperature = 20 ^{o}C.

4.12.11.2.1 Adsorption kinetics

The rate constants were therefore calculated by pseudo first-order, pseudo second-order, Elovich and fractional power kinetic models and the rate controlling steps were determined by intra-particle diffusion model. Figures 4.229 – 4.233 thus show the graphs for the pseudo first-order, pseudo second-order, Elovich, fractional power and intraparticle diffusivity kinetic plots, respectively and Table 4.38 provides the evaluated parameters of the kinetics models.

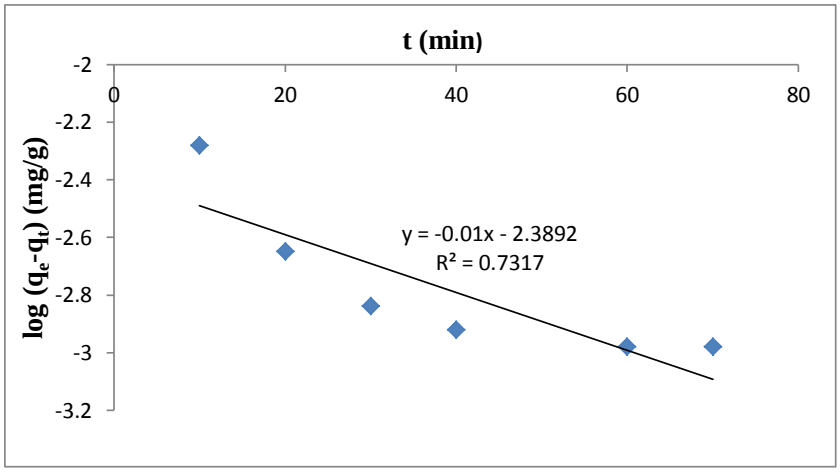

Figure 4.229: Pseudo first-order rate equation plot for TPT adsorption onto activated carbon

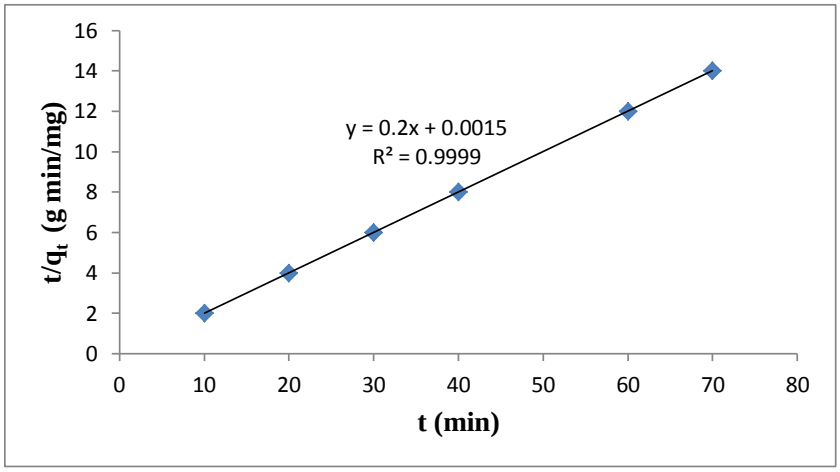

Figure 4.230: Pseudo second-order rate equation plot for TPT adsorption onto activated carbon

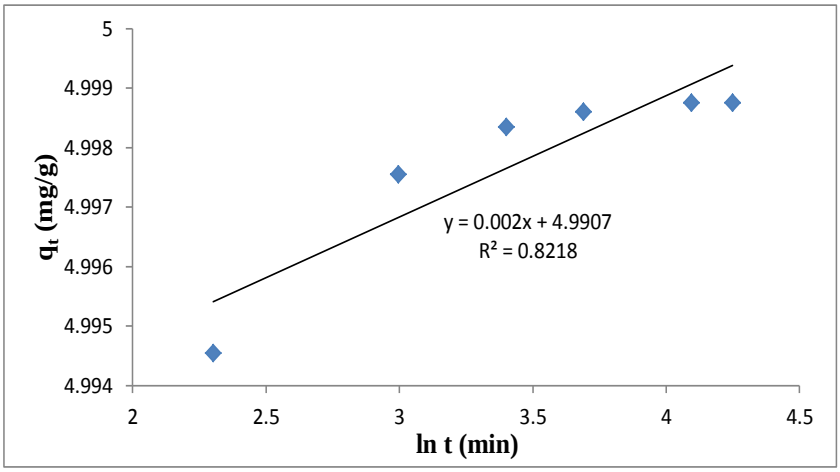

Figure 4.231: Elovich rate equation plot for TPT adsorption onto activated carbon

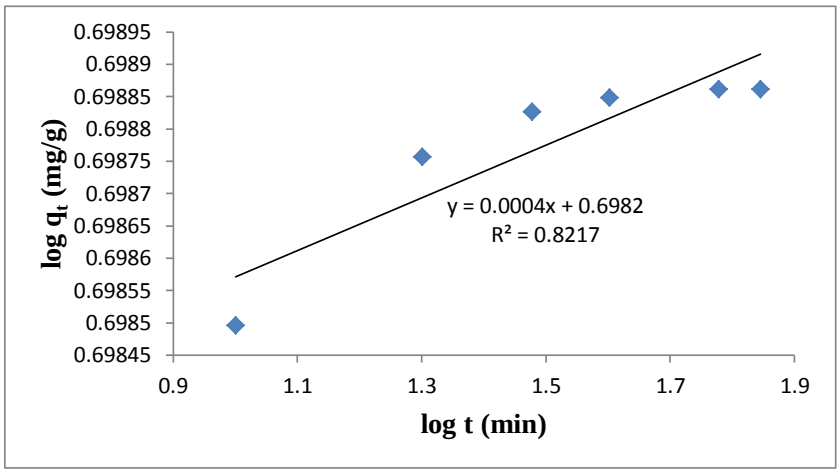

Figure 4.232: Fractional Power rate equation plot for TPT adsorption onto activated carbon

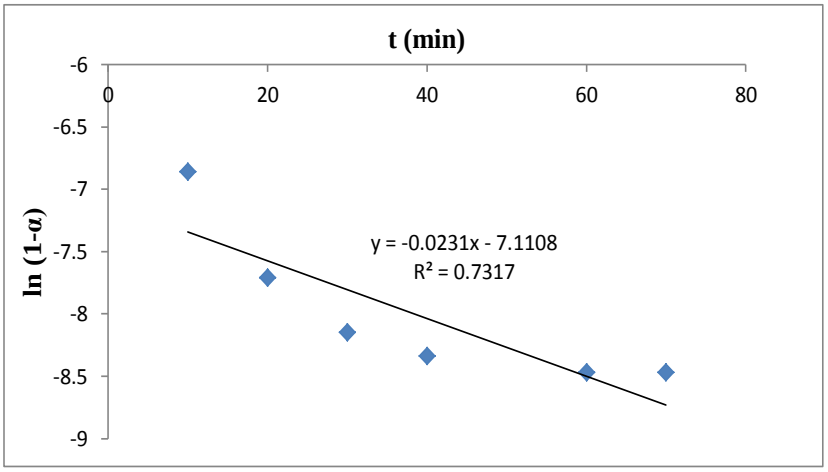

Figure 4.233: Intraparticle diffusivity plot for TPT adsorption onto activated carbon

Table 4.38: Kinetic model parameters for TPT adsorption onto activated carbon

Kinetic models	
Pseudo first-order	
k_1 (min^{-1})	0.02303
q_e (mg/g)	4.08×10^{-3}
R^2	0.7317
Pseudo second-order	
q_e (mg/g)	5.0000
h_o (mg/g/min)	666.67
k_2 (g/mg/min)	26.667
R^2	0.9999
Elovich	
β (g min/mg)	500.0
α (g min^2/mg)	2.604×10^{1086}
R^2	0.8218
Fractional Power	
v (min^{-1})	0.0004
k_3 (mg/g)	4.9911
k_3v (mg/g/min)	1.996×10^{-3}
R^2	0.8217
Intraparticle diffusivity	
k_p (min^{-1})	0.0231
R^2	0.7317

The value of correlation coefficient (R^2) of pseudo second-order kinetic model (> 0.99) is higher than the correlation coefficients of other models indicating that the kinetic model for the adsorption of TPT onto the activated carbon is pseudo second-order. The intraparticle coefficient for the adsorption of TPT by the activated carbon was also calculated and presented in Table 4.38.

The results also indicate that the power function model satisfactorily describes the time-dependence of TPT on the activated carbon since the value of the constant v is less than 1. The value of the initial adsorption rate, h_o, obtained for the pseudo second-order kinetics is 666.67 mg/g/min indicating very rapid adsorption of TPT onto the activated carbon. The amount of TPT adsorbed at equilibrium per unit weight of the adsorbent (q_e) is 5.000 mg/g and the rate constant of pseudo second - order adsorption (k_2) is 26.667 g/mg/min.

4.12.11.3 Effect of pH

The effect of pH on the adsorption of TPT onto the activated carbon was studied at pH 4 – 9. The results obtained on the effect of pH on the adsorption of TPT onto activated carbon also behave similarly as the case for TBT onto activated carbon. It was observed from Figure 4.234 that the percentage of TPT adsorbed by the activated carbon increases as the pH of the solution increases from pH 4 to pH 8, and reaches equilibration at pH ≥ 8.

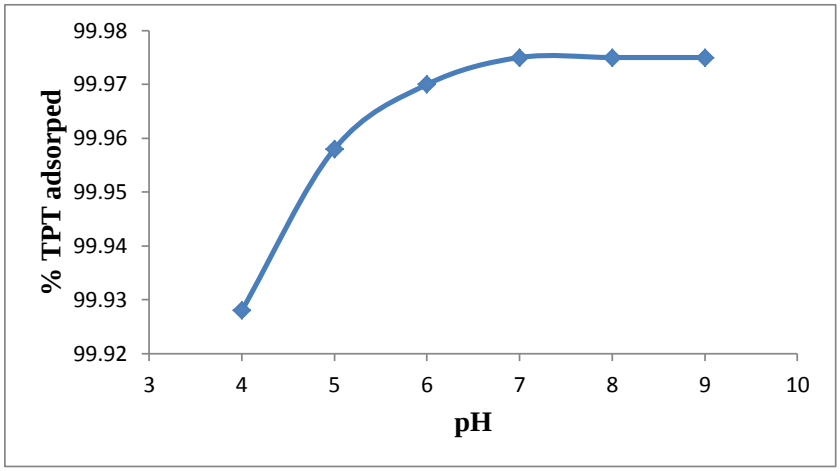

Figure 4.234: Effect of pH on TPT adsorption onto activated carbon

Experimental conditions: Concentration of TPT = 100 mg/L; Volume of TPT solution = 25 mL, Mass of activated carbon = 0.5 g; Contact time = 60 min; Stirring speed = 160 rpm, Temperature = 20 ^{o}C.

Maximum adsorption of TPT onto activated carbon was therefore recorded within the pH range of normal saline water (pH 8). About 99.98 % of TPT was removed from the initial concentration of 100 mg/L TPT by the activated carbon at a contact time of 60 min, stirring speed of 160 rpm, temperature of 20 ^{o}C and pH 8. pH 8 was chosen as the optimum pH and was utilized for further studies.

4.12.11.4 Effect of stirring speed

The stirring speed on the adsorption of TPT onto the activated carbon was studied at a stirring speed of 160 – 200 rpm. The adsorption capacity of TPT onto activated carbon steadily increases as the stirring speed of the mixture increases, reaching equilibration at 200 rpm.

About 4.9993 mg/g (99.99 %) of TPT was removed from the initial concentration of 5 mg/g TPT by the activated carbon at a contact time of 60 min, pH 8, temperature of 20 ^{o}C and a stirring speed of 200 rpm (Figure 4.235). A stirring speed of 200rpm was therefore used for further studies.

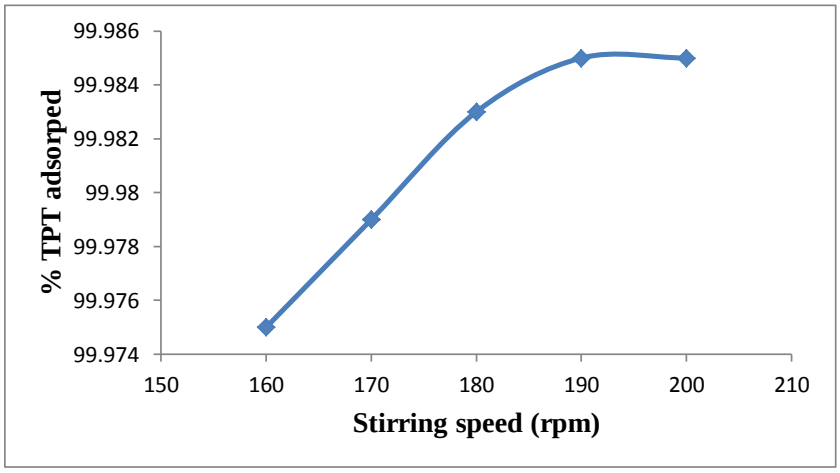

Figure 4.235: Effect of stirring speed on TPT adsorption onto activated carbon

Experimental conditions: Concentration of TPT = 100 mg/L; Volume of TPT solution = 25 mL, Mass of activated carbon = 0.5 g; Contact time = 60 min; Temperature = 20 ^{o}C.

4.12.11.5 Effect of initial concentration

The adsorption isotherms were investigated by varying the initial TPT concentration from 12.5 to 200 mg/L at optimized adsorbent dose, contact time, pH and stirring speed established after optimization of working parameters. The equilibrium data were then fitted by the Langmuir, Freundlich, Temkin and D-R isotherm models.

Figure 4.236 shows that the adsorption of TPT onto activated carbon increases as the initial TPT concentration increases from 12.5 to 200 mg/L, indicating that adsorption is also favourable for the higher TPT concentrations that have been investigated.

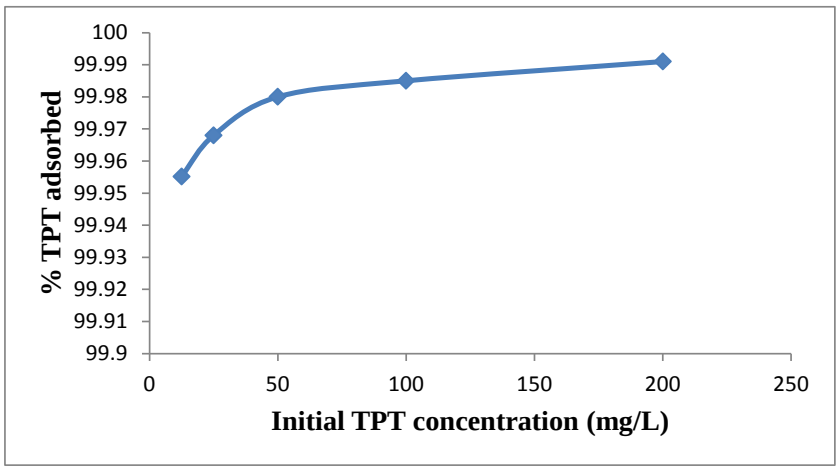

Figure 4.236: Percentage TPT adsorbed by activated carbon at various initial TPT concentrations

Experimental conditions: Volume of TPT solution = 25 mL, Mass of activated carbon = 0.5 g; pH = 8; Stirring speed = 200 rpm; Contact time = 60 min; Temperature = 20 ^{o}C.

As is the case for TBT adsorption onto the adsorbents, the increase in the adsorption capacity with an increase in initial TPT concentration is as a result of the increase in driving force due to concentration gradient developed between the bulk solution and surface of the adsorbents. At higher concentration of TPT, the active sites of the adsorbents were surrounded by much more TPT and the process of adsorption continues, leading to an increased uptake of TPT from the solution.

4.12.11.5.1 Adsorption isotherms

The graphs of the adsorption isotherms are presented in Figures 4.237 – 4.240 and parameters obtained for all the models were given in Table 4.39. The experimental data fitted well with the Freundlich and D-R models.

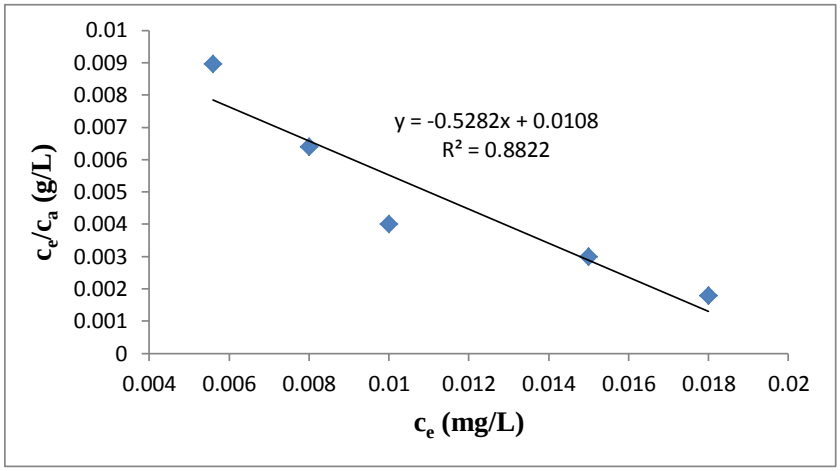

Figure 4.237: Langmuir isotherm for adsorption of TPT onto activated carbon

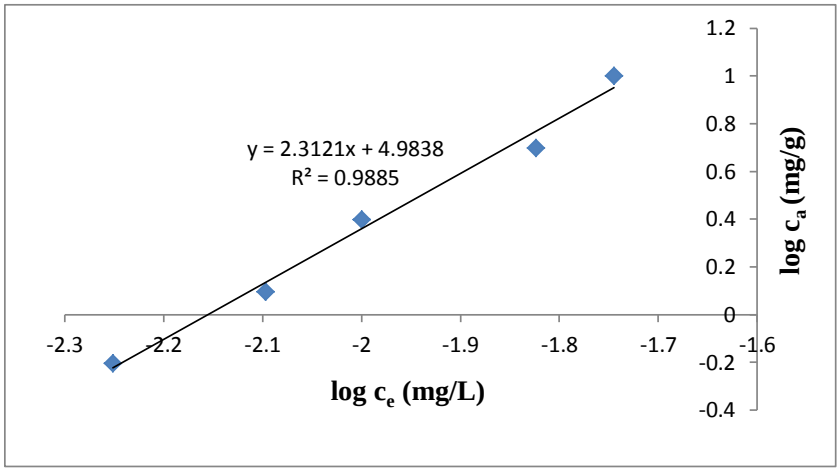

Figure 4.238: Freundlich isotherm for adsorption of TPT onto activated carbon

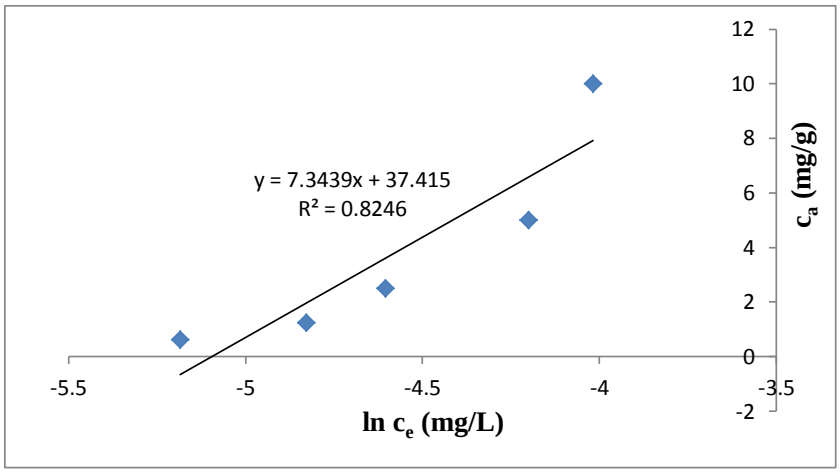

Figure 4.239: Temkin isotherm for adsorption of TPT onto activated carbon

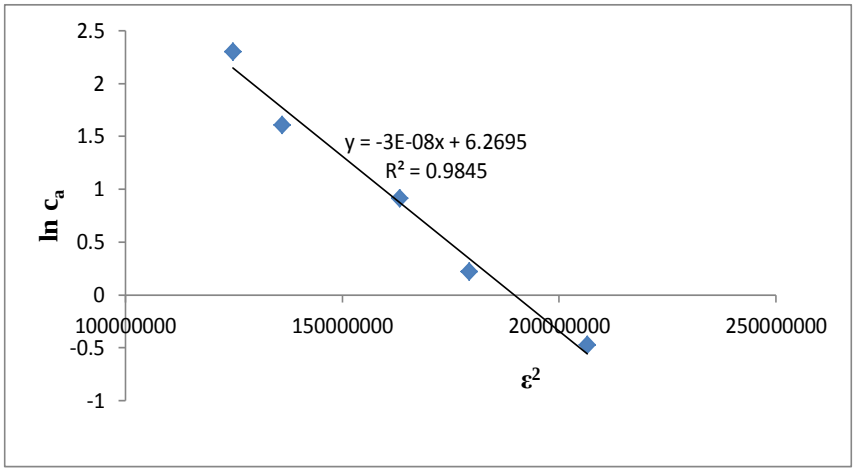

Figure 4.240: D-R isotherm for adsorption of TPT onto activated carbon

Freundlich and D-R are suitable models for describing the adsorption process because the regression coefficient (R^2) value (> 0.98) is generally higher than for other models (Table 4.39).

The value of n_F, for the activated carbon, falling in the range 1 -10 also indicates favourable adsorption. Moreover, the negative value of the Langmuir constants, A_{max} (mg/g) and k_L (L/mg) for TPT adsorption onto activated carbon indicates the inadequacy in the fitting of experimental data to Langmuir model.

Table 4.39: Isotherms constants for the adsorption of TPT onto activated carbon

Equilibrium models	
Freundlich	
k_F [mg/g (L/mg)$^{1/n}$]	96,338.52
n_F	0.4325
R^2	0.9885
Langmuir	
K_L (L/mg)	-48.907
A_{max} (mg/g)	-1.8932
R^2	0.8822
Temkin	
n_T (L/g)	7.3439
k_T (mg/L)	163.156
b_T (J/mol)	331.704
R^2	0.8246
Dubinin-Redushkevich	
k_{D-R} (J^2/mol^2)	3 x 10^{-8}
q_m (mg/g)	528.213
E (J/mol)	4082.48
R^2	0.9845

The equilibrium model constants k_F, k_L, k_T and k_{D-R} for the adsorption of TPT onto activated carbon (Table 4.39) are 96,338.52 mg/g (L/mg)$^{1/n}$, -48.907 L/mg, 163.156 mg/L and 3 x 10^{-8} J^2/mol^2, respectively.

4.12.11.6 Effect of temperature

The results obtained on the effect of temperature show that the adsorption capacity of TPT onto activated carbon increases with increase in the solution temperature (Figure 4.241). This indicates that the adsorption of TPT onto the activated carbon is endothermic. The increase in the rate of adsorption with the increase in temperature may be attributed to the strong adsorptive forces between the active sites of the adsorbents and adsorbate species and also between the adjacent molecules of the adsorbed phases.

Approx. 99.99 % of TPT was removed from the initial concentration of 100 mg/L TPT by the activated carbon at a temperature of 80 ^oC, 60 min contact time, pH 8 and a stirring speed of 200 rpm.

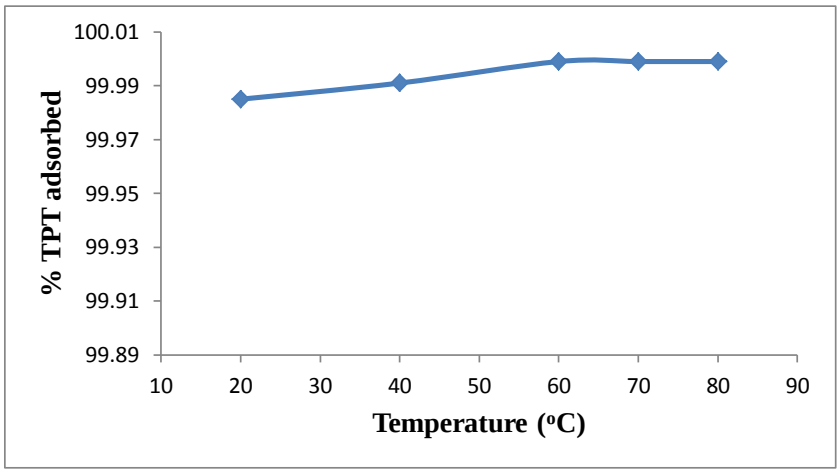

Figure 4.241: Effect of temperature on TPT adsorption onto activated carbon

Experimental conditions: Concentration of TPT = 100 mg/L; Volume of TPT solution = 25 mL, Mass of activated carbon = 0.5 g; Contact time = 60 min; pH = 8; Stirring speed = 200 rpm.

Figure 4.242 thus shows the Van't Hoff plot for the adsorption of TPT onto activated carbon. The variation in the extent of adsorption with respect to temperature has been explained on the basis of ΔH^{o} , ΔS^{o}, and ΔG^{o} as shown in Table 4.40.

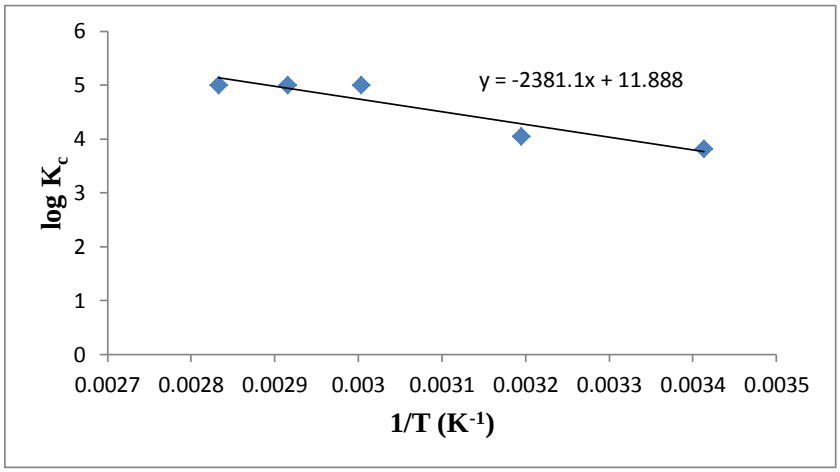

Figure 4.242: Van't Hoff Plot for the adsorption of TPT onto activated carbon

Table 4.40: Thermodynamic parameters for adsorption of TPT onto activated carbon

Temperature (°C)	ΔG° (kJ/mol)	ΔS° (J/K/mol)	ΔH° (kJ/mol)	K_c
20	-21.45	227.62	45.591	6665.7
40	-24.24			11110.1
60	-31.87			99999.0
70	-32.83			99999.0
80	-33.79			99999.0

The positive value of ΔH^{o} (45.591 kJ/mol) for the intervals of temperatures also shows that the adsorption process is endothermic. The positive value of ΔS^{o} (227.62 J/K/mol) corresponds to increase in degree of freedom of the adsorbed TPT and suggest the increase in concentration of adsorbate in solid–solution interface indicating an increase in adsorbate concentration onto the solid phase. It is also evident from Table 4.40 that ΔG^{o} values were found to be more negative as the temperature increases, this indicates that the adsorption efficiency of TPT onto activated carbon increases with increase in temperature. K_c also ranged 6665.7 – 99999.0.

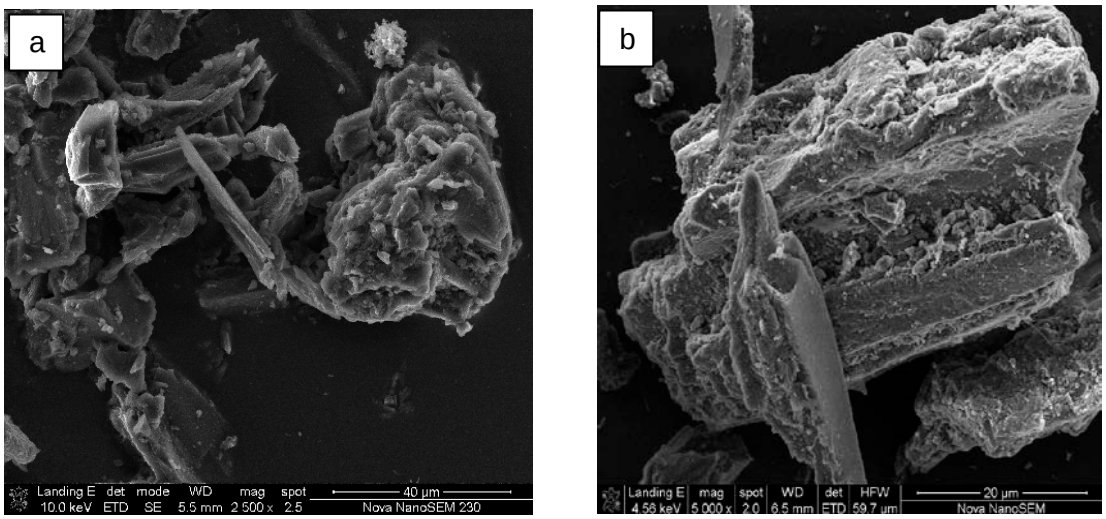

Figure 4.243: Activated carbon before (a) and after (b) TPT adsorption

Figure 4.244: Representative TPT chromatogram after adsorption of 100 mg/L TPT with 0.5g of activated carbon, contact time of 60min, temperature 20 ^{o}C and a stirring speed of 200 rpm

The SEM analysis of activated carbon before and after TPT adsorption are presented in Figure 4.243 while a representative TPT chromatogram after adsorption of 100 mg/L TPT with 0.5 g of activated carbon, contact time of 60min, temperature 20 ^{o}C and a stirring speed of 200 rpm is as shown in Figure 4.244.

4.12.12 Adsorption of TPT from TPT-contaminated artificial seawater onto fly ash

4.12.12.1 Effect of adsorbent amount

The effect of adsorbent amount on the adsorption of TPT by the fly ash is shown in Figure 4.245. It was observed that the percentage adsorption of TPT increased with increasing amount of fly ash, reaching optimum at 0.5 g for the fly ash, corresponding to 96.03 % removal. 0.5 g was therefore selected as the optimum adsorbent amount used for further studies.

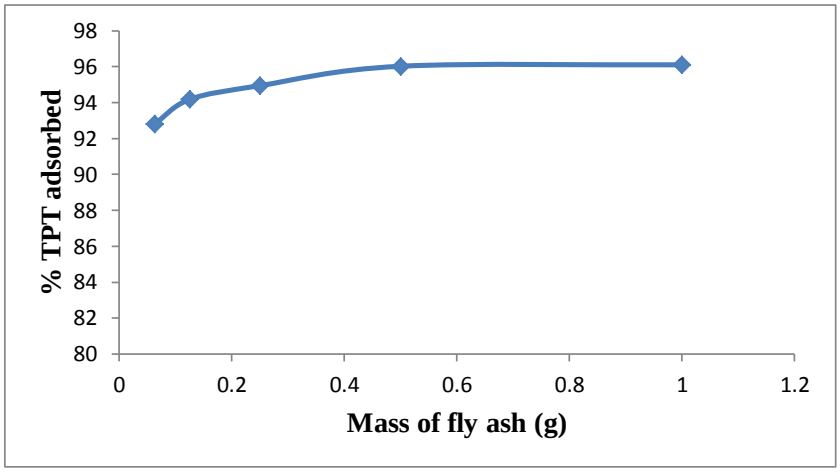

Figure 4.245: Adsorption efficiencies of TPT onto fly ash

Experimental conditions: Concentration of TPT = 100 mg/L; Volume of TPT solution = 25 mL, Contact time = 60 min; Stirring speed = 160 rpm, Temperature = 20 ^{o}C.

4.12.12.2 Effect of contact time

Figure 4.246 shows the effect of contact time on adsorption of TPT onto the fly ash. The TPT removal efficiency at different time intervals ranging from 10 – 70 min are obtained. Figure 4.246 also shows that the adsorption of TPT onto fly ash increases with time gradually and attains equilibrium after 60 minutes. The TPT removal efficiency for the fly ash reaches 4.80 mg/g (96.03 %). A contact time of 60 min was therefore fixed for further studies.

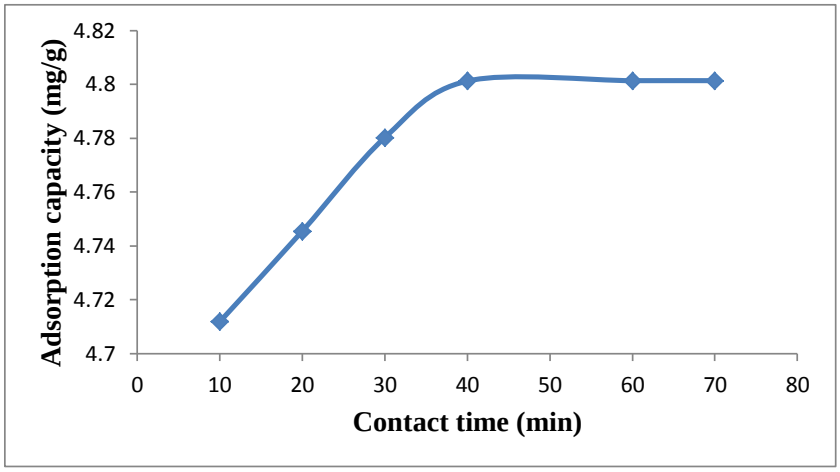

Figure 4.246: Effect of contact time on TPT adsorption onto fly ash

Experimental conditions: Concentration of TPT = 100 mg/L; Volume of TPT solution = 25 mL, Mass of fly ash = 0.5 g; Stirring speed = 160 rpm, Temperature = 20 ^{o}C.

4.12.12.2.1 Adsorption kinetics

Figures 4.247 – 4.251 show the pseudo first-order, pseudo second-order, Elovich, fractional power and intraparticle diffusivity kinetic plots, respectively and Table 4.41 provides the evaluated parameters of all the kinetic models. It is evident from the figures and table that the R^2 value obtained for pseudo second-order kinetic model is higher (R^2 > 0.99) when compared with other models, showing the applicability of the pseudo second-order kinetic model to describe the adsorption kinetic data of TPT onto the fly ash (Ayanda et al., 2013d).

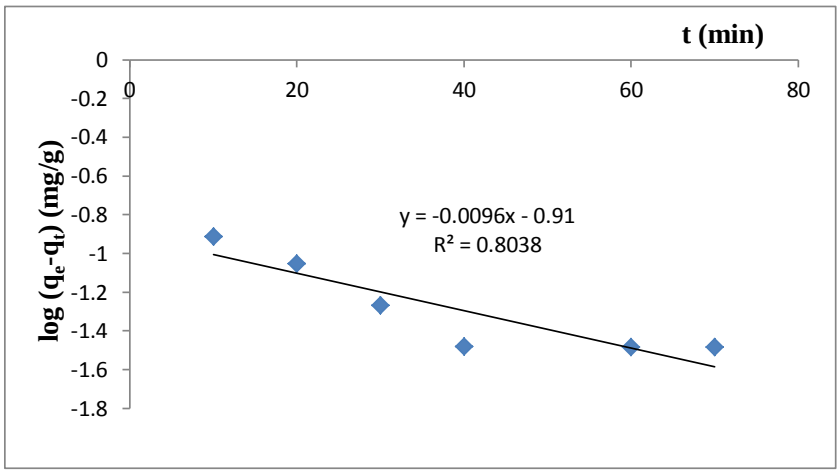

Figure 4.247: Pseudo first-order rate equation plot for TPT adsorption onto fly ash

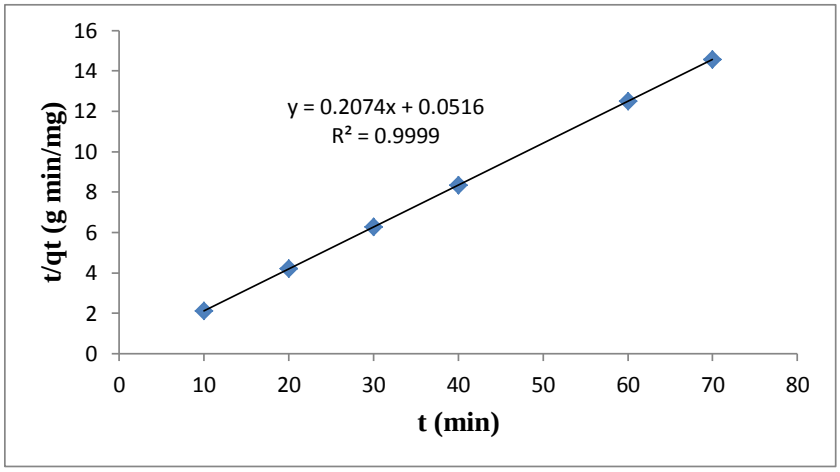

Figure 4.248: Pseudo second-order rate equation plot for TPT adsorption onto fly ash

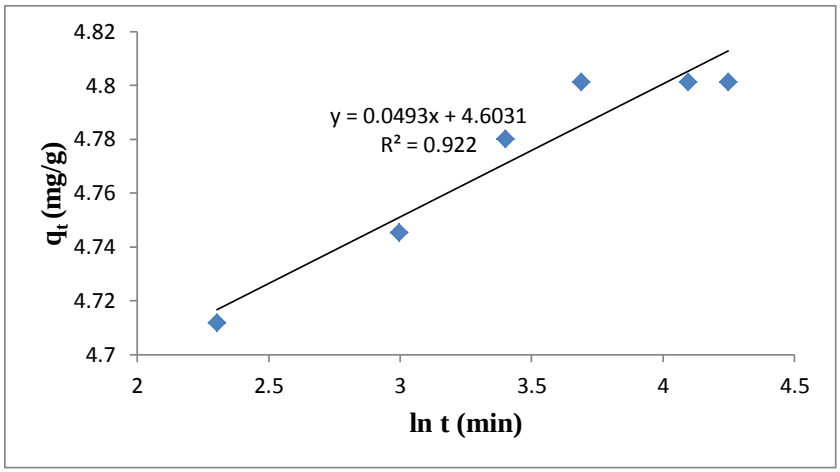

Figure 4.249: Elovich rate equation plot for TPT adsorption onto fly ash

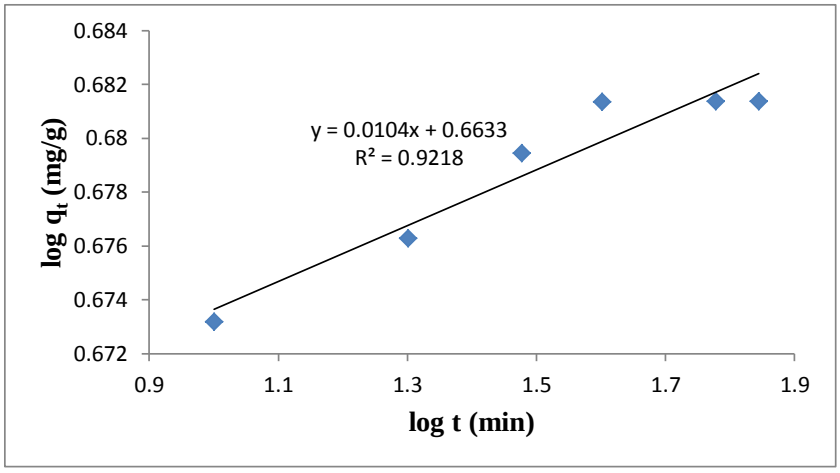

Figure 4.250: Fractional Power rate equation plot for TPT adsorption onto fly ash

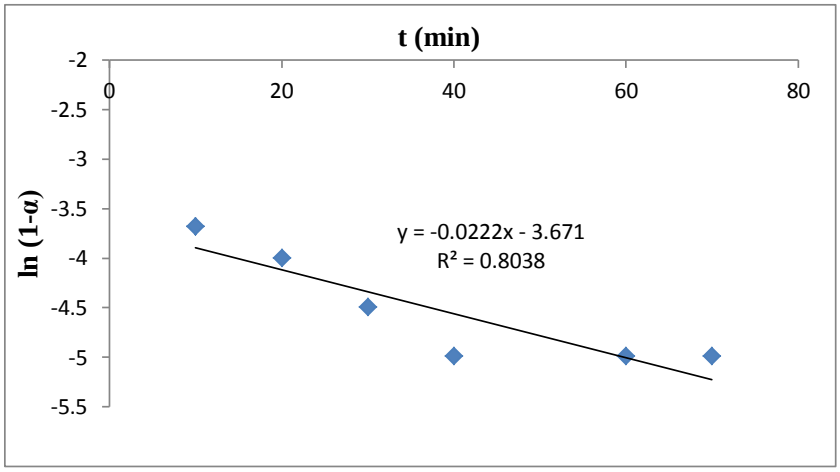

Figure 4.251: Intraparticle diffusivity plot for TPT adsorption onto fly ash

Table 4.41: Kinetic model parameters for TPT adsorption onto fly ash

Kinetic models	
Pseudo first-order	
k_1 (min^{-1})	0.0221
q_e (mg/g)	0.123
R^2	0.8018
Pseudo second-order	
q_e (mg/g)	4.8216
h_o (mg/g/min)	19.378
k_2 (g/mg/min)	0.8336
R^2	0.9999
Elovich	
β (g min/mg)	20.2839
α (g min^2/mg)	7.19×10^{41}
R^2	0.9220
Fractional Power	
v (min^{-1})	0.0104
k_3 (mg/g)	4.6057
k_3v (mg/g/min)	0.0479
R^2	0.9218
Intraparticle diffusivity	
k_p (min^{-1})	0.0222
R^2	0.8038

The intraparticle coefficient for the adsorption of TPT by the fly ash was also computed (Table 4.41). The initial adsorption rate (h_o) calculated from pseudo second-order rate equation for TPT adsorption onto fly ash is 19.378 mg/g/min. The results also indicate that the power function model satisfactorily describes the time-dependence of TPT onto fly ash since the value of the constant v is less than 1. From Table 4.41, k_1, k_2, β, α_E, k_3 and

k_p are 0.0221 min^{-1}, 0.8336 g/mg/min, 20.2839 gmin/mg, 7.19 x 10^{41} $gmin^2/mg$, 4.6057 mg/g and 0.0222 min^{-1}, respectively.

4.12.12.3 Effect of pH

The effect of pH on the adsorption of TPT onto fly ash was studied at pH 4 – 9. It was observed from Figure 4.252 that the percentage of TPT adsorbed by the fly ash increases as the pH of the solution increases from pH 4 to pH 8 and reaches equilibrium afterwards. It is therefore evident from Figure 4.252 that maximum adsorption was also recorded within the pH range of normal saline water (pH 8).

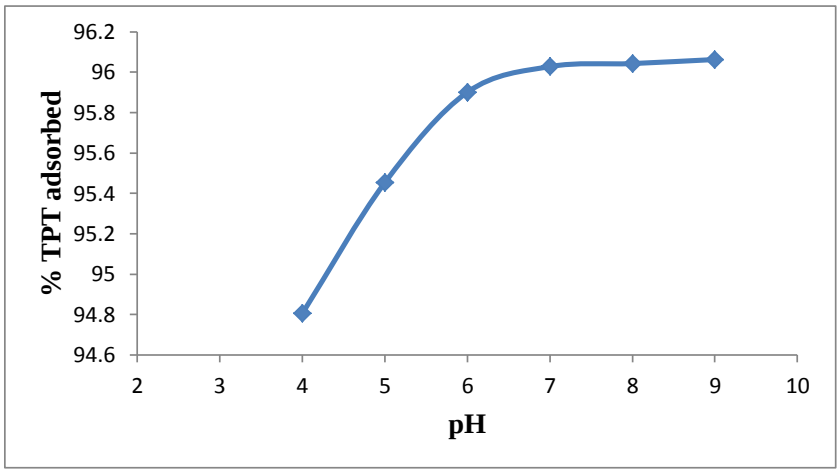

Figure 4.252: Effect of pH on TPT adsorption onto fly ash

Experimental conditions: Concentration of TPT = 100 mg/L; Volume of TPT solution = 25 mL, Mass of fly ash = 0.5 g; Contact time = 60 min; Stirring speed = 160 rpm, Temperature = 20 ^oC.

About 96.04 % of TPT was removed from the initial concentration of 100 mg/L TPT by the fly ash at a contact time of 60 min, stirring speed of 160 rpm, temperature of 20 ^oC and pH 8. pH 8 was therefore chosen as the optimum pH and was used for further studies.

4.12.12.4 Effect of stirring speed

The effect of stirring speed on the adsorption of TPT onto fly ash was studied at a stirring speed of 160 – 200 rpm. The adsorption capacity of TPT onto fly ash increases with increase in the stirring speed of the mixture and therefore attains equilibration at 200 rpm (Figure 4.161).

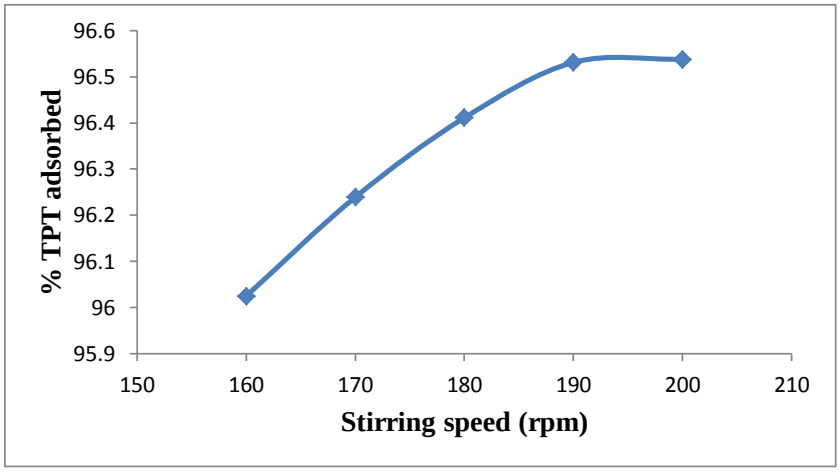

Figure 4.253: Effect of stirring speed on TPT adsorption onto fly ash

Experimental conditions: Concentration of TPT = 100 mg/L; Volume of TPT solution = 25 mL, Mass of fly ash = 0.5 g; Contact time = 60 min; Temperature = 20 ^{o}C.

4.827 mg/g (96.54 %) of TPT was therefore removed from the initial concentration of 5 mg/g TPT by the fly ash at a contact time of 60 min, pH 8, temperature of 20 ^{o}C and a stirring speed of 200 rpm (Figure 4.253). A stirring speed of 200 rpm was therefore used for further studies.

4.12.12.5 Effect of initial concentration

The effect of initial TPT concentration in the range of 12.5 to 100 mg/L on the adsorption of TPT onto fly ash was investigated. Along with pH, all parameters were kept constant in this study. It is evident from the Figure 4.254 that, as the concentration of TPT was increased, the amount of TPT adsorbed by fly ash was increased and an increase in percentage removal was also observed.

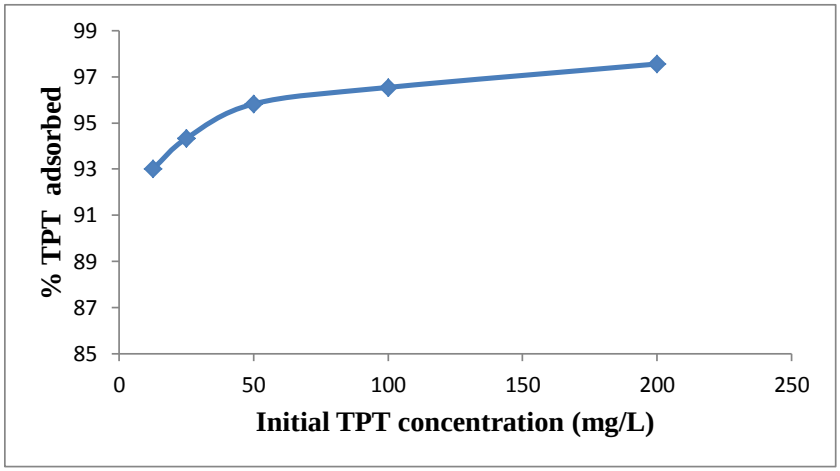

Figure 4.254: Percentage TPT adsorbed by fly ash at various initial TPT concentrations

Experimental conditions: Volume of TPT solution = 25 mL, Mass of fly ash = 0.5 g; pH = 8; Stirring speed = 200 rpm; Contact time = 60 min; Temperature = 20 ^{o}C.

The percentage TPT adsorbed increases from 93.00 – 97.55 % as the initial TPT concentration increases.

4.12.12.5.1 Adsorption isotherms

The adsorption isotherm plots are presented in Figures 4.255 – 4.258 and parameters obtained for the models were given in Table 4.42. Based on values of correlation coefficient, R^2, summarized in Table 4.42, the adsorption of TPT onto fly ash can be described by the Freundlich adsorption isotherm, probably due to the real heterogeneous nature of the surface sites involved in the process of adsorption. Han et al., 2007 also reported that the adsorption of TPT onto modified Chitosan fitted well with Freundlich adsorption isotherm.

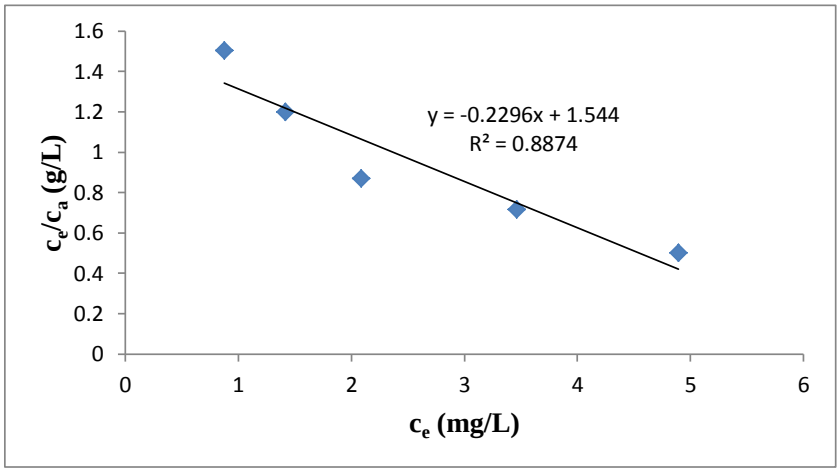

Figure 4.255: Langmuir isotherm for adsorption of TPT onto fly ash

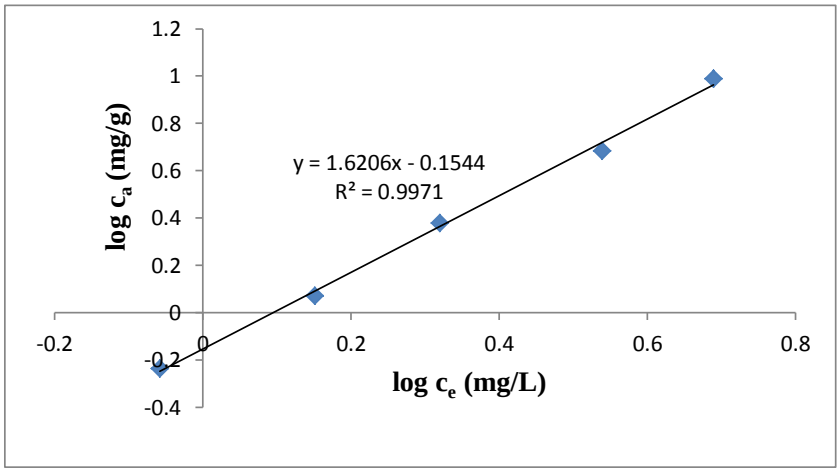

Figure 4.256: Freundlich isotherm for adsorption of TPT onto fly ash

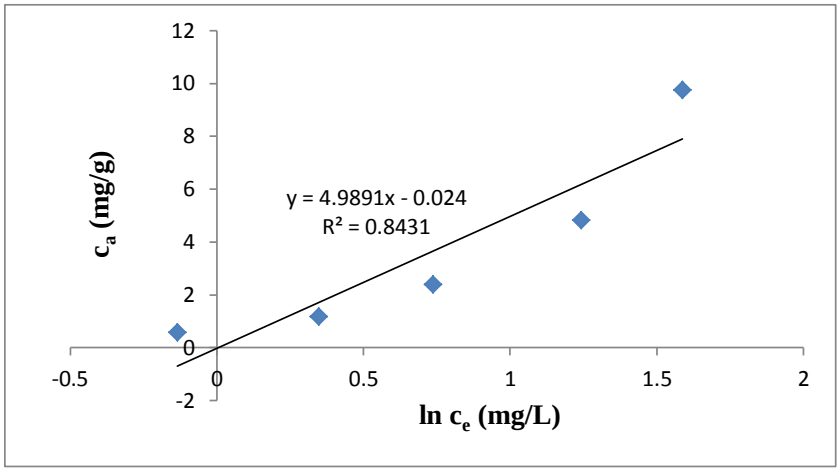

Figure 4.257: Temkin isotherm for adsorption of TPT onto fly ash

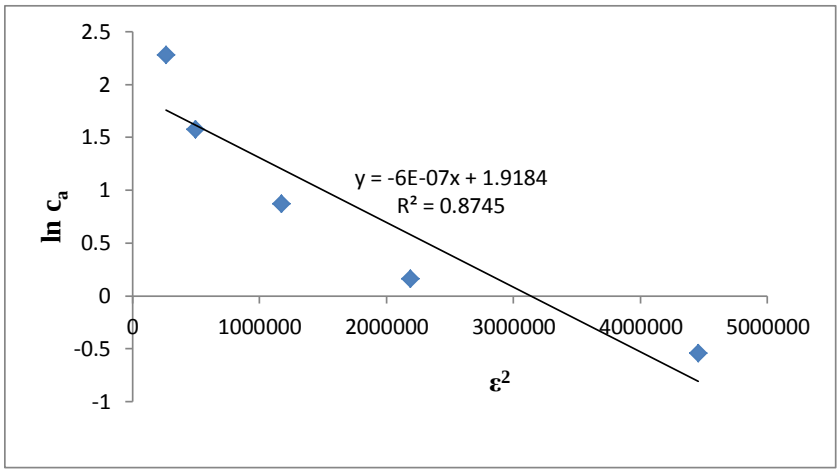

Figure 4.258: D-R isotherm for adsorption of TPT onto fly ash

Values of k_F, k_L, k_T and k_{D-R} constants obtained are 0.7008 mg/g (L/mg)$^{1/n}$, -0.1487 L/mg, 0.9952 mg/L and 6 x 10^{-7} J^2/mol^2, respectively (Table 4.42). Moreover, the negative value of the Langmuir constants, A_{max} (mg/g) and k_L (L/mg) for TPT adsorption onto fly ash indicate an inadequacy of the Langmuir model to fit the process. Thus, Freundlich model is the best model to explain the adsorption behaviour of TPT onto the fly ash.

Table 4.42: Isotherms constants for the adsorption of TPT onto fly ash

Equilibrium models	
Freundlich	
k_F [mg/g (L/mg)$^{1/n}$]	0.7008
n_F	0.6171
R^2	0.9971
Langmuir	
k_L (L/mg)	-0.1487
A_{max} (mg/g)	-4.3554
R^2	0.8874
Temkin	
n_T (L/g)	4.9891
k_T (mg/L)	0.9952
b_T (J/mol)	488.36
R^2	0.8431
Dubinin-Redushkevich	
k_{D-R} (J^2/mol^2)	6×10^{-7}
q_m (mg/g)	6.8101
E (J/mol)	912.87
R^2	0.8745

4.12.12.6 Effect of temperature

The experimental results obtained on the effect of temperature (Figure 4.259) show that the adsorption capacity of TPT onto fly ash decreases with increase in the solution temperature. This indicates that the adsorption of TPT onto fly ash is exothermic and it is in support of the work reported by Han et al., 2007 who reported the adsorption of TPT onto modified Chitosan.

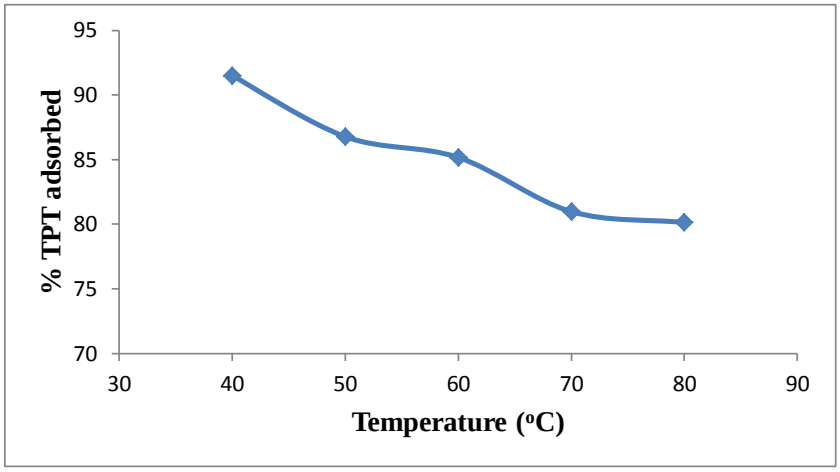

Figure 4.259: Effect of temperature on TPT adsorption onto fly ash

Experimental conditions: Concentration of TPT = 100 mg/L; Volume of TPT solution = 25 mL, Mass of fly ash = 0.5 g; Contact time = 60 min; pH = 8; Stirring speed = 200 rpm.

Approx. 80.14 % of TPT was removed from the initial concentration of 5 mg/g TPT by the fly ash at a contact time of 60 min, pH 8, stirring speed 200 rpm and temperature of 80 ^{o}C whereas 91.51 % TPT was removed by fly ash at 40 ^{o}C at the same conditions. Figure 4.260 shows the Van't Hoff plot for the adsorption of TPT onto fly ash and the variation in the extent of adsorption with respect to temperature have been explained on the basis of ΔH^{o}, ΔS^{o}, and ΔG^{o} as presented in Table 4.43.

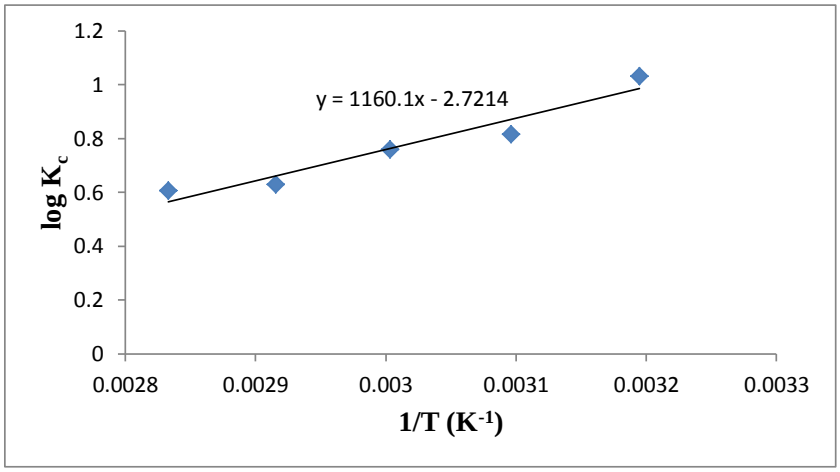

Figure 4.260: Van't Hoff Plot for the adsorption of TPT onto fly ash

Table 4.43: Thermodynamic parameters for adsorption of TPT onto fly ash

Temperature (°C)	ΔG° (kJ/mol)	ΔS° (J/K/mol)	ΔH° (kJ/mol)	K_c
40	-6.186	-52.11	-22.213	10.775
50	-5.052			6.563
60	-4.839			5.743
70	-4.131			4.258
80	-4.093			4.034

The negative value of ΔH^{o} (-22.213 kJ/mol) for the intervals of temperatures studied (Table 4.43) shows the exothermic nature of the adsorption process. The negative value of ΔS^{o} (-52.11 J/K/mol) corresponds to a decrease in degree of freedom of the adsorbed TPT and suggest the decrease in concentration of adsorbate in solid–solution interface indicating a decrease in adsorbate concentration onto the solid phase. ΔG^{o} values were found to increase as the temperature increases, which indicate non-spontaneous adsorption and the degree of spontaneity of the reaction decreases with increase in temperature.

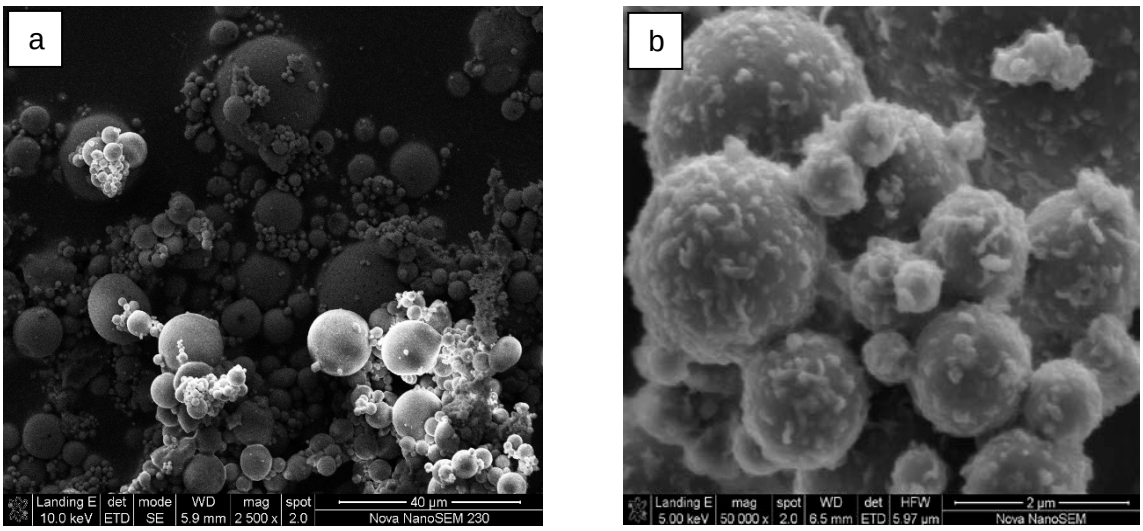

Figure 4.261: Fly ash before (a) and after (b) TPT adsorption

Figure 4.262: Representative TPT chromatogram after adsorption of 100 mg/L TPT with 0.5 g of fly ash, contact time of 60 min, temperature 20 ^{o}C and a stirring speed of 200 rpm

The SEM analysis of fly ash before and after adsorption is as presented in Figure 4.261 while a representative TPT chromatogram after adsorption of 100 mg/L TPT with 0.5 g of fly ash, contact time of 60min, temperature 20 ^{o}C and a stirring speed of 200 rpm is as shown in Figure 4.262.

4.12.13 Adsorption of TPT from TPT-contaminated artificial seawater onto nFe_3O_4

4.12.13.1 Effect of adsorbent amount

The amount of nFe_3O_4 (adsorbent dose) ranging from 0.0625 – 1.0 g per 25 mL of TPT solution was investigated on the efficiency of the adsorption process. A graph of the percentage of TPT adsorbed (C_a), mg/g onto nFe_3O_4 was plotted against the adsorbent amount (Figure 4.263).

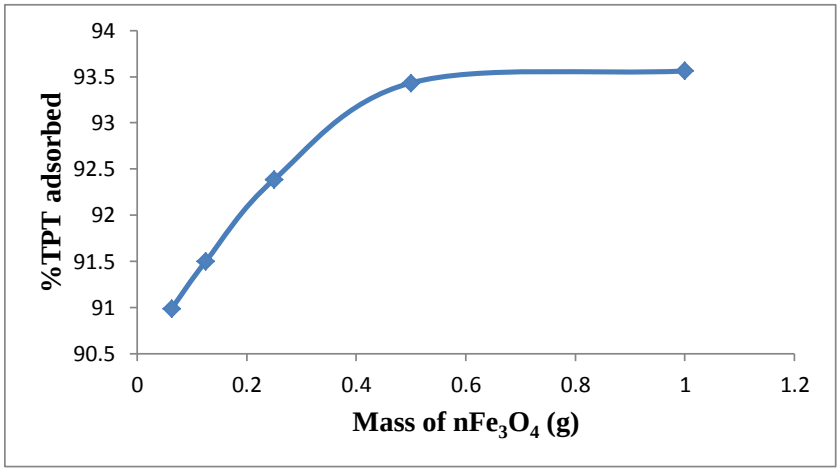

Figure 4.263: Adsorption efficiencies of TPT onto nFe_3O_4

Experimental conditions: Concentration of TPT = 100 mg/L; Volume of TPT solution = 25 mL, Contact time = 60 min; Stirring speed = 160 rpm, Temperature = 20 ^oC.

It was observed that the percentage adsorption increased with increasing nFe_3O_4 amount, reaching an optimum at 0.5 g, corresponding to 93.43 %. 0.5 g was therefore selected as the optimum nFe_3O_4 amount used for further studies (Fatoki et al., 2013).

4.12.13.2 Effect of contact time

Adsorption kinetic study of TPT from TPT – contaminated artificial seawater onto nFe_3O_4 was carried out by shaking 0.5 g of nFe_3O_4 in 25 mL of TPT solutions with an initial concentration of 100 mg/L at 20 ^oC. After pre-defined contact time (10-70 min), the aqueous samples were filtered, and the concentration of TPT in the filtrate was determined.

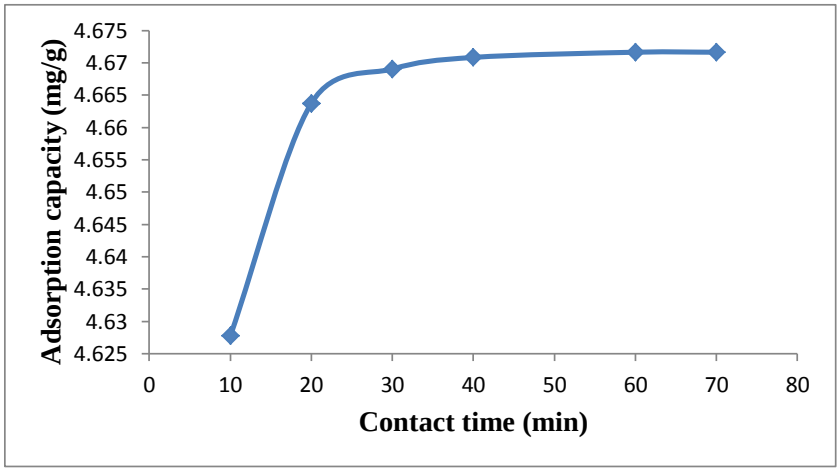

Figure 4.264: Effect of contact time on TPT adsorption onto nFe_3O_4

Experimental conditions: Concentration of TPT = 100 mg/L; Volume of TPT solution = 25 mL, Mass of nFe_3O_4 = 0.5 g; Stirring speed = 160 rpm, Temperature = 20 ^{o}C.

Figure 4.264 thus shows the effect of contact time on adsorption of TPT by nFe_3O_4. The TPT removal efficiencies at different time intervals ranging from 10 – 70 min were obtained. It was observed that equilibrium was achieved within 60 min and the corresponding TPT removal efficiency from the initial concentration of 100 mg/L TPT by the nFe_3O_4 reaches 4.67 mg/g (93.43 %).

4.12.13.2.1 Adsorption kinetics

Figures 4.265 – 4.269 show the pseudo first-order, pseudo second-order, Elovich, fractional power and intraparticle diffusivity kinetic plots, respectively while Table 4.44 provides the evaluated parameters of the kinetics models. The value of correlation coefficient (R^2) of pseudo second-order kinetic model (> 0.99) is higher than that of other models indicating that the kinetic model for the adsorption of TPT onto nFe_3O_4 is pseudo second-order. The intraparticle coefficient for the adsorption of TPT by the nFe_3O_4 was calculated and the results also indicate that the power function model satisfactorily describes the time-dependence of TPT onto the nFe_3O_4 as the value of the constant ν is less than 1.

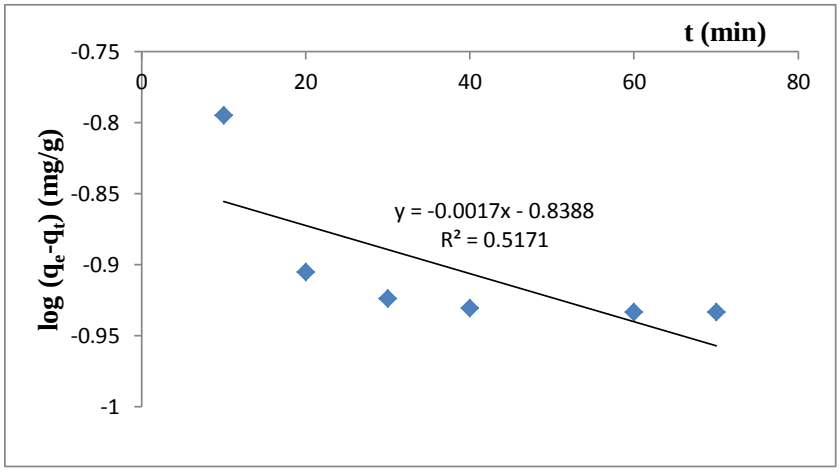

Figure 4.265: Pseudo first-order rate equation plot for TPT adsorption onto nFe_3O_4

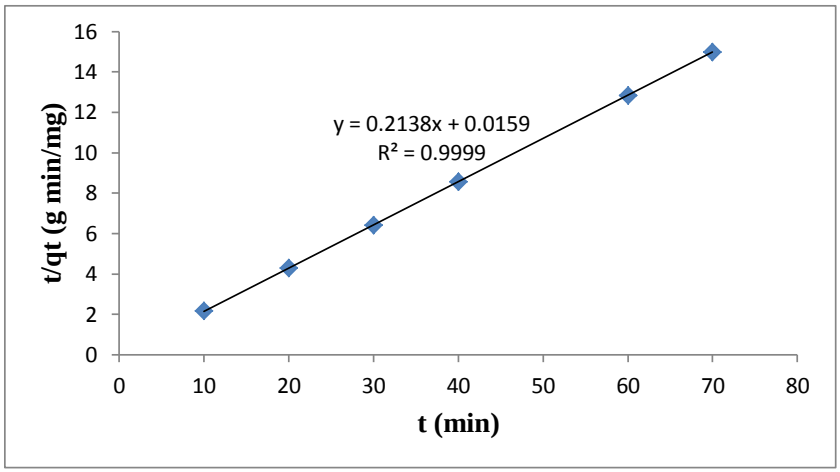

Figure 4.266: Pseudo second-order rate equation plot for TPT adsorption onto nFe_3O_4

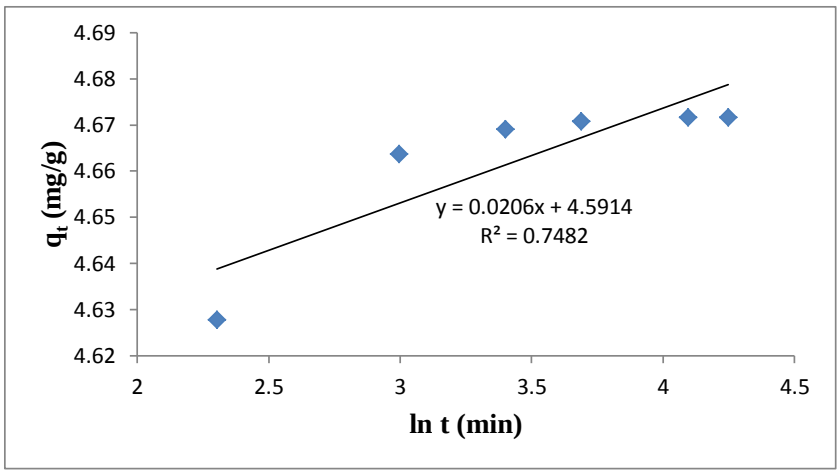

Figure 4.267: Elovich rate equation plot for TPT adsorption onto nFe_3O_4

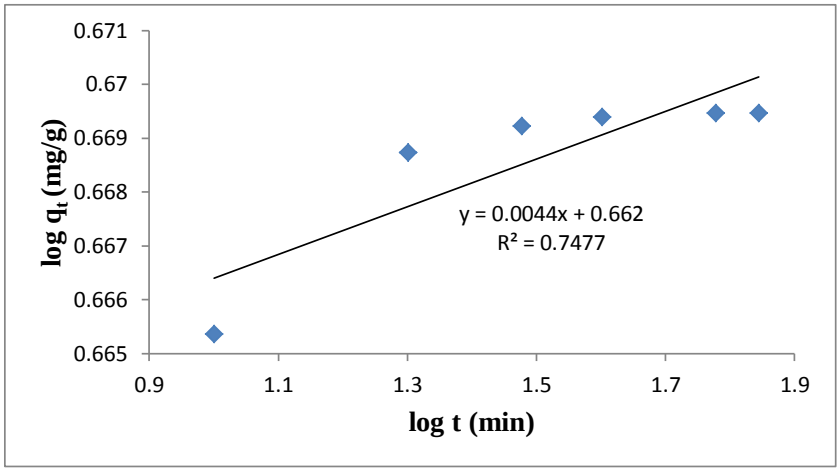

Figure 4.268: Fractional Power rate equation plot for TPT adsorption onto nFe_3O_4

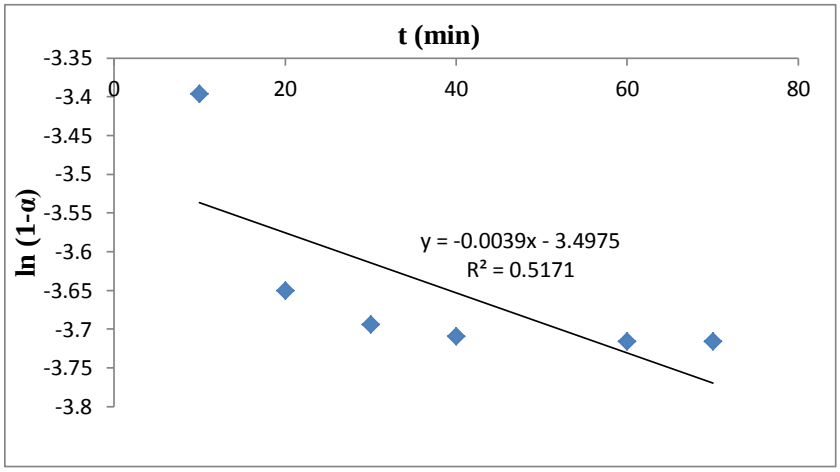

Figure 4.269: Intraparticle diffusivity plot for TPT adsorption onto nFe_3O_4

The value of the initial adsorption rates, h_o, obtained for the pseudo second-order kinetics of the adsorption of TPT onto nFe_3O_4 is 62.893 mg/g/min. The kinetic model constants k_1, k_2, β, α_E, k_3 and k_p are 3.915 x 10^{-3} min^{-1}, 2.8748 g/mg/min, 48.5436 gmin/mg, 3.042 x 10^{98} $gmin^2/mg$, 4.5920 mg/g and 0.0039 min^{-1}, respectively (Fatoki et al., 2013).

Table 4.44: Kinetic model parameters for TPT adsorption onto nFe_3O_4

Kinetic models	
Pseudo first-order	
k_1 (min^{-1})	3.915×10^{-3}
q_e (mg/g)	0.1449
R^2	0.5171
Pseudo second-order	
q_e (mg/g)	4.6773
h_o (mg/g/min)	62.893
k_2 (g/mg/min)	2.8748
R^2	0.9999
Elovich	
β (g min/mg)	48.5436
α (g min^2/mg)	3.042×10^{98}
R^2	0.7482
Fractional Power	
v (min^{-1})	0.0044
k_3 (mg/g)	4.5920
k_3v (mg/g/min)	0.0202
R^2	0.7477
Intraparticle diffusivity	
k_p (min^{-1})	0.0039
R^2	0.5171

4.12.13.3 Effect of pH

The effect of pH on the adsorption of TPT onto the nFe_3O_4 was studied at pH 4 – 9. It was observed from Figure 4.270 that the percentage of TPT adsorbed by nFe_3O_4 steadily increases as the pH of the solution increases from pH 4 to pH 8, and reaches equilibration at pH ≥ 8. It is also evident that maximum adsorption TPT onto nFe_3O_4 was recorded within the pH range of normal saline water and pH 8 was used for further studies.

About 93.65 % of TPT was removed from the initial concentration of 100 mg/L TPT by nFe_3O_4 at a contact time of 60 min, stirring speed of 160 rpm, pH 8 and a temperature of 20 ^oC.

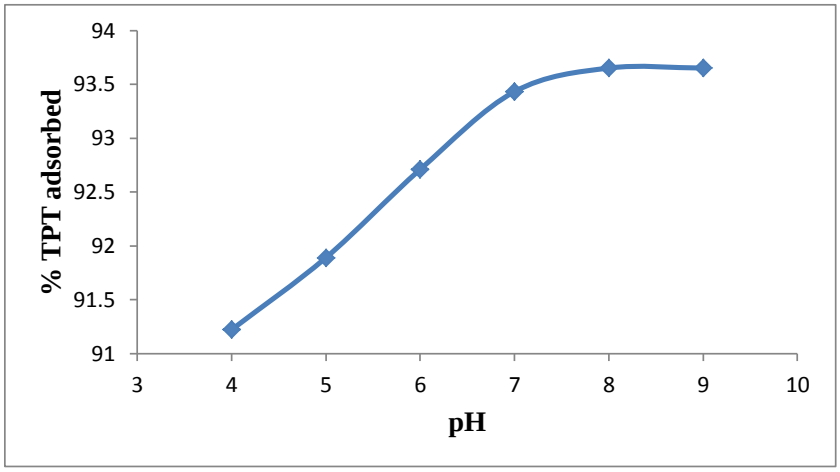

Figure 4.270: Effect of pH on TPT adsorption onto nFe_3O_4

Experimental conditions: Concentration of TPT = 100 mg/L; Volume of TPT solution = 25 mL, Mass of nFe_3O_4 = 0.5 g; Contact time = 60 min; Stirring speed = 160 rpm, Temperature = 20 ^oC.

4.12.13.4 Effect of stirring speed

The effect of stirring speed on the adsorption of TPT onto the nFe_3O_4 was studied at a stirring speed of 160 – 200 rpm. The adsorption capacity of TPT onto nFe_3O_4 increases with increasing stirring speed (Figure 4.271). The figure thus shows that about 95.50 % TPT was removed from the initial concentration of 100 mg/L TPT by nFe_3O_4 at a contact time of 60 min, pH 8, a temperature of 20 ^oC and a stirring speed of 200 rpm. 200rpm was therefore used for further studies.

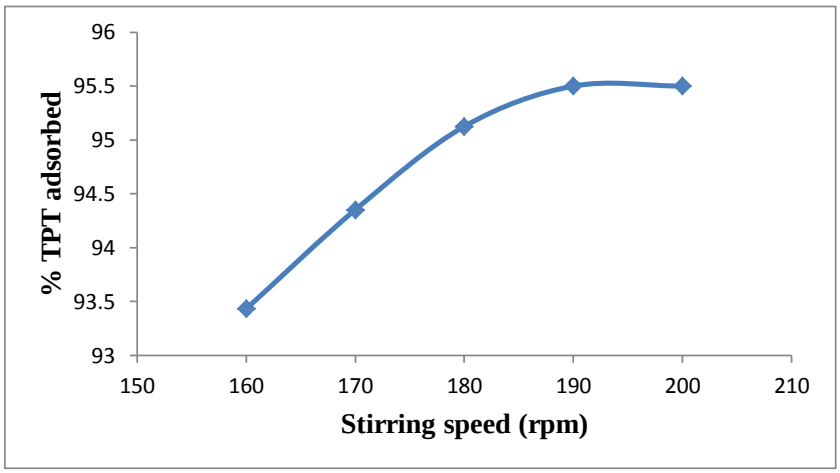

Figure 4.271: Effect of stirring speed on TPT adsorption onto nFe_3O_4

Experimental conditions: Concentration of TPT = 100 mg/L; Volume of TPT solution = 25 mL, Mass of nFe_3O_4= 0.5 g; Contact time = 60 min; Temperature = 20 ^oC.

4.12.13.5 Effect of initial concentration

The results on the effect of initial TPT concentration (Figure 4.272) show that the adsorption of TPT onto nFe_3O_4 increases as the initial TPT concentration increases from 12.5 to 100 mg/L, indicating that adsorption is also favourable for the higher TPT concentrations that have been investigated.

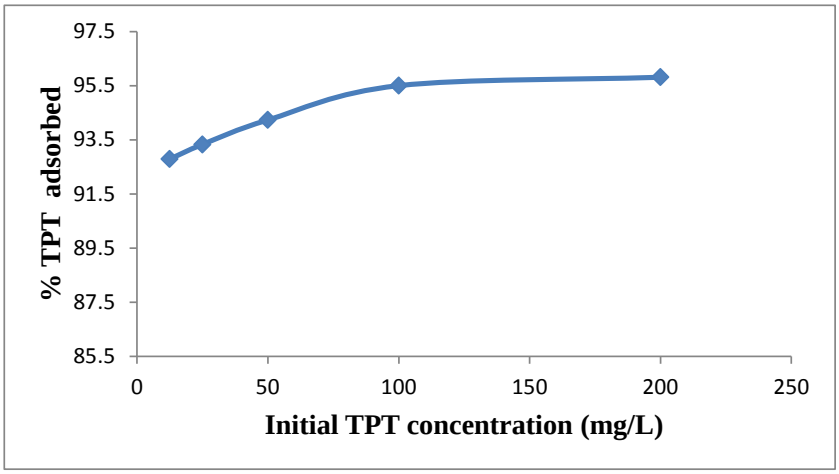

Figure 4.272: Percentage TPT adsorbed by nFe_3O_4 at various initial TPT concentrations

Experimental conditions: Volume of TPT solution = 25 mL, Mass of nFe_3O_4 = 0.5 g; pH = 8; Stirring speed = 200 rpm; Contact time = 60 min; Temperature = 20 ^oC.

The increase in the adsorption capacity of nFe_3O_4 with an increase in the initial TPT concentration can also be attributed to increase in the driving force due to concentration gradient developed between the bulk solution and surface of nFe_3O_4.

4.12.13.5.1 Adsorption isotherm

The adsorption isotherm parameters obtained from the equilibrium models for the adsorption of TPT onto nFe_3O_4 were given in Table 4.45 and the plots are presented in Figures 4.273 – 4.276. The figures and table show that the experimental data fitted well with Freundlich isotherm and the value of η_F, for the nFe_3O_4, falling in the range 1 -10 indicates favourable adsorption.

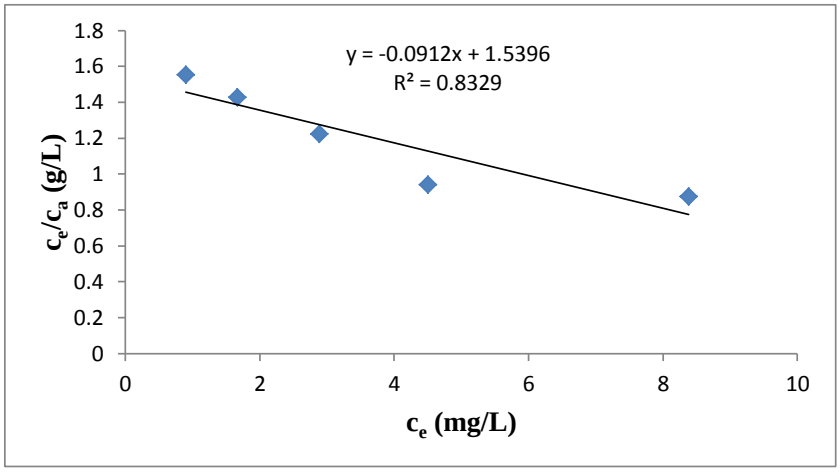

Figure 4.273: Langmuir isotherm for adsorption of TPT onto nFe_3O_4

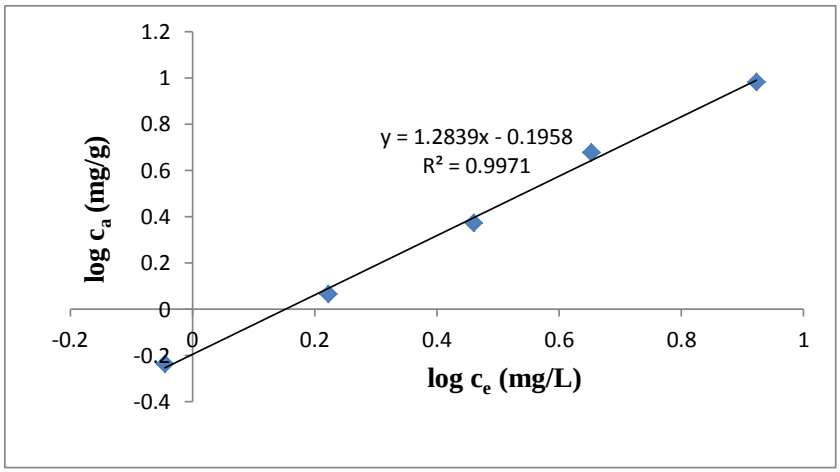

Figure 4.274: Freundlich isotherm for adsorption of TPT onto nFe_3O_4

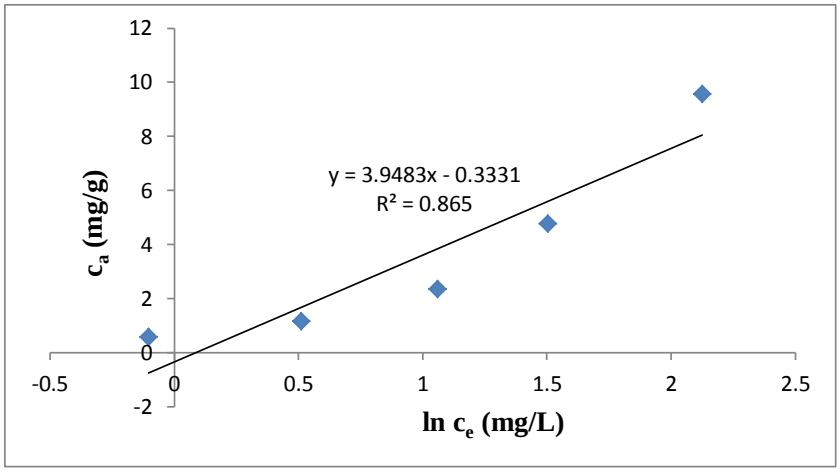

Figure 4.275: Temkin isotherm for adsorption of TPT onto nFe_3O_4

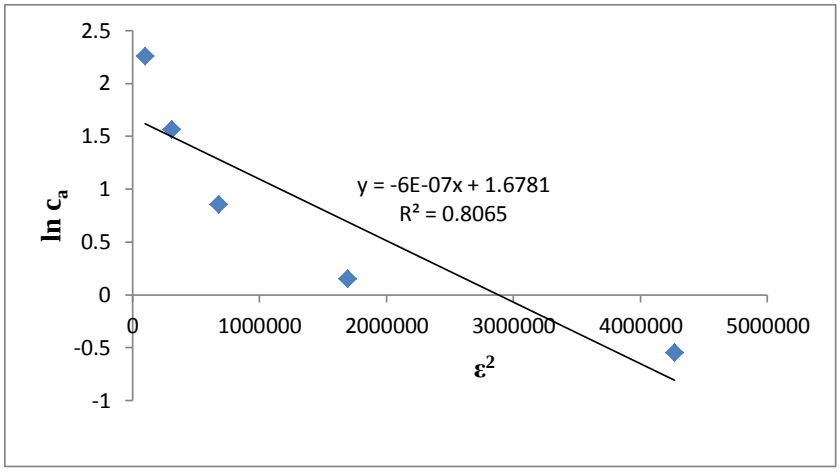

Figure 4.276: D-R isotherm for adsorption of TPT onto nFe_3O_4

Table 4.45: Isotherms constants for the adsorption of TPT onto nFe_3O_4

Equilibrium models	
Freundlich	
k_F [mg/g (L/mg)$^{1/n}$]	0.6371
n_F	0.7789
R^2	0.9971
Langmuir	
K_L (L/mg)	-0.05924
A_{max} (mg/g)	-10.9649
R^2	0.8329
Temkin	
n_T (L/g)	3.9483
k_T (mg/L)	0.9191
b_T (J/mol)	616.975
R^2	0.8650
Dubinin-Redushkevich	
k_{D-R} (J^2/mol^2)	6 x 10^{-7}
q_m (mg/g)	5.3554
E (J/mol)	912.871
R^2	0.8065

Moreover, the negative value of the Langmuir constants, A_{max} (mg/g) and k_L (L/mg) for TPT adsorption onto nFe_3O_4 indicate the inadequacy of the Langmuir model to fit the process.

4.12.13.6 Effect of temperature

The experimental results obtained on the effect of temperature for the adsorption of TPT onto nFe_3O_4 (Figure 4.277) show that the adsorption capacity of nFe_3O_4 decreases with increase in the solution temperature. This indicates that the adsorption of TPT onto nFe_3O_4 is exothermic.

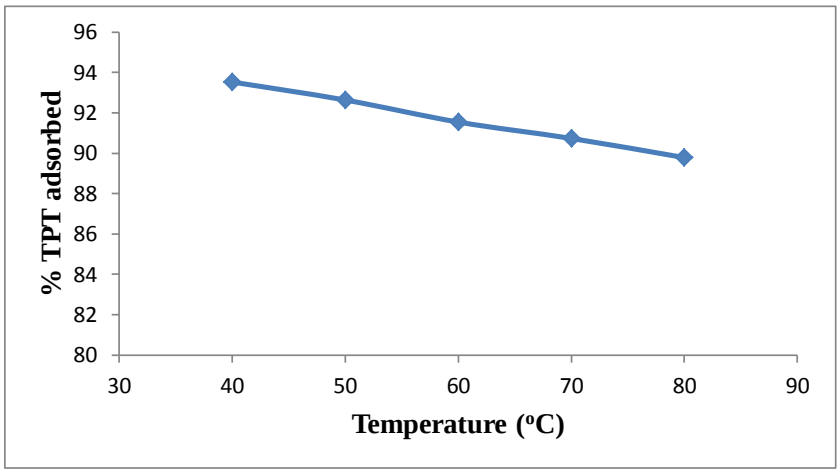

Figure 4.277: Effect of temperature on TPT adsorption onto nFe_3O_4

Experimental conditions: Concentration of TPT = 100 mg/L; Volume of TPT solution = 25 mL, Mass of nFe_3O_4 = 0.5 g; Contact time = 60 min; pH = 8; Stirring speed = 200 rpm.

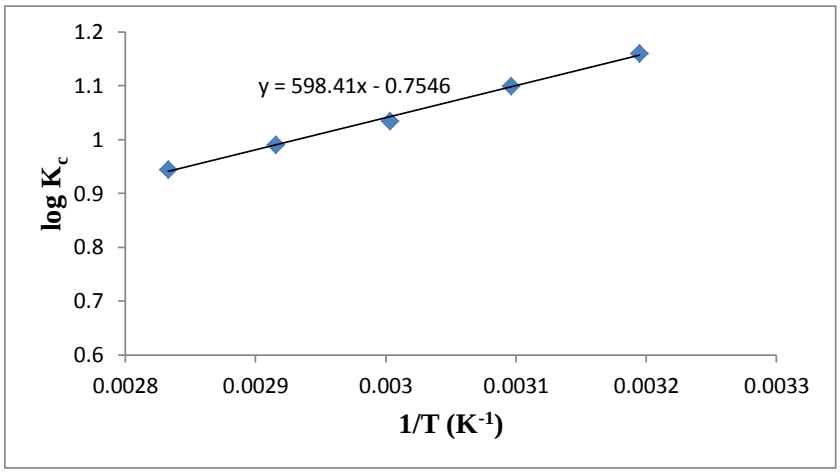

Figure 4.278: Van't Hoff Plot for the adsorption of TPT onto nFe_3O_4

Table 4.46: Thermodynamic parameters for adsorption of TPT onto nFe_3O_4

Temperature (°C)	ΔG° (kJ/mol)	ΔS° (J/K/mol)	ΔH° (kJ/mol)	K_c
40	-6.948	-14.448	-11.458	14.444
50	-6.799			12.577
60	-6.594			10.825
70	-6.505			9.790
80	-6.374			8.787

Approx. 89.78 % of TPT was removed from the initial concentration of 5 mg/g TPT by nFe_3O_4 at a contact time of 60 min, pH 8, stirring speed 200 rpm and temperature of 80 °C whereas 93.53 % TPT was removed at 40 °C at the same conditions. Figure 4.278 thus shows the Van't Hoff plot for the adsorption of TPT onto nFe_3O_4 while ΔH^o , ΔS^o, and ΔG^o are presented in Table 4.46.

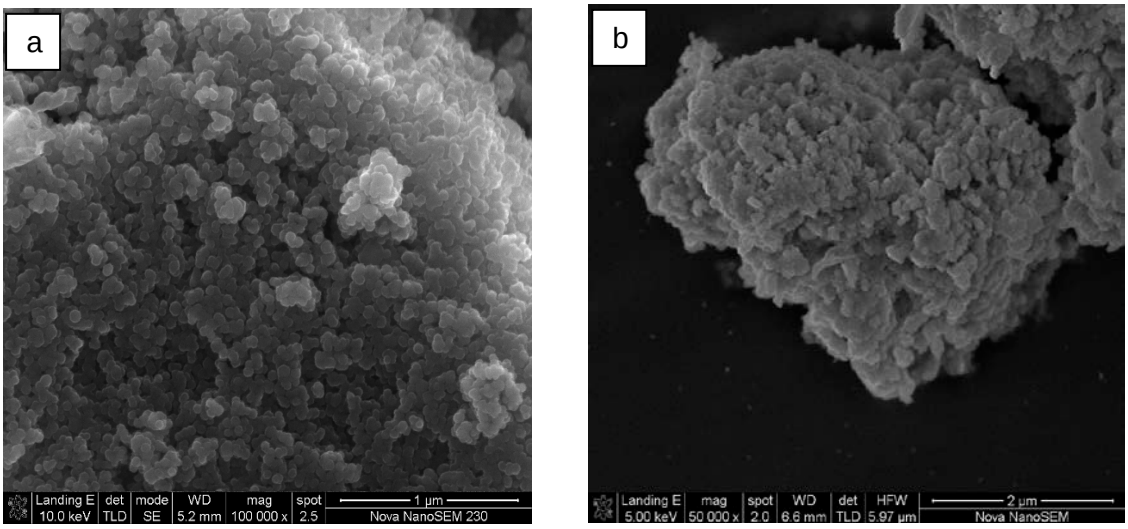

Figure 4.279: nFe_3O_4 before (a) and after (b) TPT adsorption

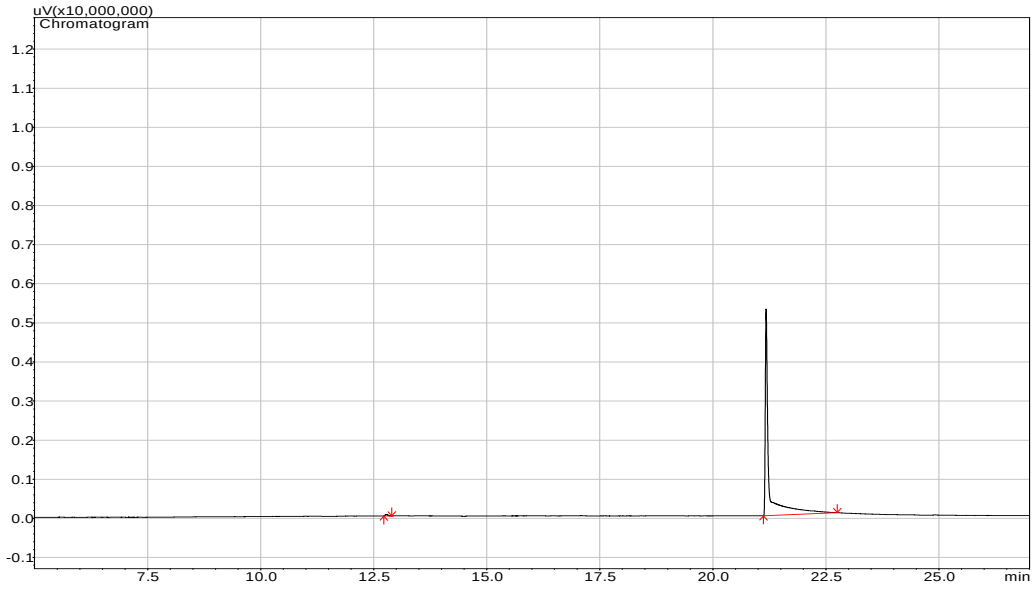

Figure 4.280: Representative TPT chromatogram after adsorption of 100 mg/L TPT with 0.5 g of nFe_3O_4, contact time of 60 min, temperature 20 ^oC and a stirring speed of 200 rpm

The negative value of ΔH^o (-11.458 kJ/mol) for the intervals of temperatures studied (Table 4.46) also shows the exothermic nature of the adsorption process. The negative value of ΔS^o (-14.448 J/K/mol) corresponds to a decrease in the degree of freedom of the adsorbed TPT and suggest the decrease in concentration of adsorbate in solid–solution interface indicating a decrease in adsorbate concentration onto the solid phase. ΔG^o values were found to increase as the temperature increases, which indicate non-spontaneous adsorption and the degree of spontaneity of the reaction decreases with increase in temperature.

The SEM analysis of nFe_3O_4 before and after adsorption (optimal condition) is presented in Figure 4.279 and the TPT chromatogram after adsorption of 100 mg/L TPT with 0.5 g of nFe_3O_4, 60 min contact time, temperature 20 ^oC and a stirring speed of 200 rpm is as shown in Figure 4.280.

4.12.14 Adsorption of TPT from TPT-contaminated artificial seawater onto $nSiO_2$

4.12.14.1 Effect of adsorbent amount

The results on the effect of $nSiO_2$ amount on the adsorption of TPT by the $nSiO_2$ as shown in Figure 4.281 indicates that the percentage of TPT adsorption increases with increasing $nSiO_2$ amount, reaching an optimum at 0.5 g, corresponding to 97.68 % removal.

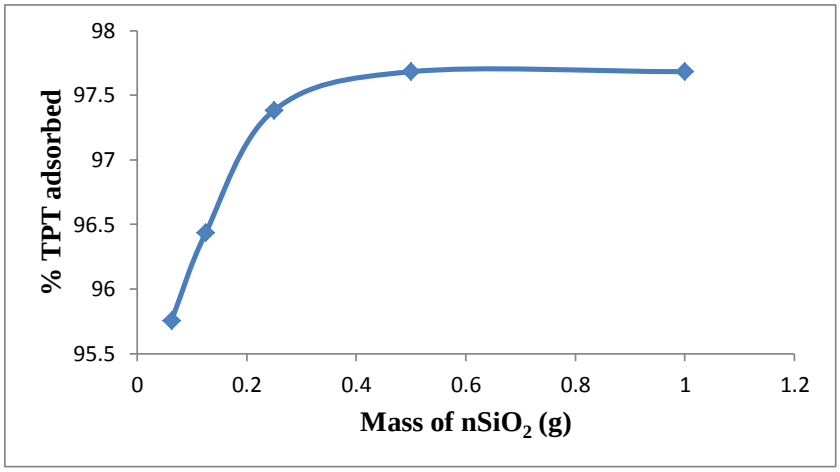

Figure 4.281: Adsorption efficiencies of TPT onto $nSiO_2$

Experimental conditions: Concentration of TPT = 100 mg/L; Volume of TPT solution = 25 mL, Contact time = 60 min; Stirring speed = 160 rpm, Temperature = 20 ^oC.

4.12.14.2 Effect of contact time

Figure 4.282 shows the effect of contact time on the adsorption of TPT onto $nSiO_2$. The TPT removal efficiency at different time intervals ranging from 10 – 70 min were obtained.

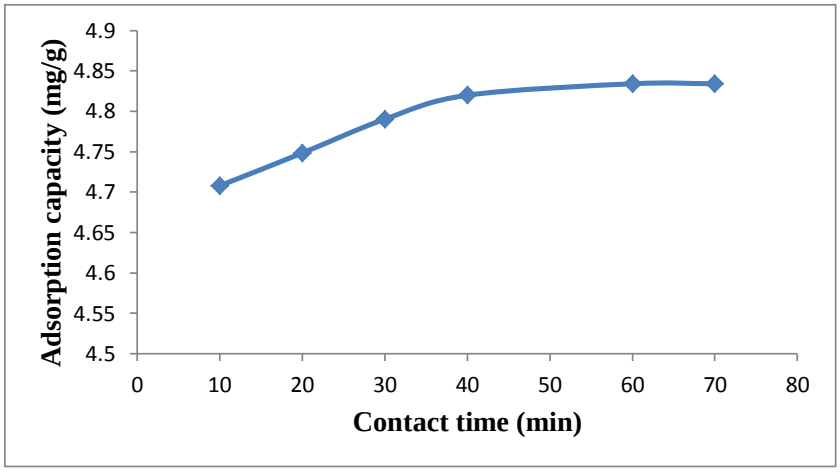

Figure 4.282: Effect of contact time on TPT adsorption onto $nSiO_2$

Experimental conditions: Concentration of TPT = 100 mg/L; Volume of TPT solution = 25 mL, Mass of $nSiO_2$ = 0.5 g; Stirring speed = 160 rpm, Temperature = 20 ^{o}C.

It was therefore observed from Figure 4.282 that equilibrium was approximately achieved within 60 min. The amount of TPT removed at a contact time of 60 min from the initial TPT concentration of 5.0 mg/g by the $nSiO_2$ is 4.83 mg/g (96.68 %). 60 min was therefore used for further studies.

4.12.14.2.1 Adsorption kinetics

Figures 4.283 – 4.287 show the pseudo first-order, pseudo second-order, Elovich, fractional power and intraparticle diffusivity kinetic plots while Table 4.47 provides the evaluated parameters of the kinetics models.

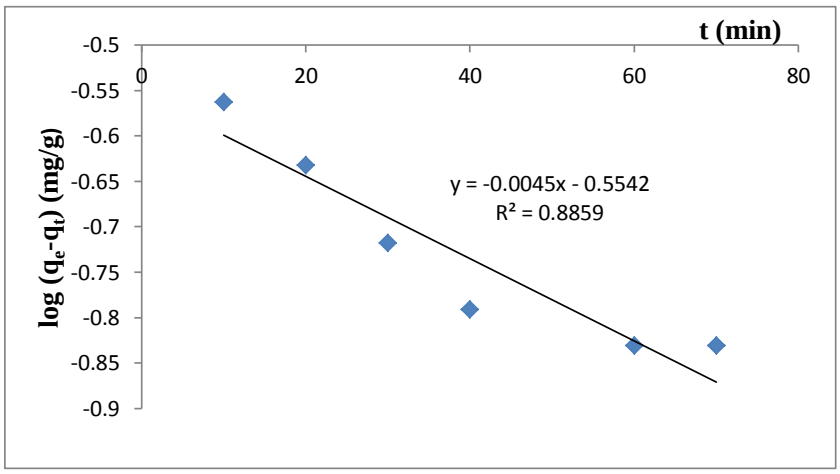

Figure 4.283: Pseudo first-order rate equation plot for TPT adsorption onto $nSiO_2$

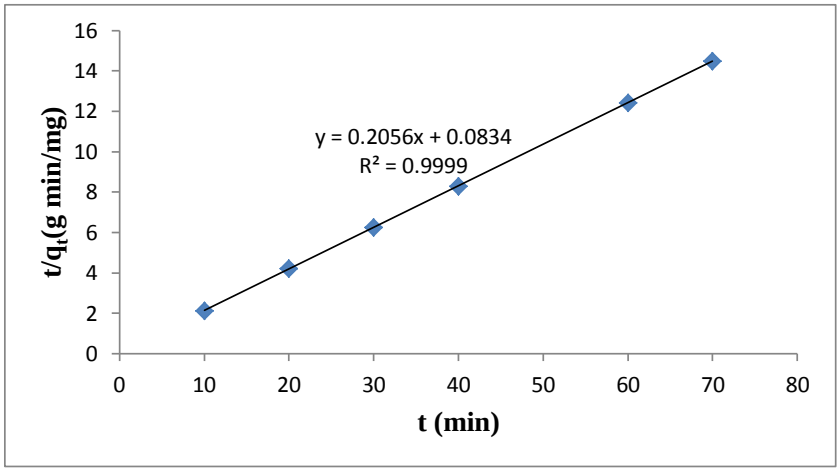

Figure 4.284: Pseudo second-order rate equation plot for TPT adsorption onto $nSiO_2$

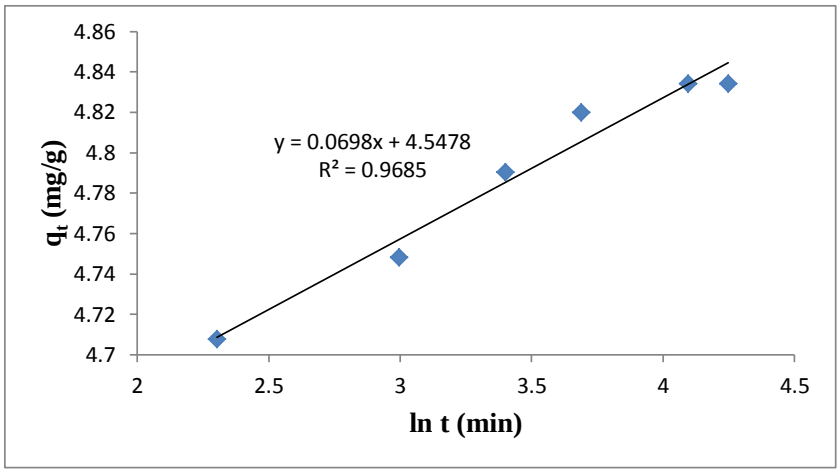

Figure 4.285: Elovich rate equation plot for TPT adsorption onto $nSiO_2$

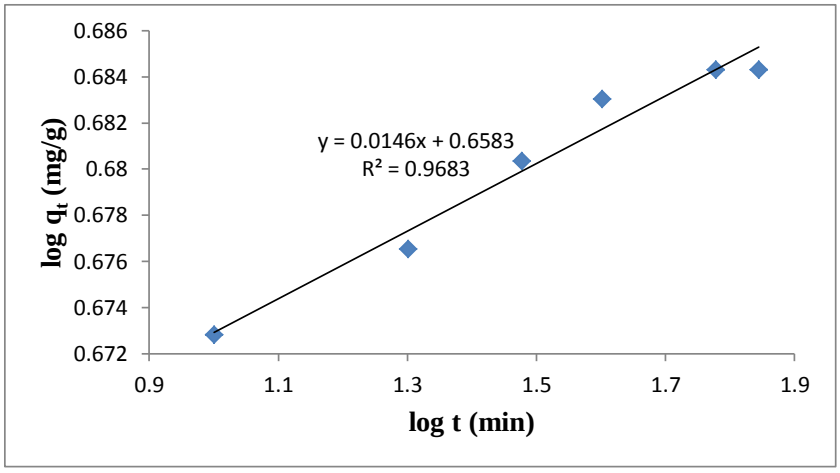

Figure 4.286: Fractional Power rate equation plot for TPT adsorption onto $nSiO_2$

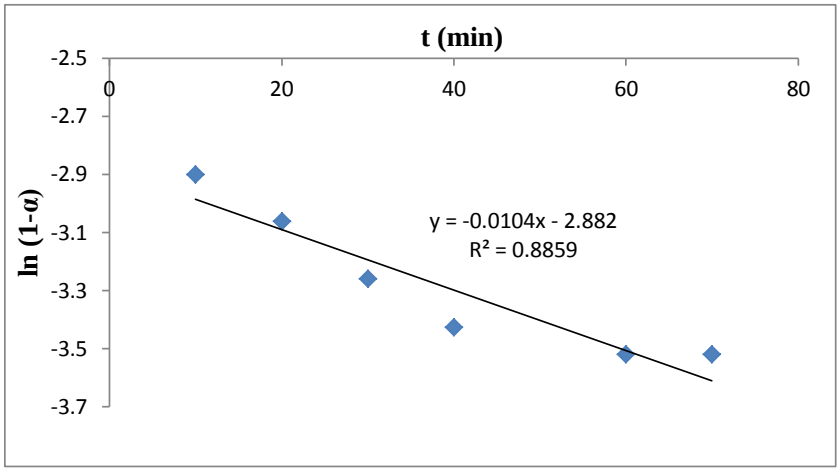

Figure 4.287: Intraparticle diffusivity plot for TPT adsorption onto $nSiO_2$

The results obtained show a very good compliance with pseudo second-order equation with high regression coefficient (> 0.99) whereas the pseudo first-order and Elovich models were not applicable as low regression coefficients (< 0.97) were observed. The results also show that the adsorption rate constant, k_2, initial adsorption rate, h_o, and equilibrium adsorption capacity, q_e, of the pseudo second-order model are 0.5079 g/mg/min, 11.99 mg/g/min and 4.8638 mg/g, respectively.

Table 4.47: Kinetic model parameters for TPT adsorption onto $nSiO_2$

Kinetic models	
Pseudo first-order	
k_1 (min^{-1})	0.0104
q_e (mg/g)	0.2791
R^2	0.8859
Pseudo second-order	
q_e (mg/g)	4.8638
h_o (mg/g/min)	11.990
k_2 (g/mg/min)	0.5079
R^2	0.9999
Elovich	
β (g min/mg)	14.3266
α (g min^2/mg)	2.84×10^{29}
R^2	0.9685
Fractional Power	
v (min^{-1})	0.0146
k_3 (mg/g)	4.5530
k_3v (mg/g/min)	0.0665
R^2	0.9683
Intraparticle diffusivity	
k_p (min^{-1})	0.0104
R^2	0.8859

A simple kinetic analysis of the adsorption of TPT onto $nSiO_2$ was also tested according to fractional power model and Table 4.47 shows the estimated parameters of the model. The results indicate that the power model satisfactorily described the time-dependent of TPT onto $nSiO_2$ as the value of the constant v is less than 1 and the regression coefficient is greater than 0.96.

The kinetic model constants k_1, k_2, β, α_E, k_3 and k_p as presented in Table 4.47 for the adsorption of TPT onto $nSiO_2$ are therefore 0.0104 min^{-1}, 0.5079 g/mg/min, 14.3266 gmin/mg, 2.84 x 10^{29} $gmin^2/mg$, 4.5530 mg/g and 0.0104 min^{-1}, respectively.

4.12.14.3 Effect of pH

The effect of pH on the adsorption of TPT onto $nSiO_2$ was studied at pH 4 – 9. It was observed from Figure 4.288 that the percentage of TPT adsorbed by $nSiO_2$ increased as the pH of the solution increases from pH 4 to pH 7, and reaches equilibration between pH 7 – 9.

Higher adsorption capacity was therefore recorded within the pH range of normal saline water. About 96.86 % TPT was removed from the initial concentration of 100 mg/L TPT by $nSiO_2$ at pH 8, a contact time of 60 min, 160 rpm stirring speed and a temperature of 20 ^oC.

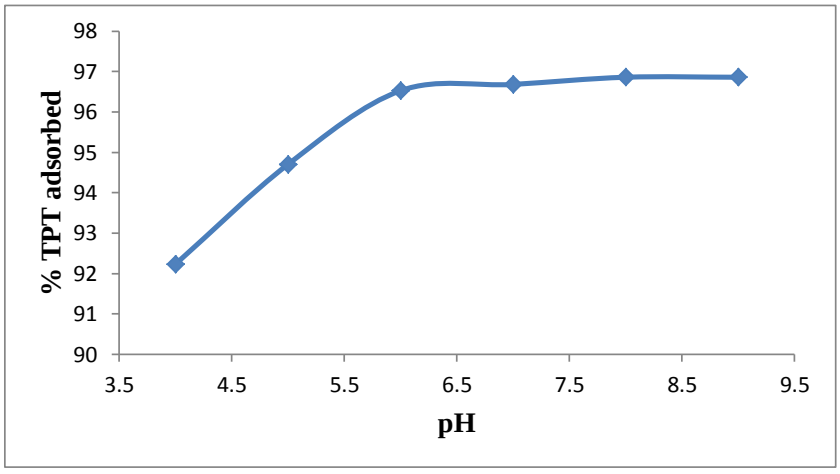

Figure 4.288: Effect of pH on TPT adsorption onto $nSiO_2$

Experimental conditions: Concentration of TPT = 100 mg/L; Volume of TPT solution = 25 mL, Mass of $nSiO_2$ = 0.5 g; Contact time = 60 min; Stirring speed = 160 rpm, Temperature = 20 ^oC.

4.12.14.4 Effect of stirring speed

The stirring speed of the adsorption process was also studied and optimized. The stirring speed on the adsorption of TPT onto $nSiO_2$ was studied at a stirring speed of 160 – 200 rpm. Figure 4.289 therefore shows that the adsorption capacity of $nSiO_2$ increases as the stirring speed of the mixture increases.

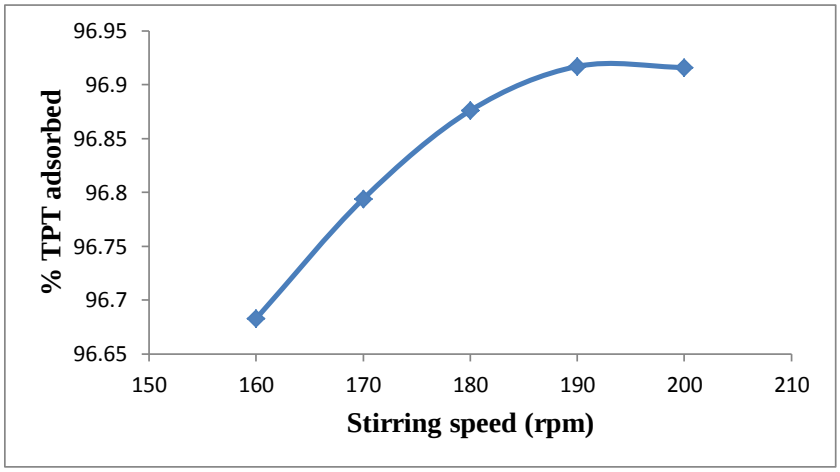

Figure 4.289: Effect of stirring speed on TPT adsorption onto $nSiO_2$

Experimental conditions: Concentration of TPT = 100 mg/L; Volume of TPT solution = 25 mL, Mass of $nSiO_2$ = 0.5 g; Contact time = 60 min; Temperature = 20 ^{o}C.

Approx. 4.846 mg/g (96.92 %) TPT was removed from the initial concentration of 5 mg/g TPT by $nSiO_2$ at a contact time of 60 min, pH 8, temperature of 20 ^{o}C and a stirring speed of 200 rpm (Figure 4.289).

4.12.14.5 Adsorption isotherms

Figure 4.290 shows that the adsorption of TPT onto $nSiO_2$ increases as the initial TPT concentration increases from 12.5 to 100 mg/L, indicating that the adsorption is also favourable for the higher TPT concentrations that have been investigated.

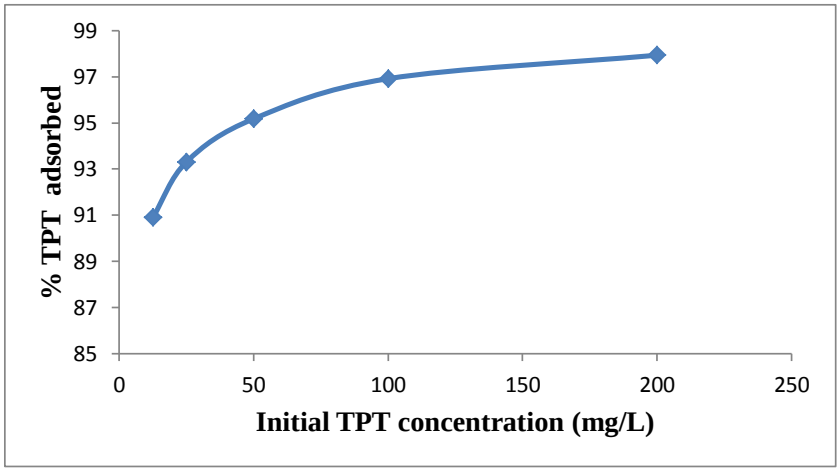

Figure 4.290: Percentage TPT adsorbed by $nSiO_2$ at various initial TPT concentrations

Experimental conditions: Volume of TPT solution = 25 mL, Mass of $nSiO_2$ = 0.5 g; pH = 8; Stirring speed = 200 rpm; Contact time = 60 min; Temperature = 20 ^{o}C.

4.12.14.5.1 Adsorption isotherms

The results obtained indicate that the Freundlich model fit the experiment data well. It is the suitable model for describing this adsorption process, as the correlation coefficient (R^2) is higher than the correlation coefficients obtained for other models (Figures 4.291 – 4.294 and Table 4.48). The value of n_F falling in the range 1 -10 also indicates favourable adsorption.

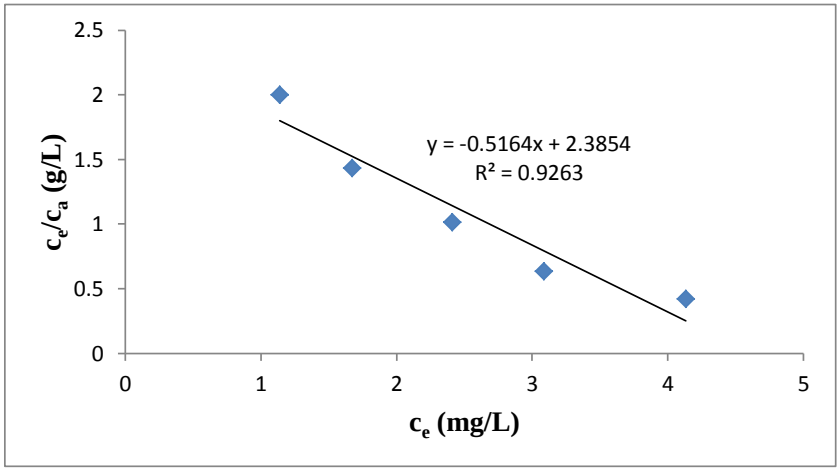

Figure 4.291: Langmuir isotherm for adsorption of TPT onto $nSiO_2$

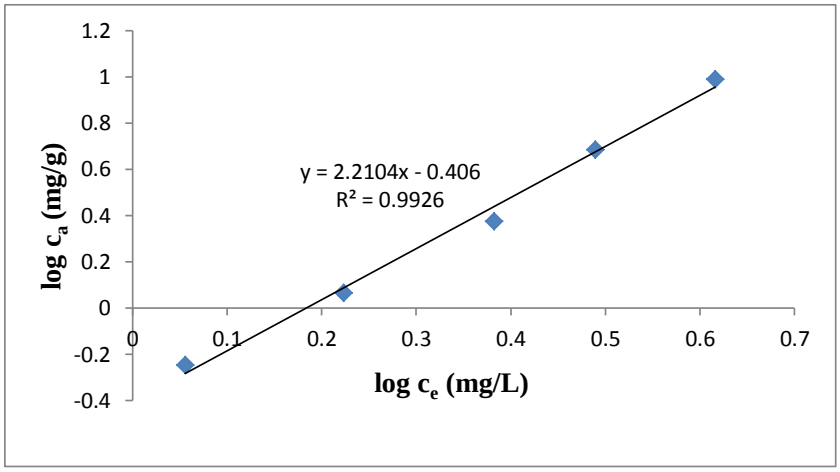

Figure 4.292: Freundlich isotherm for adsorption of TPT onto $nSiO_2$

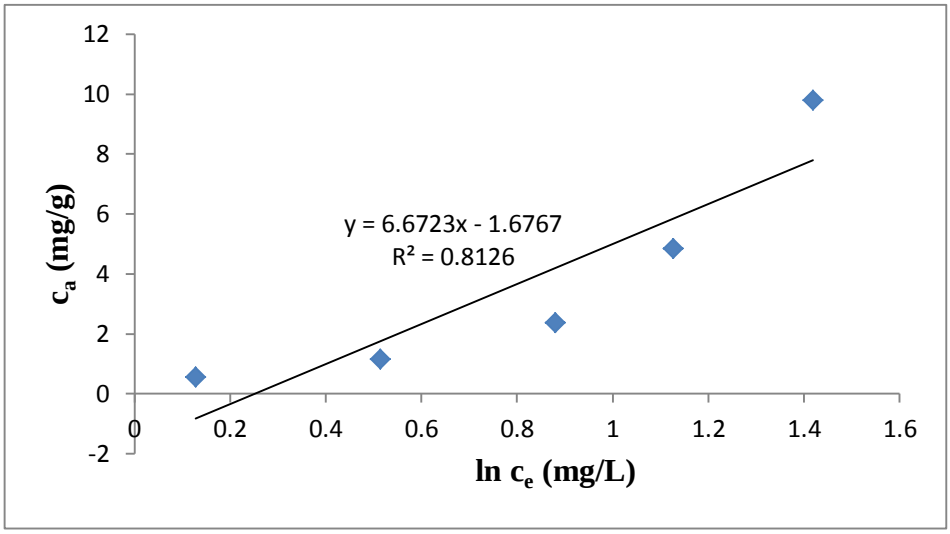

Figure 4.293: Temkin isotherm for adsorption of TPT onto $nSiO_2$

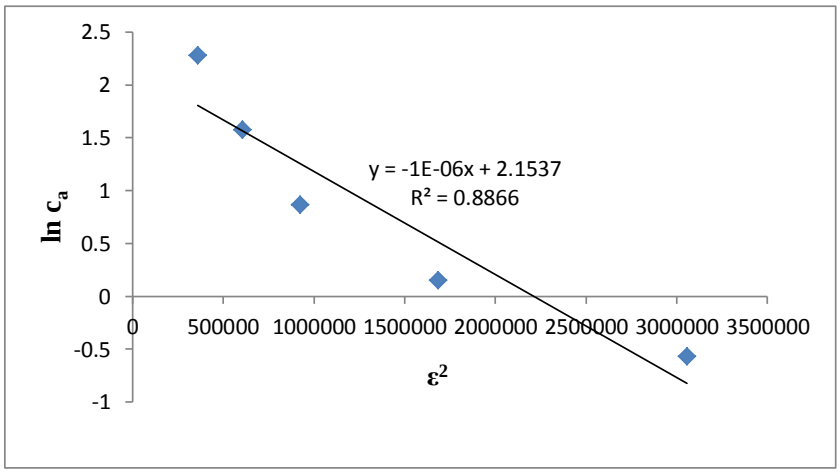

Figure 4.294: D-R isotherm for adsorption of TPT onto $nSiO_2$

The experimental data (Table 4.48) does not fit the Langmuir model, as the R^2 value is low (< 0.93) and Langmuir constants, A_{max} (mg/g) and k_L (L/mg) for TPT adsorption onto $nSiO_2$ are negative. The Temkin and D-R isotherm models also gave low R^2 value (< 0.85 for Temkin and < 0.89 for D-R) and can also not be use to describe the adsorption process. The equilibrium model constants k_F, k_L, k_T and k_{D-R} for the adsorption of TPT onto $nSiO_2$/activated carbon composite are 0.3926 mg/g $(L/mg)^{1/n}$, -0.2165 L/mg, 0.7778 mg/L and 1 x 10^{-8} J^2/mol^2, respectively.

Table 4.48: Isotherms constants for the adsorption of TPT onto $nSiO_2$

Equilibrium models	
Freundlich	
k_F [mg/g (L/mg)$^{1/n}$]	0.3926
n_F	0.4524
R^2	0.9926
Langmuir	
K_L (L/mg)	-0.2165
A_{max} (mg/g)	-1.9365
R^2	0.9263
Temkin	
n_T (L/g)	6.6723
k_T (mg/L)	0.7778
b_T (J/mol)	368.09
R^2	0.8126
Dubinin-Redushkevich	
k_{D-R} (J^2/mol^2)	1 x 10^{-6}
q_m (mg/g)	8.6167
E (J/mol)	707.106
R^2	0.8866

4.12.14.6 Effect of temperature

The experimental results obtained on the effect of temperature show that the adsorption capacity of TPT onto $nSiO_2$ adsorbent decreases with increase in the solution temperature as shown in Figure 4.295. This indicates that the adsorption of TPT onto the $nSiO_2$ is exothermic (Ayanda et al., 2013d).

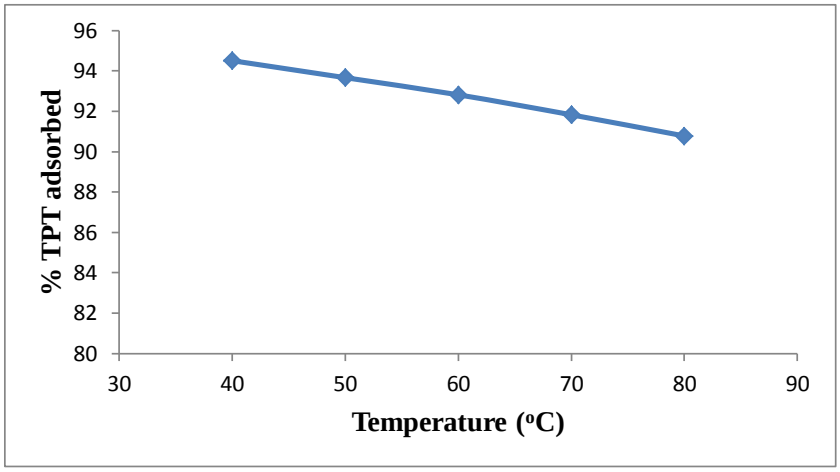

Figure 4.295: Effect of temperature on TPT adsorption onto $nSiO_2$

Experimental conditions: Concentration of TPT = 100 mg/L; Volume of TPT solution = 25 mL, Mass of $nSiO_2$ = 0.5 g; Contact time = 60 min; pH = 8; Stirring speed = 200 rpm.

Approx. 90.78 % of TPT was removed from the initial concentration of 100 mg/L TPT by $nSiO_2$ at a contact time of 60 min, pH 8, stirring speed 200 rpm and temperature of 80 °C whereas 94.51 % TPT was removed at 40 °C at the same conditions. Figure 4.296 thus shows the Van't Hoff plot for the adsorption of TPT and the variation in the extent of adsorption with respect to temperature has been explained on the basis of ΔH^{o} , ΔS^{o}, and ΔG^{o} as shown in Table 4.49.

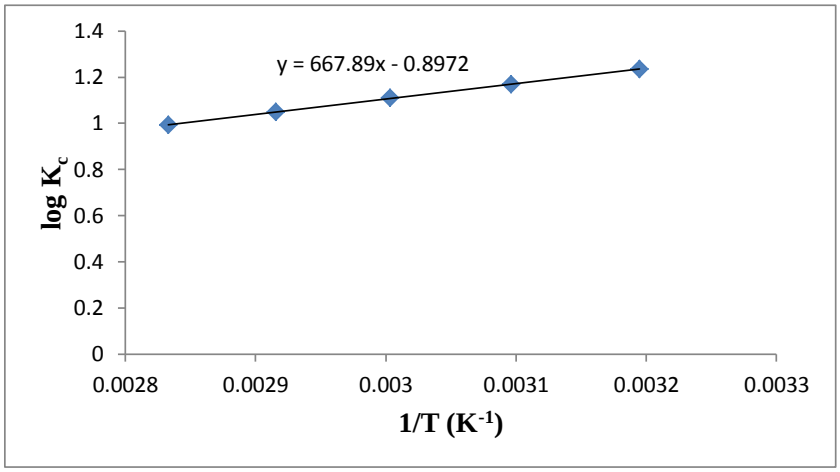

Figure 4.296: Van't Hoff Plot for the adsorption of TPT onto $nSiO_2$

Table 4.49: Thermodynamic parameters for adsorption of TPT onto $nSiO_2$

Temperature (°C)	ΔG° (kJ/mol)	ΔS° (J/K/mol)	ΔH° (kJ/mol)	K_c
40	-7.404	-17.179	-12.788	17.208
50	-7.233			14.788
60	-7.084			12.922
70	-6.898			11.235
80	-6.711			9.222

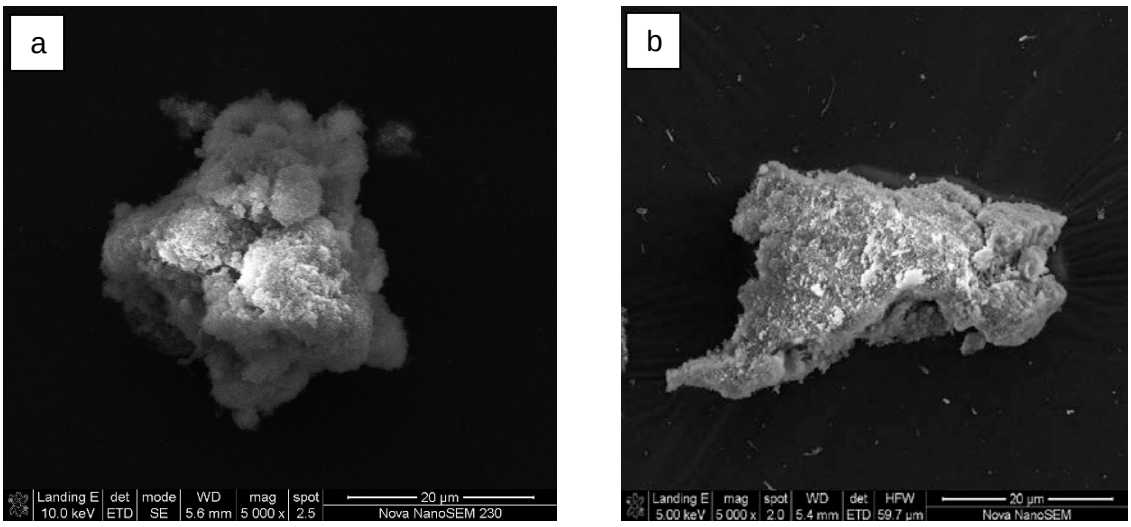

Figure 4.297: $nSiO_2$ before (a) and after (b) TPT adsorption

The negative value of ΔH^{o} (-12.788 kJ/mol) for the intervals of temperatures studied (Table 4.46) also shows that the adsorption process is exothermic. The negative value of ΔS^{o} (-17.179 J/K/mol) corresponds to a decrease in the degree of freedom of the adsorbed TPT, indicating a decrease in adsorbate concentration onto the solid phase. ΔG^{o} values were found to increase as the temperature increases, which indicate non-spontaneous adsorption and the degree of spontaneity of the reaction decreases with increase in temperature. K_c ranged 9.222 – 17.208.

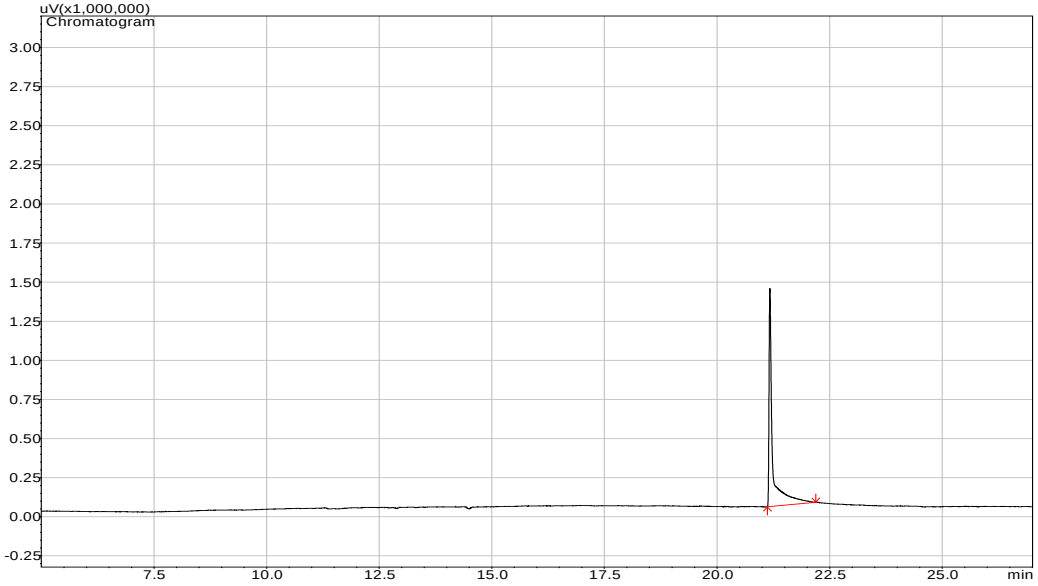

Figure 4.298: Representative TPT chromatogram after adsorption of 100 mg/L TPT with 0.5 g of $nSiO_2$, contact time of 60 min, temperature 20 ^{o}C and a stirring speed of 200 rpm

The SEM analysis of $nSiO_2$ before and after the adsorption studies is presented in Figure 4.297. A representative TPT chromatogram after adsorption of 100 mg/L TPT onto 0.5 g of $nSiO_2$ at 60 min contact time, temperature of 20 ^oC and a stirring speed of 200 rpm is as shown in Figure 4.298.

4.12.15 Adsorption of TPT from TPT-contaminated artificial seawater onto nZnO

4.12.15.1 Effect of adsorbent amount

To study the effect of nZnO amount on the adsorption of TPT from TPT – contaminated artificial seawater, the amount of the adsorbent was varied from 0.0625 – 1 g, the concentration of TPT was taken as 100 mg/L and other parameters were also kept constant. Figure 4.299 shows that the amount of TPT adsorbed and percentage removal of TPT by nZnO increases as the amount of nZnO increases from 0.0625 - 0.5 g, after which equilibration was attained.

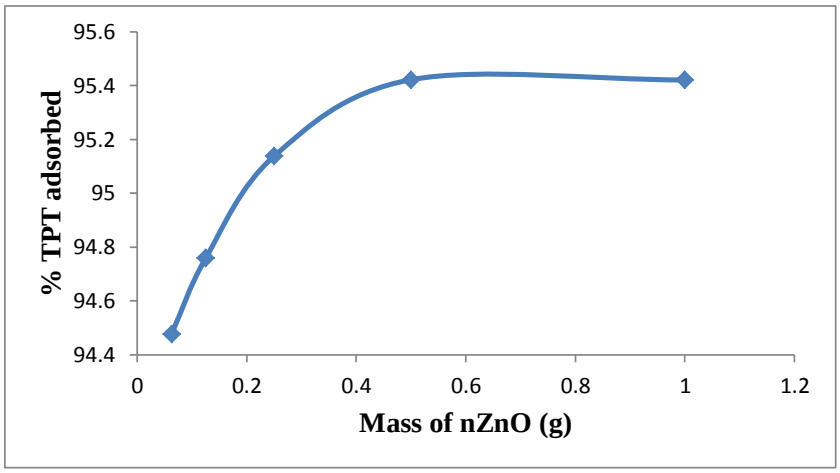

Figure 4.299: Adsorption efficiencies of TPT onto nZnO

Experimental conditions: Concentration of TPT = 100 mg/L; Volume of TPT solution = 25 mL, Contact time = 60 min; Stirring speed = 160 rpm, Temperature = 20 ^oC.

Figure 4.299 therefore shows that 0.5 g of nZnO removes 95.42 % TPT from TPT – contaminated artificial seawater.

4.12.15.2 Effect of contact time

To study the effect of contact time on the adsorption of TPT onto nZnO, the TPT concentration was 100 mg/L while, other remaining conditions such as pH, stirring speed etc. were constant. The effect of contact time was carried out at various time intervals from 10 – 70 min.

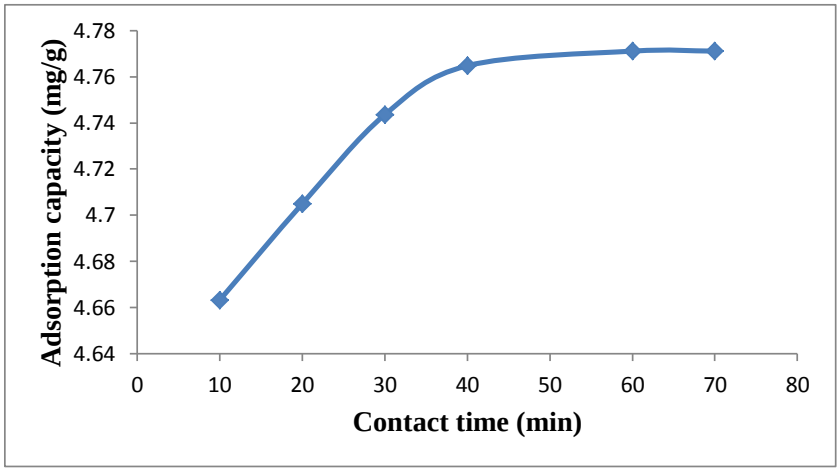

Figure 4.300: Effect of contact time on TPT adsorption onto nZnO

Experimental conditions: Concentration of TPT = 100 mg/L; Volume of TPT solution = 25 mL, Mass of nZnO = 0.5 g; Stirring speed = 160 rpm, Temperature = 20 ^{o}C.

The increase in the amount of TPT adsorbed by nZnO from 4.663 mg/g (93.27 %) to 4.771 mg/g (95.42 %) (Figure 4.300) was observed up to 60 min. After that, there is no significant change observed. 60 min was therefore fixed as the contact time for further studies.

4.12.15.2.1 Adsorption kinetics

Figures 4.301 – 4.305 thus show the pseudo first-order, pseudo second-order, Elovich, fractional power and intraparticle diffusivity kinetic plots, respectively and Table 4.50 provides the evaluated parameters of the kinetics models.

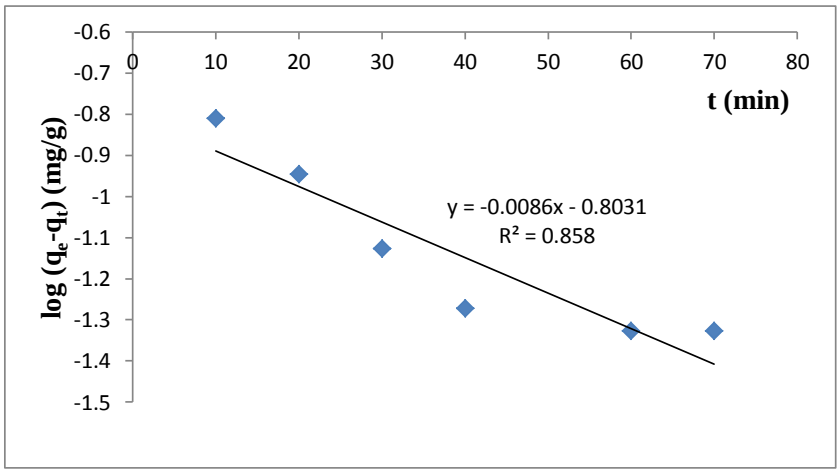

Figure 4.301: Pseudo first-order rate equation plot for TPT adsorption onto nZnO

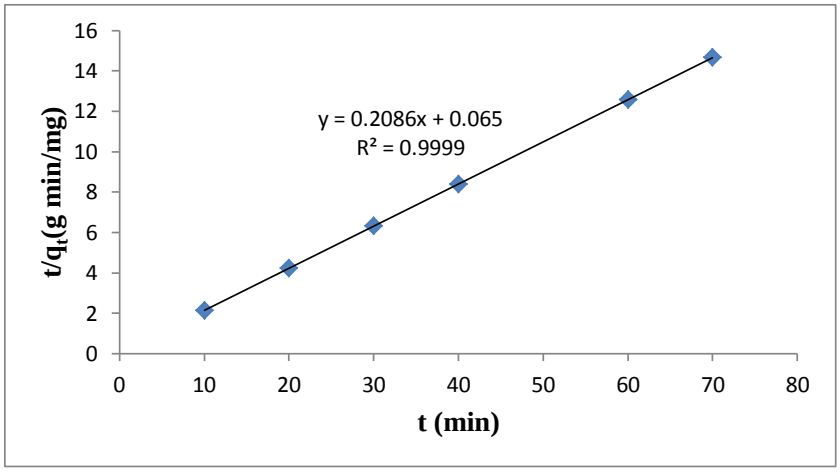

Figure 4.302: Pseudo second-order rate equation plot for TPT adsorption onto nZnO

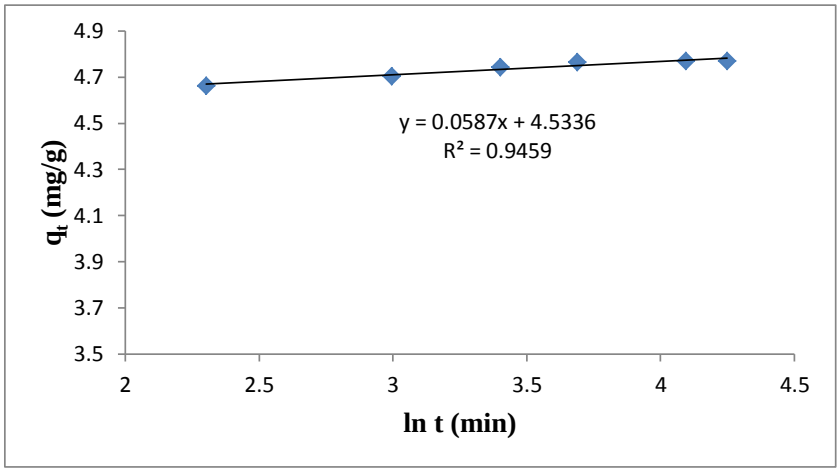

Figure 4.303: Elovich rate equation plot for TPT adsorption onto nZnO

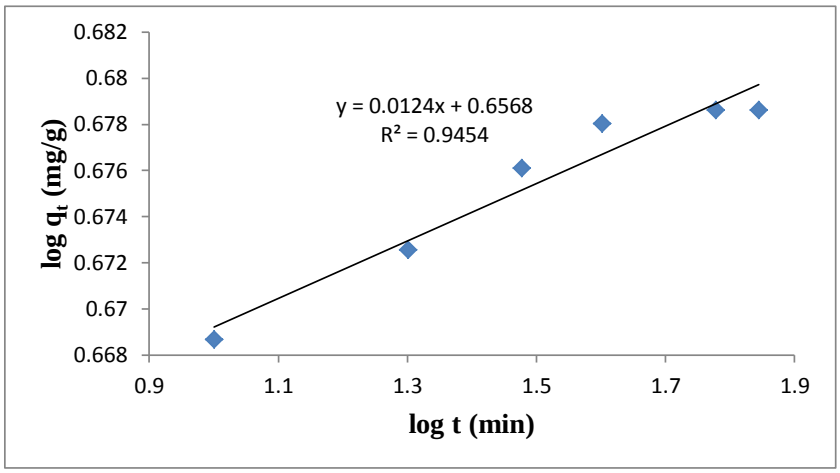

Figure 4.304: Fractional Power rate equation plot for TPT adsorption onto nZnO

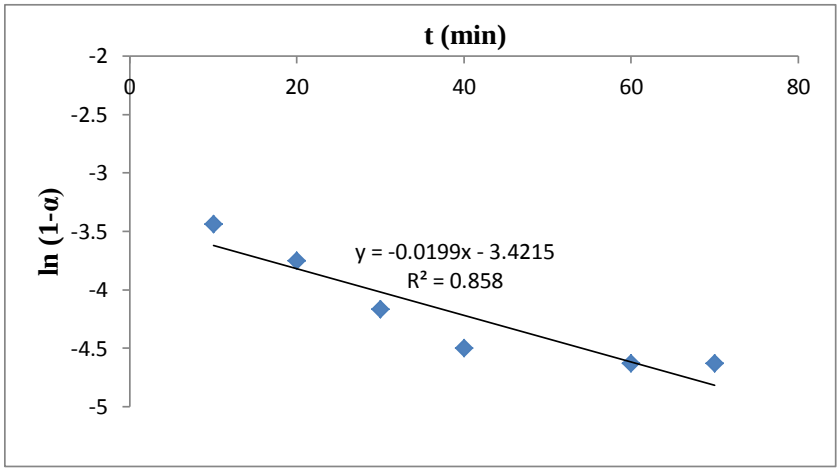

Figure 4.305: Intraparticle diffusivity plot for TPT adsorption onto nZnO

Table 4.50: Kinetic model parameters for TPT adsorption onto nZnO

Kinetic models	
Pseudo first-order	
k_1 (min^{-1})	0.0196
q_e (mg/g)	0.1574
R^2	0.8580
Pseudo second-order	
q_e (mg/g)	4.7939
h_o (mg/g/min)	15.385
k_2 (g/mg/min)	0.6694
R^2	0.9999
Elovich	
β (g min/mg)	17.0358
α (g min^2/mg)	5.935×10^{34}
R^2	0.9459
Fractional Power	
v (min^{-1})	0.0124
k_3 (mg/g)	4.5373
k_3v (mg/g/min)	0.0563
R^2	0.9454
Intraparticle diffusivity	
k_p (min^{-1})	0.0199
R^2	0.8580

The value of the correlation coefficient (R^2) of pseudo second-order kinetic model (> 0.99) is higher than the correlation coefficients of other models indicating that the kinetic model for the adsorption of TPT onto the nZnO is pseudo second-order. The intraparticle coefficient for the adsorption of TPT by the nZnO was calculated and presented in Table 4.50 and the results also indicate that the power function model satisfactorily describes the time-dependence of TPT on the nZnO since the value of the constant v is less than 1.

The value of the initial adsorption rate, h_o, obtained for the pseudo second-order kinetics is 15.385 mg/g/min. The amount of TPT adsorbed at equilibrium per unit weight of nZnO (q_e) is 4.7939 mg/g and the rate constant of pseudo second - order adsorption (k_2) is 0.6694 g/mg/min.

4.12.15.3 Effect of pH

The effect of pH on the adsorption of TPT onto nZnO was studied at pH 4 – 9. It was observed in Figure 4.306 that the percentage of TPT adsorbed by the nZnO steadily increases as the pH of the solution increases from pH 4 to pH 8, and reaches equilibration at pH ≥ 8. About 95.47 % of TPT was removed from the initial concentration of 100 mg/L TPT by nZnO at a contact time of 60 min, stirring speed of 160 rpm, temperature of 20 ^{o}C and pH 8. pH 8 was chosen as the optimum pH and was used for further studies

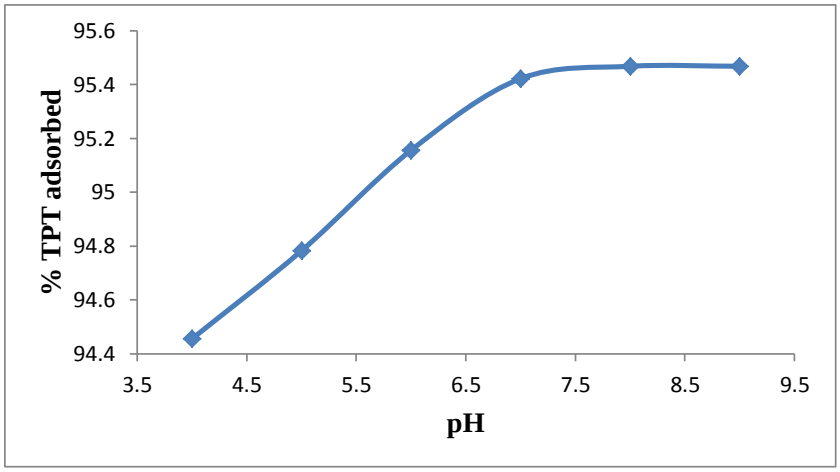

Figure 4.306: Effect of pH on TPT adsorption onto nZnO

Experimental conditions: Concentration of TPT = 100 mg/L; Volume of TPT solution = 25 mL, Mass of nZnO = 0.5 g; Contact time = 60 min; Stirring speed = 160 rpm, Temperature = 20 ^{o}C.

4.12.15.4 Effect of stirring speed

The stirring speed on the adsorption of TPT onto nZnO was studied at a stirring speed of 160 – 200 rpm. The adsorption capacity of TPT onto the nZnO increases as the stirring speed of the mixture increases. Figure 4.307 therefore show that 97.14 % of TPT was removed from the initial concentration of 100 mg/L TPT by nZnO at a contact time of 60 min, pH 8, temperature of 20 ^{o}C and a stirring speed of 200 rpm. A stirring speed of 200rpm was used for further studies.

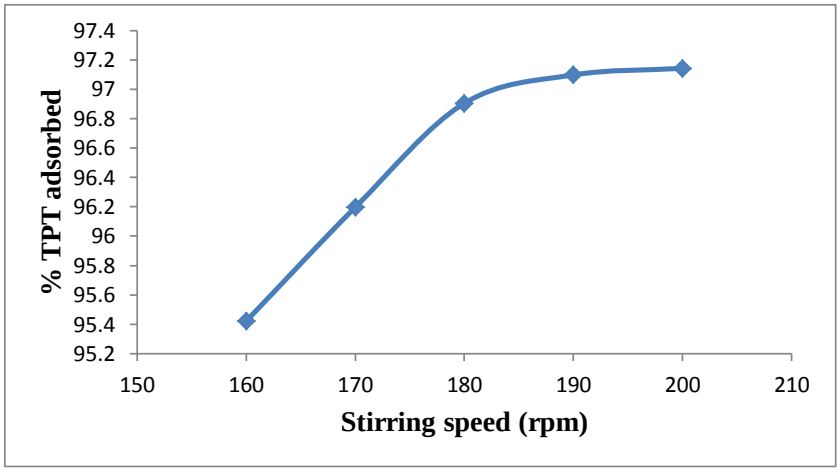

Figure 4.307: Effect of stirring speed on TPT adsorption onto nZnO

Experimental conditions: Concentration of TPT = 100 mg/L; Volume of TPT solution = 25 mL, Mass of nZnO= 0.5 g; Contact time = 60 min; Temperature = 20 ^{o}C.

4.12.15.5 Effect of initial concentration

The adsorption isotherms of the adsorption of TPT onto nZnO were investigated by varying the initial TPT concentration from 12.5 to 200 mg/L at optimized adsorbent dose, contact time, pH and stirring speed established after optimization of working parameters. The equilibrium data were fitted by Langmuir, Freundlich, Temkin and D-R isotherm models as presented in Figures 4.309 – 4.312.

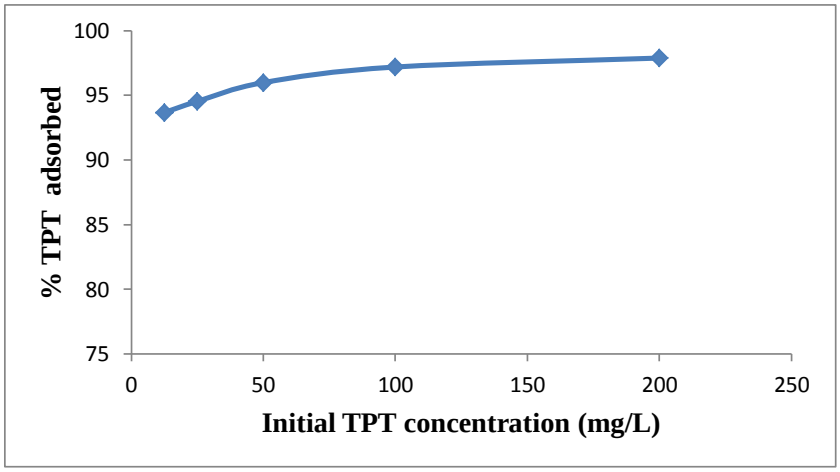

Figure 4.308: Percentage TPT adsorbed by nZnO at various initial TPT concentrations

Experimental conditions: Volume of TPT solution = 25 mL, Mass of nZnO = 0.5 g; pH = 8; Stirring speed = 200 rpm; Contact time = 60 min; Temperature = 20 ^{o}C.

Figure 4.308 therefore shows that the adsorption of TPT onto nZnO steadily increases as the initial TPT concentration increases from 12.5 to 100 mg/L, indicating that adsorption is also favourable for the higher TPT concentrations that have been investigated.

4.12.15.5.1 Adsorption isotherms

The adsorption isotherm plots are presented in Figures 4.309 – 4.312 and parameters obtained for the models were given in Table 4.51. Table 4.51 and the figures show that the experimental data fitted well with Freundlich isotherm model because the regression coefficient (R^2) (> 0.99) is higher than for other models. The value of n_F, for the nZnO, falling in the range 1 -10 also indicates favourable adsorption.

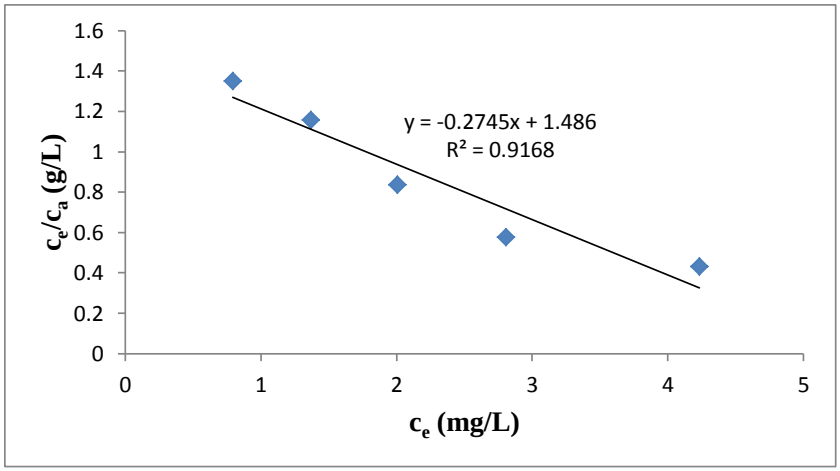

Figure 4.309: Langmuir isotherm for adsorption of TPT onto nZnO

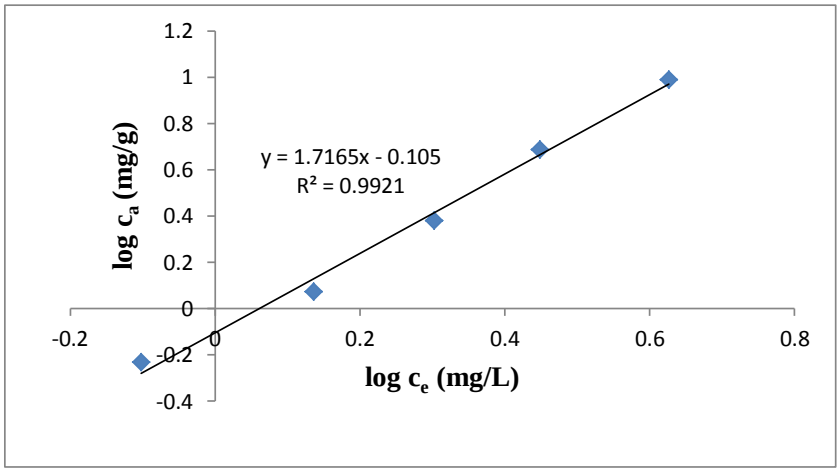

Figure 4.310: Freundlich isotherm for adsorption of TPT onto nZnO

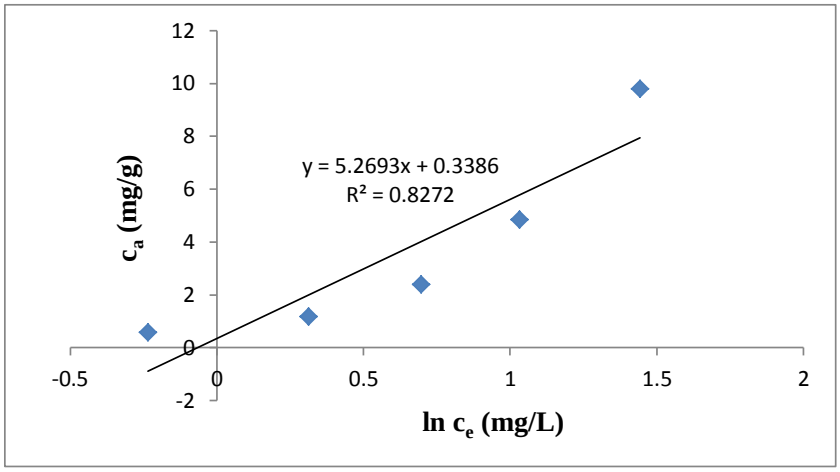

Figure 4.311: Temkin isotherm for adsorption of TPT onto nZnO

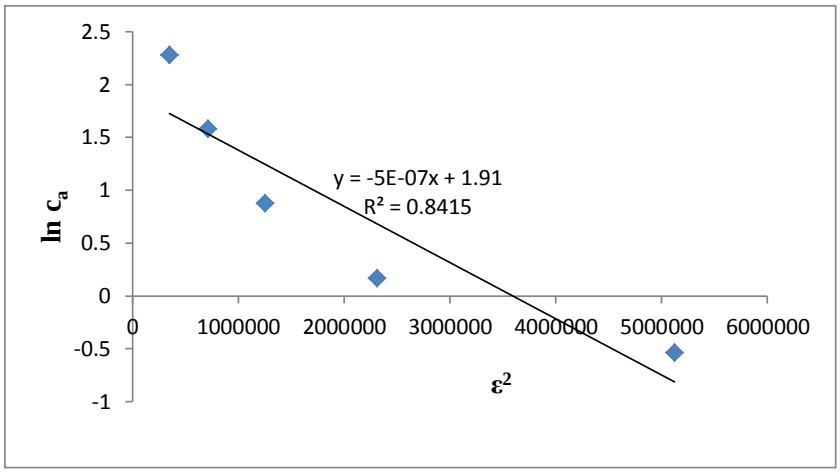

Figure 4.312: D-R isotherm for adsorption of TPT onto nZnO

The negative value of the Langmuir constants, A_{max} (mg/g) and k_L (L/mg) for TPT adsorption (Table 4.51) onto nZnO indicates the inadequacy fitting of experimental data to Langmuir model. The equilibrium model constants k_F, k_L, k_T and k_{D-R} for the adsorption of TPT onto nZnO are 0.7852 mg/g $(L/mg)^{1/n}$, -3.6429 L/mg, 1.0664 mg/L and 5 x 10^{-7} J^2/mol^2, respectively.

Table 4.51: Isotherms constants for the adsorption of TPT onto nZnO

Equilibrium models	
Freundlich	
k_F [mg/g (L/mg)$^{1/n}$]	0.7852
n_F	0.5826
R^2	0.9921
Langmuir	
K_L (L/mg)	-0.1847
A_{max} (mg/g)	-3.6429
R^2	0.9168
Temkin	
n_T (L/g)	5.2693
k_T (mg/L)	1.0664
b_T (J/mol)	462.30
R^2	0.8272
Dubinin-Redushkevich	
k_{D-R} (J^2/mol^2)	5×10^{-7}
q_m (mg/g)	6.7531
E (J/mol)	1000
R^2	0.8415

4.12.15.6 Effect of temperature

The experimental results obtained on the effect of temperature show that the adsorption capacity of TPT onto nZnO decreases with increase in the solution temperature (Figure 4.313). This indicates that the adsorption of TPT onto the nZnO is also exothermic.

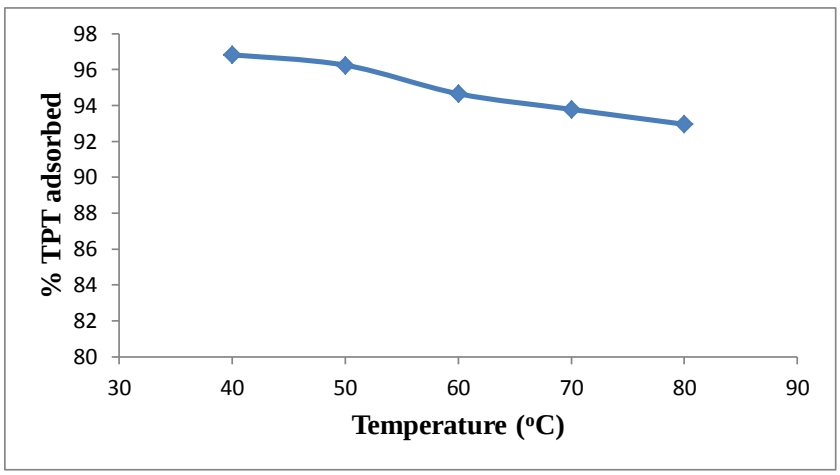

Figure 4.313: Effect of temperature on TPT adsorption onto nZnO

Experimental conditions: Concentration of TPT = 100 mg/L; Volume of TPT solution = 25 mL, Mass of nZnO = 0.5 g; Contact time = 60 min; pH = 8; Stirring speed = 200 rpm.

From Figure 4.313, approx. 92.95 % of TPT was removed from the initial concentration of 100 mg/L TPT by nZnO at a contact time of 60 min, pH 8, stirring speed 200 rpm and temperature of 80 ^{o}C whereas 96.82 % TPT was removed at 40 ^{o}C at the same conditions.

Figure 4.314 thus shows the Van't Hoff plot for the adsorption of TPT and the variation in the extent of adsorption with respect to temperature has been explained on the basis of ΔH^{o}, ΔS^{o}, and ΔG^{o} as shown in Table 4.52.

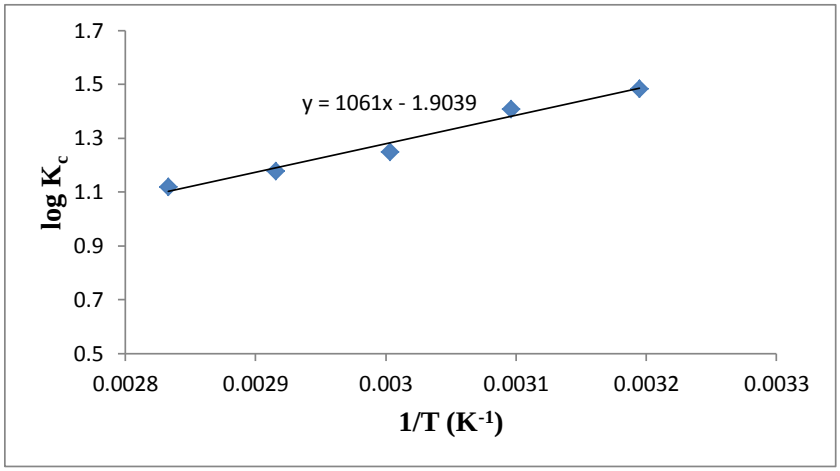

Figure 4.314: Van't Hoff Plot for the adsorption of TPT onto nZnO

Table 4.52: Thermodynamic parameters for adsorption of TPT onto nZnO

Temperature (°C)	ΔG° (kJ/mol)	ΔS° (J/K/mol)	ΔH° (kJ/mol)	K_c
40	-8.891	-36.454	-20.315	30.466
50	-8.712			25.645
60	-7.958			17.716
70	-7.740			15.093
80	-7.570			13.190

The negative value of ΔH^{o} (-20.315 kJ/mol) for the intervals of temperatures studied (Table 4.52) also shows the exothermic nature of the adsorption process. The negative value of ΔS^{o} (-36.454 J/K/mol) corresponds to a decrease in the degree of freedom of the adsorbed TPT, indicating a decrease in adsorbate concentration onto the solid phase (Ayanda et al., 2013c). ΔG^{o} values were found to increase as the temperature increases, which indicate non-spontaneous adsorption and the degree of spontaneity of the reaction decreases with increase in temperature. K_c ranged 13.190 – 30.466.

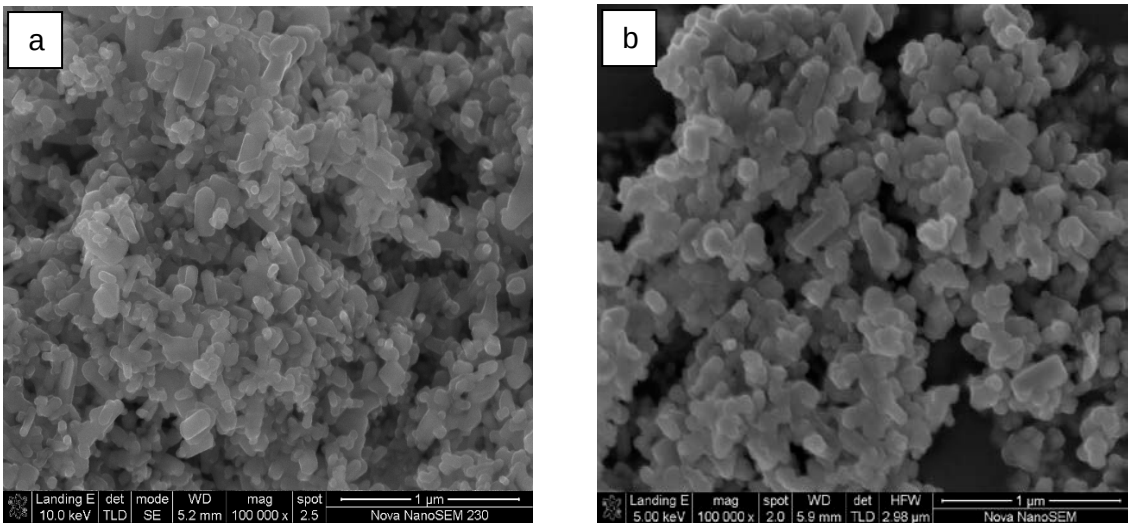

Figure 4.315: nZnO before (a) and after (b) TPT adsorption

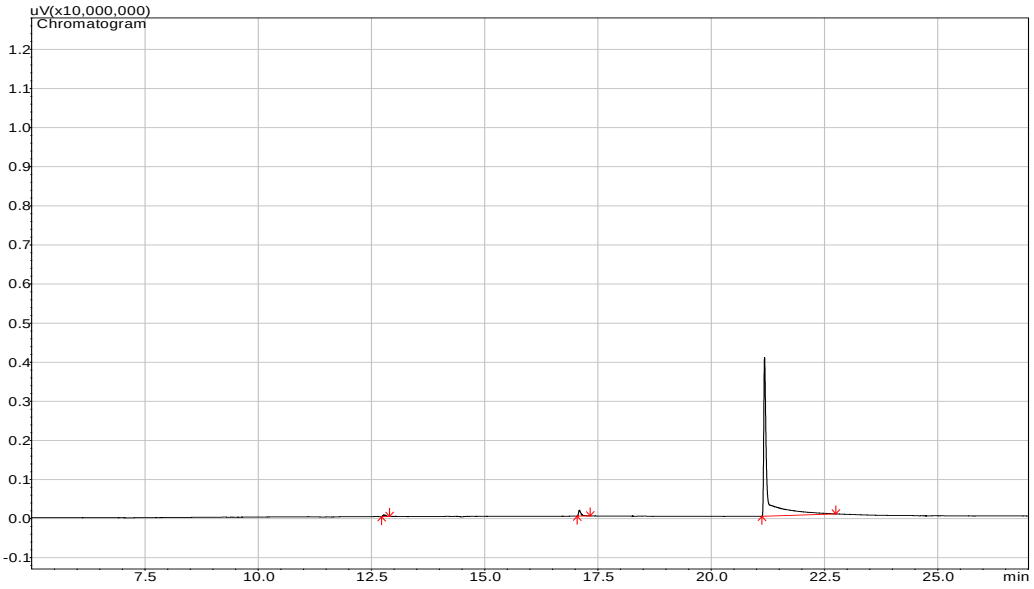

Figure 4.316: Representative TPT chromatogram after adsorption of 100 mg/L TPT with 0.5 g of nZnO, contact time of 60 min, temperature 20 ^{o}C and a stirring speed of 200 rpm

The nZnO before and after the adsorption processes were subjected to SEM analysis as shown in Figure 4.315 while a representative TPT chromatogram after adsorption of 100 mg/L TPT with 0.5 g of nZnO, contact time of 60 min, temperature 20 ^{o}C and a stirring speed of 200 rpm is as shown in Figure 4.316.

4.12.16 Adsorption of TPT from TPT-contaminated artificial seawater onto fly ash/activated carbon composite

4.12.16.1 Effect of adsorbent amount

The effect of fly ash/activated carbon composite amount on the adsorption of TPT by the composite is shown in Figure 4.317. It was observed that the percentage adsorption of TPT increases with increasing amount of fly ash/activated carbon composite, reaching optimum at 0.5 g, corresponding to 99.98 % removal. 0.5 g was therefore selected as the optimum fly ash/activated carbon composite amount used for further studies.

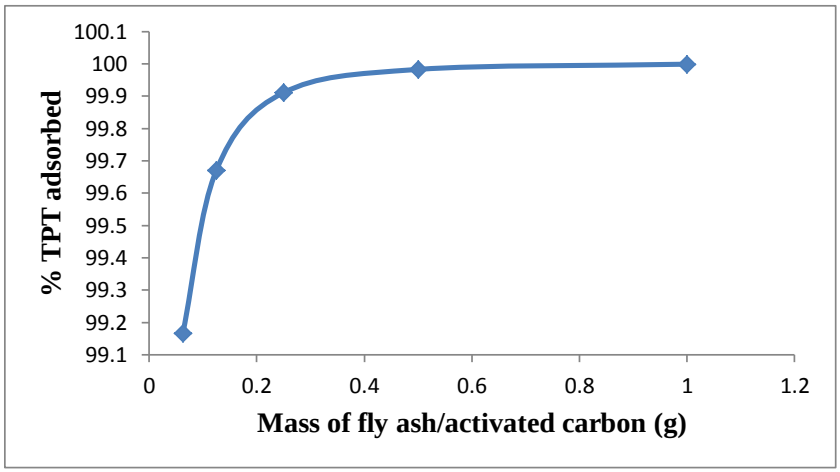

Figure 4.317: Adsorption efficiencies of TPT onto fly ash/activated carbon

Experimental conditions: Concentration of TPT = 100 mg/L; Volume of TPT solution = 25 mL, Contact time = 60 min; Stirring speed = 160 rpm, Temperature = 20 ^{o}C.

4.12.16.2 Effect of contact time

Figure 4.318 shows the effect of contact time on adsorption of TPT onto the fly ash/activated carbon composite. The TPT removal efficiency at different time intervals ranging from 10 – 70 min were obtained. The figure also shows that the adsorption of TPT onto fly ash/activated carbon composite increases with time and attains equilibrium after 60 minutes. The TPT removal efficiency for the fly ash/activated carbon composite reaches 4.9992 mg/g (99.98 %). A contact time of 60 min was fixed for further studies.

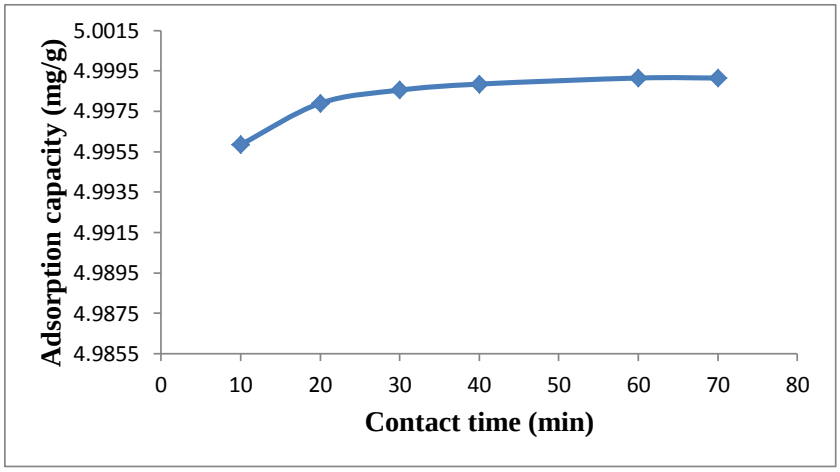

Figure 4.318: Effect of contact time on TPT adsorption onto fly ash/activated carbon

Experimental conditions: Concentration of TPT = 100 mg/L; Volume of TPT solution = 25 mL, Mass of fly ash/activated carbon = 0.5 g; Stirring speed = 160 rpm, Temperature = 20 ^{o}C.

4.12.16.2.1 Adsorption kinetics

Figures 4.319 – 4.323 show the pseudo first-order, pseudo second-order, Elovich, fractional power and intraparticle diffusivity kinetic plots, respectively while Table 4.53 shows the evaluated parameters of the kinetic models. It is evident from the figures and table that the R^2 value obtained for pseudo second-order kinetic model is higher (R^2 > 0.99) when compared with other models, showing the applicability of the pseudo second-order kinetic model to describe the adsorption kinetic data of TPT onto fly ash/activated carbon composite material.

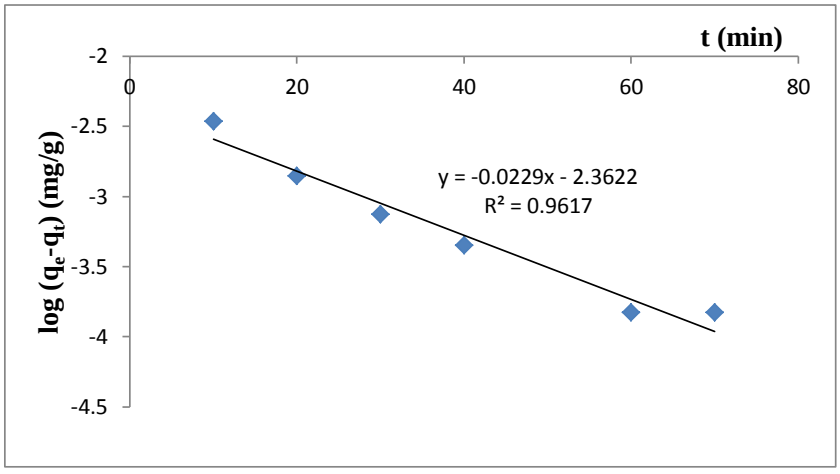

Figure 4.319: Pseudo first-order rate equation plot for TPT adsorption onto fly ash/activated carbon

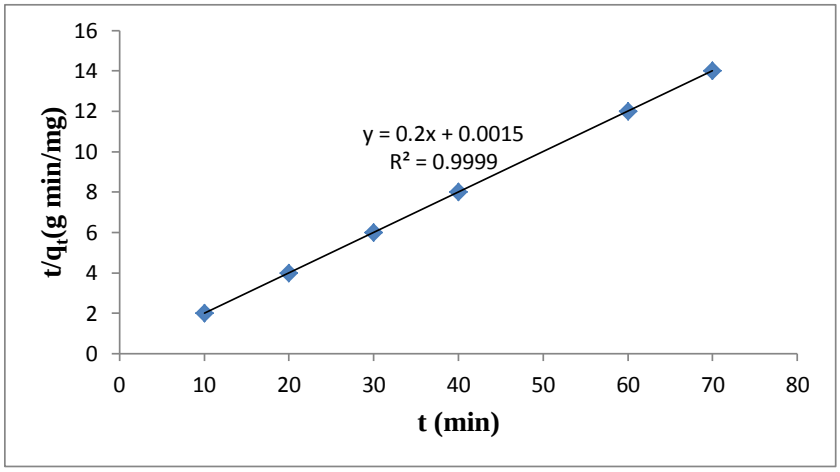

Figure 4.320: Pseudo second-order rate equation plot for TPT adsorption onto fly ash/activated carbon

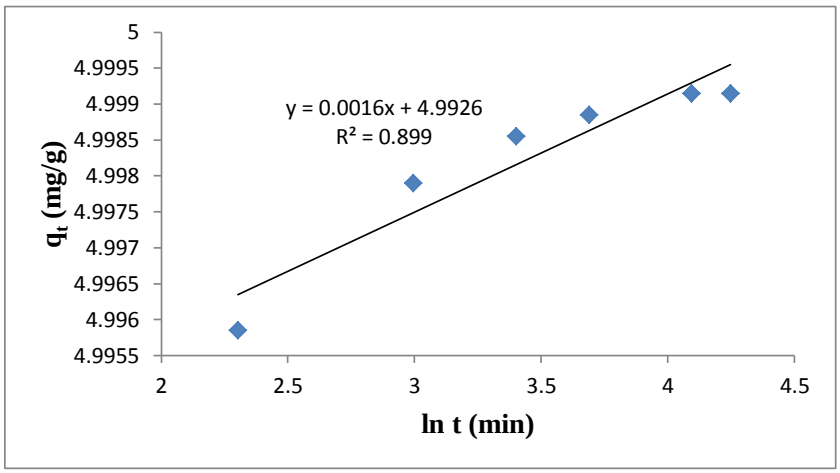

Figure 4.321: Elovich rate equation plot for TPT adsorption onto fly ash/activated carbon

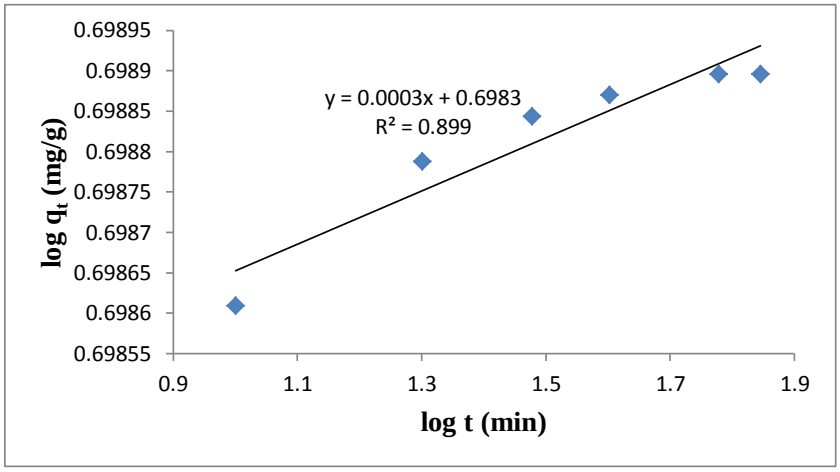

Figure 4.322: Fractional Power rate equation plot for TPT adsorption onto fly ash/activated carbon

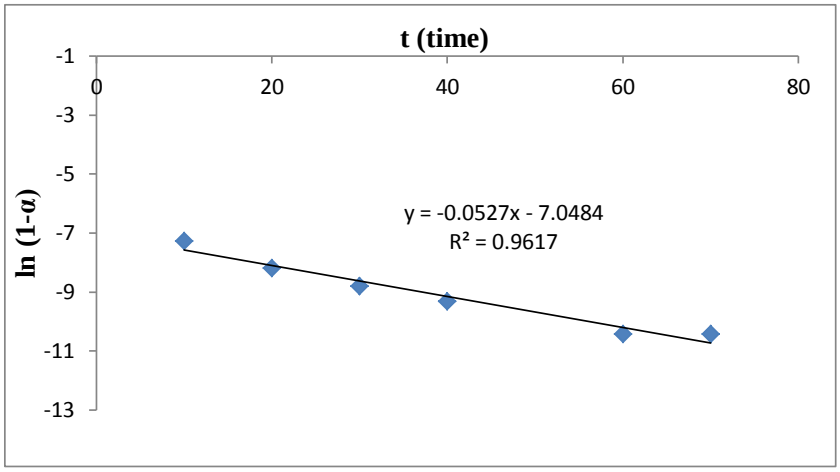

Figure 4.323: Intraparticle diffusivity plot for TPT adsorption onto fly ash/activated carbon

The intraparticle coefficient for the adsorption of TPT by fly ash/activated carbon composite was also computed (Table 4.53). The initial adsorption rate (h_o) calculated from the pseudo second-order rate equation for TPT adsorption onto fly ash/activated carbon composite is 666.67 mg/g/min. The results also indicate that the power function model satisfactorily describes the time-dependence of TPT onto fly ash/activated carbon composite since the value of the constant v is less than 1.

Table 4.53: Kinetic model parameters for TPT adsorption onto fly ash/activated carbon

Kinetic models	
Pseudo first-order	
k_1 (min^{-1})	0.0527
q_e (mg/g)	4.34×10^{-3}
R^2	0.9617
Pseudo second-order	
q_e (mg/g)	5.0
h_o (mg/g/min)	666.67
k_2 (g/mg/min)	26.67
R^2	0.9999
Elovich	
β (g min/mg)	625.0
α (g min^2/mg)	9.068×10^{1357}
R^2	0.8990
Fractional Power	
v (min^{-1})	0.0003
k_3 (mg/g)	4.9923
k_3v (mg/g/min)	1.4977×10^{-3}
R^2	0.8990
Intraparticle diffusivity	
k_p (min^{-1})	0.0527
R^2	0.9617

From Table 4.53, k_1, k_2, β, α_E, k_3 and k_p are 0.0527 min^{-1}, 26.67 g/mg/min, 625.0 gmin/mg, 9.068 x 10^{1357} $gmin^2/mg$, 4.9923 mg/g and 0.0527 min^{-1}, respectively.

4.12.16.3 Effect of pH

The effect of pH on the adsorption of TPT onto fly ash/activated carbon composite was studied at pH 4 – 9. It was observed from Figure 4.324 that the percentage of TPT adsorbed by the fly ash/activated carbon composite steadily increases as the pH of the solution increases from pH 4 to pH 8 and tends to fall afterwards. It is therefore evident from Figure 4.324 that maximum adsorption was also achieved within the pH range of normal saline water (pH 8).

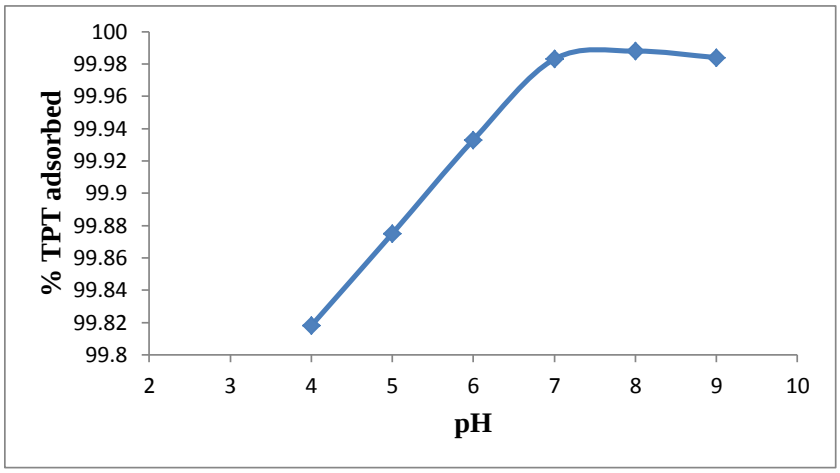

Figure 4.324: Effect of pH on TPT adsorption onto fly ash/activated carbon

Experimental conditions: Concentration of TPT = 100 mg/L; Volume of TPT solution = 25 mL, Mass of fly ash/activated carbon = 0.5 g; Contact time = 60 min; Stirring speed = 160 rpm, Temperature = 20 ^oC.

About 99.99 % of TPT was removed from the initial concentration of 100 mg/L TPT by the fly ash/activated carbon composite at a contact time of 60 min, stirring speed of 160 rpm, temperature of 20 ^oC and pH 8. pH 8 was therefore chosen as the optimum pH and was used for further studies.

4.12.16.4 Effect of stirring speed

The effect of stirring speed on the adsorption of TPT onto fly ash/activated carbon composite was studied at a stirring speed of 160 – 200 rpm. The adsorption capacity of TPT onto fly ash/activated carbon composite material increases with increase in the stirring speed of the mixture (Figure 4.325).

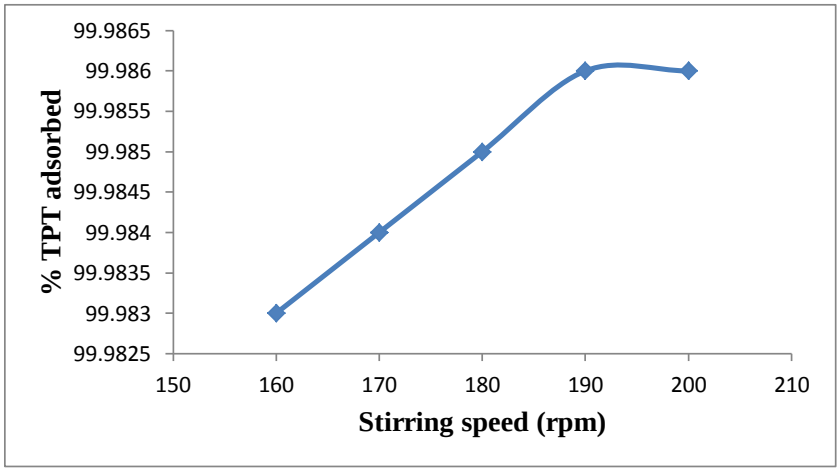

Figure 4.325: Effect of stirring speed on TPT adsorption onto fly ash/activated carbon

Experimental conditions: Concentration of TPT = 100 mg/L; Volume of TPT solution = 25 mL, Mass of fly ash/activated carbon = 0.5 g; Contact time = 60 min; Temperature = 20 ^{o}C.

4.999 mg/g of TPT (99.99 %) was therefore removed from the initial concentration of 5 mg/g TPT by the fly ash/activated carbon composite at a contact time of 60 min, pH 8, temperature of 20 ^{o}C and a stirring speed of 200 rpm. A stirring speed of 200 rpm was used for further studies

4.12.16.5 Effect of initial concentration

The effect of initial TPT concentration in the range of 12.5 to 100 mg/L on the adsorption of TPT onto fly ash/activated carbon composite was investigated. Along with pH, all parameters were kept constant in this study.

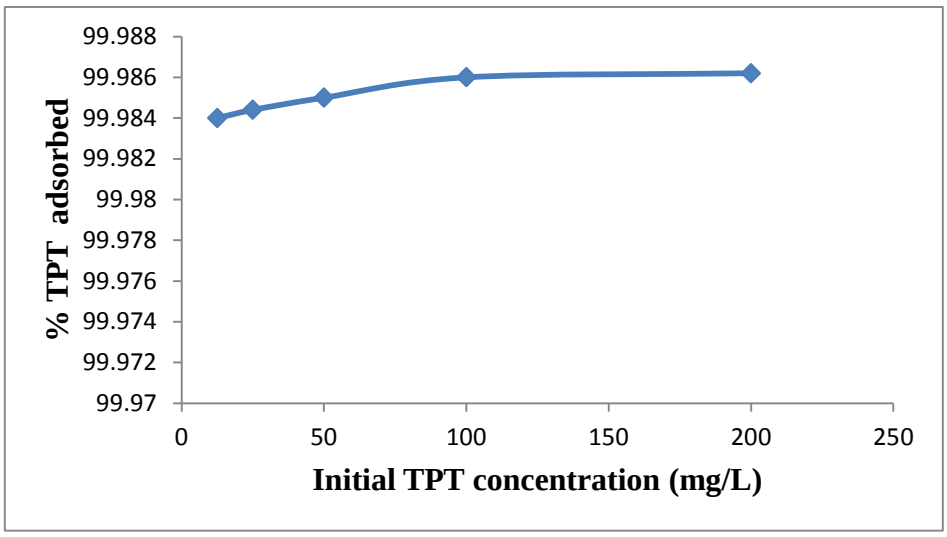

Figure 4.326: Percentage TPT adsorbed by fly ash/activated carbon at various initial TPT concentrations

Experimental conditions: Volume of TPT solution = 25 mL, Mass of fly ash/activated carbon = 0.5 g; pH = 8; Stirring speed = 200 rpm; Contact time = 60 min; Temperature = 20 ^{o}C.

It is evident from Figure 4.326 that, as the concentration of TPT increases, the amount of TPT adsorbed by fly ash/activated carbon composite increases and an increase in percentage removal was also observed. The percentage TPT adsorbed increases from 99.98 – 99.99 % as the initial TPT concentration increases.

4.12.16.5.1 Adsorption isotherms

The graphs of the adsorption isotherms are presented in Figures 4.327 – 4.330 and parameters obtained for the models were given in Table 4.54. Based on values of correlation coefficient, R^2, summarized in Table 4.54, the adsorption of TPT onto fly ash/activated carbon composite can be described by the Freundlich and D-R adsorption isotherms.

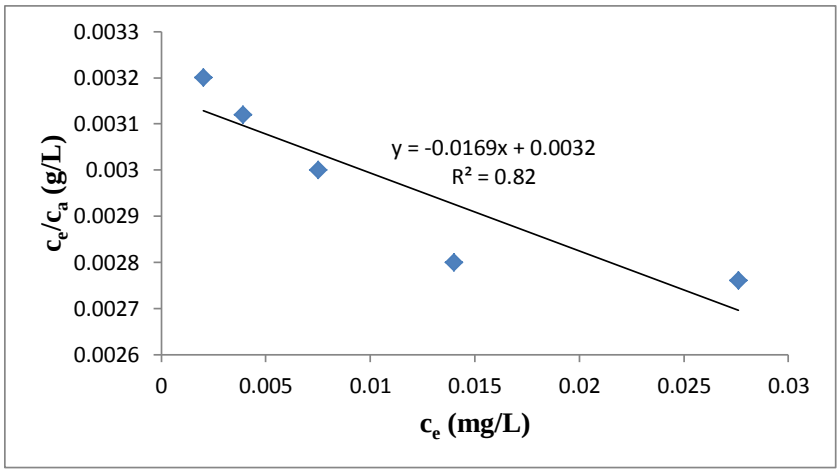

Figure 4.327: Langmuir isotherm for adsorption of TPT onto fly ash/activated carbon

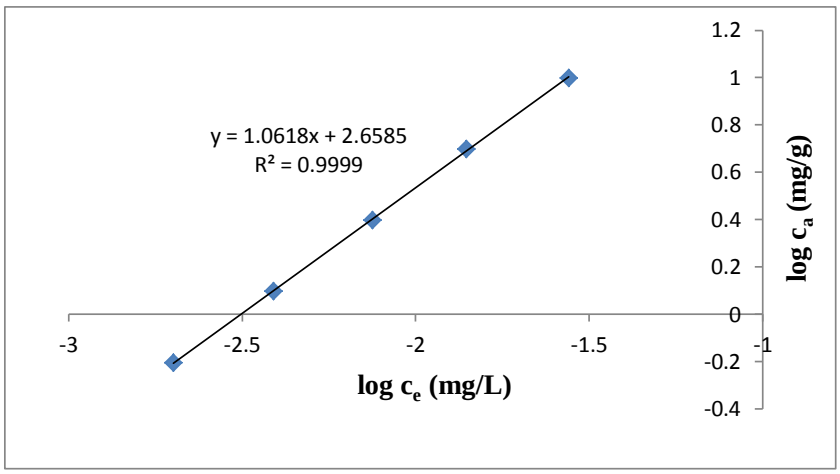

Figure 4.328: Freundlich isotherm for adsorption of TPT onto fly ash/activated carbon

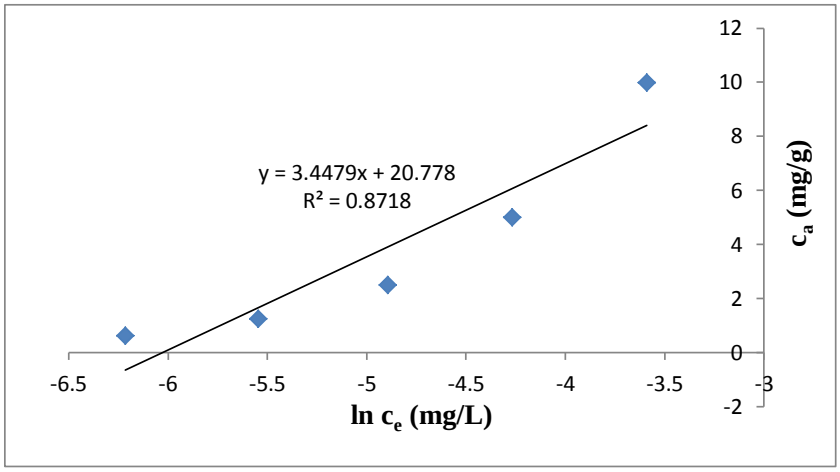

Figure 4.329: Temkin isotherm for adsorption of TPT onto fly ash/activated carbon

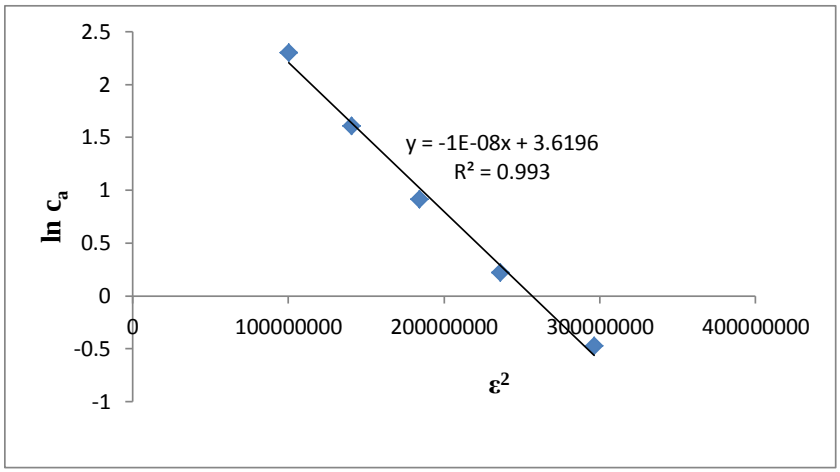

Figure 4.330: D-R isotherm for adsorption of TPT onto fly ash/activated carbon

Values of k_F, k_L, k_T and k_{D-R} constants obtained are 455.51 mg/g $(L/mg)^{1/n}$, -5.2813 L/mg, 414.17 mg/L and 1.0 x 10^{-8} J^2/mol^2, respectively (Table 4.54). Moreover, the negative value of the Langmuir constants, A_{max} (mg/g) and k_L (L/mg) for TPT adsorption onto fly ash/activated carbon composite indicates the inadequacy of the Langmuir model to fit the process. Thus, Freundlich and D-R models are the best model to explain the adsorption behaviour of TPT onto the fly ash/activated carbon composite.

Table 4.54: Isotherms constants for the adsorption of TPT onto fly ash/activated carbon

Equilibrium models	
Freundlich	
k_F [mg/g (L/mg)$^{1/n}$]	455.51
n_F	0.9418
R^2	0.9999
Langmuir	
K_L (L/mg)	-5.2813
A_{max} (mg/g)	-59.172
R^2	0.8200
Temkin	
n_T (L/g)	3.4479
k_T (mg/L)	414.17
b_T (J/mol)	706.52
R^2	0.8718
Dubinin-Redushkevich	
k_{D-R} (J^2/mol^2)	1.0×10^{-8}
q_m (mg/g)	37.323
E (J/mol)	7071.07
R^2	0.9930

4.12.16.6 Effect of temperature

The experimental results obtained on the effect of temperature (Figure 4.331) show that the TPT adsorption capacity of fly ash/activated carbon composite increases with increase in the solution temperature. This indicates that the adsorption of TPT onto fly ash/activated carbon composite is endothermic. Approx. 99.99 % of TPT was removed from the initial concentration of 100 mg/L TPT by the fly ash/activated carbon composite at a contact time of 60 min, pH 8, stirring speed 200 rpm and temperature of 80 ^oC.

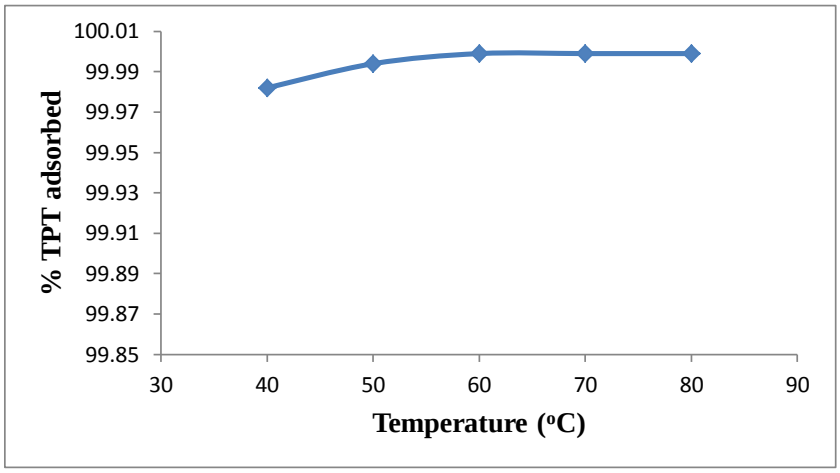

Figure 4.331: Effect of temperature on TPT adsorption onto fly ash/activated carbon

Experimental conditions: Concentration of TPT = 100 mg/L; Volume of TPT solution = 25 mL, Mass of fly ash/activated carbon = 0.5 g; Contact time = 60 min; pH = 8; Stirring speed = 200 rpm.

Figure 4.332 thus shows the Van't Hoff plot for the adsorption of TPT onto fly ash/activated carbon composite and the variation in the extent of adsorption with respect to temperature are explain on the basis of ΔH^{o}, ΔS^{o}, and ΔG^{o} as presented in Table 4.55.

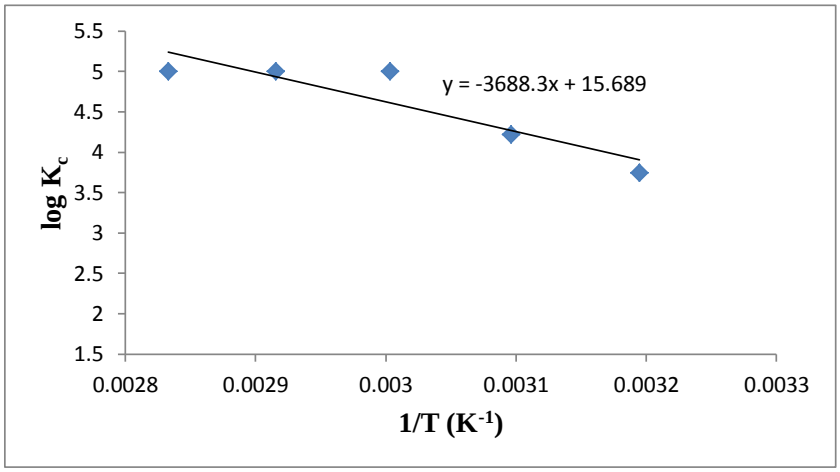

Figure 4.332: Van't Hoff Plot for the adsorption of TPT onto fly ash/activated carbon

Table 4.55: Thermodynamic parameters for adsorption of TPT onto fly ash/activated carbon

Temperature (°C)	ΔG° (kJ/mol)	ΔS° (J/K/mol)	ΔH° (kJ/mol)	K_c
40	-22.437	300.399	70.620	5554.6
50	-26.105			16665.7
60	-31.874			99999.0
70	-32.831			99999.0
80	-33.789			99999.0

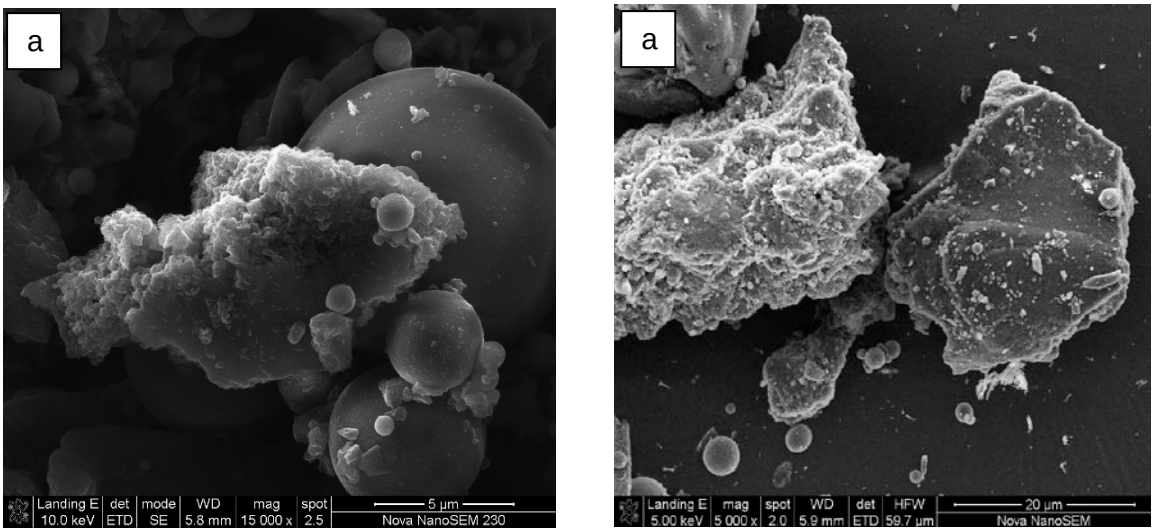

Figure 4.333: Fly ash/activated carbon before (a) and after (b) TPT adsorption

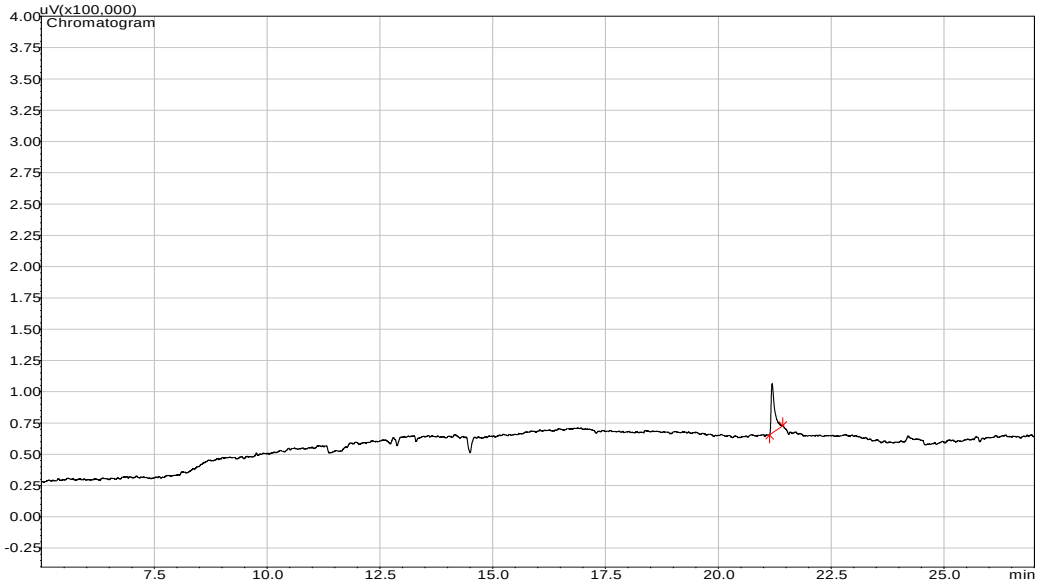

Figure 4.334: Representative TPT chromatogram after adsorption of 100 mg/L TPT with 0.5 g of fly ash/activated carbon, contact time of 60 min, temperature 20 ^{o}C and a stirring speed of 200 rpm

The positive value of ΔH^{o} (70.62 kJ/mol) for the intervals of temperatures (Table 4.55) also shows that the adsorption is endothermic. The positive value of ΔS^{o} (300.399 J/K/mol) corresponds to increase in the degree of freedom of the adsorbed TPT and suggest the increase in concentration of adsorbate in solid–solution interface indicating an increase in adsorbate concentration onto the solid phase. ΔG^{o} values were found to be more negative as the temperature increases, which indicate spontaneous adsorption and the degree of spontaneity of the reaction increases with increasing temperature. The SEM analysis of fly ash/activated carbon composite before and after adsorption is presented in Figure 4.333 while a representative TBT chromatogram after adsorption of 100 mg/L TBT with 0.5 g of fly ash/activated carbon composite, contact time of 60min, temperature 20 ^{o}C and a stirring speed of 200 rpm is as shown in Figure 4.334.

4.12.17 Adsorption of TPT from TPT-contaminated artificial seawater onto nFe_3O_4/fly ash composite

4.12.17.1 Effect of adsorbent amount

The amount of nFe_3O_4/fly ash composite material ranging from 0.0625 – 1.0 g per 25 mL of TPT solution was investigated on the efficiency of the adsorption process. A graph of the percentage of TPT adsorbed (C_a), mg/g onto nFe_3O_4/fly ash composite was plotted against the adsorbent amount (Figure 4.335).

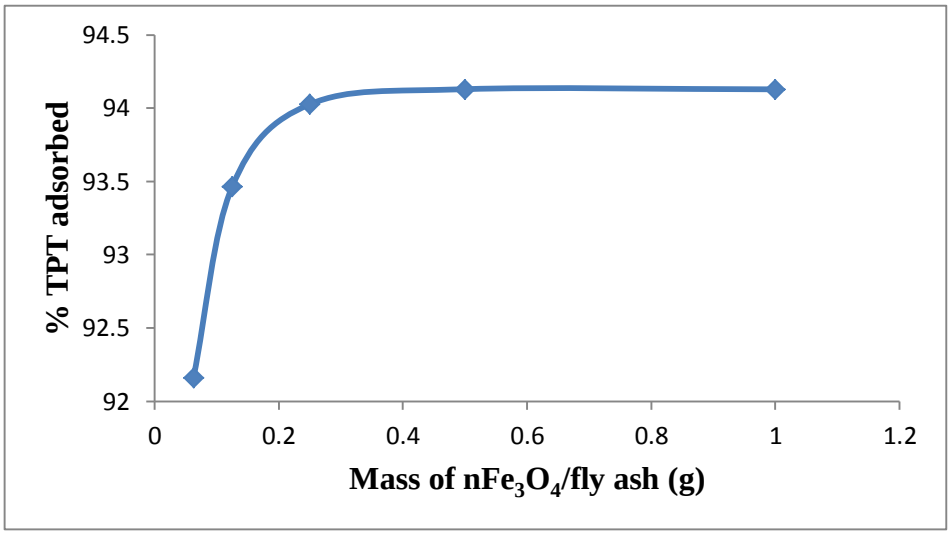

Figure 4.335: Adsorption efficiencies of TPT onto nFe_3O_4/fly ash

Experimental conditions: Concentration of TPT = 100 mg/L; Volume of TPT solution = 25 mL, Contact time = 60 min; Stirring speed = 160 rpm, Temperature = 20 ^{o}C.

It was observed that the percentage of TPT adsorbed increases with increasing nFe_3O_4/fly ash composite amount, reaching an optimum at 0.5 g, corresponding to 94.13 %. 0.5 g was therefore selected as the optimum nFe_3O_4/fly ash composite amount used for further studies.

4.12.17.2 Effect of contact time

The kinetic study of TPT onto nFe_3O_4/fly ash composite was carried out by shaking 0.5 g of nFe_3O_4/fly ash composite in 25 mL of TPT solutions with an initial concentration of 100 mg/L at 20 ^{o}C. After pre-defined contact time (10-70 min), the aqueous samples were filtered, and the concentration of TPT in the filtrate was determined.

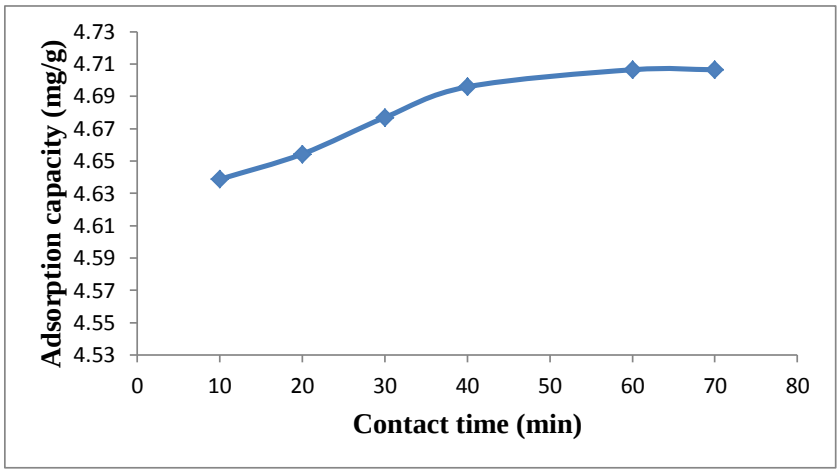

Figure 4.336: Effect of contact time on TPT adsorption onto nFe_3O_4/fly ash

Experimental conditions: Concentration of TPT = 100 mg/L; Volume of TPT solution = 25 mL, Mass of nFe_3O_4/fly ash = 0.5 g; Stirring speed = 160 rpm, Temperature = 20 ^{o}C.

Figure 4.336 thus shows the effect of contact time on adsorption of TPT by the nFe_3O_4/fly ash composite material. The TPT removal efficiencies at different time intervals ranging from 10 – 70 min were obtained. It was observed that equilibrium was achieved within 60 min and the corresponding TPT removal efficiency for nFe_3O_4/fly ash composite from the initial concentration of 100 mg/L TPT reaches 4.707 mg/g (94.13 %).

4.12.17.2.1 Adsorption kinetics

Figures 4.337 – 4.341 show the pseudo first-order, pseudo second-order, Elovich, fractional power and intraparticle diffusivity kinetic plots, respectively while Table 4.56 provides the evaluated parameters of the kinetics models. The value of correlation coefficient (R^2) of the pseudo second-order kinetic model (> 0.99) is higher than that of other models indicating that the kinetic model for the adsorption of TPT onto nFe_3O_4/fly ash composite is pseudo second-order (Fatoki et al., 2013).

The intraparticle coefficient for the adsorption of TPT by the nFe_3O_4/fly ash composite was calculated and the results also indicate that the power function model satisfactorily describes the time-dependence of TPT onto the nFe_3O_4/fly ash composite as the value of the constant v is less than 1.

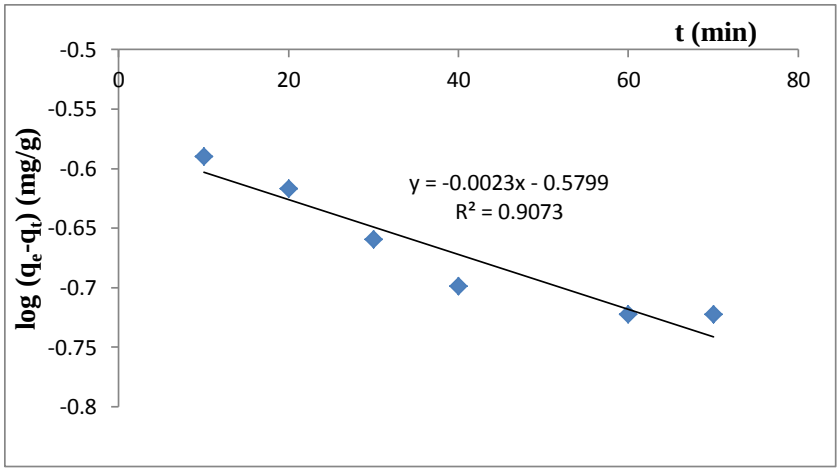

Figure 4.337: Pseudo first-order rate equation plot for TPT adsorption onto nFe_3O_4/fly ash

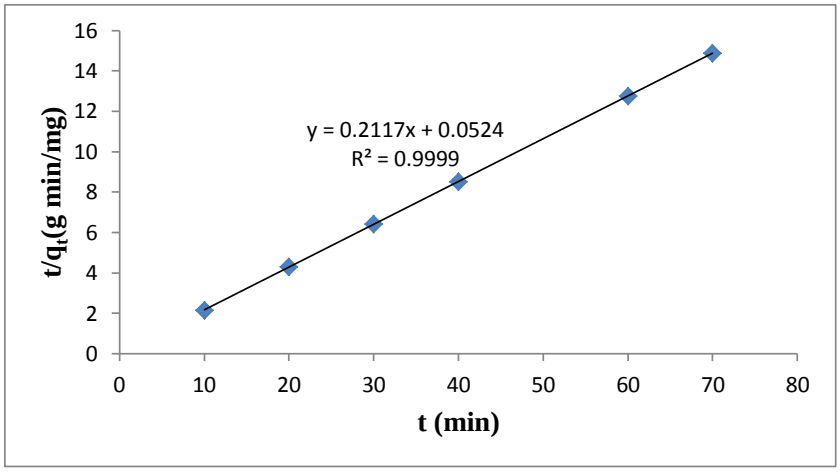

Figure 4.338: Pseudo second-order rate equation plot for TPT adsorption onto nFe_3O_4/fly ash

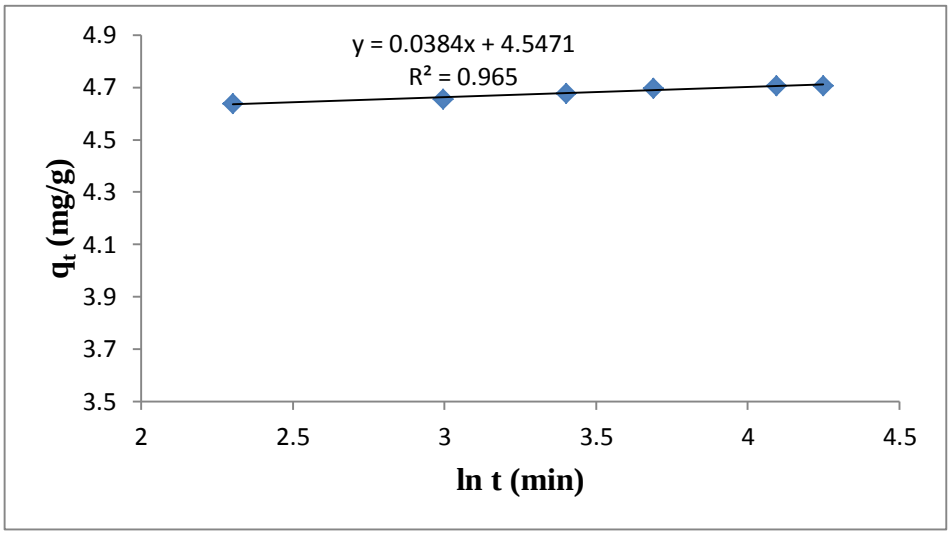

Figure 4.339: Elovich rate equation plot for TPT adsorption onto nFe_3O_4/fly ash

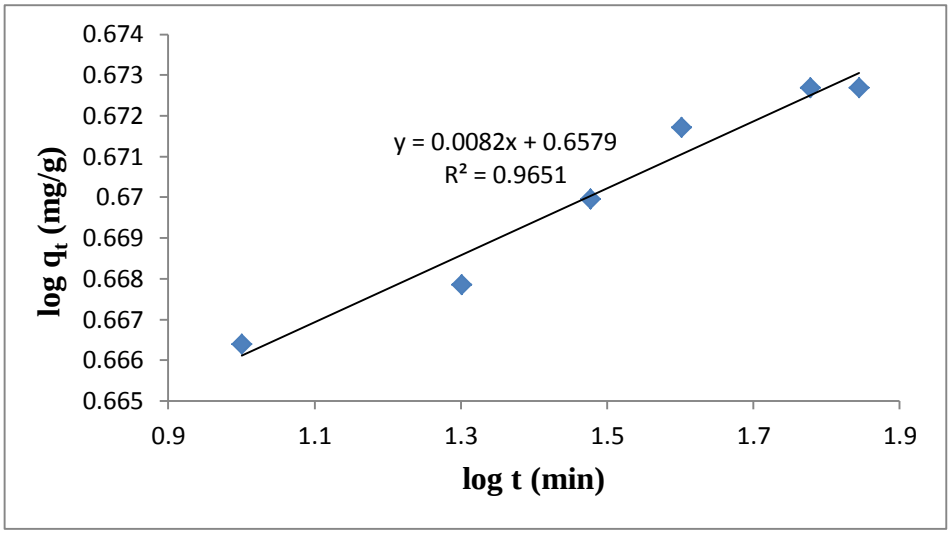

Figure 4.340: Fractional Power rate equation plot for TPT adsorption onto nFe_3O_4/fly ash

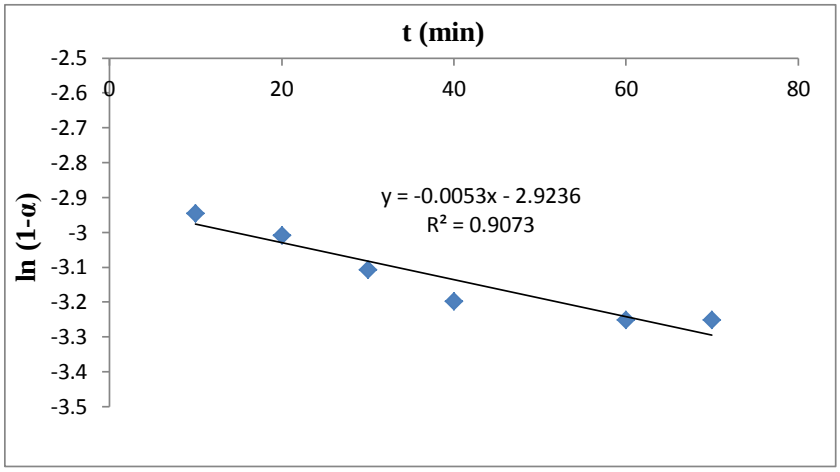

Figure 4.341: Intraparticle diffusivity plot for TPT adsorption onto nFe_3O_4/fly ash

The value of the initial adsorption rates, h_o, obtained for the pseudo second-order kinetics of the adsorption of TPT onto nFe_3O_4/fly ash composite is 19.084 mg/g/min. The kinetic model constants k_1, k_2, β, α_E, k_3 and k_p obtained as presented in Table 4.56 are 5.297 x 10^{-3} min^{-1}, 0.8553 g/mg/min, 26.042 gmin/mg, 6.954 x 10^{52} $gmin^2/mg$, 4.5488 mg/g and 0.0053 min^{-1}, respectively (Fatoki et al., 2013).

Table 4.56: Kinetic model parameters for TPT adsorption onto nFe_3O_4/fly ash

Kinetic models	
Pseudo first-order	
k_1 (min^{-1})	5.297 x 10^{-3}
q_e (mg/g)	0.2631
R^2	0.9073
Pseudo second-order	
q_e (mg/g)	4.7237
h_o (mg/g/min)	19.084
k_2 (g/mg/min)	0.8553
R^2	0.9999
Elovich	
β (g min/mg)	26.042
α ($g\ min^2/mg$)	6.954 x 10^{52}
R^2	0.9650
Fractional Power	
v (min^{-1})	0.0082
k_3 (mg/g)	4.5488
k_3v (mg/g/min)	0.0373
R^2	0.9651
Intraparticle diffusivity	
k_p (min^{-1})	0.0053
R^2	0.9073

4.12.17.3 Effect of pH

The effect of pH on the adsorption of TPT onto the nFe_3O_4/fly ash composite was studied at pH 4 – 9. The percentage TPT adsorbed by nFe_3O_4/fly ash composite steadily increases as the pH of the solution increases from pH 4 to pH 8, and reaches equilibration afterwards (Figure 4.342). pH 8 was therefore used for further studies.

Figure 4.342 therefore shows that about 95.93 % TPT was removed from the initial concentration of 100 mg/L TPT by the nFe_3O_4/fly ash composite at a contact time of 60 min, stirring speed of 160 rpm, pH 8 and a temperature of 20 ^oC.

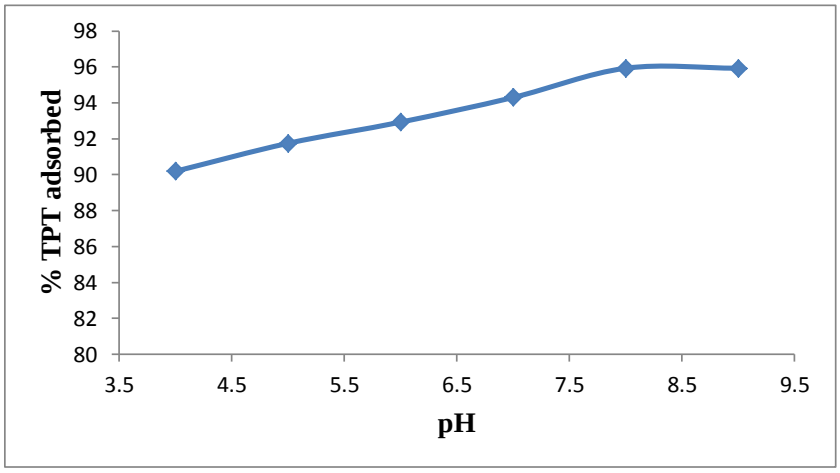

Figure 4.342: Effect of pH on TPT adsorption onto nFe_3O_4/fly ash

Experimental conditions: Concentration of TPT = 100 mg/L; Volume of TPT solution = 25 mL, Mass of nFe_3O_4/fly ash = 0.5 g; Contact time = 60 min; Stirring speed = 160 rpm, Temperature = 20 ^oC.

4.12.17.4 Effect of stirring speed

The effect of stirring speed on the adsorption of TPT onto the nFe_3O_4/fly ash composite material was studied at a stirring speed of 160 – 200 rpm. The adsorption capacity of TPT onto the composite therefore increases with increasing stirring speed as shown in Figure 4.343. The figure also shows that about 98.44 % TPT was removed from the initial concentration of 100 mg/L TPT by nFe_3O_4/fly ash composite at a contact time of 60 min, pH 8, a temperature of 20 ^oC and a stirring speed of 200 rpm. 200rpm was used for further studies.

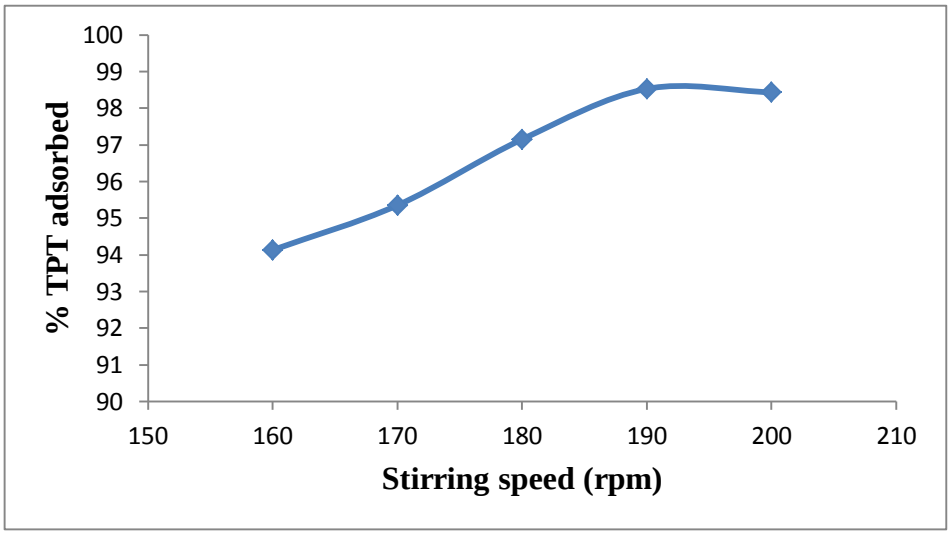

Figure 4.343: Effect of stirring speed on TPT adsorption onto nFe_3O_4/fly ash

Experimental conditions: Concentration of TPT = 100 mg/L; Volume of TPT solution = 25 mL, Mass of nFe_3O_4/fly ash = 0.5 g; Contact time = 60 min; Temperature = 20 ^oC.

4.12.17.5 Effect of initial concentration

The results obtained on the effect of initial TPT concentration (Figure 4.344) show that the adsorption of TPT onto nFe_3O_4/fly ash composite increases as the initial TPT concentration increases from 12.5 to 100 mg/L, indicating that adsorption is also favourable for the higher TPT concentrations that have been investigated.

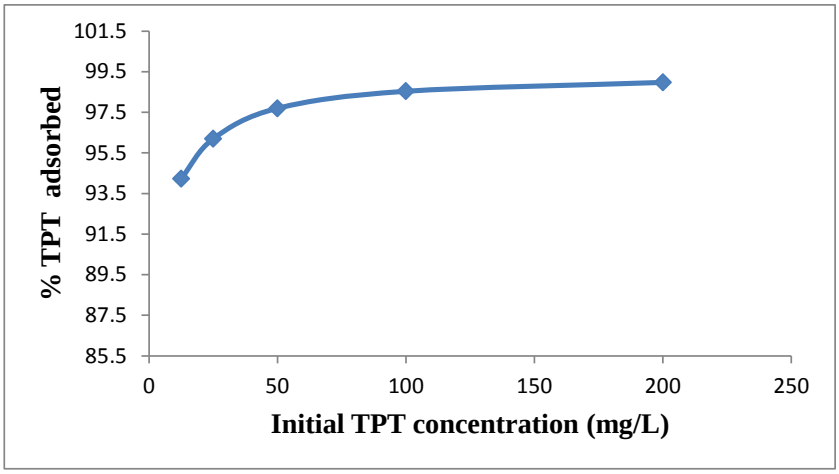

Figure 4.344: Percentage TPT adsorbed by nFe_3O_4/fly ash at various initial TPT concentrations

Experimental conditions: Volume of TPT solution = 25 mL, Mass of nFe_3O_4/fly ash = 0.5 g; pH = 8; Stirring speed = 200 rpm; Contact time = 60 min; Temperature = 20 ^oC.

4.12.17.5.1 Adsorption isotherms

The adsorption isotherm parameters obtained from the equilibrium models for the adsorption of TPT onto nFe_3O_4/fly ash composite were given in Table 4.57 and the graphs were presented in Figures 4.345 – 4.348.

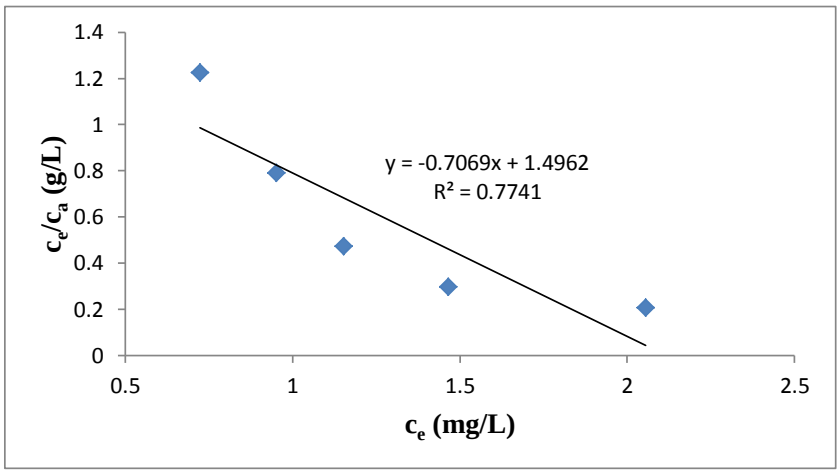

Figure 4.345: Langmuir isotherm for adsorption of TPT onto nFe_3O_4/fly ash

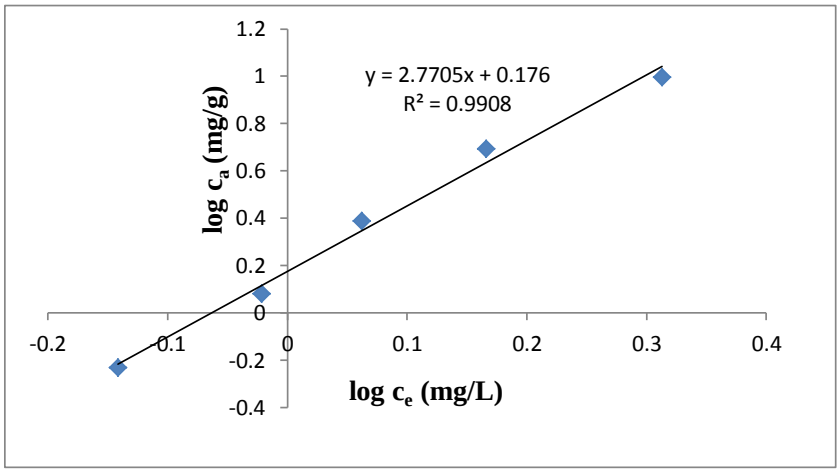

Figure 4.346: Freundlich isotherm for adsorption of TPT onto nFe_3O_4/fly ash

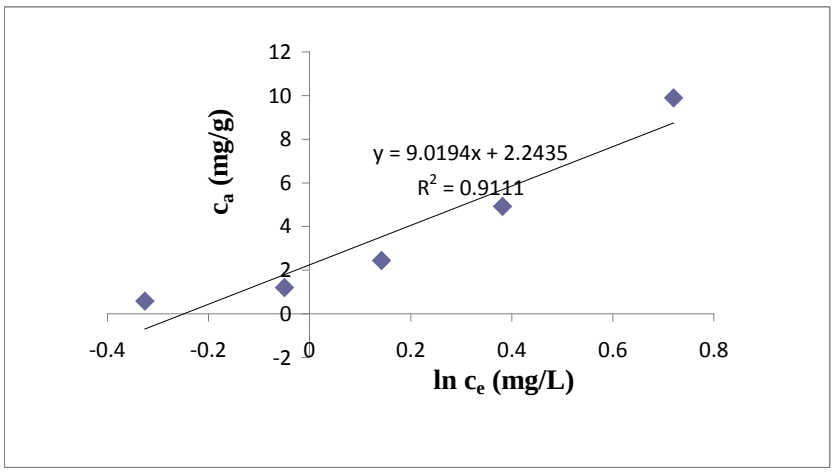

Figure 4.347: Temkin isotherm for adsorption of TPT onto nFe_3O_4/fly ash

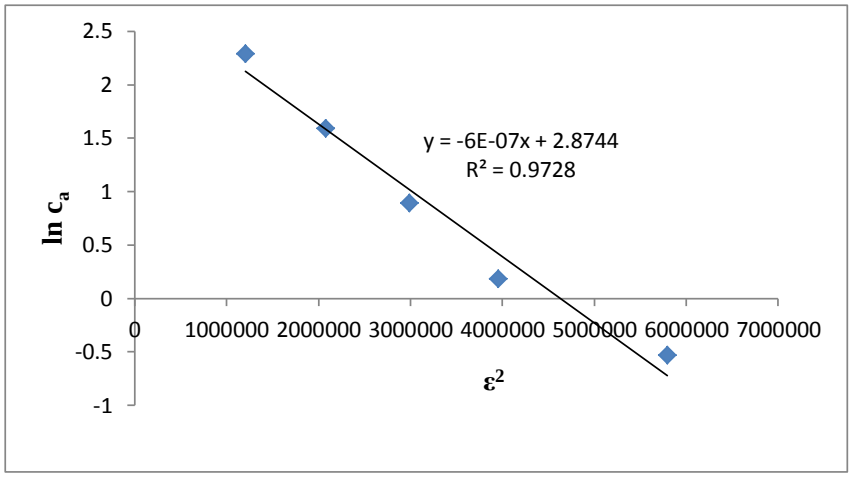

Figure 4.348: D-R isotherm for adsorption of TPT onto nFe_3O_4/fly ash

Moreover, the negative value of the Langmuir constants, A_{max} (mg/g) and k_L (L/mg) for TPT adsorption onto nFe_3O_4/fly ash composite indicates the inadequacy of the Langmuir model to fit the process. Table 4.57 also shows that the values of k_F, k_L, k_T and k_{D-R} constants obtained for the adsorption of TPT onto nFe_3O_4/fly ash composite are 1.4997 mg/g $(L/mg)^{1/n}$, -0.4715 L/mg, 1.2824 mg/L and 6.0 x 10^{-7} J^2/mol^2, respectively (Fatoki et al., 2013).

Table 4.57: Isotherms constants for the adsorption of TPT onto nFe_3O_4/fly ash

Equilibrium models	
Freundlich	
k_F [mg/g (L/mg)$^{1/n}$]	1.4997
n_F	0.3609
R^2	0.9908
Langmuir	
K_L (L/mg)	-0.4715
A_{max} (mg/g)	-1.4146
R^2	0.7741
Temkin	
n_T (L/g)	9.0194
k_T (mg/L)	1.2824
b_T (J/mol)	270.09
R^2	0.9111
Dubinin-Redushkevich	
k_{D-R} (J^2/mol^2)	6.0×10^{-7}
q_m (mg/g)	17.715
E (J/mol)	912.87
R^2	0.9728

The figures and table show that the experimental data fitted well with the Freundlich isotherm and the value of n_F, for the nFe_3O_4/fly ash composite, falling in the range 1 -10 indicates favourable adsorption.

4.12.17.6 Effect of temperature

The experimental results obtained on the effect of temperature for the adsorption of TPT onto nFe_3O_4/fly ash composite material (Figure 4.349) show that the adsorption capacity of nFe_3O_4/fly ash composite decreases with increase in the solution temperature. This indicates that the adsorption of TPT onto nFe_3O_4/fly ash composite is exothermic.

Approx. 92.99 % of TPT was removed from the initial concentration of 100 mg/L TPT by nFe_3O_4/fly ash composite at a contact time of 60 min, pH 8, stirring speed 200 rpm and temperature of 80 ^oC whereas 97.95 % TPT was removed at 40 ^oC at the same conditions. Figure 4.350 thus shows the Van't Hoff plot for the adsorption of TPT onto nFe_3O_4/fly ash composite while ΔH^o, ΔS^o, and ΔG^o are presented in Table 4.58.

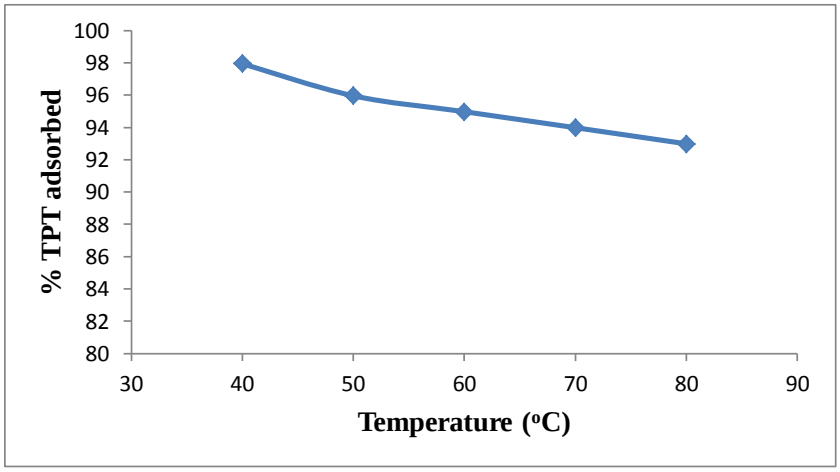

Figure 4.349: Effect of temperature on TPT adsorption onto nFe_3O_4/fly ash

Experimental conditions: Concentration of TPT = 100 mg/L; Volume of TPT solution = 25 mL, Mass of nFe_3O_4/fly ash = 0.5 g; Contact time = 60 min; pH = 8; Stirring speed = 200 rpm.

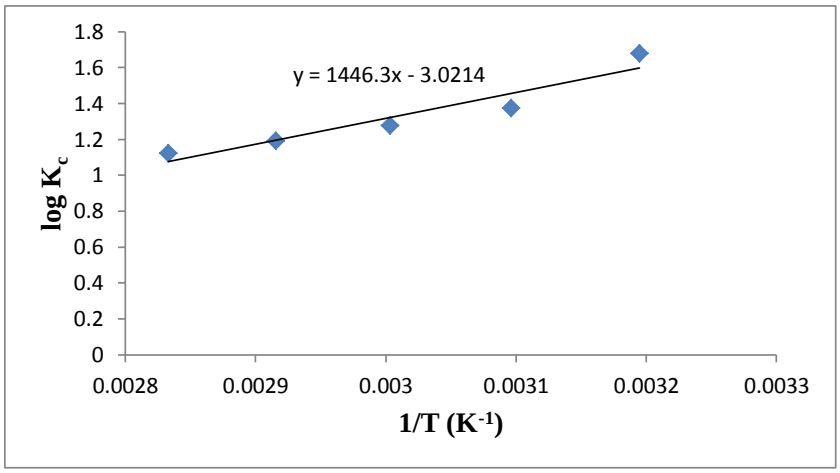

Figure 4.350: Van't Hoff Plot for the adsorption of TPT onto nFe_3O_4/fly ash

Table 4.58: Thermodynamic parameters for adsorption of TPT onto nFe_3O_4/fly ash

Temperature (°C)	ΔG° (kJ/mol)	ΔS° (J/K/mol)	ΔH° (kJ/mol)	K_c
40	-10.062	-57.851	-27.693	47.780
50	- 8.5088			23.752
60	-8.1385			18.908
70	-7.8395			15.628
80	-7.5857			13.259

The negative value of ΔH^o (-27.693 kJ/mol) for the intervals of temperatures studied (Table 4.58) also shows the exothermic nature of the adsorption process. The negative value of ΔS^o (-57.851 J/K/mol) corresponds to a decrease in the degree of freedom of the adsorbed TPT, indicating a decrease in adsorbate concentration onto the solid phase. ΔG^o values were found to increase as the temperature increases, which indicate non-

spontaneous adsorption and the degree of spontaneity of the reaction decreases with increase in temperature.

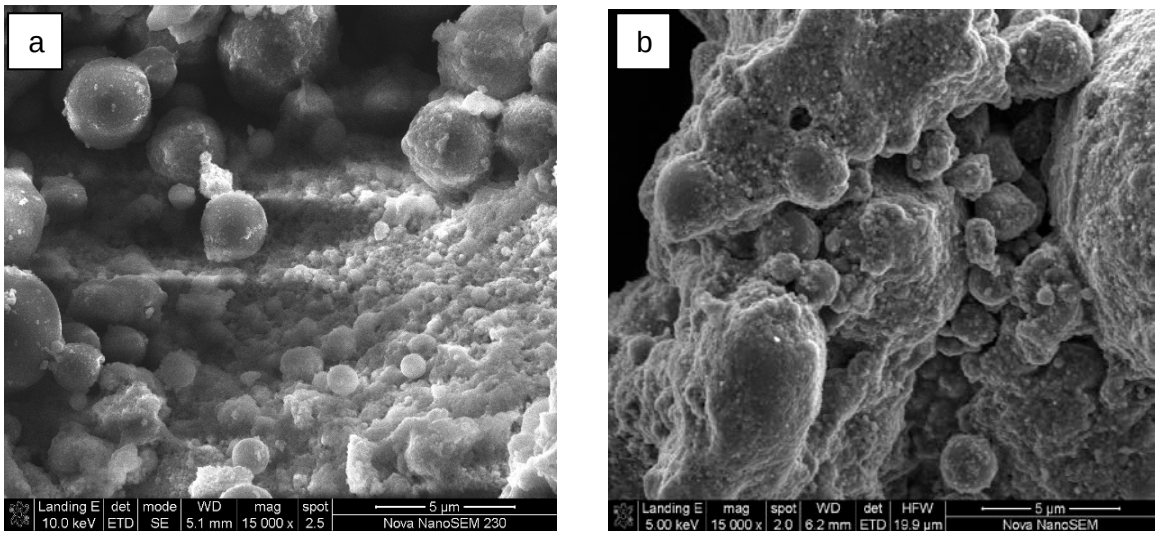

Figure 4.351: nFe_3O_4/fly ash before (a) and after (b) TPT adsorption

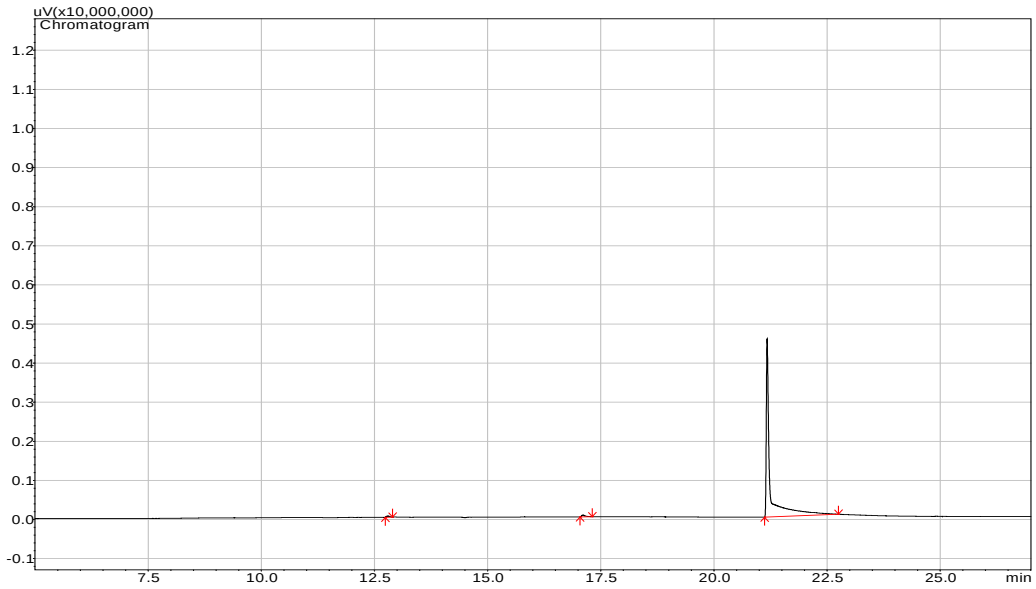

Figure 4.352: Representative TPT chromatogram after adsorption of 100 mg/L TPT with 0.5 g of nFe_3O_4/fly ash, contact time of 60 min, temperature 20 ^oC and a stirring speed of 200 rpm

The SEM analysis of nFe_3O_4/fly ash composite before and after adsorption process is presented in Figure 4.351 while the TPT chromatogram after adsorption of 100 mg/L TPT with 0.5 g of nFe_3O_4/fly ash composite, 60 min contact time, temperature 20 ^oC and a stirring speed of 200 rpm is shown in Figure 4.352.

4.12.18 Adsorption of TPT from TPT-contaminated artificial seawater onto $nSiO_2$/fly ash composite

4.12.18.1 Effect of adsorbent amount

The results on the effect of adsorbent amount on the adsorption of TPT by the $nSiO_2$/activated carbon composite as shown in Figure 4.353 indicate that the percentage of TPT adsorption increases with increasing $nSiO_2$/activated carbon composite amount, reaching an optimum at 0.5 g, corresponding to 95.90 % removal.

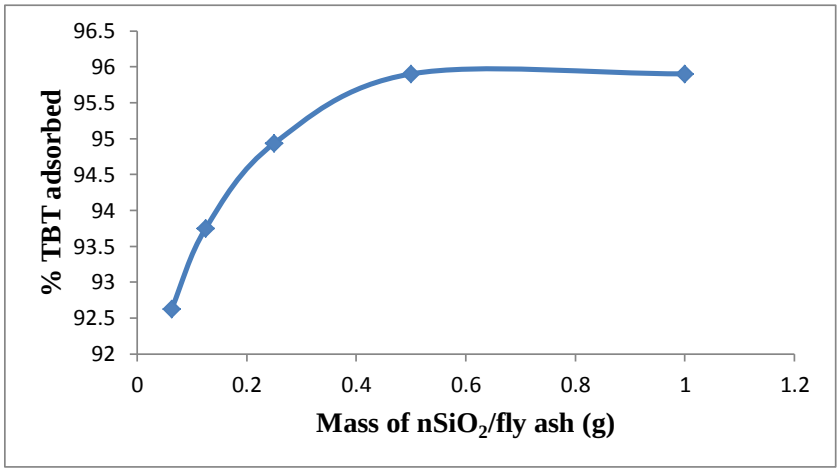

Figure 4.353: Adsorption efficiencies of TPT onto $nSiO_2$/fly ash

Experimental conditions: Concentration of TPT = 100 mg/L; Volume of TPT solution = 25 mL, Contact time = 60 min; Stirring speed = 160 rpm, Temperature = 20 ^{o}C.

4.12.18.2 Effect of contact time

Figure 4.354 shows the effect of contact time on the adsorption of TPT onto $nSiO_2$/activated carbon composite. The TPT removal efficiencies at different time intervals ranging from 10 – 70 min were obtained. It was therefore observed from Figure 4.354 that the amount of TPT adsorbed by the composite material increases with time and equilibrium was approximately achieved within 60 min. The amount of TPT removed at a contact time of 60 min from the initial TPT concentration of 5.0 mg/g by the $nSiO_2$/activated carbon composite is 4.795 mg/g (95.90 %). 60 min was therefore used for further studies.

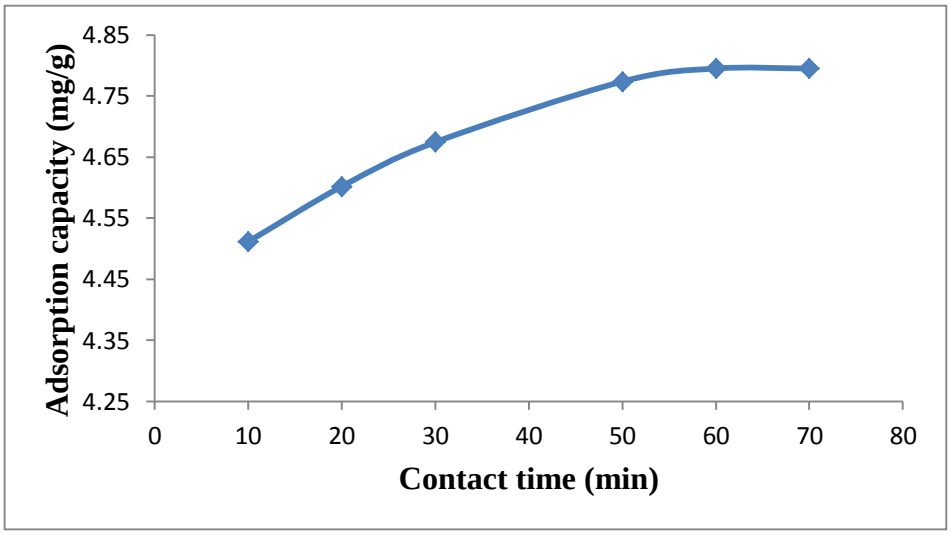

Figure 4.354: Effect of contact time on TPT adsorption onto $nSiO_2$/fly ash

Experimental conditions: Concentration of TPT = 100 mg/L; Volume of TPT solution = 25 mL, Mass of $nSiO_2$/fly ash = 0.5 g; Stirring speed = 160 rpm, Temperature = 20 ^{o}C.

4.12.18.2.1 Adsorption kinetics

Figures 4.355 – 4.359 show the pseudo first-order, pseudo second-order, Elovich, fractional power and intraparticle diffusivity kinetic plots while Table 4.59 provides the evaluated parameters of the kinetics models.

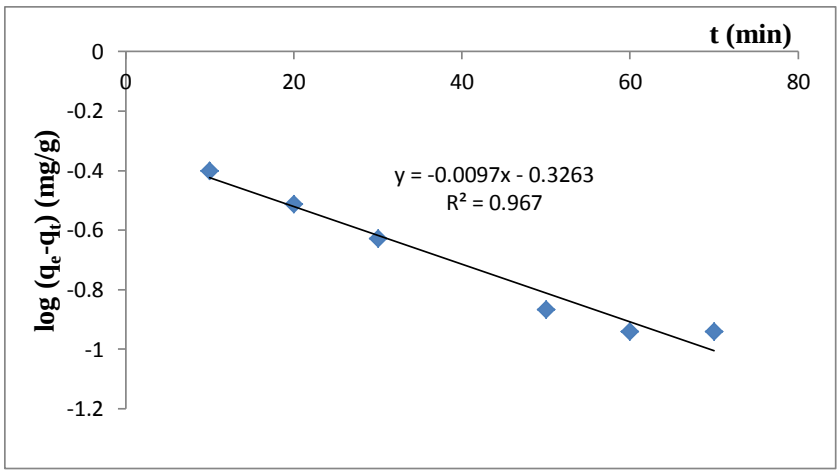

Figure 4.355: Pseudo first-order rate equation plot for TPT adsorption onto $nSiO_2$/fly ash

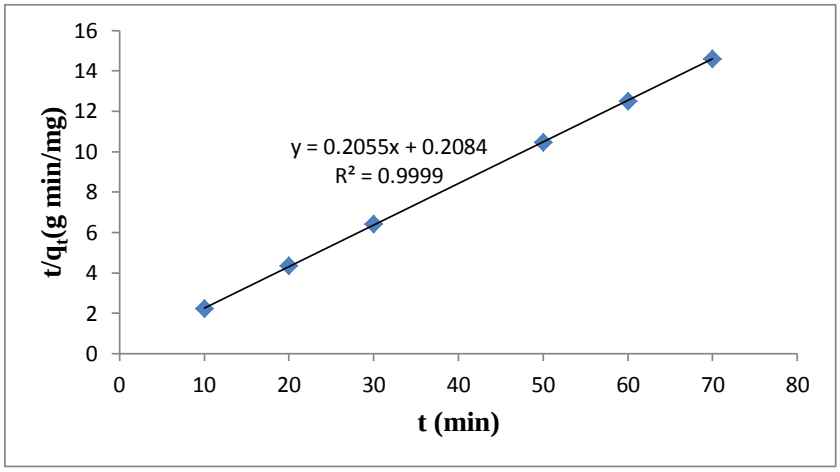

Figure 4.356: Pseudo second-order rate equation plot for TPT adsorption onto $nSiO_2$/fly ash

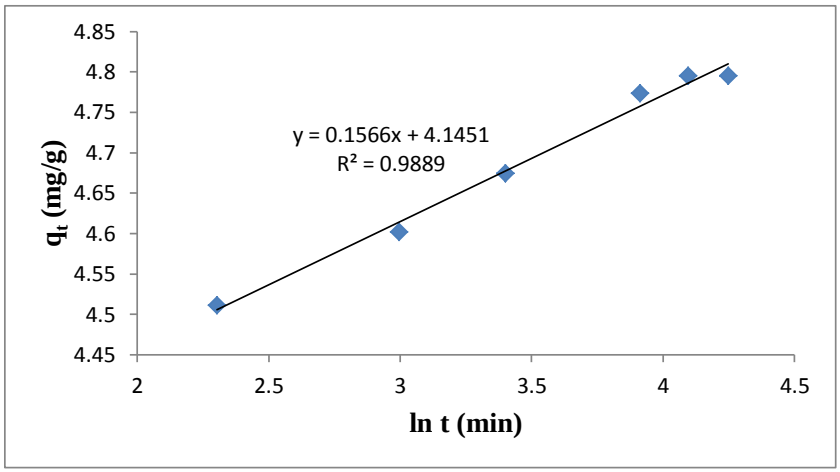

Figure 4.357: Elovich rate equation plot for TPT adsorption onto $nSiO_2$/fly ash

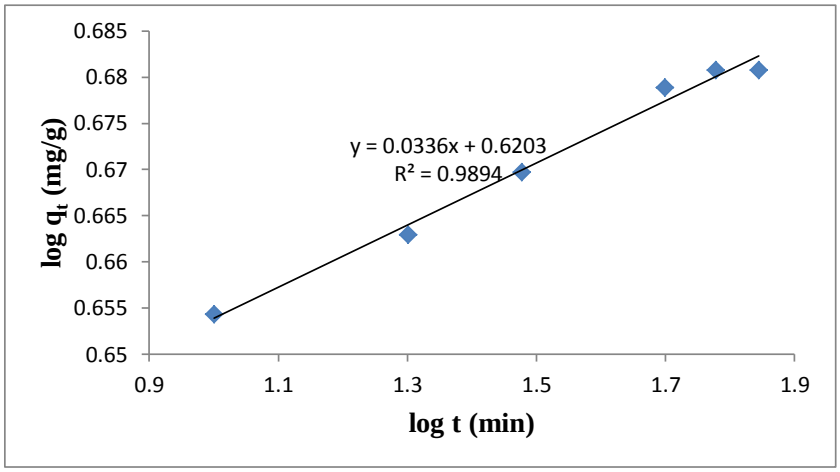

Figure 4.358: Fractional Power rate equation plot for TPT adsorption onto $nSiO_2$/fly ash

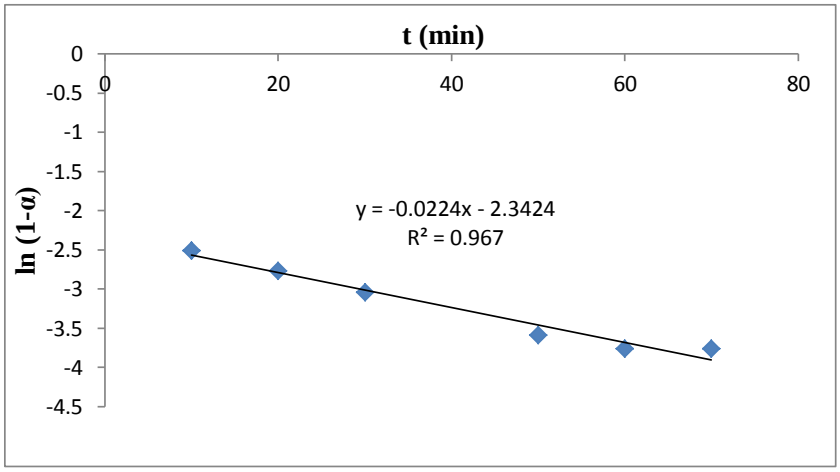

Figure 4.359: Intraparticle diffusivity plot for TPT adsorption onto $nSiO_2$/fly ash

The results obtained (Table 4.59) show a very good compliance with pseudo second-order equation with high regression coefficient (> 0.99) whereas the pseudo first-order and Elovich models were not applicable as low regression coefficients (< 0.97) were observed.

Table 4.59: Kinetic model parameters for TPT adsorption onto $nSiO_2$/fly ash

Kinetic models	
Pseudo first-order	
k_1 (min^{-1})	0.0223
q_e (mg/g)	0.4717
R^2	0.9670
Pseudo second-order	
q_e (mg/g)	4.8661
h_o (mg/g/min)	4.7985
k_2 (g/mg/min)	0.2026
R^2	0.9999
Elovich	
β (g min/mg)	6.3857
α (g min^2/mg)	1.998×10^{12}
R^2	0.9889
Fractional Power	
v (min^{-1})	0.0336
k_3 (mg/g)	4.1716
k_3v (mg/g/min)	0.1402
R^2	0.9894
Intraparticle diffusivity	
k_p (min^{-1})	0.0224
R^2	0.9870

The results also show that the adsorption rate constant, k_2, initial adsorption rate, h_o, and equilibrium adsorption capacity, q_e, of the pseudo second-order model are 0.2026 g/mg/min, 4.7985 mg/g/min and 4.8661 mg/g, respectively. A simple kinetic analysis of the

adsorption of TPT onto $nSiO_2$/fly ash composite was also tested according to fractional power model and Table 4.59 shows the estimated parameters of the model. The results indicate that the power model satisfactorily described the time-dependent of TPT onto $nSiO_2$/fly ash composite as the value of the constant v is less than 1 and the regression coefficient is greater than 0.96.

The kinetic model constants k_1, k_2, β, α_E, k_3 and k_p as presented in Table 4.59 for the adsorption of TPT onto $nSiO_2$/fly ash composite material are therefore 0.0223 min^{-1}, 0.2026 g/mg/min, 6.3859 gmin/mg, 1.998 x 10^{12} $gmin^2/mg$, 4.1716 mg/g and 0.0224 min^{-1}, respectively.

4.12.18.3 Effect of pH

The effect of pH on the adsorption of TPT onto $nSiO_2$/fly ash composite was studied at pH 4 – 9. It was observed from Figure 4.360 that the percentage of TPT adsorbed by the composite material increases as the pH of the solution increases from pH 4 to pH 8, and reaches equilibration at pH ≥ 8.

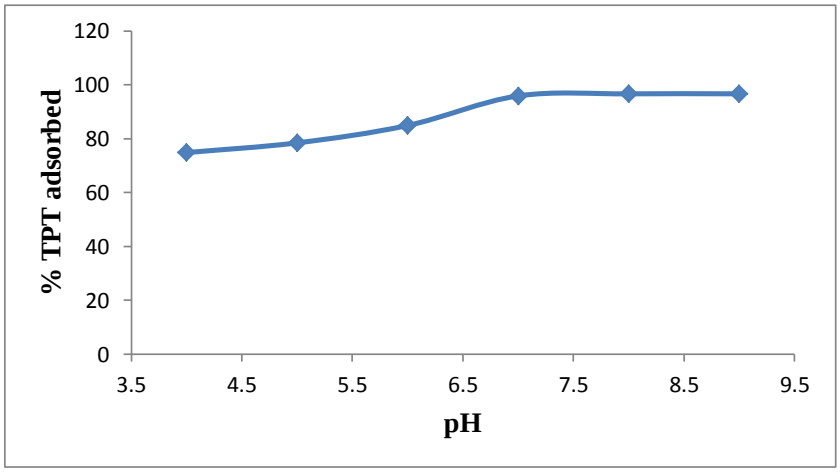

Figure 4.360: Effect of pH on TPT adsorption onto $nSiO_2$/fly ash

Experimental conditions: Concentration of TPT = 100 mg/L; Volume of TPT solution = 25 mL, Mass of $nSiO_2$/fly ash = 0.5 g; Contact time = 60 min; Stirring speed = 160 rpm, Temperature = 20 ^oC.

Maximum adsorption was therefore recorded within the pH range of normal saline water. About 96.68 % TPT was removed from the initial concentration of 100 mg/L TPT by $nSiO_2$/fly ash composite at pH 8, a contact time of 60 min, 160 rpm stirring speed and a temperature of 20 ^oC.

4.12.18.4 Effect of stirring speed

The stirring speed of the adsorption of TPT $nSiO_2$/fly ash composite was also studied and optimized. The stirring speed was studied at a stirring speed of 160 – 200 rpm. Figure 4.361 shows that the adsorption capacity of $nSiO_2$/fly ash composite increases as the stirring speed of the mixture increases from 160 rpm – 190 rpm after which equilibration was attained.

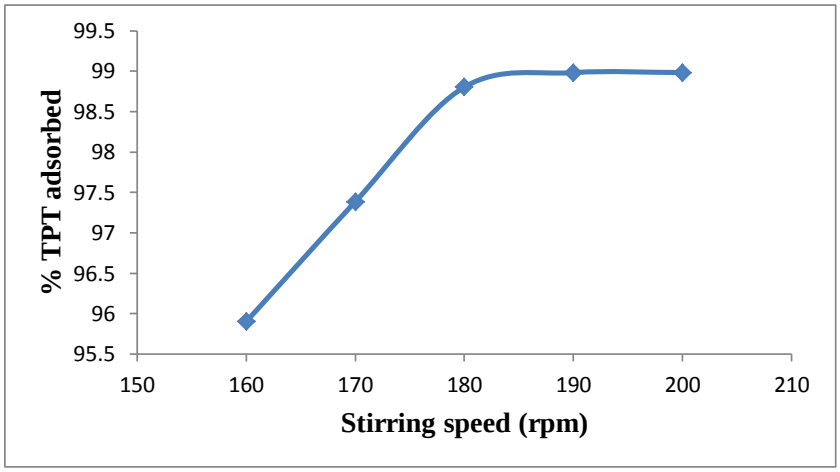

Figure 4.361: Effect of stirring speed on TPT adsorption onto $nSiO_2$/fly ash

Experimental conditions: Concentration of TPT = 100 mg/L; Volume of TPT solution = 25 mL, Mass of $nSiO_2$/fly ash = 0.5 g; Contact time = 60 min; Temperature = 20 ^oC.

Figure 4.361 therefore shows that approx. 4.9492 mg/g (98.98 %) TPT was removed from the initial concentration of 5 mg/g TPT by the $nSiO_2$/fly ash composite at a contact time of 60 min, pH 8, temperature of 20 ^oC and a stirring speed of 200 rpm.

4.12.18.5 Adsorption isotherms

Figure 4.362 shows that the adsorption of TPT onto $nSiO_2$/fly ash composite increases as the initial TPT concentration increases from 12.5 to 100 mg/L, indicating that the adsorption is favourable for the higher TPT concentrations that have been investigated.

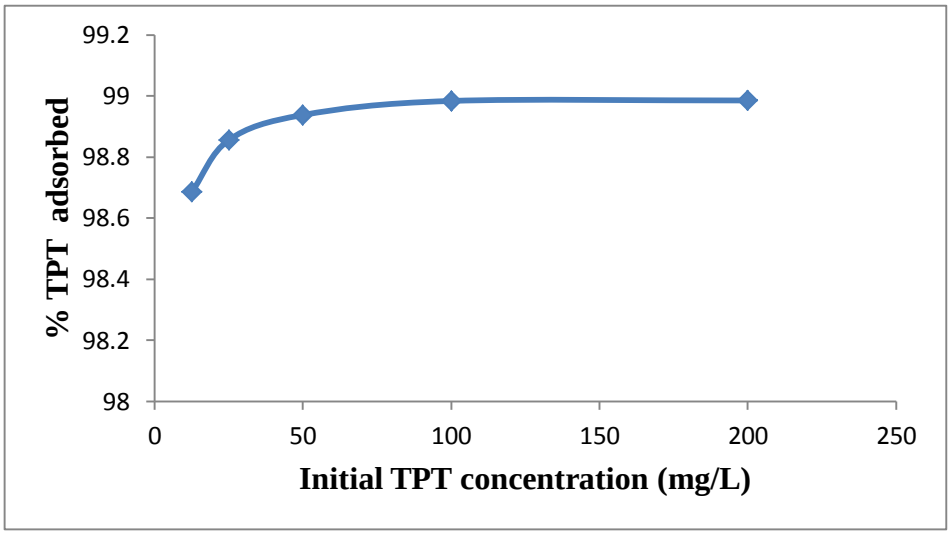

Figure 4.362: Percentage TPT adsorbed by $nSiO_2$/fly ash at various initial TPT concentrations

Experimental conditions: Volume of TPT solution = 25 mL, Mass of $nSiO_2$/fly ash = 0.5 g; pH = 8; Stirring speed = 200 rpm; Contact time = 60 min; Temperature = 20 ^{o}C.

4.12.18.5.1 Adsorption isotherms

The results indicate that the Freundlich model fit the experiment data well. It is the suitable model for describing this adsorption process because the correlation coefficient (R^2) is higher than the correlation coefficients obtained for other models (Figures 4.363 – 4.366 and Table 4.60). The value of n_F falling in the range 1 -10 also indicates favourable adsorption.

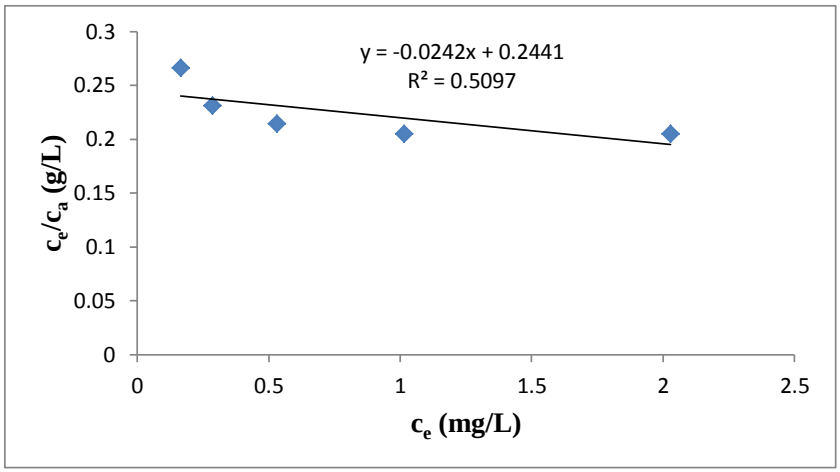

Figure 4.363: Langmuir isotherm for adsorption of TPT onto $nSiO_2$/fly ash

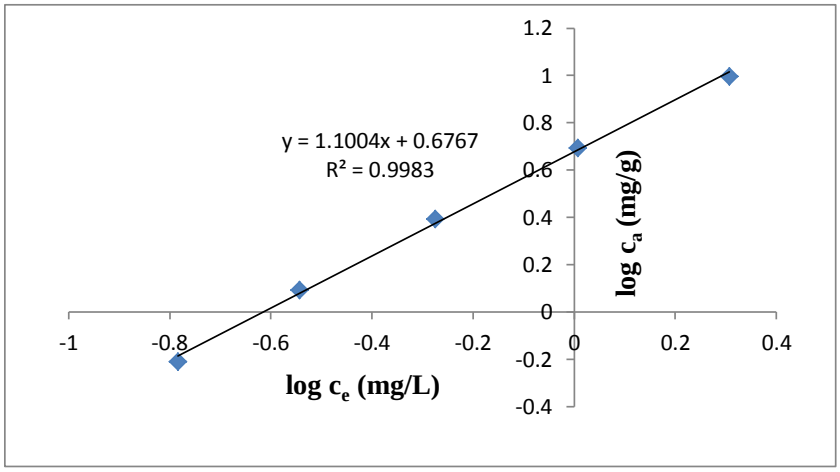

Figure 4.364: Freundlich isotherm for adsorption of TPT onto $nSiO_2$/fly ash

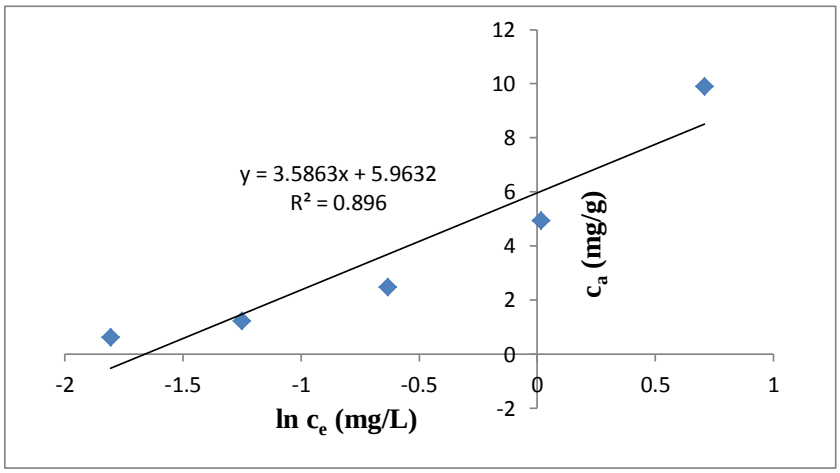

Figure 4.365: Temkin isotherm for adsorption of TPT onto $nSiO_2$/fly ash

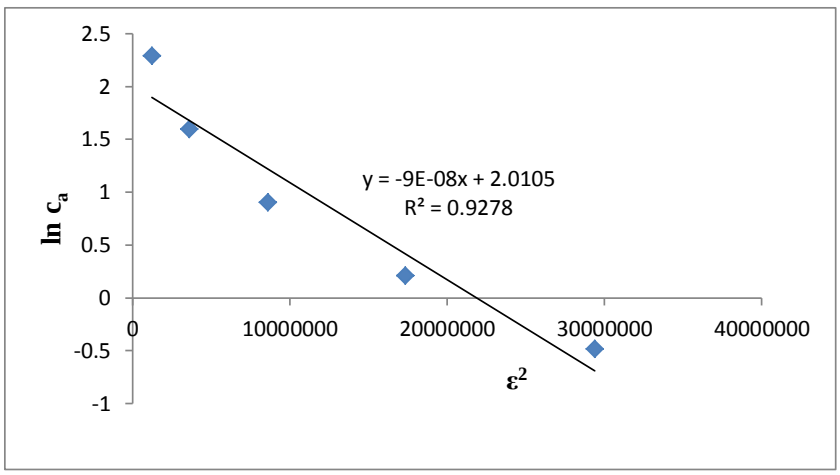

Figure 4.366: D-R isotherm for adsorption of TPT onto $nSiO_2$/fly ash

Table 4.60: Isotherms constants for the adsorption of TPT onto $nSiO_2$/fly ash

Equilibrium models	
Freundlich	
k_F [mg/g (L/mg)$^{1/n}$]	4.750
n_F	0.9088
R^2	0.9983
Langmuir	
K_L (L/mg)	-10.087
A_{max} (mg/g)	-41.322
R^2	0.5097
Temkin	
n_T (L/g)	3.5863
k_T (mg/L)	5.2739
b_T (J/mol)	679.25
R^2	0.8960
Dubinin-Redushkevich	
k_{D-R} (J^2/mol^2)	9.0 x 10^{-8}
q_m (mg/g)	7.4670
E (J/mol)	2357.02
R^2	0.9278

The experimental data (Table 4.60) does not fit the Langmuir model, as the R^2 value is low (< 0.60) and Langmuir constants, A_{max} (mg/g) and k_L (L/mg) for TPT adsorption onto $nSiO_2$/fly ash composite were negative. The Temkin and D-R isotherm models also gave low R^2 value (< 0.90 for Temkin and < 0.93 for D-R) and can also not be used to describe the adsorption process. The equilibrium model constants k_F, k_L, k_T and k_{D-R} for the adsorption of TPT onto $nSiO_2$/fly ash composite are 4.750 mg/g (L/mg)$^{1/n}$, -10.087 L/mg, 5.2739 mg/L and 9.0 x 10^{-8} J^2/mol^2, respectively (Ayanda et al., 2013d).

4.12.18.6 Effect of temperature

Experimental results obtained on the effect of temperature show that the adsorption capacity of TPT onto $nSiO_2$/fly ash composite adsorbent decreases with increase in the solution temperature as shown in Figure 4.367. This indicates that the adsorption of TPT onto the $nSiO_2$/fly ash composite is exothermic.

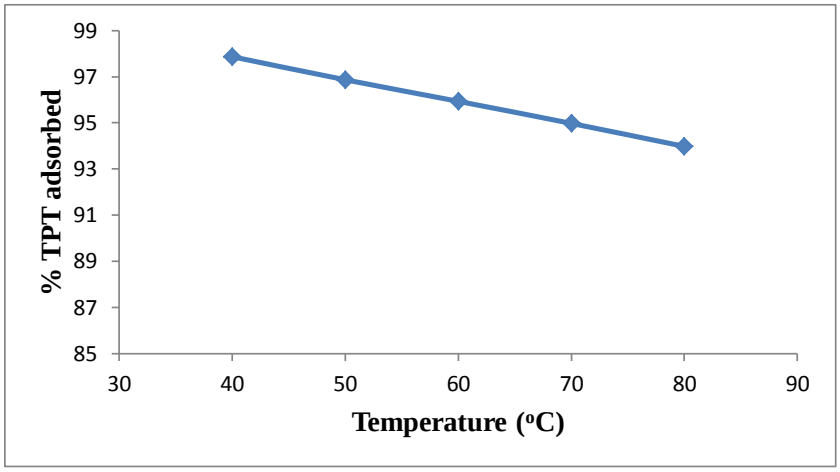

Figure 4.367: Effect of temperature on TPT adsorption onto $nSiO_2$/fly ash

Experimental conditions: Concentration of TPT = 100 mg/L; Volume of TPT solution = 25 mL, Mass of $nSiO_2$/fly ash = 0.5 g; Contact time = 60 min; pH = 8; Stirring speed = 200 rpm.

Approx. 93.98 % of TPT was removed from the initial concentration of 100 mg/L TPT by $nSiO_2$/fly ash composite at a contact time of 60 min, pH 8, stirring speed 200 rpm and temperature of 80 °C whereas 97.87 % TPT was removed at 40 °C at the same conditions. Figure 4.368 thus shows the Van't Hoff plot for the adsorption of TPT and the variation in the extent of adsorption with respect to temperature has been explained on the basis of ΔH^{o}, ΔS^{o}, and ΔG^{o} as shown in Table 4.61

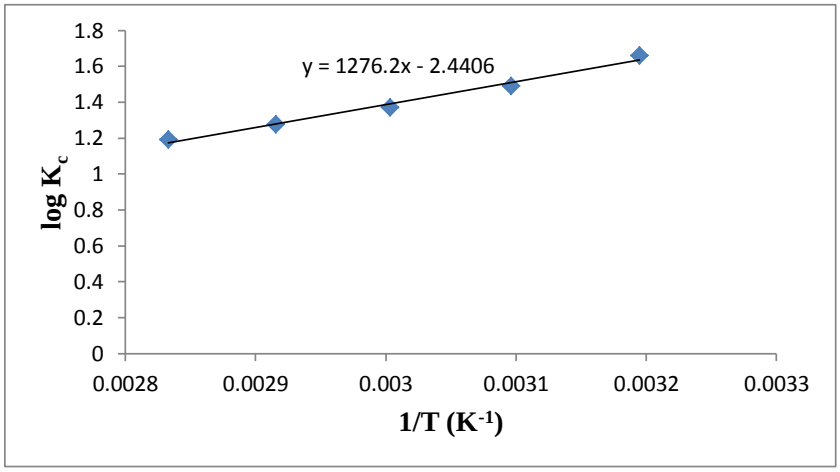

Figure 4.368: Van't Hoff Plot for the adsorption of TPT onto $nSiO_2$/fly ash

Table 4.61: Thermodynamic parameters for adsorption of TPT onto $nSiO_2$/fly ash

Temperature (°C)	ΔG° (kJ/mol)	ΔS° (J/K/mol)	ΔH° (kJ/mol)	K_c
40	-9.955	-46.731	-24.435	45.860
50	- 8.5088			30.908
60	-8.750			23.582
70	-8.381			18.901
80	-8.064			15.606

The negative value of ΔH^{o} (-24.435 kJ/mol) for the intervals of temperatures studied as presented in Table 4.61 also shows that the adsorption of TPT onto $nSiO_2$/fly ash composite is exothermic. The negative value of ΔS^{o} (-46.731 J/K/mol) corresponds to a decrease in the degree of freedom of the adsorbed TPT, indicating a decrease in adsorbate concentration onto the solid phase. ΔG^{o} values were found to increase as the temperature increases, which indicate non-spontaneous adsorption and the degree of spontaneity of the reaction decreases with increase in temperature. K_c ranged 15.606 – 45.860.

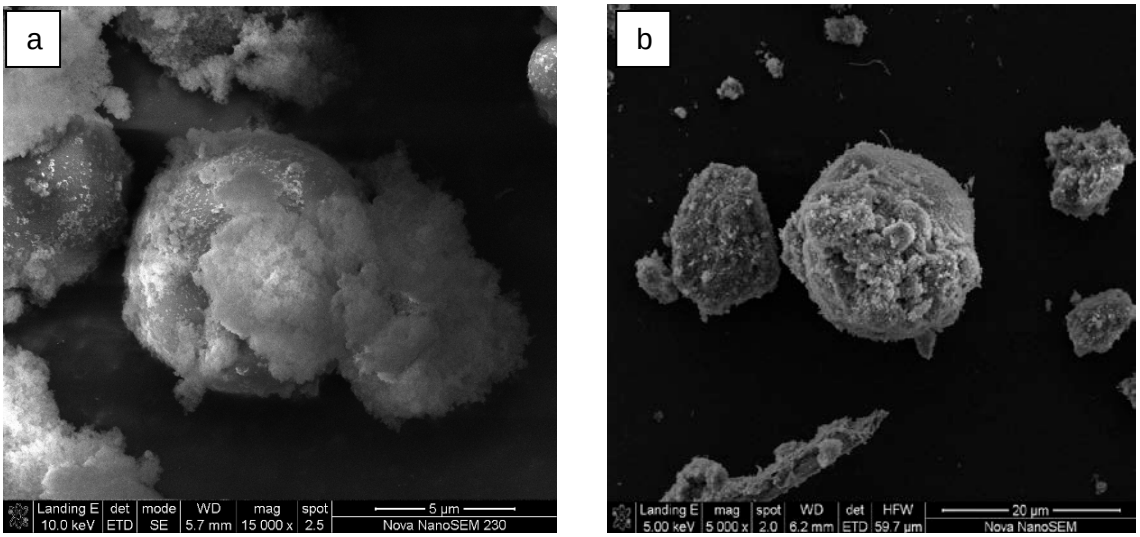

Figure 4.369: $nSiO_2$/fly ash before (a) and after (b) TPT adsorption

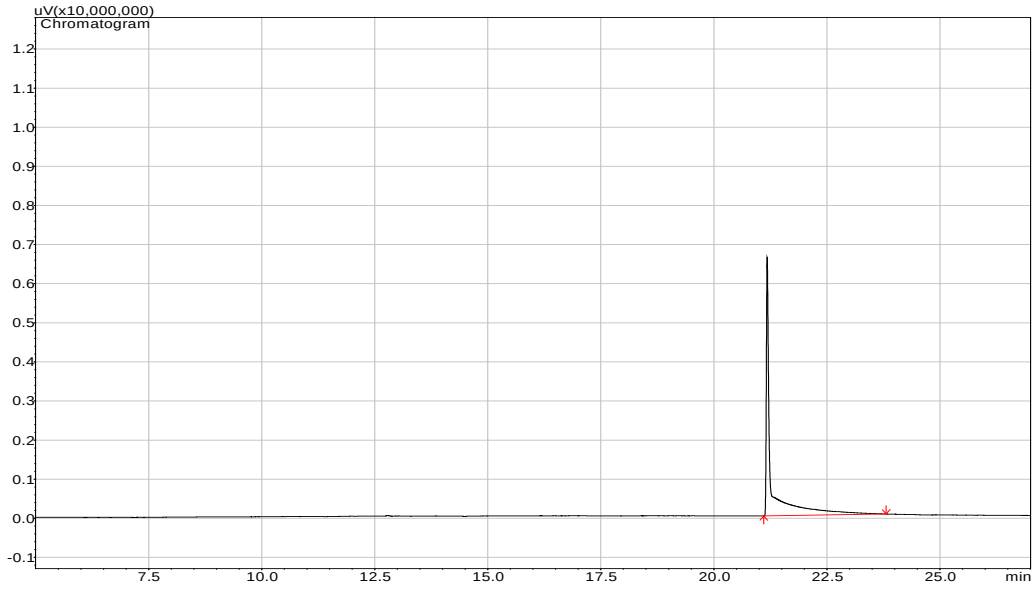

Figure 4.370: Representative TPT chromatogram after adsorption of 100 mg/L TPT with 0.5 g of $nSiO_2$/fly ash, contact time of 60 min, temperature 20 ^{o}C and a stirring speed of 200 rpm

The SEM analysis of $nSiO_2$/fly ash composite before and after the adsorption studies is presented in Figure 4.369. A representative TPT chromatogram after adsorption of 100 mg/L TPT onto 0.5 g of $nSiO_2$/fly ash composite at 60 min contact time, temperature of 20 ^oC and a stirring speed of 200 rpm is as shown in Figure 4.370.

4.12.19 Adsorption of TPT from TPT-contaminated artificial seawater onto nZnO/fly ash composite

4.12.19.1 Effect of adsorbent amount

To study the effect of adsorbent amount on the adsorption of TPT from TPT – contaminated artificial seawater, the amount of nZnO/fly ash composite was varied from 0.0625 – 1 g, the concentration of TPT was taken as 100 mg/L and other parameters were also kept constant. Figure 4.371 shows that the amount of TPT adsorbed and percentage removal of TPT by the nZnO/fly ash composite increases as the amount of nZnO increases from 0.0625 - 0.5 g after which equilibration was attained.

Figure 4.371 therefore shows that 0.5 g of nZnO/fly ash composite removes 99.63 % of TPT from TPT – contaminated artificial seawater. 0.5 g was chosen and used for further studies.

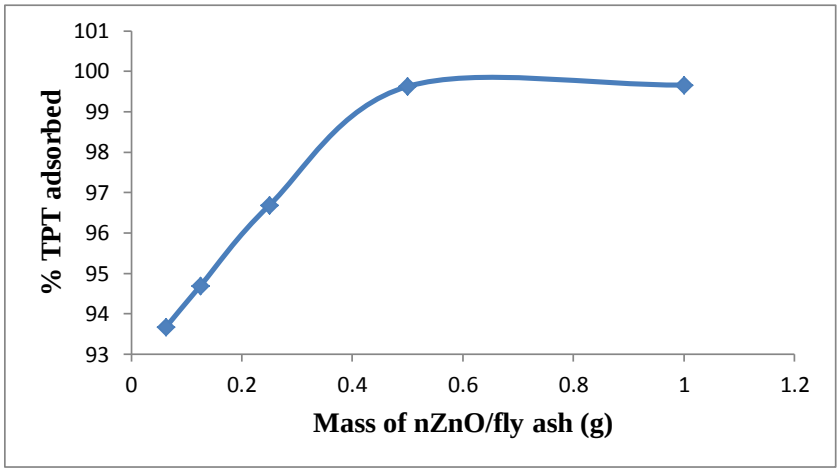

Figure 4.371: Adsorption efficiencies of TPT onto nZnO/fly ash

Experimental conditions: Concentration of TPT = 100 mg/L; Volume of TPT solution = 25 mL, Contact time = 60 min; Stirring speed = 160 rpm, Temperature = 20 ^oC.

4.12.19.2 Effect of adsorbent amount

To study the effect of contact time on the adsorption of TPT onto nZnO/fly ash composite material, the TPT concentration was 100 mg/L while, other remaining conditions such as pH, stirring speed etc. were constant. The effect of contact time was carried out at various time intervals from 10 – 70 min. The increase in the amount of TPT adsorbed by nZnO/fly ash

composite from 4.9198 mg/g (98.40 %) to 4.9814 mg/g (99.63 %) (Figure 4.372) was observed up to 60 min. After that, there is no significant change observed. 60 min was therefore fixed as the contact time for further studies

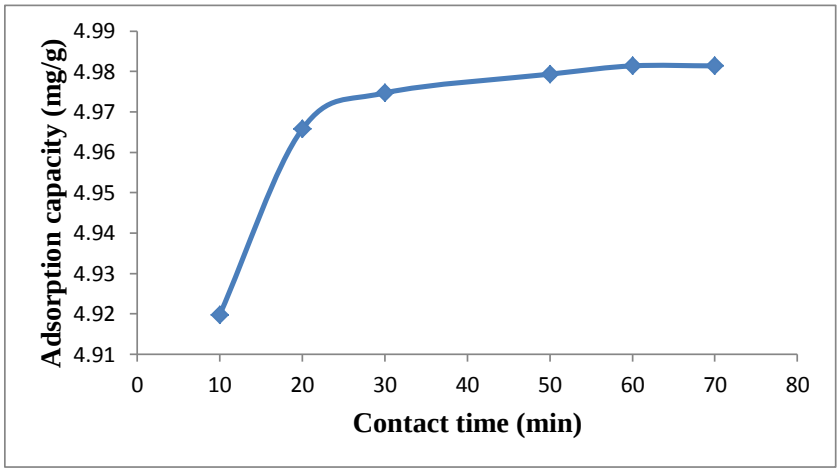

Figure 4.372: Effect of contact time on TPT adsorption onto nZnO/fly ash

Experimental conditions: Concentration of TPT = 100 mg/L; Volume of TPT solution = 25 mL, Mass of nZnO/fly ash = 0.5 g; Stirring speed = 160 rpm, Temperature = 20 ^{o}C.

4.12.19.2.1 Adsorption kinetics

Figures 4.373 – 4.377 thus show the pseudo first-order, pseudo second-order, Elovich, fractional power and intraparticle diffusivity kinetic plots, respectively and Table 4.62 shows the evaluated parameters of the kinetics models.

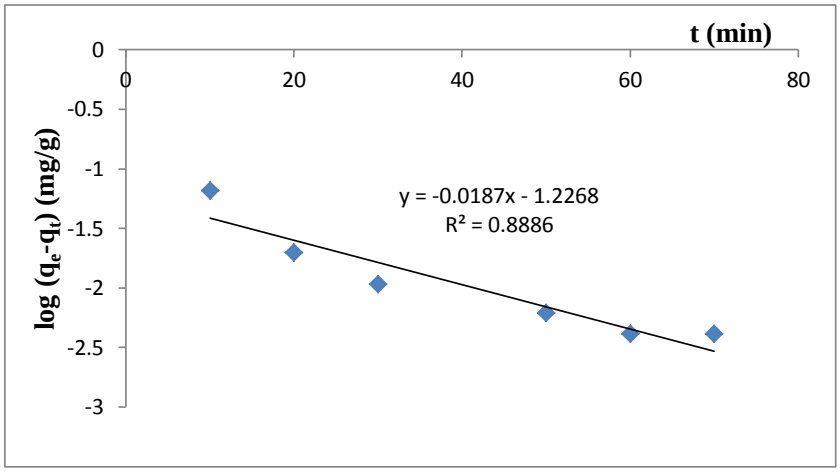

Figure 4.373: Pseudo first-order rate equation plot for TPT adsorption onto nZnO/fly ash

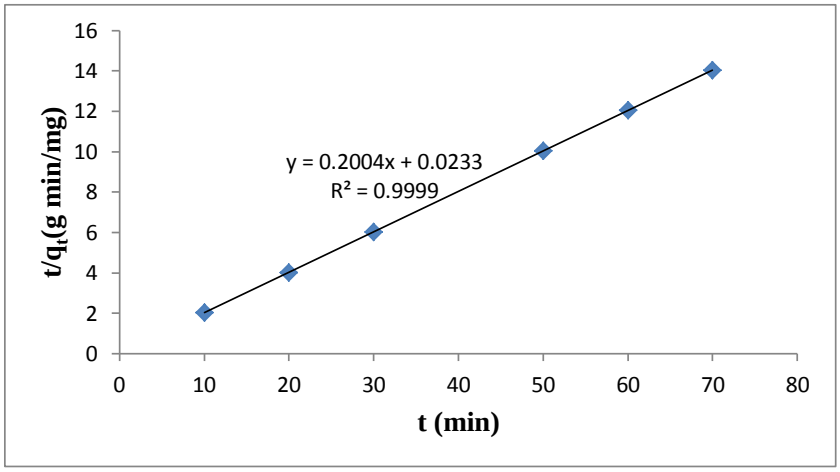

Figure 4.374: Pseudo second-order rate equation plot for TPT adsorption onto nZnO/fly ash

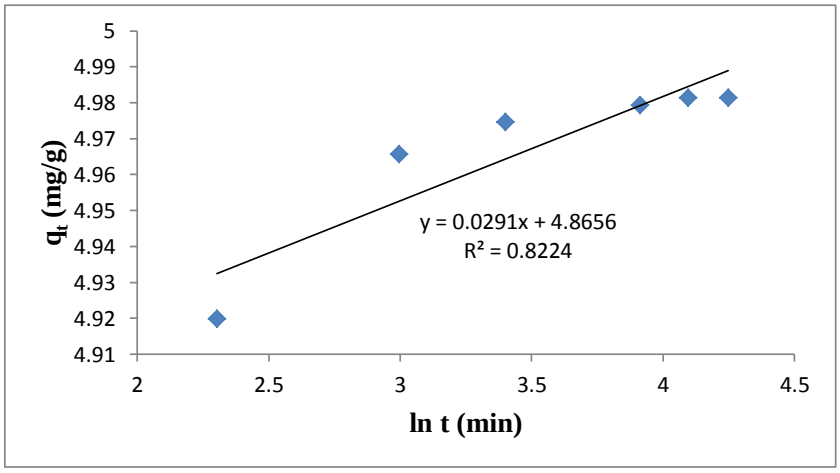

Figure 4.375: Elovich rate equation plot for TPT adsorption onto nZnO/fly ash

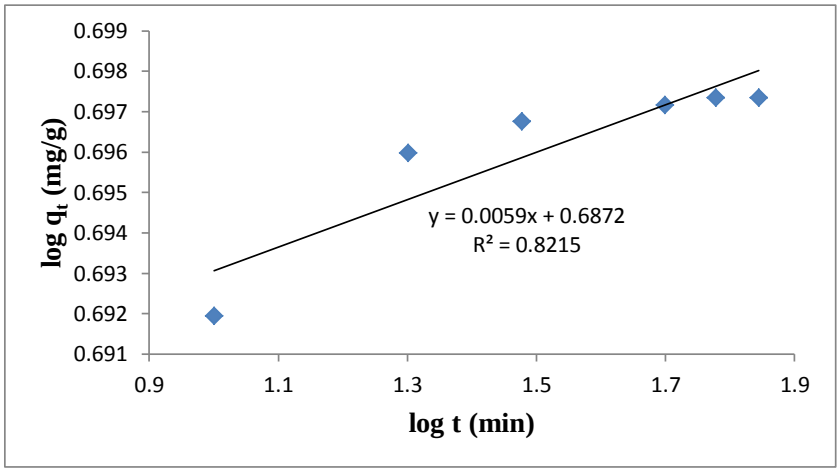

Figure 4.376: Fractional Power rate equation plot for TPT adsorption onto nZnO/fly ash

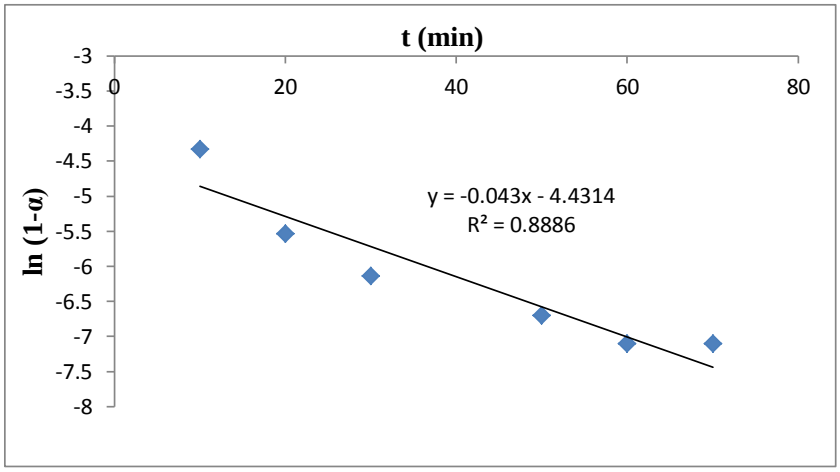

Figure 4.377: Intraparticle diffusivity plot for TPT adsorption onto nZnO/fly ash

Table 4.62: Kinetic model parameters for TPT adsorption onto nZnO/fly ash

Kinetic models	
Pseudo first-order	
k_1 (min^{-1})	0.04307
q_e (mg/g)	0.05932
R^2	0.8886
Pseudo second-order	
q_e (mg/g)	4.990
h_o (mg/g/min)	42.918
k_2 (g/mg/min)	1.7236
R^2	0.9999
Elovich	
β (g min/mg)	34.3643
α (g min^2/mg)	1.417 x 10^{74}
R^2	0.8224
Fractional Power	
v (min^{-1})	0.0059
k_3 (mg/g)	4.8663
k_3v (mg/g/min)	0.0287
R^2	0.8215
Intraparticle diffusivity	
k_p (min^{-1})	0.043
R^2	0.8886

The value of the correlation coefficient (R^2) of pseudo second-order kinetic model (> 0.99) is higher than the correlation coefficients of other models indicating that the kinetic model for the adsorption of TPT onto nZnO/fly ash composite is pseudo second-order. The intraparticle coefficient for the adsorption of TPT by the nZnO/fly ash composite was calculated and presented in Table 4.62 and the results also indicate that the power function model satisfactorily describes the time-dependence of TPT on the nZnO/fly ash composite since the value of the constant v is less than 1.

The value of the initial adsorption rate, h_o, obtained for the pseudo second-order kinetics is 42.918 mg/g/min. The amount of TPT adsorbed at equilibrium per unit weight of nZnO/fly ash composite (q_e) is 4.990 mg/g and the rate constant of pseudo second - order adsorption (k_2) is 1.7236 g/mg/min. The rate constants of other models are presented in Table 4.62.

4.12.19.3 Effect of pH

The effect of pH on the adsorption of TPT onto nZnO/fly ash composite was studied at pH 4 – 9. It was observed from Figure 4.378 that the percentage of TPT adsorbed by the nZnO/fly ash composite steadily increases as the pH of the solution increases from pH 4 to pH 8, and reaches equilibration afterwards.

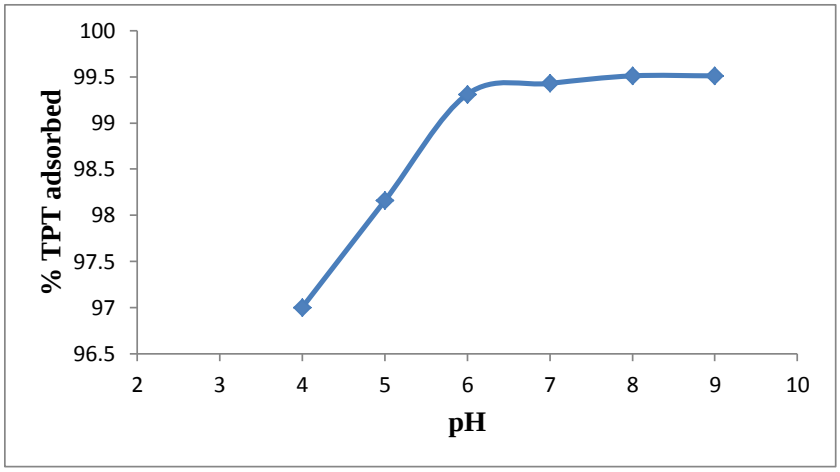

Figure 4.378: Effect of pH on TPT adsorption onto nZnO/fly ash

Experimental conditions: Concentration of TPT = 100 mg/L; Volume of TPT solution = 25 mL, Mass of nZnO/fly ash = 0.5 g; Contact time = 60 min; Stirring speed = 160 rpm, Temperature = 20 ^{o}C.

About 99.51% of TPT was removed from the initial concentration of 100 mg/L TPT by nZnO/fly ash composite at a contact time of 60 min, stirring speed of 160 rpm, temperature of 20 ^{o}C and pH 8. pH 8 was chosen as the optimum pH and was used for further studies.

4.12.19.4 Effect of stirring speed

The stirring speed on the adsorption of TPT onto nZnO/fly ash composite was studied at a stirring speed of 160 – 200 rpm. Figure 4.379 shows that the adsorption capacity of TPT onto the composite increases as the stirring speed of the mixture increases. The figure therefore shows that 99.66 % of TPT was removed from the initial concentration of 100 mg/L TPT by the nZnO/fly ash composite at a contact time of 60 min, pH 8, temperature of 20 ^{o}C and a stirring speed of 200 rpm. A stirring speed of 200rpm was used for further studies.

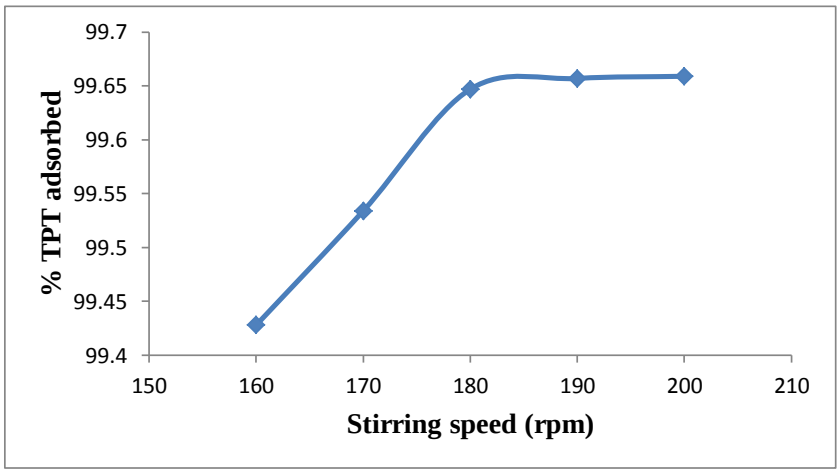

Figure 4.379: Effect of stirring speed on TPT adsorption onto nZnO/fly ash

Experimental conditions: Concentration of TPT = 100 mg/L; Volume of TPT solution = 25 mL, Mass of nZnO/fly ash = 0.5 g; Contact time = 60 min; Temperature = 20 ^{o}C.

4.12.19.5 Effect of initial concentration

The adsorption isotherms of the adsorption of TPT onto nZnO/fly ash composite were investigated by varying the initial TPT concentration from 12.5 to 200 mg/L at optimized adsorbent dose, contact time, pH and stirring speed established after optimization of all working parameters. The equilibrium data were fitted by Langmuir, Freundlich, Temkin and D-R isotherm models. Figure 4.380 therefore shows that the adsorption of TPT onto nZnO/fly ash composite increases as the initial TPT concentration increases from 12.5 to 100 mg/L.

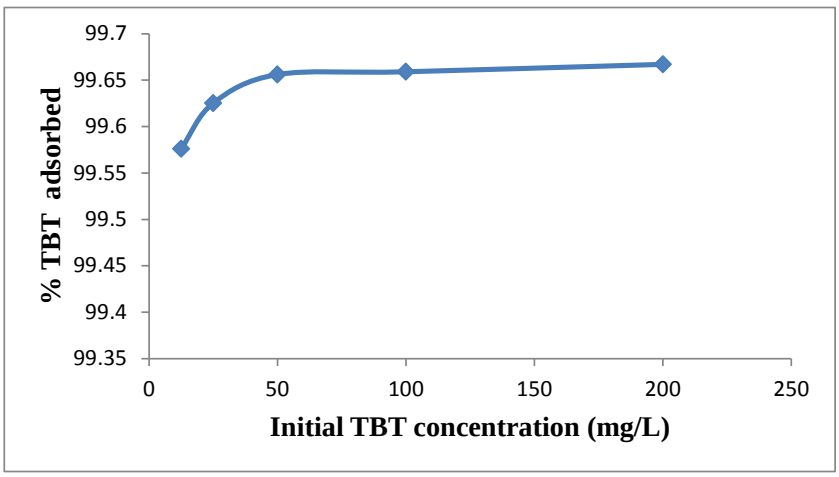

Figure 4.380: Percentage TPT adsorbed by nZnO/fly ash at various initial TPT concentrations

Experimental conditions: Volume of TPT solution = 25 mL, Mass of nZnO/fly ash = 0.5 g; pH = 8; Stirring speed = 200 rpm; Contact time = 60 min; Temperature = 20 ^{o}C.

4.12.19.5.1 Adsorption isotherms

The graphs of the adsorption isotherms are presented in Figures 4.381 – 4.384 and the parameters obtained for the models were given in Table 4.63. Table 4.63 and the figures show that the experimental data fitted well with the Freundlich isotherm model because the regression coefficient ($R^2 > 0.99$) is higher than for other models. The value of n_F, falling in the range 1 -10 also indicates favourable adsorption.

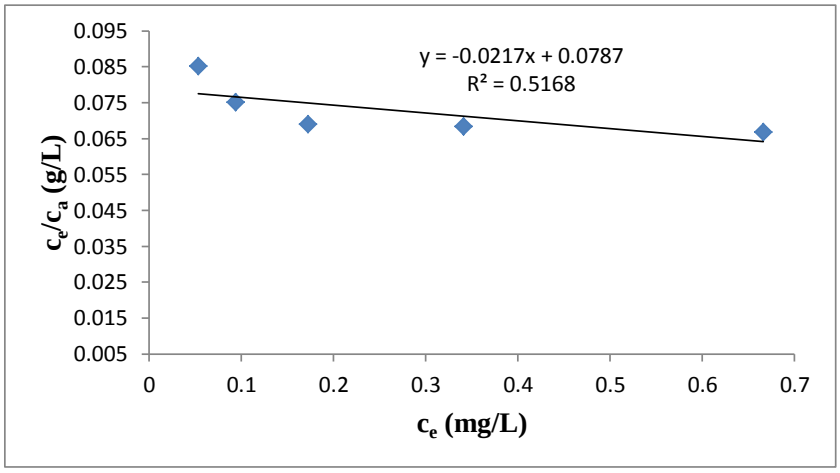

Figure 4.381: Langmuir isotherm for adsorption of TPT onto nZnO/fly ash

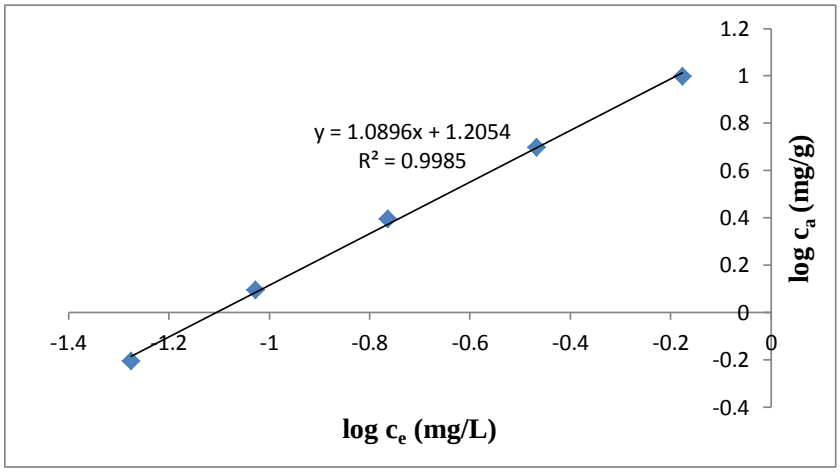

Figure 4.382: Freundlich isotherm for adsorption of TPT onto nZnO/fly ash

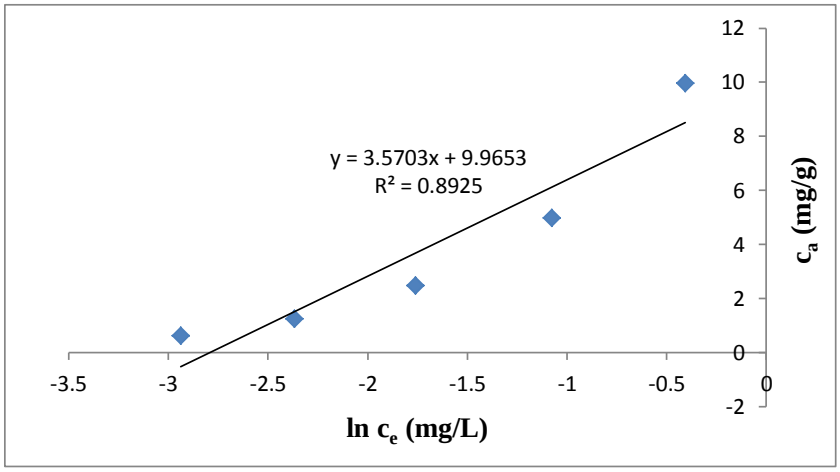

Figure 4.383: Temkin isotherm for adsorption of TPT onto nZnO/fly ash

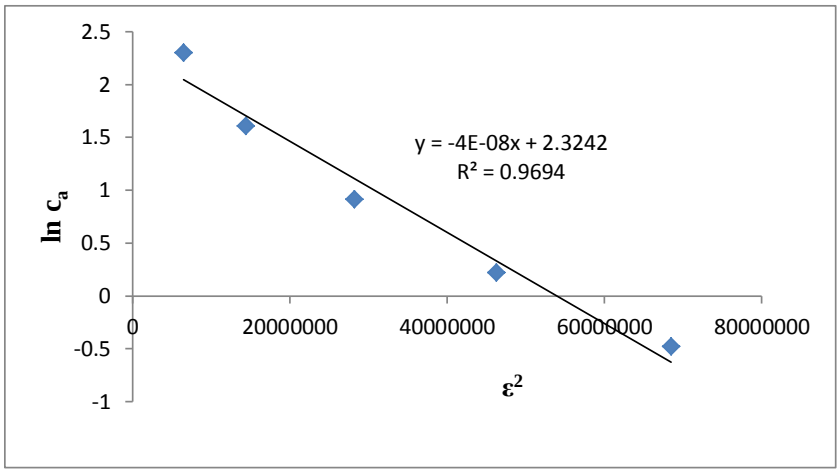

Figure 4.384: D-R isotherm for adsorption of TPT onto nZnO/fly ash

The negative value of the Langmuir constants, A_{max} (mg/g) and k_L (L/mg) for TPT adsorption onto nZnO/fly ash composite (Table 4.63) indicates the inadequacy fitting of experimental data to Langmuir model. The equilibrium model constants k_F, k_L, k_T and k_{D-R} for the adsorption of TPT onto nZnO/fly ash composite material are 16.047 mg/g $(L/mg)^{1/n}$, -0.2757 L/mg, 16.30 mg/L and 4.0 x 10^{-8} J^2/mol^2, respectively.

Table 4.63: Isotherms constants for the adsorption of TPT onto nZnO/fly ash

Equilibrium models	
Freundlich	
k_F [mg/g (L/mg)$^{1/n}$]	16.047
n_F	0.9178
R^2	0.9985
Langmuir	
K_L (L/mg)	-0.2757
A_{max} (mg/g)	-46.083
R^2	0.5168
Temkin	
n_T (L/g)	3.5703
k_T (mg/L)	16.300
b_T (J/mol)	682.296
R^2	0.8925
Dubinin-Redushkevich	
k_{D-R} (J^2/mol^2)	4.0 x 10^{-8}
q_m (mg/g)	10.2185
E (J/mol)	3535.53
R^2	0.9694

4.12.19.6 Effect of temperature

The experimental results obtained on the effect of temperature show that the adsorption capacity of TPT onto nZnO/fly ash composite decreases with increase in the solution temperature (Figure 4.385). This indicates that the adsorption of TPT onto the nZnO/fly ash is also exothermic.

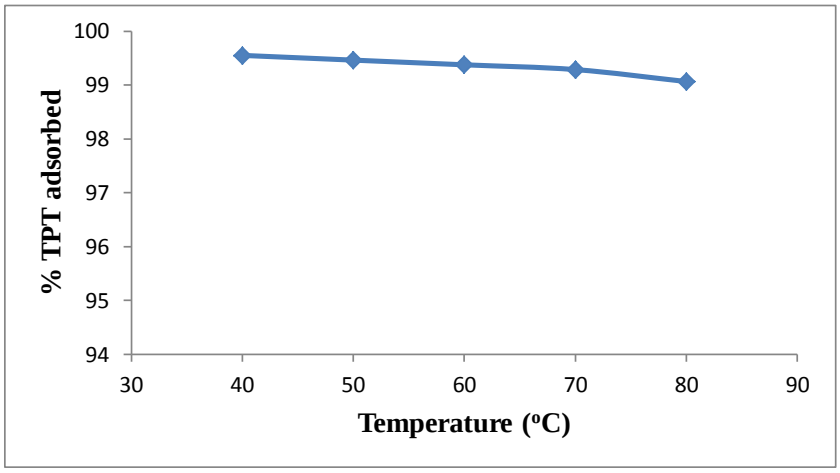

Figure 4.385: Effect of temperature on TPT adsorption onto nZnO/fly ash

Experimental conditions: Concentration of TPT = 100 mg/L; Volume of TPT solution = 25 mL, Mass of nZnO/fly ash = 0.5 g; Contact time = 60 min; pH = 8; Stirring speed = 200 rpm.

From Figure 4.385, approx. 99.07 % of TPT was removed from the initial concentration of 100 mg/L TPT by nZnO/fly ash composite at a contact time of 60 min, pH 8, stirring speed 200 rpm and temperature of 80 ^{o}C whereas 99.55 % TPT was removed at 40 ^{o}C at the same conditions. Figure 4.386 thus shows the Van't Hoff plot for the adsorption of TPT and the variation in the extent of adsorption with respect to temperature (ΔH^{o}, ΔS^{o}, and ΔG^{o}) are presented in Table 4.386.

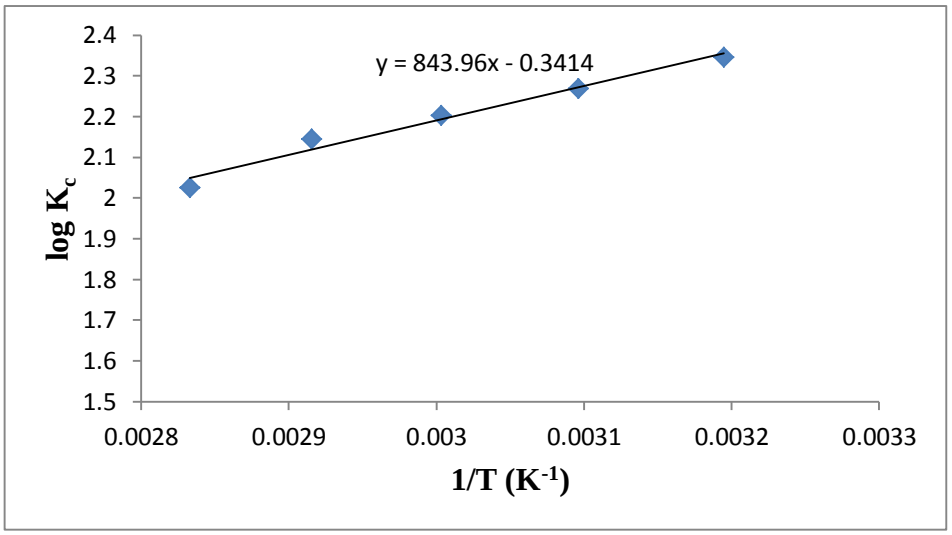

Figure 4.386: Van't Hoff Plot for the adsorption of TPT onto nZnO/fly ash

Table 4.64: Thermodynamic parameters for adsorption of TPT onto nZnO/fly ash

Temperature (°C)	ΔG° (kJ/mol)	ΔS° (J/K/mol)	ΔH° (kJ/mol)	K_c
40	-14.062	-6.5368	-16.159	222.21
50	-14.027			185.57
60	-14.042			159.51
70	-14.080			139.43
80	-13.688			106.07

The negative value of ΔH^{o} (-16.159 kJ/mol) for the intervals of temperatures studied (Table 4.64) also shows the exothermic nature of the adsorption process. The negative value of ΔS^{o} (-6.5368 J/K/mol) corresponds to a decrease in the degree of freedom of the adsorbed TPT, indicating a decrease in adsorbate concentration onto the solid phase. ΔG^{o} values were found to increase as the temperature increases, which indicate non-spontaneous adsorption and the degree of spontaneity of the reaction decreases with increase in temperature. K_c ranged 106.07 – 222.21.

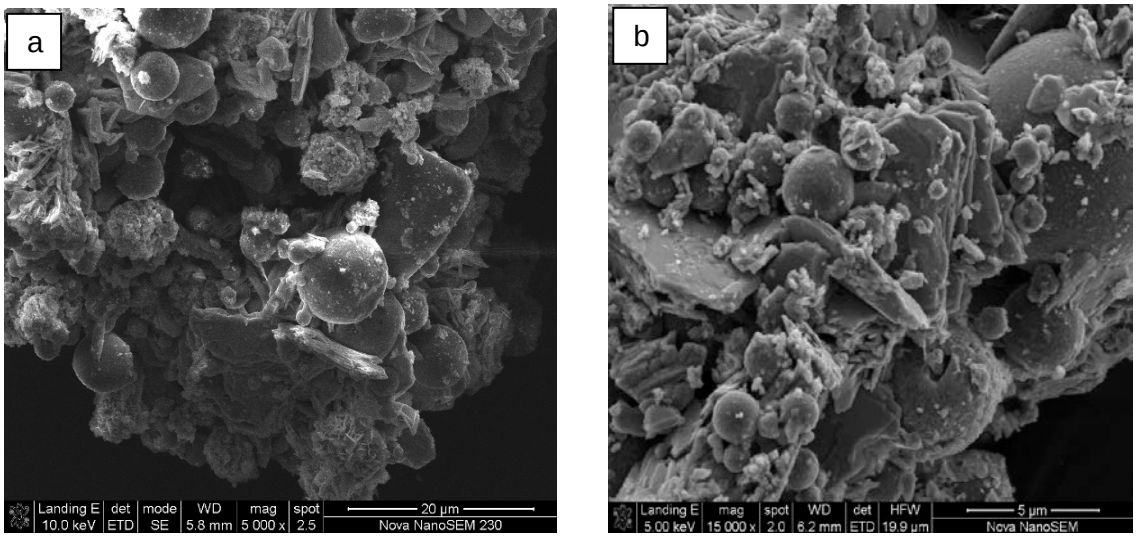

Figure 4.387: nZnO/fly ash before (a) and after (b) TPT adsorption

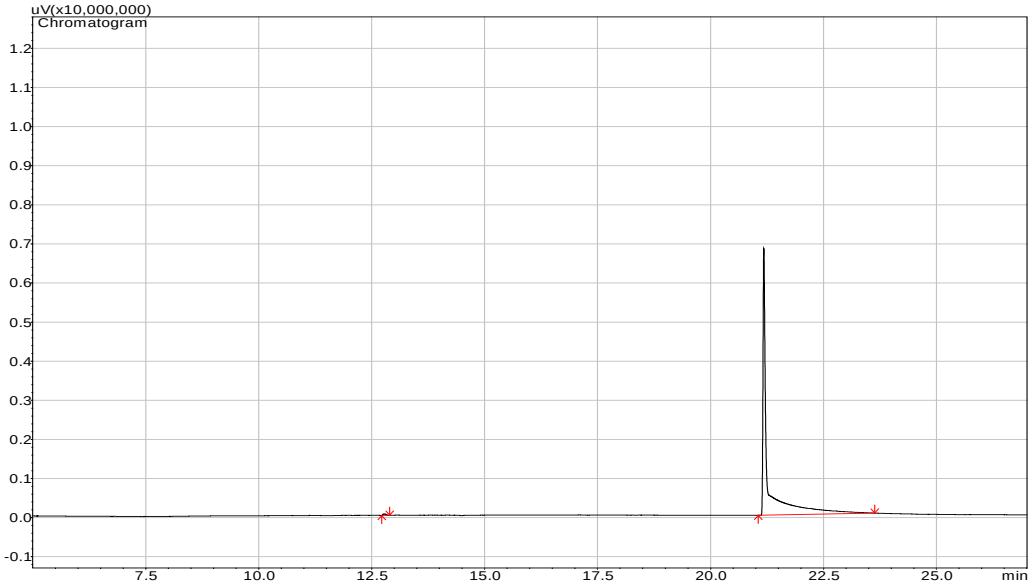

Figure 4.388: Representative TPT chromatogram after adsorption of 100 mg/L TPT with 0.5 g of nZnO/fly ash, contact time of 60 min, temperature 20 ^{o}C and a stirring speed of 200 rpm

The nZnO/fly ash composite material before and after the adsorption processes were subjected to SEM analysis as shown in Figure 4.387 while a representative TPT chromatogram after adsorption of 100 mg/L TPT with 0.5 g of nZnO/fly ash composite, contact time of 60 min, temperature 20 ^{o}C and a stirring speed of 200 rpm is as shown in Figure 4.388.

4.12.20 Comparison of TPT adsorption capacity of the precursor and composite materials

Figure 4.389 thus shows that 99.99 %, 96.54 %, 95.50 %, 96.92 %, 97.14 %, 99.99 %, 98.44 %, 98.98 % and 99.66 % TPT were removed from 25 mL of 100 mg/L TPT-contaminated artificial seawater using 0.5 g adsorbents at a contact time of 60 min, pH 8, stirring speed 200 rpm and a temperature of 20 ^{o}C by the activated carbon, fly ash, nFe_3O_4, $nSiO_2$, nZnO, fly ash/activated carbon, nFe_3O_4/fly ash, $nSiO_2$/fly ash and nZnO/fly ash composite, respectively. The adsorption of TPT onto activated carbon and fly ash/activated carbon composite is endothermic while TPT adsorption onto fly ash, nFe_3O_4, $nSiO_2$, nZnO, nFe_3O_4/fly ash, $nSiO_2$/fly ash and nZnO/fly ash composites is exothermic.

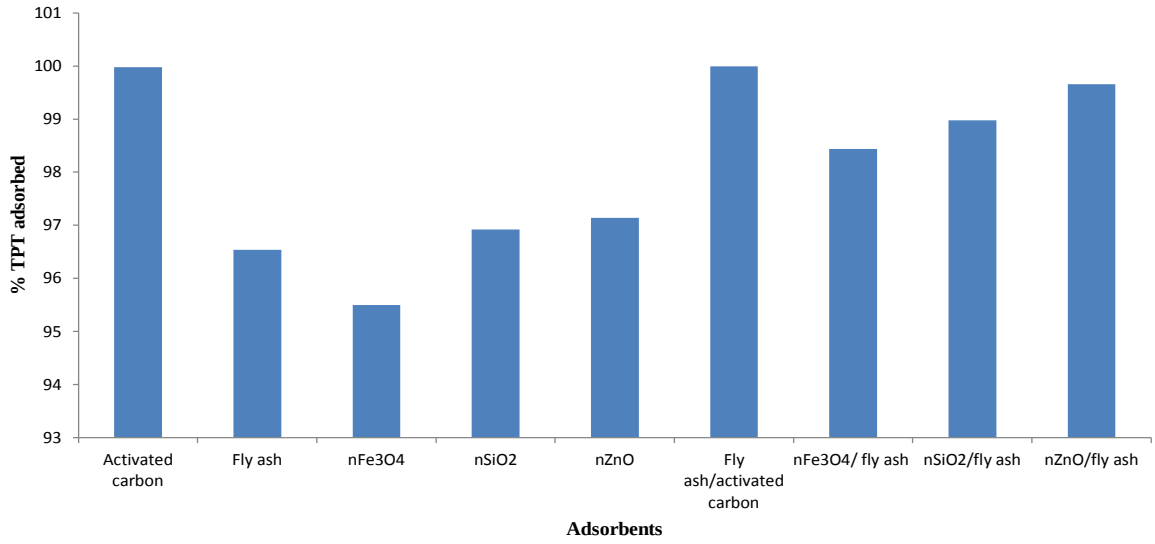

Figure 4.389: Percentage TPT removed from TPT-contaminated artificial seawater

Experimental conditions: Concentration of TPT = 100 mg/L; Volume of TPT solution = 25 mL, Mass of composite = 0.5 g; Contact time = 60 min; pH = 8; Stirring speed = 200 rpm, Temperature = 20 ^{o}C.

The value of h_o calculated from pseudo second-order rate equation for TPT by activated carbon, fly ash, nFe_3O_4, $nSiO_2$, nZnO, fly ash/activated carbon, nFe_3O_4/fly ash, $nSiO_2$/fly ash and nZnO/fly ash composites are 666.67, 19.378, 62.893, 11.990, 15.385, 666.67, 19.084, 4.799 and 42.918 mg/g min, respectively, thus indicating the higher TPT adsorption rate of activated carbon and fly ash/activated carbon composite compared to all other composites and the precursors.

The h_o values for TBT and TPT adsorption also shows that the rate at which TPT is adsorp unto the adsorbents is faster as compared to TBT. Radke et al., 2008 also reported that photolysis is faster in phenyltin derivatives as compared to butyltin compounds.

The adsorption of TPT by all the adsorbents follows a pseudo second-order kinetics model. This model depends on the assumption that chemisorption may be the rate-limiting step. In chemisorption, the TPT ions stick to the adsorbent surface by forming a chemical (usually covalent) bond and tend to find sites that maximize their coordination number with the surface. The applicability of Freundlich isotherm model to the adsorption of TPT onto the adsorbents is also based on the assumption that TPT adsorbs onto the heterogeneous surface of the adsorbents.

4.12.20.1 Application to the sorption of TPT from natural seawater

Optimal conditions for the adsorption of TPT from artificial seawater were applied to TPT removal from natural TPT – contaminated seawater (shipyard wastewater) obtained from Cape Town harbour. The physicochemical properties of the wastewater are presented in Table 4.65 and the percentage of TPT removed after adsorption of TPT contain in 25 mL of natural seawater by 0.5 g of adsorbents, contact time of 60 min and stirring speed of 200 rpm under natural condition is as shown in Figure 4.390.

Table 4.65: Physicochemical properties of TPT – contaminated natural seawater

Parameters	
Turbidity (NTU)	4.24
pH	6.75
Conductivity (mS/cm)	26.34
TDS (ppt)	13.17
Salinity (psu)	15.24
Resistivity (ohms)	38.0
TPT conc. (mg/L)	0.6432

Figure 4.390 shows that 99.90 %, 96.44 %, 95.37 %, 96.75 %, 97.03 %, 99.92 %, 98.42 %, 98.92 % and 99.58 % TPT were removed from natural seawater by activated carbon, fly ash, nFe_3O_4, $nSiO_2$, nZnO, fly ash/activated carbon, nFe_3O_4/fly ash, $nSiO_2$/fly ash and nZnO/fly ash composite, respectively. Activated carbon, fly ash/activated carbon and nZnO/fly ash composites therefore proved more efficient to the removal of TPT from TPT – contaminated natural seawater when compared with all other adsorbents.

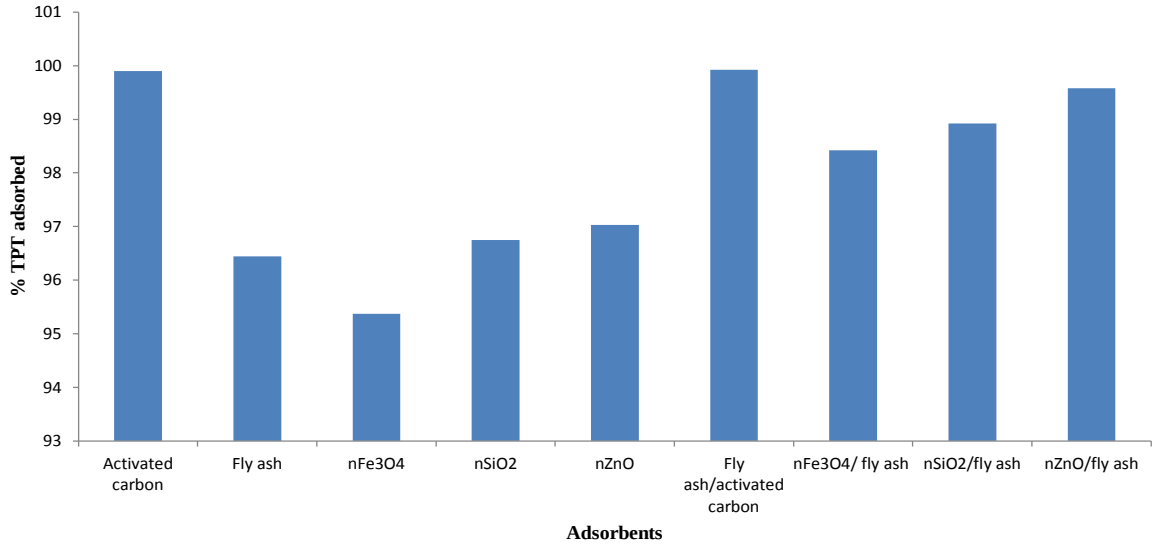

Figure 4.390: Percentage TPT removed from TPT- contaminated natural seawater

Experimental conditions: Concentration of TPT = 0.6432 mg/L; Volume of natural seawater = 25 mL, Mass of composite = 0.5 g; Contact time = 60 min; pH = ; Stirring speed = 200 rpm; Temperature = 20 ^{o}C.

The TPT removal efficiency is in the order: fly ash/activated carbon > activated carbon > nZnO/fly ash composite > $nSiO_2$/fly ash composite > nFe_3O_4/fly ash composite > nZnO > $nSiO_2$ > fly ash > nFe_3O_4 .

The percentage TPT adsorbed from the contaminated natural seawater was slightly lower than the percentage removed from TPT – contaminated artificial seawater, this could be attributed to the adsorption of other species such as metal ions that might be present in the contaminated natural seawater.

4.12.21 Adsorption of TBT from TBT- contaminated water onto nFe_3O_4/fly ash/activated carbon composite

4.12.21.1 Effect of adsorbent amount

The amount of nFe_3O_4/fly ash/activated carbon composite material ranging from 0.0625 – 1.0 g per 25 mL of TBT solution was investigated on the efficiency of the adsorption of TBT from TBT – contaminated water. A graph of the percentage of TBT adsorbed (C_a), mg/g onto nFe_3O_4/fly ash/activated carbon composite was plotted against the adsorbent amount (Figure 4.391).

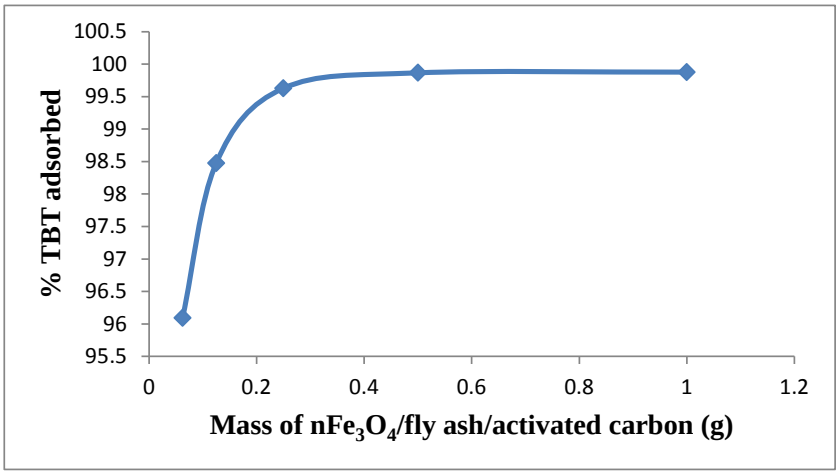

Figure 4.391: Adsorption efficiencies of TBT onto nFe_3O_4/fly ash/activated carbon

Experimental conditions: Concentration of TBT = 100 mg/L; Volume of TBT solution = 25 mL, Contact time = 60 min; Stirring speed = 160 rpm, Temperature = 20 ^oC.

It was observed that the percentage of TBT adsorbed increases with increasing nFe_3O_4/fly ash/activated carbon composite amount, reaching an optimum at 0.5 g, corresponding to 99.87 %. 0.5 g was selected as the optimum nFe_3O_4/fly ash/activated carbon composite amount used for further studies.

4.12.21.2 Effect of contact time

The kinetic study of TBT from TBT – contaminated water onto nFe_3O_4/fly ash/activated carbon composite was carried out by shaking 0.5 g of the composite in 25 mL of TBT solutions with an initial concentration of 100 mg/L at 20 ^oC. After pre-defined contact time (10-70 min), the aqueous samples were filtered, and the concentration of TBT in the filtrate determined.

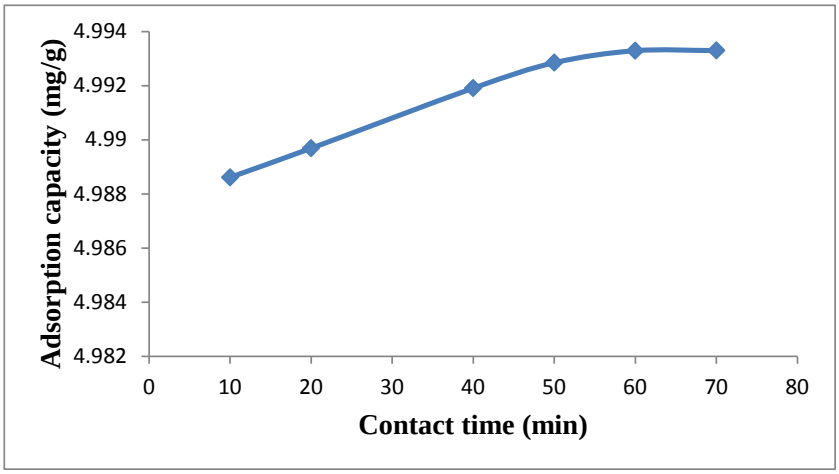

Figure 4.392: Effect of contact time on TBT adsorption onto nFe_3O_4/fly ash/activated carbon

Experimental conditions: Concentration of TBT = 100 mg/L; Volume of TBT solution = 25 mL, Mass of nFe_3O_4/fly ash/activated carbon = 0.5 g; Stirring speed = 160 rpm, Temperature = 20 ^oC.

Figure 4.392 thus shows the effect of contact time on adsorption of TBT by the nFe_3O_4/fly ash/activated carbon composite material. The TBT removal efficiencies at different time intervals ranging from 10 – 70 min were obtained. It was observed that equilibrium was achieved within 60 min and the corresponding TBT removal efficiency for nFe_3O_4/fly ash/activated carbon composite from the initial concentration of 100 mg/L TBT reaches 4.993 mg/g (99.87 %).

4.12.21.2.1 Adsorption kinetics

Figures 4.393 – 4.397 thus show the graphs of the pseudo first-order, pseudo second-order, Elovich, fractional power and intraparticle diffusivity kinetics, respectively while Table 4.66 shows the evaluated parameters of the kinetics models. The value of the correlation coefficient (R^2) of the pseudo second-order kinetic model (> 0.99) is higher than that of other models indicating that the kinetic model for the adsorption of TBT onto nFe_3O_4/fly ash/activated carbon composite is pseudo second-order.

The intraparticle coefficient for the adsorption of TBT onto nFe_3O_4/fly ash/activated carbon composite was calculated and the results also indicate that the power function model satisfactorily describes the time-dependence of TBT onto the nFe_3O_4/fly ash/activated carbon composite as the value of the constant v is less than 1.

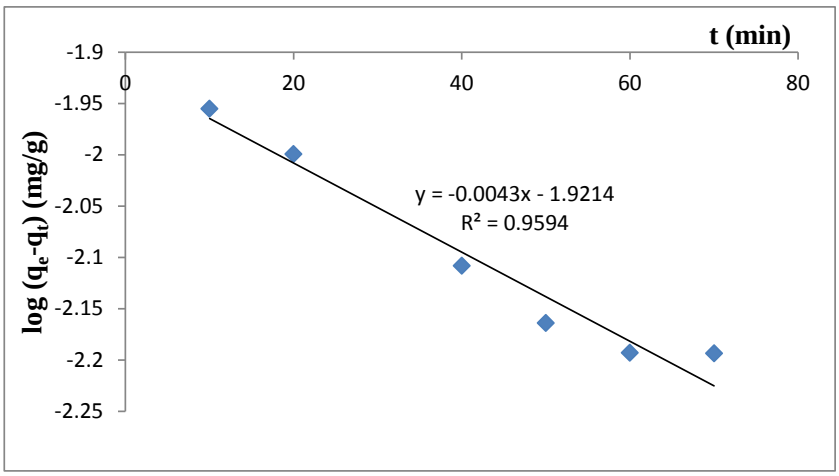

Figure 4.393: Pseudo first-order rate equation plot for TBT adsorption onto nFe_3O_4/fly ash/activated carbon

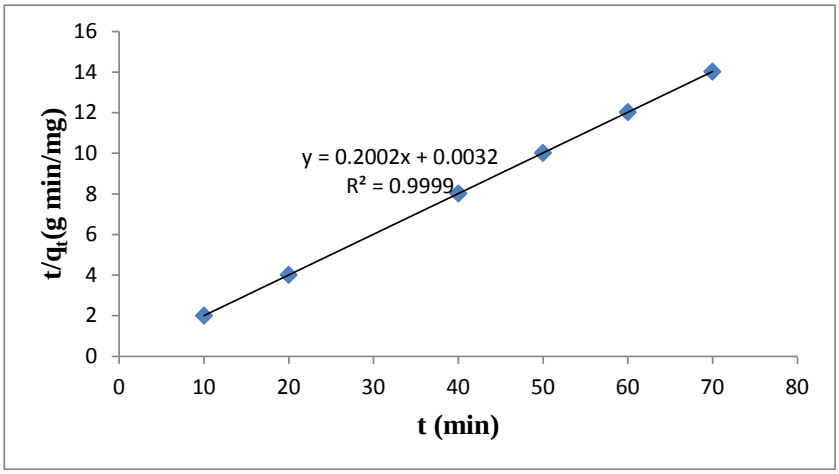

Figure 4.394: Pseudo second-order rate equation plot for TBT adsorption onto nFe_3O_4/fly ash/activated carbon

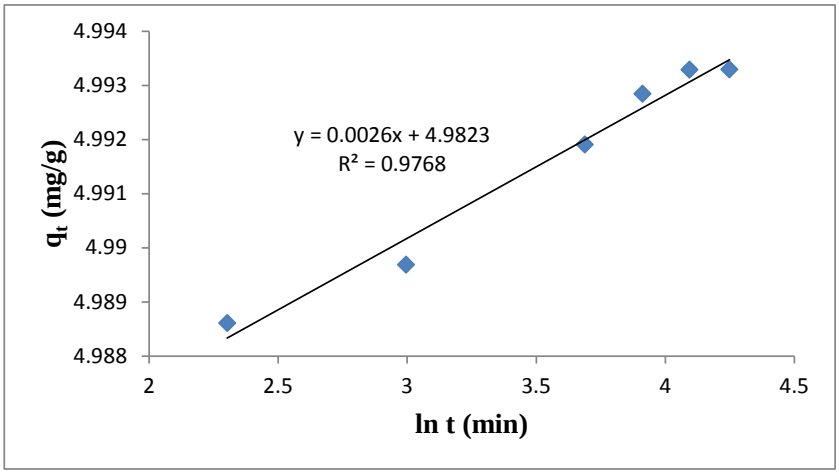

Figure 4.395: Elovich rate equation plot for TBT adsorption onto nFe_3O_4/fly ash/activated carbon

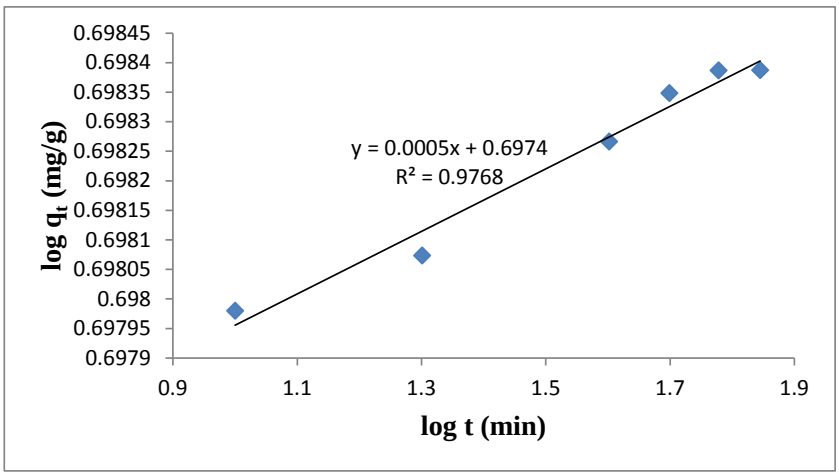

Figure 4.396: Fractional Power rate equation plot for TBT adsorption onto nFe_3O_4/fly ash/activated carbon

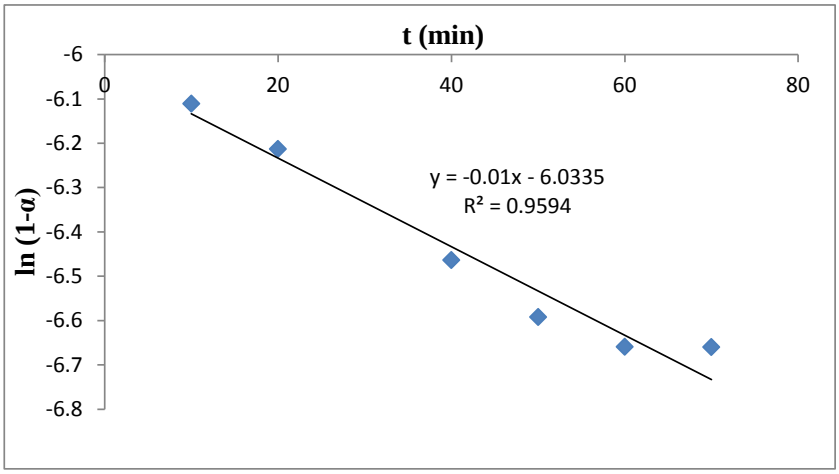

Figure 4.397: Intraparticle diffusivity plot for TBT adsorption onto nFe_3O_4/fly ash/activated carbon

The value of the initial adsorption rates, h_o, obtained for the pseudo second-order kinetics of the adsorption of TBT onto nFe_3O_4/fly ash/activated carbon composite is 312.50 mg/g/min. The kinetic model constants k_1, k_2, β, α_E, k_3 and k_p obtained as presented in Table 4.66 are 0.0099 min^{-1}, 12.525 g/mg/min, 384.62 gmin/mg, 6.5 x 10^{834} $gmin^2/mg$, 4.9820 mg/g and 0.01 min^{-1}, respectively.

Table 4.66: Kinetic model parameters for TBT adsorption onto nFe_3O_4/fly ash/activated carbon

Kinetic models	
Pseudo first-order	
k_1 (min^{-1})	0.0099
q_e (mg/g)	0.0120
R^2	0.9594
Pseudo second-order	
q_e (mg/g)	4.9950
h_o (mg/g/min)	312.50
k_2 (g/mg/min)	12.525
R^2	0.9999
Elovich	
β (g min/mg)	384.62
α (g min^2/mg)	6.5×10^{834}
R^2	0.9768
Fractional Power	
v (min^{-1})	0.0005
k_3 (mg/g)	4.9820
k_3v (mg/g/min)	0.0025
R^2	0.9768
Intraparticle diffusivity	
k_p (min^{-1})	0.01
R^2	0.9594

4.12.21.3 Effect of pH

The effect of pH on the adsorption of TBT from TBT – contaminated water onto the nFe_3O_4/fly ash/activated carbon composite was studied at pH 4 – 9. The percentage TBT adsorbed by nFe_3O_4/fly ash/activated carbon composite steadily increases as the pH of the solution increases from pH 4 to pH 8, and reaches equilibration afterwards. pH 8 was used for further studies.

Figure 4.398 therefore shows that about 99.97 % TBT was removed from the initial concentration of 100 mg/L TBT by the nFe_3O_4/fly ash/activated carbon composite at a contact time of 60 min, stirring speed of 160 rpm, pH 8 and a temperature of 20 ^oC.

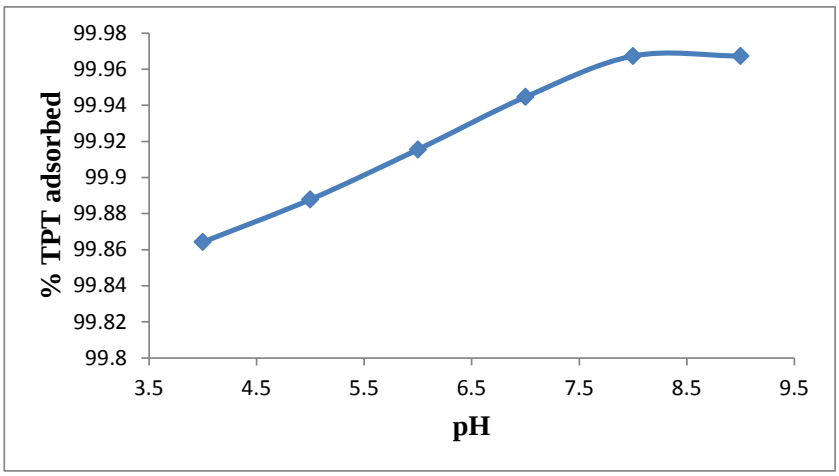

Figure 4.398: Effect of pH on TBT adsorption onto nFe_3O_4/fly ash/activated carbon

Experimental conditions: Concentration of TBT = 100 mg/L; Volume of TBT solution = 25 mL, Mass of nFe_3O_4/fly ash/activated carbon = 0.5 g; Contact time = 60 min; Stirring speed = 160 rpm, Temperature = 20 ^oC.

4.12.21.4 Effect of stirring speed

The effect of stirring speed on the adsorption of TBT from TBT – contaminated water onto the nFe_3O_4/fly ash/activated carbon composite material was studied at a stirring speed of 160 – 200 rpm. Figure 4.399 shows that the adsorption capacity of TBT onto the composite increases with increasing stirring speed from 160 rpm – 190 rpm, after which equilibration was attained.

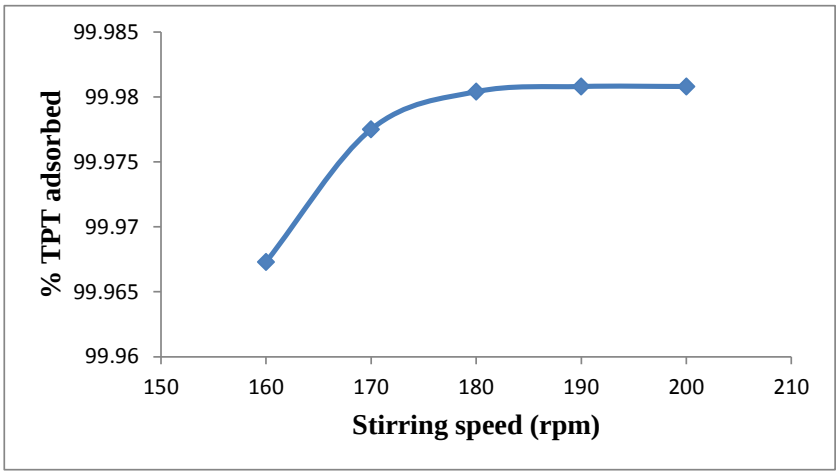

Figure 4.399: Effect of stirring speed on TBT adsorption onto nFe_3O_4/fly ash/activated carbon

Experimental conditions: Concentration of TBT = 100 mg/L; Volume of TBT solution = 25 mL, Mass of nFe_3O_4/fly ash/activated carbon = 0.5 g; pH = 8; Contact time = 60 min; Temperature = 20 ^oC.

The figure also shows that about 99.98 % TBT was removed from the initial concentration of 100 mg/L TBT by nFe_3O_4/fly ash/activated carbon composite at a contact time of 60 min, pH 8, a temperature of 20 ^oC and a stirring speed of 200 rpm. 200rpm was therefore used for further studies.

4.12.21.5 Effect of initial concentration

The results obtained on the effect of initial TBT concentration (Figure 4.600) show that the adsorption of TBT onto nFe_3O_4/fly ash/activated carbon composite increases as the initial TBT concentration increases from 12.5 to 100 mg/L, indicating that adsorption is also favourable for the higher TBT concentrations that have been investigated.

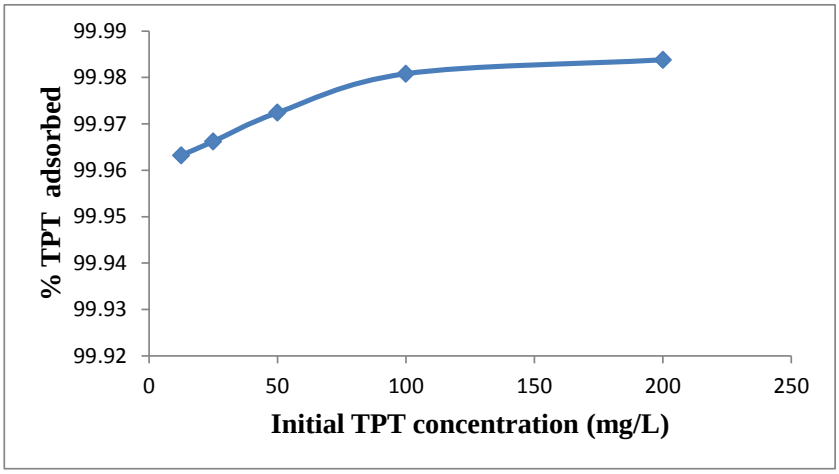

Figure 4.400: Percentage TBT adsorbed by nFe_3O_4/fly ash/activated carbon at various initial TBT concentrations

Experimental conditions: Volume of TBT solution = 25 mL, Mass of nFe_3O_4/fly ash/activated carbon = 0.5 g; pH = 8; Stirring speed = 200 rpm; Contact time = 60 min; Temperature = 20 ^oC.

4.12.21.5.1 Adsorption isotherms

The adsorption isotherm parameters obtained from the equilibrium models for the adsorption of TBT onto nFe_3O_4/fly ash/activated carbon composite were given in Table 4.67 and the graphs are presented in Figures 4.401 – 4.404. The figures and table show that the experimental data fitted well with the Freundlich isotherm and the value of n_F, for the adsorption of TBT onto nFe_3O_4/fly ash/activated carbon composite, falling in the range 1 -10 indicates favourable adsorption.

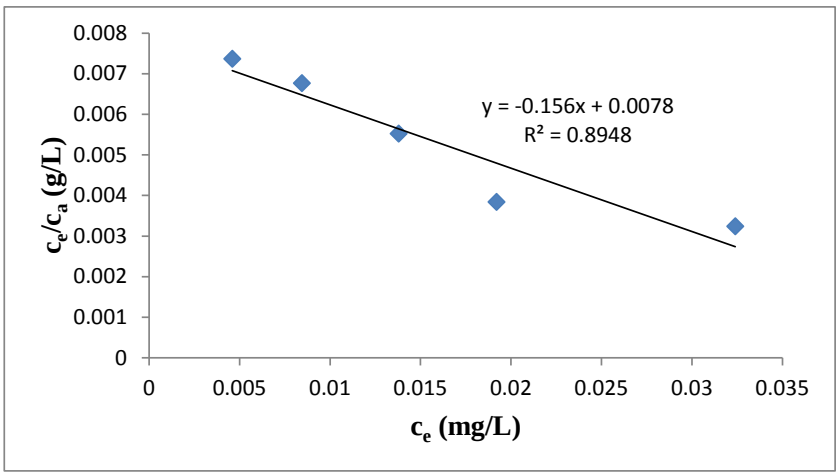

Figure 4.401: Langmuir isotherm for adsorption of TBT onto nFe_3O_4/fly ash/activated carbon

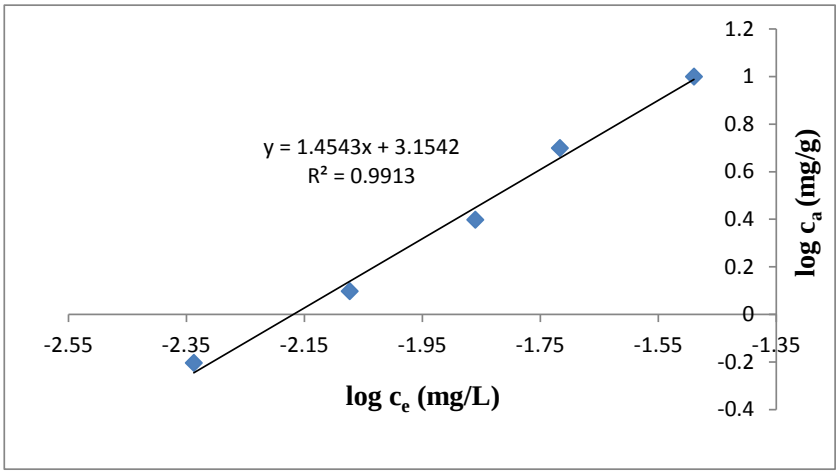

Figure 4.402: Freundlich isotherm for adsorption of TBT onto nFe_3O_4/fly ash/activated carbon

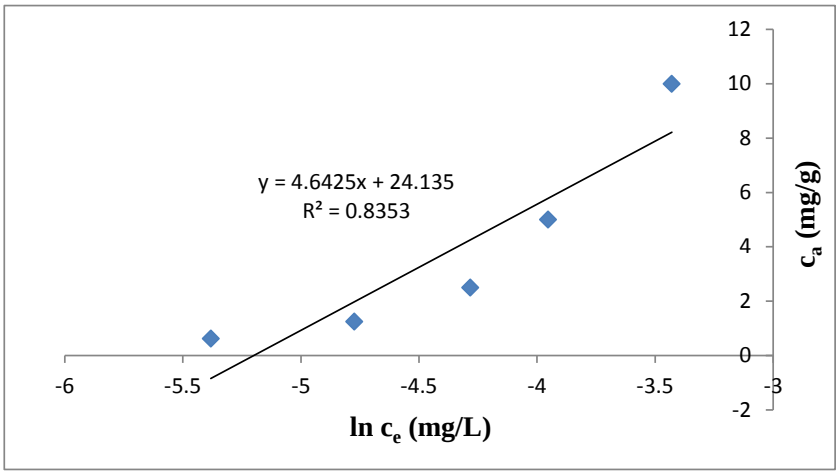

Figure 4.403: Temkin isotherm for adsorption of TBT onto nFe_3O_4/fly ash/activated carbon

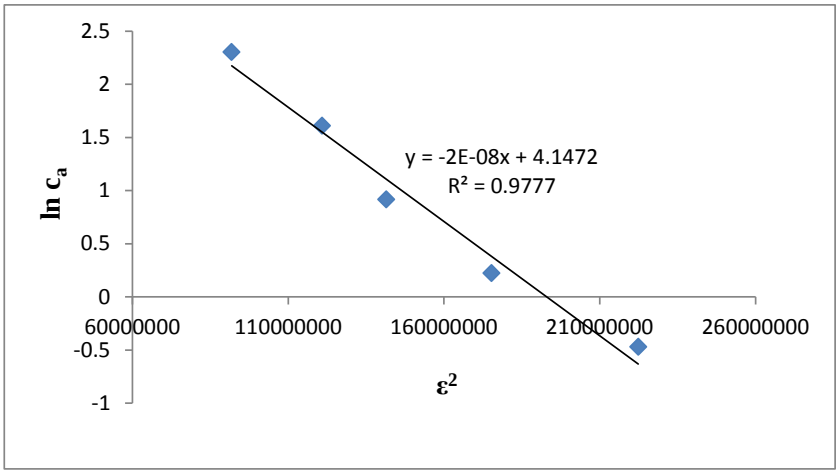

Figure 4.404: D-R isotherm for adsorption of TBT onto nFe_3O_4/fly ash/activated carbon

Table 4.67: Isotherms constants for the adsorption of TBT onto nFe_3O_4/fly ash/activated carbon

Equilibrium models	
Freundlich	
k_F [mg/g (L/mg)$^{1/n}$]	1426.3
n_F	0.6876
R^2	0.9913
Langmuir	
K_L (L/mg)	-20.0
A_{max} (mg/g)	-6.4103
R^2	0.8948
Temkin	
n_T (L/g)	4.6425
k_T (mg/L)	181.04
b_T (J/mol)	524.72
R^2	0.8353
Dubinin-Redushkevich	
k_{D-R} (J^2/mol^2)	2.0 X 10^{-8}
q_m (mg/g)	63.257
E (J/mol)	5000.0
R^2	0.9777

The negative value of the Langmuir constants, $A_{\max}$ (mg/g) and k_L (L/mg) for adsorption of TBT onto nFe_3O_4/fly ash/activated carbon composite in Table 4.67 indicates the inadequacy of the Langmuir model to fit the adsorption process. Table 4.67 also shows that the values of k_F, k_L, k_T and k_{D-R} constants obtained for the adsorption of TBT onto nFe_3O_4/fly ash/activated carbon composite material are 1426.3 mg/g (L/mg)$^{1/n}$, -20.0 L/mg, 181.04 mg/L and 2.0 x 10^{-8} J^2/mol^2, respectively.

4.12.21.6 Effect of temperature

The experimental results obtained on the effect of temperature for the adsorption of TBT onto nFe_3O_4/fly ash/activated carbon composite material (Figure 4.405) show that the adsorption capacity of nFe_3O_4/fly ash/activated carbon composite increases with increase in the solution temperature. This indicates that the adsorption of TBT from TBT – contaminated water onto nFe_3O_4/fly ash/activated carbon composite is endothermic.

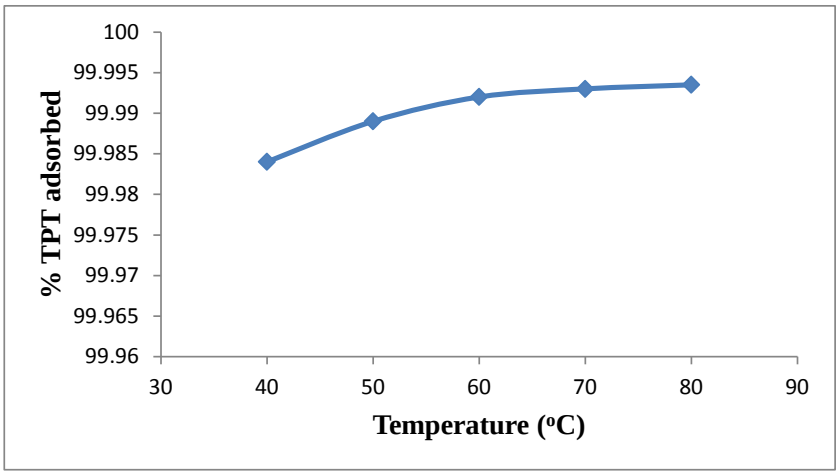

Figure 4.405: Effect of temperature on TBT adsorption onto nFe_3O_4/fly ash/activated carbon

Experimental conditions: Concentration of TBT = 100 mg/L; Volume of TBT solution = 25 mL, Mass of nFe_3O_4/fly ash/activated carbon = 0.5 g; Contact time = 60 min; pH = 8; Stirring speed = 200 rpm.

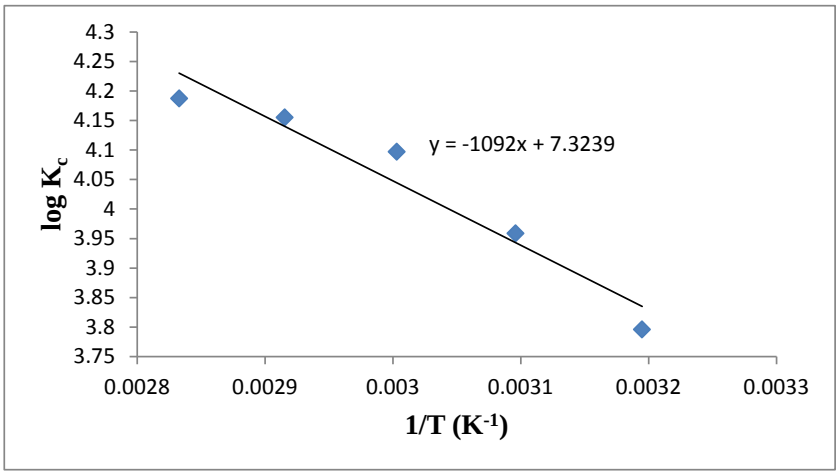

Figure 4.406: Van't Hoff Plot for the adsorption of TBT onto nFe_3O_4/fly ash/activated carbon

Approximately 99.98 % of TBT was removed from the initial concentration of 100 mg/L TBT by nFe_3O_4/fly ash/activated carbon composite at a temperature of 80 ^oC, 60 min contact time, pH 8 and a stirring speed of 200 rpm. Figure 4.406 thus shows the Van't Hoff plot for the

adsorption of TBT onto nFe_3O_4/fly ash/activated carbon composite material while ΔH^o, ΔS^o, and ΔG^o are presented in Table 4.68.

Table 4.68: Thermodynamic parameters for adsorption of TBT onto nFe_3O_4/fly ash/activated carbon

Temperature (°C)	ΔG° (kJ/mol)	ΔS° (J/K/mol)	ΔH° (kJ/mol)	K_c
40	-22.744	140.232	20.908	6249.0
50	-24.477			9089.9
60	-26.116			12499.0
70	-27.282			14284.7
80	-28.294			15383.6

The positive value of ΔH^o for the intervals of temperatures studied (20.908 kJ/mol) also shows the endothermic nature of the adsorption process. The positive value of ΔS^o (140.232 J/K/mol) corresponds to increase in degree of freedom of the adsorbed TBT onto nFe_3O_4/fly ash/activated carbon composite and suggest the increase in concentration of adsorbate in solid–solution interface indicating an increase in adsorbate concentration onto the solid phase. It is evident from Table 4.68 that ΔG^o values were found to be more negative as the temperature increases, which indicates that the adsorption efficiency of TBT onto nFe_3O_4/fly ash/activated carbon composite increases with increase in temperature.

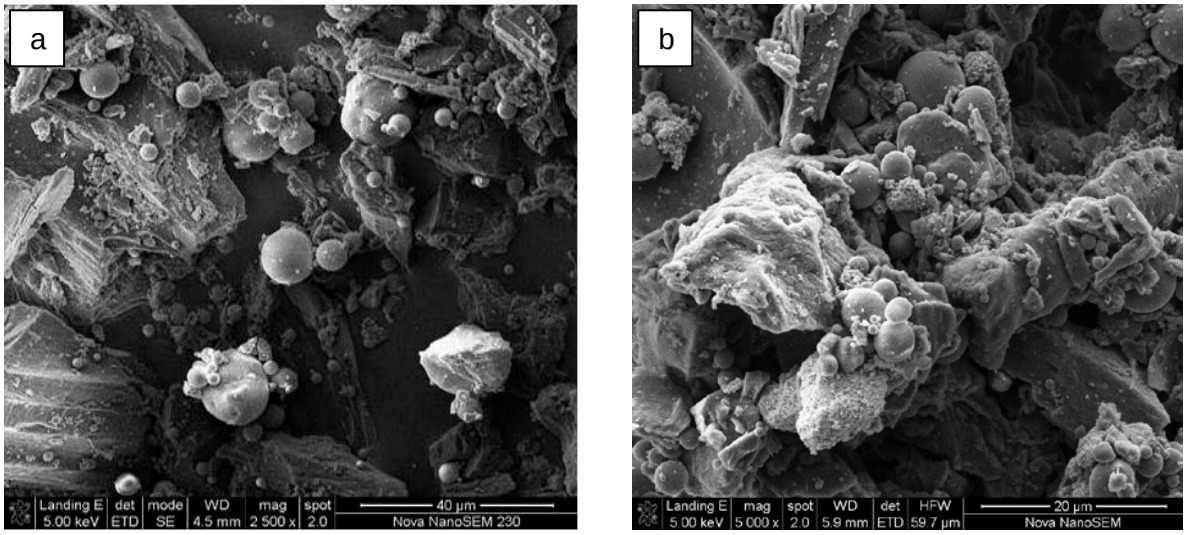

Figure 4.407: nFe_3O_4/fly ash/activated carbon before (a) and after (b) TBT adsorption

Figure 4.408: Representative TBT chromatogram after adsorption of 100 mg/L TBT with 0.5 g of nFe_3O_4/fly ash/activated carbon, contact time of 60 min, temperature 20 ^oC and a stirring speed of 200 rpm

The SEM analysis of nFe_3O_4/fly ash/activated carbon composite before and after adsorption is presented in Figure 4.407 and the TBT chromatogram after adsorption of 100 mg/L TBT with 0.5 g of nFe_3O_4/fly ash/activated carbon composite, 60 min contact time, temperature 20 ^oC and a stirring speed of 200 rpm is as shown in Figure 4.408.

4.12.22 Adsorption of TPT from TPT-contaminated water onto $nSiO_2$/fly ash/activated carbon composite

4.12.22.1 Effect of adsorbent amount

The results on the effect of adsorbent amount on the adsorption of TPT from TPT – contaminated water by the $nSiO_2$/fly ash/activated carbon composite material as shown in Figure 4.409 indicate that the percentage of TPT adsorption increases with increasing $nSiO_2$/activated carbon composite amount, reaching an optimum at 0.5 g, corresponding to 99.92 % removal.

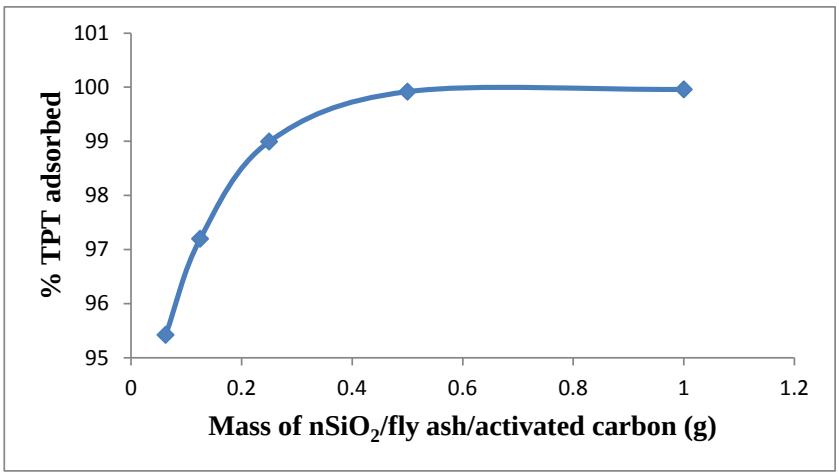

Figure 4.409: Adsorption efficiencies of TPT onto $nSiO_2$/fly ash/activated carbon

Experimental conditions: Concentration of TPT = 100 mg/L; Volume of TPT solution = 25 mL, Contact time = 60 min; Stirring speed = 160 rpm, Temperature = 20 ^{o}C.

4.12.22.2 Effect of contact time

Figure 4.410 shows the effect of contact time on the adsorption of TPT from TPT – contaminated water onto $nSiO_2$/fly ash/activated carbon composite material. The TPT removal efficiency at different time intervals ranging from 10 – 70 min were obtained.

It was therefore observed from Figure 4.410 that equilibrium was approximately achieved within 60 min. The amount of TPT removed at a contact time of 60 min from the initial TPT concentration of 5.0 mg/g by the $nSiO_2$/fly ash/activated carbon composite is 4.996 mg/g (99.92 % TPT removal). 60 min was therefore chosen for further studies.

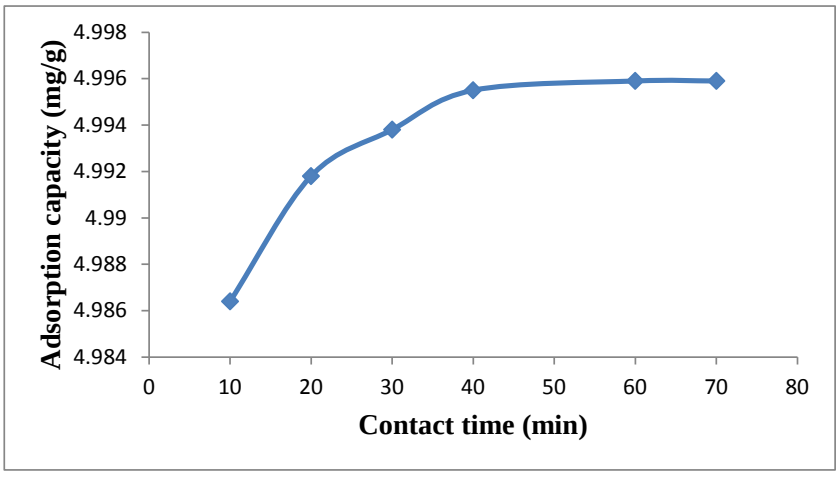

Figure 4.410: Effect of contact time on TPT adsorption onto $nSiO_2$/fly ash/activated carbon

Experimental conditions: Concentration of TPT = 100 mg/L; Volume of TPT solution = 25 mL, Mass of $nSiO_2$/fly ash/activated carbon = 0.5 g; Stirring speed = 160 rpm, Temperature = 20 ^{o}C.

4.12.22.2.1 Adsorption kinetics

Figures 4.411 – 4.415 show the pseudo first-order, pseudo second-order, Elovich, fractional power and intraparticle diffusivity kinetic plots while Table 4.69 shows the evaluated parameters of the kinetics models.

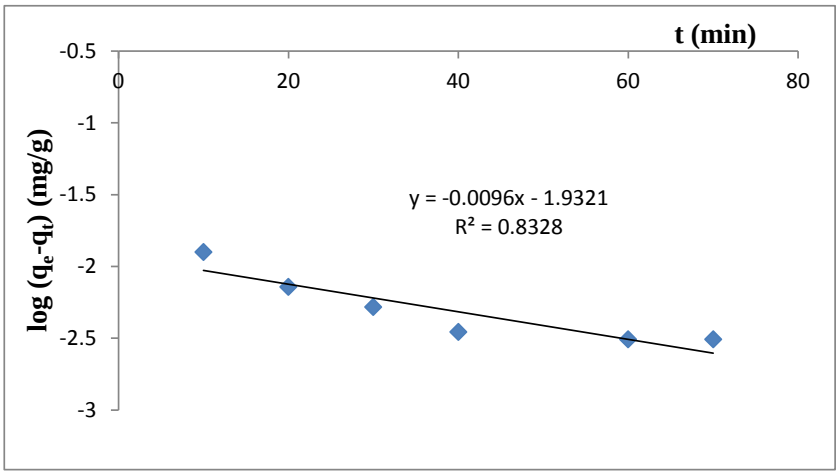

Figure 4.411: Pseudo first-order rate equation plot for TPT adsorption onto $nSiO_2$/fly ash/activated carbon

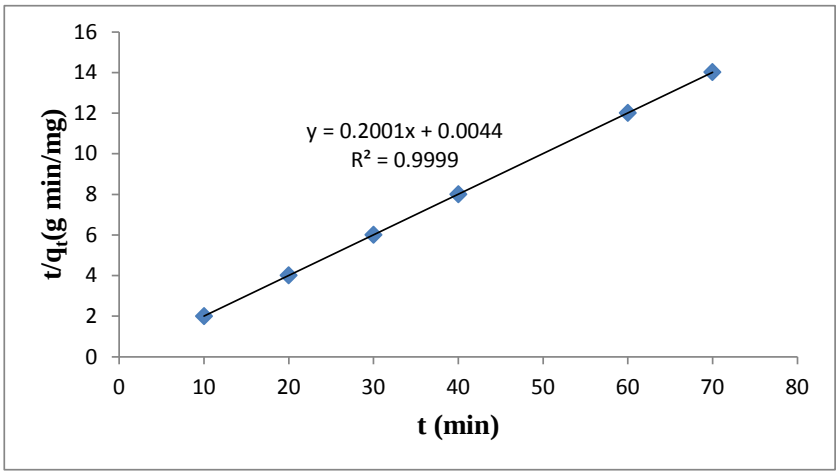

Figure 4.412: Pseudo second-order rate equation plot for TPT adsorption onto $nSiO_2$/fly ash/activated carbon

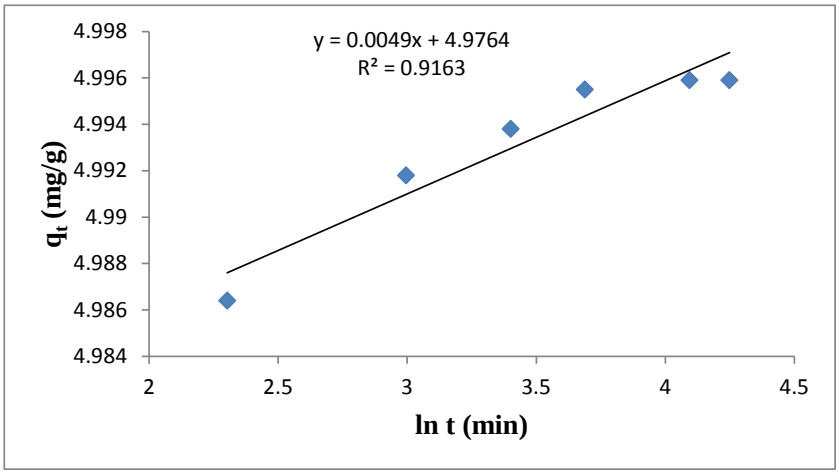

Figure 4.413: Elovich rate equation plot for TPT adsorption onto $nSiO_2$/fly ash/activated carbon

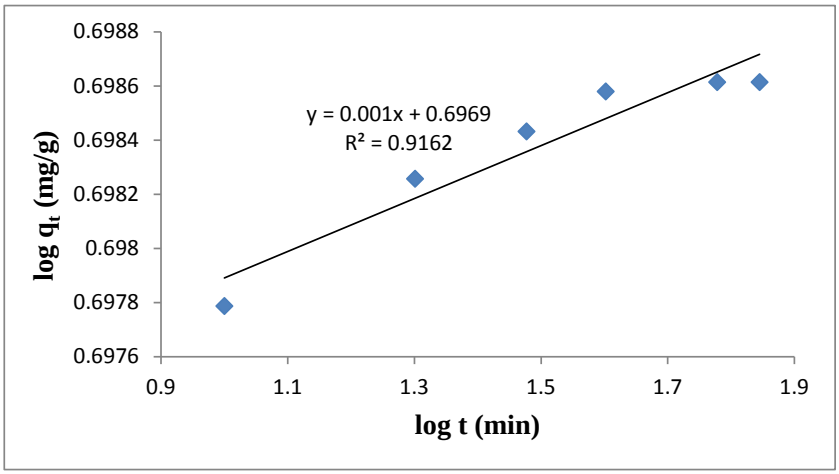

Figure 4.414: Fractional Power rate equation plot for TPT adsorption onto $nSiO_2$/fly ash/activated carbon

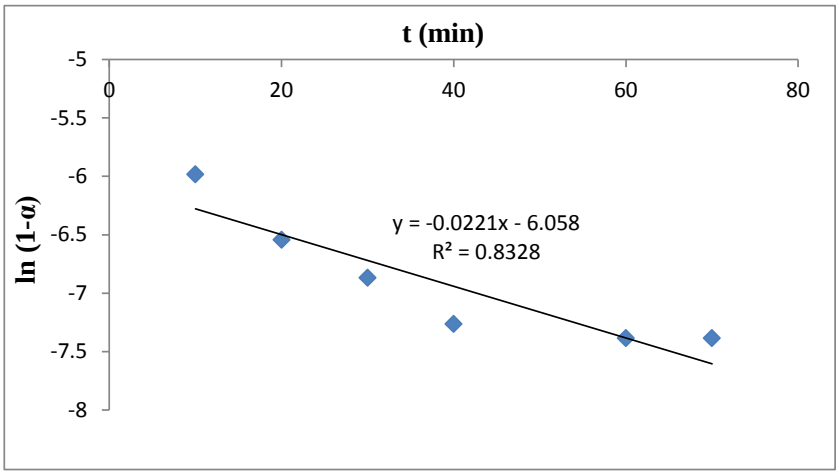

Figure 4.415: Intraparticle diffusivity plot for TPT adsorption onto $nSiO_2$/fly ash/activated carbon

Table 4.69: Kinetic model parameters for TPT adsorption onto $nSiO_2$/fly ash/activated carbon

Kinetic models	
Pseudo first-order	
k_1 (min^{-1})	0.0221
q_e (mg/g)	0.0117
R^2	0.8328
Pseudo second-order	
q_e (mg/g)	4.9975
h_o (mg/g/min)	227.27
k_2 (g/mg/min)	9.1000
R^2	0.9999
Elovich	
β (g min/mg)	204.08
α (g min^2/mg)	2.36 X 10^{443}
R^2	0.9163
Fractional Power	
v (min^{-1})	0.001
k_3 (mg/g)	4.9762
k_3v (mg/g/min)	0.0050
R^2	0.9162
Intraparticle diffusivity	
k_p (min^{-1})	0.0221
R^2	0.8328

The results obtained show a very good compliance with pseudo second-order equation with high regression coefficient (> 0.999) whereas the pseudo first-order and Elovich models were not applicable as low regression coefficients (< 0.95) were observed. The results also show that the adsorption rate constant, k_2, initial adsorption rate, h_o, and equilibrium adsorption capacity, q_e, of the pseudo second-order model are 9.100 g/mg/min, 227.27 mg/g/min and 4.9975 mg/g, respectively.

A simple kinetic analysis of the adsorption of TPT onto $nSiO_2$/fly ash/activated carbon composite was also tested according to fractional power model and Table 4.69 shows the estimated parameters of the model. The results indicate that the power model satisfactorily described the time-dependent of TPT on the $nSiO_2$/fly ash/activated carbon composite as the value of the constant v is less than 1. The kinetic model constants k_1, k_2, β, α_E, k_3 and k_p as presented in Table 4.69 for the adsorption of TPT onto $nSiO_2$/fly ash/activated carbon composite material are therefore 0.0221 min^{-1}, 9.100 g/mg/min, 204.08 gmin/mg, 2.36 x 10^{443} $gmin^2$/mg, 4.9762 mg/g and 0.0221 min^{-1}, respectively.

4.12.22.3 Effect of pH

The effect of pH on the adsorption of TPT from TPT – contaminated water onto $nSiO_2$/fly ash/activated carbon composite material was studied at pH 4 – 9. It was observed from Figure 4.416 that the percentage of TPT adsorbed by $nSiO_2$/fly ash/activated carbon composite material increases as the pH of the solution increases from pH 4 to pH 8, and reaches equilibration at pH ≥ 8.

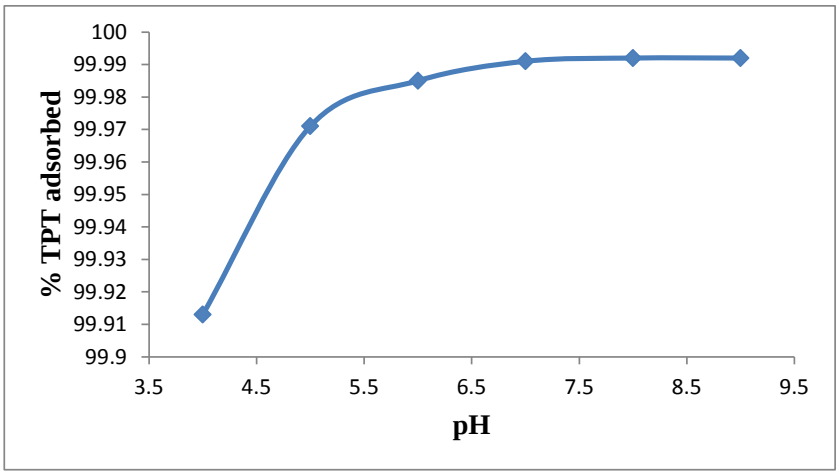

Figure 4.416: Effect of pH on TPT adsorption onto $nSiO_2$/fly ash/activated carbon

Experimental conditions: Concentration of TPT = 100 mg/L; Volume of TPT solution = 25 mL, Mass of $nSiO_2$/fly ash/activated carbon = 0.5 g; Contact time = 60 min; Stirring speed = 160 rpm, Temperature = 20 ^{o}C.

The maximum adsorption capacity was therefore recorded within pH 8. About 99.99 % TPT was removed from the initial concentration of 100 mg/L TPT by the $nSiO_2$/fly ash/activated carbon composite at pH 8, a contact time of 60 min, 160 rpm stirring speed and a temperature of 20 ^{o}C.

4.12.22.4 Effect of stirring speed

The stirring speed of the adsorption of TPT from TPT – contaminated water was also studied and optimized. The stirring speed on the adsorption of TPT onto $nSiO_2$/fly ash/activated carbon composite was studied at a stirring speed of 160 – 200 rpm. Figure 4.417 therefore shows that the adsorption capacity of $nSiO_2$/fly ash/activated carbon composite increases as the stirring speed of the mixture increases from 160 rpm – 180 rpm, after which equilibration was attained.

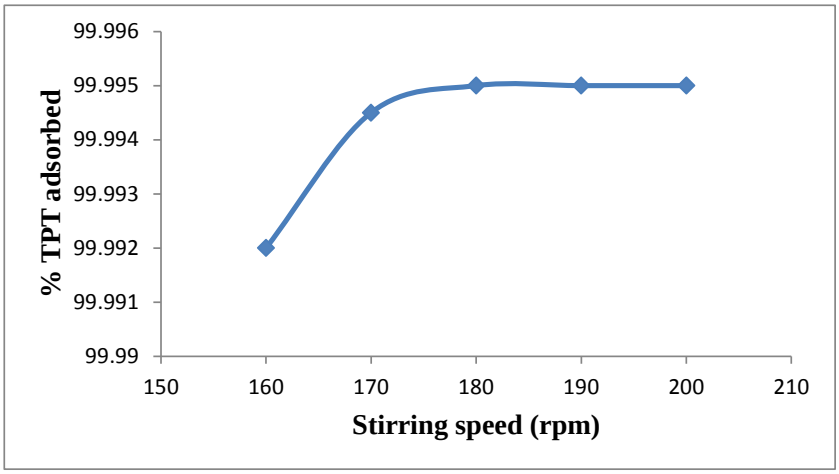

Figure 4.417: Effect of stirring speed on TPT adsorption onto $nSiO_2$/fly ash/activated carbon

Experimental conditions: Concentration of TPT = 100 mg/L; Volume of TPT solution = 25 mL, Mass of $nSiO_2$/fly ash/activated carbon = 0.5 g; Contact time = 60 min; Temperature = 20 ^oC.

Approx. 4.99 mg/g TPT (99.99 %) was removed from the initial concentration of 5 mg/g TPT by the $nSiO_2$/fly ash/activated carbon composite at a contact time of 60 min, pH 8, temperature of 20 ^oC and a stirring speed of 200 rpm (Figure 4.417).

4.12.22.5 Effect of initial concentration

Figure 4.418 shows that the adsorption of TPT from TPT – contaminated water onto $nSiO_2$/fly ash/activated carbon composite material increases as the initial TPT concentration increases from 12.5 to 100 mg/L, indicating that the adsorption is favourable for the higher TPT concentrations that have been investigated.

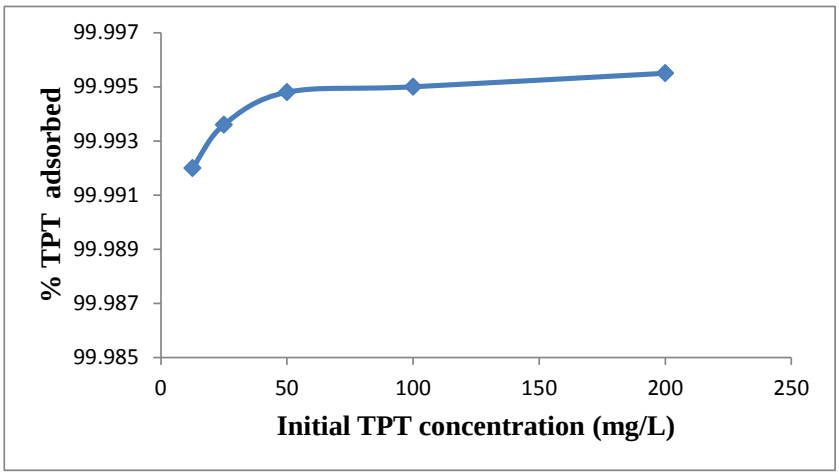

Figure 4.418: Percentage TPT adsorbed by $nSiO_2$/fly ash/activated carbon at various initial TPT concentrations

Experimental conditions: Volume of TPT solution = 25 mL, Mass of $nSiO_2$/fly ash/activated carbon = 0.5 g; pH = 8; Stirring speed = 200 rpm; Contact time = 60 min; Temperature = 20 ^oC.

The increase in the adsorption capacity with an increase in initial TPT concentration is a result of the increase in the driving force due to concentration gradient developed between the bulk solution and surface of $nSiO_2$/fly ash/activated carbon composite.

4.12.22.5.1 Adsorption isotherms

The present study indicates that the Freundlich and D-R models fit the experiment data well. They are suitable models for describing this adsorption process because R^2 values are higher than the R^2 values obtained for other models (Figures 4.419 – 4.422 and Table 4.70). The value of n_F falling in the range 1 -10 also indicates favourable adsorption.

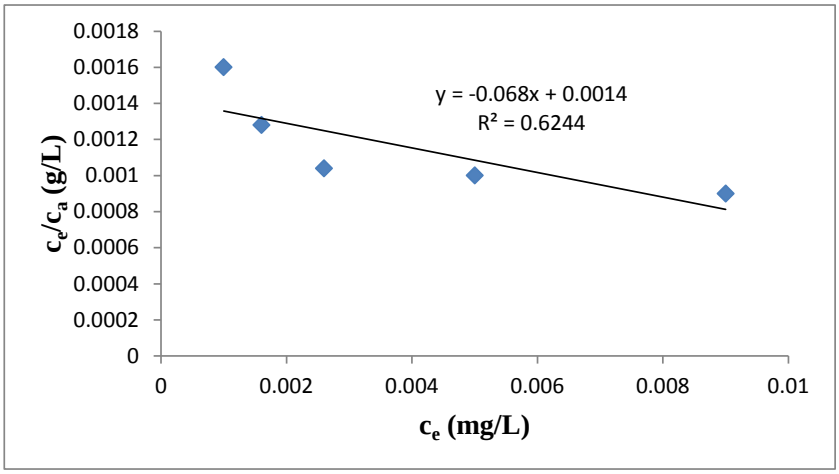

Figure 4.419: Langmuir isotherm for adsorption of TPT onto $nSiO_2$/fly ash/activated carbon

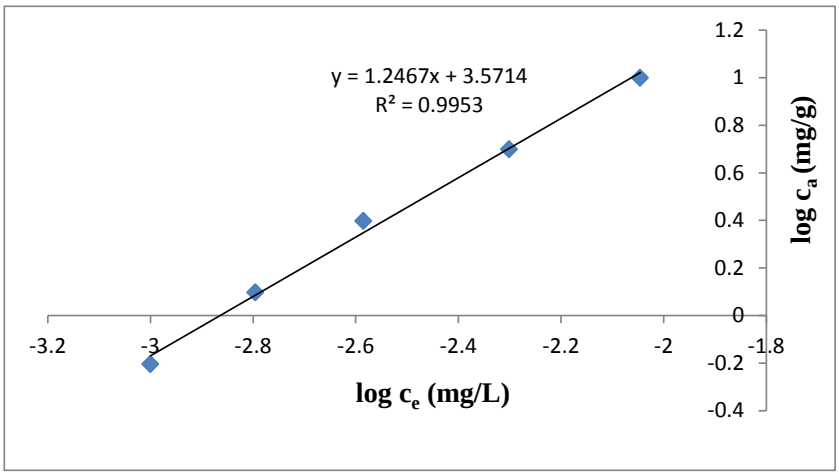

Figure 4.420: Freundlich isotherm for adsorption of TPT onto $nSiO_2$/fly ash/activated carbon

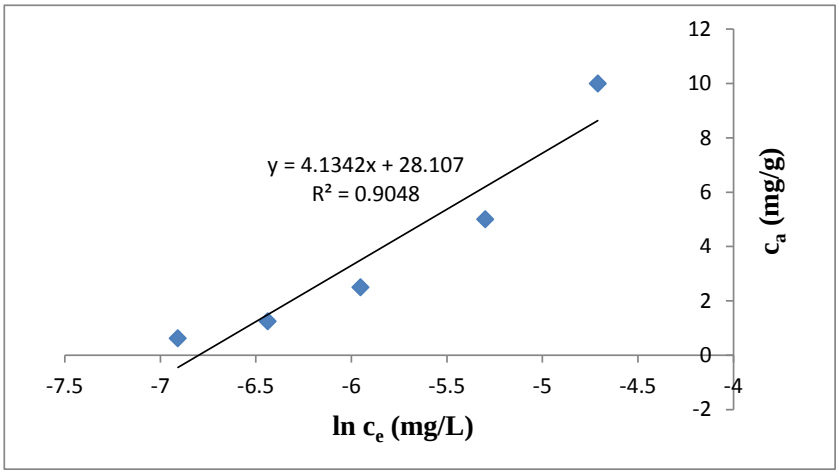

Figure 4.421: Temkin isotherm for adsorption of TPT onto nSiO$_2$/fly ash/activated carbon

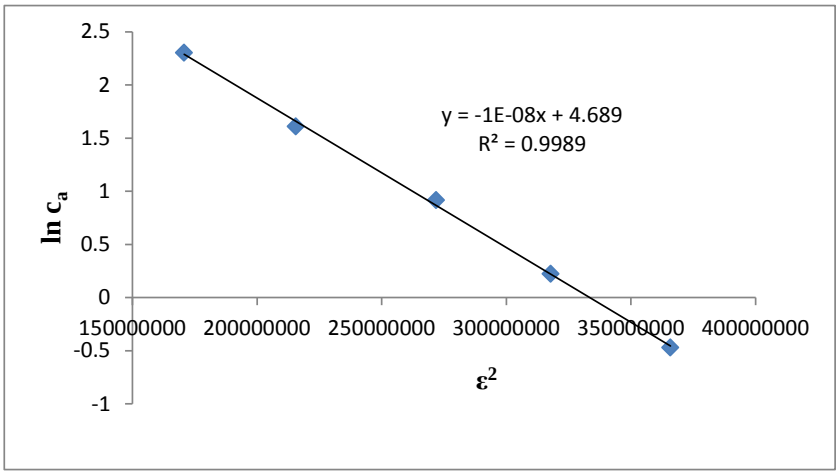

Figure 4.422: D-R isotherm for adsorption of TPT onto nSiO$_2$/fly ash/activated carbon

The experimental data (Table 4.70) does not fit the Langmuir and Temkin models, as the R^2 values obtained are very low (< 0.7 for Langmuir and < 0.91 for Temkin) and Langmuir constants, A_{max} (mg/g) and k_L (L/mg) for TPT adsorption onto nSiO$_2$/fly ash/activated carbon composite are negative. The equilibrium model constants k_1, k_2, β, α_E, k_3 and k_p for the adsorption of TPT from TPT – contaminated water onto nSiO$_2$/fly ash/activated carbon composite are 3727.4 mg/g $(L/mg)^{1/n}$, -48.567 L/mg, 896.64 mg/L and 1.0 x 10^{-8} J^2/mol^2, respectively.

Table 4.70: Isotherms constants for the adsorption of TPT onto $nSiO_2$/fly ash/activated carbon

Equilibrium models	
Freundlich	
k_F [mg/g (L/mg)$^{1/n}$]	3727.4
n_F	0.8021
R^2	0.9953
Langmuir	
K_L (L/mg)	-48.567
A_{max} (mg/g)	-14.706
R^2	0.6244
Temkin	
n_T (L/g)	4.1342
k_T (mg/L)	896.64
b_T (J/mol)	589.23
R^2	0.9048
Dubinin-Redushkevich	
k_{D-R} (J^2/mol^2)	1.0×10^{-8}
q_m (mg/g)	108.74
E (J/mol)	7071.1
R^2	0.9989

4.12.22.6 Effect of temperature

The experimental results obtained on the effect of temperature show that the adsorption capacity of TPT onto $nSiO_2$/fly ash/activated carbon composite adsorbent increases with increase in the solution temperature (Figure 4.423). This indicates that the adsorption of TPT from TPT – contaminated water onto $nSiO_2$/fly ash/activated carbon composite material is endothermic.

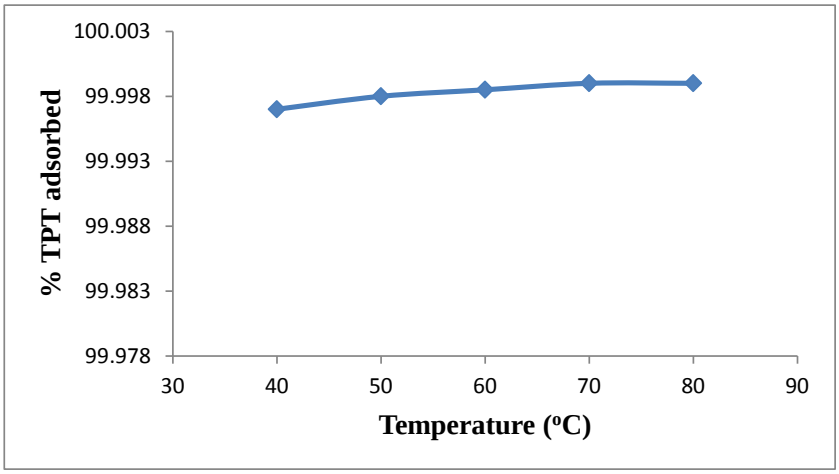

Figure 4.423: Effect of temperature on TPT adsorption onto $nSiO_2$/fly ash/activated carbon

Experimental conditions: Concentration of TPT = 100 mg/L; Volume of TPT solution = 25 mL, Mass of $nSiO_2$/fly ash/activated carbon = 0.5 g; Contact time = 60 min; pH = 8; Stirring speed = 200 rpm.

Approx. 99.999 % TPT was removed from the initial concentration of 100 mg/L TPT by $nSiO_2$/fly ash/activated carbon composite at 80 ^oC, contact time of 60 min, pH 8 and a stirring speed of 200 rpm. Figure 4.424 thus shows the Van't Hoff plot for the adsorption of TPT and the variation in the extent of adsorption with respect to temperature has been explained on the basis of ΔH^o, ΔS^o, and ΔG^o as shown in Table 4.71.

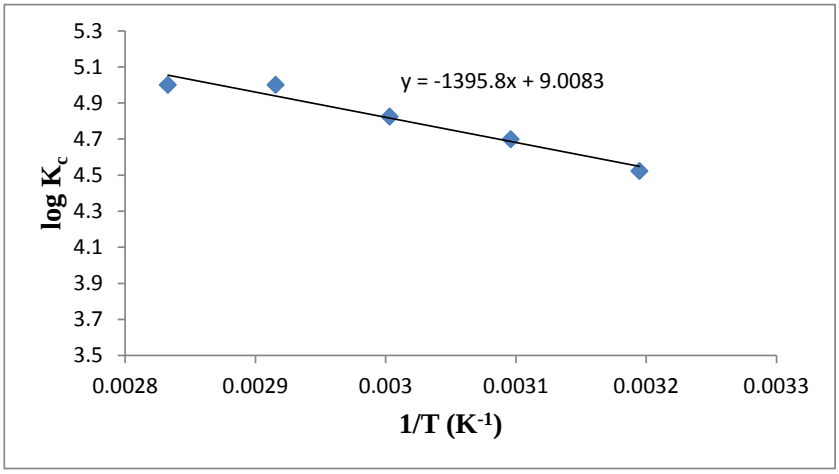

Figure 4.424: Van't Hoff Plot for the adsorption of TPT onto $nSiO_2$/fly ash/activated carbon

Table 4.71: Thermodynamic parameters for adsorption of TPT onto $nSiO_2$/fly ash/activated carbon

Temperature (°C)	ΔG° (kJ/mol)	ΔS° (J/K/mol)	ΔH° (kJ/mol)	K_c
40	-21.100	172.480	26.725	33332.3
50	-29.056			49999.0
60	-30.752			66665.7
70	-32.831			99999.0
80	-33.789			99999.0

The positive value of ΔH^o for the intervals of temperatures (26.725 kJ/mol) also shows that the adsorption of TPT from TPT – contaminated water onto $nSiO_2$/fly ash/activated carbon composite is endothermic. The positive value of ΔS^o (172.48 J/K/mol) corresponds to an increase in degree of freedom of the adsorbed TPT.

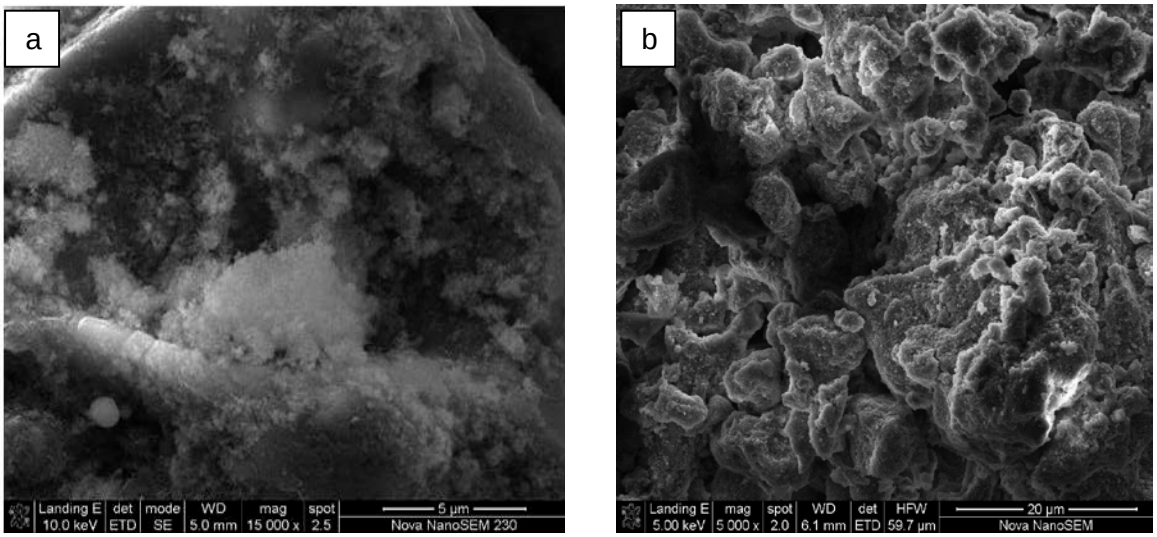

Figure 4.425: $nSiO_2$/fly ash/activated carbon before (a) and after (b) TPT adsorption

It is also evident from Table 4.71 that ΔG^{o} values were found to be more negative as the temperature increases and this indicates that the adsorption efficiency of TPT onto $nSiO_2$/fly ash/activated carbon composite increases with increase in temperature. K_c ranged 33332.3 – 99999.

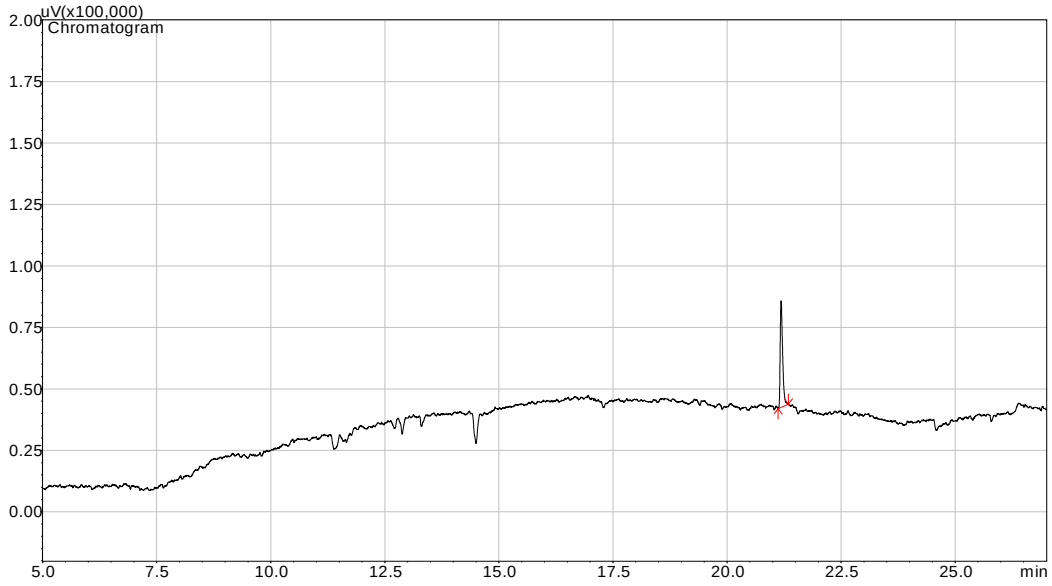

Figure 4.426: Representative TPT chromatogram after adsorption of 100 mg/L TPT with 0.5 g of $nSiO_2$/fly ash/activated carbon, contact time of 60 min, temperature 20 ^{o}C and a stirring speed of 200 rpm

The SEM analysis of $nSiO_2$/fly ash/activated carbon composite before and after the adsorption studies is presented in Figure 4.425. A representative TPT chromatogram after adsorption of 100 mg/L TPT onto 0.5 g of $nSiO_2$/fly ash/activated carbon composite material, contact time of 60min, temperature of 20 ^{o}C and a stirring speed of 200 rpm is as shown in Figure 4.426.

4.12.23 Adsorption of TBT and TPT from TBT/TPT-contaminated artificial seawater onto nZnO/fly ash/activated carbon composite

Optimal conditions for the adsorption of OTCs from artificial seawater were applied to the removal of OTCs from different TBT and TPT ratios contained in contaminated artificial seawater onto nZnO/fly ash/activated carbon composite in other to understand how the presence of one OTC affect the adsorption of the other. Figure 4.427 therefore shows that the adsorption of mixtures of OTCs depends on the concentration of individual OTCs species that are present in a medium.

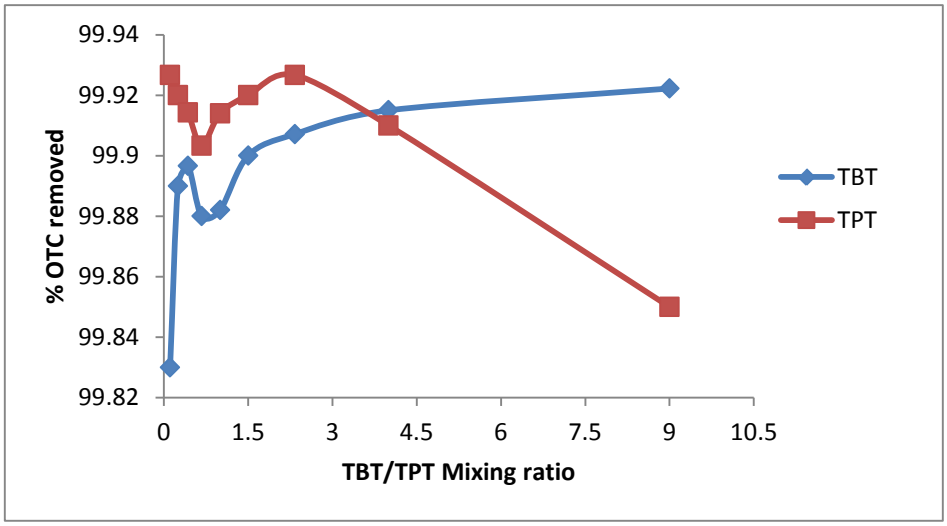

Figure 4.427: Effect of organotin mixing ratio on the adsorption

Experimental conditions: Volume of organotin solution = 25 mL; mass of nZnO/fly ash/activated carbon = 0.5 g; Temperature: 20 ^{o}C; Contact time = 60 min; pH = 8; Stirring speed = 200 rpm.

The figure and appendix E show that higher percentage of TPT was removed at lower concentration of TBT and vice versa. As the ratio of TBT to TPT increases from 0.11 – 0.43, the percentage of TPT adsorped decreases as the percentage of TBT adsorbed increases. The percentage of TBT and TPT adsorped also decreases at ratios 0.67 – 1.0 while the percentage at which both OTCs are adsorped increases from ratio 1.0 – 2.33 after which the graphs overlap around ratio 4.0. Approx. 99.89 % TBT and 99.90 TPT were removed from 25 mL of TBT/TPT-contaminated natural seawater containing 0.6423 mg/L TBT and 0.4156 mg/L TPT (TBT:TPT = 1.55) by the use of 0.5 g nZnO/fly ash/activated carbon composite at a contact time of 60 min, pH 8, 200 rpm stirring speed and temperature of 80^{o}C.

The SEM analysis of nZnO/fly ash/activated carbon composite before and after the adsorption studies is presented in Figure 4.428. A representative chromatogram after adsorption of organotin solution containing 100 mg/L TBT/TPT (1:1) with 0.5 g of nZnO/fly ash/activated carbon composite material at a contact time of 60min, temperature of 20 ^{o}C and a stirring speed of 200 rpm is as shown in Figure 4.429.

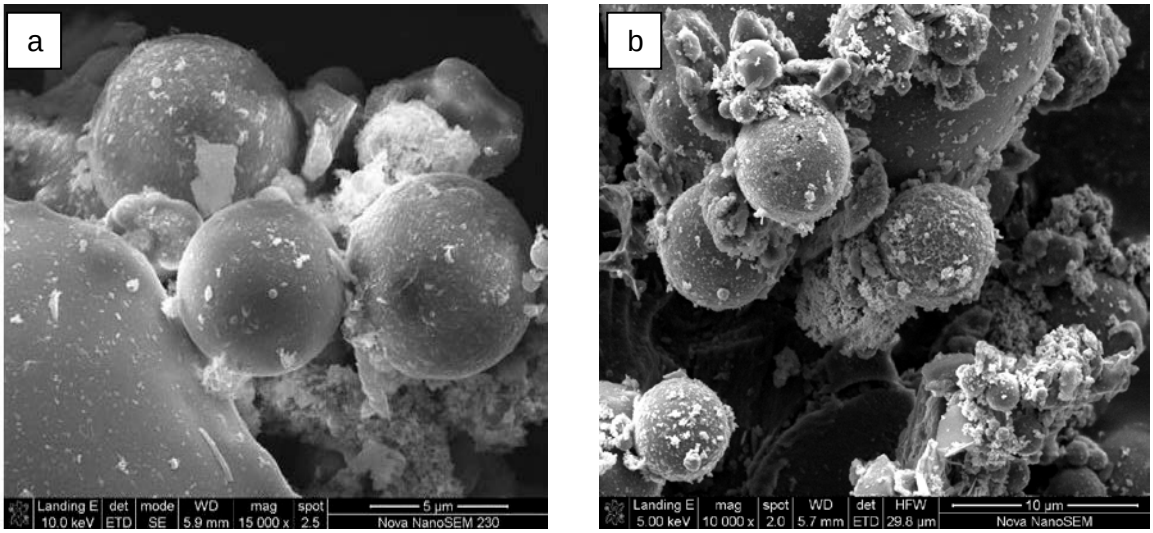

Figure 4.428: nZnO/fly ash/activated carbon before (a) and after (b) TBT/TPT adsorption

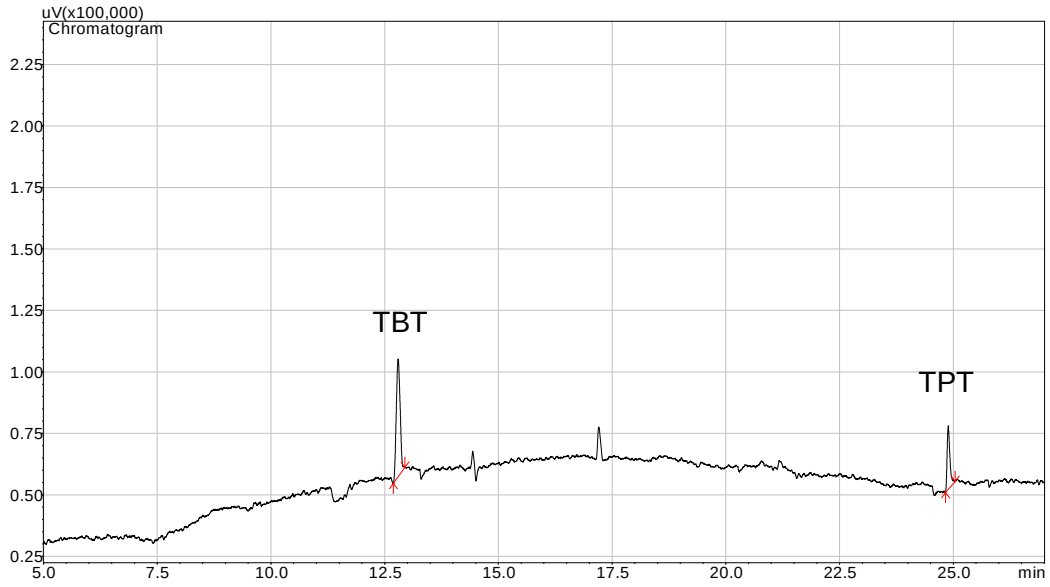

Figure 4.429: Representative TBT/TPT chromatogram after adsorption of 100 mg/L TBT/TPT with 0.5 g of nZnO/fly ash/activated carbon, contact time of 60 min, temperature 20 ^{o}C and a stirring speed of 200 rpm

4.13 Organotins confirmation by GC-MS, FTIR and EDX analysis

The full scan chromatographic elusion peaks accompanied by their MS fragmentation patterns and spectra library confirming the presence of corresponding OTC in the filtrate after adsorption of TBT onto Fe_3O_4, TBT onto silica, TPT onto nZnO, TBT onto fly ash and TPT onto fly ash are presented in Figures 4.430 – 4.434, respectively.

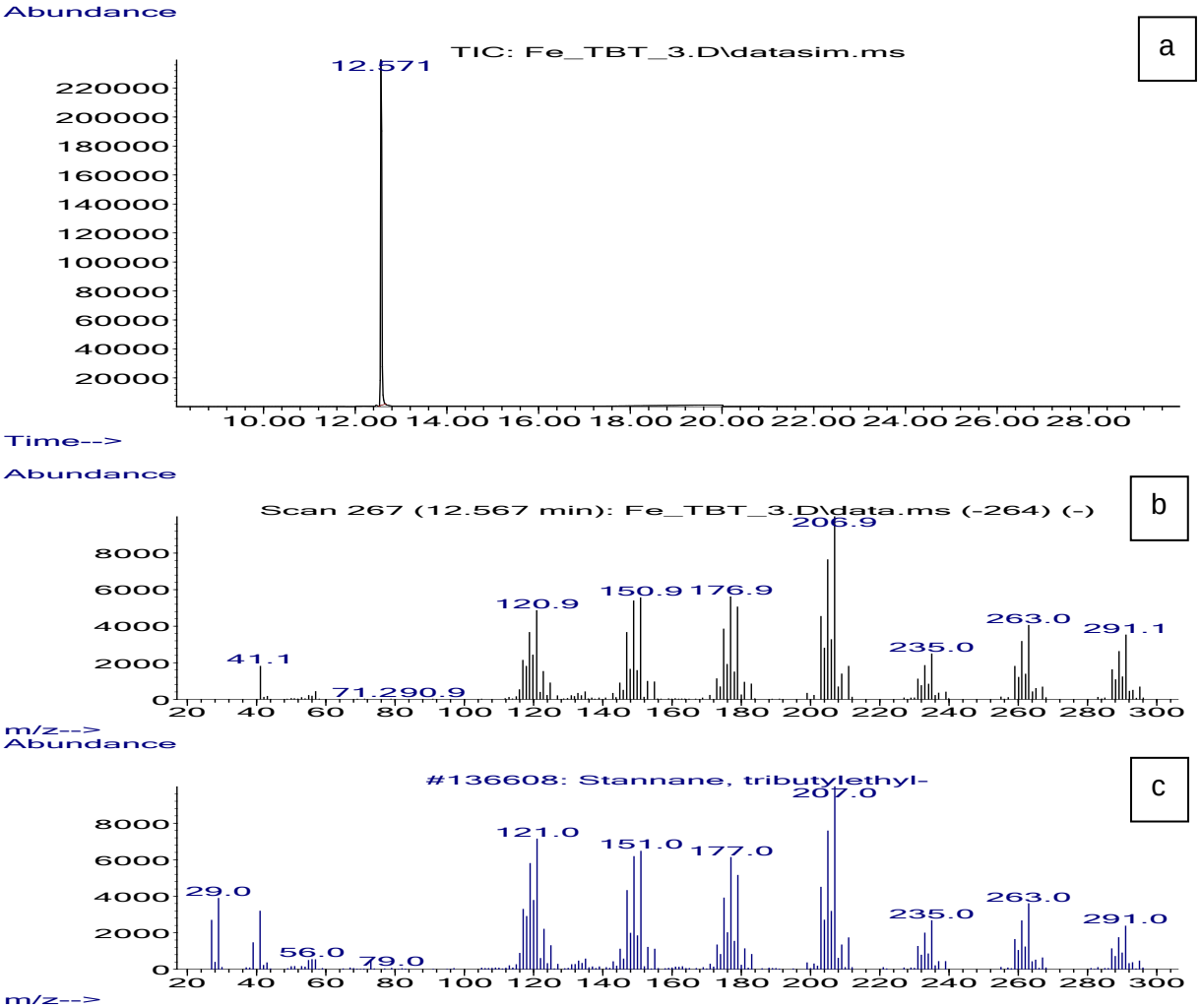

Figure 4.430: GC-MS full scan (a), spectra (b) and the library match spectra (c) after adsorption of 100 mg/L TBT with 0.5 g of nFe_3O_4, contact time of 60 min, temperature 20 ^oC and a stirring speed of 200 rpm

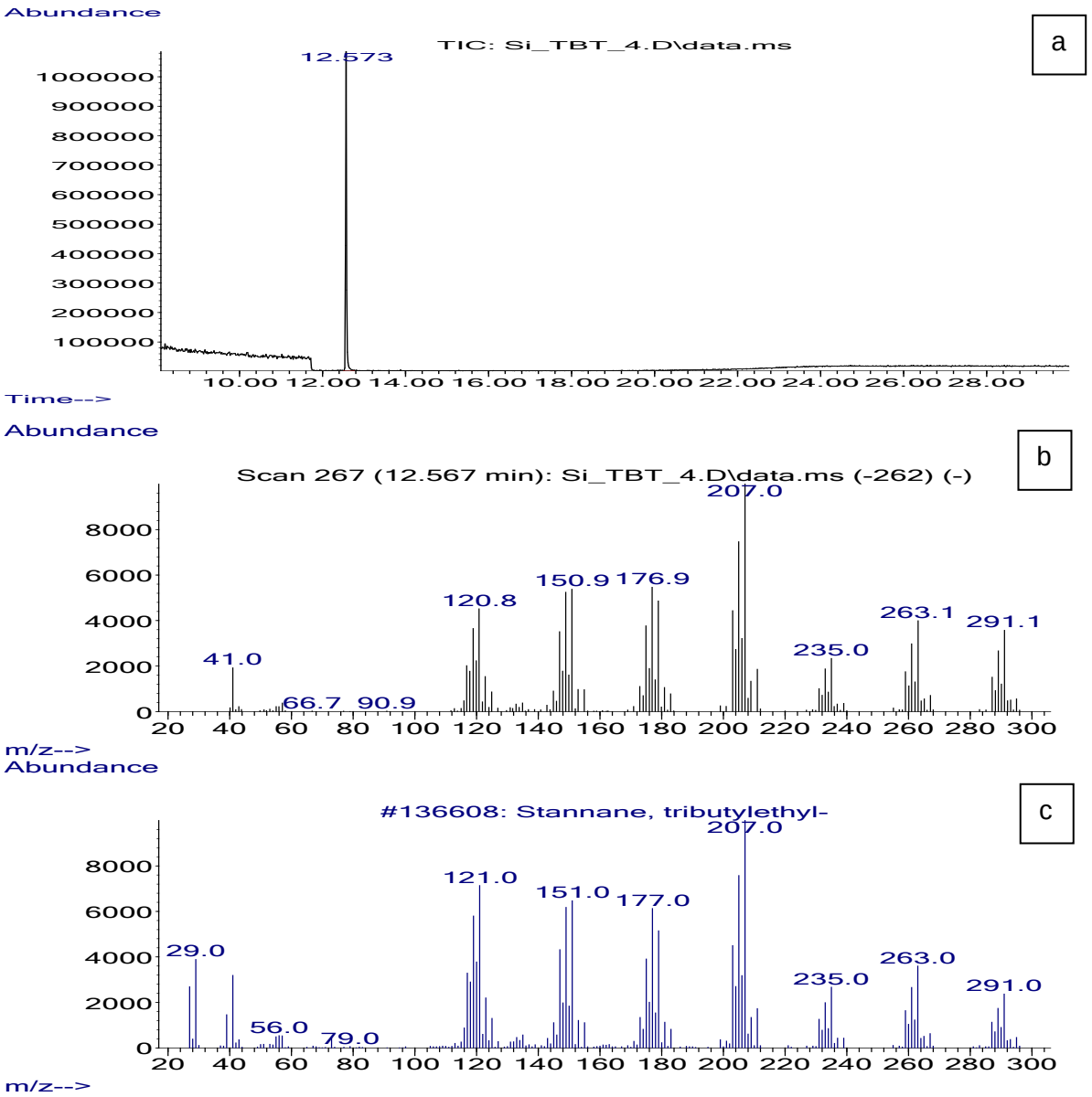

Figure 4.431: GC-MS full scan (a), spectra (b) and the library match spectra (c) after adsorption of 100 mg/L TBT with 0.5 g of $nSiO_2$, contact time of 60 min, temperature 20 ^{o}C and a stirring speed of 200 rpm

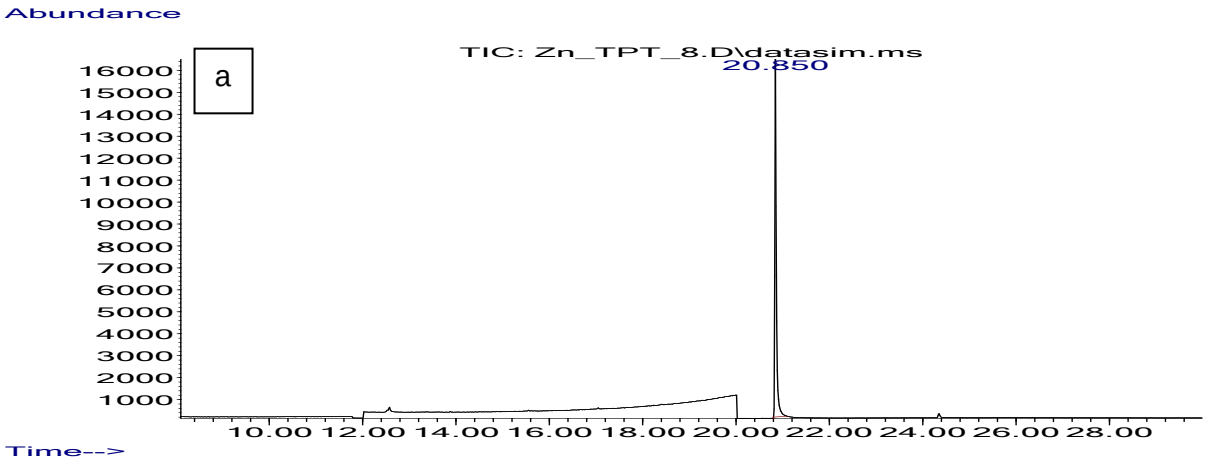

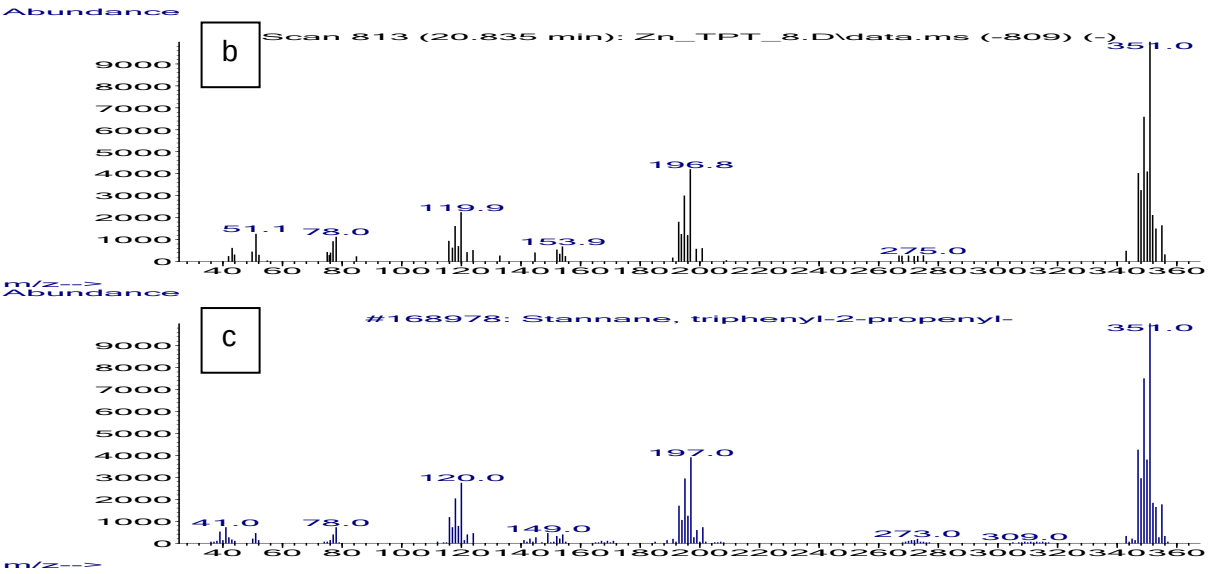

Figure 4.432: GC-MS full scan (a), spectra (b) and the library match spectra (c) after adsorption of 100 mg/L TPT with 0.5 g of nZnO, contact time of 60 min, temperature 20 ^{o}C and a stirring speed of 200 rpm

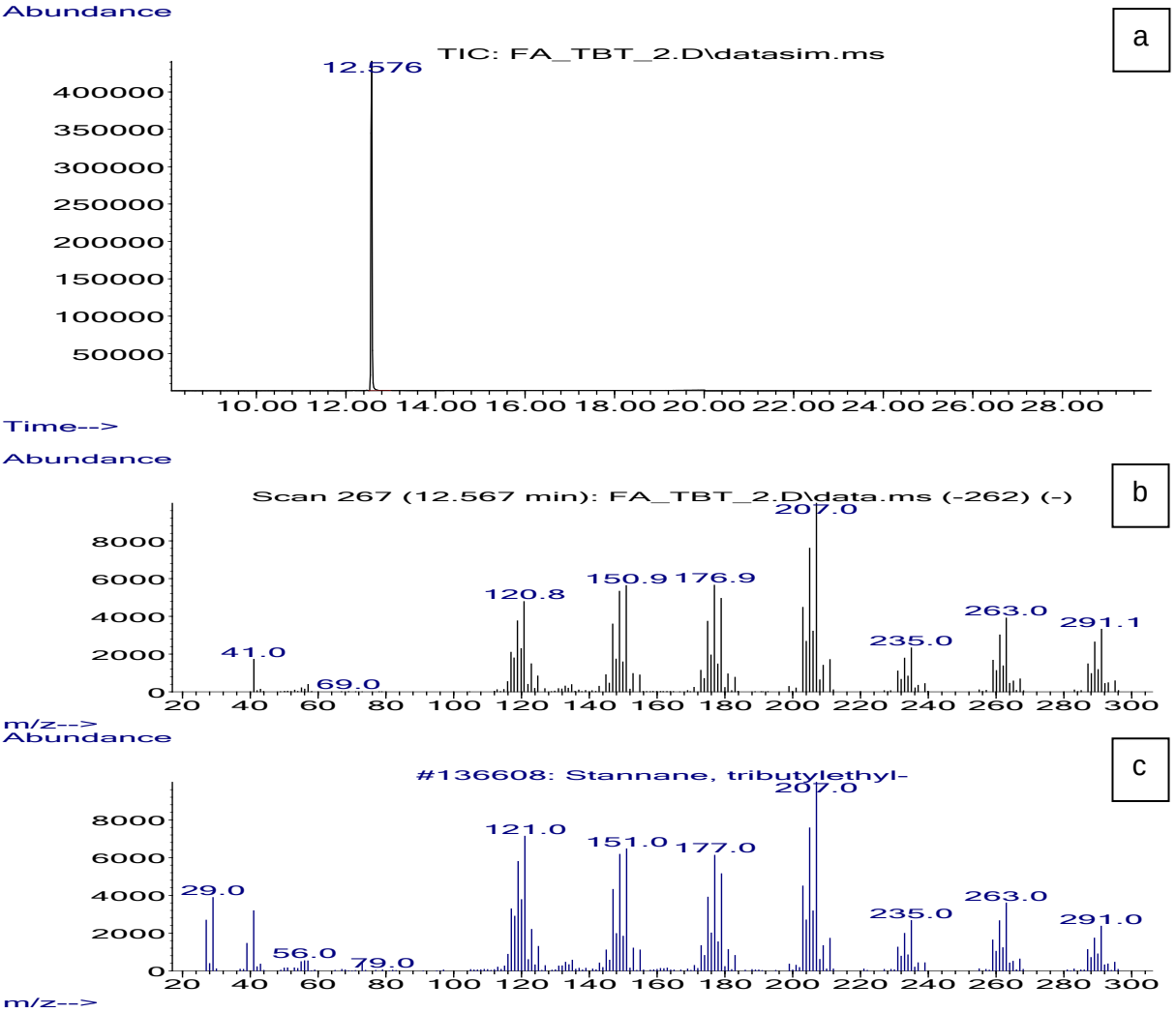

Figure 4.433: GC-MS full scan (a), spectra (b) and the library match spectra (c) after adsorption of 100 mg/L TBT with 0.5 g of fly ash, contact time of 60 min, temperature 20 ^{o}C and a stirring speed of 200 rpm

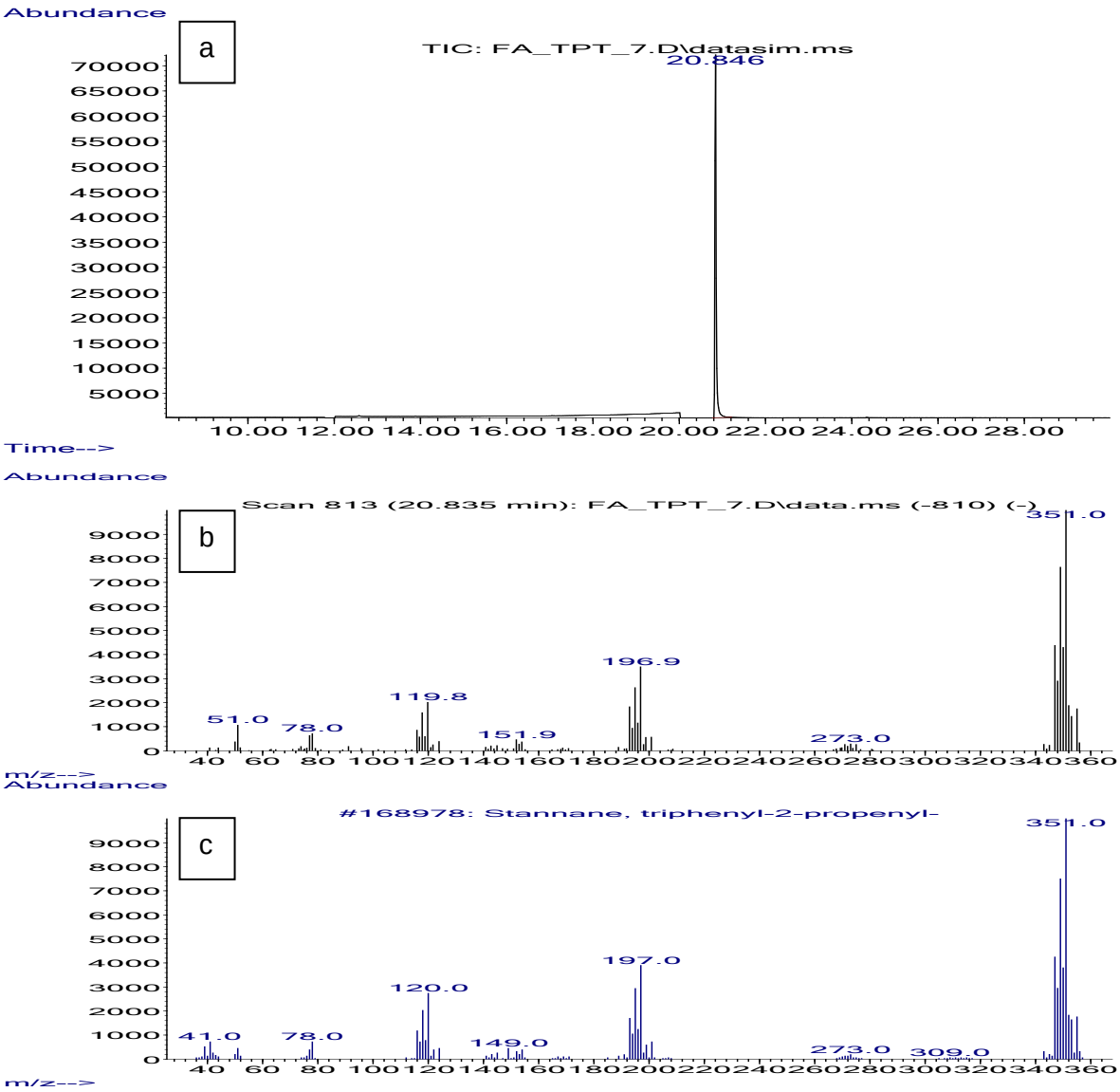

Figure 4.434: GC-MS full scan (a), spectra (b) and the library match spectra (c) after adsorption of 100 mg/L TPT with 0.5 g of fly ash, contact time of 60 min, temperature 20 ^{o}C and a stirring speed of 200 rpm

No spectra were recorded for filtrates of TBT adsorption onto nFe_3O_4/activated carbon composite, and TBT adsorption onto activated carbon, this maybe as a result of the concentration of OTC that is too low to be detected by the GC-MS. The adsorption results earlier showed that > 99.98 % OTCs were removed by these materials after adsorption.

The GC-MS analysis of these filtrates therefore confirmed that the OTCs were not degraded into other compounds or other forms of derivatives during the process of adsorption. This is because there were no other peaks found on the GC-MS full scan of the filtrates except the peaks corresponding to the OTC that remain in the filtrate after adsorption. GC-MS analysis also indicates that the adsorption of TBT and TPT does not result in the production of another severe pollutant during the treatment process.

Random residue samples (adsorbent residue after adsorption) were also analysed by FTIR but no peaks were observed as the FTIR spectrum of all the adsorbents before and after adsorption are the same. This shows that FTIR cannot be used for the elucidation of OTCs on the adsorbent residues. Some representative FTIR spectra of adsorbents before and after adsorption are presented in Appendix I.

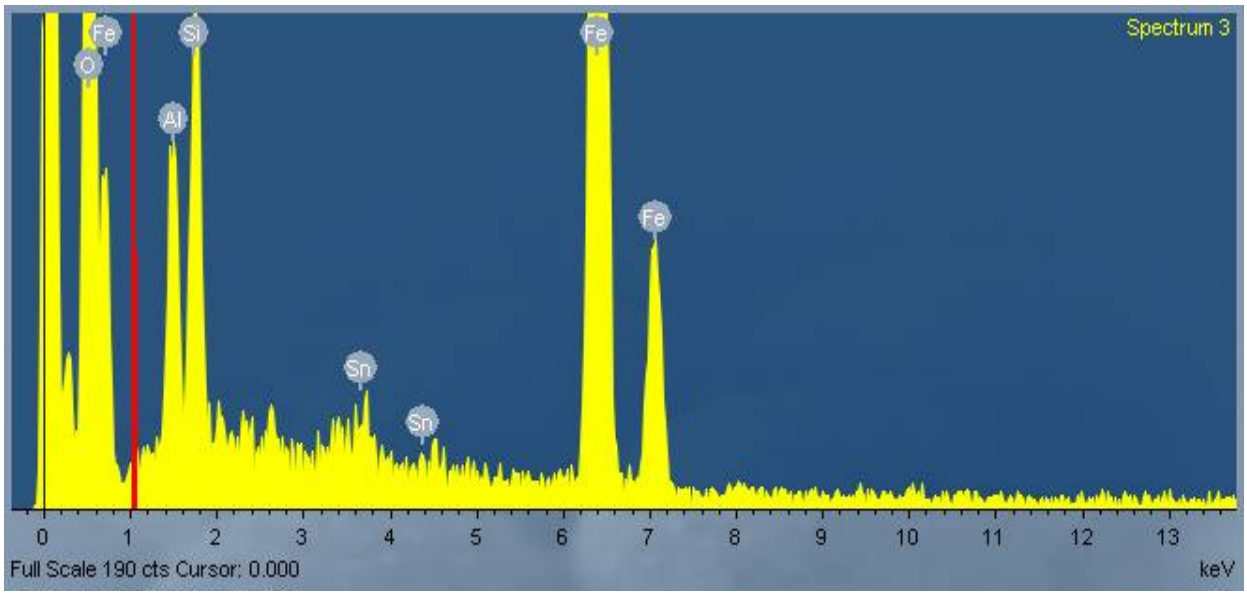

Figure 4.435: Representative EDX spectrum of the Fe_3O_4/fly ash adsorbent residue

However, the Energy-dispersive X-ray spectroscopy (EDX) analysis of the adsorbents after adsorption shows the presence of Sn on the spectra (Figure 4.435). The OTCs (TBT and TPT) present in the adsorbent residue were also desorped into 25 mL of hexane (desorption) and analysed by GC-FPD and the results obtained confirmed the presence of TBT and TPT on the adsorbent residues.

CHAPTER FIVE
CONCLUSION

OTCs are used widely for a variety of industrial and agricultural applications including pesticides, fungicides and anti-fouling agents. The extensive use of OTCs in a lot of domestic and industrial products leads to the presence of these species in all environmental media (Maguire, 1991; Donald et al., 1993; Fent, 1996). Different OTCs thus have different environmental effects and toxicities with trisubstituted OTCs being the most toxic (Ayanda et al., 2012c). Concentration as low as ng/L concentrations of TBT and TPT may result in harmful effects on marine organisms including acute poisoning and aberrance of aquatic organisms, especially larvae and consumption of seafood by man can lead to injection of these compounds. Therefore, the remediation of OTCs to > 99 % reduction from wastewater before discharge into the environment is very important. To achieve this aim, composite materials involving activated carbon, fly ash, nFe_3O_4, $nSiO_2$ and nZnO were prepared, characterized and utilized for the sorption of OTCs (TBT and TPT) from organotin – contaminated seawater and wastewater.

Experimental results obtained on characterization show that the pH values of activated carbon, $nSiO_2$, nFe_3O_4/activated carbon, $nSiO_2$/activated carbon, nZnO/activated carbon, nZnO/fly ash, fly ash/activated carbon, nFe_3O_4/fly ash/activated carbon, $nSiO_2$/fly ash/activated carbon and nZnO/fly ash/activated carbon are slightly higher than their corresponding PZC values. This suggests that the surface of these adsorbents is negatively charged and will therefore attract cations while the pH values of fly ash, nFe_3O_4, nZnO, nFe_3O_4/fly ash and $nSiO_2$/fly ash are slightly lower than their corresponding PZC values and suggests that the surface of these adsorbents is positively charged and will therefore attract anions. Ash content determination also shows that the level of inorganic materials present in the adsorbent composite materials is a function of the precursors that make up the composite materials. The XRD and FTIR analysis confirmed the absence of impurities in the precursors and the prepared composite materials while the results obtained on BET surface area and porosity determination show that the properties of the precursors are improved when the precursors are combined to form composite materials (Fatoki et al., 2012 & Ayanda et al., 2013a). The improvement in the surface area results in higher adsorption capacity of the composite materials. XRF, ICP – MS and ICP – AES results provide the elemental composition of the fly ash before its use, SEM and TEM where used to study the morphology of the precursors and composites before and after the sorption studies while FTIR was applied to reveal the systematic changes in the spectra features upon preparation of composite materials and after the adsorption studies.

The adsorption performances of the precursors and composite materials were studied in terms of kinetic and adsorption isotherms for the removal of TBT and TPT from artificial seawater and wastewater. Experimental results show that the adsorption characteristics of these adsorbents are dependent on adsorbent dose, contact time, pH, stirring speed, initial TBT concentration, and temperature. The increase in the adsorption capacity with increasing adsorbent dose is as a result of more adsorptive binding sites due to more adsorbent in the medium at higher dosages. The constant trend in the adsorption capacity after 0.5 g may be due to the saturation of adsorptive binding sites on the adsorbent surface by the adsorbate molecules (Deng et al., 2010). The contact time phenomenon is attributed to the fact that a large number of vacant surface sites are available for adsorption at the initial stage, and after a lapse of time, the remaining vacant surface sites were difficult to be occupied due to repulsive forces between the solute molecules on the solid and bulk phases (Bazrafshan et al., 2012). At low solution pH, the high concentration of H^+ ions promoted the protonation of OTCs functional groups, and thus the adsorbents became more positively charged, which inhibits the adsorption of the OTCs on it. When the solution pH increased, the solution OH^- concentration increased, which improved the interaction between the adsorbents and the OTCs molecules. Therefore, the adsorption capacity of the adsorbents was increased at higher pH value (Yu et al., 2010). The pores on the surface of the adsorbents were also unrestricted at high stirring speed making all the pores available for adsorption and the increase in the adsorption capacity with an increase in initial OTCs concentration is as a result of the increase in driving force due to concentration gradient developed between the bulk solution and surface of the adsorbents (Kumar et al., 2010). At higher concentration of OTCs, the active sites of the adsorbents were surrounded by much more OTCs and the process of adsorption continues, leading to an increased uptake of OTCs from the solution.

Kinetic models evaluated include fractional power, pseudo first-order, pseudo second-order, Elovich and intraparticle diffusivity. The kinetic data were well described by pseudo second-order model for the adsorption of TBT and TPT (from any of the medium) onto the precursors and the composite due to their high regression coefficients. The pseudo second-order kinetic model depends on the assumption that chemisorption may be the rate-limiting step. Equilibrium isotherm data were fitted using Langmuir, Freundlich, Temkin and D-R models. Freundlich model is in good agreement with all the experimental data with high R^2 values. Besides Freundlich isotherm, TBT adsorption onto nZnO/activated carbon and nFe_3O_4/activated carbon composite from TBT contaminated artificial seawater, TPT adsorption onto activated carbon and fly ash/activated carbon from TPT contaminated artificial seawater and TPT sorption onto $nSiO_2$/fly ash/activated carbon composite from TPT – contaminated water could also be described by D-R isotherm model. The magnitudes of the Freundlich constants k_F and n_F show easy separation of OTCs from the aqueous

solution and indicate favourable adsorption. The intercept value k_F is an indication of the adsorption capacity of the adsorbents while the slope $\frac{1}{n_F}$ indicates the effect of concentration on the adsorption capacity and represents the adsorption intensity (Kumar and Kirthika, 2009).

Thermodynamic analysis shows that the adsorption of TBT from TBT – contaminated artificial seawater onto activated carbon, fly ash, nFe_3O_4, $nSiO_2$, nZnO, fly ash/activated carbon, nFe_3O_4/activated carbon, $nSiO_2$/activated carbon and nZnO/activated carbon composite and adsorption of TPT onto activated carbon and fly ash/activated carbon composite from TPT – contaminated artificial seawater was endothermic while TPT adsorption onto fly ash, nFe_3O_4, $nSiO_2$, nZnO, nFe_3O_4/fly ash, $nSiO_2$/fly ash and nZnO/fly ash composites from TPT – contaminated artificial seawater was exothermic.

The SEM images before and after adsorption show that the surfaces of activated carbon, fly ash and the composites are clearly seen before adsorption whereas OTCs are deposited on the surfaces of these adsorbents after adsorption. The particles that make up the nano materials are also distinct and clearly seen before adsorption but the surface morphologies are changed after the adsorption process. Organotin confirmation by GC-MS showed that the adsorption of OTCs by the adsorbents does not result in the production of another pollutant, and new derivatives or compounds were not produced after adsorption. The SEM analysis of the adsorbents before and after the adsorption studies, the EDX analysis of the adsorbents after adsorption, and organotin analysis after desorption of TBT and TPT from the adsorbent residue into hexane therefore confirmed that OTCs are adsorbed onto the precursors and composite particles.

The experimental results show that the precursors most especially the activated carbon, and the composite materials offer great potential for the remediation of OTCs from seawater (Fatoki et al., 2013; Ayanda et al., 2013b) and wastewater with the composite materials presenting a higher organotin adsorption efficiency than the precursors due to the nature and improved properties. Although, the surface area of activated carbon is higher than that of the composite materials, however, the composites prove more efficent; this may be attributed to the combination of the adsorption characteristic of activated carbon with the catalytic properties of nano metal oxide contained in the composite materials. The practical application of optimal conditions obtained with artificial seawater to the removal of TBT and TPT from TBT – and TPT – contaminated natural seawater shows the effectiveness of the adsorbents for organotin removal from organotin – contaminated seawater (Ayanda et al., 2013c). The percentage OTCs adsorbed from contaminated natural seawater was slightly

lower than the percentage removed from contaminated artificial seawater, this could be attributed to the presence of other species such as metal ions that might be present in the OTC – contaminated natural seawater.

REFERENCES

Abdullah, A.H, Kassim, A., Zainal, Z., Hussein, M.Z, Kuang, D., Ahmad, F. and Wooi, O.S. 2001. Preparation and characterization of activated carbon from gelam wood bark (Melaleuca cajuputi). Malaysian J. Anal. Sci., 7(1): 65 - 68.

Aboul-Kassim, T.A.T. and Simoneit, B.R.T. 2001. Sorption/Desorption of organic pollutants from complex mixtures: Modeling, kinetics, experimental techniques and transport parameters. The Handbook of Environmental Chemistry, Vol. 5, Part E, Springer-Verlag Berlin Heidelberg, 1 - 74.

Adekola, F., Fédoroff, M., Geckeis, H., Kupcik, T., Lefèvre, G., Lützenkirchen, J., Plaschke, M., Preocanin, T., Rabung T., and Schild, D. 2011. Characterization of acid–base properties of two Gibbsite samples in the context of literature results. J. Colloid Interface Sci., 354: 306 - 317.

Ahmaruzzaman, M. 2010. A review on the utilization of fly ash. Prog. Energ. Combust., 36: 327 - 363.

Al-Qodah, Z. 2000. Adsorption of dyes using shale oil ash. Water Res., 34(17): 4295.

Arevalo, E. and Calmano, W. 2007. Studies on electrochemical treatment of wastewater contaminated with organotin compounds. J. Hazard. Mater., 146: 540 - 545.

Atkins, P.W. 1995. Physical Chemistry. 5th Edition, Oxford, Oxford University Press, 1995.

Ayanda, O.S. and Adekola, F.A. 2011. Comparison of some physicochemical characterization of columbite and tantalite samples from different locations in Nigeria. Chem. Sust. Dev., 19: 243 - 247.

Ayanda, O.S., Fatoki, O.S., Adekola, F.A. and Ximba, B.J. 2012a. Fate and Remediation of organotin compounds in Seawaters and Soils. Chem. Sci. Trans., 1(3): 470 - 481.

Ayanda, O.S., Fatoki, O.S., Adekola, F.A. and Ximba, B.J. 2012b. Characterization of fly ash Generated from Matla Power Station in Mpumalanga, South Africa. E-J Chem., 9(4): 1788 - 1795.

Ayanda, O.S., Baba, A.A. and Olutona G.O. 2012c. Toxicity and speciation analysis of organotin compounds. Chem. Spec. Bioavailab., 24 (4): 216 – 226.

Ayanda, O.S., Adeyi, O., Durojaiye, B. and Olafisoye, O. 2012d. Adsorption kinetics and intraparticulate diffusivities of congo red onto kola Nut pod carbon. Pol. J. Environ. Stud., 21: 1147 - 1152.

Ayanda, O.S., Fatoki, O.S., Adekola, F.A. and Ximba, B.J. 2012e. Preparation and Characterization of nZnO/Fly Ash Composite, *Technical Proceedings of the 2012 NSTI Nanotechnology Conference and Expo*, Santa Clara, California, USA, 1, pp 95-98.

Ayanda, O.S., Fatoki, O.S., Adekola, F.A. and Ximba, B.J. 2013a. Activated carbon – fly ash – nano metal oxide composite materials: Preparation, characterization and tributyltin removal efficiency. J. Chem., DOI: 10.1155/2013/148129.

Ayanda, O.S., Fatoki, O.S., Adekola, F.A. and Ximba, B.J. 2013b. Removal of Tributyltin from shipyard process wastewater by Fly ash, Activated carbon and Fly ash/activated carbon Composite: Adsorption models and Kinetics. J. Chem. Technol. Biot., DOI: 10.1002/jctb.4088.

Ayanda, O.S., Fatoki, O.S., Adekola, F.A. and Ximba, B.J. 2013c. Kinetics and equilibrium models for the sorption of tributyltin to nZnO, activated carbon and nZnO/activated carbon composite in artificial seawater. Mar. Pollut. Bull., DOI:10.1016/j.marpolbul.2013.04.001.

Ayanda, O.S., Fatoki, O.S., Adekola, F.A. and Ximba, B.J. 2013d. Utilization of $nSiO_2$, fly ash and $nSiO_2$/fly ash composite for the remediation of triphenyltin (TPT) from contaminated seawater. Environ. Sci. Poll. Res., DOI: 10.1007/s11356-013-1775-x.

Bada, S.O. and Potgieter-Vermaak, S. 2008. Evaluation and treatment of coal fly ash for adsorption application. Leonardo El. J. Pract. Technol., 37 - 48.

Bancon-Montigny, C., Lespes, G. and Potin-Gautier, M. 2000. Improved routine speciation of organotin compounds in environmental samples by pulsed flame photometric detection. J. Chromatogr. A, 896: 149-158.

Basha, S. and Murthy, Z.V.P. 2007. Kinetics and equilibrium models for biosorption of Cr(VI) on chemically modified seaweeds, Cystoseira indica. Process Biochem., 42: 1521 - 1529.

Bazrafshan, E., Mostafapour, F.K., and Zazouli, M.A. 2012. Methylene blue (cationic dye) adsorption into *Salvadora persica* stems ash. *Afr. J. Biotechnol.* 11: 16661-16668.

Beganskienė, A., Sirutkaitis, V., Kurtinaitienė, M., Juškėnas, R. and Kareiva, A. 2004. FTIR, TEM and NMR Iinvestigations of Stöber Silica Nanoparticles. Mater. Sci., 10: 287 – 290.

Boparai, H.K., Joseph, M. and O'Carroll, D.M. 2010. Kinetics and thermodynamics of cadmium ion removal by adsorption onto nano zerovalent iron particles. J. Hazard. Mater., Doi:10.1016/j.jhazmat.2010.11.029.

Bosselmann, K. 1996. Environmental law and tributyltin in the environment. In: de Mora, S.J. (Ed.), Tributyltin: Case Study of an Environmental Contaminant. Cambridge University Press, Cambridge, 237 - 263.

Boyer, I. J. 1989. Toxicity of dibutyltin tributyltin and other organotin compounds to humans and to experimental animals. Toxicology, 55: 253-298.

Brack, K. 2002. Organotin compounds in Sediments from the Göta Älv Estuary. Water Air Soil Pollut., 135: 131 - 140.

Brandli, R.C., Breedveld, G.D. and Cornelissen, G. 2009. Tributyltin Sorption of marine sedimentary black carbon and to amended activated carbon. Environ. Toxicol. Chem., 28: 503 - 508.

Brandt, R.K., Hughes, M.R., Bourget, L.P., Truszkowska, K. and Greenler, R.G. 1993. The interpretation of CO adsorbed on Pt/SiO_2 of two different particle-size distributions. Surf. Sci., 286: 15 - 25.

Campillo, N., Aguinaga, N., Viñas, P., López-García, I. and Hernández-Córdoba, M. 2004. Speciation of organotin compounds in waters and marine sediments using purge-and-trap capillary gas chromatography with atomic emission detection. Anal. Chim. Acta., 525: 273–280.

Cardwell, R. D. and Meador, J. P. 1989. Tributyltin in the environment: An overview and key issues. In: Ocean's 89 Procedings, vol 2, Organotin Symposium. Institute of electrical and electronics Engineers, Piscataway, NJ and Marine Technology Society, Washington Dc, 537-544

Claisse, F. and Blanchette, J. 2004. Physics and Chemistry of Borate Fusion – For XRF Spectroscopists. Fernand Claisse Inc. 78 pp.

Collin, J.G., Bono, A., Krishnaiah, D. and Soon, K.O. 2007. Sorption studies of methylene blue dye in aqueous solution by optimised carbon prepared from guava seeds (Psidium guajava L.). Mater. Sci.,13(1): 83 - 87.

Deng, L.Y., Xu, G.R., Yan, Z.C., Liu, Q.H., and Li, G.B. 2010. Removal effect of Cr (VI) by adsorbent made from sewage sludge. *Water Sci. Technol.,* 62: 2961–2969.

DEWHA (Department of the Environment, water, Heritage and the Arts) 2008. National Pollution Inventory Substance Profile. http://www.npi.gov.au/substances/organo-tin/health.html [22 August 2011].

Donald, O., Quevauvilla, P. and Bruchet, A. 1993. Tin and organotin speciation during wastewater and sludge treatment process. Wat. Res., 27(6): 1085-1089.

Eddleston, M., Juszczak, E., Buckley, N.A., Senarathna, L., Mohamed, F., Dissanayake, W., Hittarage, A., Azher, S., Jeganathan, K., Jayamanne, S., Sheriff, M.R. and Warrell, D.A. 2008. Multiple-dose activated charcoal in acute self-poisoning: a randomised controlled trial. Lancet, 371(9612): 579 - 87.

Eisler, R. 1989. Tin hazards to Fish, Wildlife, and invertebrates: A Synoptic Review. Biological Report 85 (1.15) Contaminant Hazard Reviews Report No. 15.

EURACHEM Guidelines (1998). The Fitness for Purpose of Analytical Methods: A Laboratory Guide to Method Validation and Related Topics, EURACHEM Guide, LGC, Teddington, 1st English ed., http://www.eurachem.ul.pt/.

Fang, L., Borggaard, O.K., Marcussen, H., Holm, P.E. and Hansen, H.C.B. 2010. The pH-dependent adsorption of tributyltin to charcoals and soot. Environ. Pollut., 158: 3642 - 3649.

Fatoki, O.S., Ayanda, O.S., Adekola, F.A., Ximba, B.J. and Opeolu, B.O. 2012. Preparation and characterization of activated carbon – nFe_3O_4, activated carbon – $nSiO_2$ and activated carbon – nZnO hybrid materials. Part. Part. Syst. Charact., 29(3): 178 - 191.

Fatoki, O.S., Ayanda, O.S., Adekola, F.A. and Ximba, B.J. 2013. Sorption of Triphenyltin Chloride to nFe_3O_4, fly ash and nFe_3O_4/fly ash Composite Material in Seawater. Clean – Soil, Air, Water. DOI: 10.1002/clen. 201300180.

Fent, K. 1996. Ecotoxicology of organotin compounds. Crit. Rev. Toxicol., 26: 1-117.

Fent, K. and Hunn, J. 1995. Organotins in freshwater harbors and rivers: temporal distribution, annual trends and fate. Environ. Toxicol. Chem., 14: 1123-1132.

Foo, K.Y. and Hameed, B.H. 2010. Insights into the modeling of adsorption isotherm systems. Chem. Eng., 156: 2 - 10.

Fungaro, D.A. and Graciano, J.E.A. 2007. Adsorption of zinc ions from water using zeolite/iron oxide composites. Adsorpt. Sci. Technol., 25(10): 729 - 740.

Gadd, G.M. 2000. Microbial interactions with tributyltin compounds: Detoxification, accumulation, and environmental fate. Sci. Total. Environ., 258: 119.

Ghasemi, Z., Seif, A., Ahmadi, T.S., Zargar, B., Rashidi, F. and Rouzbahani, G.M. 2011. Thermodynamic and kinetic studies for the adsorption of Hg(II) by nano-TiO_2 from aqueous solution. Adv. Powder Technol., 9 pp. In press.

Gianina, D., Crisan, M., Zaharescu, M., Ionescu, N.I. and Rusu, M. 2003. TEM Micrographs Fractal Analysis, 6pp. http://isis.pub.ro/iafa2003/files/5-1.pdf, (29 May 2011).

Gitari, W.M., Somerset, V.S, Petrik, L.F., Key, D., Iwuoha, E. and Okujeni, C. 2008. Treatment of acid mine drainage with fly ash: Removal and major, minor elements, SO_4 and Utilization of the solid residues for wastewater treatment. Fuel, 87(12): 2450 - 2462.

Goldberg, E.D. 1986. TBT: an environmental dilemma. Environment, 28: 17 - 44.

Golub, M. and Doherty, J. 2004. Triphenyltin as a potential human endocrine disruptor. J. Toxicol. Environ. Health, Part B Crit. Rev., 7: 281-295.

Grun, F. and Blumberg, B. 2006. Environmental obesogens: Organotins and endocrine disruption via nuclear receptor signaling. Endocrinology, 147: S50-S55.

Hala, M.T., Hanan, A.S., Nasser, H.A. and Abdel Fattah, M. K. 2009. Biosorption and biodegradation of antifouling compound tributyltin (TBT) by microalgae. Am-Eur J. Sci. Res., 4(1): 1-6.

Hamedani, N.F. and Farzaneh, F. 2006. Synthesis of ZnO nanocrystals with hexagonal (Wurtzite) structure in water using microwave irradiation. J. Sci., Islamic Repub. Iran, 17: 231 - 234.

Han, Z., Du, T. and Zhao Y. 2007. Adsorption of triphenyltin chloride on modified chitosan. J. Agro-Environ. Sc., 5: 1992 – 1995.

Harino, H., Fukushima, M., Kurpkawa, Y. and Kawai, S. 1997. Susceptibility of bacterial populations to organotin compounds and microbial degradation of organotin compounds in environmental water. Environ. Pollut., 98: 157.

Haug, G., Breedveld, G., Vangelsten, B.V. 2007. Removal of organotin compounds in dockyard wastewater by photolysis, Norwegian Geotechnological Institute, in: Anonymous (Ed.), Green North Sea Docks: Development of The Best Environmental Practice For Decontaminating Tributyltin (TBT) Containing Waters In The North Sea Region Based on Life Cycle Assessment, Reports,, INTERREG IIIB North Sea Programme.

Helena, J., Andrzej, S. and Jerzy C. 1991. Active Carbon. Ellis Horwood Ltd., London.

Ho, Y.S. 2006. Isotherms for the sorption of lead onto peat: Comparison of linear and non-linear methods. Pol. J. Environ. Stud., 15(1): 81 - 86.

Ho, Y.S. and McKay, G. 2002. Application of kinetic models to the sorption of copper (II) on to peat. Adsorpt. Sci. Technol., 20(8): 797 - 815.

Hoch, M. 2001. Organotin compounds in the environment - an overview. Appl. Geochem., 16 (s7-8): 719 - 743.

Hoch, M., Alonso-Azcarate, J., and Lischick, M. 2002. Adsorption behavior of toxic tributyltin to clay-rich sediments under various environmental conditions. Environ. Toxicol. Chem., 21(7):1390 - 1397.

Honda, K. and Takahashi, T. 2006. Organotin compound treatment. United State Patent Application Publication, 1 - 6.

Horiguchi, T., Cho, H., Shiraishi, H., Kojima, M., Kaya, M., Morita, M and Shimizu, M. 2001. Contamination by organotin (tributyltin and triphenyltin) compounds from antifouling paints and endocrine disruption in marine gastropods, RIKEN Review: Focused on New Trends in Bio-Trace Elements Research, 35: 9 - 11.

Hsieh, C.T. and Teng, H. 2000. Langmuir and Dubinin–Radushkevich analyses on equilibrium adsorption of activated carbon fabrics in aqueous solutions. J. Chem. Technol. Biot., 75(11): 1066 - 1072.

Hutson, H.D. and Yang, R.T. 1997. Theoretical basis for the Dubinin–Radushkevitch (D–R) adsorption isotherm equation. Adsorption, 3: 189 - 195.

Igwe, J.C., Abia, A.A. and Ibeh, C.A. 2008. Adsorption kinetics and intraparticulate diffusivities of Hg, As and Pb ions on unmodified and thiolated coconut fiber. Int. J. Environ. Sci. Tech., 5(1): 83 - 92.

Jha, V.K., Matsuda, M. and Miyake, M. 2008. Sorption properties of the activated carbon-zeolite composite prepared from coal fly ash for Ni^{2+}, Cu^{2+}, Cd^{2+} and Pb^{2+}. J. Hazard. Mater., 160: 148 - 153.

Kannan, K. and Lee, R. F. 1996. Triphenyltin and its degradation products in foliage and soils from sprayed pecan orchards and in fish from adjacent ponds. Environ. Toxicol. Chem., 15: 1492-1499.

Kaya, I.G.B., Duranoglu D., Beker U. and Senkal B.F. 2012. Development of polymeric and polymer-based hybrid adsorbents for chromium removal from aqueous solution, Clean – Soil, Air, Water, 40: 1222–1228.

Kimbrough, R. D. 1976. Toxicity and health effects of selected organotin compounds: A review. Environ. Health perspect.. 14: 51-56.

Knaebel, K.S. 2008. Adsorbent selection, adsorption research, Inc. Dublin, Ohio 43016, 1-21. http://www.adsorption.com/publications/AdsorbentSel1B.pdf, [19 November 2010].

Kosmulski, 2009. Compilation of PZC and IEP of sparingly soluble metal oxides and hydroxides from Literature. Adv. colloid Interface Sci., 152: 14 - 25.

Kumar, P.S. and Kirthika, K. 2009. Equilibrium and kinetic study of adsorption of nickel from aqueous solution onto bael tree leaf powder, J. Eng. Sci. Technol. 4(4): 351 – 363.

Kumar, P.S., Vincent, C., Kirthika, K. and Kumar, K.S. 2010. Kinetics and equilibrium studies of Pb^{2+} ion removal from aqueous solutions by use of nano-silversol-coated activated carbon. Braz. J. Chem. Eng. 27 (2): 339 – 346.

Langner, M., Gabrielska, J. and Przestalski, S. 2000. Adsorption of triphenyltin compounds onto phosphatidylcholine/cholesterol bilayers. Appl. Organomet. Chem., 14(1): 25 - 33.

Lespes, G., Marcic, C., LeHecho, I., Mench, M. and Potin-Gautier, M. 2003. Speciation of organotins in French beans and potatoes cultivated on soils spiked with solutions or amended with a sewage sludge. Elec. J. Env. Agricult. Food Chem., 2: 365-373.

Li, L., Quinlivan, P.A. and Knappe, D.R.U. 2002. Effects of activated carbon surface chemistry and pore structure on the adsorption of organic contaminants from aqueous solution. Carbon, 40: 2085 - 2100.

Liang, L., Luo, L. and Zhang, S. 2011. Adsorption and desorption of humic and fulvic acids on SiO_2 particles at nano and micro-scales. Colloids Surf. A, 384: 126 - 130.

Lin, J., Zhan, Y., Zhu, Z. and Xing, Y. 2011. Adsorption of tannic acid from aqueous solution onto surfactant-modified zeolite. J. Hazard. Mater. 193, 102-111.

Lu, G.Q. and Do, D.D. 1991. Adsorption properties of fly ash particles for NOx removal from flue gases. Fuel Process Technol., 27: 95 - 107.

Maarof HI, and Hameed B.H. 2004. Adsorption isotherms for phenol onto activated carbon. AJChE 4: 70 - 76.

Maes, A. and Vreysen, S. 2007. Use of sorbent materials for the removal of Cu, Zn and organotin compounds from dockyard wastewaters, in: Anonymous (Ed.), Green North Sea Docks: Development of The Best Environmental Practice For Decontaminating Tributyltin (TBT) Containing Waters In The North Sea Region Based On Life Cycle Assessment, Reports,, INTERREG IIIB North Sea Programme.

Maguire, R. J. 1991. Water pollution. Res. J. Can., 26: 243.

Mall, I.D., Srivastava, V.C. and Agarwal, N.K. 2006. Removal of Orange-G and Methyl Violet dyes by adsorption onto bagasse fly ashdkinetic study and equilibrium isotherm analyses. Dyes Pigments, 69: 210 - 223.

Matthiessen, P. and Gibbs, P. 1998. Critical appraisal of the evidence for tributyltin mediated endocrine disruption in molluscs. Environ. Toxicol. Chem., 17: 37-43.

McAllister, B. G. and Kime, D. E. 2003. Early life exposure to environmental levels of the aromatase inhibitor tributyltin causes masculinisation and irreversible sperm damage in zebrafish (Danio rerio). Aquat. Toxicol., 65: 309-316.

Meador, J. P. 1997. Comparative toxicokinetics of tributyltin in five marine species and its utility in predicting bioaccumulation and toxicity. Aquatic Toxicol., 37: 307-326.

Meador, J. P. 2000. Predicting the fate and effects of tributyltin in marine systems. Rev. Environ. Contam. Toxicol., 166: 1-48.

Meador, J. P. and Rice, C. A. 2001. Impaired growth in the polychaete *Armandia brevis* exposed to tributyltin in sediment. Mar. Environ. Res., 51: 113-129.

Meshko, V., Markovska, L., Minchev, M. and Rodrigues, A.E. 2001. Adsorption of basic dyes on granular activated carbon and natural zeolite. Water Res., 35(14): 3357.

Mimura, H., Sato, R., Sasaki, Y., Furuyama, Y., Taniike, A., Yoshida, K. and Kitatamura, A. 2008. Accelerator analysis of tributyltin adsorbed onto the surface of a tributylin resistant marine *Pseudoalteromonas* sp. Cell. Int. J. Mol. Sci., 9: 1989 - 2002.

Mizukawa, H., Takahashi, S., Nakayama, K., Sudo, A. and Tanabe, S. 2009. Contamination and Accumulation Feature of organotin compounds in Common Cormorants (Phalacrocorax carbo) from Lake Biwa, Japan. Inter. Studies Environ. Chem- Environ. Res. Asia, 153 - 161.

Mopoung, S., and Nogklai, W. 2008. Chemical and surface properties of Longan seed activated charcoal. Int. J. Phys. Sci., 3(10): 234 - 239.

Munoz, J., Baena, J.R., Gallego, M. and Valcárcel, M. 2004. Speciation of butyltin compounds in marine sediments by preconcentration on C60 and gas chromatography–mass spectrometry. J. Chromatogr. A, 1023: 175-181.

Nascimento, M., Soares, P.S.M. and Souza, V.P. 2008. Adsorption of heavy metal cations using coal fly ash modified by hydrothermal method. Fuel, 88: 1714 - 1719.

Newcombe, G., Morrison, J., Hepplewhite, C. and Knappe, D.R.U. 2002. Simultaneous adsorption of MIB and NOM onto activated carbon II. Competitive effects. Carbon, 40: 2147 - 2156.

NLM 1998. Hazardous Substances Data Bank. Bethesda, MD, US National Library of Medicine. CHEM-BANK CD-ROM, distributed by SilverPlatter International, NV.

Noh, J. S. and Schwarz, J. A. 1989. J. Colloid Interface Sci., 130: 157.

Ogata, R., Omura, M., Shimasaki, Y., Kubo, K., Oshima, Y., Aou, S. and Inou, N. 2001. Two generation reproductive toxicity study of tributyltin chloride in female rats. Toxicol. Environ. health A, 63: 127-144.

Oh, W.C., Chen, M.L. and Lim, C.S. 2007. Preparation with different mixing ratios of anatase to activated carbon and their photocatalytic performance. J. Ceram. Process. Res., 8(2):119 - 124.

Okieimen, F.E. and Orhorhoro, F. 1986. Binding Cadmium and Copper ions with chemically modified cellulosic materials. Int. J. Environ. Anal. Chem. 24: 319-325.

Oliveira, C.R., Santos, D.M., Madureira, L.A.S. and Marchi, M.R.R. 2010. Speciation of butyltin derivatives in surface sediments of three southern Brazilian harbors. J. Hazard. Mater., 181(1-3): 851-856.

Ottosen, L.M., Arevalo, E., Stichnothe, H. and Calmano, W. 2006. Ferric flocks to remove Zn and Cu from dockyard wastewater. Environ. Chem. Lett., 3(4): 164 - 168.

Panday, K.K., Prasad, G. and Singh, V.N. 1985. Copper (II) removal from aqueous solutions by fly ash. Water Res., 19(7): 869 - 873.

Park, M.O. and Hahn, Y.H. 1996. Occurrence of butyltin compounds in seawater, sediment and biosamples from the South Coast of Korea by GC-QFAAS. Inter. J. Offshore Polar Eng., 6(4): 313 - 319.

Peng, Z.G., Hidajat, K. and Uddin, M.S. 2004. Adsorption and desorption of lysozyme on nano-sized magnetic particles and its conformational changes. Colloids Surf. B, 169 - 174.

Prasad, R. and Schafran, G.C. 2006. Characterisation of tributyltin in shipyard waters and removal through laboratory and full-scale treatment. Water Res., 40(3):453 - 462.

Radke, B., Staniszewska, M., Wasik, A., Namieśnik, J. and Bolałek, J. 2008. Organotin Compounds in Marine Sediments. Pol. J. Environ. Stud., 17 (5): 643-654.

Rakhshaee, R., Giahi, M. and Pourahmad, A. 2011. Removal of methyl orange from aqueous solution by Azolla filicoloides: Synthesis of Fe_3O_4 nano-particles and its surface modification by the extracted pectin of Azolla. Chinese Chem. Lett., 22: 501 - 504.

Reynolds, K. 2004. The use of fly ash for the control and treatment of acid mine drainage. Proceedings of the 2004 Water Institute of Southern Africa (WISA) Biennial Conference. pp 956 - 961.

Ricou, P., Lecuyer, I. and Cloirec, P.L. 1999. Removal of Cu^{2+}, Zn^{2+} and Pb^{2+} by adsorption onto fly ash and fly ash/lime mixing. Water Sci. Tech., 39(10-11): 239 - 247.

Ricou, P., Lecuyer, I. and Cloirec, P.L. 2001. Experimental design methodology applied to adsorption of metallic ions onto fly ash. Wat. Res., 35(4): 965 - 976.

Rodriguez, I., Santamarina, M., Bollaín, M.H., Mejuto, M.C. and Cela, R. 1997. Speciation of organotin compounds in marine biomaterials after basic leaching in a non-focused microwave extractor equipped with pressurized vessels. J. Chromatogr. A, 774(1-2): 379-387.

Said-Pullicino, D. and Vella, A.J. 2005. Adsorption characteristics of tributyltin on municipal solid waste compost. Appl. Organometal. Chem., 19: 719 - 726.

Sathishkumar, M., Binupriya, A.R., Vijayaraghavan, K. and Yun, S. 2007. Two and three-parameter isothermal modeling for liquid-phase sorption of Procion Blue H-B by inactive mycelial biomass of Panus fulvus. J. Chem. Technol. Biotechnol., 82: 389 - 398.

Sander, H.L.T., Berth-Jan, D. and Gerard, K. 2004. Synthetic aspects of tetraorganotins and organotin(IV) halides. J. Organomet. Chem., 689: 2145 - 2157.

Sarkar, A., Bassu, A.K., Udaybhanu, G. and Rano, R., 2006. A comprehensive characterisationof fly ash from a thermal power plant in Eastern India. Fuel, 87: 259 - 77.

Sheela, T., Arthoba Nayaka, Y., Viswanatha, R., Basavanna, S. and Venkatesha, T.G. 2012. Kinetics and thermodynamics studies on the adsorption of Zn(II), Cd(II) and Hg(II) from aqueous solution using zinc oxide nanoparticles. Powder Technol., 217: 163 - 170.

Sheikh M. A., Noah, N.M., Tsuha, K. and Oomori, T. 2007. Occurrence of tributyltin compounds and characteristics of heavy metals. Int. J. Environ. Sci. Tech., 4(1): 49 - 59.

Shi, Z., Liu, F. and Yao, S. 2012. Adsorptive removal of phosphate from aqueous solutions using activated carbon loaded with Fe(III) oxide. Carbon, 50: 344.

Shin, S.K. and Song, J.H. 2011. Modeling and simulations of the removal of formaldehyde using silver nano-particles, attached to granular activated carbon. J. Hazard. Mater., 194: 385-392.

Shukla, P.R., Wang, S., Ang, H.M. and Tadé, M.O. 2009. Synthesis, characterisation, and adsorption evaluation of carbon-natural-zeolite composites. Adv. Powder Technol., 20: 245 - 250.

Sonak, S., Pangam, P., Giriyan, A. and Hawaldar, K. 2009. Implications of the ban on organotins for protection of global coastal and marine ecology. J. Environ. Manage., 90: S96 - S108.

Song, Y.C., Woo J.H., Park S.H. and Kim I.S. 2005. A study of the treating of antifouling paint waste from shipyard. Mar. Pollut. Bull., 51: 1048 - 1053.

Stenzel, M.H. 1993. Remove organics by activated carbon adsorption. Chem. Eng. Prog., 89(4): 36 - 43.

Sutcu, L. 2005. Removal of boron from waters using fly ash, M.Sc. Thesis submitted to the Graduate School of Engineering and Science of İzmir Institute of Technology, İZMİR, 1 -84.

Takimura, O., Inoue, H., Fuse, H., Murakami, K., Yamaoka, Y. and Aihara, M. 2003. Adsorption and degradation of triphenyltin by Pseudomonas chiororaphis immobilized in alginate beads. J. Jpn Soc. Water Environ., 26(11): 713 - 717.

Tesfalidet, S. 2004. Screening of organotin compounds in the Swedish Environment. Analytical Chemistry Umeå University 901 87 Umeå, 1 - 23.

Tam, N.F.Y., Chong, A. and Wong, Y.S. 2002. Removal of tributyltin (TBT) by live and dead microalgal cells. Mar. Pollut. Bull., 45: 362 - 371.

Tam, N.F.Y., Chong, A. and Wong, Y.S. 2003. Removal of tributyltin (TBT) from wastewater by microalgae. Water Pollut., 7: 1 - 12.

Tomlin, C. 1997. The pesticide manual, 11th ed. Surrey, British Crop Protection Council; Cambridge, The Royal Society of Chemistry.

Toth, J., 1971. State equations of the solid gas interface layer. Acta Chem. Acad. Sci. Hungaria, 69: 311 - 317.

Tseng, H.H., Su, J.G. and Liang, C. 2011. Synthesis of granular activated carbon/zero valent iron composites for simultaneous adsorption/dechlorination of trichloroethylene. J. Hazard. Mater., 192: 500 - 506.

Tsunoi, S., Takashi, M., Hirotaka, S., Giang Thi Huong, L., Harino, H. and Tanaka, M. 2002. Analysis of organotin compounds by grignard derivatization and gas chromatography–ion trap tandem mass spectrometry. J. Chromatogr. A, 962(1-2): 197-206.

Vidal, J.L., Vega, A.B., Arrebola, F.J., Gonzalez-Rodrıguez, M.J., Sanchez, M.C.M. and Frenich, A.G. 2003. Trace Determination of organotin compounds in Water, Sediment and Mussel Samples by Low-pressure Gas Chromatography coupled to Tandem Mass Spectrometry. Rapid Commun. Mass Spectrom., 17: 2099 - 2106.

Vimlesh, K. and Giri, A.K. 2011. Characterization of fly ash generated from Parichha Thermal Power Station in Jhansi, India. E-J Chem., 8(1): 400 - 404.

Viraraghvan, T. and Dronamraju, M.M. 1993. Removal of copper, nickel and zinc from wastewater by adsorption using peat. J. Environ. Sci. Health A: Environ. Sci. Eng., 28: 1261 - 1276.

Vreysen, S., Maes, A. and Wullaert, H. 2008. Removal of organotin compounds, Cu and Zn from shipyard wastewaters by adsorption – flocculation: A technical and economical analysis. Mar. Pollut. Bull., 56: 106 - 115.

Waite, M. E., Evans, K. E., Thain, J. E. and Waldock, M. J. 1989. Organotin concentrations in the Rivers Bure and Yare, Norfolk Broads, England. Appl. Organomet. Chem., 3: 383-391.

Wang, C., Zhao, J., Wang, X., Mai, B., Sheng, G., Peng, P. and Fu, J. 2002. Preparation, characterization and photocatalytic activity of nano-sized ZnO/SnO_2 coupled photocatalysts. Appl. Catal. B-Environ., 39: 269 - 279.

Wang, S.B. and Wu, H.W. 2006. Environmental-benign utilisation of fly ash as low-cost adsorbents. J. Hazard. Mater., 136(3): 482 - 501.

Wang, S., Ma, Q. and Zhu, Z.H. 2008. Characteristics of coal fly ash and adsorption application. Fuel, 87: 3469 - 3473.

Wang Y.S., Hsieh S.H., Lee C.H. and Horng J.J. 2013. Adsorption of complex pollutants from aqueous solutions by nanocomposite materials, Clean – Soil, Air, Water. DOI: 10.1002/clen.201200093.

Ward, C.R. and French, D. 2005. Relation between coal and fly ash mineralogy, based on quantitative x-ray diffraction methods. 2005 World of Coal Ash (WOCA), Lexington, Kentucky, USA.

Weidenhaupt, A., Arnold, C., Müller, S.R., Haderlein S.B., and Schwarzenbach, R.P. 1997. Sorption of organotin biocides to mineral surfaces. Environ. Sci. Technol., 31 (9):2603 - 2609.

Westerhoff, P., Karanfil, T. and Crittenden, J. 2006. Aerogel and iron-oxide impregnated granular activated carbon media for arsenic removal. Awwa Research Foundation and Arsenic Water Technology Partnership, USA, pp. 1-98.

WHO, 1980. Tin and organotin compounds a preliminary review. Environ. Health Crit. 15. World health Organization, Geneva, Switzerland.

WHO 1990. Tributyltin compounds. Environmental Health Criteria 116; World Health Organization, Genève, Switzerland.

Xiao, Q., Bin, H. and Man, H. 2008. Speciation of butyltin compounds in environmental and biological samples using headspace single drop microextraction coupled with gas chromatography-inductively coupled plasma mass spectrometry. J. Chromatogr. A, 1211(1-2): 135-141.

Yang, K., Lin, D.H. and Xing, B.S. 2009. Interactions of humic acid with nanosized inorganic oxides. Langmuir, 25: 3571 - 3576.

Yu-huan, Y., Hao, C. and Gang, P. 2007. Particle concentration effect in adsorption/desorption of Zn(II) on anatase type nano TiO_2. J. Environ. Sci., 19: 1442 - 1445.

Yu, J.X., Chi, R.A., Su, X.Z., He, Z.Y., Qi, Y.F and Zhang, Y.F. 2010. Desorption behaviour of methylene blue on pyromellitic dianhydride modified biosorbent by novel eluent:acid TiO_2 hydrosol. J. Hazard. Mater., 177:222-227.

Zachariadis, G.A. and Rosenberg, E. 2009. Speciation of organotin compounds in urine by GC–MIP-AED and GC–MS after ethylation and liquid–liquid extraction. J. Chromatogr. B, 877: 1140-1144.

Zawani, Z, Luqman C.A. and Thomas, S.Y.C. 2009. Equilibrium, kinetics and thermodynamic studies: Adsorption of Remazol Black 5 on the palm kernel shell activated carbon (PKS-AC). Eur. J. Sci. Res., 37(1): 67 - 76.

Zheng, Y., Zhang, J. and Wang, A. 2009. Fast removal of ammonium nitrogen from aqueous solution using chitosan-g-poly(acrylic acid)/attapulgite composite. Chem. Eng., 155: 215 - 222.

Zhang, G., Qu, J., Liu, H., Cooper, A.T. and Wu, R. 2007. $CuFe_2O_4$/activated carbon composite: A novel magnetic adsorbent for the removal of acid orange II and catalytic regeneration. Chemosphere, 68: 1058 - 1066.

APPENDICES

APPENDIX A: DATA ON THE SORPTION OF TBT FROM TBT – CONTAMINATED ARTIFICIAL SEAWATER

Activated carbon

Effect of adsorbent amount

Mass (g)	Mean ce (mg/L)	% removal
0.0625	6.801	93.199
0.125	5.852	94.148
0.25	3.8447	96.1553
0.5	0.289	99.711
1	0.273	99.727

Effect of contact time qe = 4.9996

Time	Mean ce (mg/L)	qt (mg/g)	% removal	qe-qt	log (qe-qt)	t/qt (g min/mg)	ln t (min)	log t	log qt	α	1-α	ln (1-α)
10	10.112	4.4944	89.888	0.5052	-0.29654	2.224991	2.302585	1	0.652672	0.898952	0.101048	-2.2922
20	8.38	4.581	91.62	0.4186	-0.3782	4.365859	2.995732	1.30103	0.66096	0.916273	0.083727	-2.4802
40	4.594	4.7703	95.406	0.2293	-0.6396	8.385217	3.688879	1.60206	0.678546	0.954136	0.045864	-3.0821
50	3.207	4.83965	96.793	0.15995	-0.79602	10.33133	3.912023	1.69897	0.684814	0.968007	0.031993	-3.4423
60	3.189	4.84055	96.811	0.15905	-0.79847	12.39529	4.094345	1.778151	0.684895	0.968187	0.031813	-3.4479
70	3.19	4.8405	96.81	0.1591	-0.79833	14.46132	4.248495	1.845098	0.68489	0.968177	0.031823	-3.4476

Effect of pH

pH	Mean ce (mg/L)	ca (mg/g)	% removal
3	6.787	4.66065	93.213
4	5.621	4.71895	94.379
5	4.311	4.78445	95.689
7	3.189	4.84055	96.811
8	3.062	4.8469	96.938
9	3.031	4.84845	96.969

Effect of stirring speed

Speed	Mean ce (mg/L)	ca (mg/g)	% removal
160	3.189	4.84055	96.811
170	2.104	4.8948	97.896
180	1.13	4.9435	98.87
190	0.738	4.9631	99.262
200	0.731	4.96345	99.269

Effect of initial concentration

Init. Conc.	% removal	Mean ce (mg/L)	ca mg/g	ce/ca (g/dm^3)	log ce	log ca	ln ce	1 +1/ce	ln (1+1/ce)	E	E^2	ln ca
12.5	98.904	0.137	0.61815	0.221629	-0.8633	-0.20891	-1.98777	8.29927	2.116168	5858.741	34324847	-0.48102
25	98.992	0.252	1.2374	0.203653	-0.5986	0.09251	-1.37833	4.968254	1.603068	4438.194	19697570	0.213012
50	99.136	0.432	2.4784	0.174306	-0.3645	0.394171	-0.83933	3.314815	1.198402	3317.85	11008126	0.907613
100	99.269	0.731	4.96345	0.147277	-0.1361	0.695784	-0.31334	2.367989	0.862041	2386.614	5695927	1.602101
200	99.269	1.462	9.9269	0.147277	0.16495	0.996814	0.379805	1.683995	0.521169	1442.888	2081925	2.295248

Effect of temperature					kc		- Δ G		
T K	T °C	% removal	ca (mg/g)	Mean ce (mg/L)	ca/ce	ln kc	RTlnKc	1/T	log kc
313	40	99.877	99.877	0.123	812.0081	6.69951	17434.02	0.003195	2.90956
323	50	99.918	99.918	0.082	1218.512	7.105386	19080.96	0.003096	3.08583
333	60	99.943	99.943	0.057	1753.386	7.469304	20679.23	0.003003	3.243878
343	70	99.951	99.951	0.049	2039.816	7.620615	21731.72	0.002915	3.309591
353	80	99.952	99.952	0.048	2082.333	7.641244	22425.84	0.002833	3.31855

Fly ash

Effect of adsorbent amount

Mass (g)	Mean ce (mg/L)	% removal
0.0625	30.64	69.36
0.125	21.456	78.544
0.25	11.25	88.75
0.5	10.933	89.067
1	9.595	90.405

Effect of contact time qe = 4.8942

Time	Mean ce (mg/L)	qt (mg/g)	% removal	qe-qt	log (qe-qt)	t/qt (g min/mg)	ln t (min)	log t	log qt	α	1-α	ln (1-α)
10	65.2	1.74	34.8	3.1542	0.49889	5.747126	2.302585	1	0.240549	0.35552	0.64448	-0.4393
20	45.34	2.733	54.66	2.1612	0.33469	7.317966	2.995732	1.30103	0.436639	0.55842	0.44158	-0.8174
40	15.3	4.235	84.7	0.6592	-0.1809	9.445100	3.688879	1.60206	0.626853	0.86531	0.13469	-2.0048
50	10.576	4.4712	89.424	0.423	-0.3737	11.18268	3.91202	1.69897	0.650424	0.91357	0.08643	-2.4484
60	10.833	4.45835	89.167	0.43585	-0.3607	13.45789	4.094345	1.77815	0.649174	0.91095	0.08905	-2.4185
70	10.843	4.45785	89.157	0.43635	-0.3602	15.70264	4.248495	1.84509	0.649126	0.91084	0.08916	-2.4174

Effect of pH

pH	Mean ce (mg/L)	ca (mg/g)	% removal
3	21.011	3.94945	78.989
4	17.478	4.1261	82.522
5	14.221	4.28895	85.779
7	10.833	4.45835	89.167
8	10.53	4.4735	89.47
9	10.438	4.4781	89.562

Effect of stirring speed

Speed	Mean ce (mg/L)	ca (mg/g)	% removal
160	10.833	4.45835	89.167
170	8.612	4.5694	91.388
180	6.825	4.65875	93.175
190	5.576	4.7212	94.424
200	5.468	4.7266	94.532

Effect of initial concentration

Init. Conc.	% removal	Mean ce (mg/L)	ca mg/g	ce/ca (g/dm^3)	log ce	log ca	ln ce	1 +1/ce	ln (1+1/ce)	E	E^2	ln ca
12.5	93.212	0.8485	0.5826	1.456465	-0.07135	-0.23465	-0.16429	2.17855	0.77866	2155.768	4647334	-0.5403
25	93.344	1.664	1.1668	1.426123	0.221153	0.066996	0.509224	1.600962	0.470604	1302.897	1697542	0.154265
50	93.804	3.098	2.3451	1.321052	0.491081	0.370161	1.130757	1.322789	0.279742	774.4839	599825.3	0.852328
100	94.532	5.468	4.7266	1.156857	0.737829	0.674549	1.698913	1.182882	0.167954	464.9911	216216.7	1.553206
200	94.532	10.936	9.4532	1.156857	1.038859	0.975579	2.39206	1.091441	0.087499	242.2463	58683.25	2.246353

Effect of temperature

T K	T °C	% removal	ca (mg/g)	Mean ce (mg/L)	kc ca/ce	ln kc	- Δ G RTlnKc	1/T	log kc
313	40	95.641	95.641	4.359	21.94104	3.088359	8036.781	0.003195	1.341257
323	50	95.671	95.671	4.329	22.10002	3.095579	8312.935	0.003096	1.344393
333	60	95.686	95.686	4.314	22.18034	3.099206	8580.345	0.003003	1.345968
343	70	95.729	95.729	4.271	22.41372	3.109673	8867.862	0.002915	1.350514
353	80	95.746	95.746	4.254	22.50729	3.113839	9138.626	0.002833	1.352323

nFe_3O_4

Effect of adsorbent amount

Mass (g)	Mean ce (mg/L)	% removal
0.0625	60.044	39.956
0.125	54.937	45.063
0.25	47.238	52.762
0.5	22.854	77.146
1	22.943	77.057

Effect of contact time qe = 4.4872

Time	Mean ce (mg/L)	qt (mg/g)	% removal	qe-qt	log (qe-qt)	t/qt (g min/mg)	ln t (min)	log t	log qt	α	1-α	ln (1-α)
10	47.445	2.62775	52.555	1.85945	0.269385	3.805537	2.302585	1	0.419584	0.58561	0.41439	-0.8809
20	32.401	3.37995	67.599	1.10725	0.044246	5.917247	2.995732	1.30103	0.52891	0.753243	0.246757	-1.3994
40	26.465	3.67675	73.535	0.81045	-0.09127	10.87917	3.688879	1.60206	0.565464	0.819386	0.180614	-1.7114
50	24.527	3.77365	75.473	0.71355	-0.14658	13.24977	3.912023	1.69897	0.576762	0.840981	0.159019	-1.8387
60	23.854	3.8073	76.146	0.6799	-0.16755	15.7592	4.094345	1.778151	0.580617	0.84848	0.15152	-1.8870
70	23.856	3.8072	76.144	0.68	-0.16749	18.38622	4.248495	1.845098	0.580606	0.848458	0.151542	-1.8869

Effect of pH

pH	Mean ce (mg/L)	ca (mg/g)	% removal
3	41.358	2.9321	58.642
4	29.379	3.53105	70.621
5	24.967	3.75165	75.033
7	22.854	3.8573	77.146
8	22.703	3.86485	77.297
9	22.697	3.86515	77.303

Effect of stirring speed

Speed	Mean ce (mg/L)	ca (mg/g)	% removal
160	22.854	3.8573	77.146
170	20.751	3.96245	79.249
180	19.125	4.04375	80.875
190	18.145	4.09275	81.855
200	18.067	4.09665	81.933

Effect of initial concentration

Init. Conc.	% removal	Mean ce (mg/L)	ca mg/g	ce/ca (g/dm^3)	log ce	log ca	ln ce	1 +1/ce	ln (1+1/ce)	E	E^2	ln ca
12.5	80.068	2.4915	0.500425	4.978768	0.396461	-0.30066	0.91288	1.401365	0.337447	934.2416	872807.3	-0.6923
25	80.528	4.868	1.0066	4.836082	0.687351	0.002857	1.58268	1.205423	0.186831	517.2523	267550	0.006578
50	81.052	9.474	2.0263	4.675517	0.976533	0.306704	2.24855	1.105552	0.100345	277.8108	77178.83	0.706211
100	81.933	18.067	4.09665	4.410189	1.256886	0.612429	2.89409	1.05535	0.053872	149.148	22245.14	1.41017
200	81.933	36.134	8.1933	4.410189	1.557916	0.913459	3.58723	1.027675	0.027299	75.57826	5712.073	2.103317

Effect of temperature

T K	T ^oC	% removal	ca (mg/g)	Mean ce (mg/L)	kc ca/ce	ln kc	- Δ G RTlnKc	1/T	log kc
313	40	93.725	93.725	6.275	14.93625	2.703791	7036.028	0.003195	1.174242
323	50	94.635	94.635	5.365	17.63933	2.870131	7707.513	0.003096	1.246482
333	60	96.547	96.547	3.453	27.96032	3.330787	9221.489	0.003003	1.446542
343	70	96.762	96.762	3.238	29.88326	3.397298	9688.083	0.002915	1.475428
353	80	96.782	96.782	3.218	30.0752	3.403701	9989.325	0.002833	1.478209

$nSiO_2$

Effect of adsorbent amount

Mass (g)	Mean ce (mg/L)	% removal
0.0625	26.514	73.486
0.125	20.93	79.07
0.25	15.822	84.178
0.5	12.603	87.397
1	10.205	89.795

Effect of contact time qe = 4.8076

Time	Mean ce (mg/L)	qt (mg/g)	% removal	qe-qt	log (qe-qt)	t/qt (g min/mg)	ln t (min)	log t	log qt	α	1-α	ln (1-α)
10	26.963	3.65185	73.037	1.15575	0.062864	2.738338	2.302585	1	0.562513	0.759599	0.240401	-1.4255
20	24.459	3.77705	75.541	1.03055	0.013069	5.295138	2.995732	1.30103	0.577153	0.785641	0.214359	-1.5401
40	16.822	4.1589	83.178	0.6487	-0.18796	9.617928	3.688879	1.60206	0.618978	0.865068	0.134932	-2.0029
50	14.26	4.287	85.74	0.5206	-0.2835	11.66317	3.912023	1.69897	0.632153	0.891713	0.108287	-2.2229
60	12.603	4.36985	87.397	0.43775	-0.35877	13.73045	4.094345	1.778151	0.640467	0.908946	0.091054	-2.3963
70	12.599	4.37005	87.401	0.43755	-0.35897	16.01812	4.248495	1.845098	0.640486	0.908988	0.091012	-2.3968

Effect of pH

pH	Mean ce (mg/L)	ca (mg/g)	% removal
3	30.074	3.4963	69.926
4	22.935	3.85325	77.065
5	14.201	4.28995	85.799
7	12.603	4.36985	87.397
8	12.015	4.39925	87.985
9	12.015	4.39925	87.985

Effect of stirring speed

Speed	Mean ce (mg/L)	ca (mg/g)	% removal
160	12.603	4.36985	87.397
170	10.305	4.48475	89.695
180	8.581	4.57095	91.419
190	7.503	4.62485	92.497
200	7.068	4.6466	92.932

Effect of initial concentration

Init. Conc.	% removal	Mean ce (mg/L)	ca mg/g	ce/ca (g/dm^3)	log ce	log ca	ln ce	1 +1/ce	ln (1+1/ce)	E	E^2	ln ca
12.5	91.944	1.007	0.57465	1.752371	0.003029	-0.2406	0.006976	1.993049	0.689665	1909.382	3645738	-0.55399
25	92.512	1.872	1.1564	1.618817	0.272306	0.063108	0.627007	1.534188	0.428001	1184.948	1404102	0.145312
50	92.828	3.586	2.3207	1.545223	0.55461	0.365619	1.277037	1.278862	0.245971	680.9854	463741.2	0.841869
100	92.932	7.068	4.6466	1.521112	0.849297	0.667135	1.955578	1.141483	0.132328	366.3585	134218.5	1.536136
200	92.932	14.136	9.2932	1.521112	1.150327	0.968165	2.648725	1.070741	0.068351	189.2347	35809.79	2.229283

Effect of temperature

T K	T ^oC	% removal	ca (mg/g)	Mean ce (mg/L)	kc ca/ce	ln kc	- Δ G RTlnKc	1/T	log kc
313	40	99.607	99.607	0.393	253.4529	5.535178	14404.09	0.003195	2.403897
323	50	99.766	99.766	0.234	426.3504	6.055262	16260.93	0.003096	2.629767
333	60	99.867	99.867	0.133	750.8797	6.621245	18331.33	0.003003	2.87557
343	70	99.877	99.877	0.123	812.0081	6.69951	19105.01	0.002915	2.90956
353	80	99.878	99.878	0.122	818.6721	6.707684	19685.99	0.002833	2.91311

nZnO

Effect of adsorbent amount

Mass (g)	Mean ce (mg/L)	% removal
0.0625	65.139	34.861
0.125	40.46	59.54
0.25	28.253	71.747
0.5	24.471	75.529
1	23.141	76.859

Effect of contact time

qe = 4.11825

Time	Mean ce (mg/L)	qt (mg/g)	% removal	qe-qt	log (qe-qt)	t/qt (g min/mg)	ln t (min)	log t	log qt	α	1-α	ln (1-α)
10	45.473	2.72635	54.527	1.3919	0.143608	3.667908	2.302585	1	0.435582	0.662017	0.33798	-1.0848
20	29.454	3.5273	70.546	0.59095	-0.22845	5.670059	2.995732	1.30103	0.547442	0.856505	0.14349	-1.9415
40	27.399	3.63005	72.601	0.4882	-0.3114	11.01913	3.688879	1.60206	0.559913	0.881455	0.11855	-2.1325
50	25.373	3.73135	74.627	0.3869	-0.4124	13.39998	3.912023	1.69897	0.571866	0.906052	0.09395	-2.3650
60	24.471	3.77645	75.529	0.3418	-0.46623	15.88794	4.094345	1.778151	0.577084	0.917004	0.08299	-2.4889
70	24.47	3.7765	75.53	0.34175	-0.46629	18.53568	4.248495	1.845098	0.577089	0.917016	0.08298	-2.4891

Effect of pH

pH	Mean ce (mg/L)	ca (mg/g)	% removal
3	43.614	2.8193	56.386
4	32.326	3.3837	67.674
5	26.138	3.6931	73.862
7	24.471	3.77645	75.529
8	22.5	3.875	77.5
9	22.425	3.87875	77.575

Effect of stirring speed

Speed	Mean ce (mg/L)	ca (mg/g)	% removal
160	24.471	3.77645	75.529
170	22.807	3.85965	77.193
180	21.179	3.94105	78.821
190	20.226	3.9887	79.774
200	20.103	3.99485	79.897

Effect of initial concentration

Init. Conc.	% removal	Mean ce (mg/L)	ca mg/g	ce/ca (g/dm^3)	log ce	log ca	ln ce	1 +1/ce	ln (1+1/ce)	E	E^2	ln ca
12.5	77.912	2.761	0.48695	5.66999	0.441066	-0.31252	1.015593	1.362188	0.30909	855.7402	732291.3	-0.71959
25	78.46	5.385	0.98075	5.49069	0.731186	-0.00844	1.683617	1.185701	0.17033	471.5807	222388.4	-0.01944
50	79.184	10.408	1.9796	5.25763	1.017367	0.296577	2.342575	1.09608	0.09174	253.9882	64510.01	0.682895
100	79.897	20.103	3.99485	5.03223	1.303261	0.6015	3.000869	1.049744	0.04855	134.403	18064.18	1.385006
200	79.896	40.208	7.9896	5.03254	1.604312	0.902525	3.694066	1.024871	0.02457	68.01369	4625.862	2.078141

Effect of temperature

T K	T °C	% removal	ca (mg/g)	Mean ce (mg/L)	kc ca/ce	ln kc	- Δ G RTlnKc	1/T	log kc
313	40	89.81	89.81	10.19	8.813543	2.176289	5663.319	0.003195	0.945151
323	50	94.656	94.656	5.344	17.71257	2.874275	7718.641	0.003096	1.248282
333	60	95.6	95.6	4.4	21.72727	3.078568	8523.207	0.003003	1.337005
343	70	96.796	96.796	3.204	30.21099	3.408206	9719.187	0.002915	1.480165
353	80	96.956	96.956	3.044	31.85151	3.461085	10157.74	0.002833	1.50313

Fly ash/activated carbon composite

Effect of adsorbent amount

Mass (g)	Mean ce (mg/L)	% removal
0.0625	1.602	98.398
0.125	1.27	98.73
0.25	0.637	99.363
0.5	0.419	99.581
1	0.391	99.609

Effect of contact time

qe = 4.9888

Time	Mean ce (mg/L)	qt (mg/g)	% removal	qe-qt	log (qe-qt)	t/qt (g min/mg)	ln t (min)	log t	log qt	α	1-α	ln (1-α)
10	6.158	4.6921	93.842	0.2967	-0.52768	2.131242	2.30259	1	0.671367	0.940527	0.05947	-2.8222
20	4.163	4.79185	95.837	0.19695	-0.70564	4.173753	2.99573	1.30103	0.680503	0.960522	0.03948	-3.232
40	1.184	4.9408	98.816	0.048	-1.31876	8.095855	3.68888	1.60206	0.693797	0.990378	0.00962	-4.6438
50	0.571	4.97145	99.429	0.01735	-1.7607	10.05743	3.91202	1.69897	0.696483	0.996522	0.00348	-5.6614
60	0.419	4.97905	99.581	0.00975	-2.011	12.05049	4.09435	1.778151	0.697146	0.998046	0.00195	-6.2377
70	0.42	4.979	99.58	0.0098	-2.00877	14.05905	4.24849	1.845098	0.697142	0.998036	0.00196	-6.2326

Effect of pH

pH	Mean ce (mg/L)	ca (mg/g)	% removal
3	0.704	4.9648	99.296
4	0.646	4.9677	99.354
5	0.581	4.97095	99.419
7	0.419	4.97905	99.581
8	0.401	4.97995	99.599
9	0.41	4.9795	99.59

Effect of stirring speed

Speed	Mean ce (mg/L)	ca (mg/g)	% removal
160	0.419	4.97905	99.581
170	0.336	4.9832	99.664
180	0.269	4.98655	99.731
190	0.227	4.98865	99.773
200	0.224	4.9888	99.776

Effect of initial concentration

Init. Conc.	% removal	Mean ce (mg/L)	ca mg/g	ce/ca (g/dm^3)	log ce	log ca	ln ce	1 +1/ce	ln (1+1/ce)	E	E^2	ln ca
12.5	99.488	0.064	0.6218	0.10293	-1.1938	-0.20635	-2.7489	16.625	2.810908	7782.172	60562200	-0.47514
25	99.584	0.104	1.2448	0.08355	-0.9829	0.0951	-2.2634	10.61538	2.362304	6540.186	42774033	0.218975
50	99.678	0.161	2.49195	0.06461	-0.7932	0.396539	-1.8264	7.21118	1.975633	5469.661	29917196	0.913066
100	99.776	0.224	4.9888	0.04490	-0.6498	0.697996	-1.4961	5.464286	1.698233	4701.664	22105649	1.607195
200	99.776	0.448	9.9776	0.04490	-0.3487	0.999026	-0.8029	3.232143	1.173145	3247.926	10549021	2.300343

Effect of temperature

T K	T °C	% removal	ca (mg/g)	Mean ce (mg/L)	kc ca/ce	ln kc	- Δ G RTlnKc	1/T	log kc
313	40	99.964	99.964	0.036	2776.778	7.929046	20633.61	0.003195	3.443541
323	50	99.973	99.973	0.027	3702.704	8.216819	22065.63	0.003096	3.568519
333	60	99.982	99.982	0.018	5554.556	8.622374	23871.58	0.003003	3.744649
343	70	99.983	99.983	0.017	5881.353	8.679542	24751.47	0.002915	3.769477
353	80	99.984	99.984	0.016	6249	8.740177	25651.04	0.002833	3.795811

nFe_3O_4/activated carbon composite

Effect of adsorbent amount

Mass (g)	Mean ce (mg/L)	% removal
0.0625	8.081	91.919
0.125	7.038	92.962
0.25	6.282	93.718
0.5	5.697	94.303
1	5.61	94.39

Effect of contact time qe = 4.996

Time	Mean ce (mg/L)	qt (mg/g)	% removal	qe-qt	log (qe-qt)	t/qt (g min/mg)	ln t (min)	log t	log qt	α	1-α	ln (1-α)
10	14.697	4.26515	85.303	0.73085	-0.13617	2.344583	2.302585	1	0.629934	0.85371	0.146287	-1.9222
20	11.474	4.4263	88.526	0.5697	-0.24435	4.518447	2.995732	1.30103	0.646041	0.88597	0.114031	-2.1713
40	7.084	4.6458	92.916	0.3502	-0.45568	8.609927	3.688879	1.60206	0.667061	0.92990	0.070096	-2.6579
50	6.082	4.6959	93.918	0.3001	-0.52273	10.64759	3.912023	1.69897	0.671719	0.93993	0.060068	-2.8123
60	5.697	4.71515	94.303	0.28085	-0.55153	12.72494	4.094345	1.778151	0.673496	0.94379	0.056215	-2.8786
70	5.701	4.71495	94.299	0.28105	-0.55122	14.84639	4.248495	1.845098	0.673477	0.94374	0.056255	-2.8779

Effect of pH

pH	Mean ce (mg/L)	ca (mg/g)	% removal
3	9.268	4.5366	90.732
4	8.194	4.5903	91.806
5	7.281	4.63595	92.719
7	5.697	4.71515	94.303
8	5.536	4.7232	94.464
9	5.518	4.7241	94.482

Effect of stirring speed

Speed	Mean ce (mg/L)	ca (mg/g)	% removal
160	5.697	4.71515	94.303
170	0.402	4.9799	99.598
180	0.149	4.99255	99.851
190	0.104	4.9948	99.896
200	0.08	4.996	99.92

Effect of initial concentration

Init. Conc.	% removal	Mean ce (mg/L)	ca mg/g	ce/ca (g/dm^3)	log ce	log ca	ln ce	1 +1/ce	ln (1+1/ce)	E	E^2	ln ca
12.5	99.7424	0.0322	0.62339	0.051653	-1.4921	-0.20524	-3.4358	32.0559	3.467481	9599.937	92158788	-0.4726
25	99.7932	0.0517	1.247415	0.041446	-1.2865	0.096011	-2.9623	20.34236	3.012705	8340.862	69569974	0.22107
50	99.866	0.067	2.49665	0.026836	-1.1739	0.397358	-2.7031	15.92537	2.767914	7663.141	58723722	0.9149
100	99.918	0.082	4.9959	0.016413	-1.0862	0.698614	-2.5010	13.19512	2.579847	7142.467	51014834	1.60862
200	99.919	0.162	9.9919	0.016213	-0.7905	0.999648	-1.8202	7.17284	1.970302	5454.902	29755957	2.30178

Effect of temperature

T K	T ^oC	% removal	ca (mg/g)	Mean ce (mg/L)	kc ca/ce	ln kc	- Δ G RTlnKc	1/T	log kc
313	40	99.95	99.95	0.05	1999	7.600402	19778.39	0.003195	3.300813
323	50	99.96	99.96	0.04	2499	7.823646	21009.79	0.003096	3.397766
333	60	99.977	99.977	0.023	4346.826	8.377201	23192.8	0.003003	3.638172
343	70	99.986	99.986	0.014	7141.857	8.873728	25305.23	0.002915	3.853811
353	80	99.987	99.987	0.013	7691.308	8.947846	26260.51	0.002833	3.886

$nSiO_2$/activated carbon composite

Effect of adsorbent amount

Mass (g)	Mean ce (mg/L)	% removal
0.0625	1.313	98.687
0.125	1.179	98.821
0.25	0.83	99.17
0.5	0.257	99.743
1	0.188	99.812

Effect of contact time qe = 4.9897

Time	Mean ce (mg/L)	qt (mg/g)	% removal	qe-qt	log (qe-qt)	t/qt (g min/mg)	ln t (min)	log t	log qt	α	1-α	ln (1-α)
10	0.9026	4.95487	99.0974	0.03483	-1.45805	2.018216	2.302585	1	0.695032	0.99302	0.00698	-4.9647
20	0.804	4.9598	99.196	0.0299	-1.52433	4.032421	2.995732	1.30103	0.695464	0.994008	0.005992	-5.1173
40	0.488	4.9756	99.512	0.0141	-1.85078	8.039231	3.688879	1.60206	0.696845	0.997174	0.002826	-5.8689
50	0.349	4.98255	99.651	0.00715	-2.14569	10.03502	3.912023	1.69897	0.697452	0.998567	0.001433	-6.5480
60	0.257	4.98715	99.743	0.00255	-2.59346	12.03092	4.094345	1.778151	0.697852	0.999489	0.000511	-7.5790
70	0.258	4.9871	99.742	0.0026	-2.58503	14.03621	4.248495	1.845098	0.697848	0.999479	0.000521	-7.5596

Effect of pH

pH	Mean ce (mg/L)	ca (mg/g)	% removal
3	0.324	4.9838	99.676
4	0.3	4.985	99.7
5	0.27	4.9865	99.73
7	0.257	4.98715	99.743
8	0.256	4.9872	99.744
9	0.257	4.98715	99.743

Effect of stirring speed

Speed	Mean ce (mg/L)	ca (mg/g)	% removal
160	0.257	4.98715	99.743
170	0.239	4.98805	99.761
180	0.218	4.9891	99.782
190	0.207	4.98965	99.793
200	0.206	4.9897	99.794

Effect of initial concentration

Init. Conc.	% removal	Mean ce (mg/L)	ca mg/g	ce/ca (g/dm^3)	log ce	log ca	ln ce	1 +1/ce	ln (1+1/ce)	E	E^2	ln ca
12.5	99.6	0.05	0.6225	0.080321	-1.30103	-0.20586	-2.9957	21	3.044522	8428.949	71047183	-0.47401
25	99.656	0.086	1.2457	0.069037	-1.0655	0.095413	-2.4534	12.62791	2.535909	7020.822	49291940	0.219698
50	99.724	0.138	2.4931	0.055353	-0.86012	0.39674	-1.9805	8.246377	2.109774	5841.04	34117747	0.913527
100	99.794	0.206	4.9897	0.041285	-0.68613	0.698074	-1.5799	5.854369	1.767188	4892.57	23937242	1.607376
200	99.7935	0.413	9.97935	0.041385	-0.38405	0.999102	-0.8843	3.421308	1.230023	3405.394	11596711	2.300518

Effect of temperature

T K	T °C	% removal	ca (mg/g)	Mean ce (mg/L)	kc ca/ce	ln kc	- Δ G RTlnKc	1/T	log kc
313	40	99.832	99.832	0.168	594.2381	6.38728	16621.5	0.003195	2.77396
323	50	99.866	99.866	0.134	745.2687	6.613745	17760.7	0.003096	2.872313
333	60	99.932	99.932	0.068	1469.588	7.292738	20190.4	0.003003	3.167196
343	70	99.987	99.987	0.013	7691.308	8.947846	25516.59	0.002915	3.886
353	80	99.988	99.988	0.012	8332.333	9.027899	26495.46	0.002833	3.920767

nZnO/activated carbon composite

Effect of adsorbent amount

Mass (g)	Mean ce (mg/L)	% removal
0.0625	0.952	99.048
0.125	0.679	99.321
0.25	0.491	99.509
0.5	0.37	99.63
1	0.342	99.658

Effect of contact time qe = 4.9968

Time	Mean ce (mg/L)	qt (mg/g)	% removal	qe-qt	log (qe-qt)	t/qt (g min/mg)	ln t (min)	log t	log qt	α	1-α	ln (1-α)
10	0.479	4.97605	99.521	0.0207	-1.68403	2.009626	2.302585	1	0.696885	0.995857	0.004143	-5.48641
20	0.449	4.97755	99.551	0.0192	-1.7167	4.018041	2.995732	1.30103	0.697016	0.996158	0.003842	-5.56163
40	0.391	4.98045	99.609	0.0163	-1.78781	8.031403	3.688879	1.60206	0.697269	0.996738	0.003262	-5.72538
50	0.373	4.98135	99.627	0.0154	-1.81248	10.03744	3.912023	1.69897	0.697347	0.996918	0.003082	-5.78218
60	0.37	4.9815	99.63	0.01525	-1.81673	12.04456	4.094345	1.778151	0.69736	0.996948	0.003052	-5.79196
70	0.37	4.9815	99.63	0.01525	-1.81673	14.05199	4.248495	1.845098	0.69736	0.996948	0.003052	-5.79196

Effect of pH

pH	Mean ce (mg/L)	ca (mg/g)	% removal
3	0.993	4.95035	99.007
4	0.812	4.9594	99.188
5	0.666	4.9667	99.334
7	0.37	4.9815	99.63
8	0.34	4.983	99.66
9	0.34	4.983	99.66

Effect of stirring speed

Speed	Mean ce (mg/L)	ca (mg/g)	% removal
160	0.37	4.9815	99.63
170	0.206	4.9897	99.794
180	0.102	4.9949	99.898
190	0.064	4.9968	99.936
200	0.065	4.99675	99.935

Effect of initial concentration

Init. Conc.	% removal	Mean ce (mg/L)	ca mg/g	ce/ca (g/dm^3)	log ce	log ca	ln ce	1 +1/ce	ln (1+1/ce)	E	E^2	ln ca
12.5	99.9016	0.0123	0.62439	0.019699	-1.9101	-0.20455	-4.398	82.30081	4.410381	12210.41	1.49E+08	-0.47099
25	99.9132	0.0217	1.24892	0.017375	-1.6635	0.096533	-3.830	47.08295	3.851911	10664.25	1.14E+08	0.222275
50	99.924	0.038	2.4981	0.015212	-1.4202	0.39761	-3.270	27.31579	3.307465	9156.922	83849214	0.91553
100	99.935	0.065	4.99675	0.013008	-1.1871	0.698688	-2.733	16.38462	2.796343	7741.848	59936217	1.608788
200	99.935	0.13	9.9935	0.013008	-0.8861	0.999718	-2.040	8.692308	2.162438	5986.845	35842312	2.301935

Effect of temperature

T K	T ^oC	% removal	ca (mg/g)	Mean ce (mg/L)	kc ca/ce	ln kc	- Δ G RTlnKc	1/T	log kc
313	40	99.952	99.952	0.048	2082.333	7.641244	19884.67	0.003195	3.31855
323	50	99.964	99.964	0.036	2776.778	7.929046	21292.84	0.003096	3.443541
333	60	99.977	99.977	0.023	4346.826	8.377201	23192.8	0.003003	3.638172
343	70	99.9879	99.9879	0.0121	8263.463	9.019599	25721.21	0.002915	3.917162
353	80	99.988	99.988	0.012	8332.333	9.027899	26495.46	0.002833	3.920767

APPENDIX B: DATA ON THE SORPTION OF TPT FROM TPT – CONTAMINATED ARTIFICIAL SEAWATER

Activated carbon

Effect of adsorbent amount

Mass (g)	Mean ce (mg/L)	% removal
0.0625	0.199	99.801
0.125	0.083	99.917
0.25	0.037	99.963
0.5	0.025	99.975
1	0.025	99.975

Effect of contact time qe = 4.9998

Time	Mean ce (mg/L)	qt (mg/g)	% removal	qe-qt	log (qe-qt)	t/qt (g min/mg)	ln t (min)	log t	log qt	α	1-α	ln (1-α)
10	0.109	4.99455	99.891	0.00525	-2.27984	2.002182	2.302585	1	0.698496	0.99895	0.00105	-6.8589
20	0.049	4.99755	99.951	0.00225	-2.64782	4.001961	2.995732	1.30103	0.698757	0.99955	0.00045	-7.7062
30	0.033	4.99835	99.967	0.00145	-2.83863	6.001981	3.401197	1.60206	0.698827	0.99971	0.00029	-8.1456
40	0.028	4.9986	99.972	0.0012	-2.92082	8.002241	3.688879	1.69897	0.698848	0.99976	0.00024	-8.3348
60	0.025	4.99875	99.975	0.00105	-2.97881	12.003	4.094345	1.778151	0.698861	0.99979	0.00021	-8.4684
70	0.025	4.99875	99.975	0.00105	-2.97881	14.0035	4.248495	1.845098	0.698861	0.99979	0.00021	-8.4684

Effect of pH

pH	Mean ce (mg/L)	ca (mg/g)	% removal
4	0.072	4.9964	99.928
5	0.042	4.9979	99.958
6	0.03	4.9985	99.97
7	0.025	4.99875	99.975
8	0.025	4.99875	99.975
9	0.025	4.99875	99.975

Effect of stirring speed

Speed	Mean ce (mg/L)	ca (mg/g)	% removal
160	0.025	4.99875	99.975
170	0.021	4.99895	99.979
180	0.017	4.99915	99.983
190	0.015	4.99925	99.985
200	0.015	4.99925	99.985

Effect of initial concentration

Init. Conc.	% removal	Mean ce (mg/L)	ca mg/g	ce/ca (g/dm^3)	log ce	log ca	ln ce	1 +1/ce	ln (1+1/ce)	E	E^2	ln ca
12.5	99.9552	0.0056	0.62472	0.00896	-2.2518	-0.20431	-5.1849	179.5714	5.190573	14370.42	2.07E+08	-0.47045
25	99.968	0.008	1.2496	0.00640	-2.0969	0.096771	-4.8283	126	4.836282	13389.55	1.79E+08	0.222824
50	99.98	0.01	2.4995	0.00400	-2	0.397853	-4.6052	101	4.615121	12777.25	1.63E+08	0.916091
100	99.985	0.015	4.99925	0.003	-1.8239	0.698905	-4.1997	67.66667	4.214594	11668.36	1.36E+08	1.609288
200	99.991	0.018	9.9991	0.0018	-1.7447	0.999961	-4.0174	56.55556	4.035223	11171.77	1.25E+08	2.302495

Effect of temperature

T K	T °C	% removal	ca (mg/g)	Mean ce (mg/L)	kc ca/ce	ln kc	- Δ G RTlnKc	1/T	log kc
293	20	99.985	99.985	0.015	6665.667	8.804725	21448.33	0.003413	3.823844
313	40	99.991	99.991	0.009	11110.11	9.315611	24241.85	0.003195	4.045718
333	60	99.999	99.999	0.001	99999	11.51292	31874.22	0.003003	4.999996
343	70	99.999	99.999	0.001	99999	11.51292	32831.4	0.002915	4.999996
353	80	99.999	99.999	0.001	99999	11.51292	33788.59	0.002833	4.999996

Fly ash

Effect of adsorbent amount

Mass (g)	Mean ce (mg/L)	% removal
0.0625	7.195	92.805
0.125	5.82	94.18
0.25	5.053	94.947
0.5	3.972	96.028
1	3.892	96.108

Effect of contact time qe = 4.8343

Time	Mean ce (mg/L)	qt (mg/g)	% removal	qe-qt	log (qe-qt)	t/qt (g min/mg)	ln t (min)	log t	log qt	α	1-α	ln (1-α)
10	5.763	4.71185	94.237	0.12245	-0.91204	2.122309	2.302585	1	0.673191	0.974671	0.025329	-3.6758
20	5.09	4.7455	94.91	0.0888	-1.05159	4.214519	2.995732	1.30103	0.676282	0.981631	0.018369	-3.997
30	4.395	4.78025	95.605	0.05405	-1.2672	6.275822	3.401197	1.60206	0.679451	0.988819	0.011181	-4.4936
40	3.975	4.80125	96.025	0.03305	-1.48083	8.331164	3.688879	1.69897	0.681354	0.993163	0.006837	-4.9855
60	3.972	4.8014	96.028	0.0329	-1.4828	12.49636	4.094345	1.778151	0.681368	0.993194	0.006806	-4.9900
70	3.972	4.8014	96.028	0.0329	-1.4828	14.57908	4.248495	1.845098	0.681368	0.993194	0.006806	-4.9900

Effect of pH

pH	Mean ce (mg/L)	ca (mg/g)	% removal
4	5.195	4.74025	94.805
5	4.547	4.77265	95.453
6	4.099	4.79505	95.901
7	3.972	4.8014	96.028
8	3.957	4.80215	96.043
9	3.937	4.80315	96.063

Effect of stirring speed

Speed	Mean ce (mg/L)	ca (mg/g)	% removal
160	3.975	4.80125	96.025
170	3.761	4.81195	96.239
180	3.589	4.82055	96.411
190	3.469	4.82655	96.531
200	3.462	4.8269	96.538

Effect of initial concentration

Init. Conc.	% removal	Mean ce (mg/L)	ca mg/g	ce/ca (g/dm^3)	log ce	log ca	ln ce	1 +1/ce	ln (1+1/ce)	E	E^2	ln ca
12.5	93.004	0.8745	0.581275	1.504451	-0.05824	-0.23562	-0.1341	2.14351	0.762445	2110.876	4455798	-0.54253
25	94.3344	1.4164	1.17918	1.201174	0.151186	0.07158	0.348118	1.70602	0.53416	1478.856	2187016	0.164819
50	95.824	2.088	2.3956	0.871598	0.31973	0.379414	0.736207	1.47893	0.391317	1083.385	1173724	0.873634
100	96.538	3.462	4.8269	0.717231	0.539327	0.683668	1.241846	1.28885	0.253751	702.5244	493540.5	1.574204
200	97.5535	4.893	9.75535	0.501571	0.689575	0.989243	1.587806	1.20437	0.18596	514.8407	265060.9	2.277816

Effect of temperature

T K	T °C	% removal	ca (mg/g)	Mean ce (mg/L)	kc ca/ce	ln kc	- Δ G RTlnKc	1/T	log kc
313	40	91.508	91.508	8.492	10.77579	2.377302	6186.41	0.003195	1.032449
323	50	86.777	86.777	13.223	6.56258	1.881384	5052.31	0.003096	0.817075
333	60	85.169	85.169	14.831	5.742634	1.747918	4839.219	0.003003	0.759111
343	70	80.981	80.981	19.019	4.2579	1.448776	4131.478	0.002915	0.629195
353	80	80.135	80.135	19.865	4.033979	1.394753	4093.381	0.002833	0.605734

nFe_3O_4

Effect of adsorbent amount

Mass (g)	Mean ce (mg/L)	% removal
0.0625	9.015	90.985
0.125	8.502	91.498
0.25	7.613	92.387
0.5	6.567	93.433
1	6.438	93.562

Effect of contact time

qe = 4.7882

Time	Mean ce (mg/L)	qt (mg/g)	% removal	qe-qt	log (qe-qt)	t/qt (g min/mg)	ln t (min)	log t	log qt	α	1-α	ln (1-α)
10	7.445	4.62775	92.555	0.16045	-0.79466	2.160877	2.302585	1	0.66537	0.966491	0.033509	-3.3959
20	6.725	4.66375	93.275	0.12445	-0.90501	4.288395	2.995732	1.30103	0.668735	0.974009	0.025991	-3.6500
30	6.619	4.66905	93.381	0.11915	-0.92391	6.42529	3.401197	1.60206	0.669229	0.975116	0.024884	-3.6935
40	6.583	4.67085	93.417	0.11735	-0.93052	8.563752	3.688879	1.69897	0.669396	0.975492	0.024508	-3.7088
60	6.567	4.67165	93.433	0.11655	-0.93349	12.84343	4.094345	1.778151	0.66947	0.975659	0.024341	-3.7156
70	6.567	4.67165	93.433	0.11655	-0.93349	14.984	4.248495	1.845098	0.66947	0.975659	0.024341	-3.7156

Effect of pH

pH	Mean ce (mg/L)	ca (mg/g)	% removal
4	8.778	4.5611	91.222
5	8.109	4.59455	91.891
6	7.289	4.63555	92.711
7	6.567	4.67165	93.433
8	6.348	4.6826	93.652
9	6.348	4.6826	93.652

Effect of stirring speed

Speed	Mean ce (mg/L)	ca (mg/g)	% removal
160	6.567	4.67165	93.433
170	5.648	4.7176	94.352
180	4.874	4.7563	95.126
190	4.5	4.775	95.5
200	4.5	4.775	95.5

Effect of initial concentration

Init. Conc.	% removal	Mean ce (mg/L)	ca mg/g	ce/ca (g/dm^3)	log ce	log ca	ln ce	1 +1/ce	ln (1+1/ce)	E	E^2	ln ca
12.5	92.788	0.9015	0.579925	1.554511	-0.04503	-0.23663	-0.1037	2.109262	0.746338	2066.284	4269529	-0.5449
25	93.328	1.668	1.1666	1.429796	0.222196	0.066922	0.511625	1.59952	0.469704	1300.404	1691051	0.15409
50	94.232	2.884	2.3558	1.224213	0.459995	0.372138	1.059178	1.346741	0.297687	824.1658	679249.3	0.85688
100	95.5	4.5	4.775	0.942408	0.653213	0.678973	1.504077	1.222222	0.200671	555.5693	308657.2	1.56339
200	95.811	8.379	9.58105	0.874539	0.923192	0.981413	2.125729	1.119346	0.112745	312.1403	97431.59	2.25979

Effect of temperature

T K	T ^oC	% removal	ca (mg/g)	Mean ce (mg/L)	kc ca/ce	ln kc	- Δ G RTlnKc	1/T	log kc
313	40	93.525	93.525	6.475	14.44402	2.67028	6948.822	0.003195	1.159688
323	50	92.635	92.635	7.365	12.57773	2.531928	6799.295	0.003096	1.099602
333	60	91.543	91.543	8.457	10.82452	2.381814	6594.201	0.003003	1.034409
343	70	90.732	90.732	9.268	9.789814	2.281342	6505.709	0.002915	0.990774
353	80	89.782	89.782	10.218	8.786651	2.173234	6378.097	0.002833	0.943823

$nSiO_2$

Effect of adsorbent amount

Mass (g)	Mean ce (mg/L)	% removal
0.0625	4.244	95.756
0.125	3.565	96.435
0.25	2.616	97.384
0.5	2.317	97.683
1	2.317	97.683

Effect of contact time qe = 4.9817

Time	Mean ce (mg/L)	qt (mg/g)	% removal	qe-qt	log (qe-qt)	t/qt (g min/mg)	ln t (min)	log t	log qt	α	1-α	ln (1-α)
10	5.843	4.70785	94.157	0.27391	-0.56239	2.124112	2.302585	1	0.672823	0.945017	0.054983	-2.9007
20	5.032	4.7484	94.968	0.23336	-0.63197	4.211945	2.995732	1.30103	0.676547	0.953157	0.046843	-3.0609
30	4.194	4.7903	95.806	0.19146	-0.71792	6.262656	3.401197	1.60206	0.680363	0.961568	0.038432	-3.2589
40	3.601	4.81995	96.399	0.16181	-0.79099	8.298841	3.688879	1.69897	0.683043	0.96752	0.03248	-3.4271
60	3.317	4.83415	96.683	0.14761	-0.83088	12.4117	4.094345	1.778151	0.68432	0.97037	0.02963	-3.5189
70	3.317	4.83415	96.683	0.14761	-0.83088	14.48031	4.248495	1.845098	0.68432	0.97037	0.02963	-3.5189

Effect of pH

pH	Mean ce (mg/L)	ca (mg/g)	% removal
4	7.765	4.61175	92.235
5	5.294	4.7353	94.706
6	3.472	4.8264	96.528
7	3.317	4.83415	96.683
8	3.139	4.84305	96.861
9	3.139	4.84305	96.861

Effect of stirring speed

Speed	Mean ce (mg/L)	ca (mg/g)	% removal
160	3.317	4.83415	96.683
170	3.206	4.8397	96.794
180	3.124	4.8438	96.876
190	3.083	4.84585	96.917
200	3.084	4.8458	96.916

Effect of initial concentration

Init. Conc.	% removal	Mean ce (mg/L)	ca mg/g	ce/ca (g/dm^3)	log ce	log ca	ln ce	1 +1/ce	ln (1+1/ce)	E	E^2	ln ca
12.5	90.912	1.136	0.5682	1.999296	0.055378	-0.2455	0.127513	1.880282	0.631422	1748.13	3055958	-0.56528
25	93.312	1.672	1.1664	1.433471	0.223236	0.066848	0.514021	1.598086	0.468807	1297.921	1684598	0.153922
50	95.178	2.411	2.37945	1.013259	0.382197	0.376477	0.880042	1.414766	0.346964	960.5911	922735.2	0.866869
100	96.916	3.084	4.8458	0.636427	0.489114	0.685365	1.126227	1.324254	0.280849	777.5491	604582.6	1.578112
200	97.933	4.134	9.7933	0.422125	0.61637	0.990929	1.419245	1.241896	0.21664	599.7802	359736.3	2.281698

Effect of temperature

T K	T ^oC	% removal	ca (mg/g)	Mean ce (mg/L)	kc ca/ce	ln kc	- Δ G RTlnKc	1/T	log kc
313	40	94.508	94.508	5.492	17.2083	2.845392	7404.512	0.003195	1.235738
323	50	93.666	93.666	6.334	14.78781	2.693803	7233.999	0.003096	1.169904
333	60	92.817	92.817	7.183	12.92176	2.558913	7084.508	0.003003	1.111322
343	70	91.827	91.827	8.173	11.23541	2.41907	6898.468	0.002915	1.050589
353	80	90.778	90.778	9.222	9.843635	2.286825	6711.47	0.002833	0.993155

nZnO

Effect of adsorbent amount

Mass (g)	Mean ce (mg/L)	% removal
0.0625	5.523	94.477
0.125	5.241	94.759
0.25	4.862	95.138
0.5	4.578	95.422
1	4.579	95.421

Effect of contact time

qe = 4.8183

Time	Mean ce (mg/L)	qt (mg/g)	% removal	qe-qt	log (qe-qt)	t/qt (g min/mg)	ln t (min)	log t	log qt	α	1-α	ln (1-α)
10	6.735	4.66325	93.265	0.155	-0.80967	2.144427	2.302585	1	0.668689	0.967831	0.032169	-3.4367
20	5.901	4.70495	94.099	0.1133	-0.94577	4.250842	2.995732	1.30103	0.672555	0.976485	0.023515	-3.7501
30	5.129	4.74355	94.871	0.0747	-1.12668	6.324377	3.401197	1.60206	0.676103	0.984496	0.015504	-4.1667
40	4.705	4.76475	95.295	0.0535	-1.27165	8.394984	3.688879	1.69897	0.67804	0.988896	0.011104	-4.5004
60	4.578	4.7711	95.422	0.04715	-1.32652	12.57572	4.094345	1.778151	0.678619	0.990214	0.009786	-4.6268
70	4.578	4.7711	95.422	0.04715	-1.32652	14.67167	4.248495	1.845098	0.678619	0.990214	0.009786	-4.6268

Effect of pH

pH	Mean ce (mg/L)	ca (mg/g)	% removal
4	5.544	4.7228	94.456
5	5.217	4.73915	94.783
6	4.844	4.7578	95.156
7	4.578	4.7711	95.422
8	4.532	4.7734	95.468
9	4.532	4.7734	95.468

Effect of stirring speed

Speed	Mean ce (mg/L)	ca (mg/g)	% removal
160	4.578	4.7711	95.422
170	3.803	4.80985	96.197
180	3.095	4.84525	96.905
190	2.902	4.8549	97.098
200	2.857	4.85715	97.143

Effect of initial concentration

Init. Conc.	% removal	Mean ce (mg/L)	ca mg/g	ce/ca (g/dm^3)	log ce	log ca	ln ce	1 +1/ce	ln (1+1/ce)	E	E^2	ln ca
12.5	93.672	0.791	0.58545	1.351097	-0.10182	-0.23251	-0.23446	2.264223	0.817231	2262.556	5119159	-0.53537
25	94.532	1.367	1.18165	1.156857	0.135769	0.072489	0.312619	1.731529	0.549005	1519.954	2310259	0.166912
50	95.986	2.007	2.39965	0.836372	0.302547	0.380148	0.696641	1.498256	0.404302	1119.335	1252910	0.875323
100	97.193	2.807	4.85965	0.577614	0.448242	0.686605	1.032116	1.356252	0.304725	843.6506	711746.3	1.580966
200	97.8845	4.231	9.78845	0.432244	0.626443	0.990714	1.442438	1.236351	0.212164	587.3894	345026.4	2.281203

Effect of temperature

T K	T ^oC	% removal	ca (mg/g)	Mean ce (mg/L)	kc ca/ce	ln kc	- Δ G RTlnKc	1/T	log kc
313	40	96.822	96.822	3.178	30.46633	3.416622	8891.014	0.003195	1.48382
323	50	96.247	96.247	3.753	25.64535	3.244362	8712.482	0.003096	1.409009
333	60	94.657	94.657	5.343	17.71608	2.874473	7958.155	0.003003	1.248368
343	70	93.786	93.786	6.214	15.09269	2.714211	7740.12	0.002915	1.178767
353	80	92.953	92.953	7.047	13.19044	2.579492	7570.401	0.002833	1.120259

Fly ash/activated carbon

Effect of adsorbent amount

Mass (g)	Mean ce (mg/L)	% removal
0.0625	0.834	99.166
0.125	0.329	99.671
0.25	0.089	99.911
0.5	0.017	99.983
1	0.0009	99.9991

Effect of contact time qe = 4.9993

Time	Mean ce (mg/L)	qt (mg/g)	% removal	qe-qt	log (qe-qt)	t/qt (g min/mg)	ln t (min)	log t	log qt	α	1-α	ln (1-α)
10	0.083	4.99585	99.917	0.00345	-2.46218	2.001661	2.302585	1	0.698609	0.99931	0.00069	-7.2787
20	0.042	4.9979	99.958	0.0014	-2.85387	4.001681	2.995732	1.30103	0.698788	0.99972	0.00028	-8.1806
30	0.029	4.99855	99.971	0.00075	-3.12494	6.001741	3.401197	1.60206	0.698844	0.99985	0.00015	-8.8047
40	0.023	4.99885	99.977	0.00045	-3.34679	8.00184	3.688879	1.69897	0.69887	0.99991	9E-05	-9.3156
60	0.017	4.99915	99.983	0.00015	-3.82391	12.00204	4.094345	1.778151	0.698896	0.99997	3E-05	-10.414
70	0.017	4.99915	99.983	0.00015	-3.82391	14.00238	4.248495	1.845098	0.698896	0.99997	3E-05	-10.414

Effect of pH

pH	Mean ce (mg/L)	ca (mg/g)	% removal
4	0.182	4.9909	99.818
5	0.125	4.99375	99.875
6	0.067	4.99665	99.933
7	0.017	4.99915	99.983
8	0.012	4.9994	99.988
9	0.016	4.9992	99.984

Effect of stirring speed

Speed	Mean ce (mg/L)	ca (mg/g)	% removal
160	0.017	4.99915	99.983
170	0.016	4.9992	99.984
180	0.015	4.99925	99.985
190	0.014	4.9993	99.986
200	0.014	4.9993	99.986

Effect of initial concentration

Init. Conc.	% removal	Mean ce (mg/L)	ca mg/g	ce/ca (g/dm^3)	log ce	log ca	ln ce	1 +1/ce	ln (1+1/ce)	E	E^2	ln ca
12.5	99.984	0.002	0.6249	0.003201	-2.6989	-0.20419	-6.2146	501	6.216606	17211.06	2.96E+08	-0.47016
25	99.9844	0.0039	1.249805	0.00312	-2.4089	0.096842	-5.5468	257.4103	5.550671	15367.38	2.36E+08	0.222988
50	99.985	0.0075	2.499625	0.003	-2.1249	0.397875	-4.8929	134.3333	4.900324	13566.85	1.84E+08	0.916141
100	99.986	0.014	4.9993	0.0028	-1.8539	0.698909	-4.2687	72.42857	4.282601	11856.65	1.41E+08	1.609298
200	99.9862	0.0276	9.99862	0.00276	-1.5591	0.99994	-3.5899	37.23188	3.617165	10014.35	1E+08	2.302447

Effect of temperature					kc		- Δ G		
T K	T °C	% removal	ca (mg/g)	Mean ce (mg/L)	ca/ce	ln kc	RTlnKc	1/T	log kc
313	40	99.982	99.982	0.018	5554.556	8.622374	22437.85	0.003195	3.744649
323	50	99.994	99.994	0.006	16665.67	9.721106	26105.27	0.003096	4.221823
333	60	99.999	99.999	0.001	99999	11.51292	31874.22	0.003003	4.999996
343	70	99.999	99.999	0.001	99999	11.51292	32831.4	0.002915	4.999996
353	80	99.999	99.999	0.001	99999	11.51292	33788.59	0.002833	4.999996

nFe_3O_4/fly ash composite

Effect of adsorbent amount

Mass (g)	Mean ce (mg/L)	% removal
0.0625	7.839	92.161
0.125	6.534	93.466
0.25	5.973	94.027
0.5	5.87	94.13
1	5.871	94.129

Effect of contact time qe = 4.896

Time	Mean ce (mg/L)	qt (mg/g)	% removal	qe-qt	log (qe-qt)	t/qt (g min/mg)	ln t (min)	log t	log qt	α	1-α	ln (1-α)
10	7.226	4.6387	92.774	0.2573	-0.58956	2.155776	2.302585	1	0.666396	0.947447	0.052553	-2.9459
20	6.913	4.65435	93.087	0.24165	-0.61681	4.297055	2.995732	1.30103	0.667859	0.950643	0.049357	-3.0087
30	6.461	4.67695	93.539	0.21905	-0.65946	6.414437	3.401197	1.60206	0.669963	0.955259	0.044741	-3.1069
40	6.082	4.6959	93.918	0.2001	-0.69875	8.518069	3.688879	1.69897	0.671719	0.95913	0.04087	-3.1974
60	5.87	4.7065	94.13	0.1895	-0.72239	12.74833	4.094345	1.778151	0.672698	0.961295	0.038705	-3.2518
70	5.87	4.7065	94.13	0.1895	-0.72239	14.87305	4.248495	1.845098	0.672698	0.961295	0.038705	-3.2518

Effect of pH

pH	Mean ce (mg/L)	ca (mg/g)	% removal
4	9.806	4.5097	90.194
5	8.25	4.5875	91.75
6	7.07	4.6465	92.93
7	5.697	4.71515	94.303
8	4.068	4.7966	95.932
9	4.067	4.79665	95.933

Effect of stirring speed

Speed	Mean ce (mg/L)	ca (mg/g)	% removal
160	5.87	4.7065	94.13
170	4.649	4.76755	95.351
180	2.849	4.85755	97.151
190	1.472	4.9264	98.528
200	1.565	4.92175	98.435

Effect of initial concentration

Init. Conc.	% removal	Mean ce (mg/L)	ca mg/g	ce/ca (g/dm^3)	log ce	log ca	ln ce	1 +1/ce	ln (1+1/ce)	E	E^2	ln ca
12.5	94.224	0.722	0.5889	1.226015	-0.14146	-0.22996	-0.32573	2.385042	0.869217	2406.48	5791145.5	-0.5295
25	96.1932	0.9517	1.202415	0.79149	-0.0215	0.080054	-0.04951	2.050751	0.718206	1988.398	3953728.3	0.184332
50	97.694	1.153	2.44235	0.472086	0.061829	0.387808	0.142367	1.867303	0.624495	1728.953	2989278.7	0.892961
100	98.535	1.465	4.92675	0.297356	0.165838	0.692561	0.381855	1.682594	0.520337	1440.584	2075282.4	1.59468
200	98.9725	2.055	9.89725	0.207633	0.312812	0.995515	0.720276	1.486618	0.396504	1097.745	1205044.5	2.292257

Effect of temperature

T K	T °C	% removal	ca (mg/g)	Mean ce (mg/L)	kc ca/ce	ln kc	- Δ G RTlnKc	1/T	log kc
313	40	97.95	97.95	2.05	47.78049	3.866617	10062.03	0.003195	1.679251
323	50	95.96	95.96	4.04	23.75248	3.167687	8506.576	0.003096	1.375709
333	60	94.977	94.977	5.023	18.90842	2.939607	8138.485	0.003003	1.276655
343	70	93.986	93.986	6.014	15.62787	2.749056	7839.488	0.002915	1.1939
353	80	92.987	92.987	7.013	13.25923	2.584694	7585.669	0.002833	1.122518

$nSiO_2$/fly ash composite

Effect of adsorbent amount

Mass (g)	Mean ce (mg/L)	% removal
0.0625	7.377	92.623
0.125	6.249	93.751
0.25	5.066	94.934
0.5	4.098	95.902
1	4.097	95.903

Effect of contact time qe = 4.9097

Time	Mean ce (mg/L)	qt (mg/g)	% removal	qe-qt	log (qe-qt)	t/qt (g min/mg)	ln t (min)	log t	log qt	α	1-α	ln (1-α)
10	9.77	4.5115	90.23	0.3982	-0.3999	2.216558	2.302585	1	0.654321	0.918895	0.081105	-2.5120
20	7.962	4.6019	92.038	0.3078	-0.51173	4.346031	2.995732	1.30103	0.662937	0.937308	0.062692	-2.7695
30	6.512	4.6744	93.488	0.2353	-0.62838	6.417936	3.401197	1.60206	0.669726	0.952074	0.047926	-3.0381
50	4.526	4.7737	95.474	0.136	-0.86646	10.47406	3.912023	1.69897	0.678855	0.9723	0.0277	-3.5863
60	4.098	4.7951	95.902	0.1146	-0.94082	12.51277	4.094345	1.778151	0.680798	0.976658	0.023342	-3.7575
70	4.098	4.7951	95.902	0.1146	-0.94082	14.59824	4.248495	1.845098	0.680798	0.976658	0.023342	-3.7575

Effect of pH

pH	Mean ce (mg/L)	ca (mg/g)	% removal
4	25.144	3.7428	74.856
5	21.531	3.92345	78.469
6	15.082	4.2459	84.918
7	4.098	4.7951	95.902
8	3.324	4.8338	96.676
9	3.324	4.8338	96.676

Effect of stirring speed

Speed	Mean ce (mg/L)	ca (mg/g)	% removal
160	4.098	4.7951	95.902
170	2.614	4.8693	97.386
180	1.196	4.9402	98.804
190	1.017	4.94915	98.983
200	1.016	4.9492	98.984

Effect of initial concentration

Init. Conc.	% removal	Mean ce (mg/L)	ca mg/g	ce/ca (g/dm^3)	log ce	log ca	ln ce	1 +1/ce	ln (1+1/ce)	E	E^2	ln ca
12.5	98.6856	0.1643	0.616785	0.266381	-0.78436	-0.20987	-1.80606	7.08643	1.958181	5421.346	29390996	-0.48323
25	98.856	0.286	1.2357	0.231448	-0.54363	0.091913	-1.25176	4.49650	1.5033	4161.98	17322073	0.211638
50	98.938	0.531	2.47345	0.21468	-0.27491	0.393303	-0.63299	2.88324	1.058914	2931.67	8594690	0.905614
100	98.984	1.016	4.9492	0.205286	0.006894	0.694535	0.015873	1.98425	0.685242	1897.135	3599121	1.599226
200	98.9855	2.029	9.89855	0.20498	0.307282	0.995572	0.707543	1.49285	0.400689	1109.334	1230621	2.292388

Effect of temperature

T K	T °C	% removal	ca (mg/g)	Mean ce (mg/L)	kc ca/ce	ln kc	- Δ G RTlnKc	1/T	log kc
313	40	97.866	97.866	2.134	45.86036	3.825601	9955.293	0.003195	1.661437
323	50	96.866	96.866	3.134	30.9081	3.431018	9213.732	0.003096	1.490072
333	60	95.932	95.932	4.068	23.5821	3.160488	8750.007	0.003003	1.372583
343	70	94.975	94.975	5.025	18.9005	2.939188	8381.689	0.002915	1.276473
353	80	93.978	93.978	6.022	15.60578	2.747641	8063.893	0.002833	1.193285

nZnO/fly ash composite

Effect of adsorbent amount

Mass (g)	Mean ce (mg/L)	% removal
0.0625	6.332	93.668
0.125	5.307	94.693
0.25	3.311	96.689
0.5	0.372	99.628
1	0.338	99.662

Effect of contact time qe = 4.9855

Time	Mean ce (mg/L)	qt (mg/g)	% removal	qe-qt	log (qe-qt)	t/qt (g min/mg)	ln t (min)	log t	log qt	α	1-α	ln (1-α)
10	1.604	4.9198	98.396	0.0657	-1.18243	2.032603	2.302585	1	0.691947	0.986822	0.013178	-4.32919
20	0.685	4.96575	99.315	0.01975	-1.70443	4.027589	2.995732	1.30103	0.695985	0.996039	0.003961	-5.53114
30	0.506	4.9747	99.494	0.0108	-1.96658	6.030514	3.401197	1.60206	0.696767	0.997834	0.002166	-6.13474
50	0.413	4.97935	99.587	0.00615	-2.21112	10.04147	3.912023	1.69897	0.697173	0.998766	0.001234	-6.69784
60	0.372	4.9814	99.628	0.0041	-2.38722	12.04481	4.094345	1.778151	0.697351	0.999178	0.000822	-7.1033
70	0.372	4.9814	99.628	0.0041	-2.38722	14.05227	4.248495	1.845098	0.697351	0.999178	0.000822	-7.1033

Effect of pH

pH	Mean ce (mg/L)	ca (mg/g)	% removal
4	2.997	4.85015	97.003
5	1.842	4.9079	98.158
6	0.689	4.96555	99.311
7	0.572	4.9714	99.428
8	0.49	4.9755	99.51
9	0.49	4.9755	99.51

Effect of stirring speed

Speed	ce (mg/L)	ca (mg/g)	% removal
160	0.572	4.9714	99.428
170	0.466	4.9767	99.534
180	0.353	4.98235	99.647
190	0.343	4.98285	99.657
200	0.341	4.98295	99.659

Effect of initial concentration

Init. Conc.	% removal	Mean ce (mg/L)	ca mg/g	ce/ca (g/dm^3)	log ce	log ca	ln ce	1 +1/ce	ln (1+1/ce)	E	E^2	ln ca
12.5	99.576	0.053	0.62235	0.085161	-1.2757	-0.20597	-2.9374	19.86792	2.989107	8275.527	68484346	-0.47425
25	99.6252	0.0937	1.245315	0.075242	-1.0283	0.095279	-2.3677	11.67236	2.457224	6802.976	46280478	0.219389
50	99.656	0.172	2.4914	0.069037	-0.7645	0.396443	-1.7603	6.813953	1.918972	5312.794	28225784	0.912845
100	99.659	0.341	4.98295	0.068433	-0.4673	0.697487	-1.0759	3.932551	1.369288	3790.96	14371377	1.606022
200	99.667	0.666	9.9667	0.066823	-0.1765	0.998551	-0.4065	2.501502	0.916891	2538.47	6443830	2.29925

Effect of temperature

T K	T ^oC	% removal	ca (mg/g)	Mean ce (mg/L)	kc ca/ce	ln kc	- Δ G RTlnKc	1/T	log kc
313	40	99.552	99.552	0.448	222.2143	5.403642	14061.8	0.003195	2.346772
323	50	99.464	99.464	0.536	185.5672	5.223417	14027.08	0.003096	2.268501
333	60	99.377	99.377	0.623	159.5136	5.072129	14042.5	0.003003	2.202798
343	70	99.2879	99.2879	0.7121	139.4297	4.937561	14080.45	0.002915	2.144355
353	80	99.066	99.066	0.934	106.0664	4.664065	13688.29	0.002833	2.025578

APPENDIX C: DATA ON THE SORPTION OF TBT FROM TBT – CONTAMINATED WATER

nFe_3O_4/fly ash/activated carbon composite

Effect of adsorbent amount

Mass (g)	Mean ce (mg/L)	% removal
0.0625	3.9055	96.0945
0.125	1.5255	98.4745
0.25	0.3721	99.6279
0.5	0.1342	99.8658
1	0.1233	99.8767

Effect of contact time

qe = 4.9997

Time	Mean ce (mg/L)	qt (mg/g)	% removal	qe-qt	log (qe-qt)	t/qt (g min/mg)	ln t (min)	log t	log qt	α	1-α	ln (1-α)
10	0.2278	4.98861	99.7722	0.01109	-1.95507	2.004566	2.302585	1	0.69798	0.997782	0.002218	-6.1111
20	0.2063	4.989685	99.7937	0.010015	-1.99935	4.008269	2.995732	1.30103	0.698073	0.997997	0.002003	-6.2131
40	0.1619	4.991905	99.8381	0.007795	-2.10818	8.012973	3.688879	1.60206	0.698266	0.998441	0.001559	-6.4637
50	0.1431	4.992845	99.8569	0.006855	-2.16399	10.01433	3.912023	1.69897	0.698348	0.998629	0.001371	-6.5922
60	0.1342	4.99329	99.8658	0.00641	-2.19314	12.01613	4.094345	1.778151	0.698387	0.998718	0.001282	-6.6593
70	0.1341	4.993295	99.8659	0.006405	-2.19348	14.0188	4.248495	1.845098	0.698387	0.998719	0.001281	-6.6601

Effect of pH

pH	Mean ce (mg/L)	ca (mg/g)	% removal
4	0.1358	4.99321	99.8642
5	0.1122	4.99439	99.8878
6	0.0845	4.995775	99.9155
7	0.0554	4.99723	99.9446
8	0.0327	4.998365	99.9673
9	0.0327	4.998365	99.9673

Effect of stirring speed

Speed	Mean ce (mg/L)	ca (mg/g)	% removal
160	0.0327	4.998365	99.9673
170	0.0225	4.998875	99.9775
180	0.0196	4.99902	99.9804
190	0.0192	4.99904	99.9808
200	0.0192	4.99904	99.9808

Effect of initial concentration

Init. Conc.	% removal	Mean ce (mg/L)	ca mg/g	ce/ca (g/dm^3)	log ce	log ca	ln ce	1 +1/ce	ln (1+1/ce)	E	E^2	ln ca
12.5	99.9632	0.0046	0.62477	0.007363	-2.3372	-0.20428	-5.3817	218.3913	5.386288	14912.27	2.22E+08	-0.47037
25	99.9662	0.00845	1.249578	0.006762	-2.0731	0.096763	-4.77359	119.3432	4.782003	13239.27	1.75E+08	0.222805
50	99.9724	0.0138	2.49931	0.005522	-1.8601	0.39782	-4.28309	73.46377	4.296792	11895.94	1.42E+08	0.916015
100	99.9808	0.0192	4.99904	0.003841	-1.7167	0.698887	-3.95284	53.08333	3.971863	10996.35	1.21E+08	1.609246
200	99.9838	0.0324	9.99838	0.003241	-1.4895	0.99993	-3.4296	31.8642	3.461483	9583.33	91840222	2.302423

Effect of temperature

T K	T °C	% removal	ca (mg/g)	Mean ce (mg/L)	kc ca/ce	ln kc	- Δ G RTlnKc	1/T	log kc
313	40	99.984	99.984	0.016	6249	8.740177	22744.4	0.003195	3.795811
323	50	99.989	99.989	0.011	9089.909	9.11492	24477.41	0.003096	3.95856
333	60	99.992	99.992	0.008	12499	9.433404	26116.96	0.003003	4.096875
343	70	99.993	99.993	0.007	14284.71	9.566945	27282.08	0.002915	4.154872
353	80	99.9935	99.9935	0.0065	15383.62	9.641058	28294.98	0.002833	4.187058

APPENDIX D: DATA ON THE SORPTION OF TPT FROM TPT – CONTAMINATED WATER

$nSiO_2$/fly ash/activated carbon composite

Effect of adsorbent amount

Mass (g)	Mean ce (mg/L)	% removal
0.0625	4.579	95.421
0.125	2.802	97.198
0.25	1.005	98.995
0.5	0.082	99.918
1	0.04	99.96

Effect of contact time

qe = 4.999

Time	Mean ce (mg/L)	qt (mg/g)	% removal	qe-qt	log (qe-qt)	t/qt (g min/mg)	ln t (min)	log t	log qt	α	1-α	ln (1-α)
10	0.272	4.9864	99.728	0.0126	-1.89963	2.005455	2.302585	1	0.697787	0.997479	0.002521	-5.983
20	0.164	4.9918	99.836	0.0072	-2.14267	4.006571	2.995732	1.30103	0.698257	0.99856	0.00144	-6.5429
30	0.124	4.9938	99.876	0.0052	-2.284	6.007449	3.401197	1.477121	0.698431	0.99896	0.00104	-6.8683
40	0.09	4.9955	99.91	0.0035	-2.45593	8.007206	3.688879	1.60206	0.698579	0.9993	0.0007	-7.2642
60	0.082	4.9959	99.918	0.0031	-2.50864	12.00985	4.094345	1.778151	0.698614	0.99938	0.00062	-7.3856
70	0.082	4.9959	99.918	0.0031	-2.50864	14.01149	4.248495	1.845098	0.698614	0.99938	0.00062	-7.3856

Effect of pH

pH	Mean ce (mg/L)	ca (mg/g)	% removal
4	0.087	4.99565	99.913
5	0.029	4.99855	99.971
6	0.015	4.99925	99.985
7	0.009	4.99955	99.991
8	0.008	4.9996	99.992
9	0.008	4.9996	99.992

Effect of stirring speed

Speed	Mean ce (mg/L)	ca (mg/g)	% removal
160	0.008	4.9996	99.992
170	0.0055	4.999725	99.9945
180	0.005	4.99975	99.995
190	0.005	4.99975	99.995
200	0.005	4.99975	99.995

Effect of initial concentration

Init. Conc.	% removal	Mean ce (mg/L)	ca mg/g	ce/ca (g/dm^3)	log ce	log ca	ln ce	1 +1/ce	ln (1+1/ce)	E	E^2	ln ca
12.5	99.992	0.001	0.62495	0.0016	-3	-0.20415	-6.90776	1001	6.908755	19127.32	365854215	-0.47008
25	99.9936	0.0016	1.24992	0.00128	-2.79588	0.096882	-6.43775	626	6.43935	17827.74	317828340	0.22308
50	99.9948	0.0026	2.49987	0.00104	-2.58503	0.397917	-5.95224	385.615	5.95484	16486.35	271799572	0.916239
100	99.995	0.005	4.99975	0.001	-2.30103	0.698948	-5.29832	201	5.303305	14682.53	215576641	1.609388
200	99.9955	0.009	9.99955	0.0009	-2.04576	0.99998	-4.71053	112.1111	4.71949	13066.2	170725632	2.30254

Effect of temperature

T K	T ^{o}C	% removal	ca (mg/g)	Mean ce (mg/L)	kc ca/ce	ln kc	- Δ G RTlnKc	1/T	log kc
313	40	99.997	99.997	0.003	33332.33	10.41428	27100.9	0.003195	4.522866
323	50	99.998	99.998	0.002	49999	10.81976	29055.62	0.003096	4.698961
333	60	99.9985	99.9985	0.0015	66665.67	11.10745	30751.65	0.003003	4.823902
343	70	99.999	99.999	0.001	99999	11.51292	32831.4	0.002915	4.999996
353	80	99.999	99.999	0.001	99999	11.51292	33788.59	0.002833	4.999996

APPENDIX E: DATA ON THE SORPTION OF TBT/TPT FROM TBT/TPT – CONTAMINATED ARTIFICIAL SEAWATER

Conc. TBT	Conc. TPT	TBT/TPT ratio	% TBT removed	% TPT removed
0	100	0	0	99.999
10	90	0.11	99.83	99.92667
20	80	0.25	99.89	99.92
30	70	0.43	99.89667	99.91429
40	60	0.67	99.88	99.90333
50	50	1	99.882	99.904
60	40	1.5	99.9	99.92
70	30	2.33	99.90714	99.92667
80	20	4	99.915	99.91
90	10	9	99.92222	99.85
100	0	0	99.999	0

APPENDIX F: ANALYTICAL INSTRUMENTS

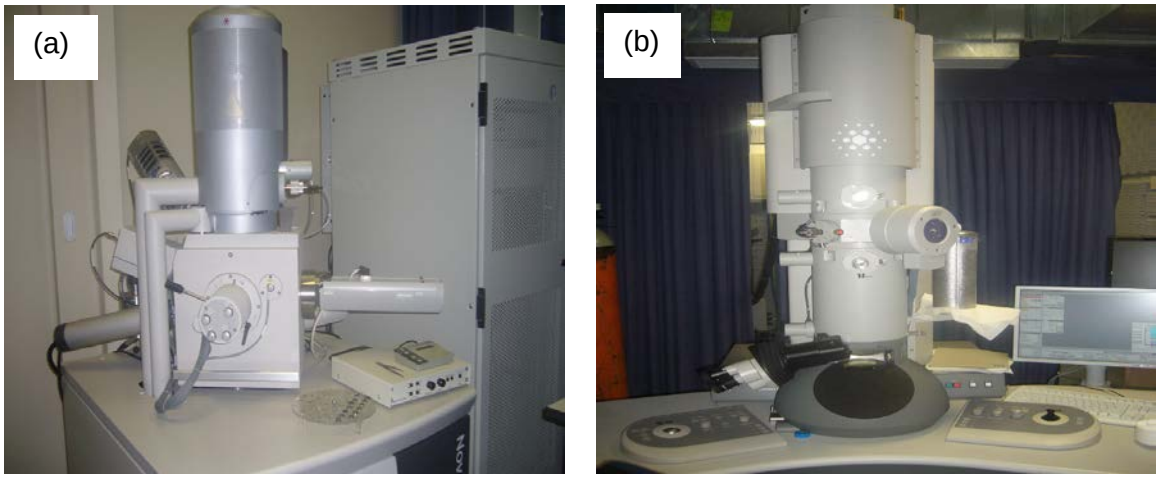

FEI^{TM} scanning electron microscope (Nova Nano SEM 230) (a) and Transmission electron microscope (TECNAI G^2 20) (b)

Euro Ea elemental analyzer

ICP-AES (Thermo Icap 6300) (d) and ICP-MS (Agilent 7700) (e)

Perkin ElmerTM Spectrum 1000 FTIR

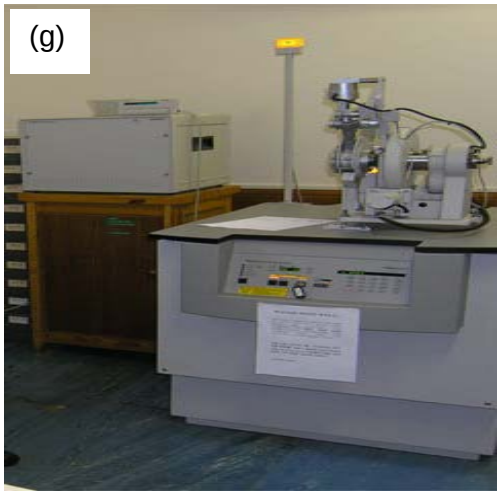

PANalytical PW 3830 diffractometer

(h)

TriStar 3000 analyzer

GC-FPD (Shimadzu GC-2010 Plus)

APPENDIX G: TBT CALIBRATION

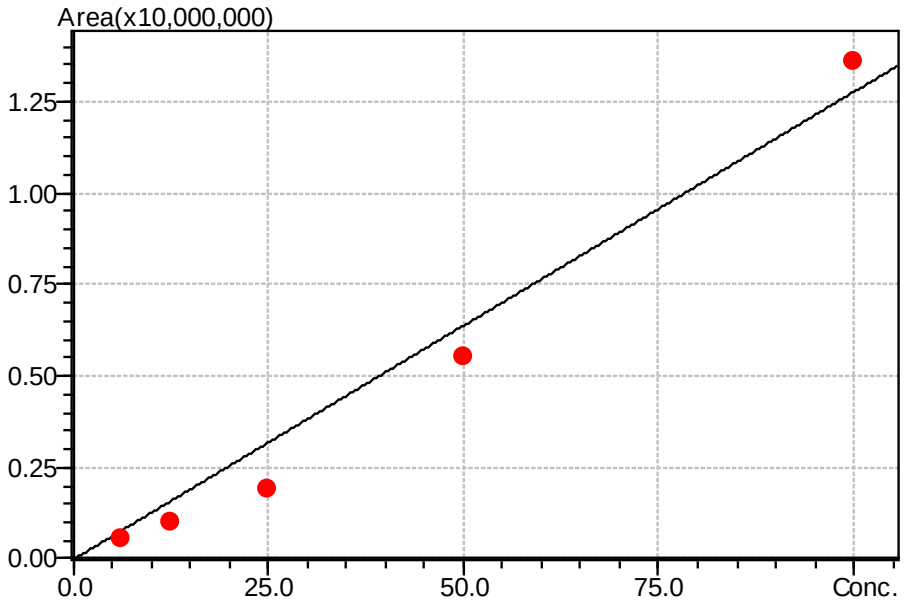

Y = 127786.8X + b
R2 = 0.9886
R = 0.9943
b = 0.0

APPENDIX H: TPT CALIBRATION

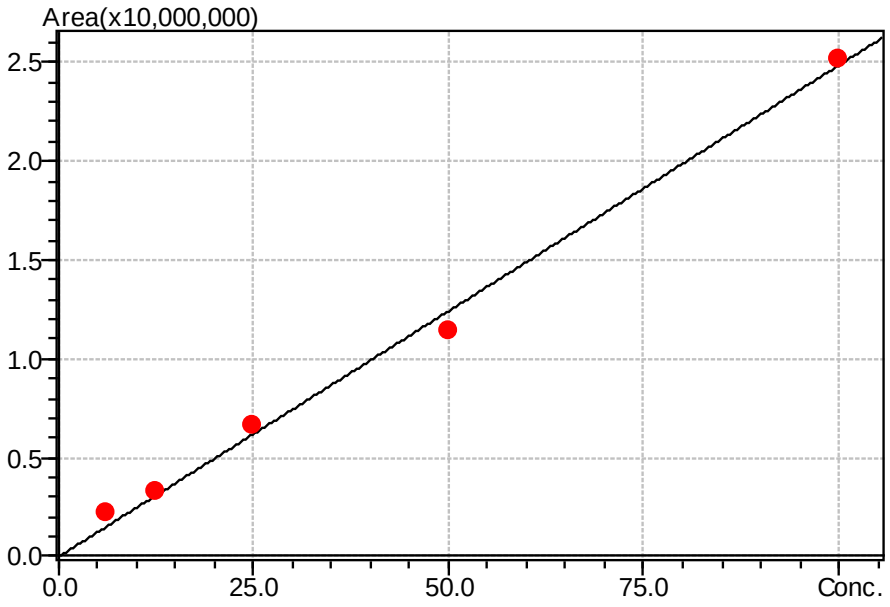

Y = 248941X + b
R2 = 0.9953
R = 0.9976
b = 0.0

APPENDIX I: SOME FTIR SPECTRA OF ADSORBENT RESIDUES BEFORE AND AFTER ORGANOTIN ADSORPTION

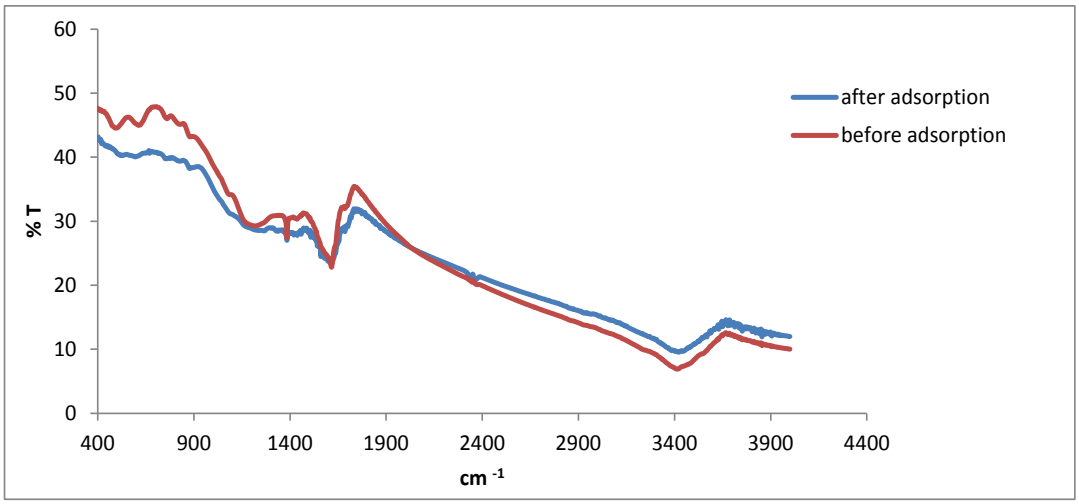

FTIR spectrum of activated carbon before and after TBT adsorption

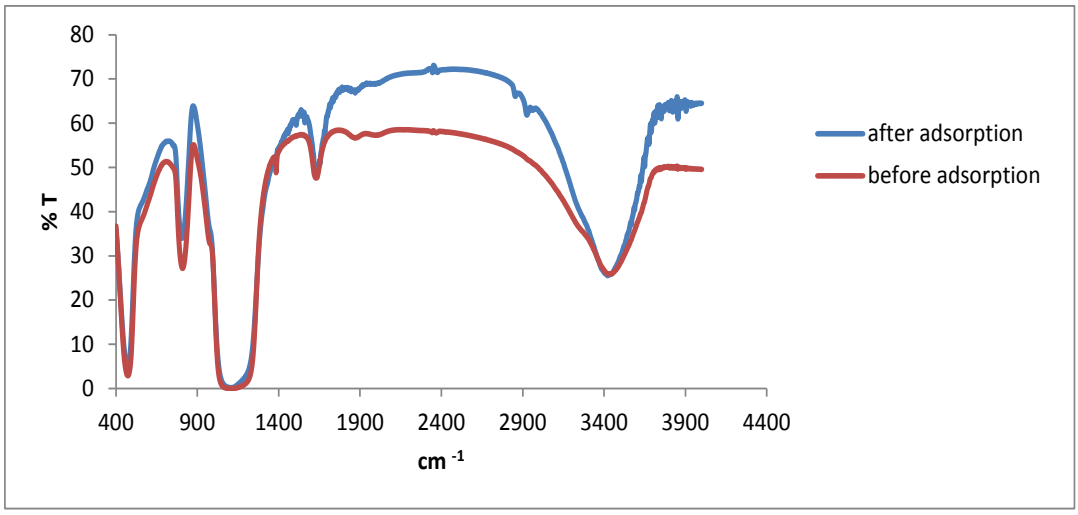

FTIR spectrum of $nSiO_2$ before and after TBT adsorption

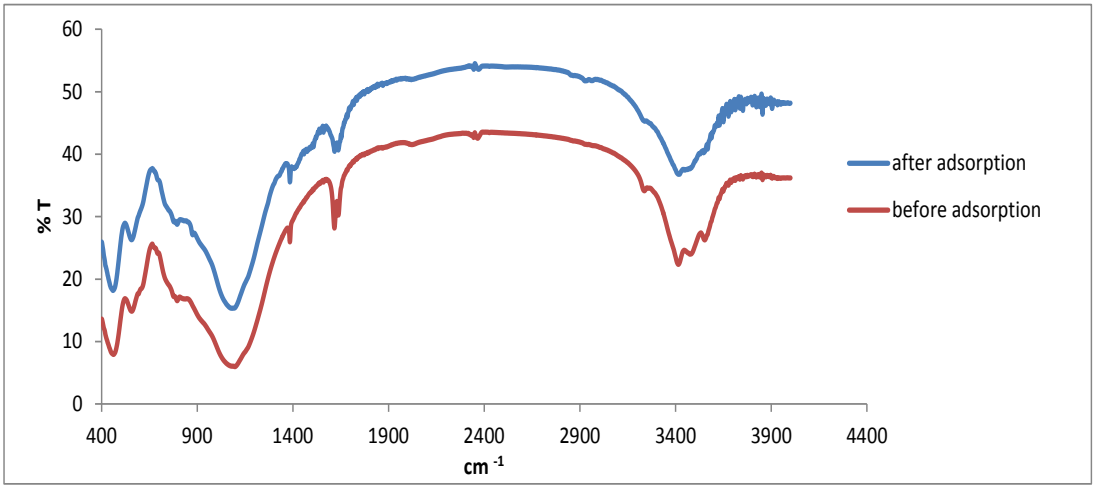

FTIR spectrum of fly ash before and after TPT adsorption

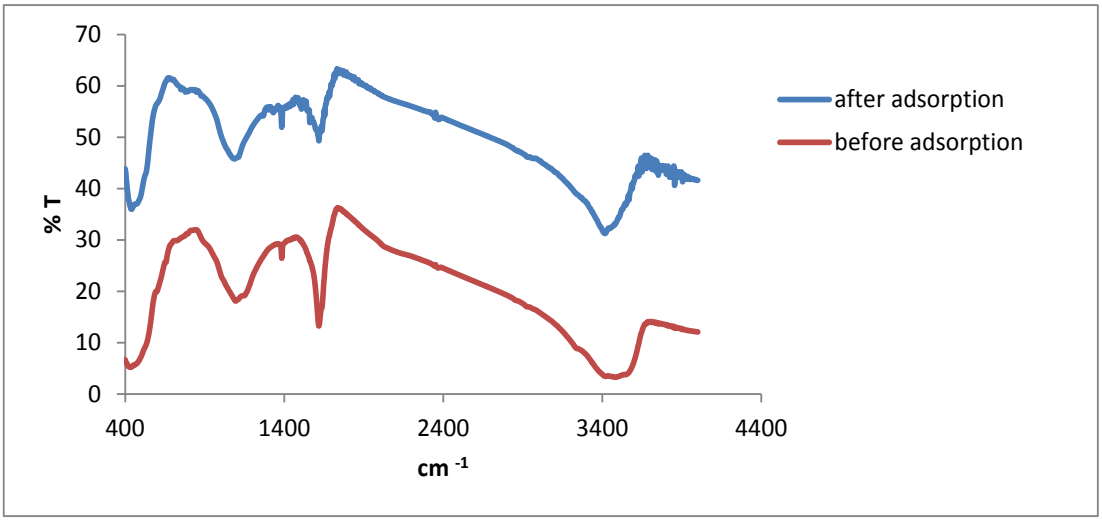

FTIR spectrum of nZnO/fly ash/activated carbon composite before and after TBT adsorption